www.icnf2019.com

Castelló, Spain
26th, 27th, 28th
June 2019

1st International Conference on Nanofluids

2nd European Symposium on Nanofluids

CONFERENCE PROCEEDINGS

1st International Conference on Nanofluids (ICNf2019)
2nd European Symposium on Nanofluids (ESNf2019)

cost EUROPEAN COOPERATION IN SCIENCE & TECHNOLOGY

Funded by the Horizon 2020 Framework Programme of the European Union

nano uptake

#icnf2019

CONFERENCE PROCEEDINGS

1st International Conference on Nanofluids (ICNf2019)

2nd European Symposium on Nanofluids (ESNf2019)

26-28 June 2019, Castelló, Spain

Organized by

Nanouptake Action (CA15119)

Universitat Jaume I

CONFERENCE PROCEEDINGS
1st International Conference on Nanofluids (ICNf2019)
2nd European Symposium on Nanofluids (ESNf2019)

DOI: http://dx.doi.org/10.6035/CA15119.03

ACKNOWLEDGEMENTS

This publication is based upon work from COST Action Nanouptake (www.nanouptake.eu), supported by COST (European Cooperation in Science and Technology).

COST (European Cooperation in Science and Technology) is a funding agency for research and innovation networks. Our Actions help connect research initiatives across Europe and enable scientists to grow their ideas by sharing them with their peers. This boosts their research, career and innovation.

www.cost.eu

cost
EUROPEAN COOPERATION
IN SCIENCE & TECHNOLOGY

Funded by the Horizon 2020 Framework Programme of the European Union

Sponsors

Exhibitors

METER

THERMTEST EUROPE

Sponsors

Ajuntament de Castelló

bp

DIPUTACIÓ DE CASTELLÓ

energies an Open Access Journal by MDPI

FYLA WE LASER THE NEW INDUSTRY

LINSEIS THERMAL ANALYSIS labotronic

UBE

UNIVERSITAT JAUME I Cátedra BP de Medio Ambiente Industrial

UNIVERSITAT JAUME I Cátedra Ciutat de Castelló

Ajuntament de Castelló

GENERALITAT VALENCIANA Conselleria d'Educació, Investigació, Cultura i Esport

Collaborators

cea

magenta H2020 FET-PROACTIVE N° 731976

LABFERRER FOOD - ENVIRONMENT - CROP

METTLER TOLEDO

PROMETEO 2016/079 GENERALITAT VALENCIANA DIGITAL LIGHT

NAITEC

UNIVERSITAT JAUME I School of Technology and Experimental Sciences - ESTCE Department of Mechanical and Engineering Construction

init

UNIVERSITAT JAUME I

Universidade Vigo

Università degli Studi della Campania Luigi Vanvitelli

UNIVERSITÉ DE RENNES 1

Index

About Nanouptake COST Action CA15119

Nanouptake – Overcoming Barriers to Nanofluids Market Uptake aims to create a Europe-wide network of leading R+D+i institutions, and of key industries, to develop and foster the use of nanofluids as advanced heat transfer/thermal storage materials to increase the efficiency of heat exchange and storage systems.

By developing of nanofluids up to higher Technological Readiness Levels (TRL) and overcoming commercial application barriers, **Nanouptake** will contribute to achieve the European Horizon 2020 Energy and Climate objectives (Societal Challenges 3: Secure, efficient and clean energy; and 6: Climate action, environment, resource efficiency and raw materials).

About ICNf2019 and ESNf2019

The 1st International Congress on Nanofluids (ICNf) and the **2nd European Symposium on Nanofluids** (ESNf) offers a series of international conferences under the auspices of the European Cooperation in Science and Technology (COST) Action - Nanouptake (CA15119, www.nanouptake.eu).

This event provides platforms for global collaboration and exchange of knowledge between researchers and engineers working on nanofluids – suspensions with particles ranging in size from 10 nm to 100 nm – and related areas.

Focuses of ICNf2019 and ESNf2019 include production and characterisation of nanofluids and liquid-based nanocomposites, nanofluid-based heat transfer and storage of thermal energy, as well as industrial applications.

Representatives of related industries are invited to ICNf2019 and ESNf2019 to enable direct knowledge transfer from science to industry.

ICNf2019 and ESNf2019 cover nanofluid aspects ranging in a wide field from basic research to real world industrial applications. Main topics include the following:

- Nanofluid materials (nanoparticles, nanoPCM, nanofluids, nanosalts, ionanofluids, etc.)
- Nanofluid preparation and characterization methods, (stability (physical and chemical effects), agglomeration, etc.)
- Nanofluid properties (thermophysical, optical, and magnetic properties)
- Heating, cooling, and refrigeration
- Phase change based heat transfer (boiling, surface coating, heat pipes, etc.)
- Storage of thermal energy
- Solar energy applications (specific black nanofluids, volumetric solar collectors, etc.)
- Numerical simulation on the microscopic and macroscopic levels
- Industrial applications
- Health, safety, and environmental issues

Organizing Committee

Chair: Leonor Hernández López (Universitat Jaume I, Spain)

Vice-Chairman: Matthias H. Buschmann (ILK Dresden gGmbH, Germany)

Lucía Buj Vicente	Universitat Jaume I
Sergio Chiva Vicent	Universitat Jaume I
Vicent Climent Jordà	Universitat Jaume I
Josep Forner Escrig	Universitat Jaume I
Alexandra Gimeno	Universitat Jaume I
Jesús Lancis Sáez	Universitat Jaume I
Sergio Martí Forés	Universitat Jaume I
Raúl Martínez Cuenca	Universitat Jaume I
Laura Menéndez Monzonís	Universitat Jaume I
Gladys Mínguez Vega	Universitat Jaume I
Rosa Mondragón Cazorla	Universitat Jaume I
Elena Mulet Escrig	Universitat Jaume I
Sohel Murshed	Universidade de Lisboa
Nuria Navarrete	Universitat Jaume I
Roberto Palma Guerrero	Universitat Jaume I
Juan S. Pérez Villanueva	Universitat Jaume I

Scientific Commitee

Leonor Hernández López	Universitat Jaume I	Spain
Matthias H. Buschmann	ILK Dresden gGmbH	Germany
Alina Adriana Minea	Technical University "Gheorghe Asachi" from Iasi	Romania
Reza Azizian	MIT, Massachusetts Institute of Technology	USA
Simona Barison	ICMATE	Italy
Camila Barreneche	Universitat de Barcelona	Spain
Siniša Bikic	University of Novi Sad	Serbia
Yulong Ding	University of Birmingham	United Kingdom
Patrice Estellé	Université Rennes 1	France
Luisa F. Cabeza	Universitat de Lleida	Spain
Ali J.Chamkha	Prince Mohammad Bin Fahd University	Kingdom of Saudi Arabia
Peter Farber	Hochschule Niederrhein University of Applied Sciences	Germany
Laura Fedele	Consiglio Nazionale delle Ricerche	Italy
Jesper Glückstad	Technical University of Denmark	Denmark
Jianying He	Norwegian University of Science and Technology	Norway
Kamel Hooman	The University of Queensland	Australia

Siamak Hosseinzadeh	Islamic Azad University	Iran
Angel Huminic	Transilvania University of Brasov	Romania
Ahmed Kadhim Hussein	Babylon University	Irak
Ali Kosar	Sabanci University	Turkey
Janusz Krupanek	Institute for Ecology of Industrial	Poland
Jesús Lancis Sáez	Universitat Jaume I	Spain
Luis Lugo	University of Vigo	Spain
Omid Mahian	Xi'an Jiaotong University	China
Oronzio Manca	Università degli Studi della Campania "Luigi Vanvitelli"	Italy
Simone Mancin	University of Padova	Italy
Raul Martínez Cuenca	Universitat Jaume I	Spain
Gladys Mínguez Vega	Universitat Jaume I	Spain
Rosa Mondragón Cazorla	Universitat Jaume I	Spain
Syed Tauseef Mohyud-Din	HITEC University Taxila Cantt	Pakistan
Sohel Murshed	Universidade de Lisboa	Portugal
Sawako Nakamae	CEA	France
Carlos Nieto de Castro	Universidade de Lisboa	Portugal
Josua P. Meyer	University of Pretoria	South Africa

Jure Ravnik	University of Maribor	Slovenia
Roger Rhiel	Instituto Nacional de Pesquisas Espaciais	Brasil
Elisa Sani	Istituto Nazionale di Ottica INO	Italy
Antonis Sergis	Imperial College	UK
Raja Sekhar Dondapati	Lovely Professional University	India
Bengt Sunden	Lund University	Sweden
Robert Taylor	University of New South Wales	Australia
Alpaslan Turgut	Dokuz Eylul University	Turkey
Dongsheng Wen	University of Leeds	United Kingdom
Somchai Wongwises	King Mongkut's University of Technology Thonburi	Thailand
Bartosz Zajaczkowski	Wroclaw University of Science and Technology	Poland
Gennady Ziskind	Ben-Gurion University	Israel
Gawel Zyla	Rzeszow University of Technology	Poland

Plenary Lectures

1) Nanofluids; Opportunities, Lack of Principle Research and Points on Accurate Publications

Mohsen Sharifpur
Associate Professor
Department of Mechanical and Aeronautical Engineering
Faculty of Engineering, Built Environment and Information Technology
University of Pretoria (UP)
South Africa

His research area includes mathematical modelling, thermal fluid behaviour and stability of nanofluids, improvement of heat transfer by nanofluids, convective multiphase flow, and computational fluid dynamics. He established a Nanofluid Research Laboratory at the University of Pretoria (UP) in 2010, which is the most active and productive nanofluids laboratory in Africa.

He is an innovative thinker and in 2016 received funds from the Technology Innovation Agency of South Africa (TIA) to construct an emergency cooling design by using nanofluids. In the same year, he published a journal article which offered a new correlation for the density of nanofluids based on nanolayer.

Professor Sharifpur has authored or co-authored of more than 70 peer-reviewed articles (published in accredited journals) and international conference papers about nanofluids. At UP, he has acted as supervisor for three post-doctoral researchers, three PhD students, and ten master's students, all of which have completed their research.

At the moment, he is supervising one post-doctoral researcher, six PhD students and one master student. Also, he guided more than 150 undergraduate final year design and project students. Professor Sharifpur acts as a reviewer for notable accredited journals and prestigious international conferences. He is registered with the Engineering Council of South Africa as a professional engineer and received a C2 rating scientist for his research activities from the National Research Founds (NRF) of South Africa.

2) Pool boiling of nanofluids

Somchai Wongwises

Professor
Department of Mechanical Engineering
King Mongkut's University of Technology Thonburi
Thailand

Somchai Wongwises is currently a Professor of Mechanical Engineering, Faculty of Engineering at King Mongkut's University of Technology Thonburi, Bangmod (KMUTT), Bangkok, Thailand. He received his Doktor Ingenieur (Dr.-Ing.) in Mechanical Engineering from the University of Hannover, Germany, in 1994. His research interests include Gas-Liquid Two-Phase Flow, Heat Transfer Enhancement, and Thermal System Design. He is a member of the technical committee and editorial board of many International Conferences and journals. He has more than 400 research papers published in ISI Journals. Professor Wongwises is the head of the Fluid Mechanics, Thermal Engineering and Multiphase Flow Research Laboratory (FUTURE).

3) Boosting solar collector performance with nanofluids: The optical properties of nanofluids

Robert Taylor

Associate Professor
School of Mechanical and Manufacturing Engineering and School of Photovoltaic and Renewable Energy Engineering
University of New South Wales
Australia

Professor Robert A Taylor's main research interest is in the development of 'next generation' solar thermal collectors. Drawing on the fields of heat transfer and nanotechnology, he is researching new/novel working fluids and materials for solar systems, with the main goal is to provide a more efficient and more economic sustainable energy solutions.

4) Tailoring radiative properties of nanofluids

Stephan Kabelac

Professor
Institute for Thermodynamics
Faculty of Mechanical Engineering
Leibniz University Hannover
Germany

Stephan Kabelac is full professor at the Institute for Thermodynamics at the Leibniz University of Hannover. Before this appointment he was heading the Institute for Thermodynamics at the Helmut-Schmidt University, the University of the Federal Armed Forces in Hamburg, Germany, from 2001 until 2011. Before that, he was the Chair of the Institute for Thermodynamics at the University of Hannover, Germany, since 1994. From 1991 – 1994 he was in the destillation and heat transfer research group at the Bayer Chemical Company AG in Leverkusen, Germany.

His research topics are connected to condensation and evaporation heat transfer in plate heat exchangers, to heat, mass and charge transport in fuel cells, to the thermodynamic evaluation of solar energy conversion devices and to the measurement of thermophysical and optical properties of nanofluids.

5) Full-spectrum solar thermal conversion and storage via photonic nanofluids

Xianglei Liu

Professor
Department of Energy and Power Engineering
Nanjing University of Aeronautics and Astronautics
China

Professor Xianglei Liu got his bachelor and Ph.D degree from Xi'an Jiaotong University and Georiga Institute of Technology, respectively. He is mainly focused on solar thermal conversion, nanoscale thermal radiation, and energy storage. He has authored more than 30 peer-reviewed journal papers and one book. He received Raymond Viskanta Young Scientist Award,EU-China Symposiums on Renewable Energy/Sustainable Energy and Energy Storage Technologies Best Poster Award.

Contents

SESSION 1
Heating

S1

SESSION 2
Cooling, Refrigeration

S2

SESSION 3
Storage of Thermal Energy

S3

Nanoencapsulation of Metallic PCMs with Atomic Layer Deposition
N. Navarrete, L. Hernández, D. La Zara, J.R. van Ommen and R. Mondragón*

Dynamic Viscosity and Surface Tension Characterization of Paraffin-in-Water Nanoemulsions
D. Cabaleiro*, S. Hamze, F. Agresti, P. Estellé*, S. Barison, L. Fedele, S. Bobbo

From MD Simulations to experimental study: Molten salt based nanofluids
A. Svobodova-Sedlackova, C. Barreneche, P. Gamallo and A. Ines Fernandez

Thermophysical characterization of novel nanoenhanced phase change materials (NEPCM) based on fatty acid and SiO_2 nanoparticles
Marc Martín, Camila Barreneche*, A. Inés Fernández

Silver dispersions in poly(ethylene glycol) as novel NePCMs for thermal energy storage
M.A. Marcos, D. Cabaleiro*, L. Fedele, S. Bobbo, L. Lugo

SESSION 4
Boiling, Phase Changed Based Heat Transfer, Surface Coating, Heat Pipes

S4

How to detect geysering of nanofluid in a thermosyphon?
A. Kujawska*, B. Zajaczkowski and M.H. Buschmann

Time and Spatially Resolved Fluid Dynamics and Heat Transfer Characterisation of Nanofluid Droplets Impacting on Heated Surfaces
A. S. Moita*, P. Pontes, F. M. Matos, Q. J. Liang, A. P. C. Ribeiro and A. L. N. Moreira

Oscillating heat pipe operated with ferronanofluid
M. Winckler, A. Potthoff, and M.H. Buschmann*

Effect of nanoparticle coating on pool boiling performance
Z. Wu*, B. Sunden

Prediction of pool boiling heat transfer coefficient for the refrigerant R141b and its solutions with surfactant and nanoparticles using limited set of experimental data
O. Khliyeva, A. Nikulin*, V. Zhelezny, N. Lukianov, Yu. Semenyuk and A.L.N. Moreira

SESSION 5
Solar Energy Applications

S5

SESSION 6

Numerical Simulation on the Microscopic and Macroscopic Levels

S6

SESSION 7

Nanofluids Materials, Nanofluid Preparation and Characterization Methods, Nanofluid Properties

S7

SESSION 8
Industrial Applications

S8

SESSION 9
Health, Safety and Environment

S9

Abstracts

SESSION 0
Nanouptake

SESSION 1
Heating — S1

SESSION 2
Cooling, Refrigeration — S2

SESSION 3
Storage of Thermal Energy — S3

SESSION 4
Boiling, Phase Changed Based Heat Transfer, Surface Coating, Heat Pipes — S4

SESSION 5
Solar Energy Applications — S5

SESSION 6
Numerical Simulation on the Microscopic and Macroscopic Levels — S6

SESSION 7
Nanofluids Materials, Nanofluid Preparation and Characterization Methods, Nanofluid Properties — S7

SESSION 8
Industrial Applications — S8

SESSION 9
Health, Safety and Environment — S9

Nanouptake: European network of nanofluid research

L. Hernández

Dept. Mechanical Engineering and Construction. Universitat Jaume I, Castelló, Spain

lhernand@uji.es

Keywords: nanofluids, heating, cooling, storage, solar applications, research network.

Abstract: Nanouptake (Overcoming Barriers to Nanofluids Market Uptake COST Action CA15119) is a networking action built under the auspices of COST, lasting for 4 years and ending by 2020. The general idea is to bring people from different European countries together to promote the substitution of classical single-phase working fluids by two-phase suspensions consisting of a base fluid and nanometre sized particles. Thus, the main objective of Nanouptake is to create a Europe-wide network of leading R+D+i institutions, and of key industries, to develop and foster the use of nanofluids as advanced heat transfer/thermal storage materials to increase the efficiency of heat exchange and storage systems used in the industry. Nanouptake participants are grouped in four main nanofluids research topics (working groups): 1) heating, 2) cooling, 3) storage and 4) boiling, solar application, modelling and others. The last advances within these topics are discussed and evaluated within the different working groups to improve the coordinated knowledge and efforts to overcome the barriers that difficult nanofluid industrial implementation. An overview on main activities (research mobilities, meetings, conferences, etc) of Nanouptake and results (joint publications, further international research proposals and projects, reports, etc) are presented.

Introduction/Background: Nanofluids (NFs) are defined as thermal energy storage (TES) or heat transfer (HT) or fluids with enhanced heat transfer properties by the addition of nanoparticles (NPs). Despite the huge effort made in the research and development of NFs in the last decade, there are still significant barriers to their market uptake by commercial implementation in industrial applications. If these barriers are overcome, NFs will be an important player in the Value Added Materials (VAM) for the energy sector with a global-orientated market of 10 billion euros/year by 2020 and 50 billion euros/year by 2050 (for all the VAMs related to energy).

NFs are advanced materials developed by nanotechnology and fall, therefore, within one of the Key Enabling Technologies (KET) supported by the European Commission. In

addition, they are mentioned in the Strategic Energy Technology Plan (SET Plan) and the Solar Thermal Electricity Technology Roadmap as potential elements to improve the efficiency of heat exchange and thermal energy storage systems, to thus contribute to meet the European Council energy objectives for 2020.

Although some NF commercial applications currently exist, most of NFs are at Technological Readiness Levels (TRL) 1 to 3. Most NF research has been conducted by research, development and innovation (R+D+i) centres through national funding without coordination. Additional coordinated research and development efforts are required to develop NFs up to higher TRL levels and to overcome commercial application barriers. These barriers are identified as: (1) Not coordinated European research efforts (2) NFs with enhanced thermal conductivity, but considerable pressure loss increment and stability problems (3) NFs not developed for specific industrial applications which maximize its capabilities (4) High cost and industrial manufacturing methods not developed (5) Incomplete NFs Life Cycle Assessment (LCA) issues (6) NFs research not supported by H2020 calls to develop specific NFs to higher TRL levels.

The objective of the NANOUPTAKE COST Action is to create a Europe-wide network of leading R+D+i centres, and of key industries, to develop and foster the use of NFs as advanced heat transfer/thermal storage materials to increase the efficiency of heat exchange and storage systems. For further details see also https://www.cost.eu/actions/CA15119/

Discussion and Results: Nanouptake is a COST Action financed by COST Association (www.cost.eu) . It started in May 2016 and will last for four years. The network of participant countries keeps growing, as during the duration of the Action, new members can enter the network: At the moment there are 25 participants countries involved (out the 38 possible members), includes 260 participants in the field of nanofluids, both from R+D+i centers and industries.

The work of NANOUPTAKE is organised in five working groups.

- WG#1 Heating systems operated with nanofluids
- WG#2 Cooling (including refrigeration) systems operated with nanofluids
- WG#3 Storage of thermal energy employing nanoparticle enhanced systems
- WG#4 Phase change of two-phase systems (solid/liquid) and solar application
- WG#5 Dissemination, publications and press work

The main activities developed within the COST Action are the following:

- Working group meetings. Including management meeting, dissemination meetings, or research meetings as congresses

· Short Term Scientific Missions (STSM), which are institutional visits aimed at supporting individual mobility, fostering collaboration between individuals.

· Training Schools, which provide intensive training in emerging research topics within the laboratories and organisations involved in the Action

· ITC Conference Grants are aimed at supporting early career investigators and PhD students from Participating ITC (Inclusiveness Target Countries, in blue in Figure 2) to attend international science and technology related conferences on the topic of the Action that are not organised by the COST Action

Many results have been obtained during the development of the Nanouptake COST Action, which are aligned with the initially defined objetives of the project. To have a better view of the results, some of the numbers of the Action are:

- 25 COST countries, 11 Inclusiveness Target Countries (ITC) and 1 International Partner Countriy are part of the Nanouptake network
- There are 260 Nanouptake participants, representing universities, research institutes and enterprises
- Four Working Group Meeting have been organized so far within the network, which a total attendance of 287 participants
- There have been 49 Short Termn Scientific Missions (STSM) involving 14 different countries
- A total of 108 people were involved in the three Training Schools performed so far
- Up to 13 young participants from ITC countries of the network had the possibility to present their research results in international conferences thanks to the grants of the action

Additionally, the dissemination to society is of a high importance for Nanouptake, that is why there is a special attention among the network regarding this issue. Many results from the network are included in its website (www.nanouptake.eu), and in addition to that:

- More than 40 digital news about Nanouptake have been released in the media
- Nanouptake has been presented in more than 9 dissemination events in congresses and meetings
- Nanouptake is present in different social networks (facebook, twitter, linkedin), where members of the action share the different activities in which they participate
- Nanouptake network also has a research profile in Researchgate, with more than 150 participants that share their nanofluids papers and joint contributions, so that the people can be updated with the latest advances in the field.

However, the most important objective of the action is that all this activities produce fruitful collaborations that promote a step forward in the research field of nanofluids. This has been the case, as during only the first two years of action all this collateral research advances have been obtained:

- A total of 46 joint publications among Nanouptake members have been obtained (1 book, 1 book of abtracts, 21 published articles, 8 under revision and 15 conference/congress papers)
- Up to 9 joint research proposals have been already submitted to international funding among Nanouptake members and 4 for of them for H2020

Still there are several challenges to be covered in the second half of Nanouptake, but the already developed collaborations within the network will facilitate the task.

Summary/Conclusions: Nanouptake networks has proved effective in promoting the research in the different energy fields of nanofluids. Many collaborations among the participants in the network have derived in joint research publications and projects. For sure the new activity of 1st International Conference on Nanofluids (ICNf2019) will also be a step further in the advances in this field.

References:

1. www.nanouptake.eu
2. https://twitter.com/nanouptake
3. https://www.facebook.com/nanouptake
4. https://www.linkedin.com/company/nanouptake/
5. https://www.researchgate.net/project/Nanouptake-COST-action
6. www.icnf2019.com

SESSION 1
Heating

S1

1st International Conference on Nanofluids (ICNf2019)
2nd European Symposium on Nanofluids (ESNf2019)
26-28 June 2019, Castelló, Spain

Assessment Study on the use of Water-Based Al_2O_3 Nanofluids in a Variety of Heat Exchangers

R. Issa

West Texas A&M University, Canyon, Texas 79016, USA

rissa@wtamu.edu

Keywords: Alumina, Nanoparticles, Convection, Heat Exchanger.

Abstract: This paper attempts to clear up some of the misconceptions regarding the heat transfer of alumina nanofluids in heat exchangers. The paper compiles experimental data from research studies conducted on water-based alumina nanofluids for shell-and-tube and corrugated plate heat exchanges. The paper examines the relation between the nanofluid Nusselt number and other parameters such as: the bulk fluid Reynolds number, nanoparticles size, nanoparticles volume concentration and nanofluid flow pattern.

Introduction/Background: Over the past few decades, a concerted effort has been made to design heat exchangers in a way to maximize their thermal performance. Altering the thermophysical properties of the original fluid by adding dispersed nanoparticles presents greater convective heat transfer enhancement. The addition of nanoparticles enhances the thermal conductivity of the nanofluid, but its enhancement is minor in comparison to the enormous enhancement in the fluid heat transfer coefficient. This is attributed to the relative velocity between the nanoparticles and the base fluid molecules caused by effects such as the temperature, concentration gradients in the fluid, shear stress, viscosity and gravity. Due to this relative velocity, the nanoparticles move all around and migrate from one region to another causing an enhancement in the convective heat transfer process.

Discussion and Results: Figures 1-a and 1-b show the alumina nanofluid Nusselt number as function of the flow Reynolds number for shell-and-tube and corrugated plate heat exchangers. As expected, the results show the nanofluid Nusselt number to increase with the increase in Reynolds number. For each type of heat exchanger, the results of the various studies seem to follow the same trend in the behavior of the data. However, there are few anomaties to this where Nusselt number was not very sensitive

to the increase in Reynolds number. In general, the results show corrugated plate heat exchangers to outperform the other heat exchanger.

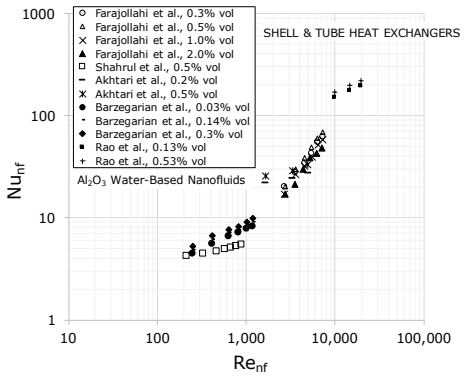

Figure 1-a. Nu_{nf} versus Re_{nf} - shell & tube

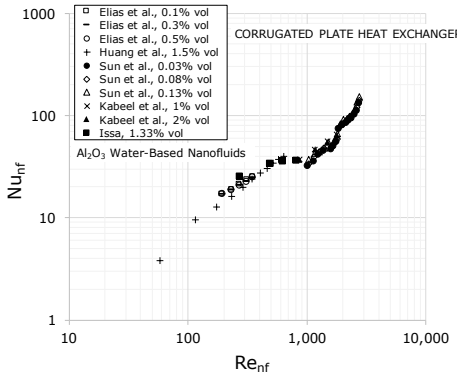

Figure 1-b. Nu_{nf} versus Re_{nf} - corrugated plate

Figures 2-a and 2-b show the alumina nanofluid Nusselt number ratio (nanofluid Nusselt number relative to the base fluid Nusselt number) as function of the alumina nanofluid particle concentration. The results show the Nusselt number ratio to increase with the concentration of the nanoparticles in the shell-and-tube heat exchangers. However, corrugated plate heat exchangers show the Nusselt number ratio to peak around 1% volume concentration and substantially drop with further increase in the nanoparticle concentration. This is likely due to the effect of having a large number of fine channels present in the plate heat exchanger where an increase in concentration can be detrimental.

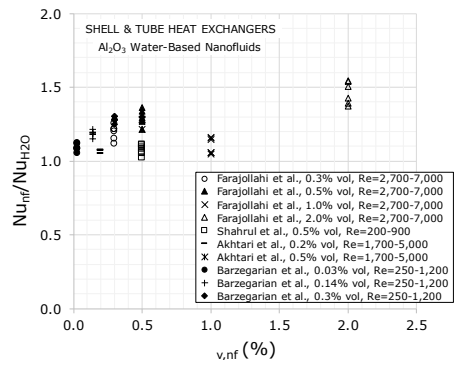

Figure 2-a. Nu_{nf}/ Nu_{H2O} versus particle concentration - shell & tube

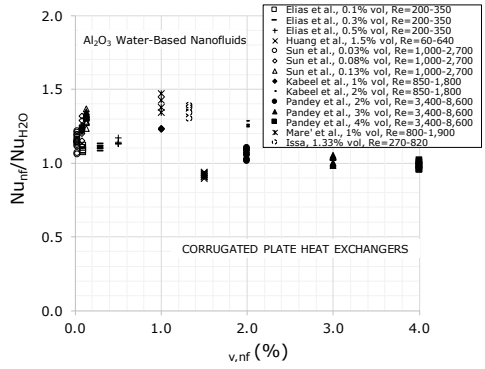

Figure 2-b. Nu_{nf}/ Nu_{H2O} versus particle concentration - corrugated plate

Figures 3-a and 3-b show results for the alumina nanofluid Nusselt number ratio as function of the nanofluid Reynolds number for the shell-and-tube and corrugated plate

heat exchangers. In general, the enhancement is clearly seen to be more significant during the transition from laminar to turbulent flow. The results also show that as the fluid becomes highly turbulent, any further increase in Reynolds number does not seem to cause further enhancement in heat transfer. Figure 4-a and 4-b show the alumina nanofluid Nusselt number ratio as function of the alumina nanoparticle size for the two heat exchangers. A decrease in the nanoparticle size appears to cause an enhancement in the fluid Nusslet number in many cases. However, there are several anomalies to this as seen in the case of Barzegarian et al. using 15 nm particles, Mare' et al. using 37 nm particles, and others.

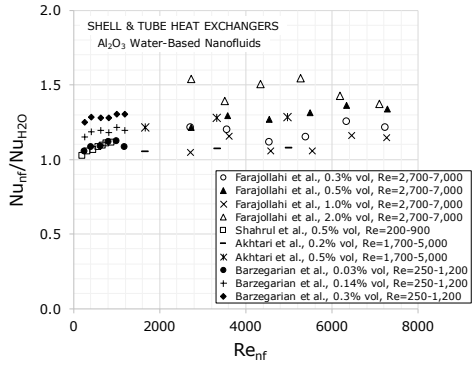

Figure 3-a. Nu_{nf}/ Nu_{H2O} vs. Re_{nf} – shell & tube

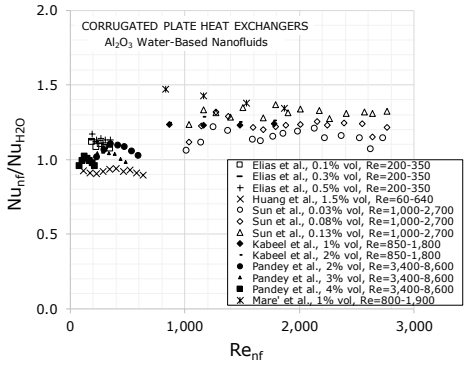

Figure 3-b. Nu_{nf}/ Nu_{H2O} versus Re_{nf} - corrugated plate

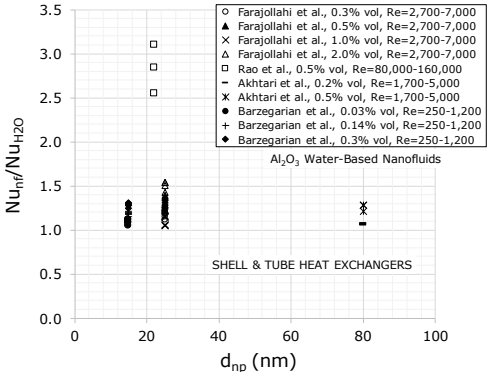

Figure 4-a. Nu_{nf}/ Nu_{H2O} versus d_{np} – shell & tube

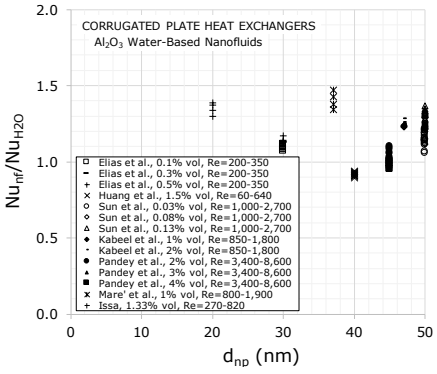

Figure 4-b. Nu_{nf}/ Nu_{H2O} versus d_{np} – corrugated plate

Summary/Conclusions: Al_2O_3 Nanofluid Nusselt number is shown to increase with Reynolds number. Corrugated plate heat exchangers are shown to outperform shell-and-tube heat exchangers. Data reveals the enhancement in the Nusselt number increases with the nanoparticle concentration for shell-andtube heat exchangers, but for plate heat exchangers an optimal concentration is found. The enhancement in heat transfer is more significant as the fluid transitions to turbulent flow. In general, there is

no clear indication that the smaller the nanoparticle size, the greater is the heat transfer enhancement.

References:

1. B. Farajollahi, S. Etemad, and M. Hojjat, Heat transfer of nanofluids in shell and tube heat exchanger, *International Journal of Heat and Mass Transfer* 53 (2010) 12-17.
2. I.M. Shahrul, I.M. Mahbubul, R. Saidur, and M. Sabri, Experimental investigation of Al_2O_3-W, SiO_2-W and ZnO-W nanofluids and their application in a shell and tube heat exchanger, *International Journal of Heat and Mass Transfer* 97 (2016) 547-558.
3. M. Akhtari, M. Haghshenasfard, and M. Talaie, Numerical and experimental investigation of heat transfer of α-Al_2O_3/water nanofluid in double pipe and shell and tube heat exchanger, *Numerical Heat Transfer* 63 (2013) 941-958.
4. R. Barzegarian, A. Aloueyan, and T. Yousefi, Thermal performance augmentation using water based Al2O3-gamma nanofluid in a horizontal shell and tube heat exchanger under forced circulation, *International Communications in Heat and Mass Transfer* 86 (2017) 52-59.
5. M. Rao, D. Sreeramulu, and D.A. Naidu, Experimental investigation of heat transfer rate of nanofluids using a shell and tube heat exchanger, *IOP Conference Series: Materials Science and Engineering* 149 (2016) 1-8.
6. M.M. Elias, R. Saidur, R. Ben-Mansour, A. Hepbasli, N.A. Rahim, and K. Jesbains, Heat transfer and pressure drop characteristics of a plate heat exchanger using water based Al_2O_3 nanofluid for 30° and 60° chevron angles, *Heat and Mass Transfer* 10 (2018) 2907-2916.
7. D. Huang, Z. Wu, and B. Sunden, Pressure drop and convective heat transfer of Al_2O_3/water and NWCNT/water nanofluids in a chevron plate heat exchanger, *International Journal of Heat and Mass Transfer* 89 (2015) 620-626.
8. A.E. Kabeel, T.A. El Maaty, and Y. El Samadony, The effect of using nano-particles on corrugated plate heat exchanger performance, *Applied Thermal Engineering* 52 (2013) 221-229.
9. S.D. Pandey, and V.K. Nema, Experimental analysis of heat transfer and friction factor of nanofluid as a coolant in a corrugated plate heat exchanger, *Experimental Thermal and Fluid Science* 38 (2012) 248-256.
10. B. Sun, C. Peng, R. Zuo, D. Yang, and H. Li, Investigation on the flow and convective heat transfer characteristics of nanofluids in the plate heat exchanger, *Experimental Thermal and Fluid Science* 76 (2016) 75-86.

11. T. Mare', S. Halelfadl, O. Sow, P. Estelle', S. Duret, and F. Bazantay, Comparison of the thermal performances of two nanofluids at low temperature in a plate heat exchanger, *Experimental Thermal and Fluid Science* 35 (2011) 1535-1543.
12. R. Issa, Thermal evaluation of water-based alumina nanofluid in an electronic heat sink application, *7th European Thermal-Sciences Conference*, Krakow, Poland, June (2016) 19-23.

1st International Conference on Nanofluids (ICNf2019)
2nd European Symposium on Nanofluids (ESNf2019)
26-28 June 2019, Castelló, Spain

Performance of TiO_2 Nanoparticles Modified Oil-paper Insulation under Accelerated Thermal Aging

M. Huang[1]*, B.L. Shan[1,2], Y.P. Ying[1,2], Y.Z Lv[3] and C.R. Li[1,2]

[1]Beijing Key Laboratory of High Voltage & EMC, North China Electric Power University, Beijing 102206, China

[2]State Key Laboratory of Alternate Electrical Power System with Renewable Energy Sources, North China Electric Power University, Beijing, 102206, China

[3]School of Energy, Power and Mechanical Engineering, North China Electric Power University, Beijing, 102206, China

*Corresponding author: hm2016@ncepu.edu.cn

Keywords: Accelerated thermal aging, TiO_2 nanoparticles, Dielectric fluids, Discharge.

Abstract: Electrical property of oil-paper insulation can be greatly improved with the modification of nanoparticles, but its stability against thermal aging has not been set foot so far. In this paper, 10-nm TiO_2 nanoparticles were used for modification and samples were thermally aged at 130°C for 36 days. Aging rate of dielectric fluid can be reduced by TiO_2 nanoparticles, but they didn't affect the variation of pressboard's degree of polymerization. The breakdown strength of nanofluid was always larger than that of mineral oil and the difference was nearly fixed to 10 kV. However, no matter whether it was under AC or lightning impulse voltage, the modification of surface discharge can't endure thermal aging, which resulted from by-products' deposition and fibre's fracture.

Introduction: Owing to its excellent electrical performance, oil-paper insulation has been widely used as the main insulating material in transformers, but recently the requirement of miniaturization, large-capacity and high-reliability for equipment has challenged the electrical property of conventional oil-paper insulation. Nanotechnology has offered a new way to improve the electrical strength. Since it was firstly found that the breakdown strength of mineral oil can be increased with Fe_3O_4 nanoparticles in 1988 [1], it has attracted more and more attention and the dielectric strength of oil-paper insulation can be significantly enhanced. However, oil and paper degrade gradually during operation due to the combined electrical, thermal and mechanical stresses [2]. Hence a new problem generates that whether modification is steady when faced to thermal stress and there has been just a few researches related to it [3-4]. They have found that the nanofulid modified by either TiO_2 [3] or Fe_3O_4 [4] nanoparticles shows a better

performance in some ways than mineral oil during thermal aging. Therefore, this paper extended the study to the performance of breakdown in dielectric fluid and surface discharge along the fluid-pressboard interface during accelerated thermal aging.

Discussion and Results: 10-nm TiO_2 nanoparticles were prepared by hydrolysis method using tetrabutyl titanate as the titanium source and they were dispersed into the previously severely processed mineral oil through ultrasonic method [3]. Then strictly dried pressboard pieces were impregnated into the nanofluid (named NF) and dielectric fluid (named OF), respectively. After these treatments, the moisture contents of both oil-impregnated pressboard (named OP) and nanofluid-impregnated pressboard (named NP) were no larger than 0.5%. Finally they were placed in nitrogen at 130°C together with some copper pieces for accelerated thermal aging.

Some aged OF and NF samples are shown in Figure 1 and they had been separately aged for 0, 12, 24 and 36 days from left to right of each fluid. It can be seen that both OF and NF's colour gradually got darker with aging. Except the un-aged one, all NP's colour was a little lighter than OP's. The variation of acidity and degree of polymerization, which are generally used as index for aging level, are illustrated in Figure 2. The acidity of both OF and NF linearly increased with aging, but NF's acidity was smaller than that of OF all the time. As to the degree of polymerization, thermal ageing resulted in an obvious decrease and it reduced from 1000 to 500 after 36 days' aging, but there seemed to be no difference between OP and NP. Because of the surface hydrophilicity [5], TiO_2 nanoparticles adsorbs aging by-products, for instance water and acid, and consequently restricts their action with oil for degradation, mineral oil's resistance to thermal aging is therefore enhanced. However, since the density of nanoparticles was very low, which was just 0.075% in volume for the nanofluid, only a tiny part of them can transport into the pressboard, and there was no strong bending force between the nanoparticles and fibre [6], they made no difference on fibre's thermal aging.

Results of fluid's breakdown, partial discharge inception voltage (PDIV) and flashover along the interface between pressboard and fluid under alternating current (AC) voltage are demonstrated in Figure 3. As aging level increased, all these properties decreased, especially the breakdown of fluid and PDIV. NF consistently possessed a higher breakdown strength than that of OP and the difference almost kept at 10 kV. For PDIV and surface flashover voltage, property improvement was very obvious at the beginning. However, there was just a small difference between OP and NP during accelerated thermal aging. The variation of dielectric strength with aging against both positive and negative lighting impulses is presented in Figure 4. No matter whether positive or

negative lightning impulse was applied, the result was similar to the surface flashover performance under AC voltage, namely, though modification with TiO_2 nanoparticles indeed improved the lightning impulse breakdown strength in the preliminary stage of thermal aging, it can't withstand thermal aging and it had little influence in the final stage. It has been known that thermal aging causes the fracture of fibre and its structure loosing, so there are more pores in pressboard and pressboard's surface becomes rough [2]. Besides, thermal aging leads to the generation of particles, part of them can be deposited on pressboard's surface. Trap energy on the surface will thereby be deepened and charge accumulation increases, making the interface between pressboard and nanofluid becomes beneficial to surface discharge. Meanwhile, the migration of by-products carries some nanoparticles out of NP, which weakens the improvement of TiO_2 nanoparticles. As a result, though NF's strength is enhanced, NP and OP's corresponding dielectric strengths are close when thermal aging level is serious.

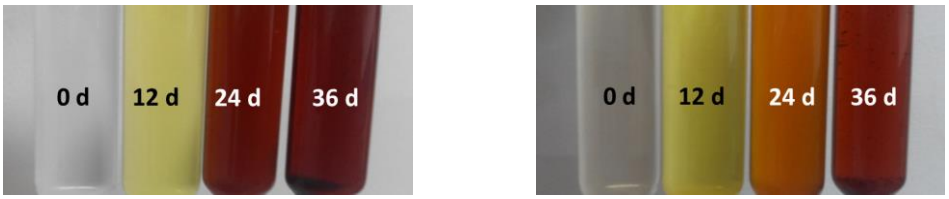

(a) OF **(b) NF**

Figure 1. Display of aged OF and NF samples

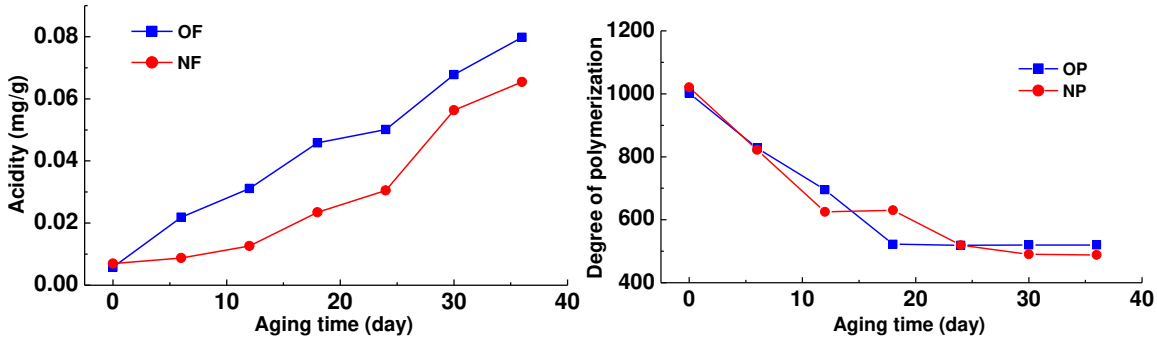

Figure 2. Variation of acidity and degree of polymerization with aging time

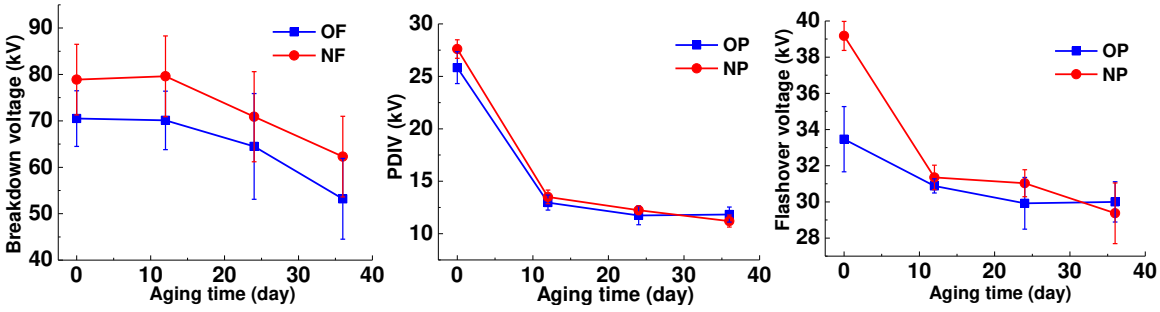

Figure 3. Variation of electrical properties under AC voltage with aging time

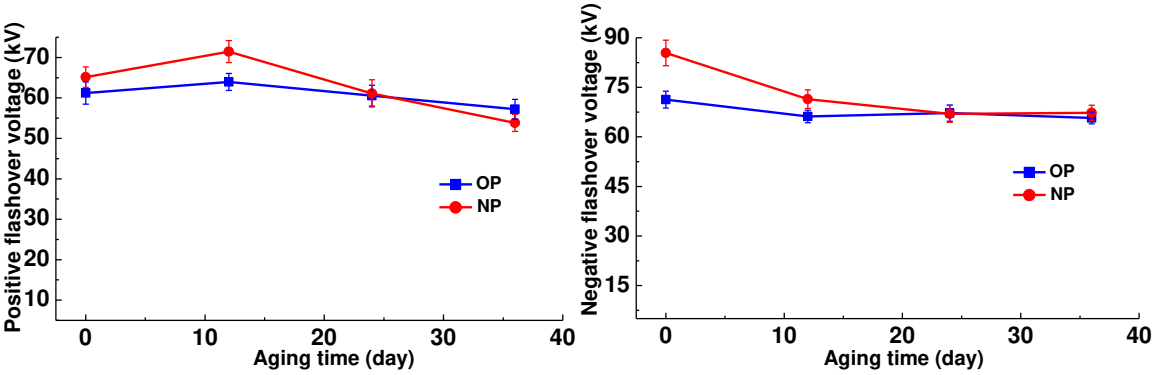

Figure 4. Variation of lightning impulse breakdown voltages with aging time

Summary: Modification with TiO_2 nanoparticles increases mineral oil's resistance to thermal aging on account of surface hydrophilicity, but it has little effect on fibre's aging. Nanofluid always owes a larger breakdown strength during thermal aging, but performance improvement of surface discharge on NP depends on aging level and it may be restricted by serious aging due to traps property degradation on the surface.

References:

1. V. Segal, A. Hjortsberg, A. Rabinovich and D. Nattrass, AC (60 Hz) and impulse breakdown strength of a colloidal fluid based on transformer oil and magnetite nanoparticles, Proceedings of the 1998 IEEE International Symposium on Electrical Insulation, Arlington, Virginia, USA, June 07-June 10, 1998.
2. A. M. Emsley, R. J. Heywood, M. Ali and C. M. Eley, On the kinetics of degradation of cellulose, *Cellulose* 4 (1997) 1-5.
3. Y. Lv, Y. Du, C. Li, B. Qi, Y. Zhong and M. Chen, TiO_2 nanoparticle induced space charge decay in thermal aged transformer oil, *Applied Physics Letters* 102 (2013) 132902.
4. V. Segal, D. Nattrass, K. Raj and D. Leonard, Accelerated thermal aging of petroleum-based ferrofluids, *Journal of Magnetism and Magnetic Materials* 201 (1999) 70-72.
5. Y. Q. Hao, Y. F. Wang and Weng Y X, Particle-size-dependent hydrophilicity of TiO_2 nanoparticles characterized by marcus reorganization energy of interfacial charge recombination, *The Journal of Physical Chemistry C* 112 (2008) 8995-9000.
6. V. Segal, A. Rabinovich, D. Nattrass, K. Raj and A.Nunes, Experimental study of magnetic colloidal fluids behavior in power transformers, *Journal of Magnetism and Magnetic Materials* 215 (2000) 513-515.

1st International Conference on Nanofluids (ICNf2019)
2nd European Symposium on Nanofluids (ESNf2019)
26-28 June 2019, Castelló, Spain

Numerical study on the thermal performance of titanium dioxide water-based nanofluid in a heated pipe

G. Sekrani[1]*, S. Poncet[1], A. Minea[2], A. Di Pasqua[3] and O. Manca[3]

[1]Mechanical Engineering Department, Université de Sherbrooke
2500 boulevard de l'Université, Sherbrooke (QC), J1K 2R1, Canada
[2]Technical University "Gheorghe Asachi" of Iasi,
Faculty of Materials Science and Engineering, Iasi, Romania
[3]Dipartimento di Ingegneria, Università degli Studi della Campania "
Luigi Vanvitelli", Via Roma 29, 81031 Aversa, Italy

*Ghofrane.sekrani@usherbrooke.ca

Keywords: Heat transfer, nanofluid, thermal performance.

Abstract: In the present paper, laminar forced convection nanofluid flows in a uniformly heated horizontal pipe are numerically carried out using the mixture model with base fluid temperature-dependent properties. The results are presented and discussed for five different values of TiO_2 nanoparticle concentrations, namely φ=0, 1, 2, 3 and 4 vol.% and three mass flowrates 6, 8 and 10 g/s. A good agreement with the experimental data is found.

Introduction: Recent advances in nanotechnology have led to the manufacturing of nanometer-sized particles referred to as nanoparticles with an equivalent diameter smaller than 100 nm. In 1995, a new class of heat transfer fluid named nanofluids has been developed by dispersing nanoparticles in traditional host fluids [1]. Colla et al. [2] experimentally investigated titania nanofluid water-based laminar flows in a uniformly heated horizontal pipe for different Reynolds numbers Re and nanoparticle concentrations φ. They noted that the nanofluid thermophysical properties were very close to the equivalent values of base fluid (water). Thus, the authors purely attributed the heat transfer enhancement to the nanoparticles migration. An experimental study of the heat transfer performance of ethylene glycol/water based TiO_2 nanofluid flowing in a circular tube was conducted by Reddy and Rao [3]. They found that the heat transfer performance enhanced with increasing φ and/or Re. He et al. [4] numerically studied the laminar convective heat transfer of TiO_2-water nanofluid flowing through a straight tube using both single phase and combined Euler and Lagrange methods. They mentioned that the convective heat transfer coefficient was mostly affected by the thermal conductivity rather than the viscosity. In the present work, we investigate the effects of

the nanoparticle concentration and the mass flow rate on convective heat transfer performance of TiO_2-water nanofluid using the mixture model.

Method: Laminar nanofluid flow inside a heated pipe is numerically investigated in the present study. The fluid is incompressible and the flow is assumed to be steady-state. The geometry corresponds to the experimental set-up developed by Colla et al. [2]. It consists of a horizontal cylindrical pipe of a length L = 2 m and a diameter D = 0.008 m, heated with a uniform heat flux, Q = 200 W, along the wall. A fully developed flow with constant temperature enters the test section. The thermophysical properties of water are considered to be temperature dependent [5]. However, the thermophysical properties of the titanium dioxide nanoparticles are considered as constants with ρ_{np}=3975 kg.m^3, Cp_{np} = 692 J.kg^{-1}.K^{-1} and k_{np} = 8.4 W.m^{-2}.K^{-1} (np: nanoparticles). The mixture model is used to model the convective nanofluid flow. For the sake of brevity, the reader can refer to the studies conducted by Sekrani et al. [5] for more details about the mixture approach. To validate the numerical solver, we initially considered pure water simulations. Six different grid distributions were tested to ensure the independence of the numerical results to the grid size. A small difference of about 1% between the coarser and the finer grids is reported for the prediction of both wall and bulk temperatures. It was therefore concluded that all the remaining simulations will be performed with the 2 million nodes. Good agreement with the experimental results of Colla et al. [2] was found with maximum errors for both the wall and bulk temperatures of 5 % and 2 %, respectively.

Results and Discussion: The axial development of the local heat transfer coefficient, h, for different nanoparticle concentrations and mass flowrates is displayed in figure 1. From the latter, one can see that for all the cases considered, the local heat transfer coefficient increases in the entrance region and then rapidly decreases with the axial distance before reaching a minimum value. When this minimum value is achieved, the local heat transfer coefficient starts to increase as the flow tends to be fully developed. Abraham et al. [6] also found the same behavior in terms of local Nusselt number. Figure 1.a shows that h increases along the domain as the nanoparticle concentration increases. For instance, at $\dot{m} = 8\ g/s$ and φ = 4 vol.%, h increases by about 42 % compared to the pure water near to the pipe exit, z = 1.875 m. In the pipe entrance region, the highest h value is depicted with the highest mass flowrate. However, after reaching the minimum value of h, the lowest $\dot{m}$ value shows the best heat transfer performance in the fully developed region. It is noteworthy that the same behavior was found for all the nanoparticle concentrations however for brevity one only presents the results for φ = 4 vol.%. The

overall performance of water based TiO_2 nanofluid in the laminar forced convection is discussed in terms of the Performance Evaluation Criterion, $\mathrm{PEC} = \frac{\dot{m}Cp_{nf}\Delta T}{\dot{V}\Delta P}$, and the overall energetic efficiency, $\eta = \frac{Nu_{nf}}{\Delta P_{nf}}\frac{\Delta P_{bf}}{Nu_{bf}}$, (bf : base fluid, nf: nanofluid). As clearly seen in figure 2.a, for all the considered mass flowrates, the overall efficiency increases as the TiO_2 concentration increases. However, at a fixed φ, the overall efficiency decreases with the increase of the mass flowrate. For example, at φ = 4 vol.%, *η* decreases by about 20% when the mass flowrate increases from 6 to 10 g/s. Adding nanoparticles to the base fluid leads to a decrease of the PEC number as it can be observed in figure 2.b. At a given TiO_2 concentration, the PEC decreases as the mass flowrate increases. For instance, at $\dot{m} = 8\ \mathrm{g/s}$, dispersing 4 vol.% of TiO_2 nanoparticles into the pure water decreases the PEC number by about 19 %.

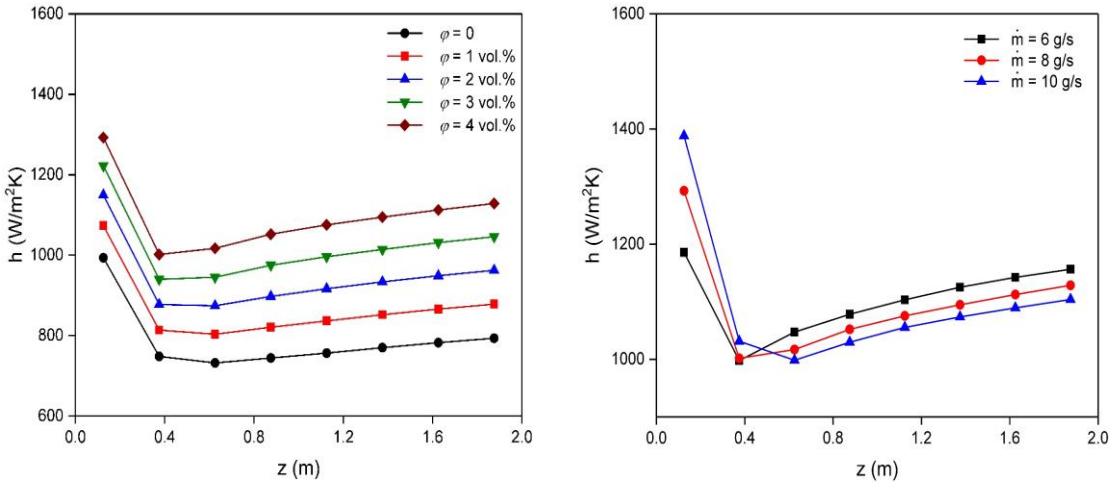

(a) **(b)**

Figure 1. Axial development of the local heat transfer coefficient h for (a) $\dot{m} = 8\ \mathrm{g/s}$ and 5 nanoparticle concentrations and (b) ϕ = 4 vol.% for three mass flowrates

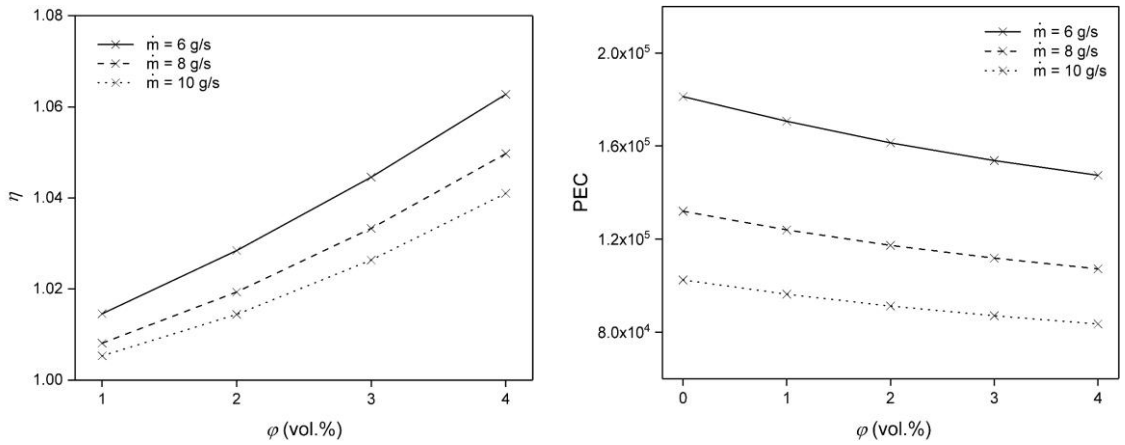

(a) **(b)**

Figure 2. Evolutions of (a) the overall efficiency η and (b) the PEC number as a function of the nanoparticle concentration for three mass flowrates.

Conclusions: Convective heat transfer in a cylindrical tube for laminar flows of TiO_2/water nanofluids was numerically investigated. The results showed that the local heat transfer coefficient and the overall efficiency were increased with the increase of nanoparticle concentration. However, the PEC number decreased at the same time. Further simulation are now carried out to improve the numerical model to take into account the agglomeration phenomenon of nanoparticles by evaluating the nanoparticle size and the volume fraction distribution using the population balance model.

Acknowledgement: G.S. and S.P. thank the support of the NSERC chair on industrial energy efficiency established at Université de Sherbrooke in 2014 and funded by Hydro-Québec, CanmetEnergy and Rio Tinto Alcan. The calculations have been done using the supercomputer Mammouth Parallèle 2 of the Compute Canada's network, which is also acknowledged.

References:

1. S.U.S. Choi and J. Eastman, Enhancing thermal conductivity of fluids with nanoparticles, *ASME International Mechanical Engineering Congress & Exhibition, American Society of Mechanical Engineers*, San Francisco 196525 (1995) 12-17.
2. L. Colla, L. Fedele and M. H. Buschmann, Laminar mixed convection of TiO_2–water nanofluid in horizontal uniformly heated pipe flow, *Int. J. Thermal Sciences* 97 (2015) 26-40.
3. M. C. S. Reddy and V. V. Rao, Experimental investigation of heat transfer coefficient and friction factor of ethylene glycol water based TiO_2 nanofluid in double pipe heat exchanger with and without helical coil inserts, *Int. Comm. Heat and Mass Transf.* 50 (2014) 68-76.
4. Y. He, Y. Men, Y. Zhao, H. Lu and Y. Ding, Numerical investigation into the convective heat transfer of TiO2 nanofluids flowing through a straight tube under the laminar flow conditions, *Applied Thermal Engineering* 29(10) (2009) 1965-1972.
5. G. Sekrani, and S. Poncet, Further investigation on laminar forced convection of nanofluid flows in a uniformly heated pipe using direct numerical simulations. *Applied Sciences*, *6*(11), (2016) 332.
6. J.P. Abraham, E.M. Sparrow and J.C.K. Tong, Heat transfer in all pipe flow regimes: laminar, transitional/intermittent, and turbulent, *Int. J. Heat Mass Transf*. 52 (2009) 557-563.

1st International Conference on Nanofluids (ICNf2019)
2nd European Symposium on Nanofluids (ESNf2019)
26-28 June 2019, Castelló, Spain

Entransy dissipation analysis and new irreversibility dimension ratio of nanofluid flow through adaptive heating elements

F. Alic[1]

[1]Faculty of Mechanical Engineering Tuzla, Department of Thermal and Fluid Technique, Bosnia and Herzegovina
*Corresponding author: fikret.alic@untz.ba

Keywords: Nanofluid, Entransy dissipation, Thermal irreversibility, Heating elements.

Abstract:

The hollow cylindrical electric heating elements of different internal diameters and temperatures are connected in series. Nanofluid flows through the hollow cylindrical elements and thus heats up. The paper analyses the geometric arrangement of cylindrical heating elements with a stepwise reduction in the internal diameter while the temperatures of their interior surfaces are varied, establishing the entransy dissipation rate and new irreversibility dimension ratio of nanofluid flow. The arrangement of heating elements in the flow direction of nanofluid affects the values of the entransy dissipation rate, thermal resistance, and new irreversibility dimension ratio.

Introduction/Background:

Today, there are a large number of different convective electric heaters for compressible and incompressible fluids. Fluid flows through the convection heating surface, while the forced convection of this fluid is heated with different intensity. The fluid velocity, the temperature of the convective surfaces, and the geometric architecture of the channel for the fluid significantly affect the heating process's efficiency. In order to increase the efficiency of convective heating of the nanofluid, an innovative solution of an electric heating system consisting of adaptive heating elements is used in this paper. Furthermore, nanofluid is used as the working medium, with different values of the nanofluid ratio, flowing at different flow rates through different, linearly connected heating elements. In this paper, an analysis of the entransy dissipation rate is carried out; the authors of [1-3] previously investigated entransy dissipation. In addition, the paper introduces a new irreversibility dimension ratio of the entransy dissipation rate and thermal entropy generation. The heating system consists of three hollow cylindrical electric heating elements through which nanofluid or base fluid flows.

Discussion and Results:

Through three hollow cylindrical heating elements (Figure 1), nanofluid flows with 293K input temperature and volumetric flow of 0.0005m^3s^{-1}. The cylindrical elements' temperature is varied at constant values of 400K, 500K, and 600K, and they are positioned differently relative to the nanofluid flow direction. The internal diameter of the cylindrical heating elements gradually decreases in the direction of nanofluid flow, from 15mm to 11mm and 7mm. The paper analyses the entransy dissipation rate, thermal entropy generation, and thermal resistance for different cases of cylindrical elements' position. The aim of this analysis is to determine how much the different temperature arrangement of cylindrical heating elements influences the generation of thermal irreversibility in a nanofluid. The energy balance of the thermal interaction between the internal surface of the heating element and the nanofluid is based on equation (1):

$$\dot{V}_{nf}\left[\varphi\rho_p c_p+(1-\varphi)\rho_f\right]dT_{nf}=\alpha d\pi\left(T_h-T_{nf}\right)dz \tag{1}$$

where $\dot{V}_{nf}$ volumetric flow rate of the nanofluid, T_{nf} nanofluid temperature, φ nanofluid ratio, ρ_f base fluid density, ρ_p nanoparticle density, c_p specific heat capacity of the nanoparticle, α convective heat transfer coefficient, and T_h surface temperature of heating element.

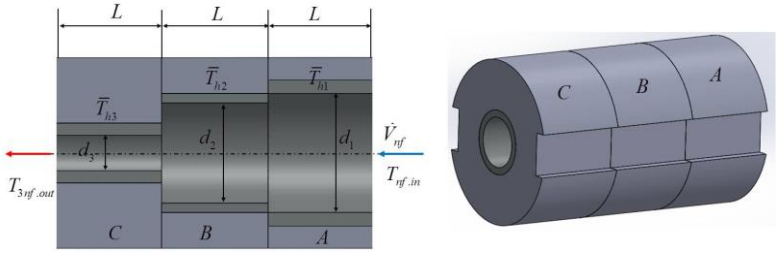

Figure 1. The in-line configuration of the three hollow cylindrical heating elements

The outlet temperature of the nanofluid of the first heating element is obtained

$$T_{nf1.out}=\bar{T}_{h1}-\left(\bar{T}_{h1}-T_{nf.in}\right)\cdot e^{-\frac{4\alpha L}{\left[\varphi\rho_p c_p+(1-\varphi)\rho_f c_f\right]w_{nf}d}} \tag{2}$$

i.e., the output nanofluid temperature from the last (third) heating element is represented by equation (3),

$$T_{nf3.out}=\bar{T}_{h3}-\left\{\left(\bar{T}_{h3}-\bar{T}_{h2}\right)+\left[\left(\bar{T}_{h2}-\bar{T}_{h1}\right)+\left(\bar{T}_{h1}-T_{nf.in}\right)\cdot e^{-\frac{4L}{d_1}\frac{\alpha_1}{w_{nf.1}\left[\varphi\rho_p c_p+(1-\varphi)\rho_f c_f\right]}}\right]\cdot e^{-\frac{4L}{d_2}\frac{\alpha_2}{w_{nf.2}\left[\varphi\rho_p c_p+(1-\varphi)\rho_f c_f\right]}}\right\}\cdot e^{-\frac{4L}{d_3}\frac{\alpha_3}{w_{nf.3}\left[\varphi\rho_p c_p+(1-\varphi)\rho_f c_f\right]}} \tag{3}$$

where T_{h1}, T_{h2}, and T_{h3} are the surface temperature for the first, second, and third cylindrical heating elements, respectively. The output nanofluid temperature from the first heating element is the input temperature for the second heating element. The entransy dissipation rate $\dot{E}_{ent}$ [4] represents a measure of the irreversibility of the heat transfer process. The entransy flow dissipation rate during heating of nanofluid can be described as

$$\Delta\dot{E}_{ent.in-out} = \frac{1}{2}\rho_{nf}\dot{V}_{nf}c_{nf}\left(T_{nf\,3.out}^2 - T_{nf.in}^2\right) \tag{4}$$

In addition, the new irreversibility dimension ratio represents the ratio of the entransy dissipation rate and the thermally generated entropy of the nanofluid in equation (5). The aim of introducing this dimensional relationship is to decide whether there is a difference between the state quantity and the process quantity in heat transfer using nanofluid.

$$\chi = \frac{\Delta\dot{E}_{ent.in-out}}{\dot{S}_{gen.\Delta T}} = \frac{\left(T_{nf\,3.out}^2 - T_{nf.in}^2\right)}{\ln\dfrac{T_{nf\,3.out}}{T_{nf.in}}} = \frac{T_{nf.in}^2}{2}\frac{\left[\left(\dfrac{T_{nf\,3.out}}{T_{nf.in}}\right)^2 - 1\right]}{\ln\dfrac{T_{nf\,3.out}}{T_{nf.in}}} = \frac{T_{nf.in}^2}{2}\frac{\left(\gamma^2-1\right)}{\ln\gamma} \tag{5}$$

On the other hand, the entransy dissipation rate is based on the total thermal resistance (equation (6)), while the characteristic parameters of heating elements and nanofluid are presented in Table 1.

$$R_{ent} = \sum_{i=1}^{3}\frac{\Delta\dot{E}_{ent.i}}{\dot{Q}_i^2} = \sum_{i=1}^{3}\frac{\left(T_{nf.i} + T_{nf.i-1}\right)}{2\rho_{nf}\dot{V}_{nf}c_{nf}\left(T_{nf.i} - T_{nf.i-1}\right)} \tag{6}$$

Table 1. The geometrical parameters of a cylindrical heating element. Physical properties of base fluid and Al_2O_3 nanoparticles.

Substances	$\rho\left[\mathrm{kgm^{-3}}\right]$	$\lambda\left[\mathrm{Wm^{-1}K^{-1}}\right]$	$c\left[\mathrm{Jkg^{-1}K^{-1}}\right]$	$d_1[\mathrm{m}]$	$d_2[\mathrm{m}]$	$d_3[\mathrm{m}]$	$L[\mathrm{m}]$
Al_2O_3	3970	40	765	0.015	0.011	0.007	0.015
Base fluid (water)	997	0.605	4180				

With the increase of volumetric flow and nanofluid ratio, the entransy dissipation rate increases, more quickly if the temperature of the heating elements increases in the nanofluid flow direction, i.e., from 400K to 500K and 600K (Figure 2).

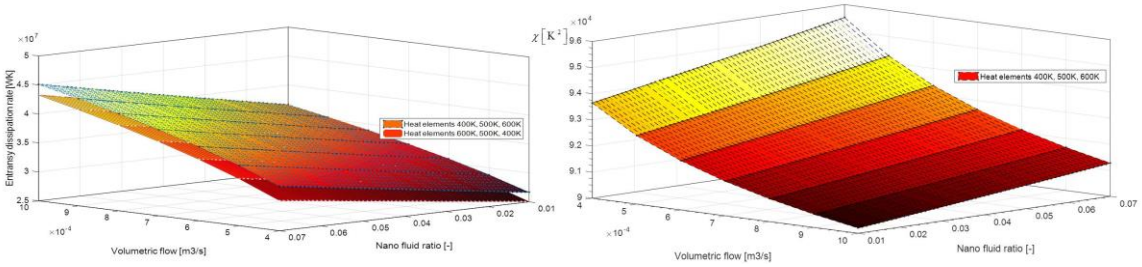

Figure 2. The entransy dissipation rate and new irreversibility dimension ratio.

The maximum values of the new dimensional relationship increase as the nanofluid ratio increases and the volumetric flow decreases. The dimensionless ratio of the thermal resistance when using nanofluid and base fluid (water) is shown in Figure 3. The same figure shows the new irreversibility dimension ratio as a function of volumetric flow and nanofluid ratio. The minimum dimensionless thermal resistance ratio for heating elements' arrangement at 600K, 500K, and 400K is established at a nanofluid rate of 0.17. Thermal resistance with nanofluid is smaller compared to the case of use base fluid. The dimensionless ratio of the new irreversibility dimension ratio (Figure 3 left) increases with the nanofluid ratio, in particular when the heating elements are arranged as 400K, 500K, and 600K in the flow direction.

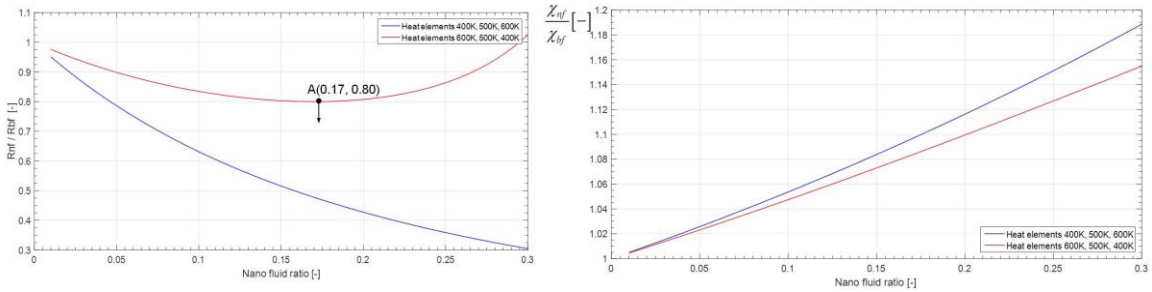

Figure 3. The dimensionless ratio of the thermal resistance and new irreversibility dimension ratio for volumetric flow 0.0005 m^3s^{-1}

Summary/Conclusions:

The analytical modelling of the entransy dissipation and thermal irreversibility using nanofluid flow through three cylindrical heating elements was analysed in this paper. The arrangement of heating elements in the flow direction of nanofluid affects the values of the entransy dissipation rate, thermal resistance, and new irreversibility dimension ratio. The new irreversibility dimension ratio represents the ratio of the entransy dissipation rate and thermal entropy generation in case of the use of nanofluid or base fluid. The established analytical model of the entransy dissipation rate and new irreversibility dimension ratio can be the basis for different thermo-technical processes. Otherwise, the obtained analytical methodology in this paper can be the basis for the optimization of the process and geometrical parameters of an innovative adaptive heating system.

References:

1. X. Qian and Z. Li, "Analysis of entransy dissipation in heat exchangers," *Int. J. Thermal Sci.*, 50 (2011), 608-614.
2. F. Alic, Entransy dissipation analysis of liquid vortex isolated by hollow cylinder, *Heat Transfer Research*, 49 (17) (2018), 1689-1704.
3. Guo, Z. Y., Zhu, H.Y., and Liang, X. G., Entransy - A physical quantity describing heat transfer ability, *Int. J. Heat Mass Transfer*, 50 (2007), 2545-2556.

1st International Conference on Nanofluids (ICNf2019)
2nd European Symposium on Nanofluids (ESNf2019)
26-28 June 2019, Castelló, Spain

Numerical investigation of pressure drop and heat transfer in nanofluids at pore length scale in open metal foams with Kelvin cell

B. Buonomo[1], A. di Pasqua[1], O. Manca[1]*, G. Sekrani[2], S. Poncet[2]

[1]Dipartimento di Ingegneria, Università degli Studi della Campania "Luigi Vanvitelli", Via Roma 29, 81031 Aversa, Italy
[2]Mechanical Engineering Department, Université de Sherbrooke 2500 boulevard de l'Université, Sherbrooke (QC), J1K 2R1, Canada

*oronzio.manca@unicampania.it

Keywords: Heat transfer, Kelvin cell, metal foams, nanofluids, pressure drop.

Abstract: In this paper a numerical analysis in metal foams with Kelvin cell model is accomplished on nanofluids using the single phase model. The examined foams are characterized by a porosity ε = 0.95 and different values of pores per inch, equal to 10 and 20 PPI. The results are presented and discussed for three different values of Al_2O_3 nanoparticle volume concentrations ϕ, equal to 0, 2 and 4%.

Introduction: Open cell foams are attractive materials for several industrial applications, such as: compact heat sinks, geothermal operations, heat exchanger and solar thermal plants. Transport phenomena in foams are highly influenced by their microstructure. Cunsolo et al. [1], using Kelvin and Weaire–Phelan ideal foam models, found that radiative characteristics of a foam were strongly dependent on struts shape of the generated foam. The effect of the morphology of a Kelvin-foam cell on convection heat transfer and effective thermal conductivity was studied by Pusterla et al. [2]. Krishnan et al. [3] accomplished a direct simulation of transport in open-cell metal foams using the Kelvin cell model. The microscopic approach allowed to obtain small-scale details and not to ignore these information as it happens in the governing equations using an engineering model.

Ambrosio et al. [4] carried out a numerical investigation on the thermal and fluid dynamic behavior of open-cell metal foams strut shape. The analysis was accomplished for real and ideal foams. The model of the ideal foams, based on the Kelvin cell model, was built with the same PPI and porosities of the real foams. The results showed that the predictions between ideal and real foams were better when the form of the ideal strut was closer to that of the real strut. Furthermore, it was highlighted that the heat transfer coefficient was major for the ligament convex shape, while a concave strut shape increased the pressure drop.

The goal of present study is the evaluation of the thermal and fluid dynamic behaviour of nanofluids in open metal foams using the Kelvin cell model.

Method: Laminar Al_2O_3-water nanofluid flow is numerically investigated in the present study. The fluid is incompressible and the flow is assumed to be steady-state. The domain is made up of a row with 32 Kelvin cells along the z-direction (Figure 1). The geometry of the ideal foams, based on the Kelvin cell model, has been generated with the free-to-use software

Surface Evolver. Fluent 15.0 is adopted to execute the numerical analyses.

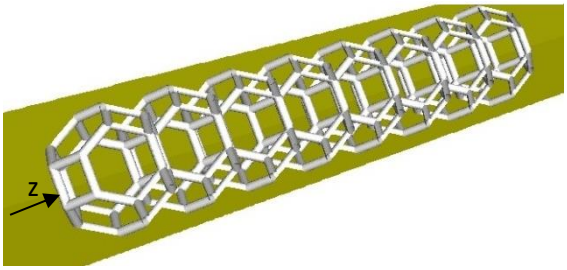

Figure 1. Numerical domain

The main characteristics of the metal foams employed are listed in the Table 1:

Table 2. Parameters of metal foams

PPI	ε	L_c [mm]	d_p [mm]	d_s [mm]
10	0.95	2.54	2.32	0.22
20	0.95	1.27	1.16	0.11

where L_c is the cell length, d_p and d_s are the pore and fiber diameter, respectively. The characteristics of the metal foams are obtained by means of the correlations presented in the work [5]. The thermophysical properties of the alumina nanoparticles are considered equal to ρ_{np}=3880 kg/m^3, c_{pnp} = 729 J/kgK and k_{np} = 42 W/mK (np: nanoparticles). The particle volume concentrations ranged from 0% to 4% and the particle diameter d_{np} is equal to 70 nm. A single-phase model approach has been adopted in order to describe the nanofluid behaviour. The choise of the correlations to calculate the nanofluid properties has been made by means of the work of Sekrani et al. [6]. The properties of the nanofluids are showed in the Table 2:

Table 2. Properties of nanofluids from ref. [6]

ϕ	ρ [kg/m^3]	c_p [J/kgK]	μ [Pas]	k [W/mK]
0%	998.2	4182	0.001003	0.60
2%	1055.8	3928	0.002002	0.61
4%	1113.5	3701	0.003429	0.68

The conditions of the problem are the following: the boundary edges are symmetric and the overflow condition is considered to the exit. The working fluid is characterized by a temperature T_0 equal to 300 K and by a velocity, indicated as v, that ranges from 0.003 m/s to 0.11 m/s. A heat flux, q_w, equal to 10000 W/m^2 is imposed on the heated walls.

Results and Discussion: The pressure drop Δp between the inlet and the outlet of the domain for several nanoparticle concentrations and for different PPI values is showed in the Figure 2.

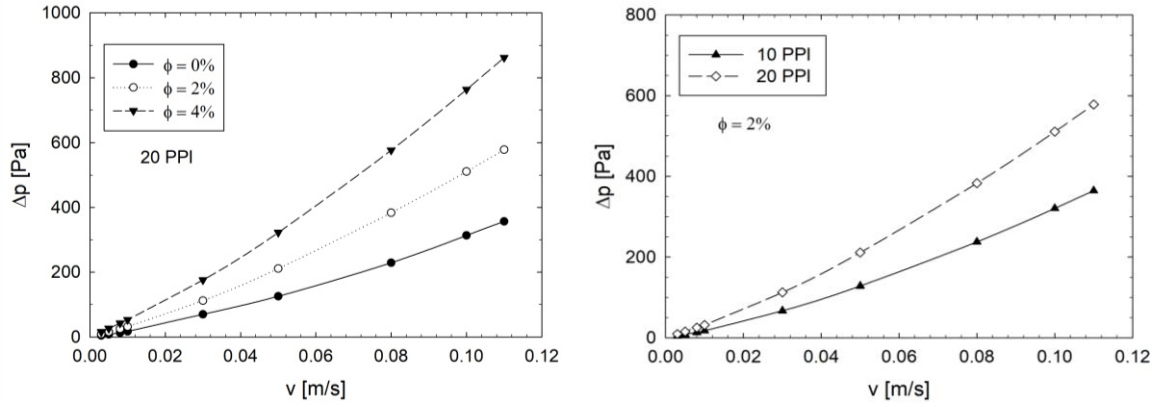

(a) **(b)**

Figure 2. The pressure drop for (a) several nanoparticles concentrations and (b) different PPI values.

One can observe as the pressure drop Δp increases both with the increase of nanoparticle concentration ϕ (Figure 2.a) and with the increment of values of pores per inch, PPI (Figure 2.b); this causes a bigger mechanical power needed to pump the working fluid.

The heat transfer coefficient, h_{sf}, between the fluid and solid phases of the metal foam, as a function of the inlet fluid velocity, is displayed in Figure 3.

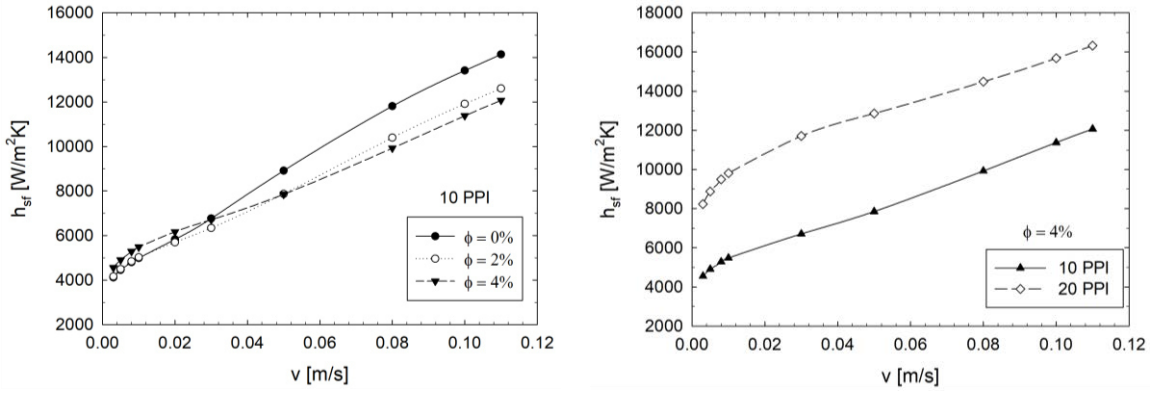

(a) **(b)**

Figure 3. The heat transfer coefficient for (a) several ϕ and (b) different PPI.

The heat transfer coefficient h_{sf} is calculated as:

$$h_{sf} = \frac{\int_{A_{sf}} qdA}{A_{sf}\left(\overline{T}_w - \overline{T}_f\right)} \quad (1)$$

where A_{sf} is the cells area, $\overline{T_f} = \frac{1}{V}\int T_f dV$ is the average fluid temperature (V = cells volume) and $\overline{T_w} = \Sigma_i \frac{1}{A_i}\int T_w dA$ is the average wall temperature (i = number of metal foam fibers).

As shown in the Figure 3.a, by increasing ϕ, the value of h_{sf} increases for lower values of velocity and then decreases with bigger velocities. Furthermore, for a fixed nanoparticles concentration, h_{sf} increases with the increment of PPI (Figure 3.b), pointing out the advantage to use a metal foam with bigger values of pores per inch.

References:

1. S. Cunsolo, M. Oliviero, W.M. Harris, A. Andreozzi, N. Bianco, W.K.S. Chiu, V. Naso, Monte Carlo determination of radiative properties of metal foams: comparison between idealized and real cell structures, *International Journal of Thermal Science* 87 (2015) 94–102.
2. S. Pusterla, M. Barbato, A. Ortona, C. D'Angelo, Numerical study of cell morphology effects on convection heat transfer in reticulated ceramics, *International Journal of Heat and Mass Transfer* 55 (25–26) (2012) 7902–7910.
3. S. Krishnan, J.Y. Murthy, S.V. Garimella, Direct Simulation of Transport in Open-Cell Metal Foam, Cooling Technologies Research Center (2006).
4. G. Ambrosio, N. Bianco, W.K.S. Chiu, M. Iasiello, V. Naso, M. Oliviero, The effect of open-cell metal foams strut shape on convection heat transfer and pressure drop, *Applied Thermal Engineering* 103 (2016) 333–343.
5. G. Incera Garrido, F.C. Patcas, S. Lang, B. Kraushaar-Czarnetzki, Mass transfer and pressure drop in ceramic foams: A description for different pore sizes and porosities, *Chemical Engineering Science* 63 (21) (2008) 5202-5217.
6. G. Sekrani, S. Poncet, P. Proulx, Modeling of convective turbulent heat transfer of water-based Al_2O_3 nanofluids in an uniformly heated pipe, *Chemical Engineering Science* 176 (2018) 205–219.

1st International Conference on Nanofluids (ICNf2019)
2nd European Symposium on Nanofluids (ESNf2019)
26-28 June 2019, Castelló, Spain

An investigation on heat transfer characteristics of the Al_2O_3-water nanofluid in an electric heater

Z. Zhai[1], D. Zheng[1], J. Wang[1]*, L. Yang[1] and B. Sundén[2]*

[1] School of Energy and Environmental Engineering, Hebei University of Technology, Tianjin 300401, China

[2] Department of Energy Sciences, Division of Heat Transfer, Lund University, Lund SE-22100, Sweden

*Corresponding authors: wjwcn00@163.com; Bengt.Sunden@energy.lth.se

Keywords: Electric heater; Nanofluid; Natural convection; Heat transfer enhancement.

Abstract: Commonly, heat transfer performance of the nanofluid is enhanced by increasing the mass fraction of nanoparticles due to an improvement of thermo-physical properties. However, more nanoparticles in the base fluid will result in an increase of the nanofluid viscosity. This research aims to investigate natural convective heat transfer for an electric heater filled with a Al_2O_3-water nanofluid. The effect of various mass fractions of the nanofluid (0.1-2.0 wet. %) on heating characteristics of the electric heater were analysed over time, and results indicate that the electric heater with the 1.0% Al_2O_3-water nanofluid has the highest heating efficiency for external environment.

Introduction/Background: Increasing demand in the enhancement of heat transfer performance results in development of active and passive heat transfer technologies in many industrial fields. Nanofluids, as a two-phase media with a certain ratio of liquid and nanoparticles, are widely concerned by many researchers especially in heat exchangers. For forced convective heat transfer, nanoparticles can significantly change the thermal-physical properties of the basic fluid [1, 2]. However, many studies focused on numerical simulations in a partially heated rectangular/annular enclosure filled with a nanofluid [3-7]. Electric heaters were used to supply the proper indoor heating instead of a central heating system, which can reduce carbon emissions. In addition, a heater with water as the base fluid is easy to recycle without pollution. This research investigates a mixture of Al_2O_3 nanoparticles and deionized water (DI-water) on heating performance of an electric heater.

Discussion and Results: A two-step method is used to compose the Al_2O_3-water nanofluid in this study. Most information of Al_2O_3 nanoparticles was provided by Beijing deke daojin company as shown in Table 1. Specific heat of nanoparticles and thermo-

physical properties of the DI-water can be found in Ref. [7]. Sodium hexametaphosphate (SHMP) as a dispersant is added into the distilled water. Mechanical stirring and ultrasonic oscillation were conducted concurrently for about 60 min.

Table 1. Thermo-physical properties of nanoparticles (25 ˚C)

Specification	Value
Appearance	White powder
Purity, %	> 99
Grain size, nm	30
Specific surface area, m^2/g	50
Density, kg/m^3	3600
Thermal conductivity, w/(m K)	35
Specific heat, J/kg K	765 [7]

The main part of the electric heater includes two horizontal tubes with a wall thickness of 2 mm and seven vertical tubes with a wall thickness of 1.5 mm. A cooling fin is located on each vertical tube. A heating rod as the heat source was put into the bottom horizontal tube. About 1.5 L base fluid or Al_2O_3-water nanofluid was added into the heater, before the experimental tests were conducted. Other geometrical information of the heater is illustrated in Fig. 1. The error of temperature measurements was caused by thermocouples (with an uncertainty of 0.1 K) and an electronic scale (with an uncertainty of 0.01 g).

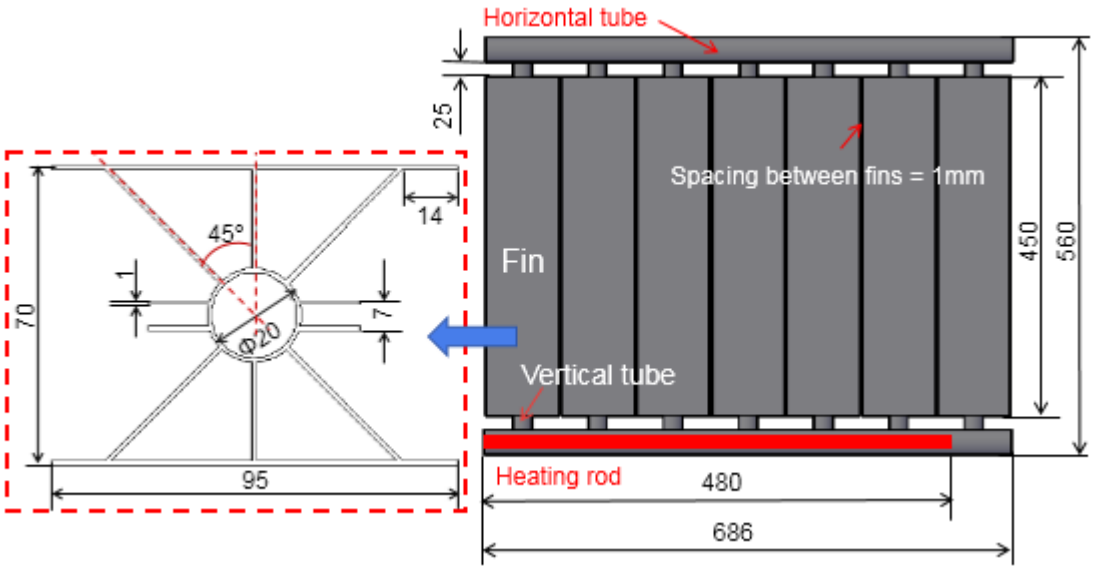

Figure 2. Dimensions of the heater and cooling fins (unit: mm)

To measure ambient temperature, the electric heater was put into an adiabatic cavity with dimensions of 1m×1m×1.5m, and thermocouples were located at four top angles of the cavity as shown in Fig. 2a. Figure 2b shows the ambient temperature around the electric heater filled with the Al_2O_3-water nanofluid. For the base fluid (DI-water), the first heating process starts at an initial temperature of 20 ˚C, and then it is terminated at an equilibrium

temperature. The equilibrium temperature is calculated based on an average value of the range from Tp-5 min to Tp+5 min, when time Tp min is the moment corresponding to the maximum heating temperature. After a heating interval of 20 minutes, a reheating process starts and ends at the similar equilibrium temperature. Compared with other results, the 1.0% Al_2O_3-water nanofluid shows a higher speed of temperature increase.

Table 2 shows that the highest ambient temperature of 61.1 ˚C is reached after a heating time of 96 minutes, and a 10.2% enhancement of heating efficiency is obtained for the 1.0% Al_2O_3-water nanofluid. Results indicated that increasing the mass fraction of the nanoparticles does not show a monotonous increase in heat transfer enhancement due to a significant effect on the viscosity.

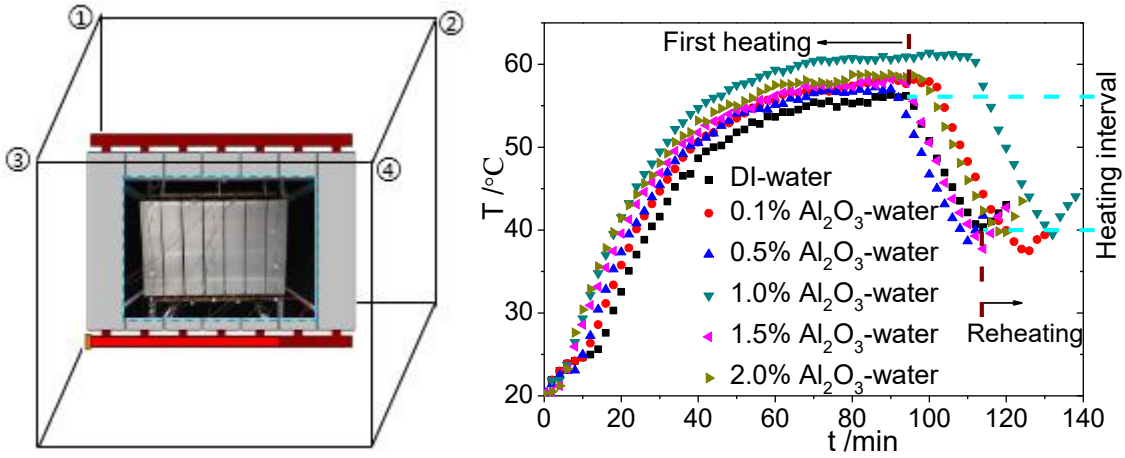

(a) Temperature sensor locations (b) Temperature test values

Figure 2. Ambient temperature testing with time

Table 2. Heating time and equilibrium temperature

Case	Equilibrium temperature, ˚C	Heating time, min	Enhancement, %
DI-water	55.4	61	/
0.1% Al_2O_3-water nanofluid	57	78	2.9
0.5% Al_2O_3-water nanofluid	58.2	90	5.1
1.0% Al_2O_3-water nanofluid	61.1	96	10.2
1.5% Al_2O_3-water nanofluid	58.8	91	6.1
2.0% Al_2O_3-water nanofluid	59.4	87	7.2

Summary/Conclusions: A 10.2% enhancement of heat transfer is obtained for an electric heater, when 1.0% Al_2O_3 nanoparticles are added into the deionized water as working medium. Moreover, the 1.0% Al_2O_3-water nanofluid shows a maximum increasing value of

the ambient temperature. A peak value of the ambient temperature is obtained when the mass fraction of nanoparticles ranges from 0.1% to 2.0%.

References:

1. V.L. Vinodhan, K.S. Suganthi and K.S. Rajan, Convective heat transfer performance of CuO–water nanofluids in U-shaped minitube: Potential for improved energy recovery, *Energ. Convers. Manage.* 118 (2016) 415-425.
2. R.S. Vajjha and D.K. Das, A review and analysis on influence of temperature and concentration of nanofluids on thermophysical properties, heat transfer and pumping power, *Int. J. Heat Mass Tran.* 55 (2012) 4063-4078.
3. S.U. Ilyas, R. Pendyala and M. Narahari, An experimental study on the natural convection heat transfer in rectangular enclosure using functionalized alumina-thermal oil-based nanofluids, *Appl. Therm. Eng.* 127 (2017) 765-775.
4. H.F. Oztop and E. Abu-Nada, Numerical study of natural convection in partially heated rectangular enclosures filled with nanofluids, *Int. J. Heat Fluid Flow* 29 (2008) 1326-1336.
5. E. Abu-Nada, Z. Masoud and A. Hijazi, Natural convection heat transfer enhancement in horizontal concentric annuli using nanofluids, *Int. Commun. Heat Mass* 35 (2008) 657-665.
6. E.B. Öğüt, Natural convection of water-based nanofluids in an inclined enclosure with a heat source, *Int. J. Therm. Sci.* 48 (2009) 2063-2073.
7. E. Abu-Nada, Z. Masoud, H.F. Oztop, and A. Campo, Effect of nanofluid variable properties on natural convection in enclosures, *Int. J. Therm. Sci.* 49(2010) 479-491.

1st International Conference on Nanofluids (ICNf2019)
2nd European Symposium on Nanofluids (ESNf2019)
26-28 June 2019, Castelló, Spain

Development of a database of heat transfer properties of nanofluids

M.E. Mondejar[1*], J. Zhang[1] and F. Haglind[1]

[1]Department of Mechanical Engineering, Technical University of Denmark, Building 403, 2800 Kgs. Lyngby, Denmark

[*]Corresponding author: maemmo@mek.dtu.dk

Keywords: database, nanofluids, heat transfer.

Abstract: This work presents the need for a standardized reporting and a database of experimental heat transfer data of nanofluids, that allow evaluating the consistency of published data in the field, and support the development of predictive general models for the heat transfer behavior of nanofluids. The first attempts to build a comprehensive database of experimental heat transfer data of nanofluids are introduced, and the main challenges for the collection of the data are enumerated. The objective is to collect experimental data published in the scientific literature and consolidate a standardized database where data can be quickly searched by base fluid, nanoparticle type, heat transfer configuration or operation ranges, and be ready for its use by researches and engineers for the analysis and simulation of nanofluids as heat transfer fluids.

Background: Evaluating the suitability of the use of nanofluids as heat transfer or working fluids requires knowledge of their heat transfer behavior over a wide range of operating conditions, or instead, models that are able to predict their heat transfer features with sufficient accuracy. Although the most widely used general heat transfer correlations have a theoretical basis, most of today's developed heat transfer correlations are empirical or semi-empirical, and require large amounts of experimental data as a basis for their development.

The rapid growth of the number of publications in the field of heat transfer of nanofluids has provided a large number of experimental data of heat transfer experiments with different types of nanofluids and configurations. Following this, several reviews that discuss heat transfer of nanofluids have been published, being 15 of them published only during 2018. Some of these review works focus on providing a general overview of the published research on experimental heat transfer of nanofluids, while others focus on specific types of nanofluids, or even configurations. For instance, Moreira et al. [1] and Choi et al. [2] present general reviews of the heat transfer applications of nanofluids in

which the increase or decrease of heat transfer is generally pointed out for each reviewed publication. Yang and Du [3] presented an equivalent analysis of the heat transfer enhancement, but dedicated only to nanofluids containing TiO_2 nanoparticles.

Though the published reviewed works provide a good overview of the publications available for specific nanofluid types, or heat transfer configurations, it is detected that they do not provide a clear view on whether data for similar systems measured by different authors are consistent, or if large deviations in the measured enhancement exist. For example, Sajid and Ali [4] reviewed recent experiments on heat transfer of nanofluids and provided a general view of the maximum achieved enhancement depending on the nanoparticle type. However this presentation of the data does not provide insight on the presence of outliers in the measurements or the consistency of datasets. In this regard, it has been pointed out that inconsistencies exist among different studies on heat transfer of nanofluids, which indicates that the impact of different factors in these processes is still not understood [5]. A database collecting experimental heat transfer data of nanofluids would allow the quick comparison of values from different sources and systems, as well as the detection of outliers or major inconsistencies. However, to the best of our knowledge, such a database is missing.

This work aims at developing a database of published experimental heat transfer data of nanofluids, as well as suggesting a standard for future data reporting in the field of nanofluids' heat transfer, therefore facilitating the data analysis and comparison. The database will consider nanofluids formed by a base fluid and a single type of nanoparticle. The data collected in the database will cover diverse flow conditions (e.g. vertical or horizontal flow, pool boiling) and geometries (e.g. tubes, plates), as well as different pressure, temperature and mass flow rate ranges. A quality control of the compiled data will be carried out, in order to avoid potential typographical errors and to spot significant outliers.

The database will be the base for the development, validation and improvement of reliable heat transfer correlations for nanofluids, as well as to provide a consistent indication on the relative level of heat transfer enhancement for different fluids and nanoparticle combinations, and heat transfer conditions. Moreover, defining a standard for the reporting of heat transfer data for nanofluids will increase the impact of credibility of future experimental data, thus ensuring their benefit for the scientific community.

Discussion and Results:

The collection of heat transfer data poses a significant challenge due to the large number of factors influencing the heat transfer phenomena (e.g. geometry, flow, media), and the diverse ways of reporting empirical data in the scientific literature (e.g. heat transfer coefficients, Nusselt numbers, or their ratios with respect to a reference fluid). This challenge increases when analyzing data of nanofluids' experiments, not only due to the addition of the nanofluids' properties, but because of the systematic inaccuracies that have been observed in the recent literature. Some of these inaccuracies are enumerated as follows: i) in most of the cases, heat transfer parameters are presented graphically in the form of plots and, normally, no access to the raw data is possible; ii) a great number of the works present heat transfer data in the form of ratios with respect to the base fluid behavior, being the reference data missing; iii) in many cases basic information about the nanofluid properties is missing (e.g. nanoparticles size, shape); iv) in some cases surfactants are used but this information is not provided or the substance is reported as unknown.

In order to standardize the existing published empirical data, and provide a base for comparison of different studies, data needs to be treated and converted. Non-dimensional magnitudes (such as the Nusselt number Nu or Péclet number Pe) are collected from the analyzed publications or calculated, if data is reported in their dimensional form. Predicted thermophysical properties for each nanofluid are used for the data conversion. All the calculated values will be built in the database and are clearly indicated.

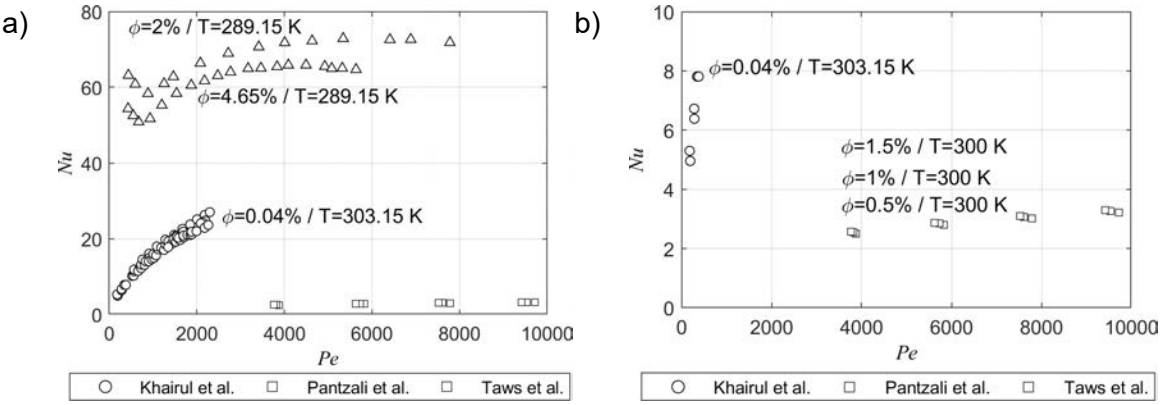

Figure 1. Comparison of heat transfer data for water+CuO nanofluids in plate heat exchangers [6–8]**. Volume fraction ϕ and temperature are indicated if given.**

Fig. 1 shows an example of comparison of heat transfer data for water+CuO nanofluids in plate heat exchangers from different sources. Thanks to the data treatment, the reported values of different magnitudes can be compared in terms of the Nu and Pe. It

can be seen that, for the higher volume fractions, the heat transferred for ϕ=2% is greater than for ϕ=4%, contrary to what is expected. For lower ϕ, values from different sources seem to agree, although differences with particle concentration are negligible.

As the database expands, it will be applied to assess the prediction performance of heat transfer correlations independently, as they are commonly derived based on limited sets of experimental data or for specific types of nanofluids.

Summary/Conclusions: The uncertainty imposed by a great number of experimental heat transfer studies on nanofluids and the observed variety of heat transfer enhancement makes it necessary the development of a database of experimental heat transfer data of nanofluids and the definition of a standard for data reporting. The database will be used for development of new heat transfer correlations, and the assessment of the existing data. This work is supported by the European Union's Horizon 2020 research and innovation programme with a Marie Skłodowska-Curie Fellowship under grant agreement No 704201 with the project NanoORC (www.nanoorc.mek.dtu.dk).

References:

[1] Moreira TA, Moreira DC, Ribatski G. Nanofluids for heat transfer applications: a review. J Brazilian Soc Mech Sci Eng 2018;40:1–29. doi:10.1007/s40430-018-1225-2.

[2] Choi TJ, Subedi B, Ham HJ, Park MS, Jang SP. A review of the internal forced convective heat transfer characteristics of nanofluids: Experimental features, mechanisms and thermal performance criteria. J Mech Sci Technol 2018;32:3491–505.

[3] Yang L, Du K. A comprehensive review on heat transfer characteristics of TiO2nanofluids. Int J Heat Mass Transf 2017;108:11–31.

[4] Sajid MU, Ali HM. Recent advances in application of nanofluids in heat transfer devices: A critical review. Renew Sustain Energy Rev 2019;103:556–92.

[5] Wang XQ, Mujumdar AS. Heat transfer characteristics of nanofluids: a review. Int J Therm Sci 2007;46:1–19. doi:10.1016/j.ijthermalsci.2006.06.010.

[6] Khairul MA, Alim MA, Mahbubul IM, Saidur R, Hepbasli A, Hossain A. Heat transfer performance and exergy analyses of a corrugated plate heat exchanger using metal oxide nanofluids. Int Commun Heat Mass Transf 2014;50:8–14.

[7] Pantzali MN, Mouza AA, Paras S V. Investigating the efficacy of nanofluids as coolants in plate heat exchangers (PHE). Chem Eng Sci 2009;64:3290–300.

[8] Taws M, Nguyen CT, Galanis N, Gherasim I. Experimental investigation of nanofluid heat transfer in a plate heat exchanger. ASME 2012 Heat Transf. Summer Conf. Collocated with ASME 2012 Fluids Eng. Div. Summer Meet. ASME 2012 10th Int. Conf. Nanochannels, Microchannels, Minichannels, 2012, p. 1–8.

1st International Conference on Nanofluids (ICNf2019)
2nd European Symposium on Nanofluids (ESNf2019)
26-28 June 2019, Castelló, Spain

Convective heat transfer enhancement by magnetic field in ferrofluids

B. Buonomo[1], D. Ercole[1], O. Manca[1]*, S. Nardini[1], S. Pragliola[1]

[1]Dipartimento di Ingegneria, Università degli Studi della Campania "Luigi Vanvitelli", Via Roma 29, 81031 Aversa, Italy

Keywords: Ferrofluid, heat transfer, forced convection, horizontal channel, magnetite nanoparticles.

Abstract: In this paper a numerical analysis of water-based ferrofluid with magnetite nanoparticles (Fe_3O_4) is accomplished under different values of magnetic field strength and for different Reynolds number. A solenoid is utilized to create a magnetic field over a region of the domain. The single-phase model is employed to simulate the behaviour of the ferrofluid. A body force is added to momentum equation in order to consider the magnetic field strength.

Introduction: The suspension of nanoparticles in conventional fluids are usually called nanofluids [1]. They were designed to improve the thermal conductivity of the basic coolant fluids. For example, the water is the most utilized coolant fluid for convectional applications but it has a thermal conductivity of more of one order of magnitude lesser than the metals. Therefore, using the suspension of solids is a good option to increase the thermal conductivity. The rise of nanofluids is recent [2] because now there is the technology to produce nanoparticles with few nanometres of diameter. The nanoparticles are suitable for suspension in fluid because they do not have the same disadvantages of macro suspensions. Among the various classes of nanofluid, the ferrofluid could be an innovative heat transfer media for industrial applications. They are stable colloidal suspension of sub-domain magnetic particles in a carrier liquid, as water [3]. They could be controlled by an external magnetic field, in fact the magnetization of nanofluids is dependent on the magnetic field and any variation induce a change of body force distribution in the ferrofluid. The ferrofluids have been the subject of several studies in literature. Kumar and Subudhi [4] have investigated the method of preparation, characterization and application of magnetic nanofluids, showing the different techniques utilized in literature. Sheikholeslami and Rokni [5] have collected the various model applied in literature to simulate the ferrofluid behaviour in different heat transfer phenomenon. A review on the experimental works on Fe_3O_4 ferrofluids in heat transfer

applications is accomplished by Hatami et. al [6]. They found a general trend on increment of Nusselt Number by increasing the Reynolds number and volume fraction.

Method: The geometrical configuration is a squared pipe with a lenght of 3 mm and the length of 1000 mm in which the ferrofluid flows. A 20mm-length solenoid is put in the centre of the pipe (between 490 mm and 510 mm from the inner surface) as showed in fig.1. The ferrofluid has a 1% of volume concentration of 40 nm-Fe_3O_4 nanoparticles and the single-phase model is applied. The fluid is electrically non-conducting in order to do not induce any electromagnetic current inside of it. To estimate the thermal properties of the nanofluids for the single-phase model, the following equations are used [7-8]:

$$\rho_{nf} = (1-\phi)\rho_{bf} + \phi\rho_p \qquad c_{p,nf} = \frac{(1-\phi)\rho_{bf}c_{p,bf} + \phi\rho_p c_{p,p}}{\rho_{nf}}$$

$$\mu_{nf} = \frac{1}{(1-\phi)^{2.5}}\mu_{bf} \qquad \frac{k_{nf}}{k_{bf}} = \frac{k_p + 2k_{bf} + 2(k_p - k_{bf})\phi}{k_p + 2k_{bf} - (k_p - k_{bf})\phi}$$

where the subscripts nf, bf and p indicate respectively the nanofluid, the base fluid and the nanoparticles. ϕ indicates the volume concentration of the nanoparticles in the base fluid, defined as the ratio between the volume of the nanoparticles and the total volume of the domain.

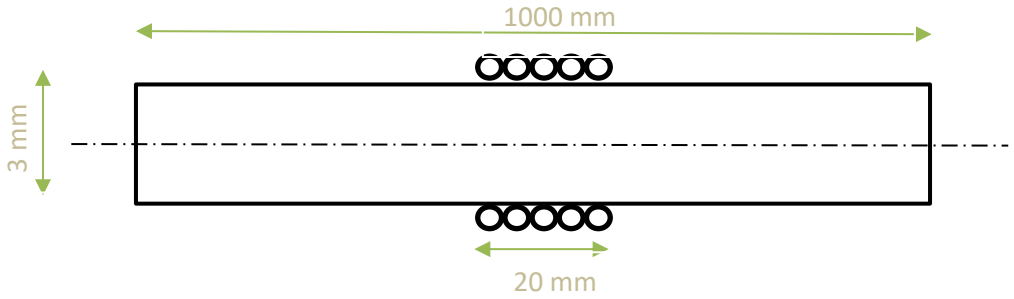

Figure 1 – Sketch of the geometrical model

The Nusselt and Reynolds number are defined using the characteristics length D of 3 mm:

$$Nu = \frac{qD}{k_{nf}(T_0 - T_m)} \tag{5}$$

$$\mathrm{Re} = \rho_{nf} VD \tag{6}$$

Where q is the wall heat flux, k_{nf} is the thermal conductivity of the ferrofluid, T_0 is the wall temperature and T_m is the mean temperature. About the boundary condition, at the inner surface the flow enters with an assigned Reynolds and a temperature of 273.16 K while

the axial surface of the pipe is an isothermal wall at 353.16 K in order to have a ΔT of 80 K. The thermal properties of the Fe_3O_4 are showed in table 1.

Table 1. Properties of the Magnetite nanoparticles

Density [kg m^{-3}]	Specific heat [J kg^{-1} K^{-1}]	Thermal conductivity [W m^{-1} K^{-1}]
5200	670	8

The governing equations are the following:

$$\frac{\partial \rho}{\partial t} + \vec{\nabla} \cdot \left(\rho \vec{V} \right) = 0 \tag{7}$$

$$\frac{\partial \left(\rho \vec{V} \right)}{\partial t} + \vec{\nabla} \cdot \left(\rho \vec{V} \vec{V} \right) = 0 = -\vec{\nabla} p + \vec{\nabla} \cdot \overset{\approx}{\tau} + \left(\vec{M} \cdot \vec{\nabla} \right) \vec{B} \tag{8}$$

$$\frac{\partial \left(\rho c_p T \right)}{\partial t} + \vec{\nabla} \cdot \left(\rho c_p T \vec{V} \right) = \vec{\nabla} \cdot \left(k \vec{\nabla} T \right) \tag{9}$$

In the momentum equation the last term on the right side of the equation is the Kelvin body force. It represents the magnetic force generated by the interaction between the external magnetic field and the ferrofluid.

Results and Discussion: The results are presented for different values of the Reynolds number at laminar regime and for different strength of the magnetic fields. In Fig. 2 are reported the convective heat transfer coefficient h, the Nusselt number and the pressure losses vs Reynolds number. It is possible to note that the presence of an external magnetic field improves the heat transfer coefficient. The pressure losses increase for higher Reynolds and for higher magnetic field strength. The Temperature fields of the ferrofluid inside the pipe is showed in Fig. 3.

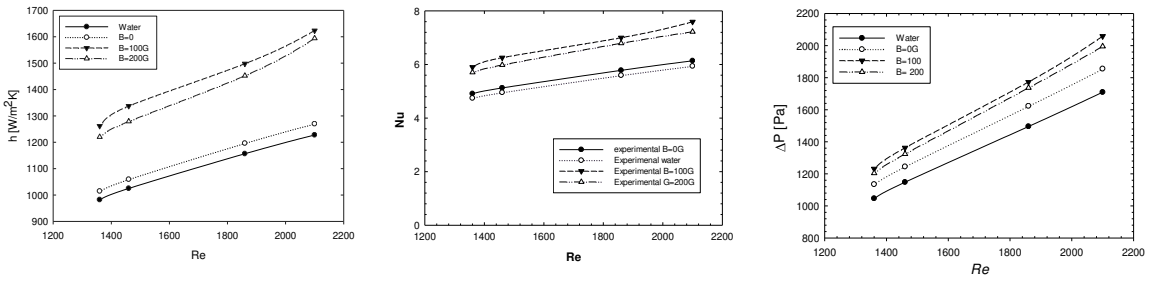

Figure 2 – convective heat transfer coefficient (a) Nusselt number (b) and pressure losses (c) for different Reynolds number for pure water and for ferrofluid at different values of magnetic fields

The deformation of the field is due to the interaction of ferrofluid with the external magnetic field that modify the direction of the flow and the temperature.

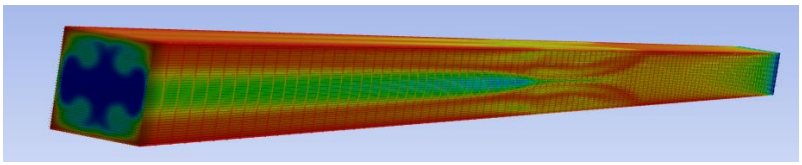

(a)

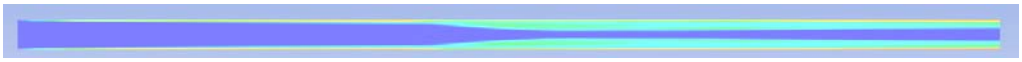

(b)

Figure 3 - Temperature fields of the ferrofluid: (a) isometric view and (b) xy-plane

References:

1. Vincenzo Bianco, Oronzio Manca, Sergio Nardini, Kambiz Vafai, *Heat Transfer Enhancement with Nanofluids*, CRC Press, New York 2015.

2. S.U.S. Choi and J. A. Eastman, Enhancing thermal conductivity of fluids with nanoparticles, *ASME International Mechanical Engineering Congress and Exposition Proceedings,* San Francisco, CA (1995) 99-105

3. R.E. Ronsenzweig, *Ferrohydrodynamics*, Dover Publications, Mincola, New York, 1997.

4. A. Kumar and S. Subudhi, Preparation, characteristics, convection and applications of magnetic nanofluids: A review, *Heat Mass Transfer* 54 (2018) 241-265

5. M. Sheikholeslami and H.B. Rokni, Simulation of nanofluid heat transfer in presence of magnetic field: A review, *International Journal of Heat and Mass Transfer* 115 (2017) 1203-1233

6. M. Hatami, S.M. Rezaei, M. T. Jing, Recent developments in magneto-hydrodynamic Fe3O4 nanofluids for different molecular applications: A review study, *Journal of Molecular Liquids* 250, (2018) 244-258

7. B.C. Pak and Y.I. Cho, Hydrodynamic and Heat Transfer Study of Dispersed Fluids with Submicron Metallic Oxide Particles, *Experimental Heat Transfer* 11 (1998) 151–170.

8. A S.Q. Zhou, R. Ni, Measurement of the specific heat capacity of water-based Al_2O_3 nanofluid, *Applied Physics Letters* 92 (2008) 093123.

1st International Conference on Nanofluids (ICNf2019)
2nd European Symposium on Nanofluids (ESNf2019)
26-28 June 2019, Castelló, Spain

Heat transfer and thermal storage improvement of nanofluids containing nanoencapsulated phase change materials

J. Gil-Font[1], Marie-Anne Hatte[1], R. Mondragón[1] and L. Hernández[1*]

[1]Departament of Mechanical Engineering and Construction, Universitat Jaume I, 12071, Castellón de la Plana, Spain

[*]Corresponding author: lhernand@uji.es

Keywords: Nanofluid, thermal oil, phase change material, heat transfer, thermal storage.

Abstract:.

In this paper, thermal energy storage capacity and heat transfer performance improvements of Nanoencapsulated Phase Change Materials (NePCMs) in a commercial thermal oil were investigated. Nanofluids combining self-encapsulated metal nanoparticles (in this case tin nanoparticles of different sizes) together with Therminol 66 (TH66) were analysed. For the NePCM, the resistance of the oxide shell to thermal cycling and the phase change enthalpy of the metal core were experimentally measured. The contribution of the latent heat can increase the total thermal energy storage of the nanofluids. The heat transfer performance of the nanofluids with respect to the base fluid was also evaluated employing theoretical values for the thermophysical properties of the involved materials, obtaining also interesting increments.

Introduction/Background:

Thermal oils play a key role in the efficiency of thermal-based industrial processes and can be used as HTF in medium and high temperature applications. However, their thermal and energy storage properties are quite poor in comparison with other fluids. A way to improve that is adding them Nanoencapsulated Phase Change Materials (NePCMs), nanoparticles with a core-shell structure in which its PCM is in the nuclei, encapsulated by a high melting point coating that prevents them from leaking when in liquid phase. Use of nePCM allows both the thermal conductivity and heat capacity of the base fluid to increase by the latent heat contribution of nePCM's cores. Furthermore, metal nanoparticles can be used as self-encapsulated nePCM using the metal oxide layer that forms naturally in most commercial synthesis processes as encapsulation. In this study, TH66 was chosen as base fluid and tin nanoparticles of different sizes were selected due to their appropiate thermal properties in the range of application of the base

fluid. Both thermal energy storage capacity and heat transfer performance of the resulting nanofluids were compared to those of the base fluid.

Discussion and Results: Tin nanoparticles with different primary particle size (100nm, 150nm and 300nm) were submitted to differential scanning calorimetry (DSC) tests in order to measure the phase change enthalpy and temperature. Nanoparticles were checked to be encapsulated by a tin oxide shell due to passivation during the manufacturing process and the enthalpy was proved to stand up to 100 thermal cycles of heating and cooling. DSC tests were carried out from 70ºC to 280ºC at a heating rate of 5ºC/min under N_2 atmosphere. Figure 1 shows the DSC curves obtained and values for the phase change enthalpy and temperature are summarized in Table 1.

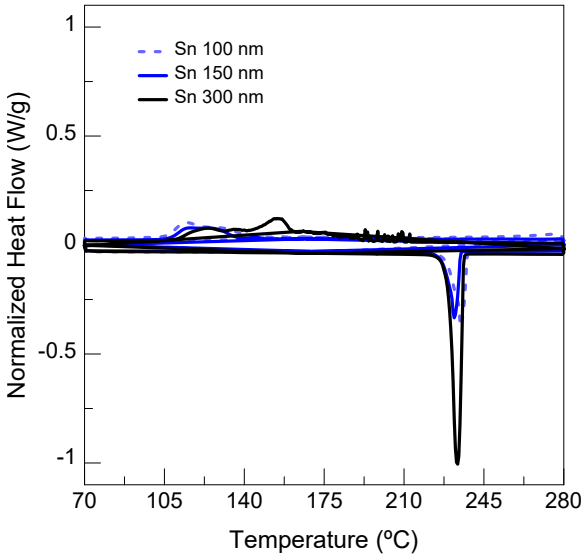

Figure 1. DSC results for tin nanoparticles

Table 1. Phase change enthalpy and melting point of NePCMs

NePCM	T_m [ºC]	ΔH_f [kJ/kg]
Sn (theoretical)	231.9	59
Sn 100nm	234.29	18.40
Sn 150nm	231.50	17.39
Sn 300nm	225.14	52.06

It can be observed that the phase change enthalpy decreases with the particle size being the Sn 300 nm the most suitable to be disperse in Therminol 66 based fluid in order to increase the energy density storage.

The total energy density storage of the nanofluid can be expressed as the summation of the sensible heat storage of the mixture and the latent heat storage due to the melting of the nePCM. The energy density storage enhancement provided for the nanofluid compared to pure Therminol 66, on a constant volume basis, was calculated by means of the following equation:

$$\Delta q_{total} = \frac{\rho_{nf} \cdot V_{nf} \left(c_{P,nf} \cdot \Delta T + \mathrm{w} \cdot \Delta H_{f,np} \right)}{\rho_{bf} \cdot V_{bf} \left(c_{P,bf} \cdot \Delta T \right)} \quad (1)$$

In Figure 2 the evolution of the energy density storage enhancement with the solid content is plotted for the three nanoparticles for ΔT=120ºC. An enhancement of 8.6% can be achieved for Sn 300 nm at 5 v.%.

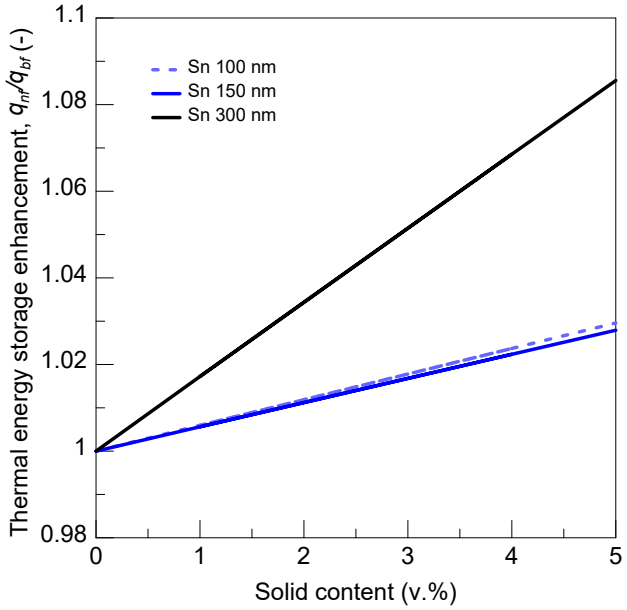

Figure 2. Evolution of thermal energy storage enhancement with solid content

The heat transfer performance of the nanofluids was evaluated through the Mouromtseff number (Mo) ratio and the heat transfer coefficient (h) ratio between the nanofluid and the base fluid. The thermal conductivity (k), viscosity (η), specific heat (c_P) and density (ρ) of the nanofluid were calculated by means of equations 1 to 4 according to the existing models, with the help of the properties provided by the supplier for pure Therminol 66. Finally, Mouromtseff number ratio was calculated with equation 5.

$$k_{nf} = \frac{k_p + 2k_{bf} + 2(k_p - k_{bf})\phi}{k_p + 2k_{bf} - (k_p - k_{bf})\phi} k_{bf} \quad (1)$$

$$\eta_{nf} = \eta_{bf}(1 + 2.5\phi) \quad (2)$$

$$c_{P,nf} = \frac{(1-\phi)\rho_{bf} c_{P,bf} + \phi \rho_p c_{P,p}}{(1-\phi)\rho_{bf} + \phi \rho_p} \quad (3)$$

$$\rho_{nf} = (1-\phi)\rho_{bf} + \phi \rho_p \quad (4)$$

$$\frac{Mo_{nf}}{Mo_{bf}} = \left(\frac{\rho_{nf}}{\rho_{bf}}\right)^{0.8} \left(\frac{c_{p_{nf}}}{c_{p_{bf}}}\right)^{0.4} \left(\frac{\mu_{nf}}{\mu_{bf}}\right)^{-0.4} \left(\frac{k_{nf}}{k_{bf}}\right)^{0.6} \quad (5)$$

Figure 3 shows the evolution of the Mouromtseff number (Mo) ratio with the solid content and temperature. It can be observed a 18.8% enhancement for 5 v.% of tin nanoparticles at 300ºC.

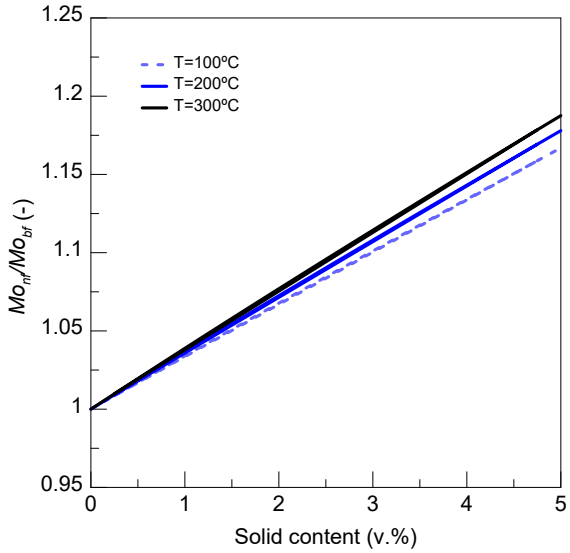

Figure 3. Evolution of Mouromtseff number ratio with solid content and temperature

The heat transfer coefficients were obtained from the Nusselt (*Nu*) number values previously calculated by using the Gnielinski correlation (6), where *Re* is the Reynolds number, *Pr* is the Prandtl number and *f* is the friction factor calculated by using the Colebrook-White equation.

$$Nu = \frac{f}{8}\frac{(\mathrm{Re}-1000)\,\mathrm{Pr}}{1+12.7\sqrt{f/8}\,(\mathrm{Pr}^{2/3}-1)} \qquad (6)$$

$$Nu = \frac{h \cdot D}{k} \qquad (7)$$

Figure 4 shows the evolution of heat transfer coefficient and its enhancement with flow rate at different solid content. An increase of 20.6% can be achieved for the nanofluid at 5 v.% of tin nanoparticles.

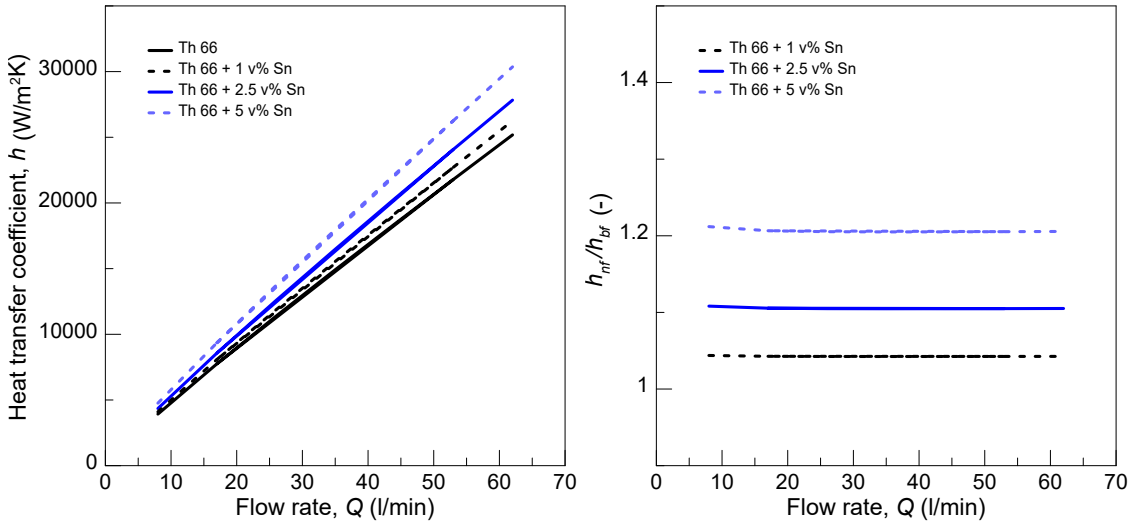

(a) **(b)**

Figure 4. (a) Evolution of heat transfer coefficient with flow rate and solid content. (b) Heat transfer coefficient enhancement with flow rate and solid content.

Summary/Conclusions:

Nanofluids based on TH66 and metal nePCM with different concentrations have been characterized and compared to the base fluid alone in terms of thermal energy storage capacity and heat transfer performance. The obtained results are promising, although more experimental measurements are required.

Acknowledgements: The authors want to thank the financial support from Universitat Jaume I (project UJI-B2016-47) and Ministerio de Economía y Competitividad (MINECO) (project ENE2016-77694-R).

References:

1. Martínez-Cuenca R, Mondragón R, Hernández L, Segarra C, Jarque JC, Hibiki T, Juliá JE. Forced-convective heat-transfer coefficient and pressure drop of water-based nanofluids in a horizontal pipe. Appl Therm Eng 2016;98:841-9.

2. Navarrete N, Gimeno-Furio A, Mondragon R, Hernandez L, Cabedo L,Cordoncillo E, Julia JE. Nanofluid based on self-nanoencapsulated metal/metal alloys phase change materials with tuneable crystallisation temperature. Sci Rep 2017;7:17580.

3. Navarrete N, Mondragón R, Wen D, Navarro ME, Ding Y, Juliá JE Thermal energy storage of molten salt- based nanofluid containing nano-encapsulated metal alloy phase change materials Energy 167 (2019) 912e920

1st International Conference on Nanofluids (ICNf2019)
2nd European Symposium on Nanofluids (ESNf2019)
26-28 June 2019, Castelló, Spain

Experimental Investigation into Cavity Flow Natural Convection of Zinc Oxide-Water Nanofluids

M. Sharifpur*, Kyoung-Yeoll Lee and J. P. Meyer

Department of Mechanical and Aeronautical Engineering, University of Pretoria, Pretoria, 0002, South Africa

*Corresponding author: mohsen.sharifpur@up.ac.za

Keywords: Nanofluids, Natural Convection, ZnO, Cavity Flow

Abstract: Nanofluids show great potential as heat transfer fluids that could benefit industries and save huge costs. Nanofluid is well known for enhancing the thermal conductivity and thermal diffusivity of the base fluid. However, there is still a lack of enough experimental results for natural convection heat transfer of nanofluids in a closed cavity. In this study, the cavity flow natural convection of zinc oxide (ZnO)-water is experimentally investigated. The ZnO nanoparticles have an average size of 20 nm, and the nanofluids were prepared for two different volume fractions of 0.36, and 1 volume percentage (vol.%). The stability of ZnO nanofluid is verified using spectrophotometer and zeta potential measurement at various temperatures and concentration of the nanofluids. The viscosity of ZnO-water nanofluid is also measured experimentally. The heat transfer efficiency of natural convection of ZnO-water nanofluid is examined experimentally in a closed square cavity at a Rayleigh number (Ra) range between 7.9E+7 and 8.9E+8. The suspension of ZnO nanoparticles in water does not enhance the natural convection heat transfer coefficient for 0.36 vol.% and 1 vol.%. Therefore, further investigation needs for the rang of less than 0.36 vol.%.

Introduction: Over the last century, many researchers of industrial and electronic cooling processes have paid attention to efficient methods of heat transfer. The higher the heat transfer coefficient (W/m2K), the more efficient the system's power output. Therefore, a new class of heat transfer mediums with higher heat transfer performance has been investigated. The innovative method of enhancing heat transfer, which was introduced by Choi [1], is to disperse nano-sized (1 to 100 nm) metallic or nonmetal particles in conventional heat transfer fluids.

The latest technology can fabricate nanoparticles that can be dispersed easily in the base fluid. To achieve thermal and cost efficient conventional heat transfer fluids, nanofluids seem to be an alternative solution for suitably meeting technological demands

in many industries, such as solar collector, nuclear reactor cooling, electronic cooling, automobiles, chemical processes and building air conditioning [2].

Low thermal conductivity of conventional fluid could be compensated for by adding nanosized particles that have a significantly higher thermal conductivity. Eastman et al. [3] reported a 40% increase in thermal conductivity by using copper nanofluid (dp < 10 nm) in ethylene glycol (EG) as a base fluid. Das et al. [4] found a 35% improvement of thermal conductivity at 50 ^{o}C by suspending 4 volume percentage (vol.%) of copper oxide (CuO) (dp = 28 nm) nanoparticles in water.

Thermal conductivity is not the only factor that influences the optimal performance of a nanofluid. Other properties of nanofluids are also affected on the performance which viscosity is on the negative side [5]. Nanofluids are proven to enhance the thermal conductivity and thermal diffusivity of the base fluids. However, each nanofluid needs to be checked in the forced or natural convection to find if there is an optimum concentration for enhancing the heat transfer. Previous experimental works show there is an optimum concentration on enhancing natural convection of nanofluids for Al_2O_3-water [6], Fe_2O_3-water [7], MWCNT-water [8] and TiO_2-water [9].

Nanofluid systems are complex, and there is still disagreement among researchers about its heat transfer efficiency. It is crucial to determine which nanofluids may enhance or deteriorate the heat transfer coefficient in an exact condition. This study aims to experimentally investigate the heat transfer efficiency of the natural convection of zinc oxide-water nanofluids in a differentially heated square enclosure for two concentrations of 0.36 vol.% and 1 vol.%.

Materials and Methods

Preparation of nanofluids and stability: The nanofluids were prepared using a two-step method, and different surfactants were examined. Finally, tetramethylammonium hydroxide pentahydrate (TAHP), which was obtained from Sigma-Aldrich in the USA, was found to formulate a stable colloid. The amount of the surfactant that was added to the nanofluid was 1 vol.% of the nanoparticles. The rest of the preparation is the same as Joubert et al. [7]. Zetasizer ZS (Malvern instrument Limited, UK) was employed to measure mean particle size as well as Zeta potential (ZP) of the suspension to confirm the stability of the nanofluids. The apparatus and the process of the measurement are the same as Ghodsinezhad et al. [7]. However, for the volume fraction 1% the ZP shows out of range, therefore, visual stability followed by viscosity measurement for 24h were done to approve the stability.

Thermophysical properties of the nanofluid: The viscosity of the nanofluid is investigated experimentally in this study. The density of the nanofluids calculated by using equation (1) and the other properties used as indicated in Joubert et al. [7]. However, Aybar et al. [10] confirmed that for the volume fraction up to 1%, most of the correlations provide almost the same value for the thermal conductivity of nanofluids.

$$\rho_{nf} = \varphi\rho_p + (1-\varphi)\rho_{bf} \qquad (1)$$

Experimental set-up: The cavity is heated from one vertical wall and cooled from the opposite wall. Other sides, including top and bottom walls, are insulated to be adiabatic. The square cavity dimensions are Height (H) 96x width (W)120x depth (L)102 mm and the details of the experimental set-up and procedure are the same as Ghodsinezhad et al. [6].

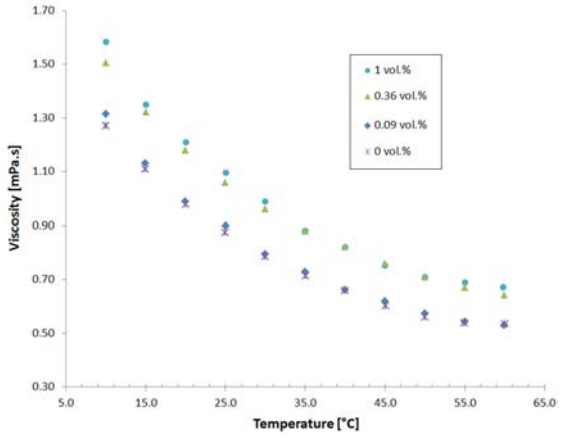

Figure 1. Viscosity of ZnO-water nanofluid

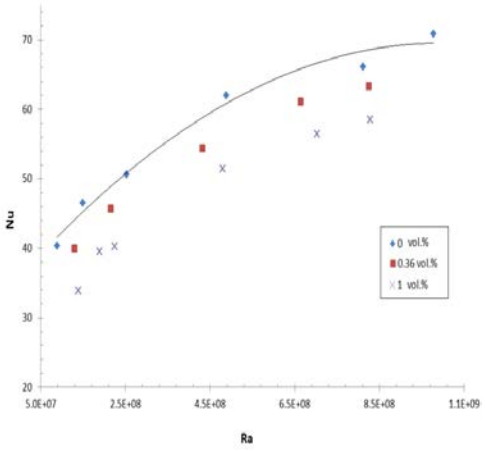

Figure 2. Nu versus Ra

Discussion and Results: The result for viscosity measurements for different volume fractions is shown in the Fig.1. Also, Fig. 2 shows the Nusselt number versus Rayleigh number. As expected, the average Nusselt number increases as the Rayleigh number increases, but the average Nusselt number decreases as the volume fraction of the nanofluid increases. Therefore, adding ZnO nanoparticles to water deteriorates the Nusselt number for natural convection when 0.36 vol.% and 1 vol.% used. The maximum uncertainty for Nusselt and Rayleigh numbers were found to be 3.05 and 4.36 %, respectively. The way to calculate the uncertainty analysis is the same as Joubert et al. [7].

Conclusions: The natural convection heat transfer in a rectangular cavity is investigated experimentally by adding a ZnO nanofluid for 0.36 vol.% and 1 vol.% concentrations. The

results show that these volume fractions do not improve the natural convection heat transfer. However, it cannot conclude that the natural convection of nanofluid deteriorates when the ZnO nanofluid used, and it needs to investigate the volume fractions less than 0.36 vol.% elaborately.

References:

1. S. Jana, A. Salehi-Khojin and W.-H. Zhong, Enhancement of fluid thermal conductivity by the addition of single and hybrid nano-additives, Thermochimica Acta, 462 (2007) 45–55.
2. J. Eastman, S. Choi, S. Li, W. Yu and L. Thompson, Anomalously increased effective thermal conductivities of ethylene glycol-based nanofluids containing copper nanoparticles, Appl. Phys. Lett., 78, (2001) 718–720.
3. S. Das, N. Putra, P. Thiesen and W. Roetzel, “Temperature Dependence of Thermal Conductivity Enhancement for Nanofluids,” J. Heat Transfer, 125 (2003) 567-574.
4. J. P. Meyer, S. A. Adio, M. Sharifpur and P. N. Nwosu, The viscosity of nanofluids: a review of the theoretical, empirical and numerical models, Heat Transfer Engineering, 37 (2016) 387-421.
5. S. Choi, Enhancing thermal conductivity of fluids with nanoparticles, *Int. Mech. Eng. Congr. Expo.*, p. 99–105, 1995.
6. H. Ghodsinezhad, M. Sharifpur, and J.P. Meyer, Experimental Investigation on Cavity Flow Natural Convection of Al_2O_3–Water Nanofluids, *International Communications in Heat and Mass Transfer*, 76 (2016) 316-324.
7. J. Joubert, M. Sharifpur, A. B. Solomon and J.P. Meyer, Enhancement in heat transfer of a ferrofluid in a differentially heated square cavity through the use of permanent magnets, *Journal of Magnetism and Magnetic Materials* 443 (2017) 149–158.
8. I. Garbadeen I, M. Sharifpur, J. F. M. Slabber and J. P. Meyer, Experimental Study on Natural Convection of MWCNT-Water Nanofluids in a Square Enclosure, *International Communications in Heat and Mass Transfer* 88 (2017) 1-8.
9. M. Sharifpur, A.B. Solomon, T. Ottermann, and J.P. Meyer, Optimum concentration of nanofluids for heat transfer enhancement under cavity flow natural convection with TiO2 – Water, *International Communications in Heat and Mass Transfer* 98 (2018) 297-303.
10. H. Ş. Aybar, M. Sharifpur, M. R. Azizian, M. Mehrabi, and J. P. Meyer, A Review of Thermal Conductivity Models of Nanofluids, *Heat Transfer Engineering* 36 (2005) 1085-1110.

SESSION 2
Cooling, Refrigeration

S2

1st International Conference on Nanofluids (ICNf2019)
2nd European Symposium on Nanofluids (ESNf2019)
26-28 June 2019, Castelló, Spain

Pool boiling CHF enhancement using a honeycomb porous plate and nanofluid

Shoji Mori[1] and Suazlan Mt Aznam

[1] Department of Mechanical Engineering, Kyushu University, Fukuoka, 819-0395, Japan

[2]International Islamic University Malaysia, Kuala Lumpur, Malaysia

*Corresponding author: morisho@mech.kyushu-u.ac.jp

Keywords: boiling, CHF enhancement, IR camera, honeycomb porous plate.

Abstract: A honeycomb-structured ceramic porous plate (HPP) was used to increase the critical heat flux (CHF) in a saturated pool boiling. Combining the HPP with a nanofluid significantly improved the CHF compared to that obtained from a plain surface in pure water, to a maximum of approximately 3.2 MW/m2. In this paper, the mechanism for the CHF enhancement was considered by measuring the temperature of the heated surface using an ITO heater and a high-speed infrared camera. As a result, the following conclusions can be made based on our data. The average temperatures at the intersecting parts of the HPP were relatively high (more than 200 °C) compared to other locations. And when the HPP was installed on the heated surface in conjunction with the nanofluid, the wall temperatures obtained under burnout conditions decreased in the order of the intersection of an HPP wall > an HPP wall between intersections > the cell. However, dryout was initiated in the cell when burnout occurred. This result implies that further CHF improvements could be achieved if the initiation of dryout at the cell can be suppressed.

Introduction/Background: Our group has previously demonstrated enhancement of the CHF of a large heated surface using a porous plate with a honeycomb structure immersed in a saturated pool boiling system based on distilled water [1-3]. A honeycomb porous plate (HPP) has been combined with a nanofluid so as to obtain a synergistic effect. This combination greatly improves the CHF, giving a value of approximately 3.2 MW/m^2 in conjunction with a copper block heater [4]. However, the CHF enhancement mechanism by an HPP together with a nanofluid is not yet fully understood. Therefore, in the present paper, changes in the temperature distribution on a heated surface over time up to the point of burnout were assessed using an indium tin oxide (ITO) heater and a high-speed infrared (IR) camera. The resulting data are used to examine the CHF enhancement mechanism obtained from combining an HPP with a nanofluid.

Experimental Apparatus and Procedure: Fig. 1 shows the experimental setup in which an ITO heater is used in order to measure the temperature distribution of the heated surface with a high-speed IR camera.

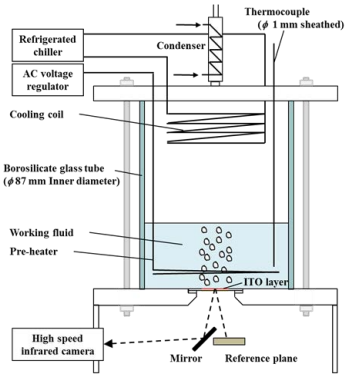

Fig. 1 Schematic diagram of the experimental apparatus including the pool boiling system and ITO heater

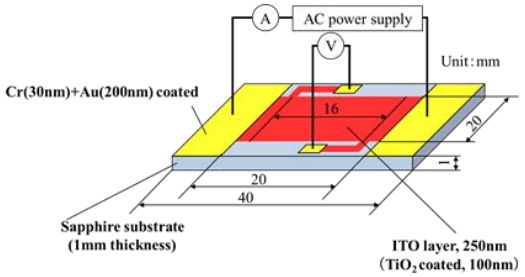

Fig. 2 ITO heater

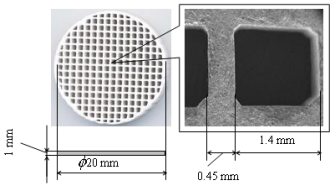

Fig. 3 Honeycomb porous plate

Fig. 2 depicts the ITO heater used in the present study. This device was fabricated by vacuum depositing a 250 nm thick ITO film on a sapphire substrate (1 × 40 × 40 mm). The heating area of the ITO unit was 20 × 20 mm.

The temperature distribution on the heated ITO surface was obtained using an IR high-speed camera with spatial and time resolutions of 130 μm and 2 ms, respectively.

Experiments were carried out using either distilled water or nanofluid as the working fluid under saturated conditions at atmospheric pressure. A sheathed heater was installed above the heated surface in the liquid bath in order to maintain the liquid temperature at the saturation temperature. During each trial, the heat flux was increased in increments of approximately 0.1 MW/m^2 until the CHF condition was reached, defined as a rapid wall temperature increase. The final heat flux in the quasi-steady state was then measured before the transition to film boiling and was taken as equal to the CHF.

Fig. 3 show the HPP used in the present study. The vapor escape channel width (equivalent to the cell width), d_V, the wall thickness of the grid, δ_S, the aperture ratio (the ratio of the open area to total area), the height, δ_h, and the diameter of the HPP were 1.3 mm, 0.4 mm, 0.55, 1.0 mm and 30.0 mm, respectively. The average pore radius of the HPP was approximately 0.17 μm.

Experimental Results and Discussion: As noted, an HPP and a nanofluid can be combined to enhance the CHF to a significant extent [4]. In order to clarify the CHF enhancement mechanism, temperature measurements were performed over time just below the HPP using the high-speed IR camera.

According to obtained boiling curves, the boiling curves demonstrate that, in the presence of the plain surface, the CHF values were higher when using the nanofluid. This enhancement is attributed to the increased surface wettability, surface roughness, and capillary wicking effect resulting from nanoparticle deposition on the heated surface, as has also been reported in previous studies. The CHF was also higher when using the HPP in both the distilled water and nanofluid. Moreover, it is interesting to observe that the highest CHF was obtained from the combination of the HPP with the nanofluid.

Fig. 4 indicates the changes in the IR images over time when using the HPP in the saturated pool boiling of the nanofluid (at 0.1 vol.%) under burnout conditions (2.84 MW/m^2). In the case of the HPP with the nanofluid, reversible dry spots can first be observed at a heat flux of 2.38 MW/m^2. Reversible dry spots were initiated in the cell part of the HPP, and small dry spots coalesced into a large irreversible dryout, leading to burnout. Frequent temperature increases occurred in the cell, although the wall temperature was reduced because the wall was easily wetted due to the nanoparticle deposition. The burnout always occurred when the wall temperature exceeded the Leidenfrost temperature, at which point the hovering period of coalesced bubbles was increased under the high heat flux and the dried area of the heating surface was not rewetted. When the HPP was installed on the heated surface in conjunction with the nanofluid, the average wall temperature under the burnout conditions decreased in the order of: the intersection of an HPP wall, an HPP wall between intersections, and the cell.

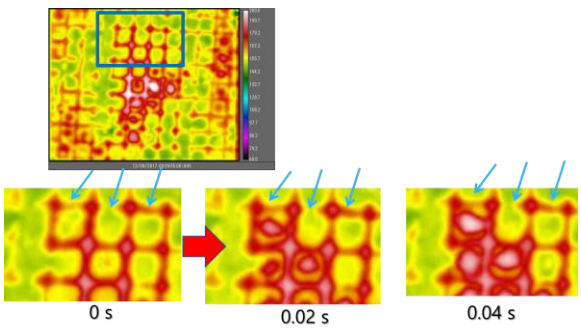

Fig. 4 Surface temperature change with time in burnout occurrence.(HPP + nanofluid , q=2.8 MW/m^2)

However, the location where dryout first occurred and at which the wall temperature first reached 300 °C was always the cell of the HPP. This result suggests that the CHF may be further improved if the initiation of dryout at the cell can be suppressed.

Conclusions

CHF enhancement resulting from a honeycomb-structured porous plate was investigated experimentally using a saturated pool boiling system in conjunction with a nanofluid. The following conclusions can be made based on the resulting data.

1. Temperature measurements by high-speed IR camera demonstrated that the average temperatures at the intersecting parts of the HPP were relatively high (more than 200 °C) compared to other locations.

2. When the HPP was installed on the heated surface in conjunction with the nanofluid, the wall temperatures obtained under burnout conditions decreased in the order of the intersection of an HPP wall > an HPP wall between intersections > the cell. However, dryout was initiated in the cell and a wall temperature of 330 °C was first obtained in this location when burnout occurred. This result implies that further CHF improvements could be achieved if the initiation of dryout at the cell can be suppressed.

Acknowledgements

This presentation is based on results obtained from a project commissioned by the New Energy and Industrial Technology Development Organization (NEDO).

References:

[1] S. Mori, K. Okuyama, Enhancement of the critical heat flux in saturated pool boiling using honeycomb porous media, International Journal of Multiphase Flow, 35(10) (2009) 946-951.

[2] S. Mori, L. Shen, K. Okuyama, Effect of cell size of a honeycomb porous plate attached to a heated surface on CHF in saturated pool boiling, in: the 14th International Heat Transfer Conference, ASME, Washington D.C., USA, 2010.

[3] S. Mori, S. Mt Aznam, K. Okuyama, Enhancement of the critical heat flux in saturated pool boiling of water by nanoparticle-coating and a honeycomb porous plate, International Journal of Heat and Mass Transfer, 80 (2015) 1-6.

[4] S. Mori, S. Mt Aznam, R. Yanagisawa, K. Okuyama, CHF enhancement by honeycomb porous plate in saturated pool boiling of nanofluid, Journal of Nuclear Science and Technology, (2015) 1-8.

1st International Conference on Nanofluids (ICNf2019)
2nd European Symposium on Nanofluids (ESNf2019)
26-28 June 2019, Castelló, Spain

Effect of the nanofluid in refrigerated showcase

J. Esarte [1], M. Aresti[1], J. Estella [1], J.Beraza [2], V. Gomara [2]

[1] NAITEC-C/ Tajonar 20-31006 Pamplona (Navarra)

[2] K-Refrigeration Group. Poligono Landaben C-A2, 31012-Pamplona (Navarra)

*Corresponding author: jesarte@naitec.es

Keywords: Nanofluid, GWP, IGWP, LCCP, refrigerant, steam compression refrigeration.

Abstract:

Steam compression refrigeration takes the last years suffering the uncertainties of the international environmental regulations relative to the fluorinated refrigerants "HFCs". Improving the energy efficiency is one of the key points in terms of compliance with these regulations and nanofluids can be a key element for it. This paper presents the effect of different nanofluids on the efficiency (COP) of a steam compression testbench that simulates a refrigerated showcase. Work that has been developed within the framework of the "REAVNan" project. The results show an improvement of around 12% for the case of nanofluid of copper nanoparticles with respect to the R449A base refrigerant.

Introduction/Background:

Environmental regulations bet on the refrigerants denominated clean (hydrocarbons, CO2, HFOs) for their zero or very low global warming potential “GWP”. However, the use of these refrigerants often undermines the energy efficiency of the equipment, "COP", in addition to requiring considerable redesigns in some cases. Considering that the total environmental impact during the equipment’s life, "LCCP", includes not only the "GWP" but also the indirect heating potential, "IGWP" (the equipment's own parameter that has to do with its energy efficiency representing 90% of impact), technological advances have to go in the improvement of energy efficiency.

Under this scenario, the industry of industrial refrigeration is forced to innovation-search for alternatives, not only in terms of refrigerant typology (environmentally friendlier) but new cooling technologies (acoustic, thermo-caloric, thermoelectric, **nanofluids** ...) that improve the efficiency and / or suppose a lower use of refrigerants.

The use of nanofluids as a coolant is a technique whose benefits have been contrasted in the field of liquid cooling in the electronic world, a field in which NAITEC is active with

the realization of different projects both national (Advanced liquid cooling in electronics) and international (NetMarketFluidics) ones, among others.

Discussion and Results:

The test bench is loaded with R449A refrigerant and left working for several hours until it reaches stability. Data of the suction, discharge, evaporator and condenser temperatures as well as the flow rate of refrigerant are continuously recorded. The compressor electrical consumption and the thermal watts drawn in the evaporator are also recorded.

Table 1. The four nanoparticles used in the nanofluid formulation

Particle	Size (nm)	Concentration (% wt)
Cu	25	1.5
Al_2O_3	20	
CuO	50	
TiO_2	30	

Under this setup, tests for different nanofluids are run.

The first test is performed with clean refrigerant in order to establish the base value of COP (1.5). Value from which to determine the COP variation that involves the use of nanofluid. For each of these nanofluids, tests are carried out with different concentrations on the refrigerant: 1, 2, 3 and 4.5% by weight. The results are shown in figure 1.

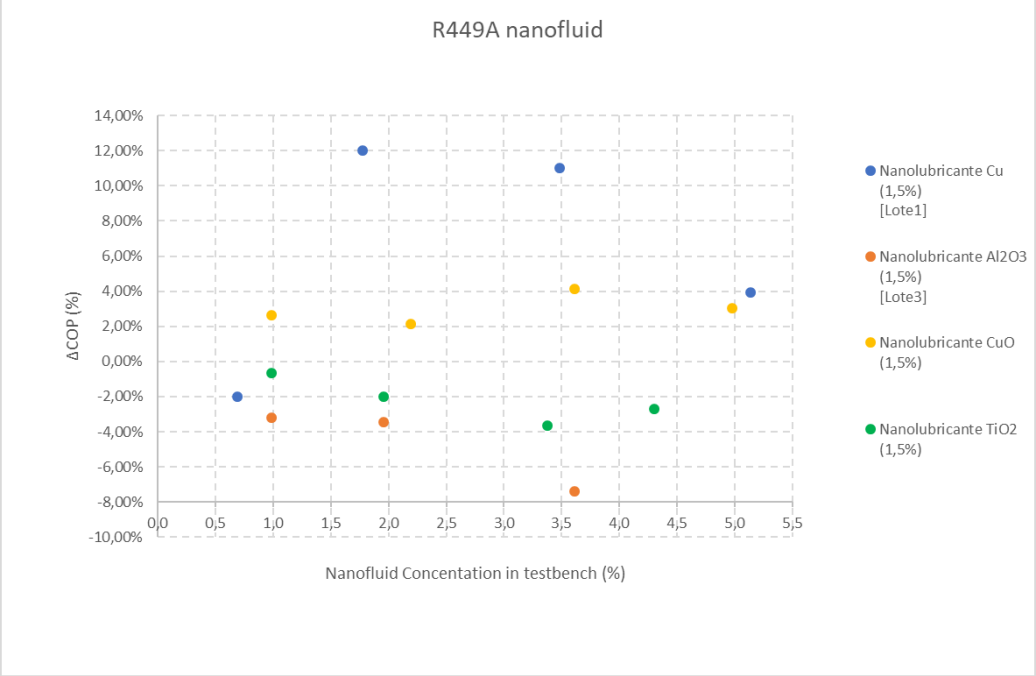

Figure 1. COP variation for different nanofluids and concentrations

It is observed that by increasing the nanoparticles concentration and the corresponding dispersants into the testbench refrigerant, the efficiency decreases. There are also formulations in which no improvement is observed with respect to the clean R449A refrigerant. Cooper nanofluid presents the most promising results as it provides the maximum COP increase whatever the concentration in the refrigerant is. By contrast, the Al_2O_3 shows the worst performance, a COP decrease. The CuO nanofluid presents a constant COP increase (around 3%) for any concentration, although this value is very low.

Summary/Conclusions:

From this work, it summarizes that the use of nanofluids as refrigerant in vapor compression cooling systems involves, in general, a COP improvement. This result is in agreement with what other researchers [1] have obtained for another type of nanoparticles and refrigerants.

Higher concentrations do not always mean a COP increase. There always appear a value from which COP decreases. In some cases, this COP seems to be unaffected by concentration, at least within a range.

Acknowledgment:

To the Government of Navarre (Spain) for the financing of the project "PT064 REAVNan" without which the development of this work would not have been possible.

References:

1. Veera Raghavalu K, Govindha Rasu N. ”Review on applications of nanofluids used in Vapour Compression refrigeration systems for COP enhancement”. IOP Conference: Materials Science and Engineering. 330 (2018) 012112.

1st International Conference on Nanofluids (ICNf2019)
2nd European Symposium on Nanofluids (ESNf2019)
26-28 June 2019, Castelló, Spain

Numerical study of the refrigeration of a plate using nanofluids at a low Reynolds number

A. Arcas-Cobos, J. Ortega-Casanova*

Andalucía Tech, Escuela de Ingenierias Industriales, Universidad de Malaga,
C/ Dr Ortiz Ramos s/n, 29071 Malaga, Spain

*Corresponding author: jortega@uma.es

Keywords: Heat transfer, nanofluids, Nusselt, pumping power, efficiency, uniformity, laminar flow, aluminium oxide.

Abstract: This paper presents the study of heat transfer between a circular plate and an impinging laminar jet of aluminium oxide nanoparticles-based fluid to obtain optimal values of plate-jet distance H/D, Reynolds number Re and volumetric nanoparticle concentration ϕ that maximize heat transfer based on the thermophysical properties correlations of Selimefendigil and Oztop [1]. The desired objectives vary from purely thermal as maximum, and average, heat transfer coefficient Nu and its uniformity σ to the purely mechanical aspects of the flow such as friction coefficient λ or pumping power Π and the combination of those requirements through efficiency η. As a result, correlations were obtained within the ranges of variables studied and optimal input parameter combination with an improvement of a 32% in heat transfer were found.

Introduction/Background: Impact jet cooling is a regular practice in industry despite the inferior heat transfer properties of fluids compared to metals. The idea of enhancing fluid cooling technologies with metal heat transfer properties was the beginning of nanofluids. Due to the lack of unique theory for heat transfer in nanofluids there have been several models to predict the thermal properties of these new fluids such as Batchelor and O'Brien [2], Hamilton and Crosser [3] or Masuda et al. [4]. However, this enhancement of heat transfer comes with the downside of some flow related problems such as stacking of nanoparticles, increasing pumping power demand and higher pressure drops. This paper studies numerically the optimization of this problem in order to achieve maximum efficiency for the geometry showed in Figure 1.

Discussion and Results: The Navier-Stokes (N-S) equations governing the problem were simplified considering a laminar, incompressible, axisymmetric, fully developed (Haggen-Poseuille velocity profile inside the jet), steady flow where Rayleight viscous dissipation is negligible compared to inner energy convection and thermophysical properties are considered homogenous, isotropic and constant [1]. Also, the problem was adimensionalized with various characteristic magnitudes, namely: jet inlet diameter

$L_c = D$, average inlet velocity $V_c = V_i$, and inlet temperature $T_c = T_i$. Finally, the N-S equations can be written as:

$$\nabla \cdot \vec{v}^* = 0, \tag{1}$$

$$\nabla \cdot (\vec{v}^* \vec{v}^*) = -\nabla p^* + \frac{1}{Re} \nabla^2 \vec{v}^*, \tag{2}$$

$$\nabla \cdot (\vec{v}^* T^*) = \frac{1}{Pe} \nabla^2 T^*, \tag{3}$$

where $\boldsymbol{p^* = \frac{p}{\rho V_i^2}}$, $\boldsymbol{Re = \frac{\rho V_i D}{\mu}}$ is the Reynolds number and $\boldsymbol{Pe = \frac{c_p \rho V_i D}{k}}$ is the Peclet number. The output parameters used to quantify the goodness of the heat transfer have been:

$$Nu = \frac{hL_c}{k}, \qquad \lambda = \frac{\tau}{(1/8)\rho V_i^2}, \qquad \Pi = \frac{pQ}{\rho V_i^3 D^2}, \qquad \eta = \frac{Nu}{\Pi}, \tag{4}$$

where $\boldsymbol{Nu}$ is the Nusselt number, $\boldsymbol{\Pi}$ the pumping power to generate the jet and $\boldsymbol{\lambda}$ the friction coefficient on the plate. The uniformity of the heat transfer will be measured by the standard deviation of $\boldsymbol{Nu}$ on the plate, $\boldsymbol{\sigma}$. Regarding $\boldsymbol{Nu}$, only the stagnation Nusselt at the symmetry axis on the plate $\boldsymbol{Nu_o}$ and the one in average along the plate $\boldsymbol{Nu_a}$ will be discussed. The thermophysical properties of the fluid under consideration, as density, viscosity, thermal conductivity and specific heat, were obtained from [1] and written in terms of the nanoparticle concentration $\boldsymbol{\phi}$. A total of 45 scenarios studying the geometry showed in Figure 1 were simulated for the following range of parameters: $\boldsymbol{Re} =$ [50,100,200], $\boldsymbol{H/D} =$ [1,2,4] and $\boldsymbol{\phi} =$ [0,1,3,6,10] %. Simulations were validated comparing Fanning's friction coefficient results from Deshpande and Vaishnav [5] and Nusselt's number from Poh et al. [6] as show in Figure 2. Also, a Grid Convergence Index studied was performed for the critical combination of $\boldsymbol{Re = 200}$, $\boldsymbol{H/D = 1, \phi = 0\%}$ due to the high velocity of the flow. Optimal grid cell size was decided using Richardson's extrapolation for shear stress across the plate's surface as show in Figure 1. The selected grid was uniform and structured with a GCI of 1.72%.

(a)

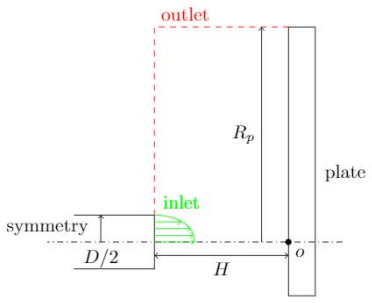

(b)

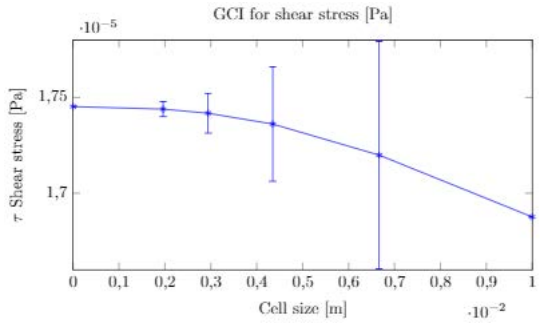

Figure 1. Sketch of the geometry (a) and grid convergence study (b).

(a)

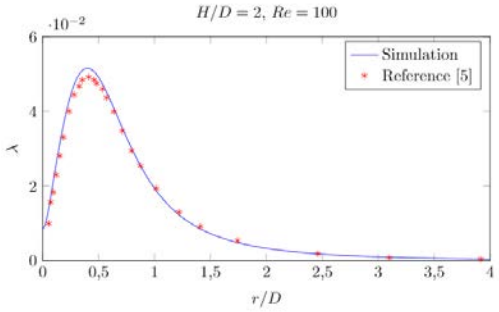

(b)

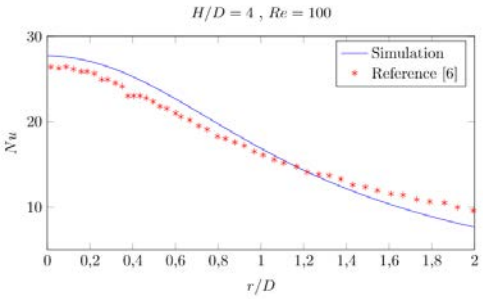

Figure 2. Validation of results with previous results by: (a) Deshpande and Vaishnav [5]; and (b) Poh et al. [6].

(a)

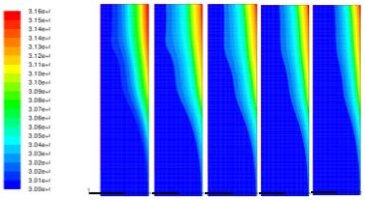

(b)

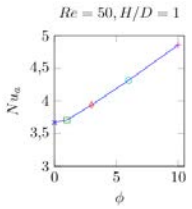

(c)

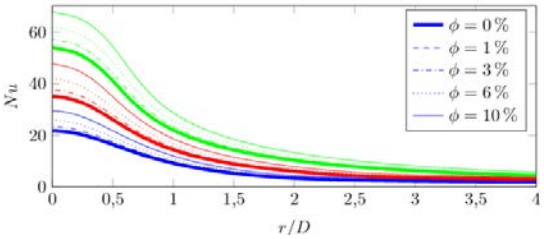

Figure 3. Temperature distribution (a); Nusselt at $Re = 50$ and $H/D = 1$ for increasing ϕ from left to right (b); Nusselt at $H/D = 1$ for $Re = 50$ (blue), $Re = 100$ (red) and $Re = 200$ (green) (c).

As an example of temperature distribution, Figure 3 depicts temperature contours for different nanoparticle concentrations and shows that the plate temperature decreases when ϕ increases, which increases refrigeration performance, as Nu_a shows in Figure 3(b). Same results are obtained as Reynolds number increases leading to the conclusion that heat transfer grows with high velocities and high concentration of nanoparticles as can be seen in Table 1, for $Re = 50$ and $H/D = 1$, and in Figure 3(c), where Nusselt profiles for $H/D = 1$ are depicted. All obtained results in terms of the output parameters were finally fitted to a global potential correlation as

$$f = A \times (H/D)^B \times (1-\phi)^C \times (Re)^D \qquad (5)$$

where A, B, C and D are constant. The obtained value of these constants, together with the mean error of the predicted values with respect the numerical ones, are shown in Table 2.

Table 1. Results obtained for H/D = 1 and Re=50.

Re	ϕ	Nu	Nu_o	σ
50	0	3.672	21.772	6.137
50	1	3.708	22.019	6.206
50	3	3.938	23.307	6.540
50	6	4.317	25.810	7.221
50	10	4.856	29.486	8.215

Table 2. Global correlation constants.

f	A	B	C	D	Error
Nu_a	0.2648	0.0128	-2.5694	0.6733	0.76 %
Nu_o	1.1097	-0.1278	-2.5524	0.7387	5.98 %
σ	0.3198	-0.1501	-2.6939	0.7316	5.53 %
λ	1.17E-6	-0.0458	-8.1227	0.8978	1.27 %
Π	3.2612	-0.1248	-0.1933	-1.2108	4.60 %

Summary/Conclusions: As a result of this study, different conclusions can be extracted especially from the potential correlation shown in (5) and Table 2:

1. Regarding the heat transfer: Maximum localized heat-transfer Nu_o occurs at minimum jet-plate distance, maximum nanoparticles concentration and maximum Reynolds number while heat transfer uniformity decreases (σ is minimum). On the other side, maximum average heat-transfer Nu_a occurs at maximum jet-plate distance, nanoparticles concentration and Reynolds number.
2. Regarding the mechanical power: Minimum mechanical power is required when jet-plate distance is maximum, nanoparticles concentration is minimum, and Reynolds number is maximum.
3. Regarding the efficiency: Maximum local and average efficiency is achieved at minimum jet-plate distance, maximum nanoparticles concentration and maximum Reynolds number.

Results show that simulations could have had a broader extent in terms of variables since optimal configurations occurs at the limits of the variables.

References:

1. F. Selimefendigil and H. F. Öztop, *Pulsating nanofuids jet impingement cooling of a heated horizontal surface*, International Journal of Heat and Mass Transfer, vol. 69, pp. 54-65, 2014.
2. G. Batchelor and R. O'brien, *Thermal or electrical conduction through a granular material*, in Proceedings of the Royal Society of London A: Mathematical, Physical and Engineering Sciences, vol. 355, pp. 313-333, The Royal Society, 1977.
3. R. L. Hamilton and O. Crosser, *Thermal conductivity of heterogeneous two-component systems*, Industrial & Engineering chemistry fundamentals, vol. 1, no. 3, pp. 187–191, 1962.

4. H. Masuda, A. Ebata, and K. Teramae, *Alteration of thermal conductivity and viscosity of liquid by dispersing ultra-fine particles. Dispersion of Al2O3, SiO2 and TiO2 ultra-fine particles.* Netsu Bussei, vol. 7, no. 4, pp. 227-233, 1993.
5. M. D. Deshpande and R. N. Vaishnav, *Submerged laminar jet impingement on a plane*, Journal of Fluid Mechanics, vol. 114, pp. 213-236, 1982.
6. H. J. Poh, K. Kumar, H. S. Chiang, and A. S. Mujumdar, *Heat transfer from a laminar impinging: jet of a power law fluid*, International communications in heat and mass transfer, vol. 31, no. 2, pp. 241-249, 2004.

1st International Conference on Nanofluids (ICNf2019)
2nd European Symposium on Nanofluids (ESNf2019)
26-28 June 2019, Castelló, Spain

Life Time Expectancy and Ageing Process of Nanofluids in Pulsating Heat Pipes

Roger R. Riehl[1*] and S M Sohel Murshed[2]

[1]National Institute for Space Research, INPE-DMC
Av. dos Astronautas 1758, São José dos Campos, SP 12227-010 Brazil
[2]Center for Innovation, Technology and Policy Research
Department of Mechanical Engineering
Instituto Superior Técnico, Universidade de Lisboa, 1049-001 Lisboa, Portugal
[*]Corresponding author: roger.riehl@inpe.br

Keywords: Thermal Management, Pulsating Heat Pipes, Lifetime Expectancy, Ageing.

Abstract: Nanofluids have been used in several thermal management systems, as they contribute to the augmentation of the heat dissipation rates in many applications, especially those where pulsating heat pipes (PHPs) are used. Long term use of this type of device is required in order to increase their reliability, which requires compatibility between the base fluid and the nanoparticle. The verification of the non-condensable gases (NCGs) generation is required as the nanofluid undergoes thermal cycling and chemical reactions are present, along with the interaction with the PHP housing material. The prediction of the amount of NCGs is required for each base fluid and nanofluid combination, which contributes to the evaluation of the life time expectancy for those devices. For this purpose, the use of the Arrhenius model is applied, which indicates the amount of NCG generated and the time related for which the PHP must undergo the ageing process. As the stability of nanofluids is strongly connected to various thermal properties, devices' thermal efficiency as well as their longevity, it is also important to employ stable nanofluids in PHPs.

Introduction: The use of nanofluids has shown to be a reliable solution to improve the thermal performances of devices especially in pulsating heat pipes (PHPs) [1]. The level of maturity of this technology has proven that nanofluids present a new line of applications for thermal management and that must be considered in current and new projects [2]. However, one must carefully consider the application of nanofluids in thermal management devices, especially those operating at saturation conditions. They inevitably undergo through chemical reactions during their thermal cycling that will direct impact the non-condensable gases (NCGs) generation, which might significantly affect their thermal performance along time. Such an important issue has been investigated in the past [3] and the basis for predicting the amount of NCGs generated, due to a given

combination of working fluid and material housing, can be properly determined [4]. Thermal management systems operating at saturation conditions require considerations regarding their life time expectancy related to the NCGs generation. If NCGs are not correctly predicted, the PHP will eventually present a decrease in its performance along time as the generated gas (usually hydrogen) will accumulate in the colder portion of the device. This will decrease the device's condensation capability, resulting in less heat removal capacity by the evaporator which, in many cases, will result in failure with the evaporator dryout, as less condensate will be transferred. Indications of this issue are shown during the device's operation, with higher temperatures observed at the evaporator for the same operational conditions as observed before, failures during start-up or temperature overshoot during operation [4]. The NCGs generation takes place mostly at the beginning of the interaction between the housing material and the working fluid, and an accelerated process can be employed to generate as much NCG as possible. This is a common process performed by heat pipes manufacturers that guarantees that the device will operate for a given amount of time without presenting the draw backs caused by NCGs. This process is part of the manufacturing and/or development of a PHP and is called *ageing*, which basically deals with the accelerated generation of NCGs (at a higher temperature) that would represent the amount of years predicted for the operation of those devices. Then, the portion of the PHP where the NCG was accumulated is removed, which ensures that the working fluid will not present in the NCGs that negatively impact their operation.

This paper, therefore, presents a methodology applied for the prediction of the amount of NCGs generated during application of nanofluids in the design of a PHP and highlights the importance of nanofluids stability for their (PHPs) performance as well as longevity.

Discussion and Results: Stability is one of the main challenges of nanofluids and it is an important requirement for their real applications, particularly in various thermal management systems such as heat pipe and channels flows [5]. The stability of nanofluids is strongly connected to the various thermal and flow properties as well as system thermal efficiency and longevity. As one of the main dispersion methods, proper sonication is a key step to obtain better dispersion of nanoparticles (NPs) and stability of nanofluids. Effect of ultrasonication parameters, such as time and amplitude on the stability of a water-based TiO_2 nanofluid, prepared by two-step method, was investigated by Cacua et al. [6] and despite very short sonication time (up to 6 minutes) and optimized amplitude setting for very small concentration (0.1 w/w%) of TiO_2 NP, almost all NPs were settled down at the bottom of the cuvettes within only 5 days. Whereas, Yu

et al. [7] prepared stable Cu/W nanofluids by chemical reduction (one-step) method and found significant increase in thermal conductivity compared to water. Thus, regardless of synthesis route employed, careful stability and degradation evaluation of nanofluids is necessary before applying them in any device, especially in close one like PHP.

The most used working fluid in PHPs is water, which is applied for a range of operational temperatures between 10 and 200°C, being this the preferred choice as base fluid for a nanofluid. However, in cases where sub-freezing temperatures must be faced by the PHP, another working fluid must be selected such as methanol, which freezes at -97.6°C and has a range of operational temperature between -80 and +100°C. However, depending on the nanoparticle selected for the nanofluid, proper consideration regarding chemical compatibility and NCGs generation must be performed, as part of the ageing process applied during the manufacturing procedure for the PHP. For the ageing process, the Arrhenius model is applied for any heat pipe operating with pure working fluids (without nanoparticles) [3]. Since nanofluids became an important contribution to new designs, their verification regarding NCGs generation must be considered. For combination of a base fluid, a nanoparticle and/or the PHP's housing material, the rate of decomposition can be estimated by the following relation

$$K = Ae^{\frac{-E_{act}}{RT}} \quad (1)$$

where K is the decomposition rate (ppm/s), A is an empirical relationship between temperature and rate coefficient (s^{-1}), E_{act} is the activation energy of the reaction, based on the combination of the working fluid and the materials involved (J/mol), R is the universal gas constant (J/mol·K) and T is the operational temperature (K). For the case of water as base fluid and copper nanoparticles, the values applied are A=0.025 s^{-1} and E_{act}=46,000 J/mol [8]. For the case of methanol as base fluid and copper nanoparticles, the values applied are A=0.030 s^{-1} and E_{act} = 67,000 J/mol [9].

The correspondent values related to the decomposition rate when using Cu/W and Cu/ methanol nanofluids are presented by Fig. 1. It is observed that, for a temperature of 100°C, the ageing process necessary for the PHP using Cu/W nanofluid will take 7 hours to generate the same amount of NCG as the Cu/ methanol nanofluid takes 15.5 days, for a life time expectancy of 10 years.

Summary: As an important method of verification the life time expectancy for a given combination of nanofluid in a PHP, the ageing process must be considered to evaluate the NCGs generation and avoid failure during operation of devices operating in saturation

conditions along its life time. Due to chemical reactions observed during the thermal cycling of those devices, such an evaluation becomes important to guarantee their thermal performance along time.

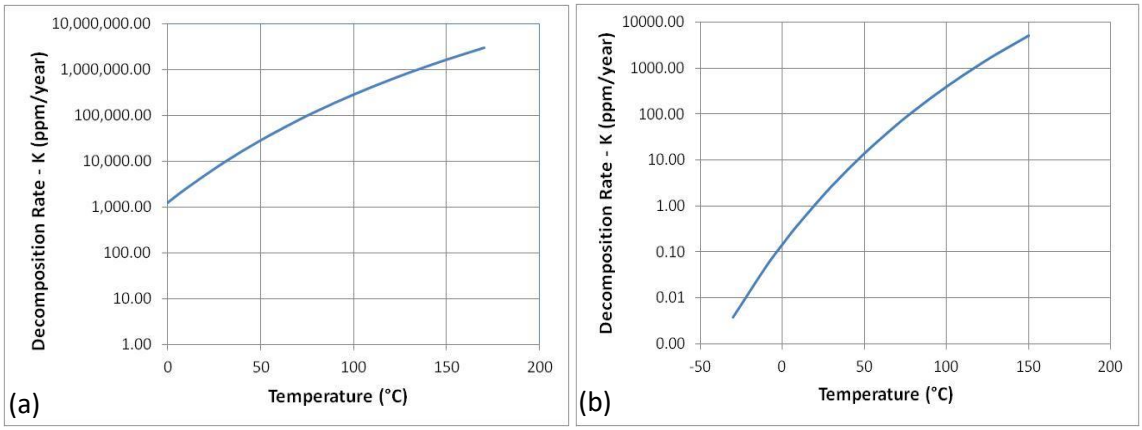

Figure 1. Decomposition rate for (a) water-copper nanofluid and (b) methanol-copper nanofluid.

References:

1. R. R. Riehl, Thermal enhancement using nanofluids on high heat dissipation electronic components, *Journal of Nanofluids* 9 (2019) 30-40.
2. M.H. Buschmann, A. Huminic, S. Mancin, R.R. Riehl and G. Huminic, State of the art of heat transfer of heat pipes and thermosyphons employing nanofluids as working fluid, *Journal of Nanofluids* 8 (2019) 253-266.
3. L.K. Tower, W.B. Kaufman, *Accelerated life tests of specimen heat pipe from communication technology satellite (CTS) project*. NASA technical memorandum, NASA TM-73846, 1977.
4. J.H., Rosenfeld, N.J., Gernert, Life test results for water heat pipes operating at 200ºC to 300ºC, *Proceedings of the STAIF-Space Technology and Applications International Forum*, Feb 10-14, Albuquerque, NM USA, 2008.
5. S.M.S. Murshed and C.A. Nieto de Castro, *Nanofluids: Synthesis, Properties and Applications*, Nova Science Publishers Inc., New York, 2014.
6. K. Cacua, F.E.B. Bioucas, S.M.S. Murshed, M.J.V. Lourenco, F.J.V. Santos and C.A. Nieto de Castro, Effects of agitation and ultrasonication on dispersion and thermal conductivity of aqueous TiO_2 nanofluids, *1st European Symposium on Nanofluids (ESNf2017)*, 8-10 October 2017, Lisbon, Portugal.
7. M-S. Liu, M. C-C. Lin, C.Y. Tsai, C-C. Wang, Enhancement of thermal conductivity with Cu for nanofluids using chemical reduction method, *International Journal of Heat and Mass Transfer* 49 (2006) 3028–3033.
8. M. J. Apted, D. G. Bennett, Timo Saari, A review of evidence for corrosion of copper by water, *Swedish Radiation Authority, Report number*: 2009:30 ISSN: 2000-0456.
9. J. Yoshihara, C. T. Campbell, Methanol synthesis and reverse water–gas shift kinetics over Cu (110) model catalysts: structural sensitivity, *Journal of Catalysis* 161 (1996) 776–782.

1st International Conference on Nanofluids (ICNf2019)
2nd European Symposium on Nanofluids (ESNf2019)
26-28 June 2019, Castelló, Spain

Magnetic field effect on thermal, dielectric and viscous properties of a transformer oil-based magnetic nanofluid

M. Rajnak[1,3], Z. Wu[2], B. Dolnik[3], K. Paulovicova[1], J. Tothova[3], R. Cimbala[3], J. Kurimsky[3], P. Kopcansky[1], B. Sunden[2], L. Wadso[4], and M. Timko[1*]

[1]Institute of experimental physics SAS, Watsonova 47, 04001 Kosice, Slovakia

[2]Department of energy sciences, Lund university, 22100, Lund, Sweden

[3]Faculty of electrical engineering and informatics, Technical university of Kosice, Letná 9, 04200, Kosice, Slovakia

[4]Devision of building materials, Lund university, 22100, Lund, Sweden

[*]Corresponding author: timko@saske.sk

Keywords: Magnetic nanofluid, Nanoparticles, Transformer oil, Thermal conductivity

Abstract: In this paper, we report on an experimental study of a transformer oil-based magnetic nanofluid. An unusual anisotropy in thermal conductivity of the nanofluid in a magnetic field is presented in regard to the field geometry. Magneto-dielectric and magneto-viscous effect in the prepared nanofluid were observed too. Suitability of the studied nanofluid for potential application in electrical engineering is considered.

Introduction/Background: Liquid dielectrics in power engineering provide electrical insulation, cooling, and serve as a diagnostic medium in electrical apparatus [1]. Transformer oils have been applied in this service for a long while. Recently, they have been facing industrial critiques due to the developments in the high voltage sector. Extreme efforts are being put into modifying the transformer oils (TO) by preparation of nanofluids [2]. Magnetic nanofluids (MNF) are of special interest, as their flow and heat transfer are controllable by magnetic field [3]. Under the applied field, the magnetic nanoparticles (MNPs) may form assemblies resulting in the change of the nanofluid's physical properties. Measurements of thermal conductivity (TC) of MNFs in magnetic field revealed the significant enhancement due to the MNP structuring [4]. From the insulating point of view, MNFs may withstand higher voltage as compared to TO [5]. Thus, the TO-based MNFs have a potential to be used as a cooling and insulating medium in power apparatus [6]. Herein, we primarily report on anisotropic TC of a MNF based on a transformer oil MOL TO 40A and Fe_3O_4 nanoparticles. Concerning the potential application in electrical engineering, the thermal study is complemented by measurements of dielectric permittivity and viscosity in dependence on a magnetic field.

Discussion and Results: Magnetite MNPs were synthesized by the well-know co-precipitation method [7]. The stabilization with oleic acid was followed by the dispersion in the TO. The concentrated MNF was finally diluted and several samples with different MNP volume fractions were prepared. Dynamic light scattering revealed a mean MNP diameter of 10 nm. The TC was measured by a thermal constants analyzer (TPS 2500S, Hot Disk AB, Sweden) using a transient plane source method (TPS). The spiral sensor with the axial and radial probing depth of 1.2 mm was inserted vertically into a Teflon container filled with the MNF. The magnetic field was generated by a pair of permanent magnets (37 mm apart) attached to the container (Fig. 1a). Its distribution (contours) simulated by the finite element method magnetics (FEMM 4.2) is presented in Fig. 1b.

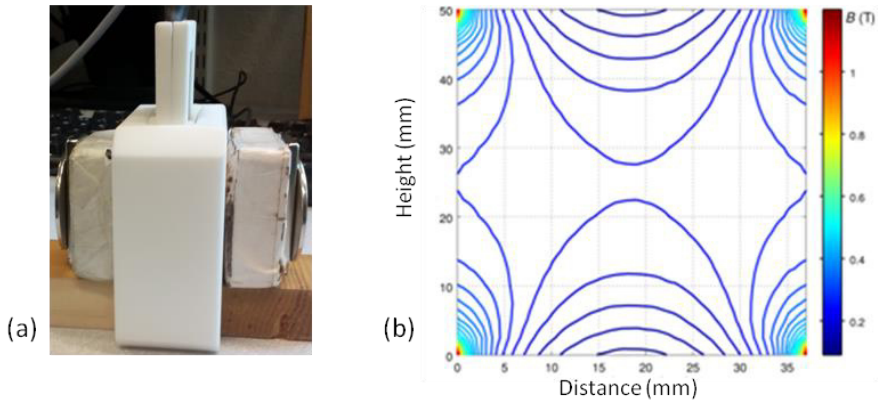

Figure 1. Hot Disk sensor holder in the Teflon container with the attached permanent magnets (a). Simulation of the magnetic field between the magnets (b).

In Fig. 2a, the increasing TC of the MNF with increasing MNP volume fraction is proven. It can be seen that the addition of 2.2 vol% of MNP results in 9.2 % increase in TC of the pure oil. It was found that the applied magnetic field increases the MNF TC in the radial direction of the sensor (perpendicularly to the magnetic field) for all samples (Fig. 2b-f). This is associated with the sample holder, sensor and magnetic field geometry. From Fig. 1, one can understand that the MNPs undergo magnetic attraction towards the container walls. Then, the concentration of MNPs is decreased in the axial (horizontal) probing depth of the sensor (as it is located in the middle of the container), leading to the decreased axial TC. On the contrary, Fig. 1b indicates higher magnetic field density in the vertical direction (the other two dimensions are set to the middle). This suggests a higher MNP concentration in the radial probing depth of the sensor resulting in the increased TC in this direction. However, the TC increments do not follow any proportional dependence on the magnetic field. Rather stochastic increase in radial TC may be attributed to a stochastic MNP concentration change (arrangement) within the probing depth when changing the magnetic field (attaching the magnets).

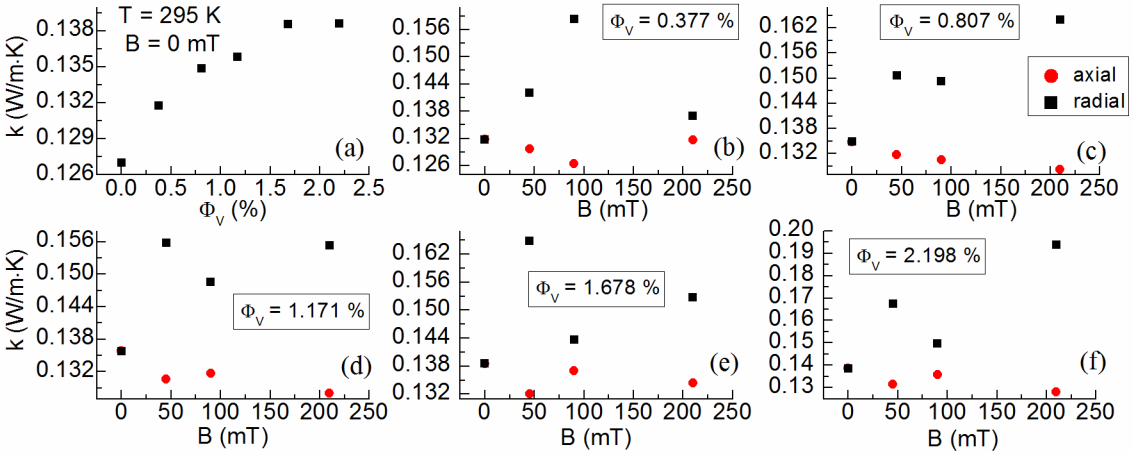

Figure 2. Thermal conductivity of the nanofluid in dependence on nanoparticle volume fraction (a). Magnetic field dependent thermal conductivity of the nanofluid samples in the radial and axial direction of the sensor.

From the dielectric point of view, the studied MNF exhibits a magneto-dielectric effect as seen from dielectric spectra in Fig. 3, obtained from an LCR meter (Agilent E4980A). The decreasing permittivity with increasing frequency of the electric field is reflecting the ceasing effect of MNP interfacial polarization processes. It is clear that upon the application of magnetic field, the real permittivity increases in both, parallel and perpendicular orientation of electric and magnetic fields. The increase is caused by the MNP assembly, the polarization of which yields the higher permittivity. However, for the most concentrated sample (2.198 vol%), the effect of parallel and perpendicular configuration is indistinguishable. The close packing of the formed assemblies in both configurations may be the reason.

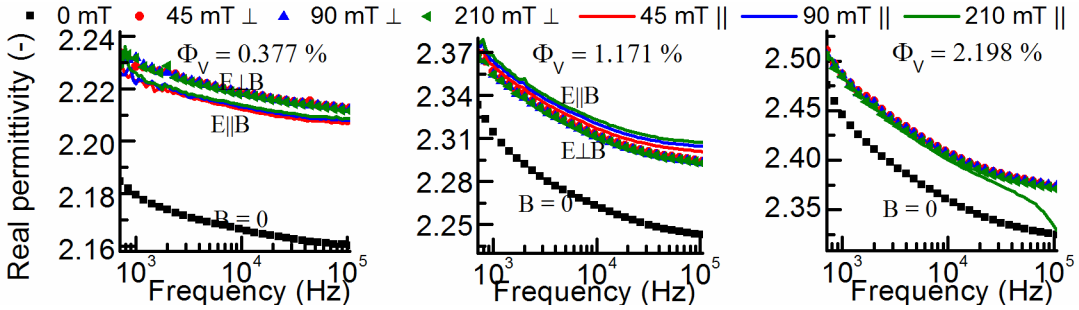

Figure 3. Frequency dependent real permittivity of the selected nanofluid samples at various magnetic field densities and orientations in regard to the electric field.

In Fig. 4, a quasi linear dependence of the MNF dynamic viscosity on MNP volume fraction is presented (Anton Paar, MCR 502). The plotted data were taken at normal laboratory temperature under the shear rate of 70 s^{-1}. The most concentrated MNF exhibits 20.4 % increase in viscosity, as compared to the pure oil viscosity. Moreover, further experimental investigation revealed the well-known magneto-viscous effect.

When applying the external magnetic field of 290 mT on the most concentrated sample, its viscosity increased again by 8.4 %. From the heat transfer point of view, these effects of increased viscosity may be considered as a drawback of the MNF. However, in gradient thermal and magnetic environments (e.g. in the vicinity of the transformer core) the positive effect of the thermomagnetic convection can still prevail over the increased viscosity.

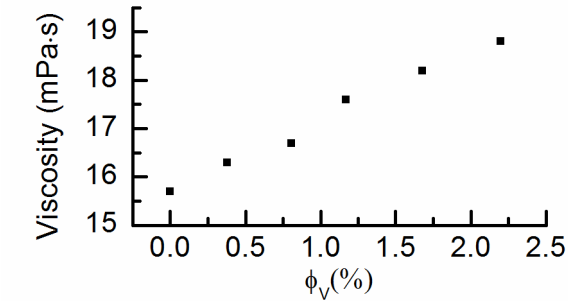

Figure 4. Nanofluid viscosity in dependence on the nanoparticle volume fraction.

Summary/Conclusions: We have proven that the thermal conductivity of the transformer oil can be enhanced by dispersing magnetite nanoparticles. The thermal conductivity of the resulting nanofluid is dependent on the magnetic field distribution. In contrast to the majority of reported studies, we observed higher thermal conductivity in perpendicular direction in regard to the magnetic field than in the parallel direction. The magnetic field controllable thermal conductivity, as well as the magneto-dielectric and magneto-viscous effects, which can give rise to the induced nanofluid flow (electrohydrodynamics, natural and thermo-magnetic convection) make the studied nanofluid suitable for cooling in electrical apparatus.

References:

1. I. Fofana and U. M. Rao, Engineering Dielectric Liquid Applications, *Energies*, 11, 10, (2018) p. 2756.
2. M. Rafiq, Y. Lv, and C. Li, A Review on Properties, Opportunities, and Challenges of Transformer Oil-Based Nanofluids, *J. Nanomater.*, 2016, (2016), p. e8371560.
3. I. Nkurikiyimfura, Y. Wang, and Z. Pan, Heat transfer enhancement by magnetic nanofluids—A review, *Renew. Sustain. Energy Rev.*, 21, (2013) pp. 548–561.
4. S. Doganay, A. Turgut, and L. Cetin, Magnetic field dependent thermal conductivity measurements of magnetic nanofluids by 3ω method, *J. Magn. Magn. Mater.*, 474, (2019) pp. 199–206.
5. U. Khaled and A. Beroual, AC Dielectric Strength of Mineral Oil-Based Fe3O4 and Al2O3 Nanofluids, *Energies*, 11, 12, (2018) p. 3505.
6. L. Pîslaru-Dănescu, A. M. Morega, G. Telipan, M. Morega, J. B. Dumitru, and V. Marinescu, Magnetic Nanofluid Applications in Electrical Engineering, *IEEE Trans. Magn.*, 49, 11, (2013) pp. 5489–5497.
7. L. Vékás, D. Bica, and M. V. Avdeev, Magnetic nanoparticles and concentrated magnetic nanofluids: Synthesis, properties and some applications, *China Particuology*, 5, 1-2, (2007) pp. 43–49.

1st International Conference on Nanofluids (ICNf2019)
2nd European Symposium on Nanofluids (ESNf2019)
26-28 June 2019, Castelló, Spain

Experimental heat transfer and pressure drop of Al_2O_3-graphene hybrid nanofluid in minichannel heat sink

Vivek Kumar[1*], Jahar Sarkar[1]
[1]Department of Mechanical Engineering, Indian Institute of Technology (B.H.U.), Varanasi, UP 221005, India
[*]vivekkr.rs.mec15@itbhu.ac.in

Keywords: Hybrid nanofluid, Minichannel heat sink, Heat transfer, Pressure drop.

Abstract: Heat transfer and pressure drop characteristics of a minichannel heat sink have been experimentally investigated by using Al_2O_3-graphene (50/50 v/v) hybrid nanofluid with 0.001% volume concentration. Heat sink consists of 10 parallel rectangular minichannels having 3 mm depth and 0.8 mm width. Effects of Reynolds number ($90 < Re < 500$) and inlet fluid temperature (20 to 40 ^oC) are studied with heat flux of 50 W/cm^2. A maximum enhancement of 40.3% at 20 ^oC has been observed for convective heat transfer coefficient with graphene/water nanofluid compared to base fluid (water). Heat transfer coefficient increases whereas pressure drop and friction factor decrease with increase in fluid inlet temperature.

Introduction: Due to significantly higher surface area to volume ratio, microchannel heat sink has a potential of heat removal up to 1000 W/cm^2 and emerged as potential thermal management device of microprocessor [1]. Hence, the fluid flow and heat transfer in mini/microchannels have emerged as an important research area. Performance can be further improved by using mono or hybrid nanofluids due to their better heat transfer characteristics. It is believed that hybrid nanofluid has better properties over mono nanofluid. Several experimental studies on heat transfer and fluid flow characteristics of nanofluid in Mini/Microchannel heat Sink (MCHS) have been conducted [2]. However, investigations on Al_2O_3-graphene based hybrid nanofluids flow in Minichannel heat sink are limited in the open literature [3]. Effect of fluid inlet temperature on the performance has been done in circular tube [4] and minichannel [5]. Best of the author's knowledge, no open literature available to show the effect of fluid inlet temperatures in the minichannel using Al_2O_3-graphene/DI water hybrid nanofluid in the laminar flow regime. The effect of Reynolds number (Re), fluid input temperature on the heat transfer and pressure drop characterization of minichannel heat sink using Al_2O_3-graphene/DI water nanofluid have been studied experimentally in the present study.

Discussion and Results: The layout of experimental setup and photograph are illustrated in Fig.1(a) and 1(b), respectively. Four main units exist in the system: flow

loop, cooling, heating and measuring unit. A circulating bath has been used just before the test section to supply fluid at certain inlet conditions. Test section includes heater with AC supply, copper plate, aluminium minichannels and acrylic plate. Cartridge heater having power of 600 W is placed at the bottom of heat sink to supply constant heat flux (50 W/cm^2). K-type thermocouples are inserted for temperature measurement. A differential pressure transducer is used to measure the pressure drop. Three fluid inlet temperatures (20°C, 30°C and 40°C) are used. After reaching thermal equilibrium, all measured temperatures have been recorded. Water based nanofluids have been prepared by two-step method by dispersing Al_2O_3 nanoparticles (45 nm diameter) and graphene nanoplates (Thickness=0.6-1.2 nm, length=0.8-0.2 µm) and sonicated in ultrasonicator for 6-8 hours without any surfactant to increase the homogeneity and stability of nanoparticles in base fluid. Hot disk TPS-500 analyser, LVDV-II+Pro Brookfield digital viscometer have been used to measure the thermal conductivity, specific heat and viscosity. Data reduction procedure has been described elsewhere by authors [5]. The total uncertainties found for estimated convection heat transfer coefficient, Nusselt number, pressure drop, friction factor, and Reynolds number are ± 3.2%, ± 4.1%, ±0.25%, ± 2.9% and ± 3.6%, respectively.

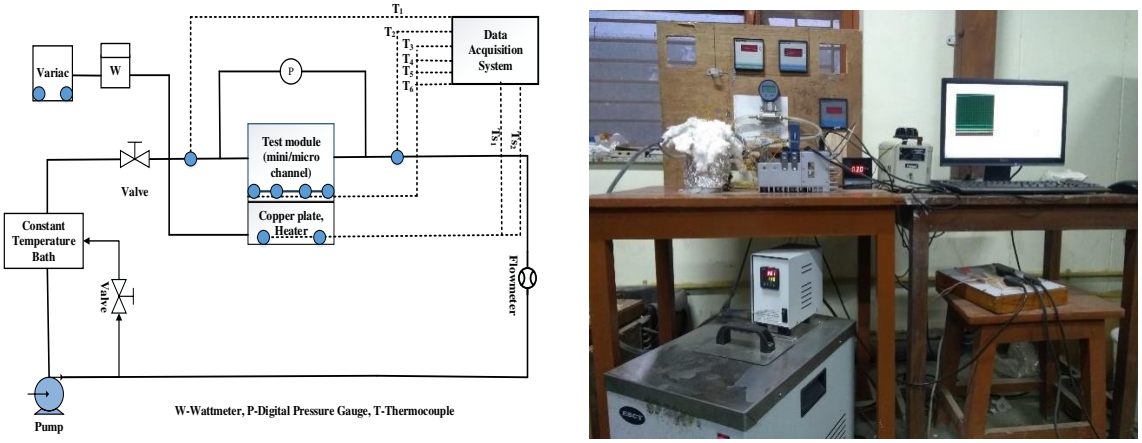

(a) (b)

Figure 1. (a) Layout of experimental work (b) experimental setup

In Figs. 2 and 3; W, A, AG and G represent water, alumina/water, hybrid (alumina + graphene)/water and grapheme/water, respectively, and 20, 30, and 40 represent the inlet temperatures. The variations of heat transfer coefficient and Nusselt number with Reynolds number for different working fluids are shown in Fig. 2(a) and Fig. 2(b), respectively. It can be observed that the heat transfer coefficient increases with increase in Reynolds number due to thickening of the thermal boundary layer. With nanoparticles addition, heat transfer coefficient increases due to several reasons including an increase

in thermal conductivity, different slip mechanisms (basically the relative motion between the nanoparticle and basefluid) and the nano-porous and nano-fin effects. The heat transfer enhancement was considerably improved at higher working temperature because of the improvement of thermal properties [5]. The maximum heat transfer coefficient is 4430.5 W/m^2.K for graphene/ DI water nanofluid at Re=490 and inlet temperature 40 °C. An increase in Nusselt number can be observed in addition of nanoparticles and this increase is due to increase in heat transfer coefficient. Nusselt number variation is similar to heat transfer coefficient with Re and for different working fluids. Maximum value of Nu is 8.6 at 40 °C for graphene/DI water nanofluid.

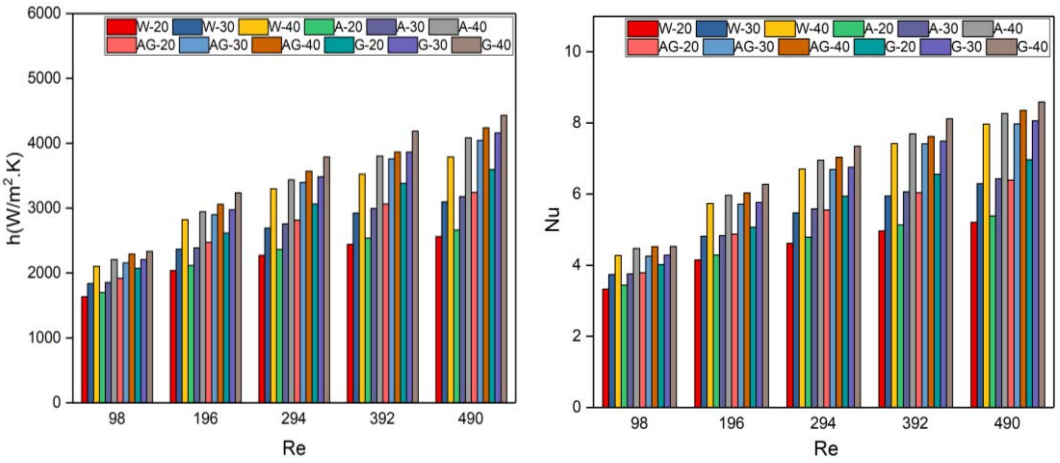

Figure 2. (a) Heat transfer and (b) Nusselt number of different fluids with Re

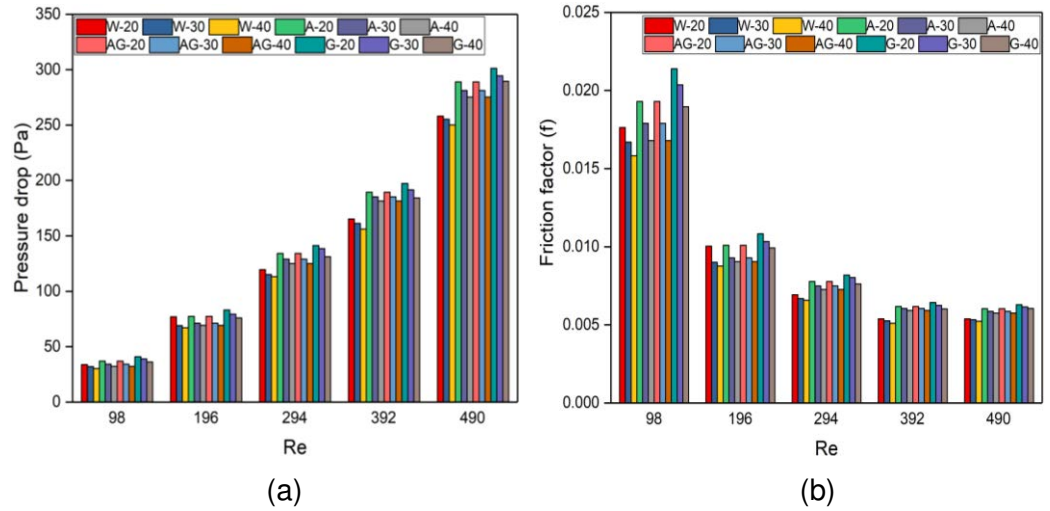

Figure 3. (a) Pressure drop and (b) Friction factor of different fluids with Re

Variations of pressure drop and friction factor with Re for different fluids at different inlet temperature are shown in Fig. 3(a) and 3(b), respectively. There is increment in pressure drop with increase in Re. By addition of nanoparticles in base fluid, pressure drop

increases due to dual effects of increasing viscosity and density. Maximum pressure drop is 301.2 N/m^2 for graphene/water nanofluid at Re=490 at 20 ^{o}C due to shape of graphene (nanoplate). There is no appreciable difference of pressure drop between Al_2O_3/water nanofluid and Al_2O_3-graphene/water hybrid nanofluid, but graphene/water nanofluid has increment of 4.23% in pressure drop from Al_2O_3-graphene/ water hybrid nanofluid. Inlet temperature has adverse effect on pressure drop due to decrease in viscosity with temperature. Friction factor decreases with increase in Reynold number due to the fact that friction factor is inversely proportional to Re for laminar flow. With the addition of nanoparticles, the friction factor increases may be due to increase in viscosity and slip mechanism. With the increase in temperature, friction factor decreases for the same Re due to decrease in viscosity.

Conclusions: Effect of inlet temperature on heat transfer and pressure drop characteristics of hybrid nanofluid in minichannel heat sink has been experimentally studied for 0.001% volume concentration. Heat transfer coefficient and Nusselt number increase with inlet temperature (20°C to 40°C) and nanoparticle dispersion in base fluid due to improvement of thermal properties. Pressure drop and friction factor increases with the Reynolds number. Both increase with nanoparticle dispersion in base fluid and decrease in inlet temperature due to increase in viscosity. Maximum pressure drop increment is 16.74 % for graphene nanofluid. The maximum value of heat transfer coefficient as well as pressure drop is for graphene/water nanofluid due to shape of graphene (nanoplate).

References:

1. S.G. Kandlikar and W.J. Grande, Evaluation of single phase flow in microchannels for high heat flux chip cooling—Thermohydraulic performance enhancement and fabrication technology, *Heat Transfer Engineering* 25 (8) (2004) 5–16.

2. A. J. Chamkha, M. Molana, A. Rahnama and F. Ghadami, On the nanofluids applications in microchannels: A comprehensive review, *Powder Technology* 332 (2018) 287–322.

3. N. Ahammed, L. G. Asirvatham and S. Wongwises, Entropy generation analysis of graphene–alumina hybrid nanofluid in multiport minichannel heat exchanger coupled with thermoelectric cooler, *Int. Journal Heat and Mass Transfer* 103 (2016) 1084–1097.

4. C. J. Ho and Y. J. Lin, Turbulent forced convection effectiveness of alumina–water nanofluid in a circular tube with elevated inlet fluid temperatures: An experimental study, *Int. Communication Heat and Mass Transfer* 57 (2014) 247–253.

5. V. Kumar and J. Sarkar, Numerical and experimental investigations on heat transfer and pressure drop characteristics of Al_2O_3-TiO_2 hybrid nanofluid in minichannel heat sink with different mixture ratio, *Powder Technology* 345 (2019) 717-727.

1st International Conference on Nanofluids (ICNf2019)
2nd European Symposium on Nanofluids (ESNf2019)
26-28 June 2019, Castelló, Spain

Performance improvement of absorption cooling systems using nanoparticles: A review

M. Venegas[1,2*], N. García-Hernando[1] and M. de Vega[1]

[1]ISE Research Group, Department of Thermal and Fluids Engineering, Universidad Carlos III de Madrid, Avda. Universidad 30, 28911 Leganés, Madrid, Spain

[2]GTADS Research Group, Department of Thermal and Fluids Engineering, Universidad Carlos III de Madrid, Avda. Universidad 30, 28911 Leganés, Madrid, Spain

[*]Corresponding author: mvenegas@ing.uc3m.es

Keywords: Nanoparticles, Absorption refrigeration, Mass transfer, H_2O-LiBr, NH_3-H_2O, NH_3-$LiNO_3$

Abstract: A review is performed about the use of nanoparticles in absorption cooling systems to improve performance. Different nanofluids are evaluated using surfactants in some cases. Main researches evaluate the mass transfer enhancement in absorbers using ammonia-water (NH_3-H_2O) and water-lithium bromide (H_2O-LiBr) as base fluid.

Introduction: Absorption cooling chillers use heat as energy source, including residual or renewable heat. The main components of absorption cycles are the absorber and the generator. They are designed for simultaneous heat and mass transfer. Most of them are large, heavy and expensive, and continuous efforts are being made to improve their design. One way to reduce their size is improving the heat and mass transfer rates by means of nanoparticles added to the working fluid. In this work a review is performed about researches published in journals up to date regarding performance improvement.

Discussion and Results: Figure 1 includes the evolution of papers published in journals along time related to the use of nanoparticles in absorption cooling chillers. Table 1 contains a summary of researches done up to date about the use of nanoparticles in absorbers. Data shown in the columns Size, Fraction, Surfactant and Maximum increase correspond to the case in which the highest mass transfer improvement was obtained.

Additional works can be found in the open literature (not included in Table 1) about whole chiller and generator performance, stability and dynamic characteristics of nanoparticles mixed with dispersants and influence of heating on absorbance, viscosity and thermal conductivity of various types of nanofluids. Also, about the combined

influence of nanoparticles and external magnetic fields in absorption. Regarding the NH_3-$LiNO_3$ solution, the enhancement of thermal conductivity by adding CNTs has been evaluated.

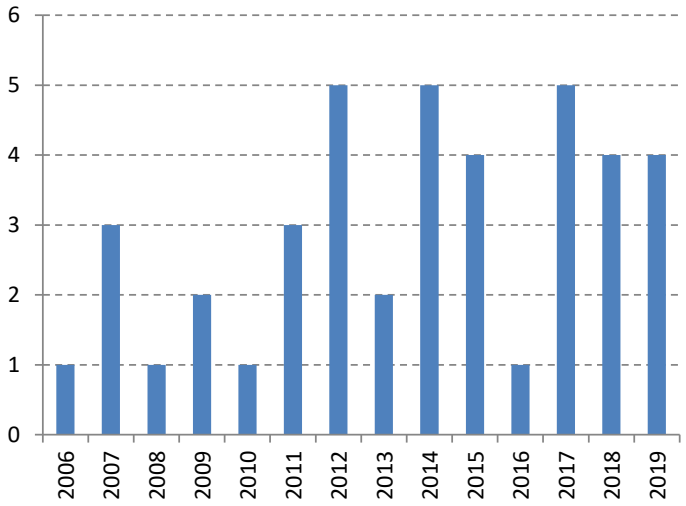

Figure 1. Number of papers published in journals along time

Table 2. Summary of researches done about absorber performance using nanoparticles

Ref.	Type	Solution	Nanoparticle	Size (nm)	Fraction	Surfactant	Maximum increase
[1]	Exp.	NH_3-$LiNO_3$	Multiwall CNT	ID: 5-10 OD: 20-30	0.01 wt%	No	1.64
[2]	Exp.	H_2O-LiBr	Fe	100	0.1 wt%	Yes	1.9
			CNT	25	0.1 wt%	Yes	2.48
[3]	Exp.	H_2O-LiBr	SiO_2	20	0.005 vol%	No	1.18
[4]	Exp.	NH_3-H_2O	Al_2O_3	< 20	0.2 wt%	Yes	1.3
			Fe_2O_3	< 30	0.2 wt%	Yes	1.7
			$ZnFe_2O_4$	< 30	0.1 wt%	Yes	1.5
[5]	Exp.	H_2O-LiBr	CuO	30-50	0.1 wt%	Yes	2.35
[6]	Exp.	NH_3-H_2O	TiO_2	15	0.5 wt%	No	1.04
[7]	Exp.	H_2O-LiBr	Cu	50	0.1 wt%	No	2.01
			Al_2O_3	25	0.1 wt%	No	1.81
			Multiwall CNT	ID: 5-10 OD: 20-40	0.1 wt%	No	1.46
[8]	Exp.	H_2O-LiBr	Fe_3O_4	20	0.05 wt%	No	2.28
[9]	Exp.	NH_3-H_2O	Al_2O_3	35	0.02 vol%	No	1.2
			CNT	25	0.02 vol%	No	1.18
[10]	Num.	H_2O-LiBr	Ag	-	10 vol%	No	1.73
[11]	Exp.	NH_3-H_2O	Cu	50	0.1 wt%	No	3.21
			CuO	47	0.1 wt%	No	3.11
			Al_2O_3	33	0.1 wt%	No	3.02

[12]	Exp.	NH_3-H_2O	Cu	< 50	0.1 wt%	Yes	5.32
			CuO	< 50	0.1 wt%	Yes	5.08
[13]	Num.	NH_3-H_2O	Cu	-	0.08 wt%	No	1.85
			Al_2O_3	-	0.08 wt%	No	1.76
[14]	Exp.	NH_3-H_2O	Multiwall CNT	20	0.22 wt%	No	1.2
[15]	Exp.	NH_3-H_2O	Multiwall CNT	10-20	0.23 wt%	No	1.162
[16]	Exp.	NH_3-H_2O	Ag	15	0.02 wt%	No	1.55
[17]	Exp.	NH_3-H_2O	Al_2O_3	20	0.2 wt%	No	1.122
			ZnO	15	0.1 wt%	No	1.132
			ZrO_2	50	0.1 wt%	No	1.105

Conclusions: Limited researches have been developed about the use of nanoparticles in absorption cooling chillers. The number of papers published has moderately increased in recent years. Major part of the works has been related to the absorber using NH_3-H_2O and secondly using H_2O-LiBr. Only three papers have evaluated the whole chiller and one the generator performance. Of the 21 papers found in the open literature evaluating performance improvement, only 6 used surfactants to increase the mass transfer, obtaining better results respect to using only nanoparticles. The best performance using H_2O-LiBr has been obtained with CNT, while Cu nanoparticles provided the best results in the case of NH_3-H_2O.

Acknowledgements: Financed by: FEDER/Ministerio de Ciencia, Innovación y Universidades – Agencia Estatal de Investigación/ _Proyecto (DPI2017-83123-R).

References:

1. C. Amaris, M. Bourouis and M. Vallès, Passive intensification of the ammonia absorption process with NH_3/$LiNO_3$ using carbon nanotubes and advanced surfaces in a tubular bubble absorber, *Energy* 68 (2014) 519-528.
2. Y.T. Kang, H.J. Kim and K.I. Lee, Heat and mass transfer enhancement of binary nanofluids for H_2O/LiBr falling film absorption process, *International Journal of Refrigeration* 31 (2008) 850-856.
3. H. Kim, J. Jeong and Y.T. Kang, Heat and mass transfer enhancement for falling film absorption process by SiO_2 binary nanofluids, *International Journal of Refrigeration* 35 (2012) 645-651.
4. L. Yang, K. Du, X.F. Niu, B. Cheng and Y.F. Jiang, Experimental study on enhancement of ammonia-water falling film absorption by adding nano-particles, *International Journal of Refrigeration* 34 (2011) 640-647.

5. G. Wang, Q. Zhang, M. Zeng, R. Xu, G. Xie and W. Chu, Investigation on mass transfer characteristics of the falling film absorption of LiBr aqueous solution added with nanoparticles, *International Journal of Refrigeration* 89 (2018) 149-158.
6. W. Jiang, S. Li, L. Yang and K. Du, Experimental investigation on enhancement of ammonia absorption process with TiO_2 nanoparticles in newly designed absorber, *International Journal of Refrigeration*, DOI: 10.1016/j.ijrefrig.2018.11.019.
7. L. Zhang, Z. Fua, Y. Liu, L. Jin, Q. Zhang and W. Hu, Experimental study on enhancement of falling film absorption process by adding various nanoparticles, *International Communications in Heat and Mass Transfer* 92 (2018) 100-106.
8. L. Zhang, Y. Liu, Y. Wang, L. Jin, Q. Zhang and W. Hu, Experimental study on the enhancement of mass transfer utilizing Fe_3O_4 nanofluids, *Journal of Heat Transfer* 140 (2018) 012404.
9. J.K. Lee, J. Koo, H. Hong and Y.T. Kang, The effects of nanoparticles on absorption heat and mass transfer performance in NH_3/H_2O binary nanofluids, *International Journal of Refrigeration* 33 (2010) 269-275.
10. S. Armou, R. Mir, Y. El Hammami, K. Zine-Dine and M. El Hattab, Heat and mass transfer enhancement in absorption of vapor in laminar liquid film by adding nano-particles, *Journal of Applied Fluid Mechanics* 10 (2017) 1711-1720.
11. J.K. Kim, J.Y. Jung and Y.T. Kang, The effect of nano-particles on the bubble absorption performance in a binary nanofluid, *International Journal of Refrigeration* 29 (2006) 22-29.
12. J.K. Kim, J.Y. Jung and Y.T. Kang, Absorption performance enhancement by nano-particles and chemical surfactants in binary nanofluids, *International Journal of Refrigeration* 30 (2007) 50-57.
13. M.B. Ben Hamida, J. Belghaib and N. Hajji, Numerical study of heat and mass transfer enhancement for bubble absorption process of ammonia-water mixture without and with nanofluids, *Thermal Science* 22 (2018) 3107-3120.
14. X. Ma, F. Su, J. Chen, T. Bai and Z. Han, Enhancement of bubble absorption process using a CNTs-ammonia binary nanofluid, *International Communications in Heat and Mass Transfer* 36 (2009) 657-660.
15. X. Ma, F. Su, J. Chen and Y. Zhang, Heat and mass transfer enhancement of the bubble absorption for a binary nanofluid, *Journal of Mechanical Science and Technology* 21 (2007) 1813-1818.
16. C. Pang, W. Wu, W. Sheng, H. Zhang and Y.T. Kang, Mass transfer enhancement by binary nanofluids (NH_3/H_2O + Ag nanoparticles) for bubble absorption process, *International Journal of Refrigeration* 35 (2012) 2240-2247.

17. W. Wu, J. Wu, Y. Wang and H. Zhang, The enhancing influence of nanoparticles on ammonia/water falling film absorption in binary nanofluids under pressure reducing conditions, *Journal of Thermal Science and Technology* 12 (2017) JTST0018.

1st International Conference on Nanofluids (ICNf2019)
2nd European Symposium on Nanofluids (ESNf2019)
26-28 June 2019, Castelló, Spain

Convective heat transfer study of graphene nanoplatelet nanofluids in a tube-in-tube heat exchanger

Javier P. Vallejo[1,2], Uxía Calviño[1,2], Ignacio Freire[1], José Fernández-Seara[2], Luis Lugo[1]

[1]Departamento de Física Aplicada, Facultade de Ciencias, Universidade de Vigo, E-36310 Vigo, Spain

[2]Área de Máquinas e Motores Térmicos, Escola de Enxeñería Industrial, Universidade de Vigo, E-36310 Vigo, Spain

[*]Corresponding author: luis.lugo@uvigo.es

Keywords: Convection heat transfer coefficient, Pressure drop, Graphene nanoplatelets, Ethylene glycol, Heat transfer.

Abstract: The heat transfer performance of different loaded sulfonic acid functionalized graphene nanoplatelet (S-GnP) nanofluids based on an ethylene glycol:water 50:50 vol% mixture (EG:W 50:50 vol%) was assessed. Firstly, the thermophysical properties needed for the analyses were experimentally determined (density, isobaric heat capacity, thermal conductivity and dynamic viscosity). Subsequently, the convection heat transfer coefficients and pressure drops were evaluated through an experimental setup with a tube-in-tube heat exchanger as main element. Finally, a dimensionless analysis of the obtained results was carried out. The 0.25 wt% S-GnP/EG:W 50:50 vol% nanofluid achieves the higher convection heat transfer performance.

Introduction/Background: The thermal conductivity enhancement of the habitually employed thermal fluids by means of the dispersion of nanoparticles has been studied from the conception of nanofluids [1]. Forced turbulent convection is the most efficient heat transfer process [2] but experimental investigations by using real heat exchangers are missing to evaluate this type of new fluids. Water and glycols are two of the most common working fluids in this field, as well as mixtures among them. Mixtures of water and ethylene glycol at 50:50 vol% are often used in applications such as the automobile engine [3], providing frost protection down to ~ 235 K [4].

In this work, three different concentrations (0.25, 0.50 and 1.0 wt%) of sulfonic acid functionalized graphene nanoplatelet, S-GnP, (provided by NanoInnova Technologies S.L., Madrid, Spain) were dispersed in ethylene glycol:water 50:50 vol% mixture, EG:W 50:50 vol%, following a two-step method. Firstly, the amounts of each component were accurately weighted. Then, the dispersions were submitted to ultrasound baths during 240 min at 20 kHz frequency and 200 W power. The thermophysical characterization of

the base fluid and the nanofluids was measured in the temperature range from 293.15 to 333.15 K. Densities, isobaric heat capacities, thermal conductivities and dynamic viscosities for base fluid and nanofluids were determined by vibrating tube, differential scanning calorimetry, transient hot wire and rotational rheometry methods, respectively.

The heat transfer coefficients and pressure drops over a tube-in-tube heat exchanger of stainless steel were obtained by means of an experimental facility composed by three hydraulic circuits: the tested fluid loop, the heating water loop and the cooling water loop [5]. The tested fluid is pumped through the inner tube of the heat exchanger being heated by the water that flows through the annular section. This heating water returns to its initial conditions by means of electric resistances, while the tested fluid by means of cooling water through an auxiliary heat exchanger. A differential pressure sensor and different temperature sensors and flow meters allow collecting all the test data. The performed tests were defined by the average tested fluid temperature (298.15, 308.15 and 318.15 K) and the tested fluid flow rate (300 to 700 $L \cdot h^{-1}$, 100 $L \cdot h^{-1}$ step). The Gnielinski correlations for concentric annular ducts determined the heating water convection coefficients [6].

Discussion and Results: The deviations between the measured thermophysical properties and those values from the literature are lower than the expanded experimental uncertainty in all cases. Figure 1 shows the thermal conductivity and dynamic viscosity behaviours as a function of temperature at several S-GnP concentrations. Quasi temperature-independent thermal conductivity enhancements reaching 4.0 % and dynamic viscosity increases of up to 35 % are found for the 1.0 wt% loading. As regards to densities, the increases reach values up to 0.27 % while heat capacity decreases up to 0.64 %.

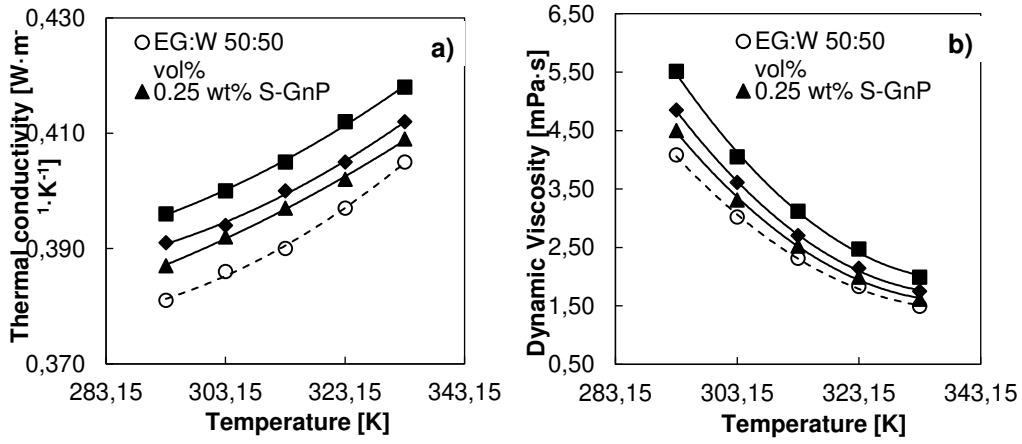

Figure 1. Thermal conductivity (a) and dynamic viscosity (b) for the different-loaded S-GnP nanofluids as a function of temperature.

Thermal conductivity enhancements were observed for all analysed S-GnP concentrations. However, 1 wt% S-GnP/EG:W 50:50 vol% nanofluid always worsens the base fluid convection heat transfer coefficients while 0.50 wt% nanofluid achieves enhancements only in some test conditions. On the contrary, 0.25 wt% loading achieves enhancements with respect to the base fluid for all the tested flow rates and temperatures. The balance between the improvement produced by the thermal conductivity increase and the worsening due to the dynamic viscosity increase explain this behaviour. Regarding pressure drop, and consequently pumping power, smooth increases were observed as concentration rises.

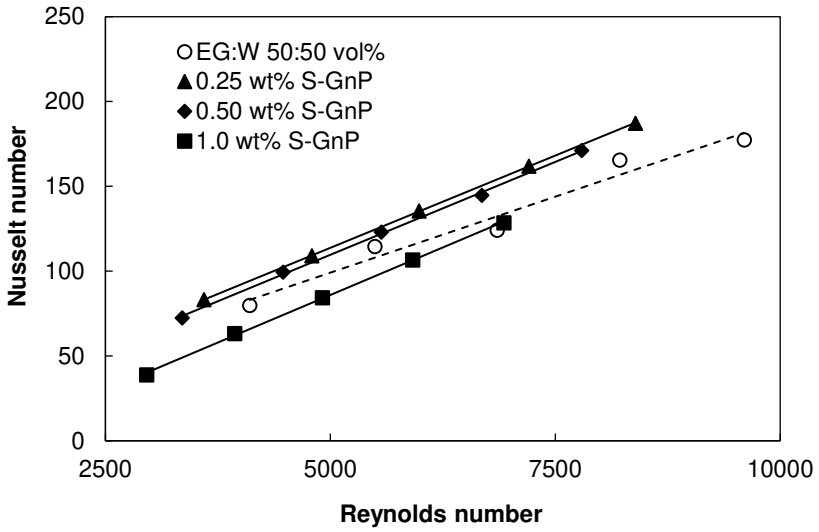

Figure 2. Nusselt number as a function of Reynolds number for the different-loaded S-GnP nanofluids at 298.15 K as tested fluid temperature.

Convection heat transfer coefficients depends on geometrical conditions of the heat exchanger, so they are not mostly extensible to other applications. Nevertheless, dimensionless analyses allow this purpose. Figure 2 shows the obtained Nusselt numbers as a function of the corresponding Reynolds numbers for the studied samples at 298.15 K. For the same Reynolds number, the 0.25 wt% and 0.50 wt% nanofluids achieve higher Nusselt numbers than the base fluid. Nevertheless, the 1.0 wt% sample worsens the base fluid results. As an example, for a Reynolds number of 6000, Nusselt numbers deviations of 16 %, 13 % and -7.4 % with respect to the base fluid are reached for 0.25 wt%, 0.50 wt% and 1.0 wt% nanofluids, respectively.

Summary/Conclusions: The thermophysical properties needed for the heat transfer performance analysis of S-GnP/EG:W 50:50 vol% nanofluids (0.25 wt%, 0.50 wt% and 1.0 wt% nanoadditive concentrations) and the base fluid were experimentally determined.

Density, isobaric heat capacity and dynamic viscosity variations of up to 0.27 %, -0.64 % and 35 %, were respectively detected for the rising loading of S-GnP while the thermal conductivity enhancements achieve 4.0 %. The heat transfer coefficients and pressure drops were obtained by means of an experimental facility that contains a tube-in-tube heat exchanger. A maximum 10.4 % convection heat transfer coefficient enhancement was obtained for the 0.25 wt% S-GnP concentration. The 0.50 wt% nanofluid only achieves improvements in some conditions while the 1.0 wt% nanofluid worsens the base fluid behaviour in all cases. The optimal concentration, 0.25 wt%, produces only slight increases in the pressure drop. Finally, a Nusselt number worsening for the 1.0 wt% S-GnP loading was detected while improvements for the 0.25 and 0.50 wt% S-GnP loadings were found.

Acknowledgements: This work was supported by “Ministerio de Economía y Competitividad” (Spain) and FEDER program through ENE2017-86425-C2-1-R project. Authors acknowledge the financial support by Xunta de Galicia through GRC ED431C 2016-034 and the provision of functionalized graphene nanoplatelets powder by Nanoinnova Technologies S.L. (www.nanoinnova.com). Authors also acknowledge EU COST Action CA15119: Overcoming Barriers to Nanofluids Market Uptake. J.P.V. acknowledges FPI Program of “Ministerio de Economía y Competitividad”.

References:

1. M. H. Ahmadi, A. Mirlohi, M. A. Nazari, R. Ghasempour A review of thermal conductivity of various nanofluids, Journal of Molecular Liquids, 265 (2018) 181-188.
2. Y. Shabany, *Heat transfer: thermal management of electronics*, CRC Press, Boca Raton, 2009.
3. C. Selvam, D. M. Lal, S. Harish, Thermophysical properties of ethylene glycol-water mixture containing silver nanoparticles, *Journal of Mechanical Science and Technology* 30 (2016) 1271-1279.
4. American Society of Heating, Refrigerating and Air Conditioning Engineers, *Handbook A. S. H. R. A. E., Fundamentals*, Atlanta, 2001.
5. J. Pérez-Tavernier, J. P. Vallejo, D. Cabaleiro, J. Fernández-Seara, L. Lugo, Heat transfer performance of a nano-enhanced propylene glycol:water mixture, *International Journal of Thermal Sciences* Accepted (2019).
6. V. Gnielinski, G2 Heat Transfer in Concentric Annular and Parallel Plate Ducts,in *VDI Heat Atlas*, Ed., VDI-Gesellschaft Verfahrenstechnik und Chemieingenieurwesen, Chapter G2, pp. 701-708, Düsseldorf, Springer, 2010.

SESSION 3
Storage of Thermal Energy

S3

1st International Conference on Nanofluids (ICNf2019)
2nd European Symposium on Nanofluids (ESNf2019)
26-28 June 2019, Castelló, Spain

Nanoencapsulation of Metallic PCMs with Atomic Layer Deposition

N. Navarrete[1], L. Hernández[1], D. La Zara[2], J.R. van Ommen[2] and R. Mondragón[1*]

[1]Departament of Mechanical Engineering and Construction, Universitat Jaume I, 12071, Castellón de la Plana, Spain

[2]Department of Chemical Engineering, Delft University of Technology, 2629 HZ, Delft, the Netherlands.

[*]Corresponding author: mondragn@uji.es

Keywords: Thermal Energy Storage, Phase Change Materials, Encapsulation, Nanofluid.

Abstract: Phase Change Materials (PCMs) are materials with a high latent heat of fusion, so they are able to store and release high amounts of energy during the melting and solidification processes. Therefore, they can be of relevance for their use in a Thermal Energy Storage step for Concentrated Solar Power plants, in order to mitigate the intermittencies of sunlight, or to improve the performance of Heat Transfer Fluids. When used as the solid phase in a nanofluid, i.e. as the nanoparticles, PCMs need to have a core-shell structure, with a PCM nucleus and a high-melting point encapsulating material that prevents the particles from collapsing into each other while in liquid phase. Metallic nanoPCMs usually have a shell of metallic oxide naturally formed by passivation in contact with oxygen. However, this layer might not be enough as encapsulation and issues of further oxidation of the nuclei due to high temperatures, thermal cycling or interaction with the base fluid can be encountered. In this work, Atomic Layer Deposition has been used to create a second encapsulating layer of silica on Sn/SnO core-shell structured nanoparticles. The composition, structure and behaviour through thermal cycling of the multi-layered nanoparticles have been analysed, as well as their performance in a thermal oil based nanofluid regarding rheometry and stability.

Introduction/Background: One of the main challenges for the use of renewable energies is the complexity in energy storage, to overcome the intermittencies of availability of the energy source. The use of Phase Change Materials (PCMs) is a good alternative as storage of thermal energy. These are materials with high phase change enthalpies. That means a considerable amount of energy needs to be supplied in order to melt the PCM, and this energy remains stored until it solidifies again.

Metals and metallic alloys are usually good PCMs. Apart from high latent heat they present high thermal conductivity, that allows for fast charge and discharge cycles, high density, that enables improvements in the thermal properties depending on the mass loading without excessively damaging the viscosity (depending on the volume concentration) [1].

In order to introduce metals as PCMs with the current technology found in the solar thermal energy industry, a good option is the use of nanofluids. These are colloidal suspension of nanometric particles that allow to include to a certain extent the physical properties of a solid while keeping the transport properties of a fluid [2]. The main requirement to use PCMs as the solid phase in a nanofluid is encapsulation of the nanoparticles. A core-shell structure is needed, with a high-melting point layer that prevents the PCM cores from collapsing into each other when in liquid phase.

Atomic Layer Deposition (ALD) is a gas-phase deposition technique that has proved useful for encapsulation of small particles [3, 4]. The untreated nanoparticles in a fluidized state are cyclically exposed to two gaseous precursors that chemisorb on their surface. After exposure to each of the precursors, a purge step is needed to remove the unreacted remainders and avoid undesired gas-phase reactions with the subsequent precursor. In this way, the deposition process is highly controlled and allows to create films of a few nanometres whose thickness can be tuned by varying the number of cycles of precursor exposure.

In this work, ALD has been used to synthesize SiO_2 encapsulations on Sn nanoparticles. Metallic nanoparticles usually have an oxide layer naturally formed by passivation that can serve as encapsulation, but also might be chemically incompatible with the base fluid or not resistant to thermal cycling, that promotes further oxidation of the nucleus. Therefore, the suitability of a second encapsulation to overcome this issues has been tested.

Discussion and Results: A silica film has been synthesized on Sn/SnO nanoparticles using ALD. The nanoparticles were cyclically exposed to $SiCl_4$ and H_2O at 40ºC, with purging steps in between. Samples were taken after 5, 10, 25 and 50 $SiCL_4$-H_2O cycles, and the progressive growth of the coating was observed according to the silica weight concentrations of 0.28%, 0.47%, 0.91% and 1.07%, respectively, measured with ICP-OES.

Visual identification of the coating was achieved by TEM imaging. In Figure 1, the multi-coated nanoparticle after 50 ALD cycles can be observed, with an EDX analysis that shows the composition of the different layers: pure Sn in the nucleus, SnO_x in the inner shell (~12

nm), and SiO_2 in the outer (~8 nm). Additionally, it was observed that the SnO_x layer is crystalline but the SiO_2 coating is amorphous.

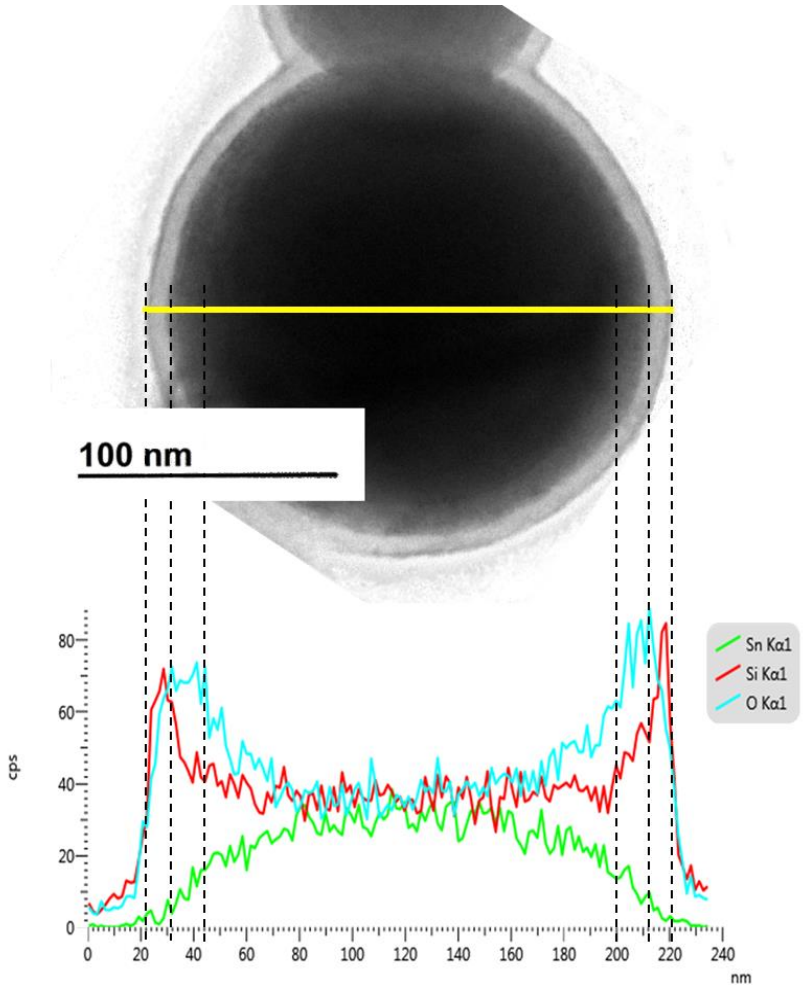

Figure 1. TEM micrograph and EDX line analysis of a Sn/SnO/SiO_2 nanoparticle.

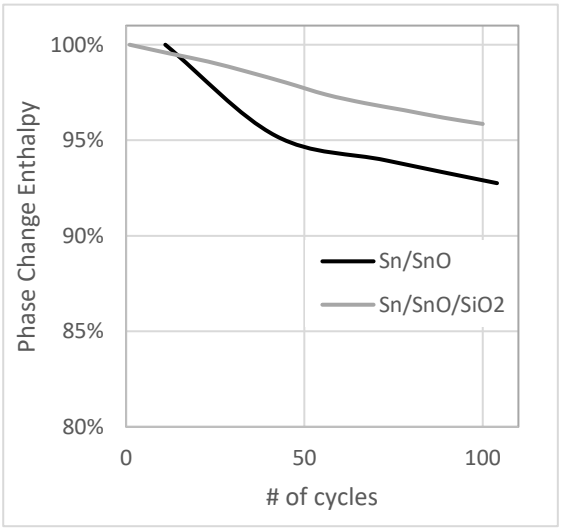

Figure 2. Evolution of phase change enthalpy through thermal cycling.

Sn/SnO and Sn/SnO_x/SiO_2 behaviour through thermal cycling have been analyzed measuring the phase change enthalpies before and after submitting the particles to 100 cycles from 70 to 280ºC. The initial enthalpy is lower for the silica coated particles ($\Delta H_{Sn/SnO}$ = 51.51 J/g, $\Delta H_{Sn/SnO_x/SiO_2}$ = 49.48 J/g), since this property depends on the mass of nanoparticles, and the ratio m_{nuclei}/m_{total} is lower due to the content in silica. However, after 100 thermal cycles the decreases in this enthalpy are of

3.84% for Sn/SnO and of 2.02% for $Sn/SnO_x/SiO_2$, as depicted in Figure 2. This indicates that the ALD coating improves the performance of the PCM cores through thermal cycling.

A summary of the analysis of the thermal properties of the nanofluids based on a thermal oil commonly used as heat transfer fluid in the solar energy industry (Therminol 66), with a 0.5 wt% of nanoparticles is presented in Table 1.

Table 1. Thermal properties of the nanofluids compared to the base oil at 120ºC.

Sample	Viscosity (mPa·s)	Increase (%)	Thermal conductivity (W/(m·K))	Increase (%)
Therminol 66	2.19	---	0.124	---
Therminol 66+Sn/SnO 0.5 wt%	2.22	+1.37	0.127	+2.42
Therminol 66+$Sn/SnO_x/SiO_2$ 0.5 wt%	2.15	-1.83	0.126	+1.61

It is observed that the variations in the viscosity of the fluid are very small and fall within the measurement uncertainty, as is expected for low concentration nanofluids. On the other hand, small enhancements in thermal conductivity can be noticed for both nanofluids with respect to the base oil.

Summary/Conclusions: A nanometric coating of amorphous SiO_2 has been synthesized in Sn/SnO nanoparticles in order to make them more suitable for their use as PCMs in nanofluids and improve their resistance to oxidation and thermal cycling.

The SiO_2 coating enhances the nanoparticle resistance to thermal cycling, reducing the losses of phase change enthalpy used to store energy, and thus enhancing its lifetime.

The coating does not affect negatively the viscosity of the nanofluids based on thermal oil at 0.5 wt% concentration, and presents a slight increase of 1.61% in thermal conductivity with respect to the base fluid.

Acknowledgements: The authors want to thank the financial support from Ministerio de Economía y Competitividad (MINECO) (project ENE2016-77694-R) and Universitat Jaume I (project UJI-B2016-47). Nuria Navarrete thanks Universitat Jaume I for a pre-doctoral fellowship (Ref. PREDOC/2016/28) and a research mobility grant (Ref. E-2018-10) that made possible the research carried in this work.

References:

1. N. Navarrete, A. Gimeno-Furio, R. Mondragon, L. Hernandez, L. Cabedo, E. Cordoncillo and J.E. Julia, Nanofluid based on self-nanoencapsulated metal/metal

alloys phase change materials with tuneable crystallisation temperature, *Scientific Reports* (2017) 1-10.

2. R. Taylor, S. Coulombe, T. Otanicar, P. Phelan, A. Gunawan, W. Lv, G. Rosengarten, R. Prasher and H. Tyagi, Small particles, big impacts: A review of the diverse applications of nanofluids, *Journal of Applied Physics* 113 (2013).
3. S.M. George, Atomic Layer Deposition: An Overview, *Chemical Rev* (2010), 110-111.
4. H. Van Bui, F. Grillo and J.R. Van Ommen, Atomic and molecular layer deposition: off the beaten track. *Chemical Communications* 53 (2017) 45-71.

1st International Conference on Nanofluids (ICNf2019)
2nd European Symposium on Nanofluids (ESNf2019)
26-28 June 2019, Castelló, Spain

Dynamic Viscosity and Surface Tension Characterization of Paraffin-in-Water Nanoemulsions

D. Cabaleiro[1,2*], S. Hamze[1], F. Agresti[3], P. Estellé[1*], S. Barison[3], L. Fedele[2], S. Bobbo[2]

[1] Université Rennes 1, LGCGM, EA3913, F-35704, Rennes, France
[2] Consiglio Nazionale delle Ricerche, ITC, Padova, Italy
[3] Consiglio Nazionale delle Ricerche, ICMATE, Padova, Italy

[*]Corresponding author: dacabaleiro@uvigo.es, patrice.estelle@univ-rennes1.fr

Keywords: Paraffin, PCM nanoemulsions, Dynamic Viscosity and Surface Tension.

Abstract: This work studies the dynamic viscosity and surface tension of phase change material nanoemulsions (PCMEs) at dispersed phase concentrations of 2, 4 and 10 wt.%. Paraffin-in-water emulsions were produced by a solvent-assisted route, starting from RT21HC commercial paraffin with a nominal melting temperature of ~20-21ºC. In the case of the 4% mass concentration, a nanoemulsion containing 3.6% in RT21HC and 0.4% in a paraffin wax with a higher melting temperature (nucleating agent) was also analysed. Dynamic viscosity strongly increases with rising concentration of dispersed phase, enhancements in this property reach 150% for the sample with 10 wt.% loading at 5ºC. Nanoemulsions exhibit surface tensions considerably lower than those of water. However, PCME values are slightly higher than surface tensions measured for the corresponding water-SDS mixtures used to produce the nanoemulsions.

Background: Phase change material nanoemulsions are a new type of nanostructured materials formulated by directly dispersing small droplets of a phase change material (PCM) into a carried fluid (CF) with the assistance of appropriate surfactants. Since PCMEs can combine the high thermal energy storage density of the PCM and the good heat transportation of the carrier fluid, these novel heat transfer fluids are potentially attractive for multiple applications such as air-conditioning or solar thermal systems. In this sense, Huang et al. [1] foresaw the possible utilization of CryoSol^{plus}20-in-water emulsions to increase the thermal storage mass of building components using capillary tube systems for cooling walls and ceilings.

The evaluation of PCME heat storage capacity relies on an accurate characterization of the temperatures at which PCM nanodroplets undergo the phase change as well as the amounts of heat absorbed or released in those thermal events. However, the study of other thermophysical properties is also necessary to estimate the flow behaviour and

heat transfer performance of these materials. Thus, reliable viscosity data are essential for an appropriate selection and operation of equipment involved in formulation, storage or pumping of nanoemulsions. Wetting behaviour may also play a major role in the case of microfluidics systems such as the capillary tubes above mentioned. Thus, knowledge of surface tension is also required to understand the balance between viscous and surface tension competing forces that usually control the actuation in micro-flows [2].

This work intends to complete the physical characterization of RT21HC-in-water emulsions. Previous analyses on phase change characteristics of these PCMEs [3] show melting transitions at ~18-20ºC and freezing temperatures at ~9-12ºC. Here, dynamic viscosity and surface tension are experimentally investigated in the range from 5 to 30ºC to analyse whether these two properties are affected by the solid/liquid state of the PCM droplets.

Materials and Sample Design: Deionized water (18.2 MΩ·cm at 25ºC) used as carried fluid was produced by a Millipore system (Billerica MA, USA). Technical grade RT21HC paraffin and RT55 wax (Rubitherm Technologies GmbH, Germany) were used as phase change material and nucleating agent, respectively. Sodium dodecyl sulfate, SDS, (98%, Sigma Aldrich) was utilized as emulsifier. PCM-in-water emulsions were produced following a solvent-assisted route proposed in Agresti et al. [4]. Studied samples contain 2, 4 and 10 wt.% of RT21HC and 0.25, 0.5 and 1.25 wt.% of SDS, respectively. An additional nanoemulsion formulated using 3.6% of RT21HC and 0.4% of RT55 (nucleating agent) as dispersed phase and 0.5% of SDS was also studied for comparison.

The hydrodynamic droplet size of PCM nanoemulsions (stored in static conditions) was monitored by Dynamic Light Scattering measurements (Zetasizer Nano-ZS90, Malvern Instruments Ltd., UK) to detect possible destabilization issues. Over the analysed period (at least a month) PCM droplets remain nanometric, with average values ~90-110 nm for PCMEs formulated at 2 and 4 wt.% concentrations and ~125-160 nm for 10 wt.% loading.

Experimental Methods: Dynamic viscosities (η) were obtained at 5 and 30ºC on a Malver Kinexus Pro rheometer (Malvern Instruments Ltd., UK) working with a cone-plate geometry (60 mm in diameter, 1º in cone angle and a gap of 0.03 mm). Temperature was controlled to within ±0.1ºC and declared uncertainty of viscosity measurements is better than 4% [5]. Surface tensions at the sample-air surface (SFT) were measured in the temperature range from 5 to 30ºC by means of a drop shape analyser DSA-30 from Krüss GmbH (Germany). A TC40 environmental chamber (also from Krüss GmbH) was used to control the

temperature with a precision of ±0.2ºC. Experimental uncertainty in surface tension obtained with this device was reported to be less than 1% [6].

Discussion and Results: Viscosity-shear rate flow curves obtained at 5ºC for water and the different nanoemulsions are presented in Figure 1.

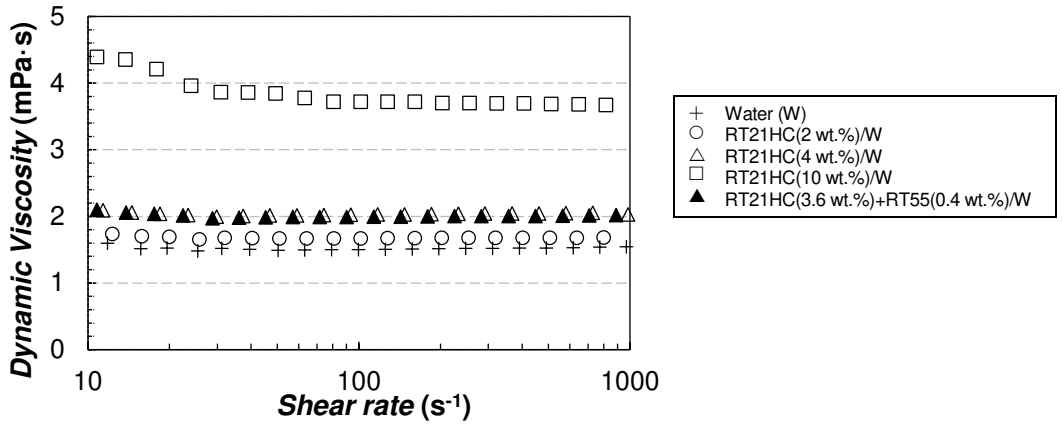

Figure 1. Flow curves obtained at 5ºC for the different samples.

As it can be observed, nanoemulsions containing 2 and 4% paraffin contents are mainly Newtonian within the studied shear rate range, while a slight pseudoplastic behaviour is observed at low shear rates for the highest concentration. A comparison of obtained viscosities at shear rates around ~100 s^{-1} shows strong increases in this property, with rises to 150% in the case of RT21HC(10 wt.%)/Water at 5ºC. Increases in dynamic viscosity are larger at 5ºC (PCM droplets are solid) than at 30ºC (liquid droplets). These differences are more remarkable at the highest mass fraction of paraffin, 10 wt.%, for which increases differ 29%.

Surface tension experimentally measured for water, a representative water+SDS mixture, bulk-RT21HC (in liquid phase) and PCM nanoemulsions are plotted in Figure 2. As expected, the addition of SDS considerably reduces the surface tension of water (Figure 2 only shows the water-surfactant mixture with 0.5 wt.% of SDS, results obtained for 0.25-1.25 wt.% concentrations are close in value since critical micelle concentration of SDS aqueous system is ~0.2-0.25 wt.%). Strong reductions in SFT (regarding the water used as base fluid) were also observed in the case of nanoemulsions. However, these last diminutions are lower than the decreases obtained for the water-surfactant mixtures with the same SDS loadings as those used to formulate the PCMEs. This behaviour (more noticeable at low temperatures) may be attributed to a preference of nanodroplets (and surfactant free in the solution) to concentrate in the bulk of the drops (instead at the sample/air surface).

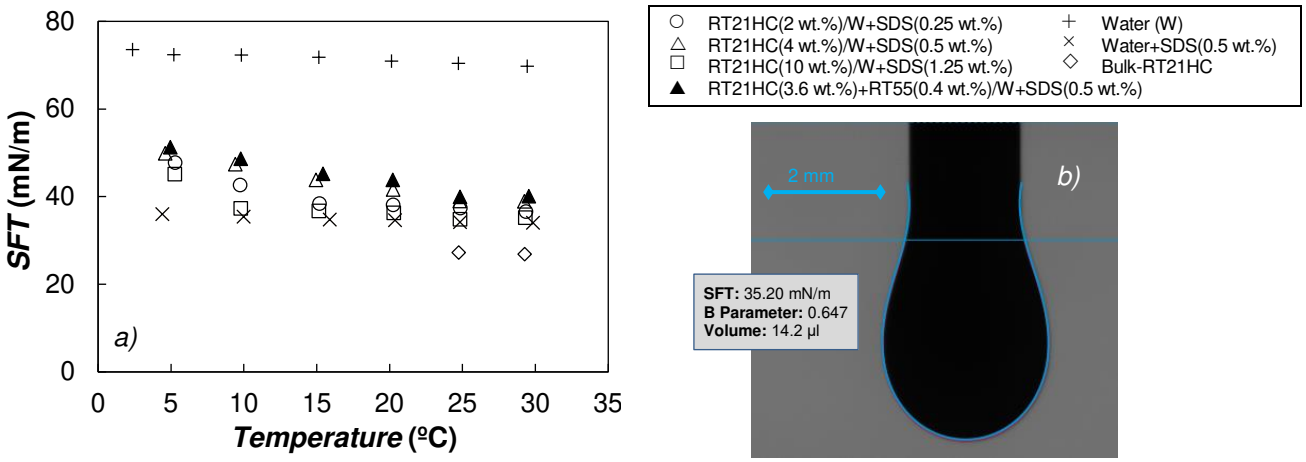

Figure 2. (a) Temperature dependence of surface tension, *SFT*, and (b) pendant drop image for the RT21HC(10 wt.%)/Water nanoemulsion.

Conclusions: Dynamic viscosity strongly rises with PCM concentration up to 150%. A slight shear-thinning behaviour was only observed for the nanoemulsion prepared at the highest concentration, while the rest of the samples are Newtonian in the studied shear rate range. SFT reduces up to 50% with the presence of paraffin droplets. However these diminutions are lower than the decreases found for the corresponding water-SDS mixtures used to produce the nanoemulsions.

Acknowledgements: This work is a contribution to the COST (European Cooperation in Science and Technology) Action CA15119: Overcoming Barriers to Nanofluids Market Uptake (NANOUPTAKE). P. Estellé acknowledges the European Union through the European Regional Development Fund (ERDF), the Ministry of Higher Education and Research, the French region of Brittany and Rennes Métropole for the financial support related to the surface tension device used in this study. D. Cabaleiro is recipient of a postdoctoral fellowship from Xunta de Galicia (Spain).

References:

1. L. Huang, C. Doetsch, C. Pollerberg, Low temperature paraffin phase change emulsions, *International Journal of Refrigeration* 33 (2010) 1583- 1589.
2. P. Estellé, D. Cabaleiro, G. Żyła, L. Lugo, S.M.S. Murshed, Current trends in surface tension and wetting behavior of nanofluids, *Renewable and Sustainable Energy Reviews* 94 (2018) 931-944.
3. D. Cabaleiro, F. Agresti, S. Barison, S. Rossi, S. Bobbo, L. Fedele, Synthesis and characterization of nano-PCM in water for phase-change secondary refrigerants applications, *The 25th IIR International congress of refrigeration-ICR2019*, August 24-30, Montréal, Canada.
4. F. Agresti, L. Fedele, S. Rossi, D. Cabaleiro, S. Bobbo, G. Ischia, S. Barison, Nano-encapsulated PCM emulsions prepared by a solvent-assisted method for solar applications, *Solar Energy Materials and Solar Cells* 194 (2019) 268-275.
5. S. Halelfadl, P. Estellé, B. Aladag, N. Doner, T. Maré, Viscosity of carbon nanotubes water-based nanofluids: influence of concentration and temperature *International Journal Thermal. Science* 71 (2013) 111-117.
6. R. Gómez-Villarejo, T. Aguilar, S. Hamze, P. Estellé, J. Navas, Experimental analysis of water-based nanofluids using boron nitride nanotubes with improved thermal properties, *Journal of Molecular Liquids* 277 (2019) 93-103.

1st International Conference on Nanofluids (ICNf2019)
2nd European Symposium on Nanofluids (ESNf2019)
26-28 June 2019, Castelló, Spain

From MD Simulations to experimental study: Molten salt based nanofluids

A. Svobodova-Sedlackova[1], C. Barreneche[1,2], P. Gamallo[3] and A. Ines Fernandez[1*]

[1] Department of Material Science and Physical Chemistry, Universitat de Barcelona, c/Martí i Franqués 1-11.08028. Barcelona.

[2] Birmingham Centre for Energy Storage & School of Chemical Engineering, University of Birmingham, Birmingham B15 2TT, UK.

[3] Computational and Theoretical Chemistry's Institute, Universitat de Barcelona (IQTC-UB), Chemistry Faculty, Universitat de Barcelona, c/Martí I Franqués 1-11.08028. Barcelona.

[*]Corresponding author: ana_inesfernandez@ub.edu

Keywords: Thermal Energy Storage (TES), nanofluids, Concentrate Solar Power (CSP), Specific Heat Capacity (Cp), Heat Transfer Fluid (HTF), solar salt

Abstract:

Currently, one of the challenges in the Thermal Energy Storage (TES) for a Concentrate Solar Power (CSP) technology is the high-temperature heat storage capacity improvement. In the last years, the so-called nanofluids attracted considerable interest in this field. Highlighted experimental studies reveal an unconventional increment in the heat capacity (*Cp*) in ionic systems when low concentration of nanoparticles are added. In this regard, the effect of doping nanoparticles is under study as well as in particular, the effect of SiO_2 nanoparticles in $NaNO_3$ molten salts specific heat. To study this phenomenon molecular dynamics simulations were carried out and the results corroborated with an experimental study with differential scanning calorimeter. The computational results, shows a formation of a thin layer rich in Na^+ cations around the nanoparticles surface, this layer increases its intensity by increasing the nanoparticle size and temperature. In unison, when increases the nanoparticles concentrations, this layering phenomenon star to disappear. In contrast, computational results and calorimetric data reveals an upper concentration limit around 4 % wt. for different nanoparticles size for the *Cp* increment, obtaining increments up to 30% when 1% of nanoparticles are added, coinciding with the maximum layering effect. This limit being when nanoparticles start to agglomerate, as shows scanning Electron Microscopy. The layering phenomenon is attributed to the *Cp* increment, becoming the most realistic explanation of this phenomenon.

Introduction/Background:

Concentrate Solar Thermal Power plants (CSP) employs Thermal Energy Systems (TES) to store energy, currently as sensible heat TES is one of the main parts of CSP, to improve their efficiency; materials with high thermal properties and high-temperature stability are needed [1,2].

The commonly known as solar salts , eutectic mixture of nitrates compound by 40% wt. sodium nitrate ($NaNO_3$) and 60% wt. potassium nitrate (KNO_3), are currently the most employed storage material and/or heat transfer fluid (HTF) [3]. These molten salts, in spite of their improved thermal properties in comparison with conventional TES/HTF materials such as mineral oils or paraffin, lower cost and best reliability. However, the main disadvantages are a low specific heat capacity, around 2 J/g·K, and the corrosion drawback making difficult the storage [4]

In 1993, Dr. Choi from the University of Illinois introduce the concept of nanofluids. Since then increasingly number of researchers worldwide are interested in this concept. The so-called nanofluids are salts (ionic systems) doped with nanoparticles [5]. The solar salt when is doped with low concentration of nanoparticles improves its specific heat capacity [6-8]. This is due to an unconventional phenomenon without a clear description, lacking theoretical explanation.

This study aims to describe this phenomenon by using molecular dynamics simulations and corroborate the obtained results with experimental measurements with differential scanning calorimetry (DSC), X-ray diffraction (XRD) and scanning electron microscopy (SEM).

Discussion and Results:

Specific heat capacity (*Cp*) calculations at 773 K are performed by Molecular Dynamics simulations. The results under different concentrations and nanoparticles nominal diameter are represented in **Figure 1a**. Both nanoparticle sizes work properly with the same concentration range: ≈ between 0.1 % wt. and 2 % wt., and the biggest *Cp* increment is observed around 1% wt. in both cases. However, nanofluids with more than 2 % wt. of nanoparticles present a *Cp* decrement even below the $NaNO_3$ value.

Figure 1b compares the DSC results and the law of mixture predicted values with the simulation values, as variations (%) respect to pure $NaNO_3$. Extraordinary *Cp* values are observed until 3 % wt. nanoparticles concentration. Afterwards, this trend decrease down

to the mixture law values. Consequently, from 3 % wt. of nanoparticles concentration the *Cp* tends to the pure $NaNO_3$, as this law predicts.

773 K. 1b) Perceptual variation (%) of computational, experimental and theoretical mixture law values, respect pure $NaNO_3$ at 773 K.

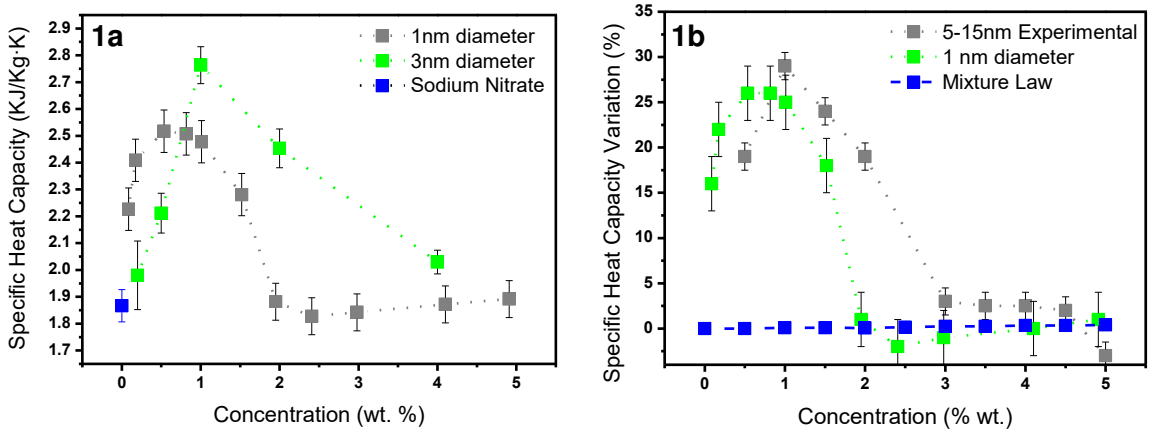

Figure 1. Computationally and experimental results of heat capacity (KJ/Kg·K) 1a) comparative between SiO_2 nanoparticles of 1 and 3 nm of diameter vs. concentrations

Instead, radial pair distributions (RPD) calculations are performed to understand the nanofluids behaviour with the 1 % wt. of nanoparticles concentrations. **Figure 2a-b**, shows a RPD between the external O^{-2} from the nanoparticles surface and the Na^{+} cation of the $NaNO_3$.

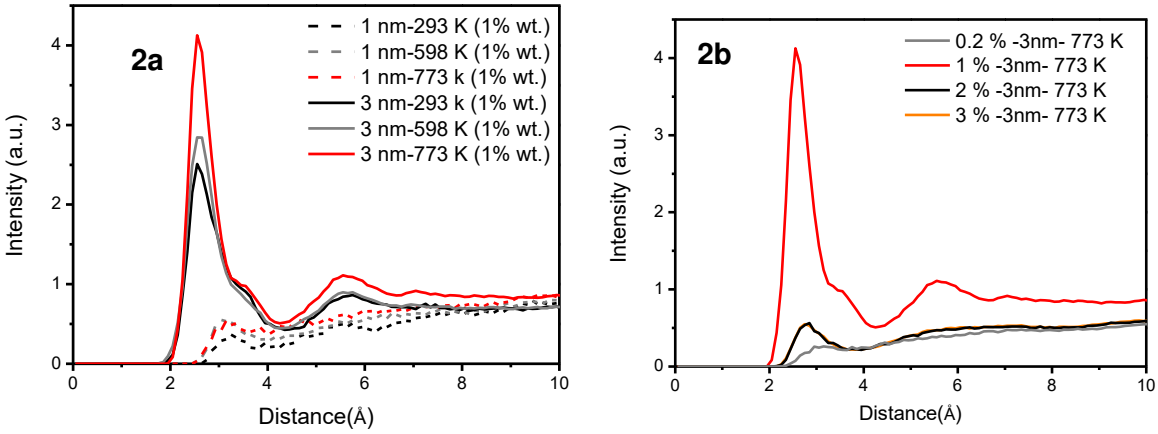

Figure 2. Radial Pair Distribution Function between external O^{-2} from SiO_2 nanoparticles and Na^{+} atoms from $NaNO_3$. 2a) Temperature vs nanoparticle nominal diameter, at 1% wt. of nanoparticles concentration. 2b) Different concentrations at same diameter and temperature.

Figure **2a** shown that when increases the nanoparticle nominal diameter and temperature a dense Na^+ cations layer are formed around the nanoparticles surface. Moreover, with the 3 nm nominal diameter nanoparticles, it can be observe the formation of Na^+ secondary structural ordinations (layers). In addition, this layering effect are increased in liquid state. On the other hand, Figure **2b** depicts the RPD at different concentrations for 3 nm nanoparticles at the same temperature, there can be observed that for lowest and highest concentrations than 1 % wt. the layering effect practically disappears.

Methods and Materials: The Molecular Dynamics (MD) simulations were carried out with Large-scale Atomic/Molecular Massively Parallel Simulator (LAMMPS) code. The trajectory of each particle is obtained by integration of Newton's equations of motion with a 1 fs timestep, during 105 time steps for equilibration, and 10^5 time steps for production. Intermolecular interactions were calculated using a Buckingham potential for dispersion forces and a Coulomb potential for electrostatic interactions

The materials characterized in this study were lab-synthetized. Sodium Nitrate (Sigma Aldrich, 99.995%) and spherical Silica nanoparticles of 5-15 nm of diameter (Sigma Aldrich, 99.5%) were used. Several formulation by combining salt and nanoparticles were obtained in the laboratory. Therefore, samples from [0, 5-10] % (w/w) concentration of nanoparticles were prepared.

Experimental analyses performed were: Cp analysis at 400ºC with DSC using a DSC 822e from Mettler Toledo with a flux of 50 mL/min of N_2, using 10 mg samples within 40-µL aluminium crucible. SEM images were obtained using a ESEM Quanta 200 FEI at 20 kW. Crystalline phases were elucidated by performing X-Ray Powder Diffraction with Panalytical PRO MRD diffractometer in transmission geometry, with Cu K_α radiation and work power of 5 kV – 40 mA.

Summary/Conclusions:

The obtained computational and experimental results in this study show the existence a range of nanoparticles concentration around between [0.2 - 2 %] wt. for the *Cp* improvement of the $NaNO_3$ based nanofluids. For instance, the maximum *Cp* increment, up to 30 %, is observed around 0.5 – 1 % wt. Moreover, analysis of the radial pair distribution, ρ(r), shows the formation of a layer on the nanoparticles surface. This fact is more promising because it may explain the great discrepancy denoted in previous studies between the computational and experimental results or between different studies under the

same experimental conditions. In conclusion, at the light of the obtained results the layering phenomenon around the nanoparticles surface is the main mechanism to explain the unconventional *Cp*.

Acknowledgments.

The work is partially funded by the Spanish government (ENE2015-64117-C5-2-R (MINECO/FEDER)). The authors would like to thank the Catalan Government for the quality accreditation given to their research group DIOPMA (2017 SGR1543). DIOPMA is certified agents TECNIO in the category of technology developers from the Government of Catalonia. The research leading to these results has received funding from the European Union's Horizon 2020 research and innovation programme under the Marie Skłodowska-Curie grant agreement No 712949 (TECNIOspring PLUS) and from the Agency for Business Competitiveness of the Government of Catalonia.

References:

1. S. S. Mostafavi, R. A. Taylor, K. Nithyanandam and Shafiei, A. Annual comparative performance and cost analysis of high temperature , sensible thermal energy storage systems integrated with a concentrated solar power plant. *Sol. Energy* 153, 153–172 (2017).
2. Y. Hou, R. Vidu and P.Stroeve, Solar Energy Storage Methods. *Ind. Eng. Chem. Res.* 50, 8954–8964 (2011).
3. R. Serrano-López, J. Fradera and S. Cuesta-López, Molten salts database for energy applications. *Chem. Eng. Process.* (2013). doi:10.1016/j.cep.2013.07.008
4. S. F. Ahmed, M. Khalid, W. Rashmi, A. Chan and K. Shahbaz, Recent progress in solar thermal energy storage using nanomaterials. *Renew. Sustain. Energy Rev.* 67, 450–460 (2017).
5. S. A. Angayarkanni, and J. Philip, Review on thermal properties of nanofluids: Recent developments. *Adv. Colloid Interface Sci.* 225, 146–176 (2015).
6. K. Khanafer, F.Tavakkoli, K.Vafai and A. AlAmiri, A critical investigation of the anomalous behavior of molten salt-based nanofluids. *Int. Commun. Heat Mass Transf.* 69, 51–58 (2015).
7. H.Tiznobaik and D. Shin, Enhanced specific heat capacity of high-temperature molten salt-based nanofluids. *Int. J. Heat Mass Transf.* 57, 542–548 (2013).
8. G. Qiao, M. Lasfargues, A. Alexiadis and Y. Ding, Simulation and experimental study of the specific heat capacity of molten salt based nanofluids. *Appl. Therm. Eng.* 111, 1517–1522 (2016).

1st International Conference on Nanofluids (ICNf2019)
2nd European Symposium on Nanofluids (ESNf2019)
26-28 June 2019, Castelló, Spain

Thermophysical characterization of novel nano-enhanced phase change materials (NEPCM) based on fatty acid and SiO_2 nanoparticles

Marc Martín, Camila Barreneche*, A. Inés Fernández

Department of Materials Science and Physical Chemistry, Universitat de Barcelona, Martí i Franqués 1–11, 08007 Barcelona, Spain

*Corresponding author: c.barreneche@ub.edu

Keywords: thermal energy storage (TES), latent heat, phase change material (PCM), fatty acids, nano-enhanced phase change materials (NEPCM)

Abstract

In the present study two fatty acids within the building application temperature range were nano-enhanced with low contents (0.5 wt.%, 1.0 wt.% and 1.5 wt.%) of silicon dioxide nanoparticles (n-SiO_2). The nano-enhanced phase change materials (NEPCM) obtained showed high thermal conductivity, melting enthalpy and specific heat capacity. The phase change temperature of these materials remained unaltered. Moreover, silica nanoparticles clustering, a plausible reason for thermal conductivity increase was observed by means of scanning electron microscopy (SEM).

Background

The use of proper thermal energy storage (TES) systems in the building sector is an opportunity to decrease both commercial and residential energy consumptions [1]. Particularly latent heat thermal energy storage (LHTES) systems are able to absorb a large amount of heat in a sharply defined temperature range. Thus, temperature of phase transition, in both melting (T_m) and solidification (T_s) processes are defined. In the same vein, enthalpy of phase change transition is considered the latent heat that can be stored, melting enthalpy (ΔH_m) and solidification enthalpy (ΔH_s) [2].

Phase change material (PCM) properties require improvement to be used in the building sector. Most fatty acids present a proper melting temperature range to be applied as PCM in building applications. Furthermore, fatty acids present impressive properties to be used as PCM, such as non-toxic, high heat storage capacity, non-flammable, congruent melting, little or non-subcooling, low vapour pressure, non-corrosive and thermally stable [3]. However, fatty acids present poor thermal conductivity, which slows down heat exchange.

Nanomaterials have shown remarkable results in many areas and thermal energy storage is no exception. For instance, Zhang et al. [4] prepared palmitic-stearic acid (PA-SA) eutectic mixtures and enhanced its thermal conductivity by 20-30% with carbon nanotubes (CNTs) addition. Thus, in the present paper a new type of nano-enhanced phase change material (NEPCM) was developed by SiO_2 nanoparticles (n-SiO_2) addition (0.5 wt.%, 1.0 wt.% and 1.5 wt.%) to two fatty acids: capric acid and eutectic mixture of capric acid (CA) and myristic acid (MA) (73.5-26.5 wt.% CA-MA). An experimental campaign was carried out to characterize thermophysical properties, i.e. specific heat capacity (C_p), thermal conductivity (k), melting temperature (T_m) and enthalpy (ΔH_m). In addition, scanning electron microscopy (SEM) was used to obtained NEPCM images.

Discussion and Results

Thermophysical properties measured include melting enthalpy, melting temperature, thermal conductivity and specific heat capacity. Table 1 summarizes results obtained for both PCM (i.e. CA and CA-MA euctectic mixture) and the corresponding PCM enhanced via n-SiO_2. Melting enthalpy measurements close to 150 J/g agreed with the values reported in the literature, [5] and [6]. As it can be seen, n-SiO_2 addition increased melting enthalpy of both fatty acids, ranging this improvement from 6.8% to 10.7%. In addition, nano-enhanced CA-MA melting enthalpy was increased by a 6.8% regardless of the nanoparticles content, whereas melting enthalpy of CA increases slightly, from 8.0% to 10.7% with nanoparticles content. Melting temperatures of both fatty acids, CA (31.5 ºC) and CA-MA (21.9 ºC), also agreed with those reported in the literature, [5] and [6]. In this case, nanoparticles slightly decreased melting temperature of both fatty acids by 1%.

The thermal conductivity of the NEPCM increases as the amount of n-SiO_2 increases. CA-MA presented an outstanding thermal conductivity increase (142%) due to the addition of 1.5 wt.% n-SiO_2. However, CA presented the highest thermal conductivity before (0.30 W/m·k) and after the addition of nanoparticles (0.5285 W/m·°C). This could be explained taking into consideration some phenomena such as Brownian motion, phonon interaction, clustering of nanoparticles and surface morphology effects, [7] and [8].

As it can be seen in Table 1, great improvements were also obtained on the sensible heat storage capabilities of NEPCM. Results show that the addition of nanoparticles increased specific heat capacity around 20% in the liquid state (40 ºC) in both fatty acids. Furthermore, adding 1.0 wt.% of n-SiO_2 produced the highest enhancement as other studies demonstrated [9-11]. The highest C_p was measured in the CA with 1.0 wt.% n-

SiO_2 (3.38 J/g·ºC). Thus, nanoparticles added to these fatty acids allow the heat storage to be more effective per unit volume in both latent and sensible storage.

Table 1. Thermophysical properties (ΔH_m, T_m, C_p, and k) in both fatty acids (capric acid and eutectic CA-MA mixture) along with the corresponding NEPCM.

Sample	ΔH_m (J/g)	T_m (ºC)	k in liquid at 45 ºC (W/m·°C)	C_p (J/g·ºC)
Capric acid	150	31.5	0.30	2.77
Capric acid + 0.5 wt.% n-SiO_2	162	31.2	0.39	3.35
Capric acid + 1.0 wt.% n-SiO_2	165	31.2	0.49	3.38
Capric acid + 1.5 wt.%) n-SiO_2	166	31.2	0.53	3.29
Eutectic CA-MA	148	21.9	0.17	2.48
Eutectic CA-MA + 0.5 wt.% n-SiO_2	158	22.0	0.25	2.99
Eutectic CA-MA + 1.0 wt.%) n-SiO_2	158	22.1	0.30	3.07
Eutectic CA-MA + 1.5 wt.%) n-SiO_2	158	22.1	0.40	3.00

According to supplier's technical data sheet, an average diameter of 5 nm to 15 nm is expected for SiO_2 nanoparticles. However, SEM images (Figure 1) show nSiO_2 forming clusters of 100 nm to 300 nm. Experimental evidences from other studies [7] strongly suggest that clustering phenomenon was the responsible for thermal conductivity enhancements demonstrated in the present study.

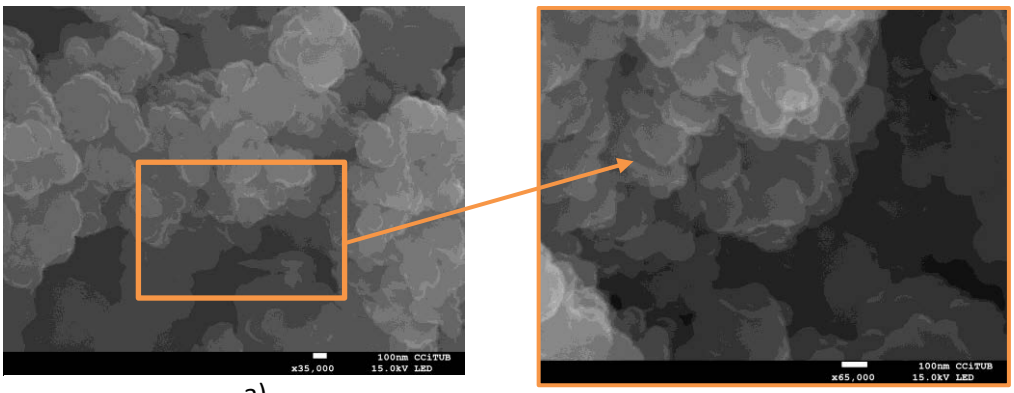

a) b)

Figure 1. SEM images of n-SiO_2 at a) x 35000 and b) x65000.

Conclusions

NEPCM were obtained with enhanced thermophysical properties by the addition of n-SiO_2. In both fatty acids, sensible (C_p) and latent heat (ΔH_m) storage capacities were increased in different proportions, around 20% and 10%, respectively. The results clearly showed an impressive thermal conductivity increase, that demonstrates an almost linear

relationship between thermal conductivity and n-SiO_2 content. Moreover, SEM images provided a reasonable explanation, clustering phenomenon, for these thermal thermophysical results.

Acknowledgments.

The work is partially funded by the Spanish government (ENE2015-64117-C5-2-R (MINECO/FEDER)). The authors would like to thank the Catalan Government for the quality accreditation given to their research group DIOPMA (2017 SGR1543). DIOPMA is certified agents TECNIO in the category of technology developers from the Government of Catalonia. The research leading to these results has received funding from the European Union's Horizon 2020 research and innovation programme under the Marie Skłodowska-Curie grant agreement No 712949 (TECNIOspring PLUS) and from the Agency for Business Competitiveness of the Government of Catalonia.

References:

1. Kalnæs and B. P. Jelle, Phase change materials and products for building applications: A state-of-the-art review and future research opportunities*, Energy and Buildings* 94 (2015) 150-176.
2. H. Mehling L. F. Cabeza*, Heat and cold storage with PCM,* Chapter 2, Springer, Berlin, Heidelberg, 2008.
3. Y. Yuan, N. Zhang, W. Tao, X. Cao, and Y. He, Fatty acids as phase change materials: A review, Renewable and Sustainable *Energy Reviews 29 (2014) 482–498.*
4. N. Zhang, Y. Yuan, Y. Yuan, X. Cao, and X. Yang, Effect of carbon nanotubes on the thermal behaviour of palmitic-stearic acid eutectic mixtures as phase change materials for energy storage, *Solar Energy 110 (2014) 64–70.*
5. A. Sharma, V. V. Tyagi, C. R. Chen and D. Buddhi*,* Review on thermal energy storage with phase change materials and applications, *Renewable and Sustainable Energy Reviews* 13 (2009) 318–345.
6. Z. Zhang, Y. Yuan, N. Zhang, and X. Cao*,* Thermophysical Properties of Some Fatty Acids/Surfactants as Phase Change Slurries for Thermal Energy Storage, *Journal of Chemical & Engineering Data* 60 (2015) 2495–2501.
7. J. W. Gao, R. T. Zheng, H. Ohtani, D. S. Zhu, and G. Chen*,* Experimental investigation of heat conduction mechanisms in nanofluids. Clue on clustering, *Nano Letters 9 (2009) 4128–4132.*

8. *D. Kim, Y.* Kwon, Y. Cho, C. Li, S. Cheong, Y. Hwang, J. Lee, D. Hong, S. Moon, Convective heat transfer characteristics of nanofluids under laminar and turbulent flow conditions, *Current Applied Physics* 9 (2009) 119-123.
9. R. Hentschke*,* On the specific heat capacity enhancement in nanofluids, Nanoscale*, Research Letters* 11 (2016).
10. M.-C. Lu and C.-H. *Huang,* Specific heat capacity of molten salt-based alumina nanofluid*, Nanoscale Research Letters 8 (2013) 292.*
11. H. Zhu, C. Zhang, S. Liu, Y. Tang, and Y. Yin*,* Effects of nanoparticle clustering and alignment on thermal conductivities of Fe_3O_4 aqueous nanofluids*, Applied Physics Letters* 89 (2006).

1st International Conference on Nanofluids (ICNf2019)
2nd European Symposium on Nanofluids (ESNf2019)
26-28 June 2019, Castelló, Spain

Silver dispersions in poly(ethylene glycol) as novel NePCMs for thermal energy storage

M.A. Marcos[1], D. Cabaleiro[1,2*], L. Fedele[2], S. Bobbo[2], L. Lugo[1]

[1] Departamento de Física Aplicada, Universidade de Vigo, 36310, Vigo, Spain

[2] Istituto per le Tecnologie della Costruzione, Consiglio Nazionale delle Ricerche, 35127, Padova, Italy

*Corresponding author: dacabaleiro@uvigo.es

Keywords: Silver nanoparticles, PEG400, NePCM, heat storage, thermal conductivity.

Abstract: The storage of thermal energy (TES), for its use in periods when demand exceeds supply, is one of the current scientific challenges. In addition to correct possible mismatches between production and consumption, TES approaches allow improving the performance of energy systems or equipment, which may reduce the consumption and undesirable effects of fossil fuels. In this sense the use of phase change materials (PCMs) has emerged as an interesting alternative. However, the poor thermal properties and/or large sub-cooling of most PMCs still prevent the practical implementation of these materials. The dispersion of nano-additives with high thermal conductivities, usually known as nano-enhanced phase change materials (NePCMs), has been proposed as a promising solution to face these limitations. The main objective of this study is to evaluate the stability and determine the thermophysical profile of poly(ethylene glycol)-based dispersions of silver nanoparticles. In particular, we would focus on the analysis of the effect that the addition of small concentrations of silver nanoparticles, up to 1.14% in mass, has on the thermal conductivity of designed materials.

Background: PCMs are classified into different groups according to the nature of the material (paraffin, fatty acids, salt hydrates, etc.). Poly(ethylene glycol)s, PEGs, exhibit large latent heat capacities at melting temperatures which can be adjusted through the molecular mass of the polymer and are potentially attractive for multiple thermal applications, including refrigeration or building facilities [1]. On the other hand, nanotechnology is establishing itself as an effective tool to design materials with improved thermal performance. For the particular case of PCMs, different authors have shown that nanoparticle addition can improve thermal conductivity and reduce the sub-cooling phenomenon. A brief review of some experimental work recently done in this field is presented below. Marcos et al. [2] formulated NePCMs as dispersions of

functionalized graphene nanoplatelets in a poly(ethylene glycol) with a mass-average molecular mass of 427 g·mol^{-1} and investigated the influence of graphene loading on solid-liquid phase change characteristics, thermal conductivity or dynamic viscosity of resulting dispersions. A comparison between the dispersion prepared at the nanoparticle concentration of 0.5 wt.% and pure PEG400 shows that, in the NePCM, thermal conductivity enhances up to 23% and the temperature interval in which melting transition occurs (according to DSC thermograms) reduces by 2.5 K. Colla et al. [3] used Al_2O_3 nanoparticles to enhance the thermal properties of two commercial paraffin waxes, RT45 and RT55 from Rubitherm®. According to experimental and numerical results, the addition of Al_2O_3 nanoparticles leads to a delay in the melting process with respect to the pure PCMs.

Metals such as silver (with thermal conductivities several orders of magnitude larger than those of most conventional thermal fluids or phase change materials) are presented as promising nanoadditives to enhance thermal properties. In addition, as particle size of additive decreases, the surface to volume ratio increases and consequently the heat transfer capacity of the resulting dispersion also improves [4]. The present study aims to experimentally analyze the influence that the addition of silver nanoparticles has on the thermal conductivity of stable NePCMs based on a poly(ethylene glycol).

Discussion and Results: A poly(ethylene glycol) with a nominal molecular mass of 400 g·mol^{-1} and analytical grade (Merk, Germany) was used as base PCM. Molecular mass and purity of pure polymer were determined by electrospray ionization mass spectrometry (APEZQe FT-ICR MS, Bruker Daltonics USA) and a mass average molecular mass of 532 g·mol^{-1} was obtained. Dry silver nanoparticles were investigated on a Transmission Electron Microscopy (TEM, JEOL JEM-1011, Japan). As can be observed in Figure 1a, nanoparticles show an average diameter ~20 nm. The hydrodynamic size of dispersed particles was measured at 298 K for the 0.01 wt.% nanofluid by means of a Malvern Zetasizer Nano ZS (Malvern Instruments, UK) based on Dynamic Light Scattering (DLS) technique. The average hydrodynamic diameter obtained by DLS is close to the sizes observed by using electronic microscopy.

In order to detect possible destabilization phenomena such as nanoparticle agglomeration, size measurements based on DLS were repeated for four weeks. Two different samples were studied following a procedure similar to that presented in Fedele et al. [5]. Two different cuvettes were filled with about 1 ml of sample. The first container was manually shaken just before performing the measurements while the other was kept in static

conditions for the whole study period. Figure 1b shows the temporal evolution of DLS measurements for both samples.

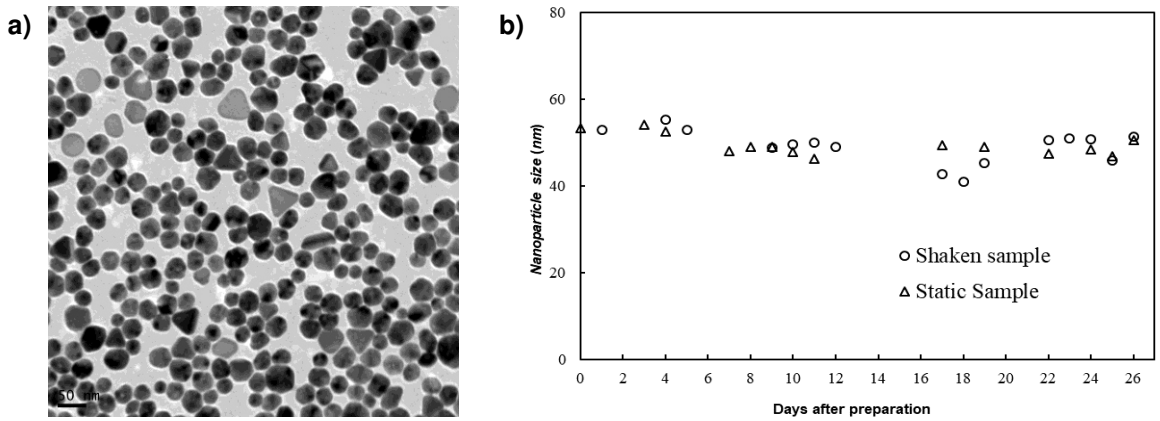

Figure 1: (a) TEM image of dry silver nanoparticles and (b) temporal evolution of average hydrodynamic size for the Ag/PEG400 dispersion at 0.01 wt.% in static and shaken conditions.

As Figure 1b shows, samples exhibit good temporal stability since particles remain dispersed without agglomeration or sedimentation, neither for the static sample nor for the shaken one.

Thermal conductivity was measured in the temperature range from 283 to 333 K using a Hot Disk Thermal Constants Analyzer® (Hot Disk AB, Sweden). Figure 2 shows the experimental results obtained for the base fluid and Ag/PEG400 nanofluids prepared at nanoparticle concentrations of 0.10, 0.50 and 1.14 wt.%.

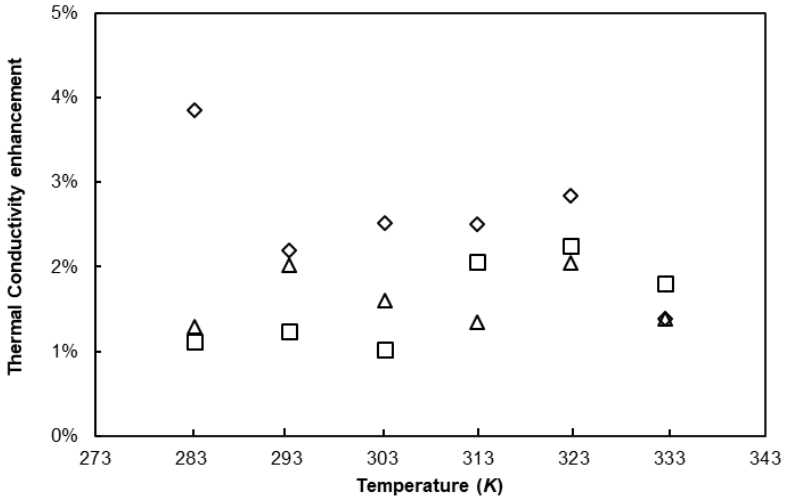

Figure 2. Thermal conductivity enhancement at different temperatures for Ag/PEG400 nanofluids at 0.10 wt.% (△), 0.50 wt.% (□) and 1.14 wt.% (◇) nanoparticle concentrations.

As can be observed in the previous figure, PCM thermal conductivity increases with the addition of silver nanoparticles. In this case, a maximum enhancement of 3.9% was measured at 283 K for 1.14 wt.% sample.

Conclusions: Silver nanoparticles dispersed in PCM determine an enhancement in the thermal conductivity that varies with the concentration. The hydrodynamic diameter of the nanoparticles in the dispersion remains constant over time indicating that no significant agglomeration occurs. This work will be completed with the study of the effect that the addition of silver nanoparticles has on sub-cooling phenomenon as well as volumetric and rheological behavior of the samples.

Acknowledgements: This work was supported by the "Ministerio de Economía y Competitividad" (Spain) and FEDER program through ENE2017-86425-C2-1-R project. Authors also acknowledge the financial support by Xunta de Galicia, GRC ED431C 2016-034. M.A.M. acknowledges EU COST for the STMS grants ref. COST-STSM-CA15119-41564 and COST-STSM-CA15119-42472. D.C. was recipient of a postdoctoral fellowship from Xunta de Galicia.

References:

1. T. Qian, J. Li, H. Ma, J. Yang, Adjustable thermal property of polyethylene glycol/diatomite shape-stabilized composite phase change material, *Polymer Composites*, 37 (2016) 854-860.
2. M.A. Marcos, D., Cabaleiro, M.J. Guimarey, M.J. Comuñas, L. Fedele, J. Fernández, L. Lugo, PEG 400-Based Phase Change Materials Nano-Enhanced with Functionalized Graphene Nanoplatelets, *Nanomaterials*, 8 (2018) 16.
3. L. Colla, D. Ercole, L. Fedele, S. Mancin, O. Manca, S. Bobbo. Nano-Phase Change Materials for Electronics Cooling Applications, *Journal of Heat Transfer*, 139 (2017) 052406.
4. V. Halté, J.Y. Bigot, B. Palpant, M. Broyer, B. Prével, A. Pérez, Size dependence of the energy relaxation in silver nanoparticles embedded in dielectric matrices, *Applied Physics Letters*, 75 (1999) 3799-3801.
5. L. Fedele., L. Colla, S. Bobbo,, S. Barison,, F. Agresti, Experimental stability analysis of different water-based nanofluids, *Nanoscale research letters* 6(1) (2011) 300.

SESSION 4

Boiling, Phase Changed Based Heat Transfer, Surface Coating, Heat Pipes

S4

1st International Conference on Nanofluids (ICNf2019)
2nd European Symposium on Nanofluids (ESNf2019)
26-28 June 2019, Castelló, Spain

How to detect geysering of nanofluid in a thermosyphon?

A. Kujawska[1*], B. Zajaczkowski[1] and M.H. Buschmann[2]

[1]Wrocław University of Science and Technology, Faculty of Mechanical and Power Engineering, St. Wyspianskiego 27, 50-370 Wrocław, Poland

[2]Institut für Luft- und Kältetechnik gGmbH, Bertolt-Brecht-Allee 20, 01309 Dresden, Germany

[*]Corresponding author: Agnieszka.Kujawska@pwr.edu.pl

Keywords: thermosyphon, geyser boiling, nanofluids, surfactant

Abstract: Thermosyphons working with nanofluids and surfactant solutions demonstrate potential to improve the efficiency of heat transfer and to reduce the risk of high mechanical load caused by geyser boiling. This paper presents the summary of the experimental study on this phenomenon and proposes a methodology of data analysis. Two carbon-based nanofluids, surfactant solution and water were tested. Nanohorns nanofluid and sodium dodecyl sulfate solution supressed the geysering for high temperatures of evaporator.

Introduction: Two-phase closed thermosyphons are one of the most effective heat transfer devices known nowadays [1]. Working fluid inside the device undergoes evaporation and condensation in a closed cycle, relying on gravity force to return the condensate to the evaporator. For some operating conditions, bubbles grow to the size of the pipe diameter and confine continuous detachment of relatively small bubbles. It leads to geysering which is schematically presented in Fig 1.

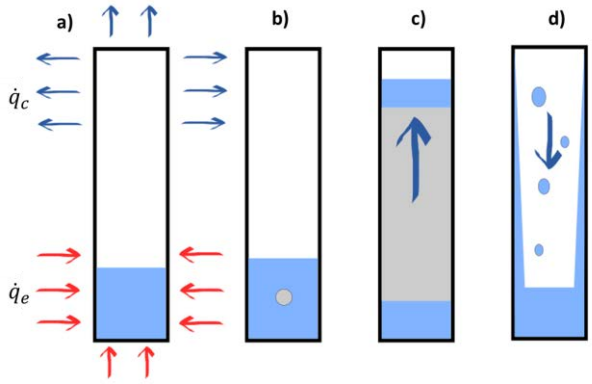

Fig. 1: Scheme of geyser boiling phenomena. Phases a) to d) as follows: superheating of the working fluid in the evaporator (a), bubble development and its quick growth (b), bubble expansion and propulsion of the fluid located above the bubble (c), and downfall return of the displaced liquid (d). Reprinted from [2] under the terms of the CC BY 4.0 (http://creativecommons.org/licenses/by/4.0/).

The process is fast, repetitive, and irregular. Its detection requires continues high-resolution pressure measurements, followed by detailed data analysis, thus it often remains unnoticed or ignored. Clear and precise definition of geyser boiling has not been formulated. There are no guidelines which pressure peaks should be recognized as geyser events. Phenomenon causes discontinuous heat transfer, high mechanical load, and may lead to shock damage to the device. All this reduce the life time of the device. Usability concerns spark the need of understanding of underlying fundamental mechanisms.

In this paper, we present the method of experimental data analysis that allows to detect occurrences of geysering regardless of the working fluid or operation conditions. We propose two parameters that can be used to identify and describe geysering behaviour. The method is tested on four working fluids: nanohorns and graphene oxide nanofluid with water and solution of sodium dodecyl sulfate which was used to stabilize both nanofluids.

Test rig and measurement procedure: Experiments were carried out using a copper two-phase closed thermosyphon. Dimensions and detailed characterisation of the device are described in [2]. For each combination of operating conditions, data was gathered at steady-state conditions for an hour. The evaporator was heated by the circulating water with temperature set on the thermostat between 30 and 85°C. Inlet temperature of cooling water was 25°C for all cases presented in this paper. Internal pressure was determined at three different locations along the condenser and adiabatic sections. All the plots presented here are based on the data from the pressure transmitter *p3* with a measurement range of 0 - 400 Pa and location nearest the boiling pool. Signal was acquired in the adiabatic section, 500 mm from the bottom of the device and 100 mm above the evaporator section. All pressure gauges work at a frequency of 1 kHz and an accuracy of ± 0.25%.

Deionized water, solution of sodium dodecyl sulfate (SDS), nanohorn and graphene oxide (GO) nanofluids were tested as working fluids. Concentrations of particles was 0.1 g/L and 0.01 g/L of SDS for both nanofluids and surfactant solution.

Discussion and Results: Sudden and significant increase in pressure occurs during each geyser event. The unsolved questions are: how big are the pressure peaks and how long lasts the waiting period between successive propulsion of the fluid located above the bubble. The first stipulation – the minimum pressure difference when compared to the average pressure conditions – must ensure that noise fluctuations from the nucleate boiling will not obscure geyser events and that too high threshold value will not allow to detect of

the spike. Return of the previously propelled liquid often causes secondary pressure fluctuations (see: left plot of Fig. 2). The waiting period indicates the minimum time between consecutive spikes, assuming that only actual geyser events are accounted.

Each working fluid shows different behaviour in the studied range of operating conditions, which makes difficult establishing the threshold line and the waiting period that work for all tested fluids. To automatize calculations, we used the probability density and assumed that all geysering values are likely to be outside the range of -2σ to 2σ (standard deviation) from the mean time-averaged pressure at given conditions. The sum of unity and standard deviation specifies the threshold line and it is called *mph* in plot titles (see: Fig. 2) [3]. Each pressure peak exceeding this value with rising trend is considered as potential geyser event.

It is necessary to determine the minimum time between subsequent geysers. Each combination of a working fluid and operating conditions requires different method. Here, the waiting period is selected using a trend analysis, followed by the naked-eye inspection of the investigated pressure distribution. This semi-manual analysis allows to determine whether numerically identified geysers match with geysers chosen visually. Fig. 2 shows the example of the same water pressure pattern (inlet temperature of heating water: 65°C) for two different waiting periods (*mpd*) with marked geysers included for calculations. Analysis of the behaviour of all working fluids was conducted following the above-described procedure.

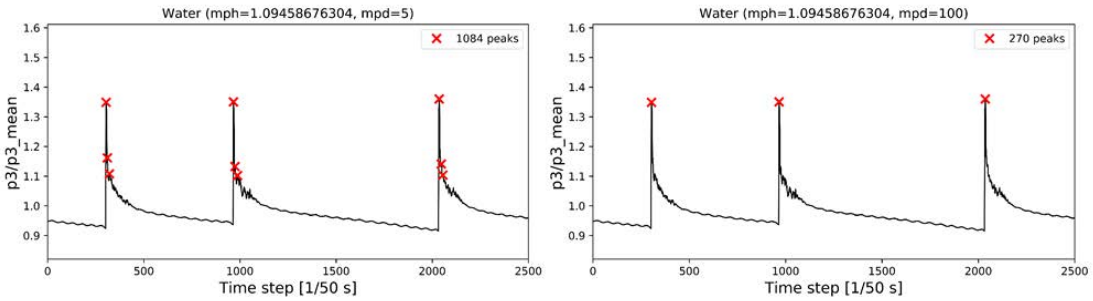

Fig 2. Geyser events included in calculations for different waiting periods (*mpd*) - left: 0.1 sec, right: 2 sec.

Averaged frequency and amplitude for detected geyser events are presented in Figure 3. In most cases, increasing frequency of events results in their reduced amplitude. Rising heat flux decreases the maximum value of pressure at peaks. The standard deviation and the threshold value decrease, and the mean amplitude of geysers is lowered. In time-dependent plots, the lowest amplitude (for example SDS solution or nanohorns at 75-85°C) is seen as random fluctuations coming from nucleate boiling with continuous detachment of

relatively small bubbles. Occasionally, small pressure peaks are detected, but it is not as obvious as in Fig. 2 with decreasing pressure before and after an event. Although GO was stabilised with the same amount of SDS as in nanohorns nanofluid, it did not inhibit geysering. It may be attributed to the attachment of SDS to graphene flakes [2]. The surface chemistry of the particles may play a key role in interacting with stabiliser.

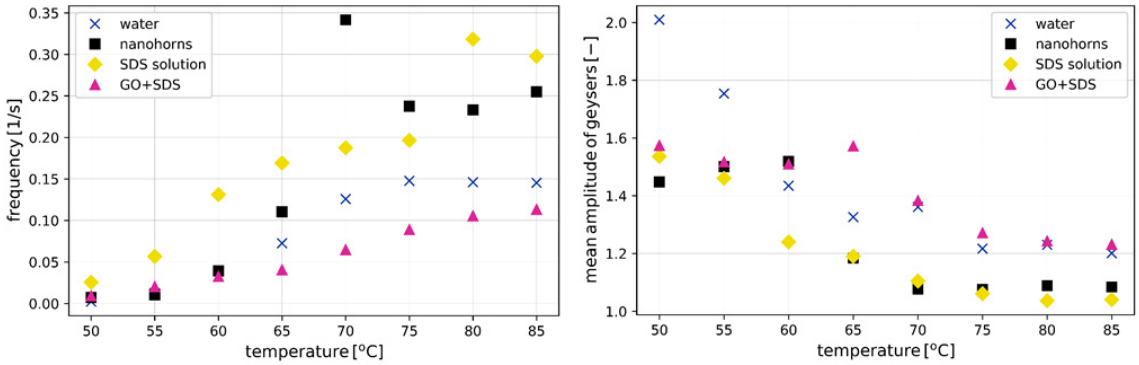

Fig 3. Averaged frequency and amplitude of detected geyser events for various working fluids dependent on inlet temperature of heating water.

Summary: Geyser events can be detected by using statistical parameters (standard deviation) for data reduction. This requires two crucial factors: the threshold value (each pressure peak exceeding this value with a rising trend is considered as a potential geyser event), and the waiting period (noise resulting from the earlier geyser event is not accounted).

This article summarises the impact of working fluid and operating conditions on geyser boiling probability in a thermosyphon. Four fluids have been tested: two carbon-based nanofluids (graphene oxide and nanohorns) stabilized with sodium dodecyl sulfate (SDS), surfactant solution and deionised water. It is shown that nanohorns nanofluid and SDS solution may almost entirely supress the geysering at high heat loads. The nucleate boiling is the leading regime under these operating conditions. The general trend is that decreasing period of events pursues reduced amplitude.

Acknowledgements: This work is a contribution to the Grant MF140079 and the NanoUptake COST Action (European Cooperation in Science and Technology) CA15119: Overcoming Barriers to Nanofluids Market Uptake. A.K. acknowledges the Nanouptake COST Action support by STSM grants no. 35922, 37694, 39240, ITC grant no. 990, and partial contribution to grant 2016/23/N/ST8/00252 from National Science Centre in Poland.

References:

1. A. Wlazlak, B. Zajaczkowski, L.M. Wilde and M.H. Buschmann, Effect of various nanofluids on thermal performance of the thermosyphon, *16th International Heat Transfer Conference (IHTC-16)*, Beijing, China, August 10-15, 2018.
2. A. Wlazlak, B. Zajaczkowski, M. Woluntarski, M.H. Buschmann, Influence of graphene oxide nanofluids and surfactant on thermal behaviour of the thermosyphon, *Journal of Thermal Analysis and Calorimetry*, https://doi.org/10.1007/s10973-018-7632-x, 2018.
3. M. Duarte: *DetectPeaks – iPython Notebook,* Available online: 09.01.2019.

1st International Conference on Nanofluids (ICNf2019)
2nd European Symposium on Nanofluids (ESNf2019)
26-28 June 2019, Castelló, Spain

Time and Spatially Resolved Fluid Dynamics and Heat Transfer Characterisation of Nanofluid Droplets Impacting on Heated Surfaces

A. S. Moita[1] *, P. Pontes[1], F. M. Matos[1], Q. J. Liang[1], , A. P. C. Ribeiro[2] and A. L. N. Moreira[1]

[1]IN+ Instituto Superior Técnico, Universidade de Lisboa. Av. Rovisco Pais, 1049-001 Lisboa, Portugal

[2]Centro de Química Estrutural, Instituto Superior Técnico, Universidade de Lisboa. Av. Rovisco Pais, 1049-001 Lisboa, Portugal

*Corresponding author: anamoita@tecnico.ulisboa.pt

Keywords: Particle-surface interactions, Wettability, Droplet dynamics, Cooling applications.

Abstract: This study addresses the simultaneous characterisation of the fluid dynamics and heat transfer mechanisms occurring during the impact of nanofluid droplets on a solid heated surface, by synchronizing high-speed video with time and space resolved infrared thermography. The effect of using gold and silver nanoparticles is evaluated on the wettability (due to particle-surface interactions) which consequently affects the fluid dynamics in the liquid film and consequently the heat transfer between the droplet and the surface. The results show an effective improvement in the heat transfer between the nanofluid droplets and the heated surface, when compared to the reference fluid (water) but only at low impact velocities (0.8m/s). These results are explained by the local wetting modifications, which affect the droplet spreading dynamics and consequently the instantaneous heat fluxes, as the droplets spread on the surface.

Introduction/Background: Thermal management dealing efficiently with high heat loads is a major challenge in several industrial applications such as in microelectronics, energy conversion and more recently in electric vehicles [1]. Spray cooling is still amongst the cooling techniques with highest potential to dissipate large heat loads, given the high heat transfer coefficients that it can dissipate (of the order of 10^4-10^5 W/m^2K) [2]. In this context, the use of complex fluids, such as nanofluids has been widely explored within the last decade, to further enhance heat transfer mechanisms [3]. However, while many researchers have focused on how adding the nanoparticles affects the bulk

properties of the nanofluids, the actual modification in the fluid flow characteristics and in the local heat transfer processes occurring at spray [4] and, at a more fundamental level, at droplet/wall interactions, are still scarcely reported in the open literature. Particularly, the nature and concentration of the particles affect the wettability at droplet-wall interactions, thus influencing the spreading dynamics and the heat transfer mechanisms. In this context, the present study concerns the detailed characterization of the effect of the nature and concentration of the nanoparticles in the dynamics and heat transfer processes occurring at the impact of nanofluid droplets on solid heated surfaces. Droplet dynamics (e.g. spreading diameter, droplet height, dynamic contact angles, contact line velocity) is evaluated together with the temperature field on the heated surface and with the heat fluxes exchanged during droplet spreading, combining high-speed visualization with time resolved infrared analysis.

Materials and Methods: Nanofluids are mainly composed by water DD, 0.5wt% CTAB - Cetyl trimethylammonium bromide and nanoparticles of gold and of silver in concentrations varying between 1% and 5%. Single droplets of these nanofluids are generated at the tip of a hypodermic needle and fall by action of gravity on a solid surface. Droplets have a fixed initial diameter of D_0 = 3mm and impact on the surface with velocities varying between U_0 = 0.8m/s and U_0 = 2m/s. The impact surface is a smooth stainless steel foil, with 20 μm thick, 20mm wide and 100mm long, which is heated by Joule effect, from ambient temperature up to 120ºC. The heat flux is continuously imposed, being the temperature controlled by a type K thermocouple and by monitoring the data provided in real time by an infrared camera. A high speed camera (Phantom v4.2) mounted to take side views of the impinging droplets, was synchronized with a high-speed thermographic camera (ONCA-MWIR-InSb from Xenics – ONCA 4696 series), which was placed bellow the heated surface. This arrangement allowed combining the analysis of droplet dynamics with the temperature fields on the heated surface and heat fluxes exchanged during droplet contact on the surface. The acquisition frequency and resolution were 2200 fps, 512×512px^2 and 1000 fps and 150×150px^2 for the high-speed video and high-speed thermographic camera, respectively. Regarding the relation μm/pixel used in the present study, the best relation was 100μm/pixel for the IR arrangement and 40μm/pixel for the high-speed arrangement. For each experimental condition considered here, five tests were performed to assure reproducibility of the experiments. High-speed and thermal images were then post-processed using in-house codes. All the calibration and post-processing procedures are detailed in [5]. Wettability was characterized by measuring static and dynamic contact angles using an optical

tensiometer (THETA from Attention). Local migration of the nanoparticles affecting local wettability was observed by a detailed analysis of the droplet-surface contact line region using Laser Scanning Fluorescent Confocal Microscopy, as in [6].

Discussion and Results: Overall the results show that for low impact velocities the cooling of the heated surface is more effectively performed by the nanofluid droplets, when compared to the water droplet. This trend is observed by the lower temperatures that are measured in the temperature profiles obtained along droplet radius, in Figure 1.

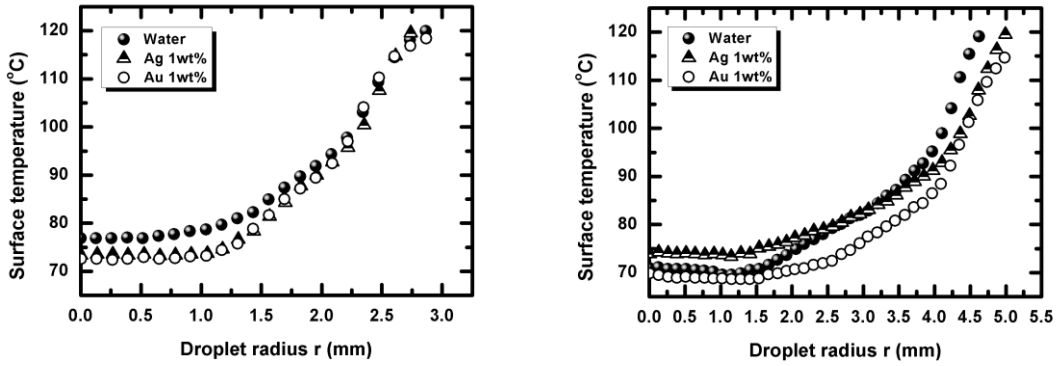

a) **b)**

Figure 1. Temperature profiles taken along the radius of water and nanofluids droplets impacting on a smooth stainless steel surface heated at 120ºC. The profiles were taken at t=8ms after impact. a) U_0=0.8m/s; b) U_0=2m/s.

In the Figure, r=0mm corresponds to the impact point of the droplet, which attains the lowest temperatures during droplet impact [5]. As the droplet spreads on the surface, the spreading liquid film thickness becomes heterogeneous and the temperature tends to raise, as one approaches the edges of the film (at larger radius values). The profiles were taken for numerous time steps after impact. Here only the profiles obtained at t=8ms after impact are shown, for illustrative purposes. The differences in the temperature profiles, which are clear in Figure 1a, i.e. at lower impact velocities (U_0=0.8m/s), become less evident at higher velocities (U_0=2m/s), as the spreading film becomes thinner and more homogeneous (Figure 1b). The lower velocities also allow secondary mechanisms of particle migration and deposition which affect the local wettability and consequently the liquid-surface contact area, which may also explain the better cooling performance of the nanofluid droplets at lower impact velocities. Laser Scanning Confocal Microscopy reveals details on these local wetting modifications, particularly the deposition of the nanoparticles on the surface, at the contact line region.

Summary/Conclusions: This paper addresses the dynamic and the transfer processes occurring at the impact of nanofluid droplets (using gold and silver nanoparticles) on a

heated surface, for cooling purposes, combining highs-peed video with time and spatially resolved IR thermography and Laser Scanning Fluorescence Confocal Microscopy. The results show that the heat transfer is enhanced by the presence of the nanoparticles, but only for low impact velocities (bellow 2m/s). This is due to specific modifications in the spreading process of the naonofluid droplets, which are significant at lower spreading velocities. These modifications are partially explained by the rheological modifications in the resulting nanofluids, but also due to local wetting variations, which affect the fluid flow within the lamella and consequently the heat transfer mechanisms.

Acknowledgements: A.S. Moita acknowledges Fundação para a Ciência e a Tecnologia FCT for financing her contract and exploratory research project through the recruitment programme FCT Investigator (IF 00810-2015). Research was partially supported by FCT under the framework of the project JICAM/0003/2017, in the context of Projecto 3599 - Promover a Produção Científica, o Desenvolvimento Tecnológico e a Inovação. Finally, the work was also partially supported by EU COST Action CA15119 (NANOUPTAKE).

References:

1. J. Kim, Spray cooling heat transfer: The state of the art., *Int. J. Heat Fluid Flow* 28-4(2007) 753-767.
2. H. Bostanci, D. Rini, J. P. Kizito and L. C. Chow, Spray cooling with ammonia on microstructured surfaces: performance enhancement and hysteresis effect, *J. Heat Transf.* 131-7(2009) 071401 (9 pages).
3. G. Duursma, K. Sefiane and A. Kennedy, Experimental studies of nanofluid droplets in spray cooling, *Heat Transf. Eng.* 30-13(2017) 1108-1120.
4. M. Maly, A. S. Moita, J. Jedelsky, A. P. C. Ribeiro and A. L. N. Moreira, Effect of nanoparticles concentration on the characteristics of nanofluid sprays for cooling applications. *J. Thermal Analysis and Calorimetry*, Article in Press (Published online 12 June 2018). https://doi.org/10.1007/s10973-018-7444-z
5. E. Teodori, P. Pontes, A. S. Moita and A. L. N. Moreira, Thermographic analysis of interfacial heat transfer mechanisms on droplet/wall interactions with high temporal and spatial resolution, *Exp. Thermal Fluid Sci.* 96(2018) 284-294.
6. D. Vieira, A. S. Moita and A. L. N. Moreira, Non-intrusive wettability characterization on complex surfaces using 3D Laser Scanning Confocal Fluorescence Microscopy, *18th International Symposium on Applications of Laser and Imaging Techniques to Fluid Mechanics. Lisbon*, Portugal, 04-07 July, 2016.

1st International Conference on Nanofluids (ICNf2019)
2nd European Symposium on Nanofluids (ESNf2019)
26-28 June 2019, Castelló, Spain

Oscillating heat pipe operated with ferronanofluid

M. Winckler[1,3] A. Potthoff[2], and M.H. Buschmann[3*]

[1]Technische Universität Dresden, 01069 Dresden, Germany

[2]Fraunhofer IKTS Dresden, Winterbergstr. 28, 01277 Dresden, Germany

[3]Institut für Luft- und Kältetechnik gGmbH Dresden, Bertolt-Brecht Allee 20, 01309 Dresden, Germany

[*]Matthias.Buschmann@ilkdresden.de

Keywords: ferronanofluid, oscillating heat pipe

Abstract: Experimental results of an oscillating heat pipe (OHP) operated with a ferronanofluid are reported. It is found, that the ferronanofluid increases the thermal performance of the OHP compared to the pure base fluid deionised water. Applying an outer magnetic field reduces the amount of heat transferred significantly. However, after removing the magnets the original situation is restored again. These findings give hope to employ ferronanofluids in combination with switchable magnetic fields to control the thermal performance of OHP's.

Introduction: Nanofluids offer new options to improve heat transfer. However, these improvements are limited due to the thinness of the particles [1]. Therefore, it is necessary to apply additional forces to enhance the influence of the nanoparticles on heat transfer.

Heat pipes are very efficient apparatus for transferring heat employing low-maintenance devices. Most recent experimental and theoretical work shows, that nanofluids employed as working fluids may increase the transferrable amount of heat in such devices [2].

The operation principles of thermosyphons, ordinary heat pipes and OHP are different. While the first two are entirely based on phase change and utilisation of latent heat an OHP provides additionally heat transfer related to the *shaker effect*. Thermal energy is transferred from the evaporator to the condenser by a bubble-slug flow which is induced by pressure instabilities occurring mainly in the evaporator. Due to this mechanism both latent and sensible heat of liquid and vaporised working fluid is available at the condenser.

Figure 1 shows the OHP-test rig developed at ILK Dresden. Centrepiece is a glass body with four loops (d_i = 3 mm). The glass body is heated in the lower part (evaporator) by a resistant heater. The condenser (upper part of device) is cooled by a water stream

(V = 6 l/h, t_{ei} = 11 °C) provided by a thermostat. After evacuation the glass body is filled with 9 ml working fluid (FR = 66 %). The employed water base ferronanofluid has a solid content of 0.9 wt. %. The magnetite (Fe_3O_4) nanoparticles have a size of 77 nm measure short after production. The suspension is electrochemical stabilised (pH-value 3.7).

Figure 1. Oscillating heat pipe – Test rig. Left glass body of OHP, centre not insulated test rig filled with DI-water (yellow rectangle highlights slug-bubble formation of working fluid) and right insulated test rig with inserted photo of slug-bubble formation of ferronanofluid. Connecting pieces for evacuation and filling are indicated by red and green arrows, flow through condenser by blue arrow.

To create the magnetic field a permanent magnet is placed on each side of the resistant heater. The nickel plated NdFeB-magnets have dimensions of 120 x 12 x 5 mm^3 each. Magnetic poles are oriented axially over the thickness (5 mm). The magnetic flux density on the surface of the magnets amounts to 0.1215 T (manufacturer information).

Experiments are carried out by changing electrical power provided to the resistance heater and measuring the heat release of the evaporator. The experimental series are.

1. reference fluid DI-water (S01),
2. ferronanofluid without magnetic field (S02),
3. ferronanofluid with magnetic field (S03), and
4. ferronanofluid without magnetic field after S03 (S04).

Results: Figure 2 shows the glass body before and after the experiments. The eye-catching change appeared in the evaporator region. The inner wall of the capillaries is obviously coated with thick magnetite debris. This coating is similar to the one found for comparable devices like the thermosyphon [2]. The adiabatic region and the condenser

show only a weak back-on. Note, that the grey-yellow coating slightly below the lower part of the condenser is a remainder of the hot melt glue which is employed to mount the glass body in the test rig.

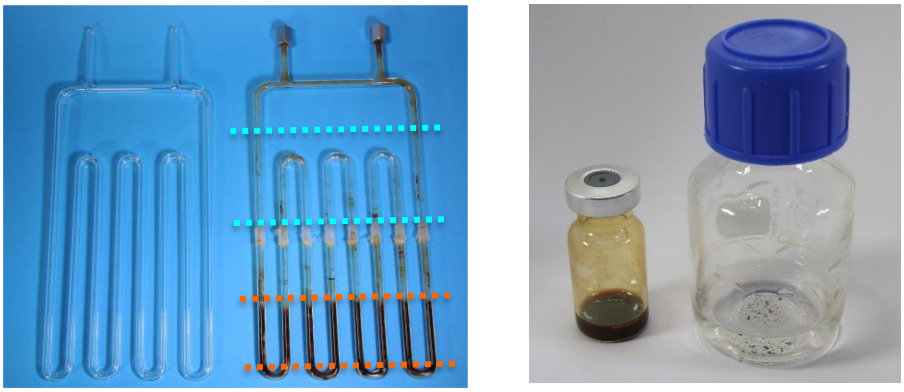

Figure 2. OHP – After experiments. Left glass body before and after experiments. Red dotted lines indicate evaporator and blue dotted lines condenser. Right ferronanofluid before (small ampulla) and after use.

The found coating of the evaporator goes along with the quality of the working fluid after use. Nearly no nanoparticles remained in the suspension (larger ampulla, Fig. 2). The brown colour of the original ferronanofluid completely disappeared. The pH-value is with about 4.1 slightly increased. A density measurement confirms, that there are nearly no magnetite nanoparticles left in the working fluid. It should be mentioned, that a few large aggregates are also found in the used suspension (see bottom of large ampulla). It is concluded, that similar to other boiling processes taking place in thermosyphons and heat pipes the nanoparticles are separated from the base fluid by phase change and forced to form a wall layer which in turn affects boiling.

Experimental results are compiled in Fig. 3. Exchanging the working fluid DI-water by ferronanofluid increases the amount of transferred heat q_c by about 4 W independently of the heat provided at the evaporator. Imposing the magnetic field leads to the surprising effect, that q_c is lowered. This effect is particularly significant for high thermal loads provided at the evaporator. Repeating the experiments after removing the magnets restores more or less the *status quo ante*. Figure 3 shows also variance and skewness of the instantaneous heat flux at the condenser. Both parameters do not any show significant differences for the four test series. Skewness and kurtosis (not shown here) indicate, that the signal is Gaussian and no geyser-like instabilities occur.

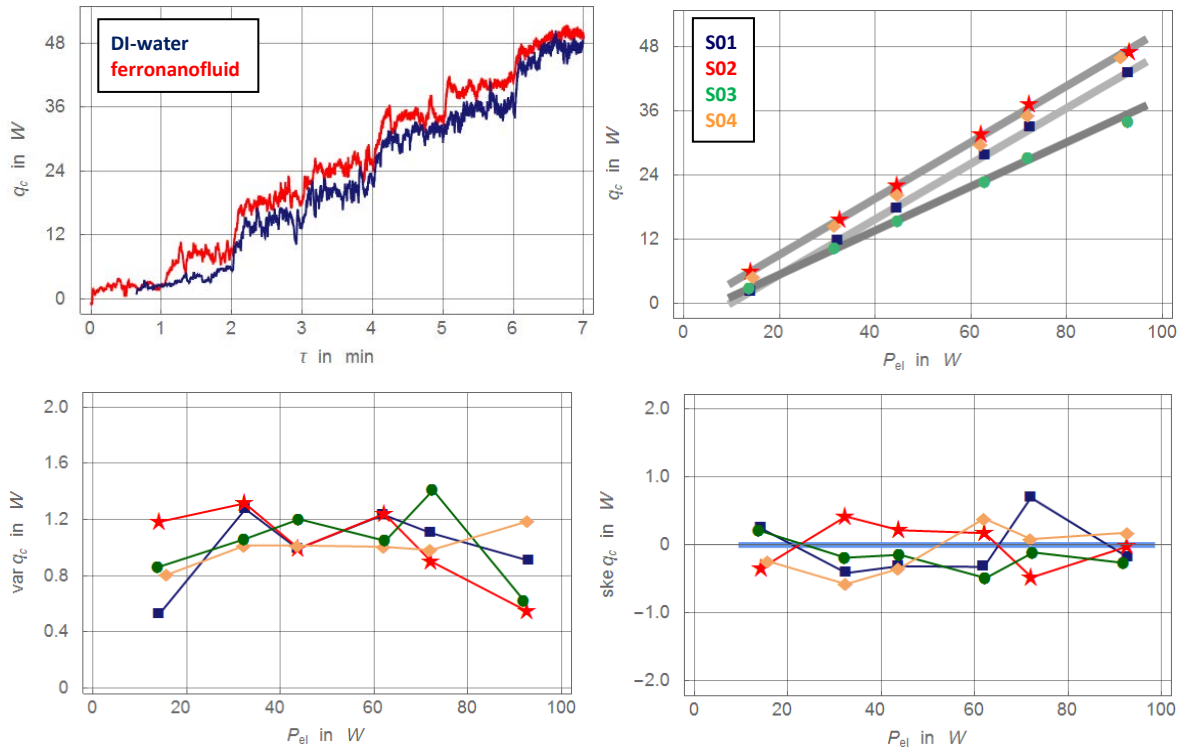

Figure 3. OHP – Experimental results. Above left obtained thermal energy at the condenser over time, right over time integrated thermal energy for the experimental series and below variance and skewness of instantaneous heat flux at condenser.

Conclusions: Experiments with an OHP indicate that

1. ferronanofluids may increase the amount of transferable heat,
2. heat transfer is supressed partly by magnet fields, and
3. the original situation is restored when the magnetic field is removed.

The results support the idea to switch OHP´s operated with ferronanofluids employing magnetic fields. However, more experiments are needed to prove the repeatability of the effects seen.

Acknowledgement: This work is part of the Grant 49VF170005.

References:

1. M.H.Buschmann, R. Azizian, T. Kempe, J.E. Juliá, R. Martínez-Cuenca, B. Sundén, Z. Wu, A. Seppälä, and T. Ala-Nissila *Correct interpretation of nanofluid convective heat transfer*, Int. J. Thermal Sci. 129 (2018) 504–531.
2. A. Wlazlak, B. Zajaczkowski, M. Woluntarski, and M.H. Buschmann *Influence of graphene oxide nanofluids and surfactant on thermal behaviour of the thermosyphon*, J. Therm. Analysis and Calorimetry (2018) 1–17.

1st International Conference on Nanofluids (ICNf2019)
2nd European Symposium on Nanofluids (ESNf2019)
26-28 June 2019, Castelló, Spain

Effect of nanoparticle coating on pool boiling performance

Z. Wu*, B. Sunden

Department of Energy Sciences, Lund University, SE-22100, Lund, Sweden

* Corresponding author: zan.wu@energy.lth.se

Keywords: Nanoparticle coating, pool boiling, bubble departure, heat transfer model, critical heat flux

Abstract: This work presents a brief summary of our recent studies on enhancing pool boiling heat transfer by nanoparticle coatings. Nanoparticles are deposited on copper substrates by an electrophoretic deposition technique. The results showed that nanoparticle coatings can enhance the heat transfer coefficient by up to 190%. Besides, a mechanistic heat transfer model was developed, with good predictive capability.

Introduction: Boiling is considered as a highly efficient approach for heat transfer dissipation at high heat fluxes. Various surface modification techniques, such as fins, surface coatings and hierarchical surfaces have been proposed to enhance boiling performance in terms of increasing heat transfer area and nucleation site density, tailoring surface wettability, and decreasing the flow resistance for bubble departure. Using nanofluids and nanostructured surfaces to enhance boiling heat transfer is an attractive method [1]. Previous studies on nanofluid boiling suggest that the heat transfer enhancement is mainly ascribed to deposition of nanoparticles on the heated surface during the pool boiling process. Nanoparticle coatings [2-3], flower-like copper oxide nanostructures [4], sintered copper surfaces with carbon nanotubes [5], and nano-textured surfaces [6] also showed large enhancement in nucleate boiling heat transfer compared to the smooth surface due to the increment in the nucleation site density.

Experimental: This work employed an electrophoretic deposition (EPD) method to modify surfaces for boiling enhancement. Please refer to our previous work [3] for a detailed description of the EPD technique. In this work, a potential of 9.5 V was applied and a deposition time of 30 minutes was used. Two types of nanoparticles were used for electrophoretic deposition, i.e., copper-zinc alloy nanoparticles (Sigma-Aldrich) of a mean particle diameter of 100 nm, and copper nanoparticles (Sigma-Aldrich) of a mean particle diameter of 126 nm. Six nanoparticles-coated surfaces were fabricated, i.e., EPD-1 deposited with 0.30 mg of copper-zinc nanoparticles, EPD-2 with 0.60 mg of copper-zinc nanoparticles, EPD-3 with 0.90 mg of copper-zinc nanoparticles, EPD-4 with

1.20 mg of copper-zinc nanoparticles, EPD-5 with 0.98 mg of copper nanoparticles, and EPD-5 with 1.50 mg of copper nanoparticles. The surface roughness and static contact angle are listed in Table 1 for the smooth surface (SS) and the six EPD surfaces.

Table 1. Tested surfaces

Surface	SS	EPD-1	EPD-2	EPD-3	EPD-4	EPD-5	EPD-6
Surface roughness Ra (μm)	0.12	0.54	0.55	1.28	1.44	2.02	1.53
Contact angle (°)	24.1	23.3	24.0	22.6	20.6	20.4	20.1

Degassing was conducted for 2 hours before the experiment. All data were collected at steady state when the deviation of the recorded temperatures was within ± 0.2 K in 5 mins. During the nucleate boiling regime, the maximum uncertainties for heat flux and heat transfer coefficient are 11.4% and 12.6%, respectively. More details of this experimental setup and data reduction can be found in Wu et al. [2]. The working fluid is HFE-7200, a well-wetting and dielectric liquid with a very low global warming potential of 55. There are only a few studies in the literature on pool boiling of such environment-friendly well-wetting and dielectric liquids.

Results and Discussion: Figure 1 presents pool boiling curves of SS and six EPD-surfaces. Compared to SS, for the modified surfaces the pool boiling curves are pushed leftwards largely; Bubbles tend to nucleate at a lower surface superheat; The heat flux increases sharply after bubble nucleation within a narrower range of surface superheat. The critical heat flux (CHF) values of SS and EPD surfaces are at a similar level, with a difference in CHF less than 10.5%, which is insignificant. Supplementary tests indicated that the wickability of HFE-7200 was almost the same on the SS and EPD surfaces. Besides, the wall superheat at CHF decreases from about 40 °C on the SS to less than 20 °C on EPD surfaces. A less temperature budget is required to dissipate the same heat flux on EPD surfaces than on SS. As shown in Fig. 2, during the nucleate boiling regime, the heat transfer coefficient increases steadily. Then HTC generally decreases when approaching CHF as intensive bubble coalescences and large vapor mushrooms prevail. The HTC was enhanced by up to 190% on EPD surfaces for HFE-7200. There are several reasons attributed to the enhancement. Firstly, from SEM images of the surfaces, there are many microscale cavities or crevices on EPD surfaces, ranging from several hundreds of nanometers to several micrometers. During the deposition process, the nanoparticles may aggregate into large particles or clusters. There are comparatively more microscale cavities which initiate boiling at a lower wall superheat and serve as active nucleation sites. For EPD surfaces, when boiling initiates, a large number of

nucleation sites are available on EPD surfaces for activation with a slight increase in wall superheat. Therefore, the heat flux increases sharply. Besides, the bubble dynamics on EPD surfaces are different from that on SS. At a similar heat flux level, bubbles depart from the surface at smaller diameters on EPD surfaces than on the SS because the corresponding wall superheat on the SS is much higher than those on EPD surfaces. Accordingly, the bubble departure frequency is higher on EPD surfaces, which tends to improve heat dissipation from the surface.

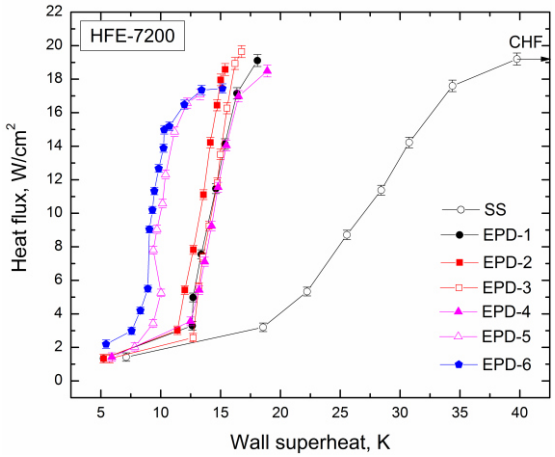

Fig. 1 Pool boiling curves

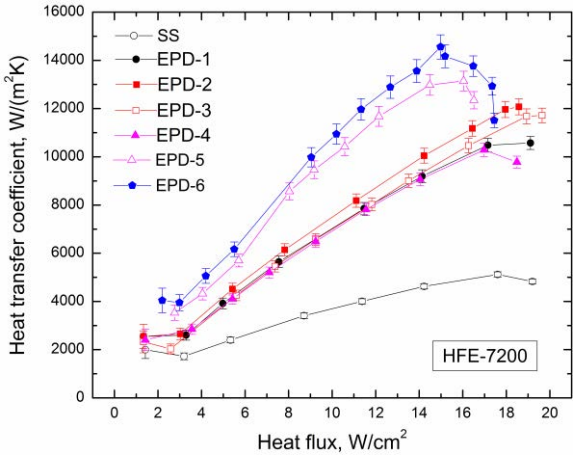

Fig. 2 Heat transfer coefficient comparisons

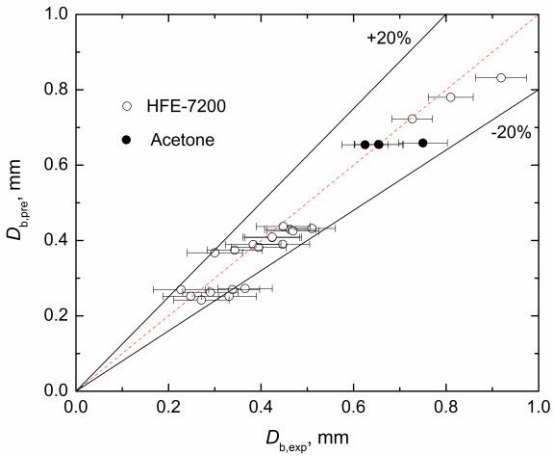

Fig. 3 Experimental and predicted D_b

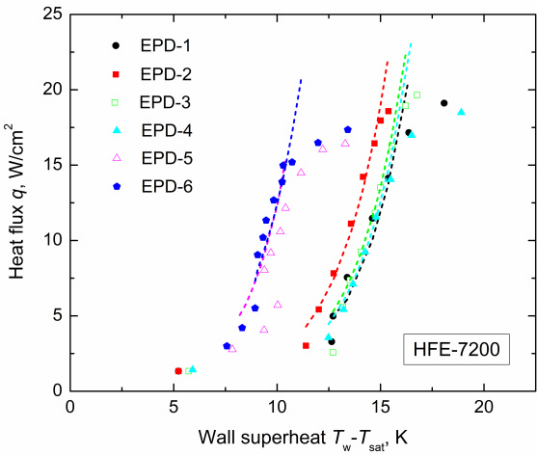

Fig. 4 Comparison of pool boiling curves

At low and medium heat fluxes where isolated bubble regime prevails, bubble departure diameters were measured from recorded images with a maximum uncertainty of 20.2%. The experimental bubble departure diameter data can be approximately predicted by our recently developed bubble departure diameter model, i.e., the Wang et al. model [7] based on a force balance on a departing bubble, as shown in Fig. 3.

A mechanistic heat transfer model was proposed by considering heat flux contributions from microlayer evaporation, transient heat conduction and micro-convection (or local convection). The overall heat flux equation is proposed as below.

$$q = q_{\mathrm{me}} + (q_{\mathrm{cond}}^{m} + q_{\mathrm{m-c}}^{m})^{\frac{1}{m}} = Na \cdot \frac{2\pi}{3}(D_{\mathrm{b}}/2)^3 \rho_{\mathrm{g}} \cdot i_{\mathrm{fg}} \cdot f$$
$$+2\sqrt{\pi \cdot f \cdot k_{\mathrm{f}} \cdot \rho_{\mathrm{f}} \cdot c_{\mathrm{pf}}}\, D_{\mathrm{b}}^2 (T_{\mathrm{w}} - T_{\mathrm{sat}}) \cdot Na \cdot \left[1 + \left(\frac{0.66\pi c}{\mathrm{Pr}^{1/6}}\right)^{m}\right]^{\frac{1}{m}} \quad (1)$$

In the above equation, bubble dynamics parameters including the bubble departure diameter D_b, the bubble departure frequency f and the active nucleation site density Na are, respectively, estimated by the Wang et al. model [7], the Peebles and Garber correlation [8] and the Hibiki and Ishii correlation [9], respectively. As given in Fig. 4, the newly developed model can predict the experimental boiling curves of modified surfaces relatively well, especially for the isolated bubble regime where bubbles are mostly isolated and bubble coalescence is not intensive. It seems that the micro-convection contribution to heat transfer may be significant for structured surfaces.

Summary: The study investigated the potential of nanoparticle-coated surfaces for enhancing pool boiling of HFE-7200 by the EPD technique. The heat transfer coefficient can be enhanced by up to 190%. A mechanistic heat transfer model was developed.

References:

1. Z. Wu, B. Sunden, On further enhancement of single-phase and flow boiling heat transfer in micro/minichannels, *Renew. Sustain. Energ. Rev.* 40 (2014) 11-27.
2. Z. Wu, A.D. Pham, Z. Cao, C. Alber, P. Falkman, T. Ruzgas, B. Sunden, Pool boiling heat transfer of n-pentane and acetone on nanostructured surfaces by electrophoretic deposition. In ASME 2018 International Mechanical Engineering Congress and Exposition. Paper No. IMECE2018-87752.
3. Z. Cao, Z. Wu, A.D. Pham, Y. Yang, S. Abbood, P. Falkman, , T. Ruzgas, C. Alber, B. Sunden, Pool boiling of HFE-7200 on nanoparticle-coating surfaces: Experiments and heat transfer analysis, *Int. J. Heat Mass Transfer* 133 (2019) 548-560.
4. Y. Im, C. Dietz, S.S. Lee, Y. Joshi, Flower-like CuO nanostructures for enhanced boiling, *Nanoscale Microscale Thermophys. Eng.* 16 (2012) 145-153.
5. J.P. McHale, S.V. Garimella, T.S. Fisher, G.A. Powell, Pool boiling performance comparison of smooth and sintered copper surfaces with and without carbon nanotubes, *Nanoscale Microscale Thermophys. Eng.* 15 (2011) 133-150.
6. S. Jun, S. Sinha-Ray, A.L. Yarin, Pool boiling on nano-textured surfaces, *Int. J. Heat Mass Transfer* 62 (2013) 99-111.
7. X. Wang, Z. Wu, J. Wei, B. Sundén, Correlations for prediction of the bubble departure radius on smooth flat surface during nucleate pool boiling, *Int. J. Heat Mass Transfer* 132 (2019) 699-714.
8. F.N. Peebles, H.J. Garber, Studies on the motion of gas bubbles in liquid, *Chem. Eng. Prog.* 49 (1953) 88-97.
9. T. Hibiki, M. Ishii, Active nucleation site density in boiling systems, *Int. J. Heat Mass Transfer* 46 (2003) 2587-601.

1st International Conference on Nanofluids (ICNf2019)
2nd European Symposium on Nanofluids (ESNf2019)
26-28 June 2019, Castelló, Spain

Prediction of pool boiling heat transfer coefficient for the refrigerant R141b and its solutions with surfactant and nanoparticles using limited set of experimental data

O. Khliyeva[1], A. Nikulin[2*], V. Zhelezny[1], N. Lukianov[1], Yu. Semenyuk[1], S.M.S. Murshed[2] and A.L.N. Moreira[2]

[1]Odessa National Academy of Food Technologies, Institute of Refrigeration, Cryotechnology and Eco-Energy, 1/3 Dvoryanskaya Str., 65082 Odessa, Ukraine

[2]Instituto Superior Técnico, Universidade de Lisboa, Center for Innovation, Technology and Policy Research, IN+, Av. Rovisco Pais 1, 1049-001 Lisboa, Portugal

[*]Corresponding author: artem.nikulin@tecnico.ulisboa.pt

Keywords: Pool boiling, Nanofluid, Heat transfer coefficient

Abstract: The main purpose of this study is to evaluate the expediency of limited set of experimental data (LSED) to increase the accuracy of heat transfer coefficient (HTC) prediction under pool boiling conditions. The analysis was performed for the pure refrigerant R141b and its solutions with the surfactant Span-80 and TiO_2 nanoparticles. The results have shown, that the joint use of LSED and existing correlations for internal boiling characteristics (IBC) helps to improve HTC prediction.

Introduction/Background: Accurate prediction of heat transfer coefficient (HTC) under pool boiling conditions is still a challenge. It is known, that the HTC can be characterized using internal boiling characteristics (IBC) (bubble departure diameter, frequency and nucleation sites density) [1]. The models, such as Stephan-Abdelsalam [2] and Tolubinsky [3] which partially take into account the IBC are usually demonstrate unsatisfactory prediction of pool boiling HTC [3,4]. However, the models using all IBC, such as RPI (Rensselaer Polytechnic Institute) can predict boiling HTC at higher level of uncertainty [4,5]. It is worth to mention, that the IBC depend both on fluid and heating surface properties. This information is quite rare and is limited to a specific set of liquid/surface combinations. Moreover, high optical density of nanofluids, even at relatively low nanoparticles concentration, makes it difficult to use optical methods for experimental study of IBC.

Taking into account the aforementioned above, the aim of our study is to test a new approach to pool boiling HTC prediction. It requires a limited set of experimental data on HTC and IBC obtained in a narrow range of experimental parameters. Thereafter, those

data can be extrapolated for a wider range of experimental parameters. We believe, that such approach is a compromise between a fully theoretical HTC prediction usually giving high uncertainty with fully experimental HTC characterization which has high time and costs consumption.

Discussion and Results: The experiments were performed with R141b and its solutions with the surfactant Span-80 (0.1 mass%) and surfactant Span-80/TiO_2 nanoparticles (0.1 mass%/0.1 mass%). The two-step method was used to prepare nanofluid. Spectral turbidimetry tests have shown that obtained nanofluid remains stable within three months with mean nanoparticle radius of 125 ± 7 nm.

The study of HTC during nucleate pool boiling was carried out using the original experimental setup [4] at 0.2, 0.3 and 0.4 MPa in the range of heat fluxes from 5 to 70 ($kW \cdot m^{-2}$). The obtained results were discussed elsewhere [3]. To study the IBC a simple experimental facility described in [3] was used at atmospheric pressure. As can be seen in Fig.1, the bubble departure diameter for R141b increase versus heat flux density, while theirs frequency demonstrate the inverse relationship. The bubble departure diameter and frequency do not change significantly versus heat flux density for R141b/Surf. and R141b/Surf./TiO_2 solutions.

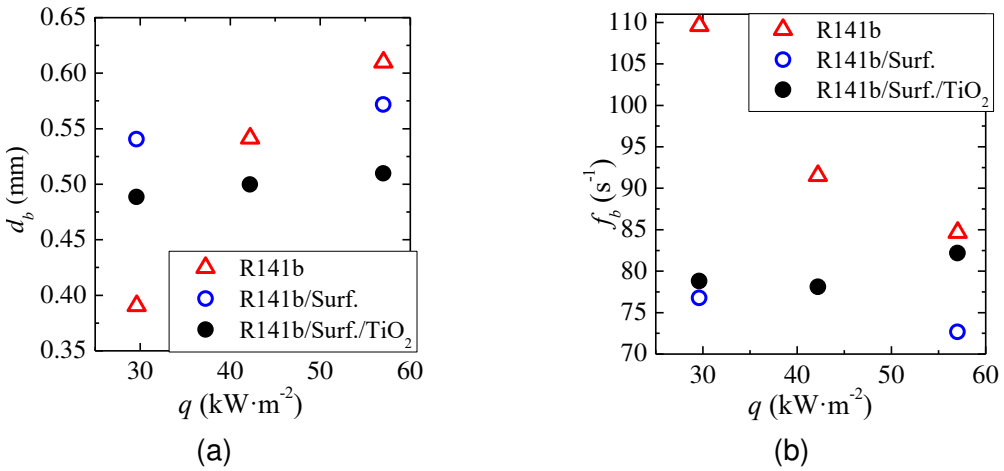

Figure 1. Bubble departure diameter (a) and frequency (b) versus heat flux density for R141b, R141b/Surf. and R141b/Surf./TiO_2

The models of Tolubinsky [3] and RPI [4] were firstly used to compare the experimental results on HTC. The following equations describe the dependence of bubble departure diameter and frequency versus pressure and rough estimate for nucleation sites density

$$\bar{d}_b = \bar{d}_{b\,0.1}\left(\frac{\sigma\left(\rho'_{0.1}-\rho''_{0.1}\right)}{\sigma_{0.1}\left(\rho'_{0.1}-\rho''_{0.1}\right)}\right)^{0.5} \qquad (1)$$

$$\bar{w}_b / \bar{w}_{b\,0.1} = \left(\rho''_{0.1} / \rho''\right)^{2.3+0.5 lg\,\pi} \tag{2}$$

$$\sqrt{n_b} = 25 \cdot 10^{-8} \left(\frac{\Delta h \cdot \rho'' \cdot \Delta T}{T_S \cdot \sigma} \right)^{1.5} \tag{3}$$

where $\bar{d}_b$, ρ', ρ'', σ, $\bar{w}_b = \bar{d}_b \bar{f}_b$ are the mean bubble departure diameter, density of the liquid and vapour, surface tension, mean velocity of bubble growth at certain pressure; $\bar{d}_{b\,0.1}$, $\rho'_{0.1}$, $\rho''_{0.1}$, $\sigma_{0.1}$, $\bar{w}_{b\,0.1}$ are the mean bubble departure diameter, density of the liquid and vapour, surface tension, mean velocity of bubble growth at $P_{0.1}$=0.1013 (MPa) respectively; $\pi = P_{0.1}/P_C$ is the reduced pressure; n_b is and nucleation sites density; Δh is heat of vaporization; ΔT is wall superheat; T_S is saturation temperature.

The results of comparison indicated to significant deviations of experimental values from calculated ones. Moreover, the models give the opposite results for the surfactant and nanoparticles effect on HTC. Such results could be explained by the effect of nanoparticles on nucleation sites density, which can increase or decrease as compared to base liquid [4].

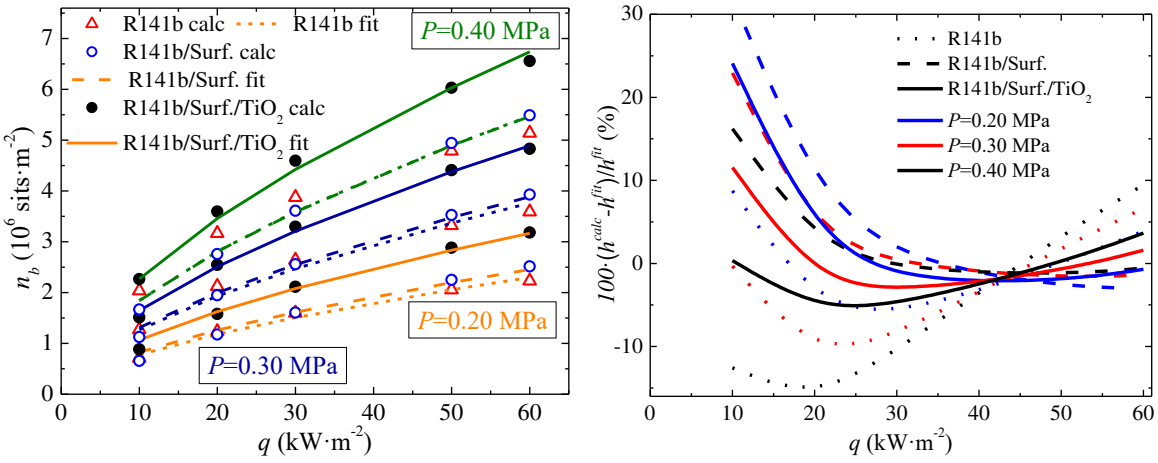

(a) (b)

Figure 2. Experimental and calculated by Eq.(4) values of nucleation sites density (a) and relative deviations of experimental and calculated values of HTC using RPI model [4,5] and Eq.(4) (b).

At the next stage, a method using RPI model to calculate a nucleation sites density was utilised [4]. The results of calculation for all studied boiling pressures are shown in Fig.2(a). Nucleation sites density for nanofluid is much higher than for pure liquid.

Nevertheless, the additive of surfactant does not change significantly the nucleation sites density. The performed analysis has shown, that the dependence of nucleation sites density versus heat flux density and pressure for all studied samples in all range of parameters is the following

$$n_b = n_{b\,0.1}\left(\frac{\Delta h\cdot\rho''}{T_S\cdot\sigma}\cdot\frac{T_{S\,0.1}\cdot\sigma_{0.1}}{\Delta h_{0.1}\cdot\rho''_{0.1}}\right)^C \qquad (4)$$

where C=1.093 is an exponent.

In the Fig.2(b) the relative deviations of experimental and calculated data on HTC within RPI model [4] and using Eq.(4) are shown. As can be seen, the deviations do not exceed 10% from 20 to 60 ($kW\cdot m^{-2}$). The increased deviations for heat flux density below 20 ($kW\cdot m^{-2}$) are probably gathered with the stochastic nature of the boiling process onset and termination.

Summary/Conclusions: For more accurate HTC prediction during boiling of pure liquids and nanofluids, it is necessary to have data on IBC. The information on IBC obtained using a limited set of experimental data at one value of pressure and two or several values of heat flux density allow to predict HTC during boiling with sufficient accuracy for many applications.

References:

1. I.L. Pioro, W. Rohsenow, S.S. Doerffer, Nucleate pool-boiling heat transfer. I: review of parametric effects of boiling surface, *International Journal of Heat and Mass transfer,* 47(23) (2004) 5033-5044.
2. K. Stephan, M. Abdelsalam, Heat-transfer correlations for natural convection boiling, *International Journal of Heat and Mass transfer* 23(1) (1980) 73–87.
3. O. Khliyeva, A. Nikulin, T. Gordeychuk, N. Lukianov, Yu. Semenyuk, An experimental study of heat transfer coefficient and internal characteristics of nucleate pool boiling of nanaofluid R141b/TiO_2, *1st European Symposium on Nanofluids (ESNf2017)*, Lisbon, Portugal, 8-10 October, (2017).
4. Nikulin A., Khliyeva O., Lukianov N., Zhelezny V., Semenyuk Y. Study of pool boiling process for the refrigerant R11, isopropanol and isopropanol/Al_2O_3 nanofluid, *International Journal of Heat and Mass Transfer*, 118 (2018) 746-757.
5. C. Gerardi, J. Buongiorno, L.-W. Hu, T. McKrell, Infrared thermometry study of nanofluid pool boiling phenomena, *Nanoscale Research Letters* 6 (1) (2011) 232.

1st International Conference on Nanofluids (ICNf2019)
2nd European Symposium on Nanofluids (ESNf2019)
26-28 June 2019, Castelló, Spain

Oxidised carbon nanohorn nanofluids for direct solar energy absorption applications: stability, optical and deposition properties

A. Gimeno-Furio[1], L. Hernandez[1], S. Barison[2], F. Agresti[2], G. Bottaro[3], D. Cabaleiro[4], L. Doretti[5], S. Mancin[6,*]

[1]Department of Mechanical Engineering and Construction, Universitat Jaume I, 12071 Castellón de la Plana, Spain

[2]CNR-ICMATE Institute of Condensed Matter Chemistry and Technologies for Energy, Corso Stati Uniti, 35127 Padova, Italy

[3]CNR-ICMATE at Dept. Chemical Science, University of Padua, Via Marzolo 1, 35131 Padova, Italy

[4]CNR-ITC Construction Technologies Institute, Corso Stati Uniti, 35127 Padova, Italy

[5]Department of Civil, Architectural and Environmental Engineering, University of Padova, 35131, Padova, Italy

[6]Department of Management and Engineering, University of Padova, 36100 Vicenza, Italy

[*]Corresponding author: simone.mancin@unipd.it

Keywords: pool boiling, contact angle, coating, stability, optical properties, solar energy

Abstract: This paper investigates two fundamental aspects of the use of carbon nanohorns and oxidised carbon nanohorns-based nanofluids for direct solar energy adsorption applications. On one hand the stability and the optical characteristics of both nanofluids were checked after a 3-month preparation period at high temperature, which comes closer to real applications. Studying both nanofluid types provided us with new knowledge about their potential use as direct solar absorbers in solar thermal collectors. Moreover, this work also investigated the effects of the oxidised carbon nanohorns-based boiling on a reference aluminium surface. During the nanofluid boiling a thin layer of nanoparticles deposited and adhered on the heated surface affecting the wettability and the optical properties of the base material.

Before and after the boiling test, scanning electron microscopy (SEM) and contact angle (CA) measurements were performed to characterize and evaluate the resulting coated surface. The boiling curves of both fluids were measured. Moreover, optical measurements of reflectance and scattering with the integrating sphere on the Al surface with the nanohorn film and on a corresponding reference copper surface were carried

out. The coated Al surfaces showed from 3 to 20 times higher solar adsorption as compared to the reference copper surface between visible and close infrared.

Introduction/Background: In recent years, solar thermal energy has attracted much interest given its thermal storage possibilities and economic appeal. Conventional solar thermal collectors transform solar radiation energy into the thermal energy of the transport medium. Typical solar collectors use a black surface to absorb incoming sunlight. Then this energy is transferred to water to form high quality pressurised steam in a boiler/heat exchanger. Thus, in general, many transfer steps (via radiation, convection, conduction and boiling) are required to follow this process and convert light energy into thermal energy for a power cycle. In order to minimise limitations, which result from following many energy transfer steps, some alternative concepts have been addressed. Of these, the idea of absorbing light inside the working fluid while generating steam has been well studied [1]. Direct steam generation can make solar plants more economic and more environmentally friendly, and would present fewer thermal losses than conventional solar plants, which would improve the cost of energy by 11% [2]. Moreover, when only light is absorbed by the working fluid, efficiency is enhanced by around 10% compared to absorbing light on a black surface, as in typical collectors [2-5].

Our proposal is to use nanofluids as working fluids either to directly absorb light and/or to enhance the harvesting capabilities of the materials used in the solar collectors. Oxidised carbon nanohorns (oxCNHs) [6] nanofluid can be considered a promising working fluid for solar collectors and it can also be used to deposit thin CNH' nanoparticles layer to enhance the absorbance properties of heat transfer materials. The aim of this paper is twofold: firstly, to study and compare the stability and optical properties of SWCNH and oxidised SWCNH suspensions in water and, secondly, to study the wettability and optical properties of a reference Al surface before and after oxidised CNH nanofluid pool boiling.

Discussion and Results: Four different nanofluids were synthesised and studied. The base fluid employed for them all was water (Millipore, 18 MΩ cm). The difference among the nanofluids lays in the type of nanoparticles, the stabilisation method and the nanoparticle concentration in nanofluids. One of them consisted of SWCNH suspended in water using sodium dodecyl sulphate (SDS, ~99%, Sigma) as a surfactant at two different SWCNH concentrations (0.005 and 0.002 %wt). The other nanofluid was also based on an aqueous suspension, but oxidised SWCNHs were used to avoid resorting to surfactants, and also at two different concentrations (0.005 and 0.002 %wt). These concentrations have been determined in previous work as being suitable for solar nanofluids [6]. SWCNHs were provided by Carbonium S.r.l. and were produced by a

process based on the rapid condensation of carbon atoms with no catalyst, giving considerably reduced production costs. The morphological characterisation of nanoparticles was made by Field Emission Scanning Electron Microscopy (FESEM) with a SIGMA Zeiss instrument (Carl Zeiss SMT Ltd, UK).

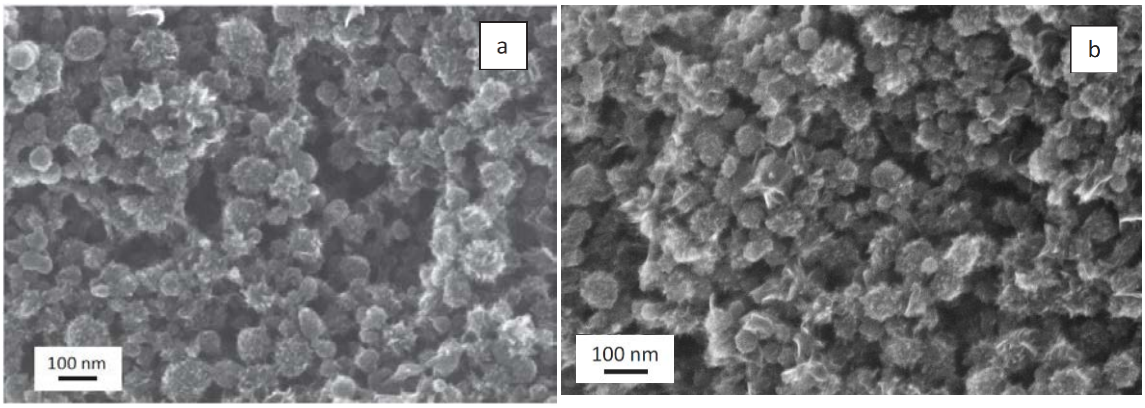

Figure 1. SEM images of SWCNH powder (a) and oxidized SWCNH (b).

Considering the stability properties, two different systems were used to measure and validate the particle size distribution in nanofluids, which repeated over time can be related to their stability. Both of them use Dynamic Light Scattering (DLS) as measuring technique and can measure at different temperatures. One of the equipment used for measuring the stability is Zetasizer Nano (Malvern Instruments) which is commonly used in literature to measure particle size distributions of nanofluids by means of DLS. The other system is the VASCO FLEX particle size analyser (Cordouan Technologies). This is a new commercial system to measure the stability of a nanofluid. The main difference between the two devices is that Vasco FLEX can analyse samples outside of apparatus, allowing for high temperature measurements (i.e. up to 300°C). A spectrophotometer (with integrating sphere) was employed to measure different optical properties of the nanofluids. The spectrophotometer used for measuring the NIR-Vis spectra of the sample is CARY 500 (Varian Devices) with the possible use of an integrating sphere. This system is chosen because different optical parameters as ballistic transmittance, reflectance, forward and backward scattering can be measured. To be able to measure the scattering of the sample, an integrating sphere is attached to the spectrophotometer.

Pool boiling tests were carried out in an experimental setup that consists of an Al surface, which was exposed to the working fluid and heated by electrical cartridge heaters. All the pool boiling experiments took place inside a confined chamber in order to avoid contamination. On the top, there is a condenser, which is directly fed with the

vapour formed. On the other hand, CA measurements were obtained by image processing. Finally, to study the effect of the pool boiling on the surface and evaluate if deposition of nanoparticles has taken place, SEM images were performed and the optical characterization of surfaces was performed by CARY5000 spectrophotometer equipped with integration sphere.

Summary/Conclusions: Stability over 3 months was evaluated at room temperature with Zetasizer Nano, with good results. Afterwards, samples were thermally treated at 75°C for 30 minutes, and their size distribution was measured again. As the results were similar to those obtained with the fresh samples, it can be concluded that the thermal treatment that goes up to 75°C does not affect their stability. Regarding optical properties, an increment from 665% to 860% in extinction within the 400-800 nm range was obtained for nanofluids in relation to their base fluid. This significant improvement was obtained even for low nanoparticle concentrations. The boiling of the oxCNH test permitted to deposit a thin layer of oxCNH nanoparticles on the heated surface. The values obtained for the CA measurements are for water 74º and oxCNH 76.3º on Al surface before the boiling and then, 70.6º and 69º for water and oxCNH, respectively, on the Al surface after the pool boiling. Moreover, the coated Al surface showed from 3 to 20 times higher solar adsorption as compared to the reference copper surface between visible and close infrared. Given their stability and optical properties, oxCNH water-based nanofluids can be good candidates as direct sunlight absorber fluids. The highlighted advantages of oxidised nanofluids are that they present higher absorbance values and do not need surfactants to be stable, which provides a more environmentally friendly nanofluid and deposition method.

References:

1. R. A. Taylor, P. E. Phelan, R. J. Adrian, A. Gunawan, and T. P. Otanicar: Characterization of light-induced, volumetric steam generation in nanofluids. Int. J. Therm. Sci. 2012, 56:1-11.
2. J. Birnbaum, M. Eck, M. Fichtner, T. Hirsch, D. Lehmann, and G. Zimmermann: A Direct Steam Generation Solar Power Plant With Integrated Thermal Storage. J. Sol. Energy Eng. 2010, 132:031014.
3. R. A. Taylor, P.E. Phelan, T.P. Otanicar, C.A. Walker, M. Nguyen: Applicability of nanofluids in high flux solar collectors. J. Renew. Sustain. Energy 2011, 3:023104.
4. R. A. Taylor, P. E. Phelan, T. P. Otanicar, R. Adrian, and R. Prasher: Nanofluid optical property characterization: towards efficient direct absorption solar collectors. Nanoscale Res. Lett. 2011, 6:225.
5. R. Pankaj and S. Subudhi: A review of studies using nanofluids in flat-plate and direct absorption solar collectos. Renewable and Sustainable Energy Reviews 2018, 84:54.
6. E. Sani, L. Mercatelli, S. Barison, C. Pagura, F. Agresti, L. Colla, P. Sansoni: Potential of carbon nanohorn-based suspensions for solar thermal collectors. Sol. Energy Mater. Sol. Cells 2011, 95:2994-3000.

1st International Conference on Nanofluids (ICNf2019)
2nd European Symposium on Nanofluids (ESNf2019)
26-28 June 2019, Castelló, Spain

On the contact angle of nanofluids

N. Çobanoğlu[1,5*], Z. H. Karadeniz[2], P. Estellé[3], R. Martínez-Cuenca[4], and M.H. Buschmann[5]

[1]İzmir Kâtip Çelebi University, Graduate School of Natural and Applied Sciences, 35620, İzmir, Turkey

[2]İzmir Kâtip Çelebi University, Department of Mechanical Engineering, 35620, İzmir, Turkey

[3] IUT Rennes, LGCGM, EA3913, F-35000 Rennes, France

[4] Departamento de Ingeniería Mecánica y Construcción, Universitat Jaume I, Castelló de la Plana 12071, Spain

[5]Institut für Luft- und Kältetechnik gGmbH Dresden, 01309 Dresden, Germany

[*]Corresponding author: nurcobanoglu@outlook.com

Keywords: Contact Angle, Nanofluid, Bond Number

Abstract: The contact angle (CA) of a liquid defines the degree of wettability. It depends on the thermophysical properties of the droplet, the forces acting on the droplet, and the substrate surface. For nanofluids (NF) nanoparticle concentration and size might be additional parameters. This study investigates several nanofluids with respect to the prediction of their CA employing correlations derived for single-phase liquids.

Introduction/Background: The contact angle of nanofluids droplets attracts attention as one of the relevant thermophysical properties needed to describe phase change processes of these suspensions properly. For practical applications it is important to prove if the CA of NF's is described correctly by existing single-phase approaches or if more sophisticated models are needed. Here two single-phase approaches are considered. One is based on the force balance on the droplet [1] and the second on its energy balance [2].

Gravity and surface force are acting on a sessile single-phase droplet. The first is due to the hydrostatic force of the variable droplet height and the second follows from external pressure and surface tension. For this Vafaei and Podowski [1] (VP-model) found

$$V = \frac{2\pi\sigma_{lg} r_d^2}{\rho g}\left(\frac{\rho g \delta}{2\sigma_{lg}} + \frac{1}{R_0} - \frac{sin\theta_d}{r_d}\right) \quad (1)$$

Here σ_{lg} and ρ denote surface tension and density, r_d and V are droplet baseline radius and volume, δ and R_0 are the apex height and curvature. θ_d is the contact angle of the droplet. A non-dimensional reformulation of (1) is obtained by introducing the Bond number *Bo* the ratio between gravitational and surface force. Two additional geometrical similarity simplexes – G_1 and G_2 – describe the droplet geometry and V^* is the nondimensional droplet volume.

$$sin\theta_d = \frac{1}{2} Bo\, G_1 + G_2 - Bo\, V^*; \qquad G_1 = \frac{\delta}{r_d}; \qquad G_2 = \frac{r_d}{R_0}; \qquad V^* = \frac{V}{2\pi {r_d}^3} \tag{2}$$

Stacy [2] stated, that for non-wetting droplets one of the characteristic length scales equals the radius at the droplet equator whereas for wetting droplets it is its wetting radius. Moreover, Kuiken [3] defined the characteristic length as the maximum half width of the droplet. Based on this the Bond number is written as:

$$Bo = \rho g {r_d}^2 / \sigma_{lg} \tag{3}$$

Yonemoto and Kunugi [4] (YK-model) derived a correlation for various-sized droplets on a solid surface by employing the energy balance.

$$\frac{\rho g \delta V}{2} = \pi {r_d}^2 \sigma_{lg}(1 - cos\theta_s) - \pi r_d \delta \sigma_{lg} sin\theta_s \tag{4}$$

A non-dimensional form is deduced by dividing (4) by the gravitational potential $\rho g \delta V/2$.

$$1 = X^* - Y^*; \qquad X^* = \frac{2\pi {r_d}^2}{\delta V} \frac{\sigma_{lg}(1-cos\theta_s)}{\rho g}; \qquad Y^* = \frac{2\pi r_d}{V} \frac{\sigma_{lg} sin\theta_s}{\rho g} \tag{5}$$

The aim of our study is to validate eqs. (2) and (5) employing water data and to check if these correlations are also valid for nanofluid droplets. For this purpose experimental data are introduced into the VF-model and the YK-model. The predicted results are than compared to the forecasts given by these correlations. Experimental data for distilled water as single phase reference fluid (DIW), and graphene oxide (GO), gold (Au) and silica (SiO_2) nanofluids are utilised. Characteristics of the nanofluids (Au and GO) employed are given in [5] and SiO_2 has 117 nm particle diameter and 2 vol. % concentration.

Discussion and Results

Geometrical parameters (δ, r_d and R_0) were obtained by CA image analysis with Fiji [6]. Spatial calibration is done for each data set by defining pixel-to-mm ratio with respect to a reference dimension.

Figures 1 and 2 show VP-model for DIW and the different nanofluids. DIW as expected for a single-phase liquid indicates good agreement with the model. Due to the extraordinary low concentration and the very small particles the gold NF shows also

reasonable good agreement. However, the VP-model seems to be not valid for GO and SiO_2 NF's. GO has large graphene flakes (≈ 800 nm length) and SiO_2 has with 2 vol. % a higher concentration which may prevent the application of the VP-model.

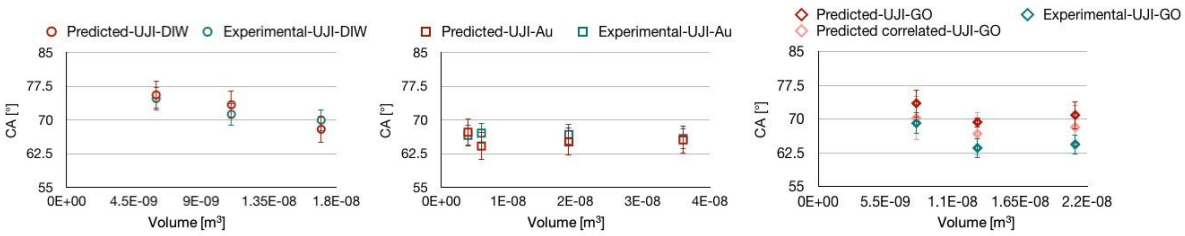

Fig. 1. VP-model for different fluids.

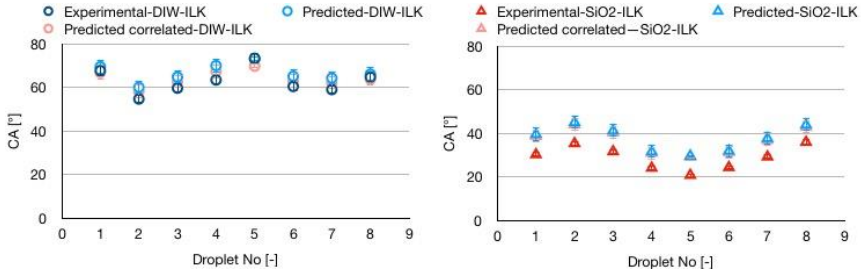

Figure 2. VP-model with experimental data of DIW and SiO_2

It is found, that the VP-models is very sensitive against tiny experimental errors following the determination of R_0. To illustrate this Fig. 2 shows additionally the results of a thought experiment where the experimental value of R_0 has been increased artificially by just 2 %. With this minute correction the GO-data collapse much better with the VP-model.

Strictly speaking the YK-model describes only spherical droplets. Therefore, employing the correlation for $\theta_s = f(r_d, r_{ds}, \theta_d)$ given in [1] eq. (4) is rewritten.

$$1 + cos\theta_s = \frac{sin^2\theta_d}{G_1(BoV^* + sin\theta_d)} \tag{6}$$

The contact angle for spherical droplets is denotes by θ_s and its baseline radius by r_{ds}.

Figure 3 shows results for the modified YK-model for DIW, gold and GO nanofluids. The model reproduces the experimental data by up to 4% mean absolute deviation. However, the results for the SiO_2-nanofluid (Fig. 4) indicate again that a single-phase model is not suitable for a highly concentrated nanofluid.

Summary/Conclusions: With this study the attempt is undertaken to validate two models describing the correlation between contact angle, geometrical parameters and forces /

energy balance on the droplet for nanofluid droplets. The task is difficult because the measurement of the needed geometrical parameters demands high quality.

In general it is found, that the contact angle of a single-phase liquid depends on the Bond number, the non-dimensional droplet volume and two geometrical similarity simplexes. This

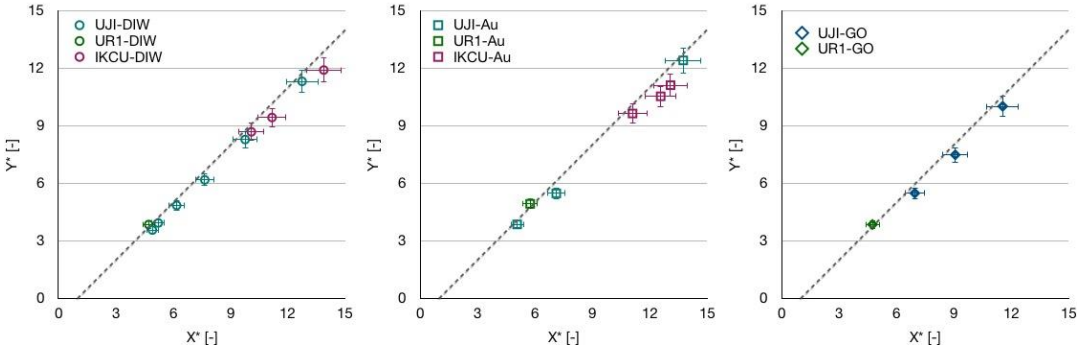

Fig. 3. YK-model for experimental data at various volumes.

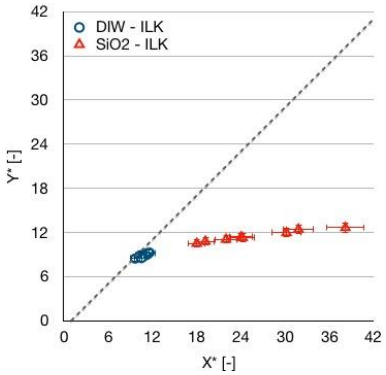

Fig. 4. YK-model for experimental data of DIW (dark blue) and SiO_2 (red).

approach holds also for diluted nanofluids like the gold NF investigated. However, for high concentrated suspensions as the silica nanofluids analysed significant differences are found. The reason is probably, that additional effects like disjoining pressure, convective flows inside the droplet etc. affect CA. Further research is needed to resolve these effects properly.

References:

1. S. Vafaei and M. Podowski, Analysis of the relationship between liquid droplet size and contact angle. *Advances in Colloid and Interface Science* 113 (2005) p. 133-146.
2. R. Stacy, *Contact angle measurement technique for rough surfaces*, (2009), (PhD thesis) Michigan Technological University.
3. H. Kuiken, A single-parameter method for the determination of surface tension and contact angle, *Colloids and surfaces* 59 (1991) 129-148.

4. Y. Yonemoto and T. Kunugi, *Wettability model for various-sized droplets on solid surfaces.* Physics of Fluids 26 (2014) 082110.
5. M. Hernaiz et al., The contact angle under zero-gravity characterises nanofluids correctly, *Journal of Colloid and Interface Science*, 2019 (submitted).
6. J. Schindelin, I. Arganda-Carreras, E. Frise, V. Kaynig, M. Longair, et al., *Fiji: an open-source platform for biological-image analysis,* Nature methods 9 (2012) 676.

1st International Conference on Nanofluids (ICNf2019)
2nd European Symposium on Nanofluids (ESNf2019)
26-28 June 2019, Castelló, Spain

Effect of Nanoparticle Layer Coating on Heat Transfer Performance of Heat Pipe

T. Okawa*, M. Wang and K. Enoki

The University of Electro-Communications
1-5-1, Chofugaoka, Chofu-shi, Tokyo 182-8585, Japan

*Corresponding author: okawa.tomio@uec.ac.jp

Keywords: Heat pipe, Nanoparticle layer, Wick, Heat transfer enhancement

Abstract: In order to enhance the heat transfer performance, the inside wall of a container or a screen mesh of a cylindrical heat pipe was coated with a silica nanoparticle layer. When the screen mesh was coated, the thermal resistance decreased drastically (about 50%). This indicates that the nanoparticle layer enhanced wicking performance of screen mesh. When the container inside wall was coated, reduction of the thermal resistance was less significant but the heat pipe worked well even when the screen mesh was removed. This demonstrates that the nanoparticle layer on the wall acted as a very thin wick.

Introduction/Background: Heat pipe is a simple and efficient heat transfer device that uses continuous evaporation and condensation of working fluid [1]. Recently, it was experimentally showed that the heat transfer performance of heat pipe can be enhanced if nanometer-sized particles are dispersed in working fluid [2-5]. A main reason of the heat transfer enhancement is considered that nanoparticle deposition occurred in the heat pipe to enhance wick performance. Separately, Umehara et al. [6] showed that nanoparticle layer can easily be formed on the surface if a high-temperature body is immersed in nanofluid. The nanoparticle layer is thin, cheap and exhibits strong capillarity. It is therefore expected that nanoparticle layer is pre-coated on the wick device and/or the container inner wall, the heat transfer performance of heat pipe can be enhanced. In view of this, the nanoparticle-layer pre-coated heat pipe is fabricated and its heat transfer performance is experimentally explored in this work.

Nanoparticle Layer Formation on the Screen Mesh: A screen mesh made of brass was heated to 800 ºC in a constant temperature reservoir; it was then immersed into distilled water-silica nanofluid. The particle concentration was 0.4 kg/m^3. To form nanoparticle layer on whole surface, this process was repeated three times. The screen mesh was placed on the inner surface of a cylindrical copper container of 8 mm in outer

diameter, 0.5 mm in wall thickness, and 100 mm in length. After supplying the working fluid in the tube (the filling rate was about 15%), the two ends were closed to construct a heat pipe.

Nanoparticle Formation on the Container Inner Wall: The copper tube was covered with polyimide tape for electric insulation, wrapped helically with a nichrome wire for heating, and covered with a fluorine tape for thermal insulation. The tube was then immersed in the distilled water-silica nanofluid; alternating current was supplied to the nichrome wire to cause nucleate boiling on the inner surface of the tube. Through these procedures, a nanoparticle layer was formed on the inner surface of the copper tube. The mass of deposited nanoparticles was measured about 1.5-2 g/m^2.

Measurement of Heat Transfer Performance: An experimental apparatus used to measure the heat transfer rate is shown schematically in Fig. 1. In the figure, the left-hand-side of the heat pipe is the evaporation section and the right-hand-side the condensation section (the heat pipe was arranged horizontally). Heating and cooling were carried out using a nichrome wire heater and a fan, respectively. The heating section was thermally insulated and copper fins were set on the cooling section. The temperature measurements were conducted using type-K thermal couples at 5, 15, 25, 40, 50, 60, 75, 85 and 95 mm from the left end of the heat pipe. The electric power applied to the nichrome wire Q was set within 3-25 W. The thermal resistance of the heat pipe R was defined by R=ΔT/Q where ΔT is the temperature difference between the evaporation and condensation sections.

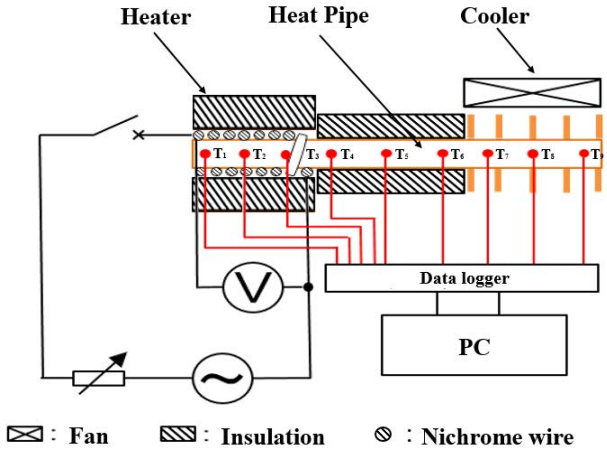

Figure 1. Schematic diagram of experimental apparatus

Results and Discussion: Figures 2(a)-(c) show the values of ΔT and R measured in the experiments. Here, the three successive letters denote the type of heat pipe as follows.

- 1st (inner surface of container): B→Bare, N→Nanoparticle layer pre-coated.
- 2nd (screen mesh): B→Bare, N→Nanoparticle layer pre-coated, X→ removed.
- 3rd (working fluid): W→Water, N→Nanofluid.

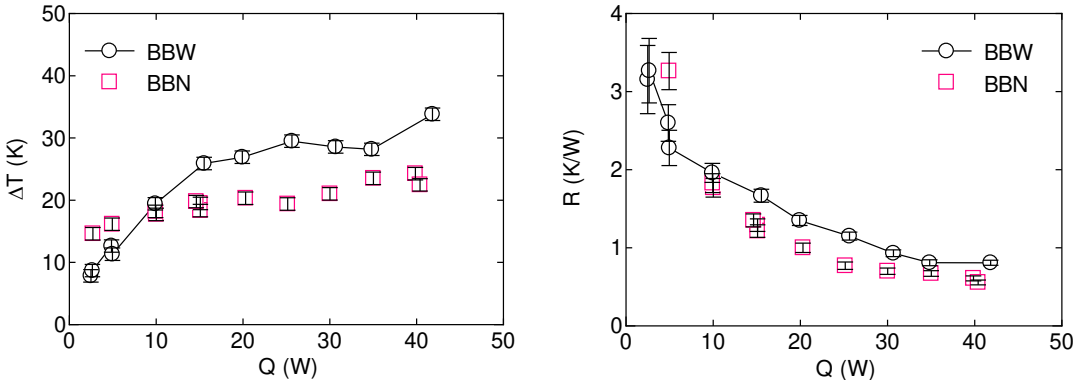

(a) Effect of working fluid

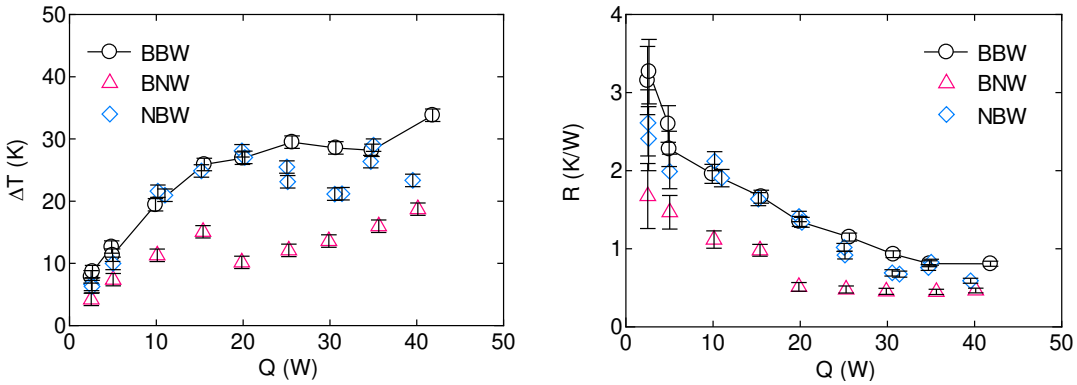

(b) Effect of nanoparticle-layer pre-coating

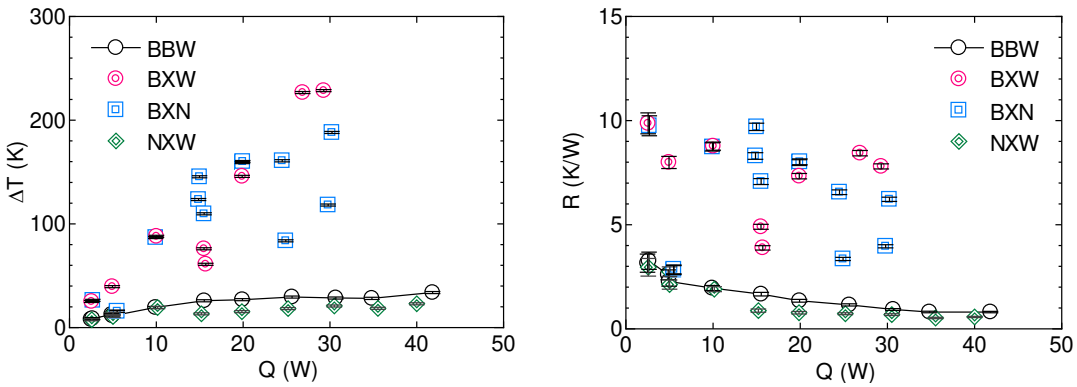

(c) Heat transfer performance when the wick device (screen mesh) was removed

Figure 2. Measurement results of heat transfer performance (error bars show the measurement errors estimated by error propagation analysis)

Figure 2(a) indicates that overall heat transfer performance of BBN is better than BBW. This is consistent with the previous studies [2-5]. Next, it can be seen in Fig. 2(b) that the

values of R for BNW is substantially smaller than those for BBW (about 50% in average), indicating that the nanoparticle layer significantly enhanced the wicking performance of the screen mesh. Reduction of R is also seen for NBW particularly when Q was high but it is less significant in comparison with BNW. The experimental results when the screen mesh was removed are presented in Fig. 2(c). For BXW and BXN, ΔT and R increased noticeably as expected since no wicking device was placed in the container. It is however interesting to note that for NXW, slight improvement in heat transfer performance can be seen in comparison with BBW. This indicates that the wire mesh can be removed since the nanoparticle layer pre-coated on the container inner wall acts as a wick. This is a preferable feature from the viewpoint of space-saving particularly for the cooling of small electronic devices since the nanoparticle layer is very thin (about 100μm in this study).

Summary/Conclusions: Effects of nanoparticle layer pre-coating on the heat transfer performance of a heat pipe were experimentally explored. Main conclusions are:

- When the nanoparticle layer was pre-coated on the wick device, the thermal resistance was reduced significantly (about 50%). Nanoparticle-layer pre-coating on a wick device in heat pipe is hence considered effective to improve the heat transfer performance through wicking enhancement.
- For the heat pipe with nanoparticle-layer pre-coating on the container inner wall, good heat transfer performance was achieved even when the wick device (screen mesh) was removed. This is considered a preferable feature in cooling of small electronic devices such as a cell-phone since the nanoparticle-layer can be regarded as a very thin wick.

Acknowledgement: This work was supported by JKA and its promotion funds from KEIRIN RACE.

References

1. A. Faghri, Review and advances in heat pipe science and technology, *Journal of Heat Transfer* 134 (2012) 123001.
2. R. Sureshkumar, S.T. Mohideen and N. Nethaji, Heat transfer characteristics of nanofluids in heat pipes: A review, *Renewable and Sustainable Energy Reviews* 20 (2013) 397-410.
3. O.A. Alawi, N.A. C. Sidik, H.A. Mohammed and S. Syahrullail, Fluid flow and heat transfer characteristics of nanofluids in heat pipes: A review, *International Communications in Heat and Mass Transfer* 56 (2014) 50-62.

4. N.K. Gupta, A.K. Tiwari and S.K. Ghosh, Heat transfer mechanisms in heat pipes using nanofluids - A review, *Experimental Thermal and Fluid Science* 90 (2018) 84-100.
5. M. Ghanbarpour, N. Nikkam, R. Khodabandeh, M.S. Toprak and M. Muhammed, Thermal performance of screen mesh heat pipe with Al2O3 nanofluid, *Experimental Thermal and Fluid Science* 66 (2015) 213-220.
6. Y. Umehara, K. Enoki, W. Liu and T. Okawa, Effect of surface properties on quenching characteristics of high-temperature body, 10th International Symposium on Measurement Techniques for Multiphase Flow, ISMTMF-R001-113, 2017.

SESSION 5
Solar Energy Applications

S5

1st International Conference on Nanofluids (ICNf2019)
2nd European Symposium on Nanofluids (ESNf2019)
26-28 June 2019, Castelló, Spain

Stability and optical analysis of carbon black thermal oil-based nanofluid as direct solar energy absorber

A. Gimeno-Furio[1*], L. Hernandez[1], N. Navarrete[1] and R. Mondragon[1]

[1]Department of Mechanical Engineering and Construction, Universitat Jaume I, Av. Vicent Sos Baynat, s/n 12071 Castelló, Spain

[*]Corresponding author: afurio@uji.es

Keywords: solar absorbers, carbon black, thermal oil, nanofluids.

Abstract: Carbon nanoparticles are very useful in solar thermal applications, since they absorb much of the solar spectrum, are cheap and have excellent optical properties. Carbon nanoparticles-thermal oil-based nanofluid was prepared using two-step method with diphenyl sulfone as surfactant to achieve that nanoparticles remain suspended even at high temperatures. The stability was studied using two Dynamic Light Scattering systems at room and high temperature and also evaluated before and after exposing the nanofluid to a thermal treatment so that conditions closer to those in real applications were replicated.

The results of this study contribute to the knowledge about these solar nanofluids stability and their promising use as an alternative to the conventional solar collectors.

Introduction/Background: Concentrated Solar Power (CSP) plants, which convert the sun radiation as heat, are widely used in applications ranging from hot water supply to large-scale electricity production. Clean energy demand is growing continuously and solar thermal processes are expected to be a potential source of energy in the future [1]. A new idea of the solar thermal collectors was described by [2], introducing the concept in which solar radiation is absorbed and transported by the same working fluid. The majority of the heat transfer fluids used (HTF) (water, glycols, oils, etc.) are transparent for the most part of the solar spectrum [3] because of that some additives can be added to the working fluid to enhance the absorption properties of it. The addition of nanoparticles appears as a potential alternative to improve the absorption properties of the heat transfer fluid. The properties that make the nanofluids an appropriate candidate for direct solar thermal energy absorption applications are the clogging and fouling avoidance when they pass through pumps and pipes [4].

Recent works have demonstrated that more promising applications of nanofluids could be utilising their optical properties, which are highly adjustable [5]. Indeed, the use of nanofluids as both solar collector and heat transfer fluids is intended to improve efficiencies and reduce costs in solar thermal systems.

One of the main obstacles when using nanofluids, is the stability of the colloids. Among others, the most common method to obtain a stable nanofluid is through the use of surfactants [6]. Usually, dynamic light scattering (DLS) technique is employed to measure the size of the nanofluid. Particle size distribution can be measured over the time and comparing the results, the stability can be determined. In this case, as carbon black (CB) nanoparticles are added to Therminol 66 thermal oil (TH66), dyphenil sulfone (DS) as surfactant has been chosen according to the literature [7].

The aim of this work is to quantitatively study the high-temperature stability of CB nanofluids for use in direct solar absorption. For that purpose, two different systems were used based on DLS technique to compare and set-up a new DLS system.

Discussion and Results: Particle size distribution of the CB thermal oil-based sample was obtained by DLS technique using two equipment and at two different temperatures (25°C and 85°C). The results obtained in both equipment are presented below at room and high temperature:

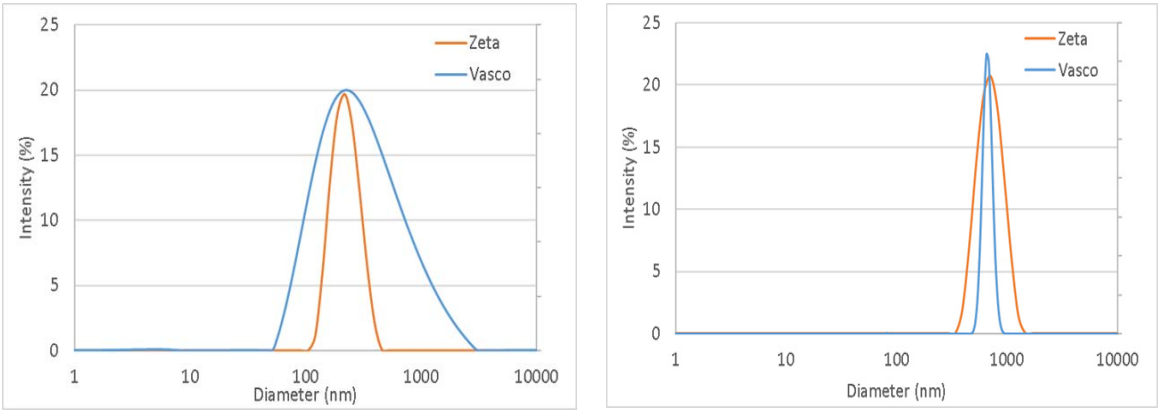

Figure 1. Particle size distribution of CB nanoparticles suspended in TH66 at room (left) and high (right) temperature in two different devices: Zetasizer Nano (orange line) and VASCO FLEX (blue line)

From the results obtained in Fig. 1, it is possible to confirm the convergence of the size results in Zetasizer and VASCO systems. However, the curves of both equipment are

centered on the same point; this value is different at room than at high temperature. It can be obtained that the higher the temperature the bigger the diameter. The fact that particle size becomes bigger with the temperature is due to the agglomeration. Nanoparticles aggregate forming clusters whose diameter is greater than that of the dispersed nanoparticles.

Consequently, in order to get a deeper study of the stability at high temperature, the sample was thermally treated at 85°C for 30 minutes in the stove. After this treatment, particle size distribution of the samples was measured again at room temperature and at 85°C. Fig. 2 clearly indicates that once the samples are thermally treated, the nanoparticles agglomerate and remain stable, without forming larger agglomerates and without settle.

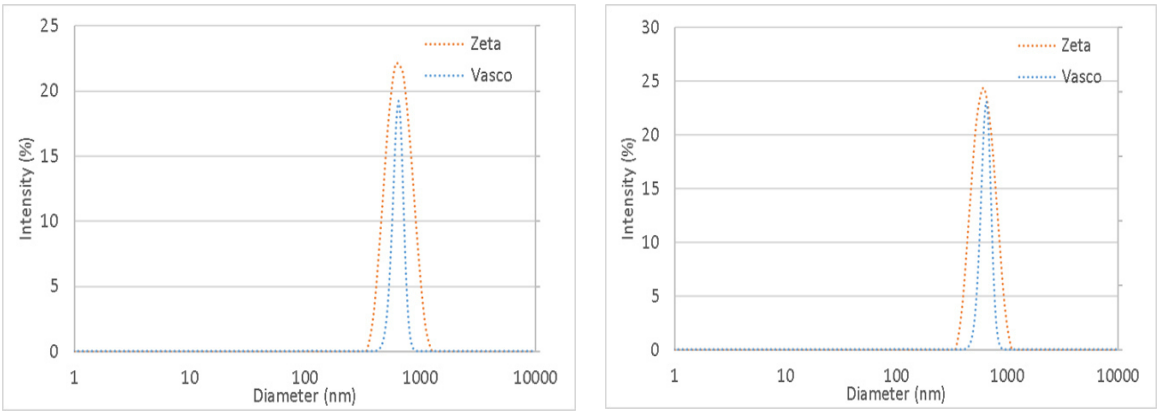

Figure 2. Particle size distribution of the thermally treated CB nanoparticles suspended in TH66 at room (left) and high (right) temperature in two different devices: Zetasizer Nano (orange line) and VASCO FLEX (blue line)

Zaverage values of each measurement have been compiled in a table to have a better understanding about the particle size.

Table 1. Zaverage of the samples before and after the thermal treatment measured at 25°C and 85°C in two different systems.

Temperature	25°C		85°C	
	Zeta	**Vasco**	**Zeta**	**Vasco**
Before thermal treatment	210	310	666	600
After thermal treatment	607	661	623	600

It is extracted that the mean size of the CB nanoparticles before being treated and measured at room temperature is around 260 nm. However, the averaged diameter after the nanofluid exposed to the thermal treatment measured at 25°C and 85°C, and when it has not been treated but measured at 85°C is around 630nm. It clearly indicates that nanoparticles have agglomerate due to the effect of the temperature.

Summary/Conclusions: In order to measure the stability of the nanofluid at different temperatures, two DLS systems were used. Particle size distribution was evaluated at room temperature with Zetasizer and VASCO FLEX, with good results since both equipment were in concordance. Afterwards, the sample was thermally treated at 85°C for 30 minutes in a stove, and its size was measured again. The results obtained were very different to those obtained with the fresh samples, then it can be concluded that the temperature play an important role when working with this nanofluid. It is also needed to remark that once the nanofluid has been treated, the clusters produce are stable with the temperature.

All the measurements before and after the thermal treatment were performed in both devices. The agreement obtained between both systems' results ensures the repeatability of this measurement.

References:

1. C. Philibert, Interactions of policies for renewable energy and climate 22 (2011)
2. J.E. Minardi, H.N. Chuang, Performance of a "black" liquid flat-plate solar collector. Sol. Energy 17 (1975) 179-183.
3. T.P. Otanicar, P.E. Phelan, J.S. Golden, Optical properties of liquids for direct absorption solar thermal energy systems. Sol. Energy 83 (2009), 969–977.
4. R.A. Taylor, P.E. Phelan, T.P. Otanicar, R. Adrian, R. Prasher, Nanofluid optical property characterization : towards efficient direct absorption solar collectors. Nano Express 6 (2011), 1-11.
5. R. Taylor, S. Coulombe, T. Otanicar, P. Phelan, A. Gunawan, Small particles, big impacts: A review of the diverse applications of nanofluids. J Appl. Phys 113 (2013) 011301.
6. W. Yu and H. Xie, A review on nanofluids: preparation, stability mechanisms and applications. J. Nanom. 2012 (2011), 1-17.
7. A. Gimeno-Furio, N. Navarrete, R. Martinez-Cuenca, J.E. Julia, L. Hernandez, Influence of high temperatre exposure on the thermal and optical properties of thermal oil-based solar nanofluids. J. Nanof. 7 (2018), 1-8.

1st International Conference on Nanofluids (ICNf2019)
2nd European Symposium on Nanofluids (ESNf2019)
26-28 June 2019, Castelló, Spain

An overview of phase change material nano-emulsions and their applications

S. Bobbo[1*], D. Cabaleiro[1,2], F. Agresti[3], S. Barison[3], S. Rossi[1], L. Fedele[1]

[1] Consiglio Nazionale delle Ricerche, ITC, Padova, Italy

[2] Dpt. Física Aplicada, Universidade de Vigo, Vigo, Spain

[3] Consiglio Nazionale delle Ricerche, ICMATE, Padova, Italy

[*]Corresponding author: sergio.bobbo@itc.cnr.it

Keywords: phase change material, nanoemulsion, slurry, encapsulation, applications.

Abstract: Phase change material nanoemulsions were largely investigated in the last years as potential heat transfer fluids. This review work aims at giving an overview of properties and potentialities of these fluids, considering their problems, some strategies to overcome them and the potential applications of these fluids in different sectors and for different temperature ranges.

Introduction/Background: Phase change material emulsions (PCMEs) or phase change slurries were largely investigated in the last years as potential heat transfer fluids [1]. They are mainly based on water, containing nano- or micro-droplets of phase change materials (PCMs), properly dispersed/encapsulated, typically by surfactants. PCMEs possess much larger energy storage capacity than currently used chilled water based systems and exploit higher thermal conductivity than bulk PCM reservoirs. Numerous formulations and preparation methods have been tested in literature and various properties have been investigated including droplet size, phase change transition characteristics, specific heat, viscosity, thermal conductivity, density, etc. Main issues in the PCMEs development are the stability with freeze-thaw cycles and mechanical shear and the subcooling, that is the PCME cooling below PCM melting point without experiencing crystallization. Various strategies to face these issues have been proposed so far. Moreover, various applications have been foreseen in different temperature ranges. This work reviews the PCME characteristics as well as the potential applications to give an overview of PCME properties and potentialities.

Discussion and Results: A PCM nanoemulsion is mainly composed by a PCM as the dispersed phase in the form of fine droplets in a carrier fluid such as water, dispersed

with the help of surfactants/emulsifiers that reduce the surface tension and can entrap/encapsulate the PCM. There can be various types of emulsions, based on PCM in water or in oil, and the properties strongly depend on droplets size, going from microemulsions (from few µm down to few hundred nm), to nanoemulsions (around or below 100 nm). Thanks to the plethora of phase change materials of different types (paraffins, sugars, alcohols, salts, etc.) and to the wide range of melting temperatures, PCM can be fruitfully dispersed in water or oils opening up numerous possible applications, having demonstrated in many cases an increase in fluid heat capacity fluid.
Various preparation methods were developed, as high-energy methods (high-shear stirring, ultrasonication, high pressure homogenization, etc.), low energy methods, where the nanoemulsions are produced as a result of a phase transition/inversion during emulsification (phase inversion temperature, emulsion inversion point, etc.), or some combined methods including both high and low energy methods. An example of nanoemulsion and of droplet morphology during phase inversion temperature is reported in Figure 1, where some spherical nano-droplets were observed before inversion and they became elongated (worm-like) nano-micelles after inversion.

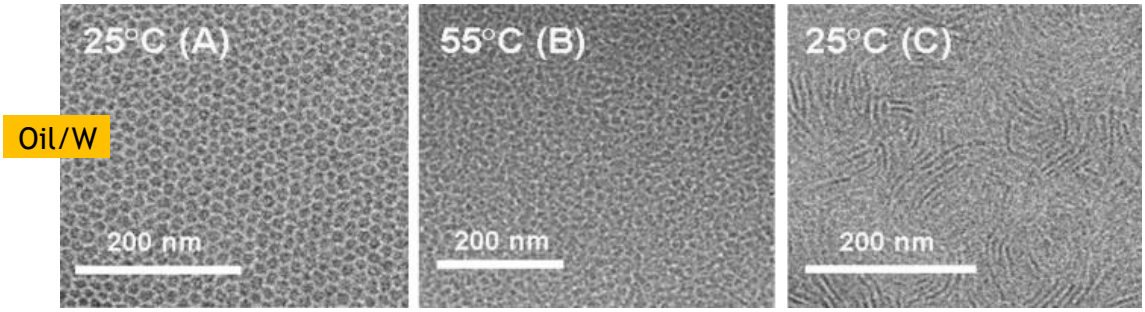

Figure 1. Cryo-TEM images of an emulsion (5% (w/w) lauryl acrylate and 7% (w/w) Brij 96V) at (A) room temperature, before inversion; (B) 55 °C, above the phase transition temperature; (C) room temperature, after inversion (from [2]).

One of main issues of PCME is their stability, which is typically investigated with time, under freeze-thaw cycles, under mechanical shear or against electrolyte charges, by DLS, visual inspection and/or turbidity. A further issue in PCME development is the subcooling. Subcooling can be reduced by using a nucleating agent. The nucleating agent and its fraction has important effect both on the melting and nucleation temperature. Various nucleating agents were investigated as similar PCM with higher melting temperature or nanoparticles of other materials as metals, metal oxides, carbon nanostructures, etc. Figure 2 shows and example of reduction of subcooling of a commercial paraffin emulsion by introducing a carbon nanostructure as nucleating agent.

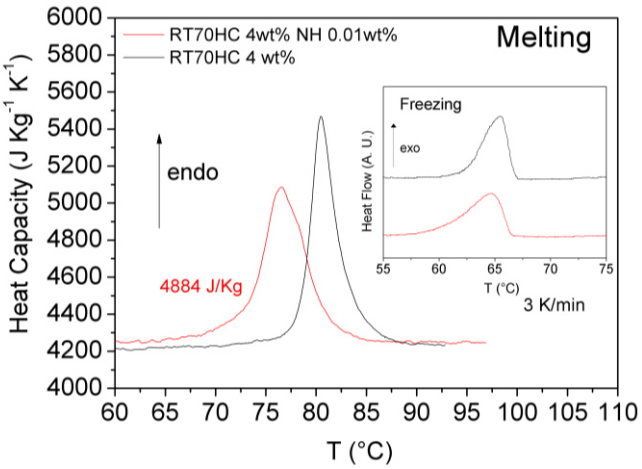

Figure 2. DSC heating profile (from [3]) of an emulsion containing 4wt% of a 70°C melting commercial paraffin (from Rubitherm) and the same with 0.01 wt% of carbon nanohorns (cooling curves in inset).

Various properties of PCME were investigated and will be illustrated, being differently influenced by PCM droplets, as isobaric heat capacity, thermal conductivity, viscosity and rheological behaviour and density. As, for example, to viscosity, typically the viscosity increases with PCM concentration and droplet size and, as a consequence, a good compromise between increase in heat capacity and in viscosity has to found.

These fluids have been so far investigated for various applications as in heating, ventilating and air conditioning (HVAC) systems [4], solar thermal storage (where various temperatures ranges between 30 and 100°C were tested), waste heat recovery and heat transfer (typically around 20, 50 or 60-65°C), intelligent building (where PCM were tested for various applications between 0 and about 90°C), etc. [5,6].

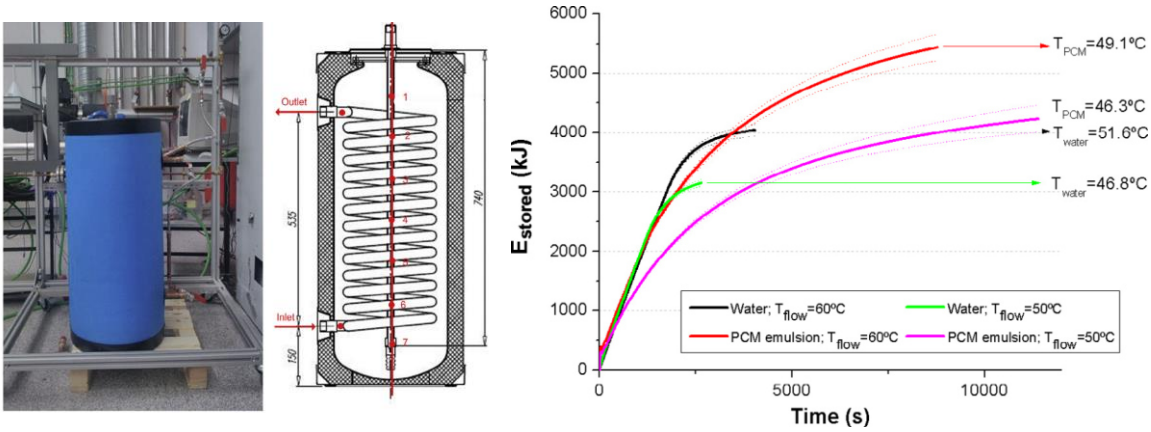

Figure 3. The tank where Delgado et al. [7] tested a paraffin (60%) in water PCME (left) and the thermal energy stored by the tank containing the PCM emulsion and by the tank containing water for different tests (right).

Figure 3 shows an example of an application studied by Delgado et al. [7] of a commercial tank with a helical coil heat exchanger and containing a low cost PCME, that was experimentally analysed as a thermal energy storage system in terms of volumetric energy density and heat transfer rate. The PCME showed an energy density 34% higher than the water tank, which makes it a promising solution.

Summary/Conclusions: An overview of properties and potentialities of PCME is given. The practical implementation of PCMEs seems feasible, but some problems must be faced before a competitive edge over conventional carrier fluids. More combined studies on stability, subcooling and viscosity are required since these three properties are somewhat related and a balance among them is essential.

References:

1. J. Shao, J. Darkwa, G. Kokogiannakis, Review of phase change emulsions (PCMEs) and their applications in HVAC systems*, Review Energ. Build.* 94 (2015) 200–217.
2. L. Spernath et al., Phase transitions in O/W lauryl acrylate emulsions during phase inversion, studied by light microscopy and cryo-TEM, *Colloids Surf. A* 332 (2009) 19–25.
3. F. Agresti, L. Fedele, S. Rossi, D. Cabaleiro, S. Bobbo, G. Ischia, S. Barison, Nano-encapsulated PCM emulsions prepared by a solvent-assisted method for solar applications, submitted to *Solar Energy Materials & Solar Cells*.
4. M. Hany Abokersh, et al., Review of the phase change material (PCM) usage for solar domestic water heating systems (SDWHS), *Int. J. Energy Res.* 42 (2018) 329.
5. S. Puupponen, A. Seppala, O. Vartia, K. Saari, T. Ala-Nissila, Preparation of paraffin and fatty acid phase changing nanoemulsions for heat transfer, *Thermochim. Acta* 601 (2015) 33–38.
6. Z. Qiu, X. Ma, P. Li, X. Zhao, A. Wright, Micro-encapsulated phase change material (MPCM) slurries: Characterization and building applications, *Renew. Sust. Energ. Rev.* 77 (2017) 246–262.
7. M. Delgado et al., Experimental analysis of a low cost phase change material emulsion for its use as thermal storage system, *Energy Conver. Manag.* 106 (2015) 201–212.

1st International Conference on Nanofluids (ICNf2019)
2nd European Symposium on Nanofluids (ESNf2019)
26-28 June 2019, Castelló, Spain

Stability and thermal properties study of 2D-metal chalcogenides-based nanofluids for concentrating solar power

P. Martínez-Merino[1*], R. Alcántara[1], T. Aguilar[1], J.J. Gallardo[1], I. Carrillo-Berdugo[1], R. Gómez-Villarejo[1], C. Fernández-Lorenzo[1] and J. Navas[1*]

[1]Departamento de Química Física, Facultad de Ciencias, Universidad de Cádiz, E-11510 Puerto Real (Cádiz), Spain

[*]Paloma Martínez-Merino: paloma.martinez@uca.es

Keywords: concentrating solar power, nanofluids, 2-D nanomaterial, liquid phase exfoliation, stability, thermophysical properties.

Abstract

Nanofluids are considered colloidal systems with improved thermophysical properties such as thermal conductivity, thermal diffusivity, heat capacity or convective heat transfer coefficient compared to conventional fluids. Accordingly, in recent years the interest of these systems has increased in many fields such as refrigerants, automotive lubricants and also as heat transfer fluid in thermosolar systems. In this work, nanofluids based in 2D nanostructures of WS_2 have been prepared by Liquid Phase Exfoliation (LPE) in order to improve the heat transfer of the thermal oil typically used in Concentrating Solar Power (CSP) plants. Results show a great stability for these nanofluids over the time and an enhancement of up to 20% in the heat transfer process. These results reveal that nanofluids prepared could improve the overall efficiency of CSP plants if they were used as heat transfer fluid.

Introduction/Background

Concentrating Solar Power (CSP) technologies are one of the renewable technologies that play a major role in solving the present and future electricity problems [1]. The main problem of these technologies is its elevated cost [2]. One of the research lines in this topic is the replacement of the heat transfer fluid used in CSP plants by nanofluids to improve the overall efficiency of CSP plants. Taylor et al. [3] suggested the idea of using nanofluids in absorber tubes of solar collectors, resulting in an increase of 5-10% in nanofluid efficiency compared to conventional fluids. Sokhansefat [4] and Mwesigye [5] investigated the improvement of heat transfer in a cylinder-parabolic collector tube using a synthetic oil with Al_2O_3 nanoparticles, showing an improvement in thermal efficiency of

7% with the use of nanofluid. Most of the works found in the literature use water or ethylene glycol as base fluid, but there are few studies of nanofluids based on the eutectic mixture of diphenyl and biphenyl oxide typically used in CSP plants. In this work, this eutectic mixture will be called HTF. In addition, one of the challenges is to get nanofluids stable over time. With this purpose, in this work, nanofluids based on 2D nanostructures have been prepared since the surface area of these nanostructures is higher than that of the nanostructures with spherical morphology [6]. WS_2 nanomaterial is used because it has a high thermal conductivity (34.5 $Wm^{-1}K^{-1}$) [7]. Liquid Phase Exfoliation method is used to obtain nanofluids and Polyethylene glycol (PEG) is used as a surfactant to get a great stability. A study was carried out changing PEG concentration and ultrasonic time. Morphological characterization was performed by Transmission Electron Microscopy (TEM). The TEM analysis was performed using a JEM-2100F microscope supplied by Jeol©. The stability was studied by UV-Vis spectroscopy and particle size evolution for 15 days. Thus, UV-Vis spectra were recorded between 400 and 850 nm, and the extinction coefficient was evaluated at 629 nm, where a band assigned to WS_2 is found. Particle size measurements were performed using the dynamic light scattering (DLS) technique. Finally, thermal properties were studied to evaluate the efficiency of the nanofluids in CSP plants. Isobaric specific heat measurements were performed using the temperature-modulated differential scanning calorimeter (TMDSC) technique, using a calorimeter supplied by TA Instruments©, model Q-20. Thermal conductivity was measured using the Laser Light Flash Technique (LFA 1600 equipment, supplied by Linseis Thermal Analysis©).

Results and Discussion

TEM images (Figure 1) show that the structures present in the nanofluids are nanosheets with lateral dimensions between 50-80 nm, which means that exfoliation process has been effective. Nanofluids present high values of extinction coefficient which means that the radiation absorption capacity of these fluids is better than conventional fluids used in CSP (Figure 2). The analysis of extinction coefficient revealed a slight decrease during the first three days in all nanofluids, after which the nanostructures remain stable in the fluid. In turn, the highest values of extinction coefficient are observed in the nanofluids prepared with higher PEG concentration, which indicates that more material has been exfoliated and therefore the exfoliation process was more effective in these cases. The particle sizes measured by DLS are around 200-230 nm during the 15 days of characterization. This behaviour can be related to low levels of agglomeration

and sedimentation. Thus, the analysis of extinction coefficient and particle size show a high stability for these nanofluids, which is one of the great objectives for its application.

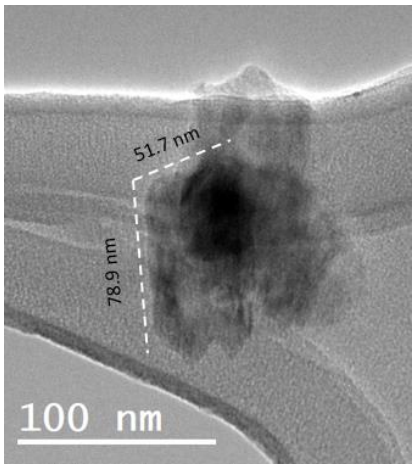

Figure 1. TEM images of WS_2 nanosheets

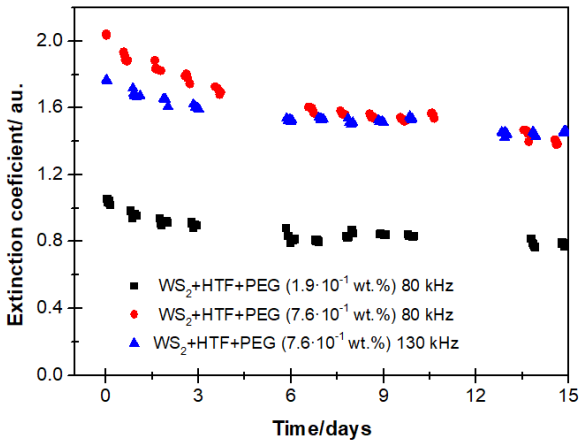

Figure 2. Evolution with time of the extinction coefficient values at λ=629 nm from UV-Vis spectra

Regarding to thermal properties, the heat transfer enhancement was determined using the Dittus-Boelter correlation (Figure 3) which considers that the coefficient of heat transfer enhancement can be expressed as a function of the density, conductivity, specific heat and viscosity of the nanofluid and base fluid:

$$h_{nf}/h_{bf} = \left(\frac{\rho_{nf}}{\rho_{bf}}\right)^{0.8}\left(\frac{k_{nf}}{k_{bf}}\right)^{0.6}\left(\frac{C_{p(nf)}}{C_{p(bf)}}\right)^{0.4}\left(\frac{\mu_{nf}}{\mu_{bf}}\right)^{-0.4}$$

It is considered that the efficiency is improved when $h_{nf}/h_{bf} > 1$. Results show improvements of heat transfer around 20% in all nanofluids compared to the base fluid.

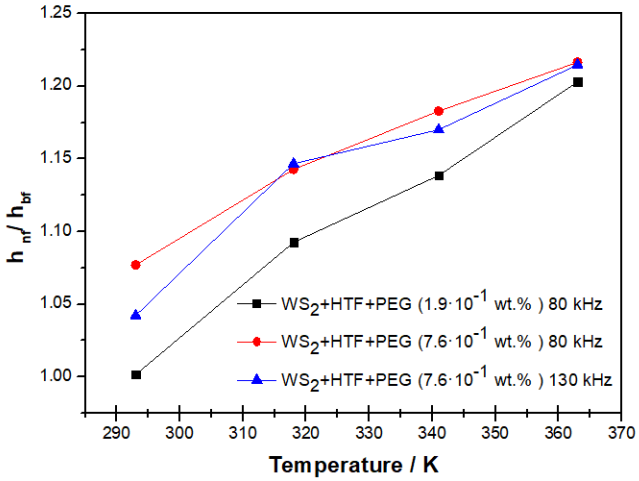

Figure 3. Ratio of heat transfer coefficient

Conclusions

In this work, nanofluids have been prepared based on 2D nanostructures of WS_2. It is observed that the best conditions to carry out the exfoliation process and obtain stable nanofluids with improved thermal properties are the surfactant concentration and ultrasonic frequency. The thermal properties of the organic oil typically used in CSP is improved by 20% with the presence of 2D nanostructures of WS_2. These results reveal that these nanofluids could be used in CSP plants.

References:

1. D. A. Baharoon, H. A. Rahman, W. Z. W Omar, S. O. Fadhl, Historical development of concentrating solar power technologies to generate clean electricity efficiently – A review, *Renewable and Sustainable Energy Reviews*, 41 (2015) 996-1027.
2. G. R. Timilsinaa, L. Kurdgelashvili, P. A. Narbel, Solar energy: Markets, economics and policies, *Renewable and Sustainable Energy Reviews*, 16 (2012) 449-465
3. R. A. Taylor, P. Phelan, T.P. Otanicar, C.A. Walker, M. Nguyen, S.Trimble, R. Prasher, Applicability of nanofluids in high flux solar collectors, *Journal of Renewable and Sustainable Energy,* 3 (2011) 023104.
4. T. Sokhansefat, A. B. Kasaeian, F. Kowsary, Heat transfer enhancement in parabolic trough collector tube using Al_2O_3/synthetic oil nanofluid, *Renewable and Sustainable Energy Reviews*, 33 (2014) 636-644.
5. A. Mwesigye, Z. Huan, J. P. Meyer, Thermodynamic optimisation of the performance of a parabolic trough receiver using synthetic oil–Al_2O_3 nanofluid, *Applied Energy*, 156 (2015) 398-412.
6. J. Navas, P. Martínez-Merino, A. Sánchez-Coronilla, J. J. Gallardo, R. Alcántara, E. I. Martín, J. C. Piñero, J. R. León, T. Aguilar, J. Hidalgo Toledo and C. Fernández-Lorenzo, MoS_2 nanosheets vs. nanowires: preparation and a theoretical study of highly stable and efficient nanofluids for concentrating solar power, *Journal of Materials Chemistry A*, 6 (2018) 14919-14929.
7. R. Yan, J. R. Simpson, S. Bertolazzi, J. Brivio, M. Watson, Thermal conductivity of monolayer molybdenum disulfide obtained from temperature-dependent, Raman spectroscopy, *ACS Nano*, 8 (2014) 986-993.

1st International Conference on Nanofluids (ICNf2019)
2nd European Symposium on Nanofluids (ESNf2019)
26-28 June 2019, Castelló, Spain

Influence of two carbon-based nanosheets on the optical properties of nanofluids

E. Sani[1*], J. P. Vallejo[2], L. Mercatelli[1], M.R. Martina[1], D. Di Rosa[1,3], A. Dell'Oro[4], L. Lugo[2]

[1] CNR-INO National Institute of Optics, Largo E. Fermi, 6, I-50125 Firenze, Italy

[2] Departamento de Física Aplicada, Facultade de Ciencias, Universidade de Vigo, E-36310 Vigo, Spain

[3] Department of Energy, Systems, Territory and Constructions Engineering (D.E.S.T.eC.), University of Pisa, Largo L. Lazzarino, I-56122 Pisa, Italy

[4] INAF, Astrophysical Observatory of Arcetri, Largo E. Fermi 5, I-50125 Firenze, Italy

[*]Corresponding author: elisa.sani@ino.cnr.it

Keywords: Graphene nanoplatelets, functionalization, colloidal stability, optical absorption, nonlinear optical properties, solar energy

Abstract: The knowledge of stability and optical properties of nanofluids is needed for many applications, like their use in future solar energy exploitation systems. This work reports on the comparative study of two different sets of aqueous nanofluids, consisting in the dispersion of polycarboxylate chemically modified graphene nanoplatelets (P-GnP) and sulfonic acid-functionalized graphene nanoplatelets (S-GnP). The suspensions revealed a good long-term stability and positive light extinction properties. Moreover, non-linear optical behaviour under high input intensities was determined.

Introduction/Background: Energy is one of the most appealing application fields of nanofluids. In particular, dark nanofluids are considered promising for solar energy exploitation. Among the large variety of nanoparticles and base fluids which have been investigated in the literature, the family of carbon-based nanostructures has emerged as particularly promising. Graphene is one of most intriguing carbon allotropes [1]. Graphene nanoplatelets or nanosheets consist of small flakes of several-layer staked graphene that partially inherit the good properties of graphene with a much lower production cost [2]. Graphene nanoparticles are naturally hydrophobic. They can be stably suspended in water after chemical modifications of their surface, e.g. by oxidation or by different types of functionalization [3,4].

In this work, we report on the comparative characterization of optical properties of two sets of water-based nanofluids composed by different functionalized graphene

nanoplatelets. These suspensions were characterized through a stability analysis based on zeta potential and dynamic light scattering (DLS) measurements. Then, we focused on optical properties both at low and high input energies.

Discussion and Results: Polycarboxylate chemically modified graphene nanoplatelets, P-GnP, and Sulfonic acid-functionalized graphene nanoplatelets, S-GnP, were suspended in Milli Q-grade water, at nanoadditive concentrations of 0.005 wt%, 0.025 wt% and 0.05 wt%. The size and morphology of the nanoadditives were characterized by transmission electron microscopy (TEM). The stability of the dispersions was investigated by zeta potential and dynamic light scattering analyses. Optical properties of nanofluids were investigated both in linear conditions and under high intensity laser irradiation.

Figure 1a shows the spectral extinction coefficient of both nanodditive types at the same 0.025% concentration. The same plot also includes the extinction coefficient of pure water, for reference. We can notice that both nanoadditives considerably increase the transmittance with respect to the pure base fluid. For the same values of nanopowder loading, the extinction coefficient is considerably higher for P-GnP nanofluids than in S-GnP nanofluids in the whole investigated wavelength range. The shape of the UV plasmonic peak and of its tail appear different for the two samples according to the different functionalization. The evidenced spectral features were found extremely important for sunlight absorption, as shown in Fig. 1b, where the sunlight extinction fraction (EF) is plotted. It corresponds to the fraction of incident sunlight *I(λ)* [5] which is extinct in the fluid after a propagation path of length x, and it is given by the expression [6, 7]:

$$EF(x) = 1 - \frac{\int_{\lambda_{min}}^{\lambda_{MAX}} I(\lambda) \cdot e^{-\mu(\lambda)x} d\lambda}{\int_{\lambda_{min}}^{\lambda_{MAX}} I(\lambda) d\lambda}$$

where $\mu(\lambda)$ is the spectral extinction coefficient and λ_{min} and λ_{MAX} are the minimum and maximum wavelength, 300 and 2500 nm, respectively.

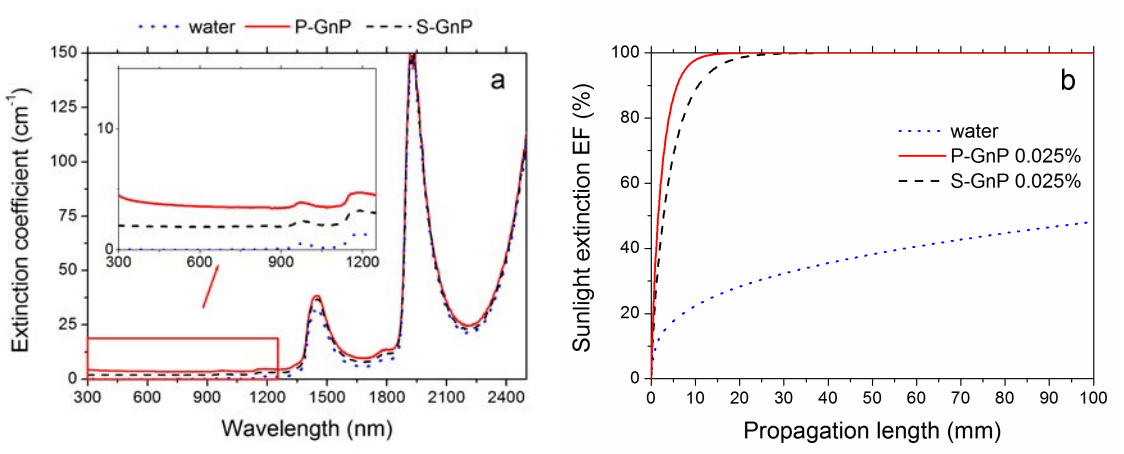

Figure 1. (a) Spectral extinction coefficient of the 0.025 wt% nanofluids from 300 to 2500 nm wavelength; (b) Sunlight extinction fraction for the same samples, as a function of the path length of sunlight inside the nanofluid.

Figure 2 shows the energy measurements for the lowest investigated concentrations of both nanofluid types at the wavelength of 355 nm. Similar trends were obtained at the other test wavelengths (532 and 1064 nm). We can appreciate a marked nonlinear behaviour. For all experiments, the P-GnP samples show both the lowest starting linear transmittance and the most pronounced nonlinearity.

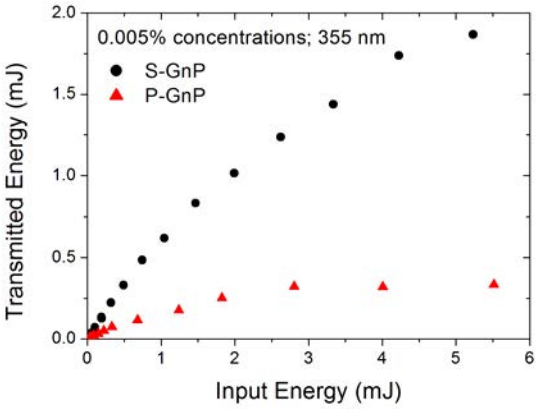

Figure 2. Transmitted energy as a function of the incident energy at the lowest concentration and under 355 nm light irradiation, for both functionalized graphene nanoplatelet types.

Summary/Conclusions: Two set of different suspensions in water, based on polycarboxylate chemically modified graphene nanoplatelets (P-GnP) and Sulfonic acid-functionalized graphene nanoplatelets (S-GnP) were tested at three different concentrations (0.005 wt%, 0.025%wt and 0.05 wt%). Dispersions, especially of P-GnP, showed a good

long-term stability. We evaluated the potential of samples for direct solar absorber applications, obtaining a high sunlight absorption, with some differences among the samples connected to the concentration and to the different functionalization of nanoadditives. The nonlinear optical measurements evidenced a non-linear behaviour for both nanoadditive types and at the three test wavelengths (ultra-violet, visible, and near-infrared), demonstrating appealing broadband characteristics. These results open interesting perspectives for the further application of these nanofluids in solar vapor generation and solar desalination.

Acknowledgements: This work was partially supported by EU COST Action CA15119: Overcoming Barriers to Nanofluids Market Uptake (NANOUPTAKE) in the framework of the Short Term Scientific Mission program. This work was also partially supported by "Ministerio de Economía y Competitividad" (Spain) and FEDER program through ENE2014-55489-C2-2-R and ENE2017-86425-C2-1-R projects. J. P. V. acknowledges FPI Program of "Ministerio de Economía y Competitividad". Thanks are due to Mr. M. D'Uva and Mr. M. Pucci (INO-CNR) for technical assistance.

References:

1. A.K. Geim and K.S. Novoselov, The rise of graphene, *Nature Materials* 6 (2007) 183.
2. E. Sani, J. P. Vallejo, D. Cabaleiro, and L. Lugo, Functionalized graphene nanoplatelet-nanofluids for solar thermal collectors, *Solar Energy Materials and Solar Cells* 185 (2018) 205.
3. Y. Si and E. T. Samulski, Synthesis of Water Soluble Graphene, *Nano Letters* 8 (2008) 1679.
4. S. Park, J. An, R. D. Piner, I. Jung, D. Yang, A. Velamakanni, S. T. Nguyen, and R. S. Ruoff, Aqueous Suspension and Characterization of Chemically Modified Graphene Sheets, *Chemistry of Materials* 20 (2008) 6592
5. Standard Tables for Reference Solar Spectral Irradiances: Direct Normal and Hemispherical on 37° Tilted Surface, Active Standard ASTM G173. ASTM G173 - 03 (2012).
6. E. Sani, L. Mercatelli, S. Barison, C. Pagura, F. Agresti, L. Colla, and P. Sansoni, "Potential of carbon nanohorn-based suspensions for solar thermal collectors," Solar Energy Materials and Solar Cells 95 (2011) 2994.
7. E. Sani, S. Barison, C. Pagura, L. Mercatelli, P. Sansoni, D. Fontani, D. Jafrancesco, and F. Francini, "Carbon nanohorns-based nanofluids as direct sunlight absorbers," Optics Express 18 (2010) 5179.

1st International Conference on Nanofluids (ICNf2019)
2nd European Symposium on Nanofluids (ESNf2019)
26-28 June 2019, Castelló, Spain

Experimental study of photothermal boiling in graphite nanofluid

P.G. Struhalin[1], P. Kosinski[2], V. Popsueva[3], K.V. Kutsenko[1] and B.V. Balakin[1,3*]

[1]NRNU Moscow Engineering Physics Institute, Russia, Inst. Nucl. Phys. Eng., Moscow, Kashirskoe sh.31

[2]University of Bergen, Dpt. Phys. Tech., Norway, Bergen, Allegaten 55

[2]Western Norway University of Applied Sciences, Dpt. Mech. Mar. Eng., Norway, Bergen, Inndalsveien 28

[*]Corresponding author: Boris.Balakin@hvl.no

Keywords: solar steam, direct absorption collector, nanofluid, graphite

Abstract: The process of nanoparticle-assisted solar evaporation has already found applications for disinfection and desalination. In this paper, we present experimental data for a photo-thermal system with a continuous production of solar steam, where the condensate is recycled back into the process. The maximum thermal efficiency was 54% at 2.0% particle concentration.

Introduction/Background: Although the idea of radiative evaporation of nanofluids is relatively straightforward, the process was firstly established *in-situ* only less than a decade ago [1]. Since that time, there have been only a few subsequent studies (e.g. [2]), which addressed various technical uncertainties of the process. The nanofluid stability, condensate recyclability and toxicity of the steam are among the important problems, which limit the use of the solar steam for different industrial applications. There is a certain progress observed in this direction at the lab-scale, where numerous experiments are performed in order to screen the nanofluid composition. The objective of these studies is to optimize the process for a simplified standalone nanofluid batch.

In our experiments the nanofluid was produced using a two-step method, sonicating graphite nanoparticles, dispersed in distilled water, in an ultrasound bath. The sample size was 300 ml and the concentration of the nanoparticles was in the interval 0.1--14.0 % wt. The nanoparticles were produced via fine grinding of 1-mm grains of MPG-7 graphite powder [3] using the ball mill. The static light scattering (SLS) test of the nanofluid sample (ANALYSETTE NanoTec Fritsch 22) resulted in an average particle

size below 2 μm. The nanofluid was evaporated under irradiation of three light sources 400 W Osram with radiant heat flux q = 12 W/m^2.

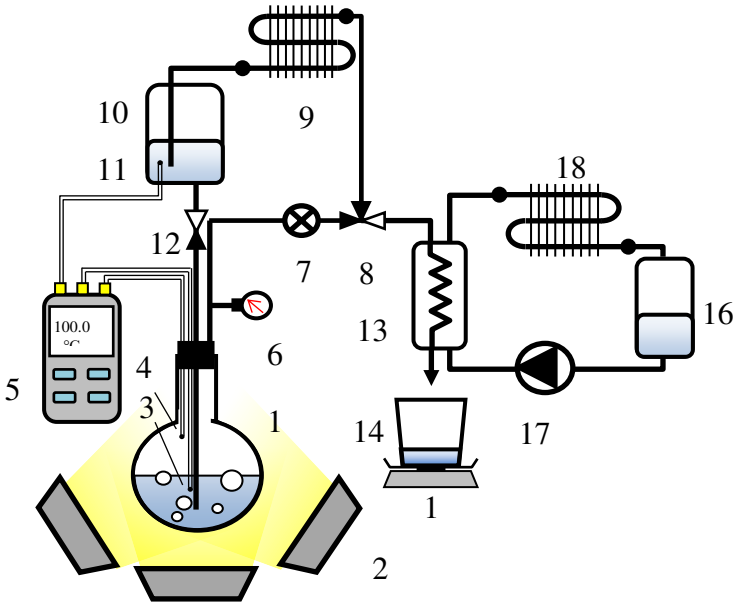

Figure 1. A schematic description of the experiment

The experimental system, shown in Fig. 1, consisted of two closed lines. The main continuous-operation line, included 500 ml transparent flask of borosilicate glass 1, closed at the top with a plug. The plug had several ports for: the steam intake line, the condensate return line and two sensor line openings. The steam that was produced in the flask, went through a vertical pipe section and further condensed in the air radiator 9. The condensate was directed to an expansion tank 10, open to the atmosphere. The condensate recycled back to the boiling nanofluid due to the hydrostatic pressure in the condensate tank, located 1.5 m above the flask. The return line was equipped with the check valve 12. The second line, opened with the directional valve 8, was used to take samples of condensate. In this line we placed a spiral pipe-in-pipe heat exchanger 13 for rapid condensation of steam, where forced convection of cold water was established by pump 17. The cooling water was taken from tank 16 and cooled in radiator 18. The measurement system consisted of: manometer 6, thermocouples 3, 4, 11, precision scale 15 and flow meter 7. All the pipes were thermally insulated.

Discussion and Results: At the beginning of the experiments we experienced a short start-up phase of around 20 min during which the recirculation was unstable. This was due to condensation of steam in the pipes, initially present at ambient condition. When the lines were heated, the system came to a steady state with a continuous recirculation

of condensate back into the process. The experimental condition was stable for longer than five hours.

In Fig. 2 (left) we plot the flow rate of the nanofluid-produced steam against the concentration of nanoparticles. As it follows from the plot, there is a detectable maximum of steam generation at particle concentration close to 1%. For lower concentrations, the steam flow rate was less due to the lower particle surface absorbing the radiant heat. On the other hand, an increase of the concentration above the optimum reduced the optical depth of the system and so enhanced the radiative thermal losses.

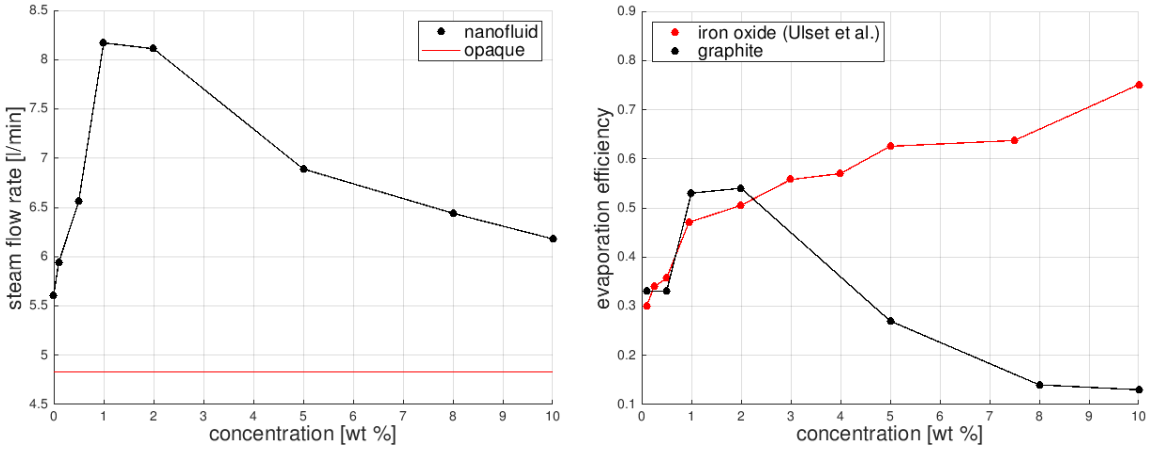

Figure 2. Steam generation (left) and evaporation efficiency (right) dependent on particle concentration

The steam generation results are also compared to the data from a supplementary study, where the outer surface of the flask was painted in black so that it became totally opaque (emissivity ~ 0.8). As it follows from the experimental results for pure water, the nanoparticle-assisted photothermal steam generation is in average 40% more intensive than conventional boiling at the glass surface.

Further, the SLS analysis of the nanofluid samples was performed and revealed that the particle size for the freshly produced nanofluid was below 2.0 μm, while the particles agglomerated after the boiling up to 5 μm. The SLS study of the steam condensate did not point to existence of nanoparticles there.

The evaporation efficiency, given as the ratio of the amount of heat, used for evaporation of water from the nanofluid, to the in-coming heat, is shown in Fig. 2 (right) for different nanoparticle concentrations. The last quantity was calculated from the temporal history of nanofluid temperature in the flask during the start-up. As it comes from the figure, the maximum of the photothermal performance is shifted as less heat is absorbed in the nanofluid at 2% than at 1%. The maximum efficiency was 54%; the photothermal boiling

was therefore more efficient at low concentrations than for the iron oxide nanofluid, considered in our previous work [4]. The produced "luminate" steam was capable to operate a small-scale model turbine, mounted in a by-pass line (not shown in Fig. 1).

Summary/Conclusions: In this paper, we demonstrate the possibility to maintain the process of photothermal steam generation from the graphite nanofluid in a closed recirculate laboratory system. The maximum efficiency of the process was 54% at 2% of the particles in the system, which was more efficient than the process of steam generation for a conventional, opaque "solar" receiver. The steam was free of the nanoparticles. These results demonstrate that the process of photothermal boiling in nanofluids could be potentially utilized in energy technology.

Acknowledgments: This study was supported by Russian Science Foundation (project No. 17-79-10481).

References:

1. O. Neumann, A.S. Urban, J. Day, S. Lal, P. Nordlander and N.J. Halas, Solar vapour generation enabled by nanoparticles, *ACS Nano* 7 (2013) 42–49.
2. G. Ni, N. Miljkovic, H. Ghasemi, X. Huang, S.V. Boriskina, C.-T. Lin, J. Wang, Y. Xu, M.M. Rahman, T.J. Zhang and G. Chen, Volumetric solar heating of nanofluids for direct vapor generation, *Nano Energy* 17 (2015) 290–301.
3. V. Chebotarev, I. Fomin, R. Pavlichenko, A. Skibenko, V. Tereshin, V. Vojtsenya, The prospects of using carbon-graphite materials as construction elements of the microwave plasma diagnostic in a fusion reactor, *Journal of Nuclear Materials* 212-215 (1994) 1157 – 1162.
4. E.T. Ulset, P. Kosinski, Y. Zabednova, O.V. Zhdaneev, P.G. Struchalin and B.V. Balakin, Photothermal boiling in aqueos nanofluids, *Nano Energy* 50 (2019) 339-346.

1st International Conference on Nanofluids (ICNf2019)
2nd European Symposium on Nanofluids (ESNf2019)
26-28 June 2019, Castelló, Spain

Single slope solar still productivity enhancement using phase change material and copper oxide (CuO) nanoparticle

Varun Kumar Sonker[1*], Arnab Sarkar[1], Jyoti Prasad Chakraborty[2]
[1]Department of Mechanical Engineering, Indian Institute of Technology (B.H.U.),
[2]Department of Chemical Engg. & Tech., Indian Institute of Technology (B.H.U.),
Varanasi, UP 221005, India
[*]varunkrs.rs.mec15@itbhu.ac.in

Keywords: Solar distillation, Phase change material, Nanoparticles.

Abstract: An improvement in the quality of heat transfer rate in the basin of solar still stores latent heat as a thermal energy enhances the efficiency of solar still. In this study, nanoparticles were mixed in lauric acid as a phase change material (PCM) to increases the thermal conductivity of the latter compared to the base material. The mixing of nanoparticles with the lauric acid changes the thermophysical properties of the used lauric acid. The thermophysical properties as density, viscosity and thermal conductivity showed increasing value in contrast to the specific heat where it reduced relatively. Three observation (without pcm, with pcm and pcm with nanoparticles) were done on single slope solar still to study the effect of distillation productivity. The mixing of nanoparticles to pcm increased the rate of heat transfer, resulting in higher distillate.

Introduction: Now a day the provision of pure drinking water is becoming a challenging issue in many areas of the world. In arid and urban areas, drinking water is very scarce and living of a human being in these areas strongly depends on how such water can be made available. Solar distillation has been in practice for a long time. In 15th century solar radiation exposed for water heating, evaporate and condensate [1]. In 16th century, the first documented work on solar still was done by Arab Alchemist [2]. In 1870, the first American patent on solar still was granted for experimental work of Wheelers and Evans [3]. After two years in 1872, an engineer from Sweden namely was Carlos Wilson, designed and built the first large solar distillation plant in Las Salinas, Chile for large-scale distilled water production [4]. In 1970 Talbert et al. Presented the historical background of solar still [5] and Delyannis reviewed the major plant of solar still around the world in 1973 [6]. For instance, nanoparticles have been used in thermal application because they have high specific heat, high thermal conductivity, and high thermal absorptivity especially at low temperature [7].

Discussion and Result: The schematic and vivid description of the single slope solar still is shown in fig (a) with experimental setup in fig (b) respectively. Copper cylinder loaded pcm are shown in fig (c) and fig (d) shows the proper mixing of nanoparticle in lauric acid. The pcm loaded copper cylinder were placed in basin of solar still at proper distance. Six copper cylinders were constructed with 7 cm diameter and 7 cm height. Each copper cylinder has to allow filling with lauric acid as thermal energy storage with 1% weight of pcm sealed with high temperature rubber cork. The experiments have been conducted in the month of November in the time duration of 09.00 am to next day morning (08.00 am). The hourly variations of temperature were noted by using PT100 thermocouples. Also, the solar intensity in W/M^2 through solar power meter, relative humidity (%) by hygrometer and distillate have been measured. Commercial grade of lauric acid used as latent heat storage material because of wide range of availability and low cost. The solar radiation is transmitted through the glass cover and it is absorbed by the pcm and basin. Part of the energy absorbed by the basin is transmitted by the convection to the basin water.

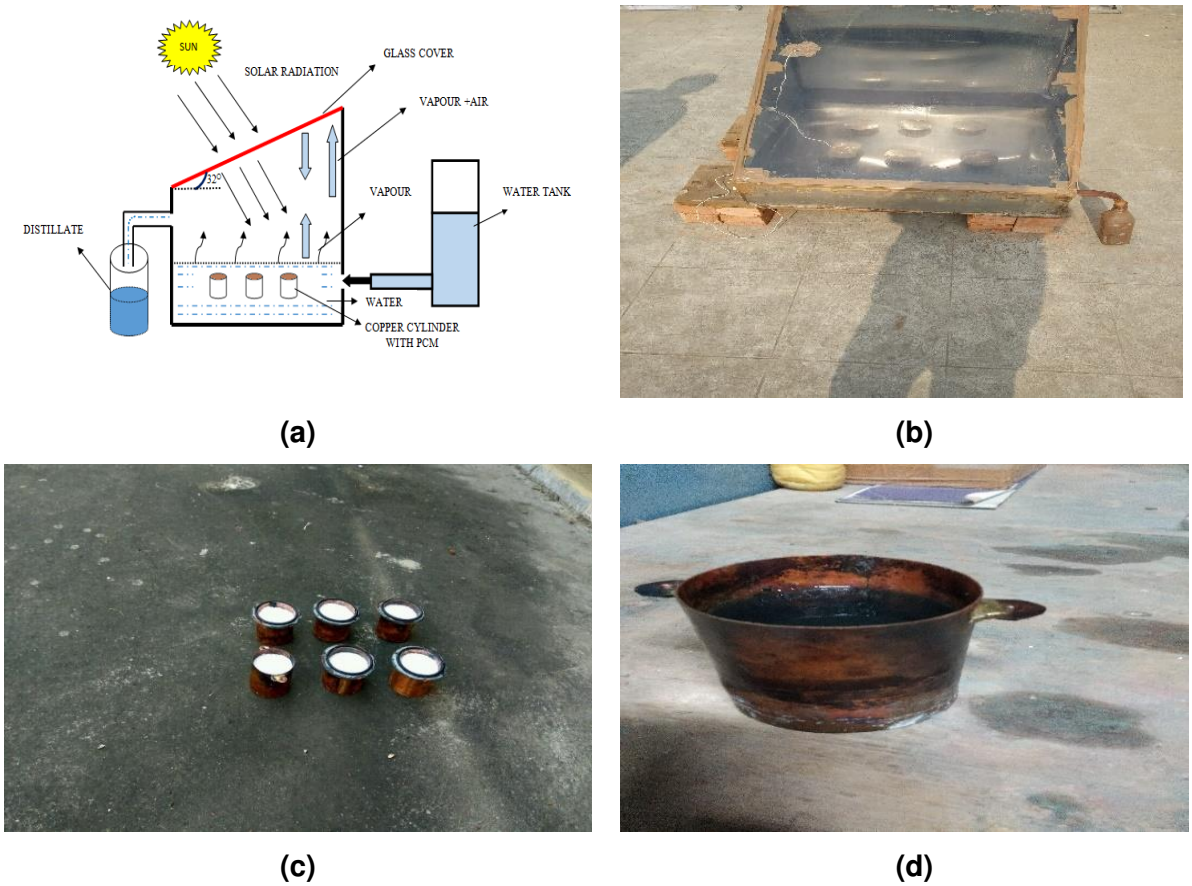

Figure 1. (a) Schematic diagram of experimental setup (b) Single slope solar still (c) Copper cylinder loaded with PCM (d) Mixing of PCM with nanoparticle

As the copper cylinder are heated. Heat is first stored as a sensible heat until the pcm reaches its melting point. At this time, pcm starts to melt and after complete melting of the pcm, the heat will be stored in the melted pcm as a sensible heat. After the sunset, when the solar radiation decrease, the solar still components start to cool down and the liquid pcm transfers heat to the basin liner and from the latter to the basin water until the pcm completely solidified. The pcm act as a heat source for the basin water during low intensity of solar radiation as well as during the night; consequently, the solar still continues to produce pure water after sunset even thin layers of basin water.

Table 1. Thermo-physical properties of phase change material (PCM)

Material properties	Lauric acid ($CH_3(CH_2)_{10}COOH$)
Melting temperature, ^{0}c	42-46 ^{0}c
Latent heat of fusion kj/kg	178
Solid density, kg/m^3	862
Thermal conductivity, W/m ^{0}c	0.16
Specific heat capacity, kj/kg ^{0}c	2.10

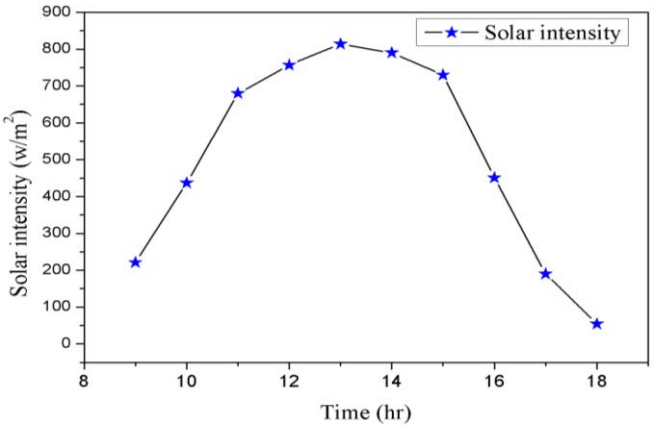

(a)

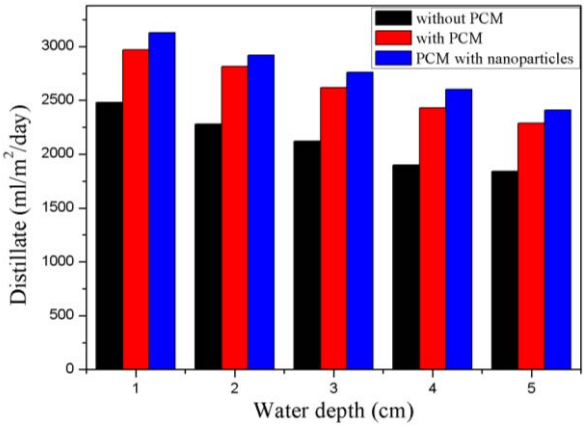

(b)

Figure 2. (a) Solar intensity with time and (b) Distillate at different water depth

The yield of single slope solar still was investigates experimentally for Varanasi city at Uttar Pradesh, India. The parameters that effects the distillate as the solar intensity has been shown in fig 2(a) and fig 2(b) shows pure water productivity per day with simple solar still, solar still with pcm and coupled with nanoparticles. The thermophysical properties of pcm also depicted in table 1.

Conclusion: In this research, work, lauric acid and nanoparticles combination were added to a single slope solar still to find their impact on distillate. The thermophysical properties of the mixed nanoparticles with lauric acid was investigated and evaluated. We found that simple single slope solar still daily productivity was 2.48 Litre/m^2/day and with heat storage, daily productivity was 2.97 Litre/m^2/day, while addition of nanoparticles in pcm found the maximum distillate 3.13 Litre/m^2/day at different water depth in same climatic conditions. However, latent and sensible heat storage in the pcm from sunshine to until sunset and then these energies are returned to the distillation system resulting in the better productivity. Increased thermal conductivity of pcm added with nanoparticles significantly enhances distillate.

References:

1. Giorgio Nebbia and Gabriella Nebbia Menozzi, Early experiments on water desalination by freezing, Desalination, 5(1) (1968) 49–54.
2. Augustin Mouchot, La Chaleur solaire et ses Applications industrielles Solar Energy — The French Connection part one, 1869.
3. Wheeler NW, Evans WW. Evaporating and distilling with solar heat. US Patent No. 102.633; 1870.
4. Harding J. Apparatus for solar distillation. Proc Inst Civil Eng, London 1883;73:284–8.
5. S. Talbert, J. Eibling and G. Lof, Manual on Solar Distillation of Saline Water, US Department of the Interior, OSW, R&D, Report No. 546, 1970.
6. A.A. Delyannis, Solar stills provide an island's inhabitants with water, Sun at Work, 10(1) (1965).
7. M.J. Biercuk, M.C. Llaguno, M. Radosavljevic, J.K. Hyun, A.T. Johnson, Carbon nanotube composites for thermal management, Appl. Phys. Lett. 80 (2002) 2767–2769, http://dx.doi.org/10.1063/1.1469696.

1st International Conference on Nanofluids (ICNf2019)
2nd European Symposium on Nanofluids (ESNf2019)
26-28 June 2019, Castelló, Spain

Rheology and microstructure of silica nanoparticle suspensions in nitrate molten salts

A. DeFilippo[1], M. Zurita[2*], M. Durth[1] and S. Fereres[1*]

[1]Abengoa, Energía Solar 1, 41014, Seville, Spain

[2]Universidad Loyola Andalucia, Energía Solar 1, 41014 Seville, Spain

[*]Corresponding author: sonia.fereres@abengoa.com, mzurita@uloyola.es

Keywords: Nanofluids, Molten Salts, Aggregation, Viscosity.

Abstract: The rheological response of silica nanoparticle suspensions in solar salt has been experimentally characterized in a parallel plate viscometer. The measured viscosity dependence on particle volume fraction is compared to analytical calculations. However, the resulting intrinsic viscosity values for fractal-like clusters leads to an inconsistent description of the suspension microstructure. Results suggests that anisotropy of clusters cannot be neglected and that aggregates possibly restructure under large shear rates to form clusters with a fractal dimension below values expected for a Diffusion Limited Cluster-Cluster Aggregate (DLCA) mechanism. The experimental results also show that above a threshold in nanoparticle volume fraction, our suspensions exhibit both shear thinning and shear thickening behaviour. We conclude significant cluster restructuring takes place as shear rate is varied, indicating the need of deepening our understanding of the role of non-hydrodynamic particle-particle interactions in ionic systems.

Introduction/Background: Molten salts are extensively used as heat transfer fluids and thermal energy storage media in solar thermal plants. Although they operate over a wide temperature range and are thermally stable up to high temperatures, they typically have poor heat transfer properties. Consequently, researchers have tried improving their transport properties by adding nanoparticles to the molten salts. Thermal conductivity [1,2] and specific heat capacity [3] have been some of the most sought out property enhancements. However, suspension stability and detrimental large viscosity increments remain as major technological challenges that preclude utilization of nanoparticle suspensions in commercial solar thermal plants.

It is well established that nanoparticle aggregation and the formation of large, tenuous fractal-like aggregates is responsible of the substantial enhancements in heat transfer properties and viscosity values of nanoparticles suspensions. However, merely

qualitative estimates linking viscosity enhancements to state of aggregation has been so far reported. Simultaneous computation of microstructure evolution and particle stresses through Stokesian Dynamics simulations have proven a powerful theoretical tool to understand rheological response of particle suspensions [4]. Here, we make use of our previously computed intrinsic viscosity of dilute suspensions of fractal-like clusters [5] to infer the state of aggregation from experimental viscosity results.

Discussion and Results: Figure 1 shows the dependence of normalized viscosity η/η_0 on primary particle volume fraction ϕ for two suspensions of silica nanoparticles in a solar salt mixture (60-40 wt.% $NaNO_3$-KNO_3).

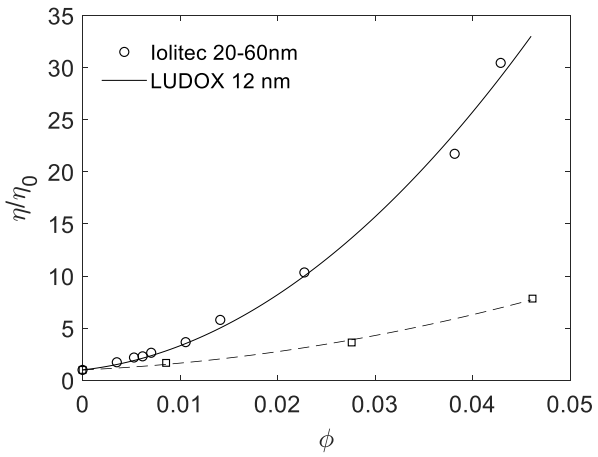

Figure 1. Viscosity of two suspensions of silica nanoparticles in Solar Salt, as a function of nanoparticle volume fraction ϕ. Results are normalized by pure salt viscosity at the temperature of the test (330 °C) and correspond to a shear rate $\dot{\gamma}$=1000 1/s. Circles: Iolitec, 20 nm – 60 nm particles. Squares: 12 nm LUDOX particles. Curve fits correspond to Eq. (1) in the text.

Classical theories cannot explain viscosity dependence on primary particle volume fraction as clusters form. Instead, modelling clusters as spherical particles with an effective volume fraction, ϕ_a , we expect:

$$\frac{\eta}{\eta_0} = 1 + 2.5\phi_a + 7.6\phi_a^2 = 1 + 2.5\left(\frac{\phi_a}{\phi}\right)\phi + 7.6\left(\frac{\phi_a}{\phi}\right)^2\phi^2 \qquad (1)$$

as corresponding to a second order expansion in volume fraction in the large shear rate limit [6]. The model allows only one free parameter in a fit to a second order polynomial. Nevertheless, goodness of the fit is excellent and, interestingly, fitting does not improve if both coefficients in linear and quadratic terms are allowed to vary. Moreover, restricting our fit to the unique ϕ_a/ϕ parameter reduces the confidence interval of the fit to a narrow range (see Table 1). In turn, this allows us to make predictions about suspension microstructure.

Table 1. Fit of experimental viscosity data to a Batchelor Eq. (1) and inferred microstructure information

Nanoparticles	ϕ_a/ϕ	N	ϕ_{gel}	R-square	95% confidence bounds
Iolitec 10-20 nm	41.2	1062	0.023	0.9927	41.0-42.3
Ludox	17.2	198	0.071	0.9966	16.4-17.9

A rigorous effective aggregate volume fraction can be assigned to aggregates in the limit of negligible cluster-cluster interactions. Suspension viscosity can then be obtained as [7]:

$$\frac{\eta}{\eta_0} = 1 + \frac{\langle S_{xy} \rangle}{\dot{\gamma}\eta_0} n_a \tag{2}$$

where $\langle S_{xy} \rangle$ is the time and ensemble averaged particle stresslet in simple shear with velocity field $\boldsymbol{v} = \dot{\gamma} y \mathbf{e_x}$, and n and $n_a = n/N = 6\phi/(\pi a^3)$ are the number densities of, respectively, primary particles and of aggregates. N is cluster size measured in terms of the number of primary particles that comprise the aggregate.

We accurately computed $\langle S_{xy} \rangle$ for large ensembles of varying size N fractal-like aggregates generated using a tunable cluster-cluster aggregation algorithm with fractal dimension and prefactors given $D_f = 1.8, k_0 = 1.3$. Normalized results lead to:

$$\frac{\langle S_{xy} \rangle}{N S_{sphere}} = 1.1 N^{0.52} \tag{3}$$

where the stresslet of a spherical particle in simple shear flow is given by $S_{sphere} = \frac{5}{12} \pi \dot{\gamma} \eta_0 a^3$. Inserting this result in Eq. (3), we obtain:

$$N = \left(\frac{1}{1.1} \frac{\phi_a}{\phi} \right)^{1/.52} \tag{4}$$

which leads to the estimated values of N in Table 1. Solid volume fractions are above expected gelation limit, ϕ_{gel}, which shows the inadequacy of an equivalent spherical particle formulation and/or aggregates with fractal dimensions below DLCA values.

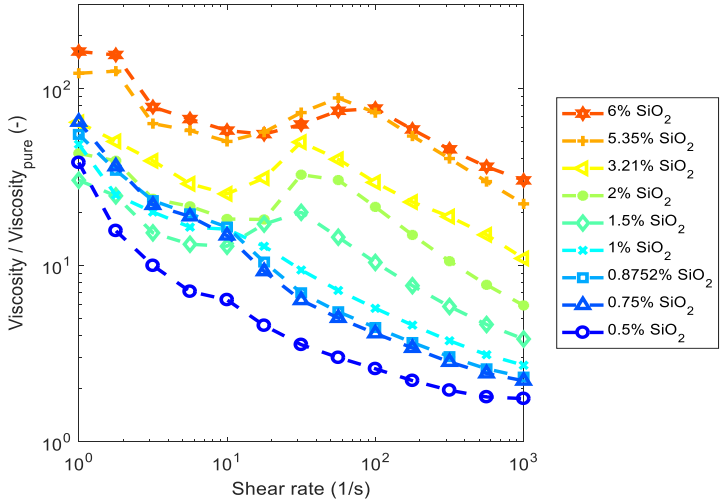

Figure 2. Normalized nanofluid viscosity vs. shear rate for a range of solar salt SiO_2 suspensions with varied particle mass fractions at 330°C

Viscosity of molten salts with suspended nanoparticles depends on particle loading and shear rate. Figure 2 shows normalized nanofluid viscosity versus shear rate for suspensions for varying mass fractions of nanoparticles at 330 °C. For particle mass loadings of 1% and below, the mixture exhibits shear thinning over the entire shear rate range tested. At particle mass loadings greater than 1%, the mixture undergoes shear thickening between about 20 1/s and 100 1/s. As particle loading increases, the highest shear rate at which shear thickening occurs increases. To this date, we have not seen shear thickening behaviour reported for molten salt nanofluids. However, shear thickening is common in colloidal structures and appears a result of increased clustering at lower shears and breakage of the clusters at higher shear.

Summary/Conclusions: The rheological response of silica nanoparticle suspensions in solar salt has been experimentally characterized. Viscosity dependence on particle loading and shear rate is measured and compared to predictions using Stokesian Dynamics simulations. Computed intrinsic viscosity values of dilute suspensions of fractal-like clusters are used to infer the state of aggregation from the experimental viscosity results. However, inconsistencies appear, indicating that a more complex cluster-restructuring mechanism is taking place, highlighting also the need for further investigation.

References:

1. Y. Ueki Y, N. Fujita, M. Kawai M, and M. Shibahara, Thermal conductivity of molten salt-based nanofluid, *AIP Advances* 7 (2017) 055117.
2. B. Ma, and D. Banerjee, Experimental measurements of thermal conductivity of alumina nanofluid synthesized in salt melt, *AIP Advances* 7, (2017) 115124.
3. P. Andreu-Cabedo, R. Mondragon, L. Hernandez, R. Martinez-Cuenca, L. Cabedo, and E.J. Julia, Increment of specific heat capacity of solar salt with SiO2 nanoparticles, *Nanoscale Research Letters* 9 (2014) 582.
4. J.F. Brady, and G. Bossis, Stokesian Dynamics, *Annual Review of Fluid Mechanics* 20 (1988) 111–157.
5. M. Ravina, A. DeFilippo, S. Fereres, and M. Zurita-Gotor, Microstructural effects on the rheological behaviour of nanofluids, *7th European Conference on Computational Fluid Dynamics (ECFD 7)*, Glasgow, UK, 2018.
6. G.K. Batchelor, and J.T. Green, The determination of the bulk stress in a suspension of spherical particles to order c^2, Journal of Fluid Mechanics 56 (1972) 401–427.
7. M. Zurita-Gotor, J. Bławzdziewicz, and E. Wajnryb, Motion of a rod-like particle between parallel walls with application to suspension rheology, Journal of Rheology 51 (2007) 71–97.

1st International Conference on Nanofluids (ICNf2019)
2nd European Symposium on Nanofluids (ESNf2019)
26-28 June 2019, Castelló, Spain

Experimental and theoretical approach of stability and thermophysical properties of NiO-nanofluids for solar energy applications

T. Aguilar[1*], A. Sánchez-Coronilla,[2] E. I. Martin,[3] P. Martínez-Merino,[1] R. Gómez-Villarejo,[1] I. Carrillo-Berdugo,[1] J.J. Gallardo,[1] R. Alcántara,[1] J. Navas[1]

[1]Departamento de Química Física, Facultad de Ciencias, Universidad de Cádiz.

[2]Departmento de Química Física, Facultad de Farmacia, Universidad de Sevilla.

[3]Departmento de Ingeniería Química, Facultad de Química, Universidad de Sevilla.

[*]Corresponding author: mariateresa.aguilar@uca.es

Keywords: NiO, nanofluid, stability, thermal properties, density functional theory.

Abstract

Nanofluids could be a promising alternative to the typical HTF used in a CSP. In this work, stability and thermal properties of NiO-nanofluids are analysed from an experimental a theoretical viewpoint. Results showed an improvement of stability due to the use of surfactants as stabilizers and an enhancement of thermal conductivity up to 96%. DFT leaded a better understanding of their stability and improved thermal conductivity.

Introduction

Nanofluid is the trending material, which is studied at the present, with the aim to improve their thermal properties to be used in concentrating solar power (CSP) plants. Many researches have studied the effect of different nanoparticles such as metal [1] or metal oxide [2] and the effect of the stability of nanoparticles along time on the base fluid. Furthermore, stability is not only important to avoid damage on the pipes, that transport nanofluids, but also in the improvement of their thermal properties. This work is focused on the experimental and theoretical study of the stability and thermal properties of nanofluids prepared with different mass concentrations of commercial NiO ($1{\cdot}10^{-4}$, $5{\cdot}10^{-4}$ and $10{\cdot}10^{-4}$ %wt.). Nanoparticles were dispersed into a eutectic mixture of biphenyl ($C_{12}H_{10}$, 26.5%) and diphenyl oxide ($C_{12}H_{10}O$, 73.5%), which is the typical heat transfer fluid (HTF) used in CSP plants, commercially known as Dowtherm A. Furthermore, two kinds of surfactants: Benzalkonium Chloride (BAC) and 1-Octadecanethiol (ODT) in a ratio 1:0.75:0.75 (NPs:BAC:ODT) were added in order to improve the dispersion and

stability of nanoparticles in the HTF. Stability of colloidal suspensions were analysed by means of UV-Vis spectroscopy, that can provide a measurable characterization of stability by evaluating the absorbance of a suspension [3] and Dynamic Light Scattering (DLS), to determine the sedimentation process by means of the study of particle size measurements. To a better understanding of the stability of nanofluids, a theoretical study based on density functional theory (DFT) was performed to comprehend the interaction of the ODT and BAC surfactants with molecules of the base fluid (DFT) and with NiO (100) surface (DFT-periodic). Hydrogen bonds between the surfactants and the base fluid were analysed by using the Quantum Theory of Atoms in Molecules (QTAIM). Finally, thermal conductivity of nanofluids was measured at several temperatures using the laser flash technique (LFA 1600 equipment, supplied by Linseis Thermal Analysis©).

Results and discussion

The physical stability of nanofluids was analysed by means of the evolution of coefficient extinction along seven days (see Figure 1A). It can be see a decrease until the third day after preparation of nanofluids and then remains stable. Nanofluid with the lowest concentration of nanoparticles ($1 \cdot 10^{-4}$% wt. NiO)) was the most stable as the decrease in the extinction coefficient is lesser than the others and showed the highest value after seven days. Particle size was analysed as the sedimentation process is closely linked with the size of agglomerates in the base fluid. Figure 1B shows particle size of nanofluids. In all cases, size of nanoparticles increases up to the third day, the values remain stable from then. The results are in agreement with those from UV-Vis spectroscopy. A theoretical study to understand the role played by the surfactants in the stability of nanofluids interaction energies of BAC and ODT by means of their two terminal extremes with diphenyl oxide and biphenyl was performed. The most favoured interaction corresponds to the structural configuration shows in Figure 1C for BAC-diphenyl oxide/biphenyl and Figure 1D for ODT-diphenyl oxide/biphenyl. QTAIM analysis corroborated the formation of H bridges with diphenyl oxide and biphenyl molecules through the study of the properties at the bond critical point (BCP), such as electron density (ρ) and its Laplacian ($\nabla^2\rho$). From these results it is possible to recognise the preferred area for the interaction of the surfactants with the HTF molecules: the BAC through the area of the terminal benzene and the ODT through the –SH. Furthermore, interaction of surfactant with the surface of NiO was studied through the interaction energies (E_{int}) of their two extremes. Figures 1E and 1F show the most stable interaction of the plane (100) NiO with BAC and ODT, respectively. The values of the energies exhibited two stables interaction for BAC as surfactant trough terminal methyl and the

ring benzene on the Ni, which values were E_{int}(Ni-methyl)= -10.542 kcal/mol and E_{int}(Ni-phenyl)= -7.622 kcal/mol, respectively. In the case of ODT, the only favoured interaction is the one corresponding to –SH group of the ODT on the Ni site E_{int}(Ni-SH) = -3.018 kcal/mol.

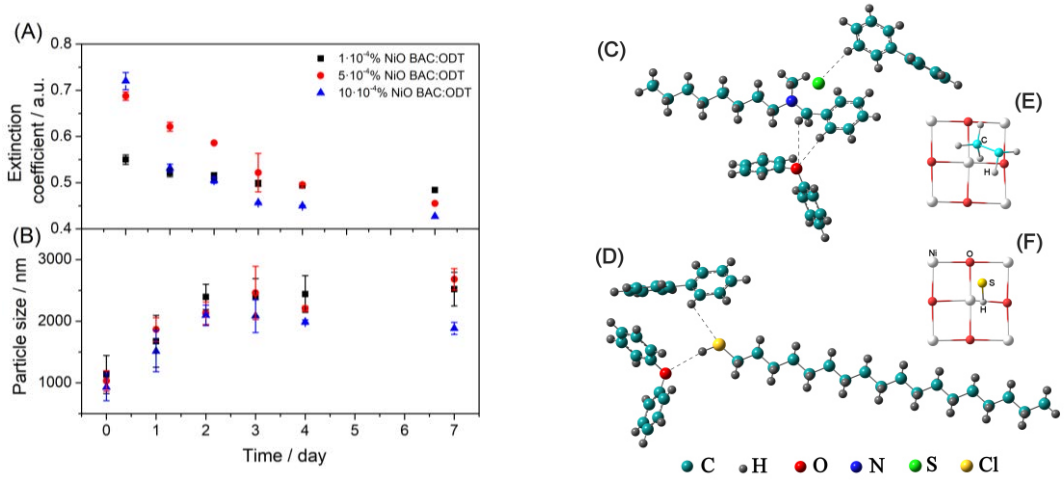

Figure 1. Stability of NiO-nanofluids during seven days, A) Extinction coefficient of nanofluids at 700 nm B) Particle size of nanofluids. Optimized structures in solvent phase of the most favored interaction between base fluid and BAC (C) and ODT (D) and local geometry in 2D for the most stable interactions of BAC (E) and ODT (F) with the surface NiO (100).

The most interesting property related to heat transfer efficiency is thermal conductivity.[3, 4] and the suspension of nanoparticles in HTF is known to lead to an increase in this value. Thus, thermal conductivity was measured for nanofluids in a range between 293 and 363 K. Figure 2A shows experimental thermal conductivity of nanofluids. It is possible to observe how thermal conductivity of the base fluid decreases as the temperature rises, however, nanofluids indicate an opposite trend, as thermal conductivity increase with temperature. Values of *k* reaching an improvement up to 96% at 363 K for the nanofluid with lesser nominal mass concentration of nanoparticles, which was the most stable nanofluid study from coefficient extinction and particle size. The improvement of thermal conductivity could be associated with Brownian motion and generated at molecular level.

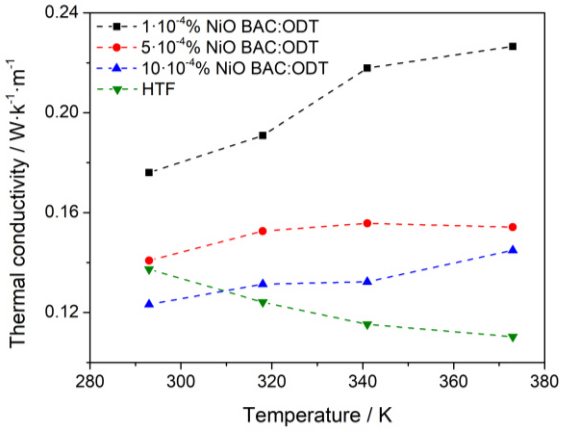

Figure 2. Experimental thermal conductivity of NiO-nanofluids.

Conclusion

In this work were prepared nanofluids based on NiO nanoparticles. Nanomaterial was dispersed in a eutectic mixture of diphenyl oxide and biphenyl (a common thermal oil used in a CSP plant) with a mixture of BAC and ODT surfactants to stabilize nanoparticles. Nanofluids showed stability from the third day after preparation, being concentration of $1{\cdot}10^{-4}$% NiO (p/p) the most stable nanofluid. Furthermore, the role played by interaction NiO-surfactant-base fluid was studied from DFT, concluding the most stable configurations were through phenyl group of BAC and O atom of diphenyl oxide and –SH group of ODT and O atom of diphenyl oxide for interaction surfactant base fluid. To explain interaction NiO-surfactant the most favoured configurations were Ni-Methyl and Ni-HC (Phenyl) for BAC as surfactant and Ni-SH for ODT as surfactant. Finally, the presence of stable nanoparticles leads to enhanced thermal properties at higher temperature, reaching up to 96% at 363 K for nanofluid with $1{\cdot}10^{-4}$% NiO (p/p) and a change in the typical trend of thermal conductivity of the base fluid.

References:

1. R. Gómez-Villarejo, E.I. Martín, J. Navas, A. Sánchez-Coronilla, T. Aguilar, J.J. Gallardo, R. Alcántara, D. De los Santos, I. Carrillo-Berdugo, C. Fernández-Lorenzo, Ag-based nanofluidic system to enhance heat transfer fluids for concentrating solar power: Nano-level insights, *Applied Energy* 194 (2017) 19-29.
2. A. Mwesigye, Z. Huan, J.P. Meyer, Thermodynamic optimisation of the performance of a parabolic trough receiver using synthetic oil–Al_2O_3 nanofluid, *Applied Energy* (2015) 398-412.

3. W. S. Sarsam, A. amiri, M. N. N. Zubir, H. Yarmand, S. N. Kazi, A. Badarudin. Stability and thermophysical properties of water-based nanofluids containing triethalnolamine-treated graphene nanoplatelets with different specific surface areas. *Colloid surface A.* 500 (2016) 17-31.
4. M. Chandrasekar, S. Suresh, T. Senthilkumar, Mechanisms proposed through experimental investigations on thermophysical properties and forced convective heat transfer characteristics of various nanofluids – A review, *Renewable and Sustainable Energy Reviews* 16(6) (2012) 3917-3938.

1st International Conference on Nanofluids (ICNf2019)
2nd European Symposium on Nanofluids (ESNf2019)
26-28 June 2019, Castelló, Spain

TiO_2-based nanofluids for concentrated solar energy: preparation, stability and thermal properties

T. Aguilar[1*], A. Yasinskiy,[2] P. Martínez-Merino,[1] I. Carrillo-Berdugo,[1] R. Gómez-Villarejo,[1] J.J. Gallardo,[1] R. Alcántara,[1] J. Navas[1]

[1]Departamento de Química Física, Facultad de Ciencias, Universidad de Cádiz, Puerto Real, Cádiz, Spain

[2]Department of Non-ferrous Metals Metallurgy, School of Non-Ferrous Metals and Materials Science, Siberian Federal University, Krasnoyarsk, Russia

[*]Corresponding author: mariateresa.aguilar@uca.es

Keywords: metal oxide, nanofluid, preparation, stability, thermal properties.

Abstract

This study presents the preparation of TiO_2-nanofluids by means of two different methods: a solvothermal synthesis for using the one-step method, and the dispersion of nanoparticles using an ultrasonic probe. Nanofluids showed high stability during one month and enhanced thermal properties, reaching an improvement up to 51.7 and 31.4% at higher temperatures.

Introduction

Nowadays, one of the most interesting research line is focusing on the enhancement of thermal properties of heat transfer fluid (HTF) used in concentrating solar power (CSP) in order to reduce the costs or improve the overall efficiency of CSP plants. Recent studies have reported achieving enhanced thermal performance by the addition of nanoparticles (NPs) to the HTF to obtain nanofluids [1, 2]. However, the challenge in the preparation of nanofluids is keeping colloidal suspensions stable for a long time, since nanomaterials tend to be attracted each other, as the reduction of their particle sizes increases the Van der Waals forces of attraction. Thus, the stability of nanofluids is the key to understand their practical applications, and the presence of nanoparticles in the base fluid along time will determine the improvement in thermal performance and lifetime of the nanofluid [3, 4]. Preparation of nanofluids can be performed by different techniques, however those can be included in two main groups: one-step and two-step methods. One step-method (1SM) involves synthesizing the nanomaterial into the base fluid, while in two-step method (2SM) nanoparticles are synthesized and then dispersed in the base fluid. When nanofluids are prepared by 2SM, it is necessary the addition of surfactants (SAA, *Surface Active Agent*) in order to facilitate the dispersion of NPs and thus prevent their agglomeration and

sedimentation. A decrease in the amount of nanomaterial available in the nanofluid capable to ease the transport of heat would cause a decrease of thermal properties. Instead, nanofluids whose NPs are prepared directly in the base fluid do not usually need the addition of SAA and, nevertheless, they are significantly more stable than the previous ones. It is due to the fact that by means of this methodology the drying processes, that cause the sintering of nanoparticles, are removed. In this work, nanofluids were prepared by means of ultrasonic probe (2SM) and a solvothermal synthesis (1SM) to obtain TiO_2-nanofluids in a HTF (usually called as Dowtherm A, i.e. the eutectic mixture of biphenyl and diphenyl oxide), typically used in CSP plants. For nanofluids prepared using 2SM, different nanoparticle mass concentrations ($1 \cdot 10^{-4}$, $2.5 \cdot 10^{-4}$ and $5 \cdot 10^{-4}$% wt.) were studied. Also, in order to disperse and stabilize the nanofluids, 1-Octadecanethiol (ODT) was added as surfactant with a ratio 1:1 (NPs:SAA). Moreover, TiO_2 was synthesized inside of the same HTF by using a small proportion of benzylic alcohol and titanium isopropoxide as reactants. Stability of nanofluids was studied by UV-Vis spectroscopy and particle size evolution along 28 days. UV-Vis spectra were recorded and the extinction coefficient was evaluated at 450 nm, as at this wavelength light scattering and photon absorption processes take place. A change in this positions means a variation of number of nanoparticles are available within the nanofluid. Particle size measurements were performed using the dynamic light scattering (DLS) technique. Finally, thermal conductivity was studied to evaluate how this property can be affected by stability of nanofluids. Thermal conductivity was measured using the Laser Flash Technique (LFA 1600 equipment, supplied by Linseis Thermal Analysis©).

Results and discussion

Stability of TiO_2-nanofluids was studied along 28 days by using UV-Vis spectroscopy and Dynamic Light Scattering (DLS), in order to record extinction coefficient and particle size, respectively. Both, nanofluids prepared by 1SM and 2SM, underwent a lowering of extinction coefficient up to fifth and third day after its preparation, respectively, to then stabilize. Although, TiO_2-nanofluids prepared using as 1SM (solvothermal synthesis) as 2SM method (ODT as surfactant), hardly exhibited changes after one month, dispersion of nanoparticles obtained by means of 1SM seemed to be higher than nanofluids prepared by 2SM. A high dispersion of nanoparticles indicates the presence of more number of nanoparticles in the core of the fluid. Furthermore, values of particle size of TiO_2-NFs, from DLS technique, not only were lower than 300 nm but also their sizes not increased during 28 days after preparation. TiO_2-nanofluids (2SM), see Figure 1A, showed values between 200 and 250 nm. Also, TiO_2-nanofluid (1SM) showed the lower

particle size, 160-170nm (see Figure 1B). It explains why extinction coefficient remained stable, since the lowest particle size the lowest precipitation of nanoparticles. Therefore, nanofluids prepared using one step method showed lower particle size than the nanofluids prepared by using the two step method.

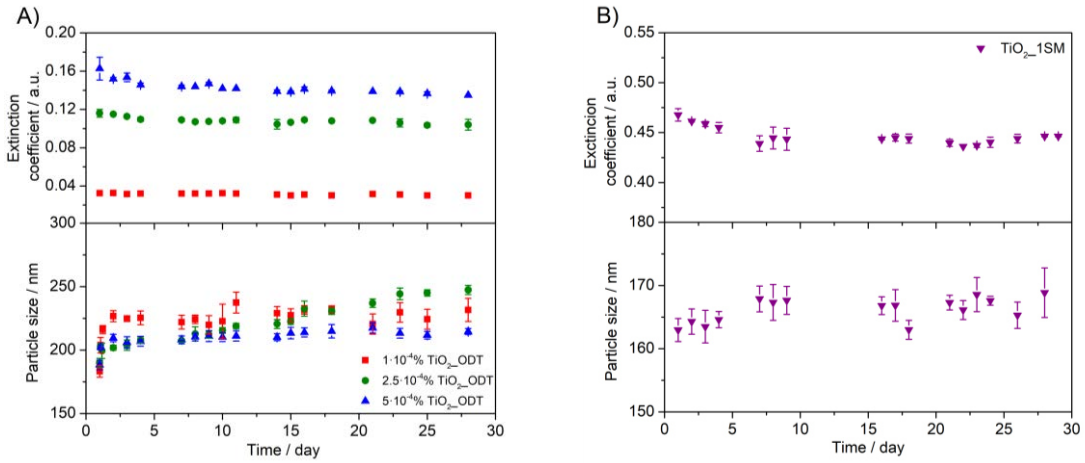

Figure 1. Stability of TiO_2-nanofluids during 28 days, A) TiO_2 –nanofluids prepared by 2SM and B) TiO_2-nanofluid prepared by 1SM (Up: extinction coefficient at 450 nm, Down: particle size).

In the other hand, thermal conductivity of nanofluids was analysed, as an enhancement of this property has a positive effect on heat transfer performance [2, 5]. Samples and base fluid were examined using the LFA technique. Figure 2 shows the ratio (k_r) between the thermal conductivity of TiO_2-nanofluids (k_{nf}) and the base fluid (k_{bf}), this relationship revealing the behaviour of thermal conductivity with temperature. k_r > 1 means the nanofluids studied present enhanced thermal conductivity. Incorporation of TiO_2-NPs increased thermal conductivity of NFs. The raise became more strongly marked with temperature increase, reaching improvement up to 52.7 y 31.4%, for TiO_2_2SM y TiO_2_1SM, respectively, at the highest temperature.

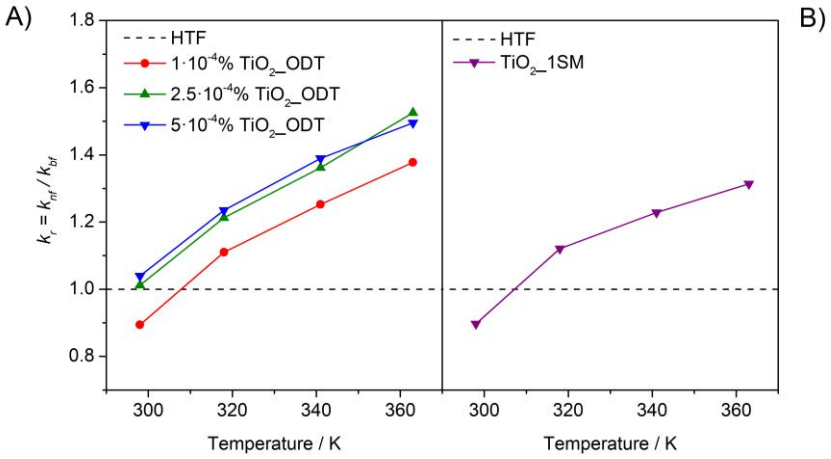

Figure 2. Relative thermal conductivity of TiO_2-nanofluids, A) TiO_2 –nanofluids prepared by 2SM and B) TiO_2-nanofluid prepared by 1SM.

Conclusion

In this study were obtained stable nanofluids based on the dispersion of titanium dioxide nanoparticles in a HTF, typically used in a CSP, using a two-step method and adding surfactants (ODT) to stabilize nanoparticles. Furthermore, TiO_2-NPs were successfully synthesized inside of the same HTF by means of a solvothermal method. Nanofluids showed high stability, which was determined through the study of their extinction coefficient and particle size. It was determined that both, the 2SM using surfactant as a stabilizer and 1SM, showed the ability to stabilize the NPs in the medium. This improvement favored the presence of nanoparticles for longer in the fluid that involved an improvement in thermal properties. Finally, thermal conductivity was improved for both kinds of nanofluid, up to 52.7%.

References:

1. A. Mwesigye, Z. Huan, J.P. Meyer, Thermodynamic optimisation of the performance of a parabolic trough receiver using synthetic oil–Al_2O_3 nanofluid, *Applied Energy* (2015) 398-412.
2. S. Lee, S.U.S. Choi, S. Li, J.A. Eastman, Measuring Thermal Conductivity of Fluids Containing Oxide Nanoparticles, *Journal of Heat Transfer* 121(2) (1999) 280-289.
3. R. Sadeghi, S.G. Etemad, E. Keshavarzi, M. Haghshenasfard, Investigation of alumina nanofluid stability by UV–vis spectrum*, Microfluidics and Nanofluidics* 18 (5) (2015) 1023-1030.
4. A. Nasiri, M. Shariaty-Niasar, A. Rashidi, A. Amrollahi, R. Khodafarin, Effect of dispersion method on thermal conductivity and stability of nanofluid, *Experimental Thermal and Fluid Science* 35 (4) (2011) 717-723.
5. D.-H. Yoo, K.S. Hong, H.-S. Yang, Study of thermal conductivity of nanofluids for the application of heat transfer fluids, *Thermochimica Acta* 455 (1) (2007) 66-69.

1st International Conference on Nanofluids (ICNf2019)
2nd European Symposium on Nanofluids (ESNf2019)
26-28 June 2019, Castelló, Spain

Influence of Nanofluids in the Performance of a Pilot Solar Collector

L.V. Pereira[1], X. Paredes[2*], C.A. Nieto de Castro[2] and M.J.V. Lourenço[2]

[1] UC Leuven – Limburg, Management en Technologie-Campus Gasthuisberg, Herestraat 49, 3000 Leuven, Belgium

[2] Centro de Química Estrutural, Faculdade de Ciências, Universidade de Lisboa 1749-016 Lisboa, Portugal

[*]Corresponding author: xpmendez@ciencias.ulisboa.pt

Keywords: Nanofluids, Thermal solar collector, Melanin; Efficiency.

Abstract: In this work, we conduct a practical comparison of the different performances of several heat transfer fluids in a simple, home-made solar collector that allows for great control and analysis of the experiments. As baseline for the comparison, measurements with water, commercially available ethylene glycol and a mixture of both are used. Nanoparticles of the natural pigment melanin are then added and an evaluation of its impact on the base fluid is discussed. The efficiency of the solar collector was found to increase 12% with this nanofluid.

Introduction: Heat transfer processes account for a notable part of the total global energy consumption. Improving these processes for better efficiency can help reduce the energy usage or improve output. Engineers have made headways in the design of the heat exchangers themselves, but we are still facing a variety of challenges regarding the fluids being used in this equipment. A dispersion of appropriate solid particles can help improve the final performance of a base fluid depending on how this addition affects its thermophysical properties (mainly thermal conductivity, viscosity and heat capacity) and, depending on the application, its optical properties (particularly sunlight absorption).

One of the many uses for heat transfer fluids is in flat-plate solar collectors, widely used for water heating in residential buildings. An active system uses a pump to circulate the heating fluid while a passive one uses the thermosiphon principle, with the liquid being transported by natural convection. Solar water heating systems can be further subdivided in direct systems, where the fluid being circulated is the water to be heated, and indirect systems, where the water is heated through a heat exchanger and the fluid being circulated is not physically in contact with the water. The authors will not dwell on the advantages and disadvantages posed by any of these systems. For our study, we

have used a simple home-made flat-plate collector with a pump (active) and a heat exchanger (indirect) in order to test the performance changes that arise from the introduction of melanin nanoparticles in different base fluids.

Materials and method:

The solar collector model is made of polystyrene foam for the casing, copper tubing with a diameter of 2 mm rolled up in a double cone shape, sandwiched between two 0.1 m by 0.1 m plates. The absorber plate can be made of aluminium, copper or copper treated with a black photosensitive pigment developed and patented [1], containing melanin of natural origin from cuttlefish. It is completely naturally degradable and has good thermal properties. The transparent cover is made of a biopolymer with corn starch as its main ingredient; biodegradable, cheap and easy to make.

A peristaltic pump takes care of circulating the fluid from the solar collector to the water reservoir that is a simple glass recipient inside insulating foam where more rolled up 2 mm copper tube is used to facilitate the heat exchange.

To measure the temperature in different parts of the setup, Pt-100 resistance thermometers will be used, calibrated between 20 and 80ºC, to within 0.08 K connected to a multiplexer to measure the ambient temperature, the reservoir temperature and the temperature under the absorber plate every ten seconds.

The fluids used to gauge the influence of the melanin nanoparticles are ultrapure type 1 water, commercially available ethylene glycol (Motul-Inugel Optimal Ultra), and a 40/60 mixture of the ethylene glycol with water. We check the effects of the addition of melanin nanoparticles produced at our laboratory.

The methodology used follows that reported previously [2] for graphene nanofluids. The circuit itself is first filled in with the heat transfer fluid. Afterwards the system goes through a cycle where first, the fluid under the absorber plate heats up, followed up by a period where it is circulated so that the heat is transferred to the water reservoir. This cycle takes place four times. For every heating fluid the complete test is repeated three times. As these experiments were performed in winter, the heating source used was a controlled flux air dryer.

The efficiency of the solar collector, defined as the ratio of the usable thermal energy to the incident solar energy can be calculated using the following equation:

$$\eta = \frac{\dot{m}C_p}{AG_T}(T_{out} - T_{in}) \quad (1)$$

where $\dot{m}$ is the mass flow rate, C_p the heat capacity of the fluid/nanofluid, *A* the collector area, G_T the solar irradiance (heat flux) (~1000 W/m^2), and T_{out} and T_{in} the average temperatures of the in and out flow streams in the collector.

The heat capacity of the nanofluid can be calculated from the proposed mixing rule given by Equation (2).

$$C_{p_{nf}} = \phi_{np}C_{p_{np}} + (1 - \phi_{np})C_{p_{bf}} \quad (2)$$

Melanin, the nanomaterial extracted from cuttlefish was described in reference [3], has a C_p around 2 Jg^{-1}K^{-1} at room temperature and 6 Jg^{-1}K^{-1} at 100ºC. The nanofluid was prepared with a 1% w/w concentration of melanin NP's in water (corresponds to a volume fraction of 0.382).

If the same mass flow rate is used, we can calculate the efficiency of the solar collector with respect to that of water, under the same solar irradiance (or heat flux applied):

$$\frac{\eta_{HTF}}{\eta_{Water}} = \frac{C_{p_{HTF}}}{C_{p_{Water}}} \frac{(T_{out} - T_{in})_{HTF}}{(T_{out} - T_{in})_{Water}} \quad (3)$$

Discussion and Results:

The relative efficiency of the solar collector used can be observed in Table 1.

Table 1. Relative efficiency of solar collector for different heat transfer fluids

HTF	Water	EG	EG+water	Nanofluid
C_p/Jg^{-1}K^{-1}	4.157	2.40	3.58	4.10
$T_{out} - T_{in}$	2.19	1.65	2.13	2.49
η_{HTF}/η_{Water}	1	0.43	0.84	1.12

It is clear that the nanofluid of melanin in water is more efficient (12%) than water, in the same conditions. Another way of visualizing this effect is by measuring the temperature change of the water reservoir. This is the most important parameter to analyse the performance of the fluid, namely the difference in the out temperature and the highest temperature achieved in the water reservoir. This way we can see how much heat has been transferred to the water (including heat losses in the pipes. An example of the temperature variation in the water reservoir is shown in figure 1, where similar results using water as the HTF and the Nanofluid are compared.

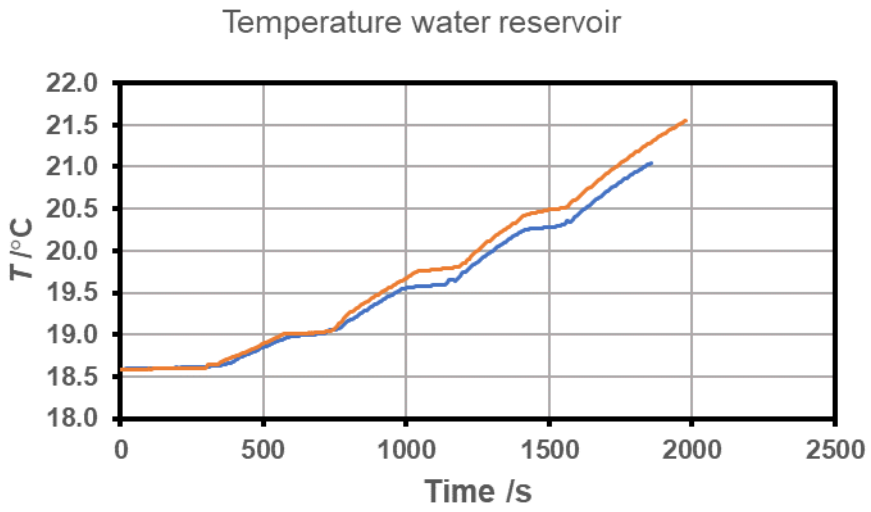

Figure 2. Example of temperature increase in the water reservoir

Summary/Conclusions: Our current results indicate that the addition of the nanoparticles, increases efficiency of the solar collector by 12% and that the temperature change in the water reservoir is greater (0.3ºC), just in 30 minutes. The main contribution is the use of natural melanin particles, from cuttlefish, and not synthetic nanomaterials, due to their environmental and toxicological concerns. Further tests with other nanofluids will be performed soon, with a different time scale.

References:

1. Klemens Massonne (BASF), Salomé Vieira (FCUL), Maria José Lourenço (FCUL), Carlos Nieto de Castro (FCUL), "Use of Melanin or Melanin Particles for Solar Thermal Energy Conversion", Patent Number EP 3 228 192 A2, published 11.10.2017.
2. F.E.B. Bioucas, S.I.C. Vieira, M.J.V. Lourenço, F.J.V. Santos, C. A. Nieto de Castro, Performance of heat transfer fluids with nanographene in a pilot solar collector, *Solar Energy* 172 (2018) 171–176
3. S. I. C. Vieira, M. Araújo, R. André, P. Madeira, M. Humanes, M. J. V. Lourenço and C. A. Nieto de Castro, Sepia melanin: a new class of nanomaterial with anomalously high heat storage capacity obtained from a natural nanofluid, J. Nanofluids 2, (2013) 104–111.

1st International Conference on Nanofluids (ICNf2019)
2nd European Symposium on Nanofluids (ESNf2019)
26-28 June 2019, Castelló, Spain

Solar Radiation Harvesting via Flat Plate Collectors: Nanofluid Figure of Merit against Thermal Efficiency

Alper Mete Genc[1], Elif Begum Elcioglu[2], Ziya Haktan Karadeniz[3], Mehmet Akif Ezan[4] and Alpaslan Turgut[4]

[1] İzmir Katip Çelebi University, The Graduate School of Natural and Applied Sciences, Department of Mechanical Engineering, Çiğli 35620 İzmir, Turkey

[2] Eskisehir Osmangazi University, Sivrihisar Vocational School, Mechanics Program, Sivrihisar 26600, Eskisehir, Turkey

[3] İzmir Katip Çelebi University, Department of Mechanical Engineering, Çiğli 35620 İzmir, Turkey

[4] Dokuz Eylul University, Engineering Faculty, Mechanical Engineering Department, Tinaztepe Campus, Buca 35397 Izmir, Turkey

[*]Corresponding author: ebelcioglu@ogu.edu.tr

Keywords: Solar Collector, Nanofluid Figure of Merit, Energy Harvesting, Thermal Efficiency.

Abstract: Nanofluids benefit from solid nanoparticle content in increasing their heat transfer coefficients, while suffering from increased pumping power requirement and colloidal instabilities due to the same reason. To assess the bounds of nanofluid effectiveness, it is important to realistically specify the benefits of nanofluid over its base fluid, and relate these benefits to system efficiency. In this work, we compared different nanofluids use in a flat plate solar collector (FPSC) for laminar flow, based on thermal efficiency and Mouromtseff number comparisons. Results showed that nanofluid thermophysical properties manifest in FPSC thermal efficiency as well as FOM's. Al_2O_3, TiO_2, graphene, and SWCNT based nanofluids outperformed H_2O, while SiO_2 and polystyrene based nanofluids yielded performances lower than that provided by H_2O alone.

Introduction/Background: The ever-increasing need for high-efficiency energy systems directed the global perspective to new materials with tunable properties, such as nanofluids. Figure of Merits (FOM's) have been proposed to assess whether nanofluid use would be meaningful. These FOM's [1] depend on heat transfer coefficient (h), viscosity (μ), density (ρ), thermal conductivity (k), specific heat (c_p), flow conditions, geometry, and temperature; necessitating accurate measurement of properties. Figure 1 summarizes some of the nanofluid FOM's [2–4]. In order to judge whether a nanofluid is

beneficial than its base fluid as a coolant; $(FOM)_P$, $(FOM)_h$, $(FOM)_T$, and $(FOM)_Q$ should be >1 [2], and Mo_{nf}/Mo_{bf} >1 (see Figure 1).

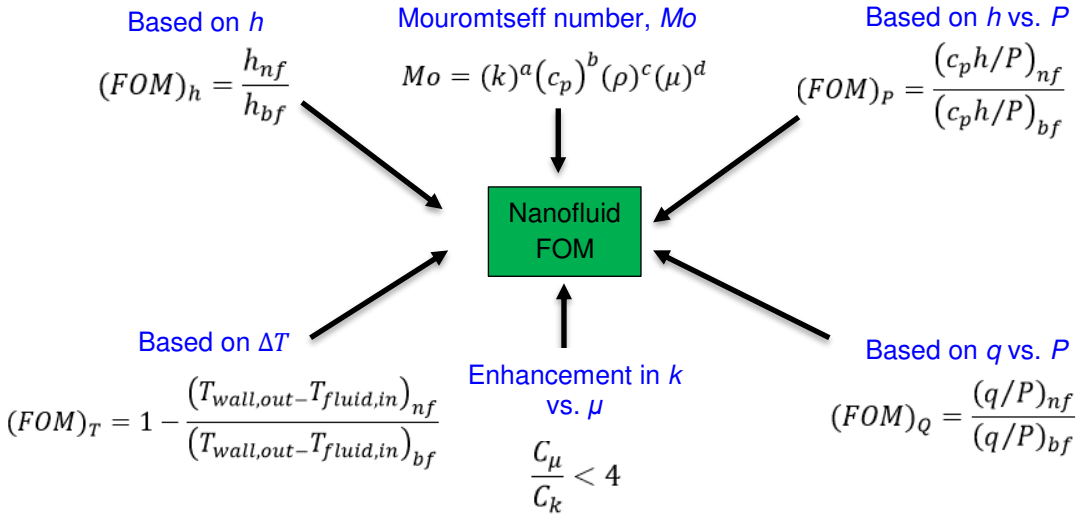

Figure 1. Widely used nanofluid FOM's.

Solar-thermal energy conversion is regarded as a leading application where nanofluids could be promising. Genc et al. [5] reported on the use of Al_2O_3-H_2O nanofluid in a FPSC and concluded that it outperformed H_2O for flow rates < 0.016 kg/s. Mirzaei [6] reported that CuO-H_2O outperformed H_2O for the flow rates considered in a FPSC. Colangelo et al. [7] approached to the topic from stability point of view, and reported that nanoparticle sedimentation could be reduced by varying tube cross section.

In this work we considered a FPSC with a working fluid of either of the following with H_2O as the base fluid: Al_2O_3 [8]; TiO_2 [9]; SiO_2, polystyrene and Al_2O_3 [10], graphene nano-platelet [11]; and SWCNT [12], in numerically evaluating FPSC efficiency, along with FOM discussions. The solar irradiation and ambient temperature are defined according to monthly average daily weather of Izmir, Turkey. The inlet temperature of the working fluids to the FPSC is assumed constant (25 °C). The mass flow rate is set to 0.008 kg/s kg/s.

Discussion and Results: Genc et al. [5] reported that, Al_2O_3-H_2O nanofluid outperformed H_2O at low flow rates (0.004 kg/s and 0.008 kg/s) and efficiency improvement scaled up until the flow rate reached 0.016 kg/s (at which H_2O experiences turbulent, Al_2O_3-H_2O experiences laminar flow). For >0.016 kg/s, nanoparticle addition adversely affected FPSC efficiency (compared to that with H_2O) due to viscous loss and increased pump power requirement. Having observed this trend in Al_2O_3-H_2O benchmark case, here we focus on laminar flow where use of nanofluid is appeared to be

advantageous at 0.008 kg/s. Figure 2 compares FPSC thermal efficiency for different nanofluids. Efficiency decreases with nanoparticle addition for the case of SiO_2- and polystyrene-based nanofluids, and slowly increases for SWCNT-based nanofluids; while enhancements are more pronounced for Al_2O_3, TiO_2, and especially for graphene nano-platelet based nanofluids.

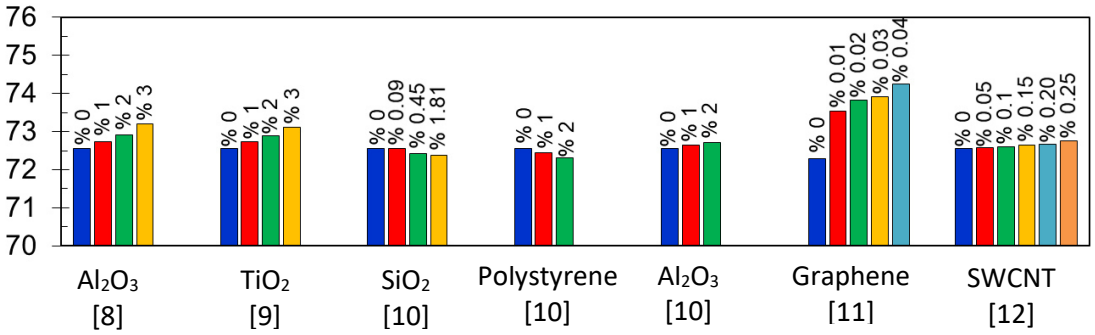

Figure 2. Thermal efficiency of a FPSC for nanofluid studies for laminar flow.

Thermal efficiency depends on nanoparticle and base fluid thermophysical properties (Figure 2). Except for SiO_2- and polystyrene-based nanofluids, efficiency is positively correlated to nanoparticle fraction. Figure 3 depicts a Mo number based comparison. Mo ratio for laminar flow increases with increasing particle concentration except for SiO_2- and polystyrene-H_2O nanofluids due to their lower thermal conductivity. It should be pointed out that the amount of change is in the same scaled order of magnitude for FOM and thermal efficiency except for SWCNT-based nanofluids.

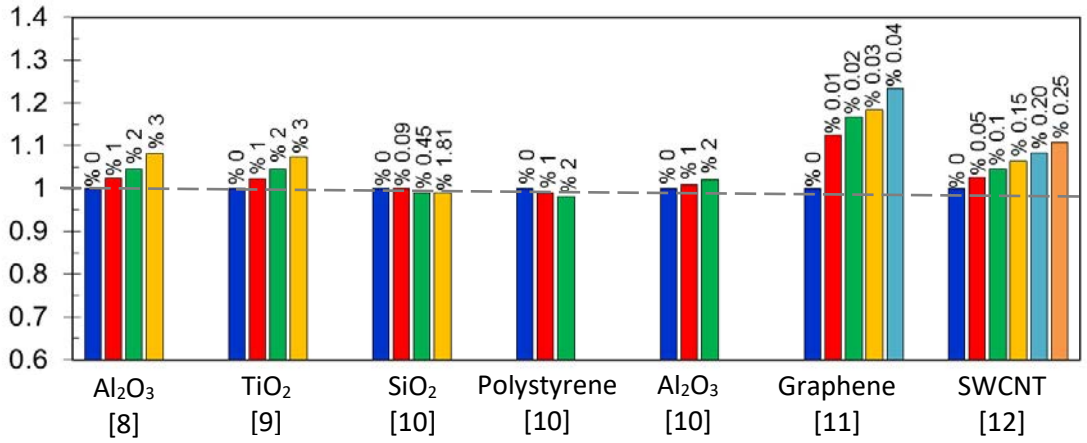

Figure 3. Mo ratio for laminar flow.

Summary/Conclusions: Based on the analyses performed, the following conclusions are drawn:

- Mo_{nf}/Mo_{bf} >1 for Al_2O_3, TiO_2, graphene, and SWCNT based nanofluids, while it is <1 for SiO_2 - and polystyrene based nanofluids. Based on this criterion, the latter two are considered not suitable for use in a FPSC under the conditions studied.

- Although individual nanofluid thermophysical properties are not primary concerns in terms of applications (Mo ratio), their unified impact (thermal efficiency) may alter the benefit in the use of nanofluids as in the case of SWCNT-based nanofluids.
- Stability deterioration may alter theoretically predicted thermophysical properties and heat transfer coefficient of nanofluids [13]. Applications require employment of nanofluids for a certain time and correlating colloid state parameters (e.g., nanofluid storage time, zeta potential range, etc.) to FOM would be a valuable future work.

References:

1. W. Yu, D. M. France, E.V. Timofeeva, D. Singh and J.L. Routbort, Comparative review of turbulent heat transfer of nanofluids, *Int. J. Heat Mass Transf*. 55 (2012) 5380–5396.
2. L. Yu, D. Liu, A Study of Thermal Effectiveness of Laminar Forced Convection of Nanofluids, in Proc. ASME 2012 Int. Mech. Eng. Congr. Expo. IMECE2012, Houston, Texas, USA, 2012: pp. 1–12.
3. R. Prasher, D. Song, J. Wang and P. Phelan, Measurements of nanofluid viscosity and its implications for thermal applications, *Appl. Phys. Lett*. 89 (2006) 1–3.
4. E. Timofeeva, W. Yu, D.M. France, D. Singh and J.L. Routbort, Nanofluids for heat transfer : an engineering approach, *Nanoscale Res. Lett*. 6 (2011) 1–7.
5. A. M. Genc, M. A. Ezan and A. Turgut, Thermal performance of a nanofluid-based flat plate solar collector: A transient numerical study, *Appl. Therm. Eng*. 130 (2018) 395–407.
6. M. Mirzaei, Experimental investigation of CuO nanofluid in the thermal characteristics of a flat plate solar collector, *Environ. Prog. Sustain. Energy*. 38 (2019) 260–267.
7. G. Colangelo, E. Favale, A. De Risi and D. Laforgia, A new solution for reduced sedimentation flat panel solar thermal collector using nanofluids, *Appl. Energy*. 111 (2013) 80–93.
8. A. Turgut, Ş. Sağlanmak and S. Doğanay, Experimental Investigation on Thermal Conductivity and Viscosity of Nanofluids: Particle Size Effect, *J. Fac. Eng. Archit. Gazi Univ*. 31 (2016) 95–103.
9. A. Turgut, I. Tavman, M. Chirtoc, H.P. Schuchmann, C. Sauter and S. Tavman, Thermal Conductivity and Viscosity Measurements of Water-Based TiO_2 Nanofluids, *Int. J. Thermophys*. 30 (2009) 1213–1226.
10. V. Mikkola, S. Puupponen, H. Granbohm, K. Saari and A. Seppälä, Influence of particle properties on convective heat transfer of nanofluids, *Int. J. Therm. Sci*. 124 (2018) 187–195.
11. S. Iranmanesh, H. Chyuan, B. Chin, E. Sadeghinezhad, A. Esmaeilzadeh and M. Mehrali, Thermal performance enhancement of an evacuated tube solar collector using graphene nanoplatelets nanofluid, *J. Clean. Prod*. 162 (2017) 121–129.
12. M. A. Sabiha, R. M. Mostafizur, R. Saidur and S. Mekhilef, Experimental investigation on thermo physical properties of single walled carbon nanotube nanofluids, *Int. J. Heat Mass Transf*. 93 (2016) 862–871.
13. I.M. Mahbubul, E.B. Elcioglu, M.A. Amalina and R. Saidur, Stability , thermophysical properties and performance assessment of alumina – water nanofluid with emphasis on ultrasonication and storage period, *Powder Technol*. 345 (2019) 668–675.

1st International Conference on Nanofluids (ICNf2019)
2nd European Symposium on Nanofluids (ESNf2019)
26-28 June 2019, Castelló, Spain

Particle-Wall Interaction Effects on Low-Flux Nanofluid-Based Direct Absorption Solar Collectors

Omar Z. Sharaf[1], Ashraf N. Al-Khateeb[2], Dimitrios C. Kyritsis[1], and Eiyad Abu-Nada[1*]

[1]Department of Mechanical Engineering, Khalifa University of Science and Technology, P.O. Box 127788, Abu Dhabi, UAE

[2]Department of Aerospace Engineering, Khalifa University of Science and Technology, P.O. Box 127788, Abu Dhabi, UAE

[*]Corresponding author: eiyad.abunada@ku.ac.ae

Keywords: volumetric solar absorption, direct absorption solar collector, Eulerian-Lagrangian simulation, two-phase nanofluid flow

Abstract: Four-way-coupled Eulerian-Lagrangian modelling was used in order to describe the particle-fluid, particle-particle, and particle-wall interactions in low-flux, nanofluid-based direct absorption solar collectors (DASCs). Based on the capacity of Eulerian-Lagrangian modeling to account for the discrete nature of nanoparticles, the optical, thermal, and particle concentration effects of particle-wall interactions are revealed for different flow Reynolds numbers and particle volume fractions. As a result of particle-wall interactions, particle deposition was shown to noticeably affect the local particle concentration in vicinity of the upper and lower collector surfaces. This, in turn, affected the absorption and thermal efficiencies of the collector, which are closely related to the particle distribution profile at the collector upper surface.

Introduction/Background: Direct absorption solar collectors (DASCs) based on the suspension of trace amounts of nanoparticles in a base fluid are an emerging type of solar thermal collectors that provide an alternative to conventional surface-based collectors [1]. Due to the superior optical and thermal properties of nanofluids [2], DASCs allow for the direct volumetric absorption of solar radiation within a nanofluid that functions both as the solar radiation absorber and heat transfer medium.

The majority of DASC studies in the literature are based on fully-continuous modelling where the nanofluid is assumed to be a homogeneous mixture of nanoparticles and base-fluid [3]. Fully-continuous models are simple and computationally-efficient; however, they are unable to capture the discrete nature of nanoparticles. Therefore, there is a need for discrete simulation techniques in order to accurately model physical

phenomena such as non-homogenous local particle concentrations, lateral particle migration, temperature and velocity slips between fluid and particle, particle-particle interactions, and particle-wall interactions and deposition. Eulerian-Lagrangian modelling is a hybrid continuous-discrete approach based on the treatment of the fluid phase from a continuum perspective and the particulate phase from a discrete perspective [4]. In this approach, closure relations are used for the momentum, heat, and mass interchange between the two phases.

In this work, a transient, four-way-coupled hybrid Eulerian-Lagrangian model is developed to characterize the nanofluid flow, heat transfer, solar radiation volumetric absorption, particle local distribution, and particle deposition in low-flux DASCs. Computational particles that represent clouds of real nanoparticles with identical properties are utilized in conjunction with a vorticity-stream function representation of the continuous phase. The main focus of this study is on particle-wall interactions and their thermal, optical, and particle concentration effects in low-flux DASCs.

Discussion and Results: A schematic of the nanofluid-based low-flux DASC is shown in Fig. (1). The nanofluid is contained within an insulated enclosure with a top low-iron glass-cover and an externally-insulated, internally-reflective bottom surface. Incident radiation is normal to the surface of the collector and attenuation of the incident solar radiation is dissipated in the form of local heat release. The fluid flow is two-dimensional, incompressible, laminar, and Newtonian. Moreover, all particles are treated as point-masses and taken to be spherical in shape, single-sized, and non-rotating.

The particle number concentration, normalized with respect to the total number of particles in the computational domain, is shown in Fig. (2) at Reynolds number (Re) of 0.1, particle-wall normal restitution coefficient (r) of 0.90, mean particle volume fraction (ϕ_p) of 0.001%, and particle diameter (D_p) of 10 nm. Due to particle deposition on the upper and lower surfaces, the local particle concentration is noticeably affected in vicinity of channel walls, where steep concentration gradients can be observed.

Deposited nanoparticles on the collector upper surface are optically-active, that is, they contribute to the extinction of solar radiation within the collector. In order to quantify the effects of particle deposition on collector performance, we use two performance metrics; namely, absorption efficiency η_{abs} and thermal efficiency η_{th}, defined as follows:

$$\eta_{abs} = \frac{Q_{abs}}{Q_{inc}}, \quad (1)$$

$$\eta_{th} = \frac{Q_{use}}{Q_{abs}}, \quad (2)$$

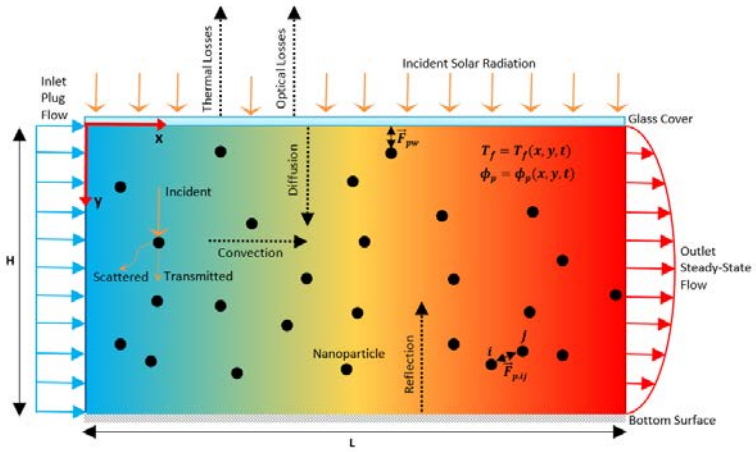

Figure 1. Schematic of the nanofluid-based direct absorption solar collector

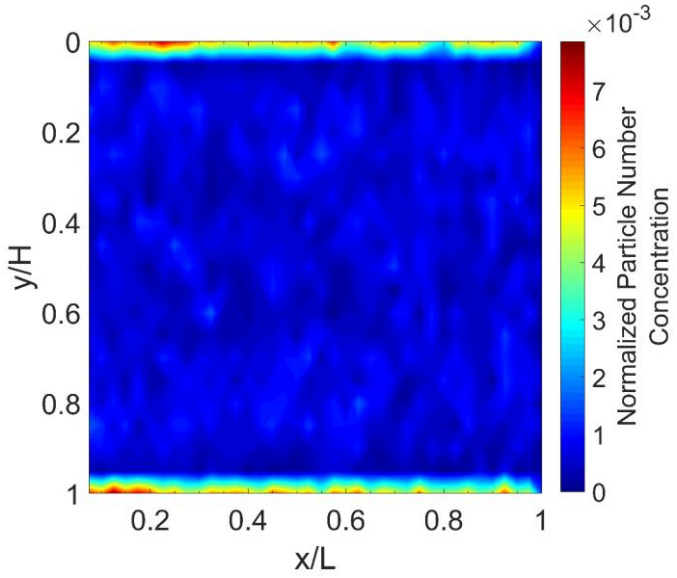

Figure 2. Normalized particle number concentration distribution within the DASC $(\boldsymbol{Re = 0.1, r = 0.90, \phi_p = 0.001\%, D_p = 10\ \mathrm{nm}})$

where Q_{inc} is incident solar power, Q_{abs} is absorbed solar radiation by the nanofluid, and Q_{use} is useful thermal power carried by the nanofluid. η_{abs} is a measure of the bulk nanofluid ability to absorb incident solar radiation during its multiple passes within the collector, whereas η_{th} is the ratio of useful thermal energy carried by the nanofluid to the solar radiation absorbed by the nanofluid. Figure (3) shows the absorption and thermal efficiencies for different Re and ϕ_p for the cases of $r = 0.90$ (imperfectly-elastic collisions with particle deposition) and $r = 1.0$ (perfectly-elastic collisions with no particle deposition). Our results show that η_{abs} and η_{th} are lower when particle deposition takes place relative to the case when there is no particle deposition (Fig. (3a,c)). This is especially true for η_{abs} at low Re and ϕ_p (Fig. (3a)). This can be attributed to the fact that

particle deposition leads to more surface absorption of solar radiation at the collector upper wall (where thermal losses to the surroundings take place) at the expense of bulk volumetric absorption. On the other hand, η_{abs} and η_{th} are relatively unaffected by particle deposition, regardless of Re and ϕ_p (Fig. (3b,d)). Fig. (3a) also shows that at low ϕ_p, an increase in Re unexpectedly improves η_{abs} for the case of $r = 0.90$. This is a result of the reduced particle deposition rate as Re increases, which limits the role of lateral Brownian particle migration since the flow becomes more convection-dominated.

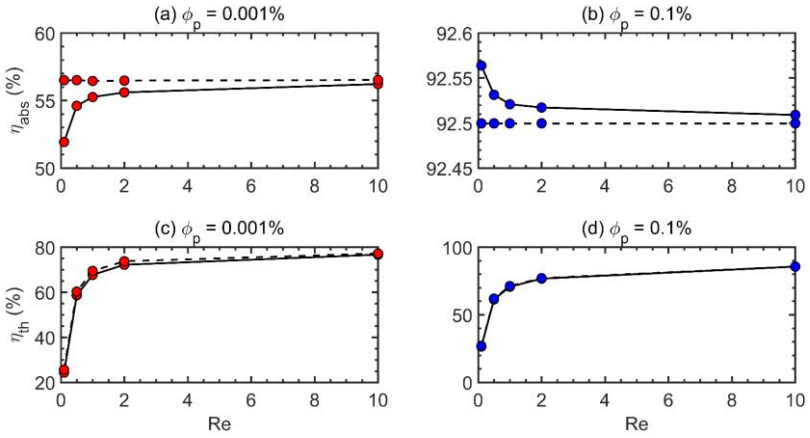

Figure 3. DASC absorption and thermal efficiencies as a function of Re and ϕ_p for the cases of $r = 0.90$ (solid lines) and $r = 1.0$ (dashed lines) $(D_p = 10\ \mathrm{nm})$

Conclusions: Using four-way-coupled Eulerian-Lagrangian modelling, particle-wall interactions were found to cause particle deposition and steep particle concentration gradients in the solid walls' vicinity of direct absorption solar collectors. Particle deposition resulted in augmented surface absorption of solar radiation at the expense of bulk volumetric absorption, which, in turn, affected the absorption and thermal efficiencies of the collector.

References:

1. S.-H. Lee, T. J. Choi and S. P. Jang, Thermal efficiency comparison: Surface-based solar receivers with conventional fluids and volumetric solar receivers with nanofluids, *Energy* 115 (2016), 404-417.
2. Y. Kameya and K. Hanamura, "Enhancement of solar radiation absorption using nanoparticle suspension," *Solar Energy* 85 (2011), 299-307.

3. X. Xu, C. Xu, J. Liu, X. Fang and Z. Zhang, "A direct absorption solar collector based on a water-ethylene glycol based nanofluid with anti-freeze property and excellent dispersion stability," *Renewable Energy* 133 (2019), 760-769.
4. C. T. Crowe, *Multiphase flow handbook*, Taylor & Francis, Boca Raton, FL, 2006.

SESSION 6

Numerical Simulation on the Microscopic and Macroscopic Levels

S6

1st International Conference on Nanofluids (ICNf2019)
2nd European Symposium on Nanofluids (ESNf2019)
26-28 June 2019, Castelló, Spain

Numerical analysis of heat transfer enhancement of EG-Si_3N_4 nanofluid in forced convection laminar pipe flow

E. Berberović[1*] and S. Bikić[2]

[1]Polytechnic faculty, University of Zenica
Fakultetska 1, 72000 Zenica, Bosnia and Herzegovina

[2]Faculty of Technical Sciences, University of Novi Sad
Trg Dositeja Obradovića 6, 21000 Novi Sad, Serbia

[*]Corresponding author: eberberovic@ptf.unze.ba

Keywords: EG-Si_3N_4 nanofluid, numerical, laminar, heat transfer.

Abstract: Heat transfer characteristics of ethylene glycol-based silicon nitride (EG-Si_3N_4) non-Newtonian nanofluid in laminar flow under forced convection and constant heat flux are analysed. Heat transfer is characterized in terms of Nusselt number and heat transfer coefficient for various concentrations of Si_3N_4 nanoparticles. Computational modelling is performed using software OpenFOAM®. The analysis shows promising results for enhancement of heat transfer of the EG-Si_3N_4 nanofluid compared to pure EG base fluid.

Introduction/Background: The research in nanofluids has been intensified over the past years, due to their proven potential in heat transfer applications, such as industrial heat exchangers, solar collectors or thermal energy storage systems [1], with water and ethylene glycol being commonly used as base fluids in the experimental studies [2] and numerical CFD studies [3]. Nanofluid is commonly modelled as a Newtonian fluid, however the available literature lacks investigations of nanofluids which show a more complex rheological behaviour. This study focuses on numerical analysis of heat transfer of such a non-Newtonian nanofluid (EG-Si_3N_4) in laminar flow in a smooth horizontal pipe.

Discussion and Results: The computational model consists of the steady-state governing equations for the conservation of mass, linear momentum and energy in forced convection regime, neglecting the temperature induced density changes

$$\nabla \cdot \left(\rho \mathbf{U} \right) = 0 \,, \tag{1}$$

$$\nabla \cdot \left(\rho \mathbf{U}\mathbf{U} \right) = -\nabla p + \nabla \cdot \tau \,, \tag{2}$$

$$\nabla \cdot \left(\rho c_p \mathbf{U} T \right) = \nabla \cdot \left(k \nabla T \right). \tag{3}$$

In the above equations ρ is the nanofluid density, **U** is its velocity, p is the pressure, τ is the viscous stress tensor, c_p is the specific heat, k is the thermal conductivity and T is the temperature. The density and the specific heat of the nanofluid are modelled as weighted averages based on the volumetric concentration of nanoparticles. The rheology and the thermal conductivity of the EG-Si_3N_4 nanofluid are modelled by the expressions [4]

$$\tau = \tau_0 + K\gamma^n, \quad k = \left(1 + 2.87\varphi_v\right) k_{bf}, \tag{4}$$

where γ is the strain rate and the parameters τ_0, K and n depend on the Si_3N_4 nanoparticle volumetric concentration φ_v [4]. The horizontal pipe is modelled as a 2D axisymmetric slice with one cell in the azimuthal direction. The problem described by Eqns. (1)-(4) was solved with the finite volume-based software OpenFOAM® and following boundary conditions:

- inlet, $\mathbf{U}=(U_{in},0,0)$, $\nabla p=0$, $T=T_{in}$,
- pipe wall, $\mathbf{U}=(0,0,0)$, $\nabla p=0$, $\nabla T = q/k$, q being the given heat flux at the pipe wall,
- outlet, $\nabla \mathbf{U}=0$, $p=p_{out}$, $\nabla T = qD\pi / \left(\dot{m} c_p\right)$.

The mean fluid temperature in the pipe cross section S, the convective heat transfer coefficients and the Nusselt number are evaluated from the following expressions

$$T_m = \int_S \rho c_p T \mathbf{U} \cdot \mathrm{d}\mathbf{S} \Big/ \int_S \rho c_p \mathbf{U} \cdot \mathrm{d}\mathbf{S}, \quad h = -k\nabla T_{wall} / \left(T_{wall} - T_m\right), \quad \mathrm{Nu} = hD/k. \tag{5}$$

The model is verified against the known analytical solutions [5], the experimental results of [6] and the empirical result of [7]. Figure 1 shows the computed velocity profile and the friction factor for laminar flow of water. The pipe geometry and fluid properties are the same as in [6], with Re=965 and q=1000 W/m^2. The results converge with increasing mesh resolution and the model correctly predicts the analytical velocity profile and friction factor f=64/Re=0,0663.

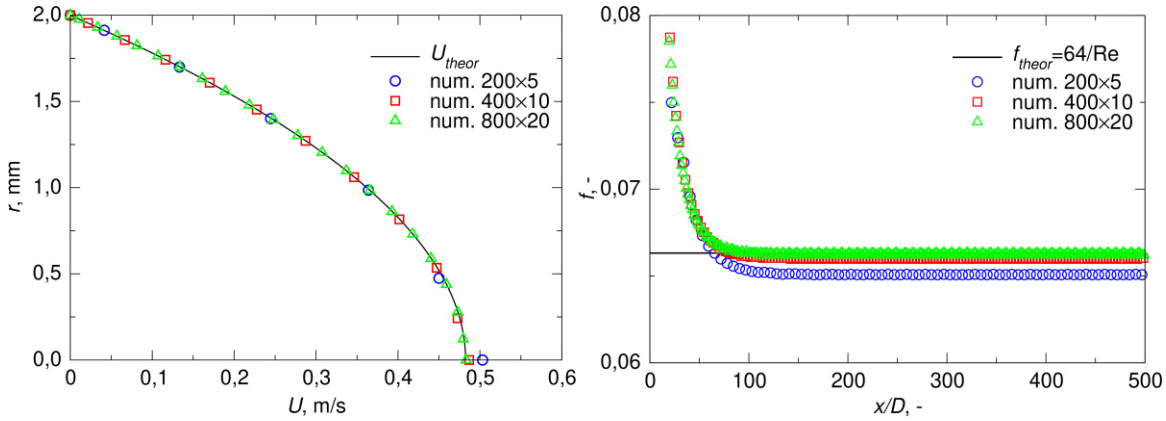

Figure 1. The computed velocity profile (left) evaluated at *x*/*D*=625 and friction factor (right) for laminar flow at Re=965

The dimensionless radial temperature distribution in the pipe and the local Nusselt number along the pipe are plotted in Fig. 2. Again, the computational results converge with increasing the mesh resolution, the analytical solution Nu=4.36 is correctly predicted and the results compare very well with the experimental results of [6] and the empirical correlation from [7].

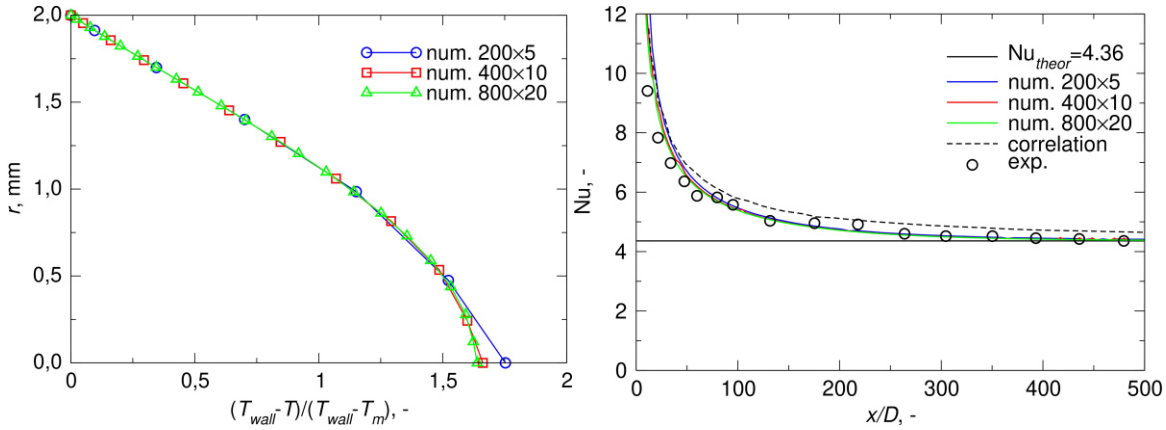

Figure 2. The computed dimensionless temperature profile (left) evaluated at *x*/*D*=625 and Nusselt number (right) for laminar flow at Re=965

After the verification with respect to the hydrodynamics and heat transfer, simulations of the laminar flow of the EG-Si_3N_4 nanofluid are performed. The geometry is given by the pipe length of 2 m and the diameter of 4 mm, with the imposed wall heat flux of 10 kW/m^2. The computed velocity profile and convective heat transfer coefficient of EG as base fluid and of EG-Si_3N_4 with various nanoparticle concentrations are plotted in Fig. 3 for the volume flow rate $Q=6\cdot10^{-5}$ m^3/s, corresponding to Re=1500 for the base fluid.

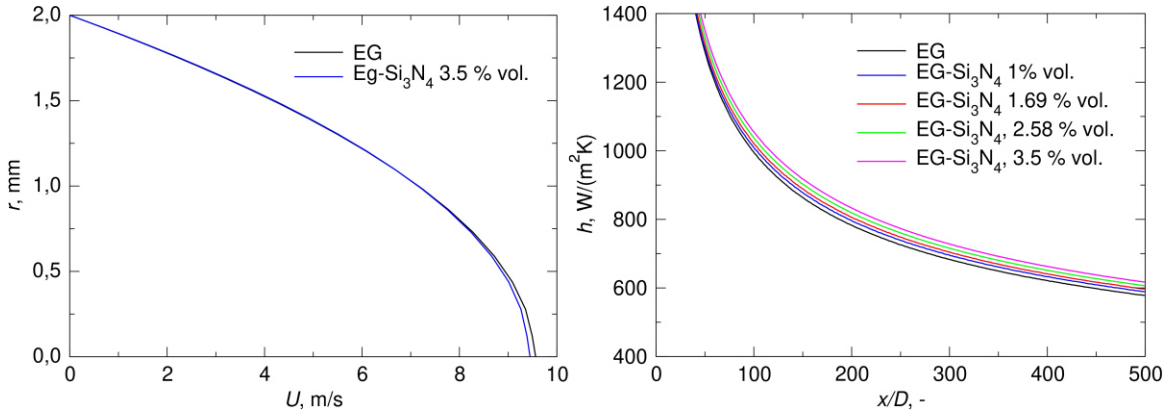

Figure 3. The computed velocity profile (left) evaluated at x/D=500 and heat transfer coefficient (right) at Q=6·10^{-5} m^3/s and various nanoparticle concentrations

It is clearly seen from the flattened velocity profile that the non-Newtonian shear thinning behaviour is correctly reproduced in the computational model, while the heat transfer coefficient increases with increasing the nanoparticle concentration. In addition, further computations were performed for the highest nanoparticle concentration of φ_V=3,5% in the range of Reynolds numbers from 200 to 2100, corresponding to the base fluid. It is found that the heat transfer coefficient increases with increasing the volume flow rate showing enhancement up to 6.5% compared to EG as the base fluid.

Summary/Conclusions: Heat transfer characteristics of EG-Si_3N_4 nanofluid in laminar pipe flow subject to forced convection and constant heat flux have been analysed. The computational model was verified against analytical and available experimental and empirical results. In contrast to previous studies, the nanofluid has been modelled as a non-Newtonian shear thinning fluid for various concentrations of Si_3N_4 nanoparticles. The obtained results show noticeable enhancement of heat transfer coefficient up to 6.5% for the EG-Si_3N_4 nanofluid compared to pure EG. The heat transfer coefficient increases with increasing the concentration of the Si_3N_4 nanoparticles and with increasing the Reynolds number of the flow. Future research should include temperature dependence of nanofluid thermal properties.

References:

1. G. Huminic, A. Huminic, Application of nanofluids in heat exchangers: A review, *Renewable and Sustainable Energy Reviews* 16 (2012) 5625-5638.
2. B.A. Bhanvase, M.R. Sarode, L.A. Putterwar, K.A. Abdullah, M.P. Deosarkar, S.H. Sonawane, Intensification of convective heat transfer in water/ethylene glycol based

nanofluids containing TiO_2 nanoparticles, *Chemical Engineering and Processing* 82 (2014) 123-131.

3. M. Akbari, N. Galanis, A. Behzadmehr, Comparative analysis of single and two-phase models for CFD studies of nanofluid heat transfer, *International Journal of Thermal Sciences* 50 (2011) 1343-1354.
4. G. Zyla, J. Fal, S. Bikić, M. Wanic, Ethylene glycol based silicon nitride nanofluids: An experimental study on their thermophysical, electrical and optical properties, *Physica E Low-dimensional Systems and Nanostructures* 104 (2018) 82-90.
5. T.L. Bergman, A.S. Lavine, F.P. Incropera, D.P. Dewitt, Fundamentals of heat and mass transfer, John Wiley & Sons Inc., Hoboken, New Jersey, 2011.
6. J.P. Meyer, M. Everts, Single-phase mixed convection of developing and fully developed flow in smooth horizontal circular tubes in the laminar and transitional flow regimes, *International Journal of Heat and Mass Transfer* 117 (2018) 1251-1273.
7. R.K. Shah, A.L. London, *Laminar Flow Forced Convection in Ducts*, Academic Press, New York, 1978.

1st International Conference on Nanofluids (ICNf2019)
2nd European Symposium on Nanofluids (ESNf2019)
26-28 June 2019, Castelló, Spain

Molecular Dynamics Simulation of Water Based Nanofluids Viscosity

V. Rudyak[1,2,3], S. Krasnolutskii[1], A. Belkin[1], E. Lezhnev[1]

[1]Novosibirsk State University of Architecture and Civil Engineering

Leningradskay Str., 113, Novosibirsk, 630008, Russian Federation

[2]Novosibirsk State University, Novosibirsk, Russian Federation

[3]Siberian Federal University, Krasnoyarsk, Russian Federation

[*]Corresponding author: valery.rudyak@mail.ru

Keywords: Nanofluid, Viscosity, Correlation Functions, Molecular Dynamics.

Abstract: Viscosity of the water and water based nanofluids with cuprum nanoparticles was studied by molecular dynamics method. It was shown that the simulation accuracy is of the order of the experimental one. The dependence of the nanofluid viscosity on particles volume concentration and their size was studied. The mechanisms of the impulse transfer (viscosity) of water and water base nanofluid were compared.

Introduction/Background: Nanofluids is actively studied last two decades. Today it is clear that transport properties of nanofluids are not described by the classical theories for the course dispersed fluid (Einstein's, Maxwell's, etc. theories). Viscosity and thermal conductivity of nanofluids depend not only on volume concentration of particles but also on their size and material [1,2]. These properties of nanofluids are reliably studied experimentally. However, the measurements of the thermophysical properties of nanofluids give only integral information about their transport processes and as a rule do not answer the question about the mechanisms of these processes. To study the mechanisms of transport processes the molecular dynamics (MD) method must be used. On the other hand, the nanofluid is very complex system with particles of micro- and nanosizes. Usually the nanoparticles are modelled by clusters of different size. But cluster is not nanoparticle because in liquid it may change (and change!) its size and shape. In addition, the atoms of such cluster can be replaced by the base fluid molecules. In real physical experiment we have stable nanoparticles, these particles have constant shape and size. In order to simulate the transport processes in such nanofluids, it is necessary to determine correctly the interaction potentials of nanoparticles with base fluid molecules and between each other. Such potentials were

constructed early in our papers [3,4]. The present paper is devoted to molecular dynamics simulation of the viscosity of nanofluids. We consider real water based nanofluids with Cu nanoparticles. The volume concentration of nanoparticles varied up to 5% and size of nanoparticles was equal to 2, 4 and 8 nm.

Discussion and Results: In our simulation, we employed the standard molecular dynamics method. We used the original SibMD package that was applied earlier for solving various problems of transport processes of nanofluids (see papers [1, 2] and references therein). The simulation was carried out in a cubic cell with periodic boundary conditions. The success of the molecular dynamics modeling is determined by the interparticles interaction potentials. It is well known that water is very complex fluid. Many complex intermolecular potentials were developed to study the different properties of the water (see [5,6] and references therein). These potentials have many unknown parameters therefore such potentials cannot be used to simulate the transport properties of nanofluids. For this reason, it is still impossible to model well enough viscosity and thermal conductivity of water in a wide range of temperatures and pressures. Currently, to simulate the viscosity of nanofluids, we must use the simplest interaction potentials for molecules and particles. Therefore, in this paper the interaction of molecules of the carrier liquid (water) was described by the Lennard-Jones 6-12 potential. The interactions of water molecules with nanoparticle and nanoparticles between each other were described by the RK [3] and RKI [4] potentials, respectively.

The shear viscosity coefficient η was calculated by means of the fluctuation-dissipation theorem (the Green–Kubo formula) which expresses the viscosity coefficient through correlation function χ of the stress tensor. Since the phase trajectories of the system are locally unstable and mixed in the molecular dynamic simulation the obtained results must be averaged over the ensemble of independent phase trajectories. In this study, averaging was carried out over 1000 independent phase trajectories. The integration step was equal to one femtosecond.

The simulation of the water viscosity under normal conditions was the first task of this work. We studied the dependence of the simulation accuracy on the number of molecules used. The number of molecules *N* was varied from 4000 to 64000. The viscosity coefficient achieved its plateau value [7] during 5 picoseconds. The simulation accuracy was determined by the comparison of the calculated and experimental [8] data. The obtained data are presented in Table 1. The relative simulation error was show in the last row. Using 64000 molecules we obtain the accuracy of the order of the experimental one.

The next task was the MD study of the viscosity coefficient of water based nanofluids with different size copper nanoparticles. It was shown that viscosity coefficient grows with increasing the volume concentration of the nanoparticles. The viscosity increase is much greater than that predicted by classical theories (Einstein's [9], Batchelor's [10], etc.). The viscosity enchantment achieves about 40% for the nanofluid with 4 nm particles at concentration equals to 5%. The nanofluid viscosity increases with decreasing particle size.

Summary/Conclusions: The first main conclusion of this study is very simple. The Lennard-Jones potential permits to simulate the viscosity of water with good accuracy. Developing this approach we can study successfully the transport coefficients of nanofluids. However we use special potentials [3,4], because the nanoparticles are not clusters. Finely, to achieve a good accuracy we have to use at least several tens of thousands molecules in the simulation cell. On the other hand the interactions of the nanoparticles between each other have almost no effect on the viscosity coefficient. The analysis of different contributions showed that despite the high increase in the overall viscosity coefficient compared to the base fluid, the kinetic part decreases. This decrease is caused by decreased molecular density in the nanofluid. It should be noted that the fluid is dense, therefore the kinetic contribution into the momentum transfer is small, about 11% for water, and 6–7% for the nanofluids. The potential contribution of molecules in the nanofluids is also slightly reduced. Thus, the increase in the viscosity caused mainly by nanoparticle–molecule interactions and the correlations between molecule–molecule and molecule–nanoparticle interactions.

To generalize the obtained conclusions to other water based nanofluids the effect of the interparticles interaction potentials was studied. For this purpose, the parameters of the nanoparticle atoms interaction potential were varied. It is shown that as the the depth of the potential well increases, the viscosity of the nanofluids also increases.

In the last part of the work the structure of nanofluid is studied. Using molecular dynamics simulation, the radial distribution functions of the water and water based nanofluids were obtained and compared. Nanofluids are found to be more ordered than the based fluid, with the degree of order of the base fluid increasing with increasing particle concentration. On the other hand the number density of the nanoparticles growths quickly with decreasing their size. Thus, the short-range order in a nanofluid is the greater, the smaller the nanoparticle size. This is the main reason why the viscosity of the nanofluid increases with decreasing particle size.

This work was supported by the Russian Foundation for Basic Research (17-01-00040 and 17-58-45023).

Table 1. The comparison of calculated η and experimental η_e data for the water viscosity

N	4000	8000	16000	64000
η, Pa·s	$8.17 \cdot 10^{-4}$	$8.37 \cdot 10^{-4}$	$8.46 \cdot 10^{-4}$	$8.77 \cdot 10^{-4}$
η_e, Pa·s	$8.902 \cdot 10^{-4}$	$8.902 \cdot 10^{-4}$	$8.902 \cdot 10^{-4}$	$8.902 \cdot 10^{-4}$
Δ, %	8.47	6.02	4.95	1.5

References:

1. V.Ya. Rudyak and A.V. Minakov, Thermophysical properties of nanofluids, *Eur. Phys. J. E* 41 (2018) 15.
2. V.Ya. Rudyak, Modern understanding of the thermophysical properties of nanofluids and features of their flows *J. Nanofluids* 8 (2019) 1-15.
3. V.Ya. Rudyak and S.L. Krasnolutskii, Diffusion of nanoparticles in a rarefied gas, *Technical Physics* 47 (2002) 807-813.
4. V.Ya. Rudyak, S.L. Krasnolutskii and D.A. Ivanov, The interaction potential of nanoparticles, *Doklady Physics* 57 (2012) 33-35.
5. W.L. Jorgensen, J. Chandrasekhar and J.D. Madura, Comparison of simple potential functions for simulating liquid water, *J. Chem. Physics* 79 (1983) P. 926-935.
6. A. Zen, Y. Luo, G. Mazzola, L. Guidoni, S. Sorella, Ab initio molecular dynamics simulation of liquid water by quantum Monte Carlo, *J. Chem. Physics* 142 (2015) 144111.
7. V.Ya. Rudyak, A.A. Belkin, D.A. Ivanov and V.V. Egorov, The simulation of transport processes using the method of molecular dynamics. Self-diffusion coefficient, *High Temperature* 46 (2008) 30-39.
8. K. Krynicki, C.D. Green and D.W. Sawyer, Pressure and temperature dependence of self-diffusion in water, *Faraday Discussions of the Chemical Society* 66 (1978) 199-208.
9. A. Einstein, Eine neue Bestimmung der Molekiildimensionen, *Annalen der Physik* 19 (1906) 289-306.
10. G.K. Batchelor, The effect of Brownian motion on the bulk stress in a suspension of spherical particles*, J. Fluid Mech.* 83 (1977) 97-117.

1st International Conference on Nanofluids (ICNf2019)
2nd European Symposium on Nanofluids (ESNf2019)
26-28 June 2019, Castelló, Spain

Stochastic analysis of nanofluid simulations

J. Ravnik[1*], A. Šušnjara[2], J. Tibaut[1] D. Poljak[2], M. Cvetković[2]

[1]University of Maribor, Faculty of mechanical engineering, Slovenia

[2]University of Split, Faculty of electrical engineering, mechanical engineering and naval architecture, Croatia

[*]Corresponding author: jure.ravnik@um.si

Keywords: Computational fluid dynamics, Stochastic collocation method, Variance based sensitivity analysis.

Abstract: In this paper we couple a computational fluid dynamics simulation of flow and heat transfer of nanofluids with stochastic modelling of input parameters. An effective properties numerical model is used to describe nanofluid flow. We simulate the flow and heat transfer in a heated pipe, for which experimental measurements are available. In order to assess the influence of input parameters on the simulation results, we employ the stochastic collocation method (SCM) as a wrapper around the deterministic code. In this way, we are able to propagate the uncertainty from input to output parameters. First, we identify the two most important parameters using the "One-at-a-time" principle and then, the full tensor SCM was used to assess the stochastic mean, variance and Sobol-like indices for sensitivity analysis.

Introduction: Cooling is one of the major challenges in development of efficient devices. In order for the heat transfer to be as efficient as possible, the choice of a working fluid is also very important. The thermal properties of the working fluid largely determine heat transfer characteristics. As thermal conductivity of water, oil and other working fluids are low, nanofluids were introduced. Nanofluid is a suspension consisting of uniformly dispersed and suspended nanometre-sized (10--50nm) particles in a base fluid. Nanofluids have a very high thermal conductivity at a very low nanoparticle concentrations and exhibit considerable enhancement of convection.

The stochastic collocation method (SCM) is a nonintrusive, sampling based method with strong mathematical foundations [5]. The polynomial representation of the stochastic output leads to significantly reduced number of simulations with respect to traditional Monte Carlo method. These features enable the use of SCM as a wrapper around the well-known deterministic code for nanofluid flow and heat transfer. Besides the

stochastic mean and variance of the flow fields, the stochastic framework is used for sensitivity analysis (SA) of the model. The SA is based on variance and it is conducted in two steps. Firstly, the "one-at-a-time" principle is used to reduce the dimensionality of problem and then the Sobol like indices are calculated thus leading to more detailed SA of the model.

Nanofluid model: In this paper we present a stochastic interpretation of results coming from a computational fluid dynamics simulation of nanofluid flow and heat transfer. Laminar steady flow is considered, for which incompressible Navier-Stokes equations are solved under the Boussinesq approximation where buoyancy is induced by changes of density. Ansys CFX was used to perform simulations. Nanofluid is modelled as a new fluid having effective properties. Nanoparticle volume fraction is used to estimate the TiO_2 nanofluid properties using established models [2] and temperature dependent properties of water and nanoparticles.

Flow in a heated pipe is considered. The geometry and boundary conditions are such that they replicate the experiment [1]. Flow and heat transfer on the nanofluid as well as heat transfer through the copper pipe material is simulated. We take the particle volume fraction and the wall heat flux to be the random variables subjected to stochastic analysis.

Stochastic modelling: The stochastic model consists of *d* input parameters modelled as random variables (RV), organised in input vector: $\boldsymbol{X} = [x_1, \dots, x_d]$. The SCM is based on the polynomial approximation of the considered output *Y* in the *d* dimensional stochastic space: $\hat{Y}(\boldsymbol{X}) = \sum_{k=1}^{N} L_k(\boldsymbol{X}) \cdot Y^{(k)}$, where $L_k(\boldsymbol{X})$ are the Lagrange basis functions and $Y^{(k)}$ are is the output realization for the *k*-th input point. The interpolation points (SC points) in each dimension are calculated according to Gauss-Legendre quadrature rule. The interpolation in the multivariate dimension space is done by using the tensor product of basis functions. The stochastic mean is calculated according to the formula known from the statistics:

$$\mu\left(\hat{Y}(\boldsymbol{X})\right) = \int_D \hat{Y}(\boldsymbol{X}) p(\boldsymbol{X}) d\boldsymbol{X} = \sum_{k=1}^{N} Y^{(k)} w_k$$

where weights w_k are pre-computed for each collocation point $\boldsymbol{w_k} = \int_{\mathbf{D}} \boldsymbol{L_k(X)p(X)dX}$. The $p(\boldsymbol{X})$ stands for joint probability density function, $p(\boldsymbol{X}) = \prod_{k=1}^{d} p(X^{(k)})$. The formula for stochastic variance is obtained accordingly and the final form is given as:

$$Var\left(\hat{Y}(\boldsymbol{X})\right) = \sum_{k=1}^{N} \left(Y^{(k)}\right)^2 w_k - \mu^2$$

A more detailed description of the SCM is available in [4].

Results: We numerically repeated the experiment [1] using heating of 200 W, mass flow rate 6 g/s and nanoparticle mass fraction 1%. We made the stochastic analysis considering two input parameters: the heat flux (q) and the nanoparticle volume fraction (φ). A uniform distribution of 10% variation from the nominal value is assumed. We consider 3 collocation points and 5 collocation points. In the first case this yield 3x3=9 flow simulations and in the second one 5x5=25 simulations. In Figure 1, we show the temperature profiles calculated for 3 and 5 collocation points, along the wall of the pipe together with the standard deviation obtained from the stochastic analysis and compare those to experimental values [1].

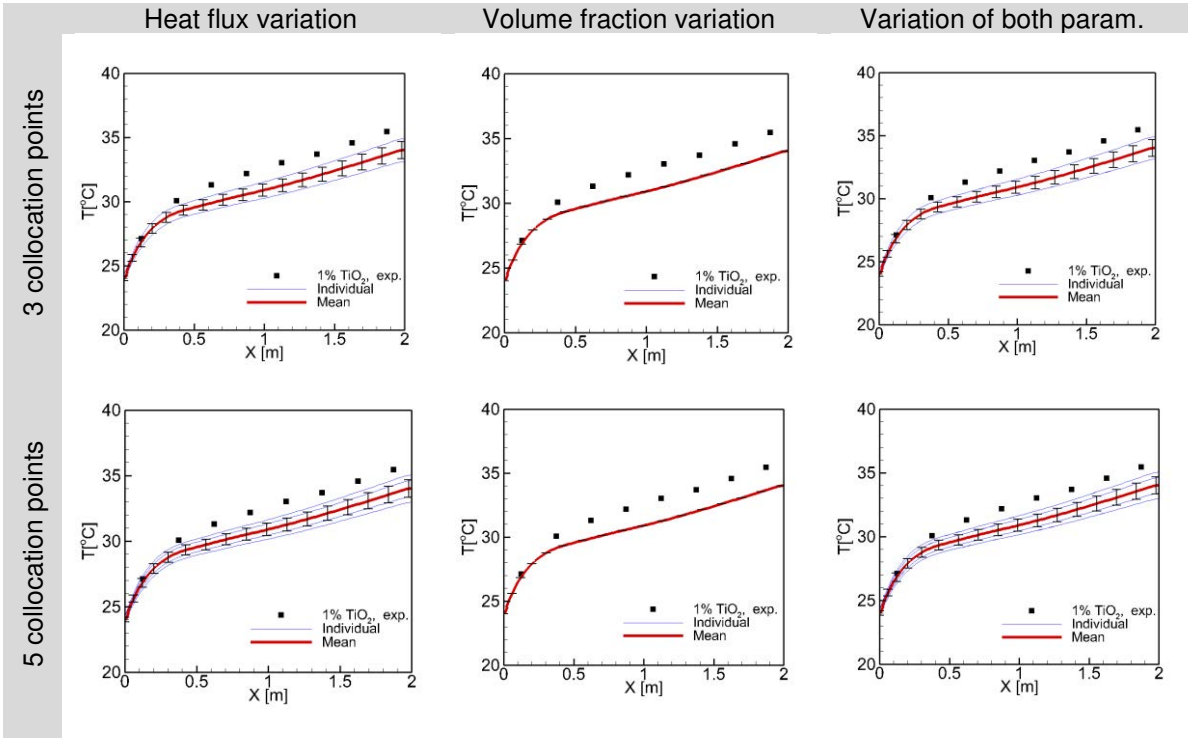

Figure 1. Temperature profiles with standard deviation along the wall of the pipe, for 3 (top) and 5 (bottom) collocation points, for constant φ and variated q (left), constant q and variated φ (middle) and all numerical test cases (right).

The results show, that the heat flux has the most influence on the results of the numerical simulation. The variation in the temperatures for each case in very high. On the other hand, variation of the volume fraction does not significantly influence the temperature profile. The results show that there is little difference in standard deviations and means obtained with 3 and 5 collocation point stochastic analysis. In Figure 2 we determine, that the velocity profile is unaffected by parameter changes, a much larger effect can be seen on the temperature profiles.

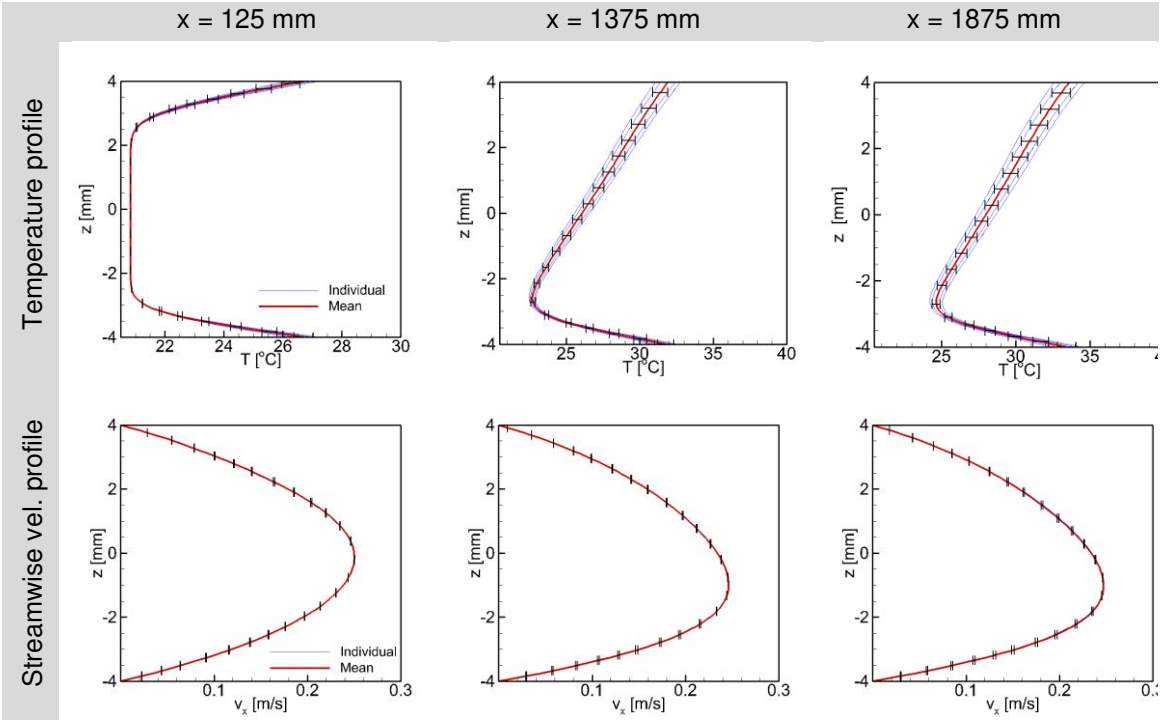

Figure 2. Temperature profiles (top) and streamwise velocity profiles (bottom) at different vertical cross-section along the pipe.

Conclusions: Using stochastic uncertainty analysis as a wrapper around a deterministic flow and heat transfer simulation tool, gives engineers a non-intrusive tool to assess the accuracy of simulations and estimate the importance of individual parameters. Using stochastic collocation method, we significantly reduce the number of required simulations. This is especially important in nanofluid simulations, as such simulations are computationally intensive. We applied the method to simulation of nanofluid flow in a pipe. We were able to identify the heat flux as the input parameter, which affect the nanofluid flow results most significantly. Nanoparticle volume faction plays a less significant role.

References:

1. L. Colla, L. Fedele, and M. H. Buschmann. Laminar mixed convection of TiO_2-water nanofluid in horizontal uniformly heated pipe flow. *International Journal of Thermal Sciences*, 97:26–40, 2015
2. J. Ravnik, A. Susnjara, J. Tibaut, D. Poljak, M. Cvetkovic, Stochastic modelling of nanofluid heat transfer, *4th workshop UNEMA*, Split, Croatia, 2018
3. A. Saltelli, et al. Variance based sensitivity analysis of model output. Design and estimator for the total sensitivity index, *Comput Phys Commun,* Vol. 181, No. 2, pp. 259-270, 2010
4. D. Xiu. "Fast Numerical Methods for Stochastic Computations: A Review", *Commun Comput Phys*, Vol. 5, No. 2-4, pp. 242-272, 2009.

1st International Conference on Nanofluids (ICNf2019)
2nd European Symposium on Nanofluids (ESNf2019)
26-28June 2019, Castelló, Spain

Nanoparticles in ionic liquids: numerical evaluation of heat transfer behavior in laminar flow

E.I. Chereches[1*],M. Chereches[1],A. Dima[1]and A.A.Minea[1]

[1]Technical University "Gh. Asachi" of Iasi, Bd. D. Mangeron no. 63, Iasi, Romania

[*]elena_ionela97@yahoo.com

Keywords: nanoparticles, ionic liquids, heat transfer, ionanofluids.

Abstract: Developing materials that efficiently combine cutting-edge technology with competitive costs so as to meet technical, economic and, last but not least, environmental challenges are a must in the field of materials engineering and beyond. Ionic liquids are heat transfer fluids that offer a wide range of advantageous properties. One of the most recent application of these complex ionic liquids and nanomaterial systems is the ionanofluids. In this paper we performed a numerical study of the laminar flow of a fluid through a pipeline, accompanied by thermal transfer. The problem is typically addressed by validating the model on experimental bases and then implementing four less studied fluids, namely two ionic liquids and two ionanofluids (obtained by adding 1% multi walled carbon nanotubes - MWCNT). The numerical results presented confirm the theory of the definite advantages of adding nanoparticles to conventional liquids.

Introduction: An ionic liquid is a liquid salt and in certain contexts, the term has been limited to salts whose melting point is below a certain temperature, such as 100°C (212°F) [1]. Ionic liquids are considered to be low-conducting liquids with high-viscosity, non-ionizing, and very low vapor pressure [2]. Their properties are varied: many of them have low combustibility, are thermally stable, with wide liquid regions and favourable solvation properties for a series of polar and non-polar compounds [3]. An ionanofluid is defined as a stable dispersion of nanomaterial particles (tubes, rods, spheres, etc.) in an ionic liquid and the first article on the thermal properties of ionanofluids was published in 2009 [4]. The first record of the functionalization of carbon nanotubes (CNT) in ionic liquids was presented by Aida et al. [5,6] who discovered that carbon nanotubes (CNT) and ionic liquids can be mixed to form gels called "Bucky gels", now considered in the ionanofluid category. Sheveylyova et al. [7] measured the caloric capacity of $[C_4mim][BF_4]$ and $[C_4mim][PF_6]$ with MWCNT produced by gaseous catalytic precipitation in the temperature range 80-370 K. However, the amount of ionanofluids obtained was

around 12 wt% of the concentrated nanomaterial, but surprisingly the same improvement (8%) was obtained, which was also achieved with 1 wt% MWCNT. An interesting phenomenon has been observed by Liu et al. [8] and Wang et al. [9], where the addition of MWCNT and graphene nanoparticles resulted in a reduction in viscosity. Concerning ionanofluids containing MWCNT, the thermal conductivity of various pure ionic liquids according to temperature was measured by Franca et al. [10]. Ribeiro et al. [11] found that the thermal conductivity of each studied ionic liquid decreased linearly within the temperature range studied, a phenomenon also found in the literature on ionic liquids.

Discussion and Results: The numerical approach consists of a study of forced laminar flow and heat transfer for two ionic liquids and two ionanofluids in a pipe, as can be seen in Figure 1. The pipe has a radius of 0.0294m and a length of 6.045m. The fluid enters into the pipe with constant velocity (calculated based on Re for each fluid) and with a temperature of 298.15K. The heated area of the walls is from: x=1.83 m at x=4.27 m. while the wall heat flux is constant at 5210.85W/m^2.

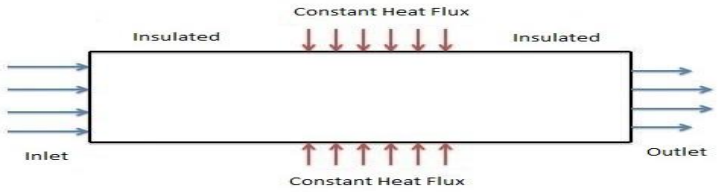

Figure 1. Description of the case studied – pipe cross section.

The fluid flow is characterized by the Reynolds number:

$$\mathrm{Re} = \frac{w \cdot d}{\nu} \tag{1}$$

where: w – the average fluid velocity, [m/s]; d–the characteristic length of the flow,[m];υ – the kinematic viscosity of the fluid,[m^2/s]. In our case d = 0.05588m. A numerical analysis was performed for different Reynolds numbers, Re = 500, and Re = 1000 respectively, in laminar flow – see the transport equations in Ansys [12]. The properties of the considered fluids are shown in Table 1, while the validation was performed in terms of Nu. Results for the Nusselt number at x = 2.67 m and x = 6.045 m from inlet are shown in Figure 2.

Table 1. Thermophysical Properties of ionic liquids and ionanofluids at 298.15K.

Code	Fluids	Specific heat (J/Kg*K)	Density (Kg/m^3)	Thermal conductivity (W/m*K)	Dynamic viscosity (N s/m^2)	Kinematic viscosity (m^2/s)
IL 1	[C_{4mim}][NTf_2]	1372.44	1441.34	0.117	0.0285	1.977e-5

IL 2	[C_{2mim}][$EtSO_4$]	1615	1241.37	0.175	0.05001	4.0280e-5
INF1	[C_4mim][NTf_2]+ 1%MWCNT	1396.03	1423	0.129	0.03158	2.21925e-5
INF2	[C2mim][EtSO4] + 1%MWCNT	1642.72	1226.06	0.189	0.05398	4.40272e-5

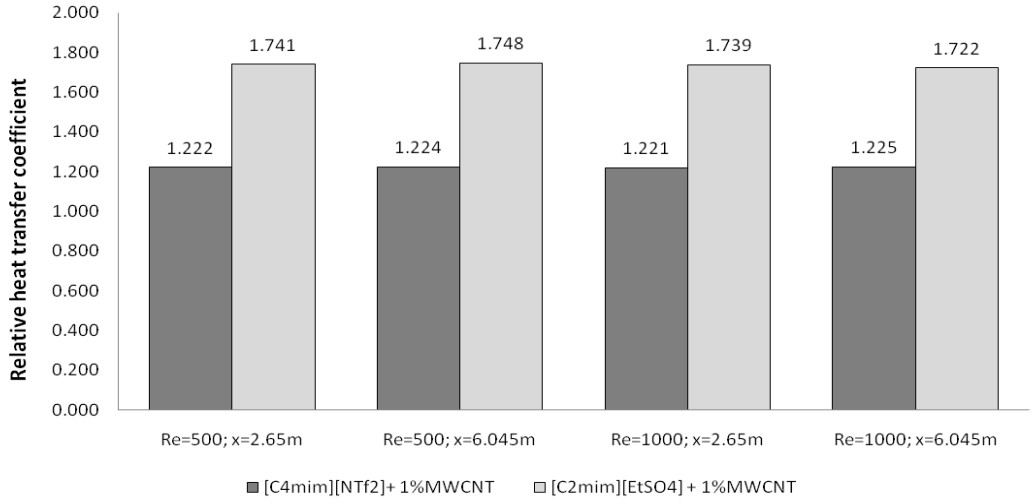

Figure 2. Heat transfer coefficient enhancement in comparison with base fluid

The heat transfer performance of ionic liquid and ionanofluid was defined by the convective heat transfer coefficient (h), which was extracted from the code post-processing module:

$$h = \frac{Nu \cdot K}{L} \tag{3}$$

Where Nu is Nusselt number, k is the thermal conductivity and L is the diameter of the pipeline.

Where h is the heat transfer coefficient by convection, L is the diameter and k is the thermal conductivity. The relative heat transfer coefficient is plotted in Figure 2 and is defined as:

$$h_{relative} = \frac{h_{ionanofluid}}{h_{liquid}} = \frac{Nu_{ionanofluid} \cdot K_{ionanofluid}}{Nu_{liquid} \cdot K_{liquid}} \tag{4}$$

Conclusions: This research follows a numerical procedure to outline the benefits of nanoparticle enhanced fluids over conventional fluids for heat transfer.By introducing 1% MWCNT into the ionic liquid [C_4mim][NTf_2] an increase of the convection heat transfer coefficient of 22.2 % and 22.4% is noticed, for Re of 500 at a distance x = 2.65m and x = 6.045m,respectively. For the same ionic liquid, an increase of the convection thermal transfer coefficient of 22.1% and 22.5%, respectively, for Re of 1000 was observed. For ionanofluid [C_2mim][$EtSO_4$] + 1% MWCNT and Re=500, an increase in the heat transfer coefficient of 74.1% -74.8% was noticed.

References:

1. T.Fukushima and T.Aida, Ionicliquids for soft functional materials with carbon nanotubes,*Chem. A Eur. J*. 13 (2007) 5048–5058.
2. F. Endres and S.Z. El Abedin, Air and water stable ionic liquids in physical chemistry,*Phys. Chem. Chem. Phys*. 8 (2006) 2101-2116.
3. H.L. Ngo, K. LeCompte, L. Hargens and A.B. McEwen, Thermal properties of imidazolium ionic liquids, *Thermochim. Acta* 357–358 (2000) 97-102.
4. C.A.Nieto de Castro, M.J.V.Lourenço, A.P.C.Ribeiro, E.Langa, S.I.C.Vieira, P.Goodrichand and C. Hardacre, Thermal Properties of Ionic Liquids and Ionanofluids of Imidazolium and PyrrolidiniumLiquids,*J. Chem. Eng. Data*55(2)(2010) 653–661.
5. T.Fukushima, A.Kosaka, Y.Ishimura, T.Yamamoto, T.Takigawa, N.Ishiiand and T. Aida, Molecular Ordering of Organic Molten Salts Triggered by Single-Walled Carbon Nanotubes,*Science* 300 (5628) (2003) 2072-2074.
6. T.Fukushima and T. Aida, Ionic Liquids for Soft Functional Materials with Carbon Nanotubes,*Chemistry-A European Journal*13(18) (2007)5048-5058.
7. M.P.Shevelyova, Y.U.Paulechka, G.J. Kabo, A.V.Blokhinand and G. Kabo, Physicochemical Properties of Imidazolium-Based Ionic Nanofluids: Density, Heat Capacity, and Enthalpy of Formation,*J. Phys. Chem. C*117 (2013) 4782−4790.
8. J.Liu,F.Wang, L. Zhang, X.Fang and Z. Zhang, Thermodynamic properties and thermal stability of ionic liquid-based nanofluids containing graphene as advanced heat transfer fluids for medium-to-high-temperature applications,*Renew. Energy* 63(2014)519–23.
9. F.Wang, L.Han, Z.Zhang, X.Fang, J.Shi and W. Ma, Surfactant-free ionic liquid-based nanofluids with remarkable thermal conductivity enhancement at very low loading of grapheme, *Nanoscale Res. Let*. 7(2012)314–320.
10. J. M. P.França, F.Reis, S. I. C.Vieira, M. J. V.Lourenço, F. J. V.Santos, C. A.Nieto de Castro and A. H. Pádua, Thermophysical Properties of Ionic Liquid Dicyanamide (DCA) Nanosystems. *J. Chem. Thermodyn*. 79(2014) 248–257.
11. A.P.C.Ribeiro,S.I.C.Vieira,P.Goodrich, C.Hardacre, M.J.V.Lourenço and C.A. Nieto de Castro, Thermal conductivity of [Cnmim][(CF3SO2)2N] and [C4mim][BF4] IoNanofluids with carbon nanotubes – Measurement, theory and structural characterization, *J. Nanofluids*2(2013) 55–62.
12. AnsysWorkbech version 17.

1st International Conference on Nanofluids (ICNf2019)
2nd European Symposium on Nanofluids (ESNf2019)
26-28 June 2019, Castelló, Spain

Numerical simulation of mixed convection of a nanofluid with different numerical models

J. Tibaut[1*], T. Tibaut[2], J. Ravnik[1]

[1]University of Maribor, Faculty of mechanical engineering, Slovenia

[2]University of Ljubljana, Faculty of mechanical engineering, Slovenia

[*]Corresponding author: jan.tibaut@um.si

Keywords: *Nanofluids, single-phase model, mixture model, pipe flow, natural convection, forced convection*

Abstract: In this paper, we present a numerical study of laminar mixed convection of a nanofluid in a pipe and compare the results to experimental measurements. Mechanisms that control the behaviour of nanoparticles in the base fluid and the fluid motion are not very well known. Thus, it is important to know, which mathematical model describes the nanofluid best.

Introduction/Background: Nanofluids are a mixture of a base fluid and nanometre sized particles. The base fluid is usually water. Two approaches can be considered in order to simulate flow of a suspension of particles: the Euler-Euler method and the Euler-Lagrange method. In this study, we used the first method. The fluid and the particles are considered as continuous phase. We used the single-phase model and the mixture model. An investigation using the single-phase model was presented by Ravnik et al. [1]. They simulated the fluid motion with the boundary-domain integral numerical method. In the single-phase model, the properties of the fluid are obtained from empirical correlations. On the other hand, the mixture model is more complex. The model was presented by Buongiorno [2]. In the mixture model an additional conservation equation is employed in order to solve the dispersion of nanoparticles in the fluid. Khalili et al. [3] employed the mixture model to simulate the flow of a nanofluid in a circular enclosure. Numerical simulations were performed using both type of models in order to simulate the flow of a nanofluid in a heated pipe. We used the same test case as it was presented in the experimental study of Colla et al. [4].

Numerical models: Three conservation laws were employed in order to simulate the fluid flow and heat transfer. Firstly, the continuity equation for incompressible fluid, secondly the momentum conservation equation was used to solve the pressure and velocity vector field and thirdly the energy equation was employed to solve the

temperature field. In the mixture-model an additional conservation equation is used to solve the volume fraction.

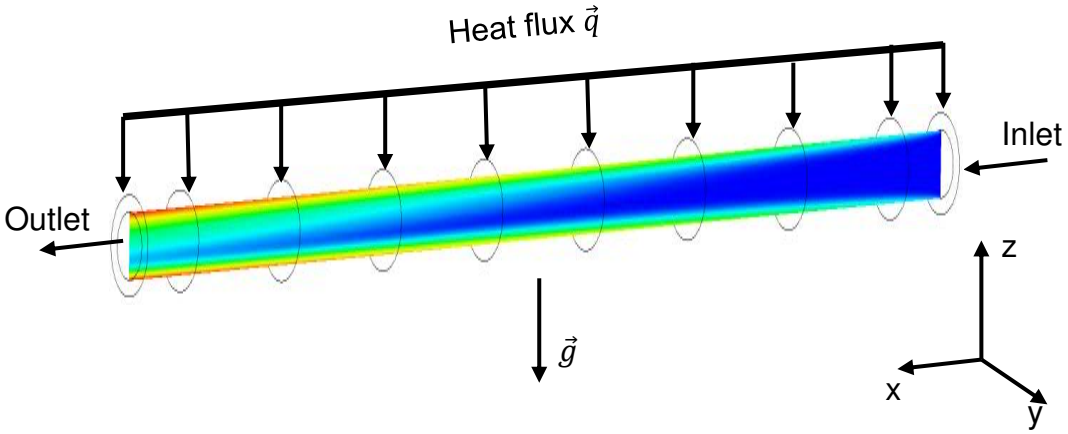

Figure 1. A representation of the boundary conditions and a temperature isolines on the cross-section x-z

In the single-phase model the nanofluid is considered as a homogeneous mixture. The density of the nanofluid, heat capacity, viscosity, thermal conductivity and thermal expansion coefficient were modelled according to the models given in [1].

In the mixture model [2], the additional volume fraction conservation equation is presented in this form:

$$(\vec{v}\cdot\vec{\nabla})\varphi = -\vec{\nabla}(\vec{j}_B + \vec{j}_T), \tag{6}$$

φ is the particle volume fraction, $\vec{j}_B$ is the Brownian motion and $\vec{j}_T$ is the thermophoresis. If we write the equation with the Fick and Fourier's laws of diffusion, we get this form:

$$(\vec{v}\cdot\vec{\nabla})\varphi = -\vec{\nabla}(\rho_{np}D_B\vec{\nabla}\varphi + \rho_{np}D_T\vec{\nabla}T), \tag{7}$$

where D_B is the diffusion coefficient of the Brownian motion and D_T is the diffusion coefficient of the thermophoresis. The D_B coefficient is solved with the Stokes-Einstein equation, that was presented in [2]:

$$D_B = \frac{k_B T}{3\pi\mu_f d_p}, \tag{8}$$

where k_B is the Boltzmann constant, T is the temperature and d_p is the particle diameter. The model for D_T is [2]:

$$D_T = 0.26\frac{k_f(T)}{2k_f(T)+k_{np}}\frac{\mu_f(T)}{\rho_{np}}\frac{\varphi}{T}, \tag{9}$$

The mass flow rate, heat flux and particle volume fraction were set in the same way as in the experiment. The mass flow rate was $6\frac{g}{s}$, the volume fraction was 0.027 (mass fraction 1%) and 0.065 (mass fraction 2.5%). The pipe was heated at the wall with 23889 $[\frac{W}{m^2}]$. Numerical simulations were performed with Ansys CFX numerical solver. The solver solves the system of linear equations with the Fine volume method.

Results and discussion:

For the mixture model, we set two different cases. In the first case, the boundary condition of the volume fraction at the inlet of the pipe was homogeneous. For the second case the volume fraction as inlet was non-homogeneous. A sigmoid function was used at the inlet of the pipe to describe the particle volume fraction. The shape of the sigmoid function was set up in a way that the volume fraction increased towards the bottom of the pipe

In Figure 1 we present the boundary conditions of the set numerical test case and the temperature profile on the cross section x-z for the non-homogeneous boundary condition on the inlet of the pipe.

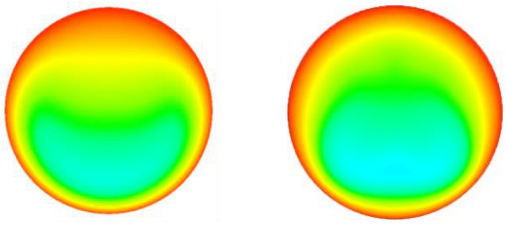

Figure 2. The isotherms of the single-phase model (left) and the mixture model (right) on a cross-section of the pipe at the distance of 1.825 m from the inlet.

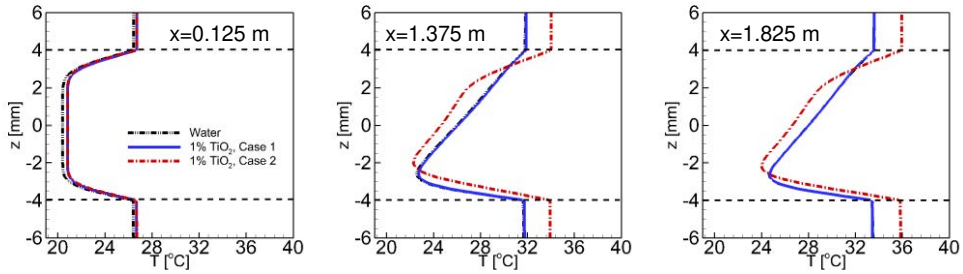

Figure 3. The temperature profiles for three different cross sections, pure water, the single-phase model (Case1) and the mixture-model (Case 2) with non-homogeneous boundary condition.

In Figures 2 and 3 we present the temperature profiles and isotherms at different positions in the pipe. We observed that there is a difference between the two numerical models in the temperature profile.

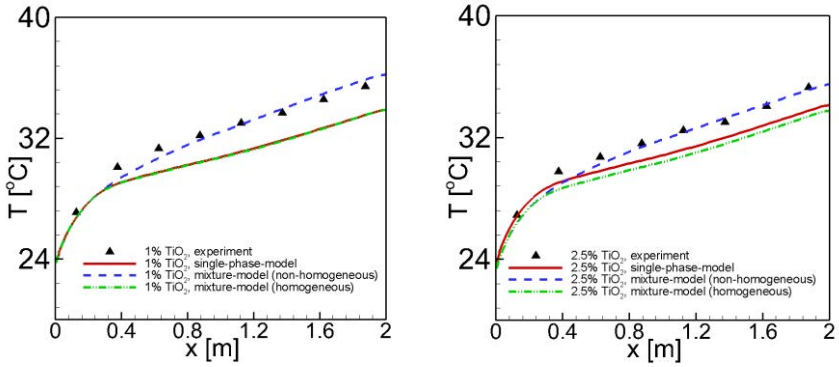

Figure 4. The temperature at the wall of the pipe for different models.

In Figure 4 we present the results of the pipe wall temperature for different numerical simulations: We observed that the mixture model with the non-homogeneous volume fraction boundary condition has shown good agreement with the experiment.

Conclusions:

We can conclude that single phase model and mixture model with constant inlet particle volume fractions both lead to poor agreement with the experiment. By changing the inlet particle volume fraction distribution we were able to capture experimental values well.

References:

1. Ravnik, J. & Škerget, L. A numerical study of nanofluid natural convection in a cubic enclosure with a circular and an ellipsoidal cylinder, International Journal of Heat and Mass Transfer, 89 pp. 596–605, 2015.
2. Buongiorno, J. Convective Transport in Nanofluid, Journal of heat transfer, 128(March 2006), pp. 240–250, 2006.
3. Khalili, E., Saboonchi, A. & Saghafian, M. Natural Convection of Al2 O3 Nanofluid Between Two Horizontal Cylinders Inside a Circular Enclosure, Heat Transfer Engineering, 38(2), pp. 177–189, 2017.
4. Colla, L., Fedele, L. & Buschmann, M. H. Nanofluids suppress secondary flow in laminar pipe flow, v International Conference on Heat Transfer and Fluid Flow pp. 1–4, 2015.

1st International Conference on Nanofluids (ICNf2019)
2nd European Symposium on Nanofluids (ESNf2019)
26-28 June 2019, Castelló, Spain

Numerical analysis of the cooling of a flat plate using nanofluids at a high Reynolds number

E. M. Garcia-Merida, J. Ortega-Casanova*

Andalucía Tech, Escuela de Ingenierías Industriales, Universidad de Málaga,

C/ Dr Ortiz Ramos s/n, 29071 Málaga, Spain

*Corresponding author: jortega@uma.es

Keywords: nanofluid, aluminum, heat transfer, CFD, impinging jet, correlations.

Abstract: In this paper, the numerical analysis of an impinging jet of Al2O3-water nanofluid at a high Reynolds number is carried out using ANSYS Fluent. The main purpose of the paper is to describe the effects on heat transfer throughout a parametrical analysis by varying the jet-to-plate distance and the volume fraction of nanoparticles in the nanofluid. The Reynolds number is constant and equal to 23000, based on the jet diameter, so that a turbulence model has been used. In order to assess the effect that changing the parameters have in the heat transfer, the Nusselt number at the stagnation point and the average Nusselt number at the plate are used, as well as its uniformity by means of the standard deviation. Heat transfer enhancement is up to around 22% for a jet-to-plate-distance four times the diameter of the jet and a 10% of nanoparticles in volume fraction. This configuration also has the highest uniformity. Finally, some numerical correlations have been obtained for the average Nusselt number on the plate using Matlab.

Introduction/Background: The evolution of cooling technologies has always been constrained due to the relatively low thermal conductivity of fluids compared to solids (thermal conductivity of aluminum is around 400 times bigger than conductivity of water) in many applications: electronics, engines, power generation, etc. Despite the addition of solid particles to base fluids had been previously studied theoretically and experimentally, the use of nano-sized particles was not considered until 1990s [1], meaning the beginning of the nanofluids. There have been many proposed models for the properties of nanofluids considering both complex and simple mechanisms, but properties such as density or heat capacity are usually given by the volumetric fractions proportionally. Impinging jets are a common cooling technology extensively studied numerically for high Reynolds numbers during the last years [2]. In this numerical study, a Al_2O_3 nanofluid (one of the most studied) is used in a submerged impinging jet

projected at Reynolds 23000 to a heated flat plate (see Figure 1a). The main parameters of the study are the diameter of the jet, the jet-to-plate distance and the volume fraction of nanoparticles.

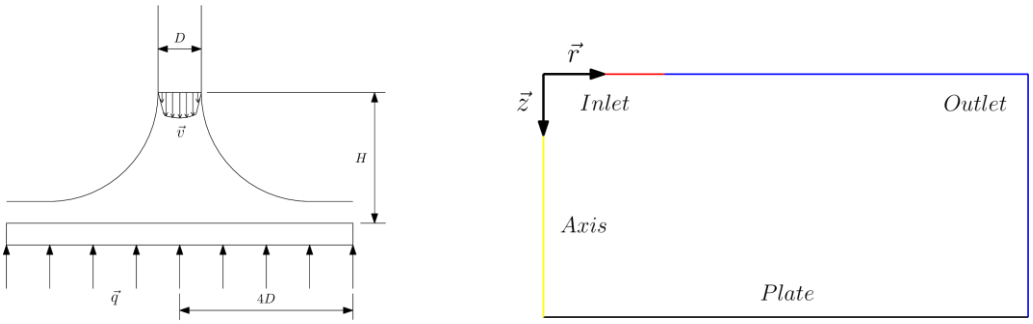

(a) **(b)**

Figure 1. Geometry (a) and boundaries of the problem (b).

Discussion and Results: Considering a steady, incompressible, axisymmetric, turbulent flow and ignoring gravity, the Reynolds-Averaged Navier-Stokes (RANS) equations are:

$$\frac{\partial \hat{V}_i}{\partial \hat{x}_i} = 0, \tag{1}$$

$$\frac{\partial(\hat{V}_i\hat{V}_j)}{\partial \hat{x}_j} = -\frac{1}{\rho}\frac{\partial \hat{P}}{\partial \hat{x}_i} + \nu\frac{\partial}{\partial \hat{x}_i}\left[\frac{\partial \hat{V}_i}{\partial \hat{x}_j} + \frac{\partial \hat{V}_j}{\partial \hat{x}_i}\right] + \frac{\partial(-\hat{v}_i'\hat{v}_j')}{\partial \hat{x}_j}, \tag{2}$$

$$\frac{\partial}{\partial \hat{x}_i}\left[\hat{V}_i(\rho\hat{e} + \hat{P})\right] = \frac{\partial}{\partial \hat{x}_i}\left[K_{eff}\frac{\partial \hat{T}}{\partial \hat{x}_j}\right] + \Phi, \tag{3}$$

where $\hat{V}_i$, with $i = r, \theta, z$ are the average radial, azimuthal and axial components of the velocity, $\hat{v}_i$ is the turbulent component of the instant velocity ($\hat{v} = \hat{V} + \hat{v}'$), $\hat{P}$ is the pressure, T is the temperature, $\hat{e}$ is the internal energy per unit mass. ϵ is the Diract Delta function, K_{eff} ($K_{eff} = K + K_t$) is the effective thermal conductivity considering turbulence thermal conductivity $K_t = c_p\mu_t/Pr_t$, c_p is the specific heat of the fluid, Pr_t is the Prandtl number for turbulence, Φ is the viscous dissipation term and ν is the kinematic viscosity. The heat flux at the plate is constant, $q = 100\,W$. Some non-dimensional performance parameters have been obtained: to quantify the quality of the heat transfer, the Nusselt number based on the diameter; for the pumping pressure, a non-dimensional power (Π); and to evaluate the overall quality of the solution, a non-dimensional efficiency has been defined (η):

$$Nu = \frac{hD}{K}; \qquad \Pi = \frac{pQ}{\rho D^2 U^3}; \qquad \eta = \frac{Nu}{\Pi}, \tag{4}$$

where h is the film coefficient at the plate, D the diameter of the jet, K the thermal conductivity, Q the volume flow, U a characteristic velocity and ρ the density. The Nusselt number both averaged at the plate (Nu_{avg}) and at the stagnation point (Nu_0) have been

used to compare different configurations, as well as the standard deviation σ to quantify its uniformity. The nanofluid has been considered as a one-phase fluid where nanoparticles and liquid are in thermal equilibrium and move at the same velocity, as done in [3]. While density and heat capacity are given by the volume fraction of nanoparticles proportionally, the dynamic viscosity and the conductivity have been obtained from correlations [2,8]. 15 case scenarios have been simulated for $Re = 23000$ by changing the volume fraction $\phi = [0, 1, 3, 6, 10]\%$ and the ratio $H/D = [1, 2, 4]$. A GCI study has been carried out using 3 different grids for the most critical case, $H/D = 1$ without nanoparticles, where the highest velocities are accomplished. Figure 2(a) shows the convergence of the solution using Richardson's extrapolation for Nu_{avg}, finally using $N_2 = 210$ radial cells ($GCI = 0{,}0043\%$). Figure 2(b) shows the validation of the configuration, comparing the Nusselt number at the plate against [4]. For turbulence modelling, different models have been compared (Figure 3a) to experimental data from [5,6,7], finally choosing the SST-Transition with Kato-Launder modification because of its lower percentage average error against the experimental data.

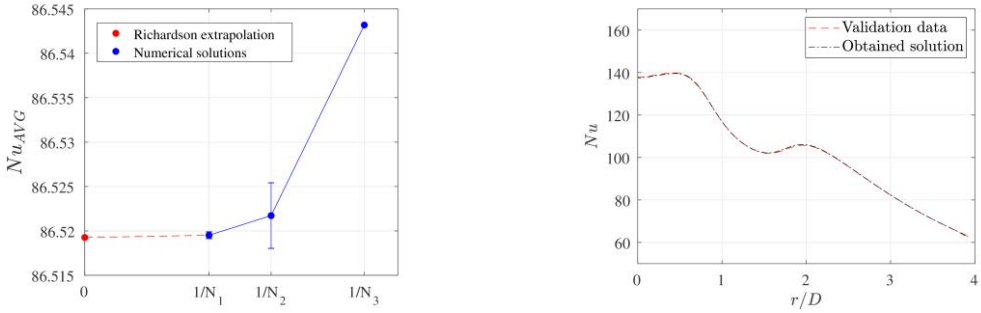

(a) **(b)**

Figure 2. GCI (a), and validation with [4] (b).

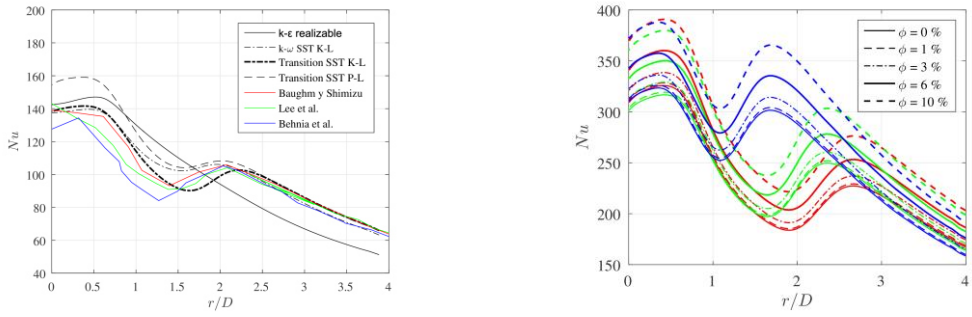

(a) **(b)**

Figure 3. Turbulence models comparison against experimental data, with air as working fluid (a), and radial Nusselt number distribution for different ϕ and $H/D = 1$ (red), $H/D = 2$ (green) and $H/D = 4$ (blue) (b).

As main result of the simulations, the Nusselt number has been plotted against the non-dimensional radius of the plate in Figure 3(b), which clearly shows that the heat transfer quality increases when ϕ increases. As complement to Figure 3, Table 1 shows that Nu_{avg}

increases with distance and that the heat transfer is more uniform (lower σ). Table 1 also shows some regular dependency of Nu_{avg} with ϕ and H/D, thus potential correlations have been prepared for all the non-dimensional parameters. As example, the correlation for Nu_{avg} and the mean error with respect to the numerical values are:

$$Nu_{avg} = 2.047 \cdot 10^2 \left(\frac{H}{D}\right)^{7.083 \cdot 10^{-2}} \cdot \left(1 - \frac{\phi}{100}\right)^{-1.872} ; \; Error = 0.715\% \qquad (5)$$

Table 1. Results for Nu_{avg} and σ (uniformity).

H/D	1					2					4				
ϕ [%]	0	1	3	6	10	0	1	3	6	10	0	1	3	6	10
Nu_{avg}	207.45	209.24	216.13	230.70	251.33	214.67	216.53	223.66	238.72	260.02	228.76	230.73	238.29	254.24	276.75
σ	53.88	54.29	55.83	59.11	63.82	46.14	46.48	47.77	50.54	54.53	38.67	38.95	40.04	42.38	45.79

Summary/Conclusions: some of the most important conclusions from this study are:

1. Improvement of the heat transfer as ϕ and H/D increase, resulting in a bigger film coefficient and a more uniform refrigeration. Nu_{avg} is a 21% bigger for the same geometry with a 10% volume fraction of nanoparticles compared to only water. Uniformity (σ) increases around a 14,5% when doubling the jet-to-plate distance.
2. The use of simplified one-phase, thermal-equilibrium macroscopic models for the thermophysical properties of nanofluids allow a fast CFD analysis with illustrative results that can provide understanding of their behavior.
3. For practical applications, the efficiency and uniformity of the heat transfer will be limited mainly by the available space.

References:

1. S.U.S. Chol, and J.A. Estman, Enhancing thermal conductivity of fluids with nanoparticles, *ASME-Publications-Fed* 231 (1995) 99-106.
2. J. Wienand, A. Riedelsheimer and B. Weigand, Numerical study of a turbulent impinging jet for different jet-to-plate distances using two-equation turbulence models*, European Journal of Mechanics-B/Fluids* 61 (2017) 210-217.
3. F. Selimefendigil and H.F. Öztop, Pulsating nanofluids jet impingement cooling of a heated horizontal surface, *International Journal of Heat and Mass Transfer* 69 (2014) 54-65.
4. J. Ortega-Casanova and S.I. Castillo-Sanchez, On using axisymmetric turbulent impinging jets swirling as Burger's vortex for heat transfer applications. Single and

multi-objective vortex parameters optimization, *Applied Thermal Engineering* 121 (2017) 103-114.

5. J.W. Baughn, and S. Shimizu, Heat transfer measurements from a surface with uniform heat flux and an impinging jet, *Journal of Heat Transfer* 111.4 (1989) 1096-1098.
6. L.D. Hee et al., Turbulent heat transfer from a flat surface to a swirling round impinging jet, *International Journal of Heat and Mass Transfer* 45.1 (2002) 223-227.
7. M. Behnia, S. Parneix, and P.A. Durbin, Prediction of heat transfer in an axisymmetric turbulent jet impinging on a flat plate, *International journal of heat and mass transfer* 41.12 (1998) 1845-1855.

1st International Conference on Nanofluids (ICNf2019)
2nd European Symposium on Nanofluids (ESNf2019)
26-28 June 2019, Castelló, Spain

Specific Heat Capacity Enhancement in a Nanofluid Studied via Molecular Dynamics Computer Simulation

S. Engelmann and R. Hentschke*

School of Mathematics and Natural Sciences, Bergische Universität Wuppertal, D-42097 Wuppertal, Germany

*Corresponding author: hentschk@uni-wuppertal.de

Keywords: nanofluid, heat capacity enhancement, computer simulation, phonon spectral density.

Abstract: Molten salts are used as heat transfer fluids and for short term heat energy storage in solar power plants. Experiments show that the specific heat capacity of the base salt is significantly enhanced by adding small amounts of certain nanoparticles. This effect, which is technically interesting and economically important, is not yet understood. Our aim is the theoretical investigation of the specific heat capacity in the aforementioned nanofluids on the molecular level using simulations. Here we present results for liquid potassium nitrate doped with silica nanoparticles. The system indeed shows the experimentally observed enhancement of its specific heat. In addition, we can trace the effect via the spectral density distribution of the nanofluid in comparison to the base liquid.

Introduction/Background: Nanofluids, i.e. solvents doped with suspended nanoparticles, show altered thermophysical properties. These changes are sometimes quite remarkable in the sense that the effects are much greater than expected on the basis of models, which describe the properties of interest in terms of a weighted sum of the corresponding properties of the individual components [1]. Typically the nanoparticle content varies between 0.1% to 5% by weight. Among these thermophysical properties are the thermal conductivity, viscosity, or the specific heat capacity [2]. This makes nanofluids particularly interesting in heat transfer applications - especially in the context of solar thermal technologies [3,4].

The thermodynamic property of interest in this study is the specific heat capacity, i.e. the heat capacity in units of J/(gK), of the heat transfer fluid, which should be as high as possible [5]. In a previous paper [6] one of us has given a comprehensive overview of the attendant literature. In summary, it is probably safe to say that the specific heat capacity of salt mixtures is enhanced by every type of nanoparticle used. Details of the methods of preparation may vary (e.g., the temperatures during drying of the samples). Quite

independent of these variations c_P-enhancements are between 10 to 30% on average. However, a molecular theory explaining the above effects of nanoparticles on the specific heat capacity of heat transfer fluids does not yet exist.

Here we present the results of molecular dynamics simulations, employing the computation package LAMMPS [7], to model a single SiO_2-particle immersed in liquid KNO_3 inside a cubic volume applying periodic boundaries. We choose this system, because it exhibits an increase of c_P as has been shown experimentally [8,9]. The force field for KNO_3 and its parameters were taken from Ref. [10]. All intermolecular interactions are described by a Buckingham/Coulomb potential with a cut-off radius of 9Å. Long-range Coulomb interactions are calculated using the PPPM method [11] (partial charges: q_{Si}=1.91, q_O=-0.9352, and q_H=0.4238). Otherwise the silica force field is modelled according to Refs. [12,13,14]. Interactions between silica and salt are modelled via the Lorentz-Berthelot mixing rules.

Discussion and Results: Figure 1 shows a key result, i.e. the isochoric heat capacity, c_V, of KNO_3 doped with SiO_2 vs. w_{np}, the weight fraction nanoparticles, at T=700K. The radius of the silica particle used here is 0.9 nm. There are two sets of data points. The upper data set is the direct result of the molecular dynamics simulations, which yields the classical c_V via the equilibrium fluctuations of the energy in the canonical ensemble. The straight dashed line is the usual linear interpolation formula based on the specific heat capacities of the individual components. Note that the data in the range w_{np}<0.1 fall systematically above this line. Thus, our simulations do show a discernible increase of c_V in this w_{np}-regime, which is in accord with the experimental 6%-enhancement obtained in Ref. [7]. This is highlighted by the shading bounded by the linear fit from below and the solid line from above.

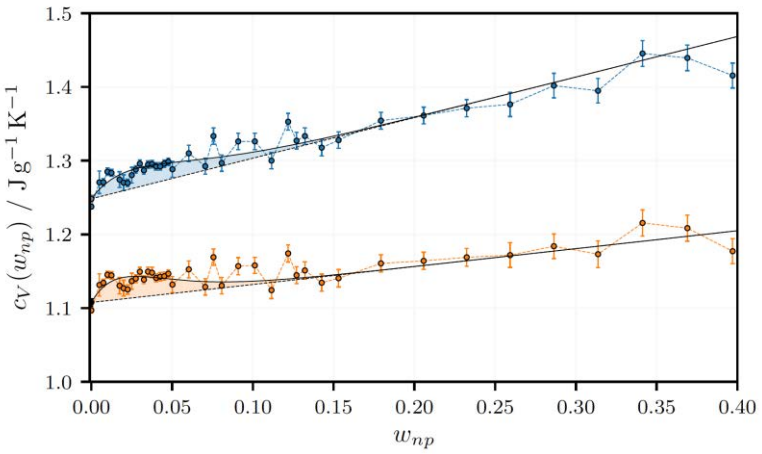

Figure 1. Isochoric heat capacity, c_V, of KNO_3 doped with SiO_2 vs. w_{np}, the weight fraction nanoparticles at 700K. Blue: results from classical energy fluctuations in the canonical ensemble; orange: results including quantum corrections. The shading corresponds to the c_V-enhancement observed at low w_{np} fitted via the interactive mesolayer model developed previously in Ref. [6].

A useful quantity, which allows to study the influence of the nanoparticles on vibrational modes, is the spectral density $g(\nu)$, which essentially is the Fourier transform of the atomic velocity auto-correlation function. The effect of the addition of nanoparticles on $g(\nu)$ is most revealing if we study the difference spectra $\Delta g = g_{nanofluid} - g_{basefluid}$ shown in an overview form in Fig. 2. Notice the rather broad feature at small frequencies, corresponding to longer wavelength collective modes, in contrast to the rather narrow features at higher frequencies due to molecular modes. Closer inspection reveals a contribution from both types of additional modes to the heat capacity enhancement.

Summary/Conclusions: In summary, the effect of nanoparticles on the heat capacity, as well as on other physicochemical properties, of liquids is not colligative. Even qualitatively it depends on particle type and size, possibly morphology. In other respects it is basic and almost universal, i.e. it affects the liquid and the solid phase alike and it is observed over a wide range of base fluids of small molecules as well as polymers. Here we have studied a particular system only. But the theoretical framework developed in the course of this work allows us to focus on three aspects - the generation of additional shear modes entering through the Frenkel frequency, anharmonicity, and possibly a shift of the Debye frequency - within the recent phonon theory of liquids [15,16]. In particular, the presence of the particles causes additional low frequency vibrational modes, apparently in line with a reduction of the Frenkel frequency. In addition we find that the presence of nanoparticles

enhances existing molecular modes in the base liquid, causing the observed 'hump' of the specific heat capacity at low particle concentrations.

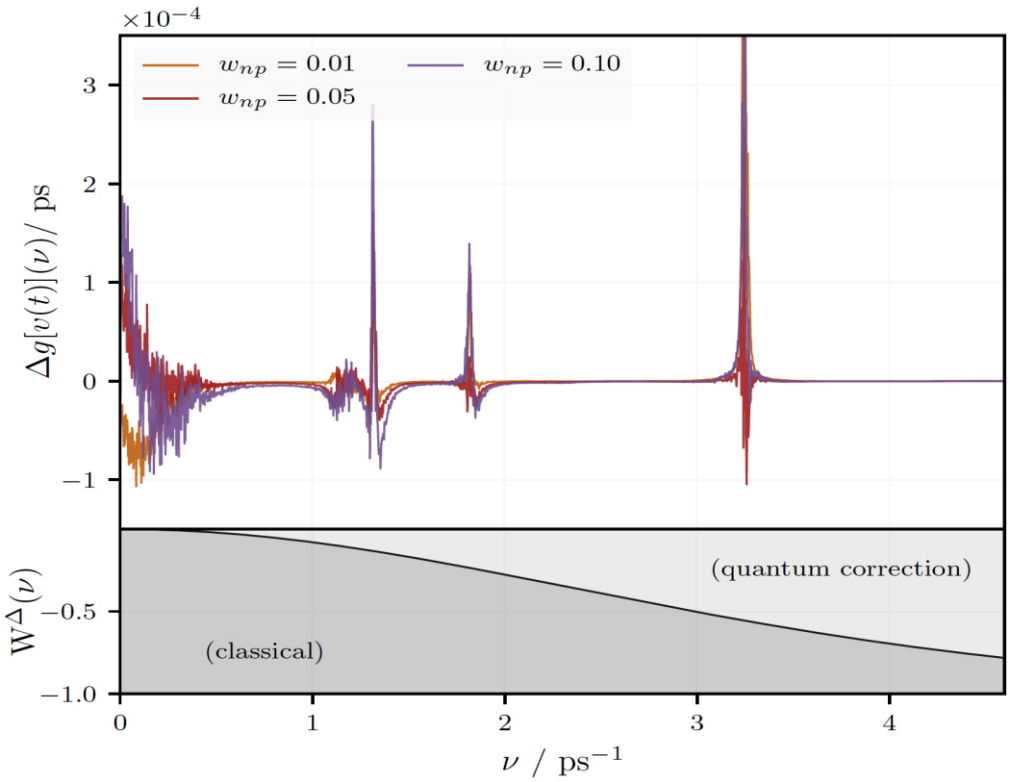

Figure 2. Difference spectral density, $\Delta g(\nu)$, vs. frequency, ν, obtained for doped KNO_3. Here the spectrum obtained for neat KNO_3, obtained under otherwise identical conditions, is subtracted from the spectral density of the doped systems. The lower portion of the graph shows the relative weights of classical and quantum contributions to the heat capacity.

Acknowledgements: This work was supported through DFG-grant HE 1545/18-1.

References:

1. K. Khanafer and K. Vafai, A critical synthesis of thermophysical characteristics of nanofluids. *International Journal of Heat and Mass Transfer* 54 (2011) 4410-4428.
2. S. U. Ilyas, R. Pendyala, A. Shuib and N. Marneni, A Review on the Viscous and Thermal Transport Properties of Nanofluids. *Adv. Materials Research* 917 (2014), 18-27.
3. M. Thirugnanasambandam, S. Iniyan and R. Goic, A review of solar thermal technologies. *Renewable and Sustainable Energy Reviews* 14 (2010), 312-322.
4. N. Ali, J. A. Teixeira and A. Addali, A Review on Nanofluids: Fabrication, Stability, and Thermophysical Properties. *Journal of Nanomaterials* (2018), Article ID 6978130, 33 pages, 2018. https://doi.org/10.1155/2018/6978130.

5. I. M. Shahrul, I. M. Mahbubul, S. S. Khaleduzzaman, R. Saidur and M. F. M. Sabri, A comparative review on the specific heat of nano fluids for energy perspective. *Renewable and Sustainable Energy Reviews* 38 (2014) 88-98.
6. R. Hentschke, On the specific heat capacity enhancement in nanofluids. *Nanoscale Research Letters*, 11 (2016) 1-11.
7. S. Plimpton, Fast parallel algorithms for short-range molecular dynamics. *J. Comp. Phys.* 117 (1995) 1-19.
8. M. Chieruzzi, A. Miliozzi, T. Crescenzi, L. Torre and J. M Kenny, A new phase change material based on potassium nitrate with silica and alumina nanoparticles for thermal energy storage. *Nanoscale Research Letters* 10 (2015) 273-283.
9. G. Qiao, M. Lasfargues, A. Alexiadis and Y. Ding, Simulation and experimental study of the specific heat capacity of molten salt based nanofluids. *Applied Thermal Engineering* 111 (2016) 1517-1522.
10. S. Jayaraman, A. P. Thompson, O. A. von Lilienfeld, E. J. Maginn, Molecular simulation of the thermal and transport properties of three alkali nitrate salts. *Industrial & Eng. Chem. Res. 49* (2010) 559-571.
11. R. W. Hockney and J. W. Eastwood, Computer simulation using particles. Taylor & Francis: New York (1988).
12. F. S. Emami, et al. Force field and a surface model database for silica to simulate interfacial properties in atomic resolution. *Chemistry of Materials* 26 (2014) 2647-2658.
13. T.-C. Lim, Alignment of Buckingham parameters to generalized Lennard-Jones potential functions. *Zeitschrift für Naturforschung* A 64 (2009) 200-204.
14. S. Engelmann, PhD Thesis, University of Wuppertal (2019).
15. D. Bolmatov, V. V. Brazhkin and K. Trachenko, The phonon theory of liquid thermodynamics. *Scientific Reports* 2 (2012) 421.
16. K. Trachenko and V. V. Brazhkin, Heat capacity at the glass transition. Physical Review B 83 (2011) 014201.

1st International Conference on Nanofluids (ICNf2019)
2nd European Symposium on Nanofluids (ESNf2019)
26-28 June 2019, Castelló, Spain

Mechanical Reliability of Core-Shell Nanoparticles for thermal energy storage by Finite Element Method

J. Forner-Escrig[1], R. Mondragón[1*] and R. Palma[1]

[1]Department of Mechanical Engineering and Construction, Universitat Jaume I, Av. de Vicent Sos Baynat, s/n 12071 Castellón de la Plana, Spain

[*]Corresponding author: mondragn@uji.es

Keywords: Finite Element Method, Monte Carlo analysis, Thermoelasticity, Nanoparticles, Phase change materials.

Abstract: Nowadays, possible applications of nanoencapsulated phase change materials (nePCM) focuses on thermal energy storage facilities such as concentrated solar power (CSP) plants. From a practical point of view, one of the problems encountered is that the shell, which confines the PCM in the core-shell nanoparticle, fails due to the thermal stresses developed during the heating/cooling cycles. On this ground, the aim of the present work is to develop a numerical tool by combining a finite element (FE) code –previously developed by the authors- and Monte Carlo (MC) techniques in order to perform a sensitivity analysis (SA). In particular, the SA provides those variables that should be controlled in the design and synthetization of PCM given that SA quantifies the material properties and/or geometrical dimensions that have the most direct impact on the failure of the nanoparticle shell. Finally, a mechanical reliability study is carried out to ensure the resistance of the shell by using standard procedures based on MC techniques. In conclusion, the results of the present work could be used by the experimental community for designing reliable PCM.

Introduction: Thermal energy storage systems are currently under research as they can contribute to solve the difference between supply and demand of energy. More specifically, heat storage systems based on nanofluids are focusing great efforts of the scientific community. Nanofluids are the result of combining a heat transfer fluid and nanoparticles to enhance the heat transfer and storage properties of the mixture. Nanoencapsulated phase change materials (nePCM) are used as nanoparticles for these purposes. One of the concerns about nePCM is adjusting the value of the shell thickness since a compromise between mechanical strength and heat storage must be achieved. Numerical simulations seem to be a valuable –complementary to experiments- tool to determine what geometrical and/or material properties have the most direct impact on the mechanical strength of nanoparticles.

Methodology: The authors of this work have developed a model considering mechanical and thermal with phase change fields. In order to obtain the numerical formulation of the problem within the finite element method, the governing equations are expressed in weak forms by means of standard finite element (FE) procedures (see [1] for more detail) and then they are discretised. The FE formulation is implemented in the research code FEAP, which belongs to the University of California at Berkeley (USA). In this work, the governing equations are composed by linear momentum and thermal balances. For the sake of brevity, these equations are no reported in the present work, for more details see [2].

Afterwards, a sensitivity analysis (SA) is performed by combining the Monte Carlo (MC) and the FE method. SA allows finding and quantifying what material and/or geometrical parameters exert an influence on Rankine's equivalent stress, which is the mechanical failure criteria used in the present work. More detail on SA can be found in [3].

The scalar parameters that quantify the SA are the input parameters of the FE model and they are listed in Table 1.

Table 1. Scalar parameters for the SA

Property	Notation
Solid core mass density	Θ_1
Liquid core mass density	Θ_2
Solid core heat capacity	Θ_3
Liquid core heat capacity	Θ_4
Solid core thermal conductivity	Θ_5
Liquid core thermal conductivity	Θ_6
Core Young's modulus	Θ_7
Core Poisson's ratio	Θ_8
Core coefficient of thermal expansion	Θ_9
Core melting temperature	Θ_{10}
Latent heat	Θ_{11}
Shell thickness	Θ_{12}
Shell mass density	Θ_{13}
Shell heat capacity	Θ_{14}
Shell thermal conductivity	Θ_{15}
Shell Young's modulus	Θ_{16}
Shell Poisson's ratio	Θ_{17}
Shell coefficient of thermal expansion	Θ_{18}
Shell melting temperature	Θ_{19}

Discussion and Results: In this work, spherical tin nanoparticles encapsulated in tin oxide are considered. The domain of study is a single nanoparticle, which is mechanically fixed at its centre; thermally a time-dependent temperature is prescribed on surface.

The diameter and shell thickness of the considered nanoparticles are 103 nm and 9.78 nm, respectively. These nanoparticles are increasingly linearly heated from a reference temperature of 343 K up to a value of 523 K. The uncertainties considered for the listed parameters in Table 1 vary between 5-10% around nominal values, which are reported in [2]. Uncertainties of input parameters are normally distributed except that of shell thickness, which is distributed as a uniform random variable. Results from numerical simulations are shown in Figures 1 and 2:

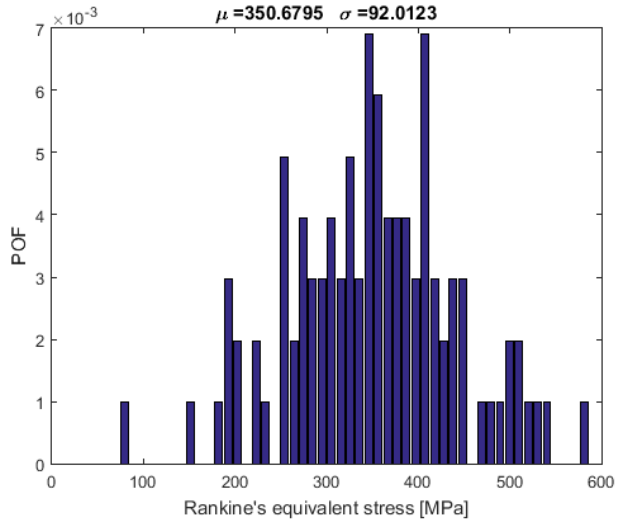

Figure 1. Probability of failure of the nanoparticle shell.

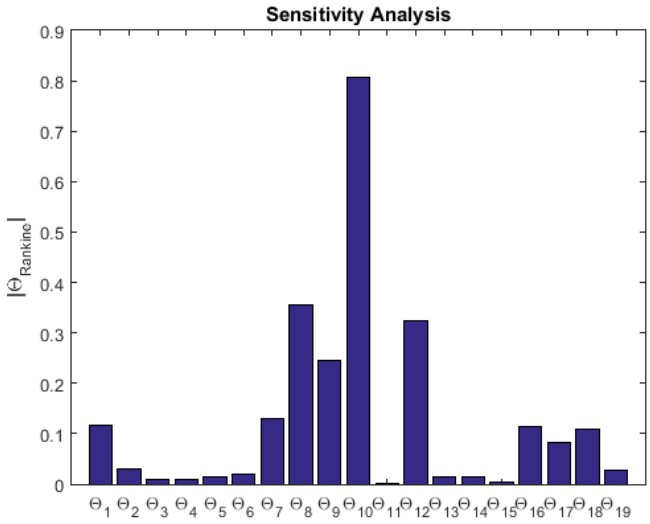

Figure 2. Sensitivity Analysis of Rankine's equivalent stress.

Figure 1 represents the probability of failure of the nanoparticle shell for each of the Rankine's equivalent stresses obtained from MC simulations. As observed, since the tensile strength of the nanoparticle shell is assumed to be 803 MPa, the probability of failure is null, which agrees with experimental observations since the synthetization of these nePCMs is well achieved.

Figure 2 represents the SA of Rankine's equivalent stress. From the figure, it can be determined that the parameter exerting the most direct impact on the failure of the nanoparticle shell is the melting temperature of the PCM, which is represented by Θ_{10}. Two more parameters whose influence is not negligible appear to be Poisson's ratio of the PCM and the shell thickness of the nanoparticle.

Conclusions: In this article, a SA is carried out by the combination of FE and MC analyses. From numerical simulations, it can be concluded that for tin nanoparticles encapsulated in tin oxide, the parameters that have a more direct impact on the failure of the shell nanoparticle due to thermal stresses are: melting temperature of the PCM, Poisson's ratio of the PCM and the shell thickness. Therefore, these are the physical parameters to be closely controlled when synthesizing tin nanoparticles.

Acknowledgements: This research was partially funded by Ministerio de Economía y Competitividad (MINECO) of Spain through the project ENE2016-77694-R and Universitat Jaume I through the project UJI-B2016-47. Josep Forner-Escrig thanks Ministerio de Ciencia, Innovación y Universidades of Spain and Fondo Social Europeo for a pre-doctoral fellowship through Grant Ref. BES-2017-080217 (FPI program). This work has been developed by participants of the COST Action CA15119 Overcoming Barriers to Nanofluids Market Uptake (NANOUPTAKE).

References:

1. O. Zienkiewicz and R. Taylor, *The Finite Element Method 7th Edition*, Butterworth-Heinemann, 2013
2. J. Forner-Escrig, R. Mondragón, R. Palma, Finite element formulation to investigate thermomechanical behaviour in nanoencapsulated phase change materials. *Submitted for publication*.
3. A. Saltelli, M. Ratto, T. Andres, F. Campolongo, J. Cariboni, D. Gatelli, M. Saisana and S. Tarantola, *Global Sensitivity Analysis. The Primer*, John Wiley & Sons, Ltd., 2008.

1st International Conference on Nanofluids (ICNf2019)
2nd European Symposium on Nanofluids (ESNf2019)
26-28 June 2019, Castelló, Spain

Numerical investigation for heat transfer of TiO_2-water nanofluid in a laminar heated pipe flow

P. Farber, J. Burggraf, K. R. Karpaiya and P. Ueberholz

IMH - Institute of Modelling and High-Performance Computing,
Hochschule Niederrhein University of Applied Sciences,
Reinarzstraße 49, 47805 Krefeld, Germany

Keywords: Euler-Lagrange, Brownian force, thermophoresis, two-phase flow

Abstract: The mathematical modelling of heat transfer in nanofluids based on the effects of additional particle forces was investigated with CFD simulations of TiO_2-water nanofluid in a heated pipe flow. The additional particle forces analysed were Brownian force, thermophoresis, Saffman lift force and Magnus force. The results were validated with an existing experimental work [1] and show that two-phase Euler-Lagrange simulation models reproduce the experiment better than single-phase simulation. The effects of additional particle forces on the heat transfer of nanofluids are negligible.

Introduction/Background: In general, nanofluids simulation models can be classified into single-phase and two-phase flows. In the single-phase flow, the mixture of base fluid and nanoparticles are considered as a continuum with effective material properties [2]. In terms of two-phase flow, the base fluid and nanoparticles are modelled as two separate phases. The efficiency of these single-phase and two-phase flow approaches has been investigated in several numerical studies. These studies [3, 4] concluded that the two-phase approach is more promising than the single-phase model in predicting convective heat transfer of the nanofluids. In the two-phase approach, it was proven through these studies [5, 6] that the Euler-Lagrange approach shows better accordance to experimental results in comparison to the Euler-Euler approach. The experimental work used in this study [1] was chosen as reference due to its accurate measurements as well as the multitude of temperature measurement points. A TiO_2-water nanofluid was employed in this work for its weak changes in thermophysical properties when compared with the base fluid water. The experimental work concluded that the heat transfer of nanofluids deteriorates along the heated pipe; Colla et. al. hypothesized that Brownian motion and thermophoresis of nanoparticles are responsible for this phenomenon. Thus, this numerical study focuses on investigating the effects of additional forces on the heat transfer of nanofluids based on the Euler-Lagrange approach with reference to the experimental data.

The pipe geometric model is a 2000mm long copper pipe with a diameter of 8mm and a run-in length of 375mm (Figure 1). It is constructed and meshed using ANSYS ICEM 18.2. The commercial CFD-code ANSYS Fluent 19.0 was used as the solver. Figure 1 shows the boundary conditions for the simulation. Shell conduction was activated for the pipe wall. The applicability of the constructed mesh is analysed with 3D grid convergence study with pure water which yielded simulation results with near perfect accuracy [1]. A grid convergence study with nanoparticles was tested with axisymmetric 2D-simulations in order to keep the numerical effort low. Based on these studies, a grid with 1,252,803 cells was selected for the 3D simulations of the nanofluids.

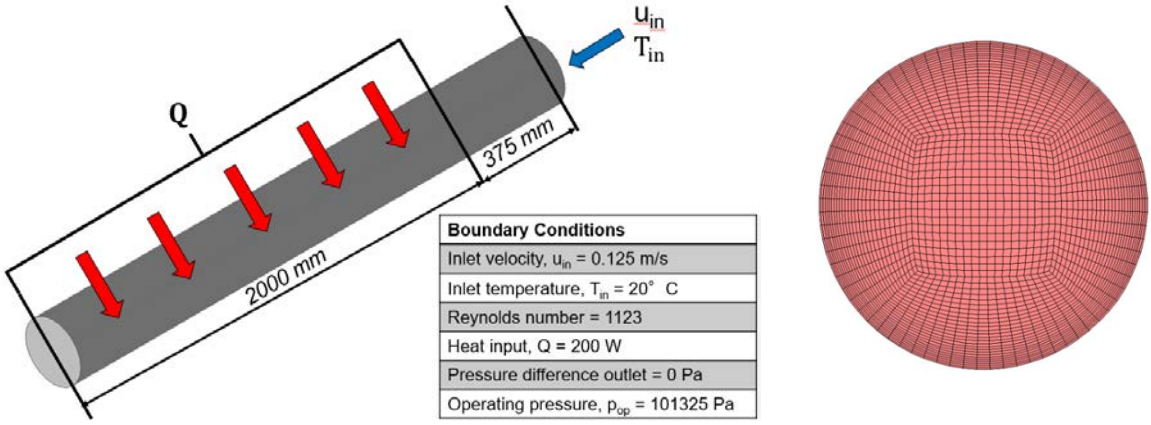

Boundary Conditions
Inlet velocity, u_{in} = 0.125 m/s
Inlet temperature, T_{in} = 20° C
Reynolds number = 1123
Heat input, Q = 200 W
Pressure difference outlet = 0 Pa
Operating pressure, p_{op} = 101325 Pa

Figure 1. Experimental boundary conditions and meshed pipe geometry

The mass, momentum and energy equations and the particle force and energy balance for the Euler-Lagrange approach used in this study were obtained from [7]. The material properties of the base fluid water [8] and TiO_2-nanoparticles [9] were interpolated by means of the Newton method, whereas for the copper wall [10], the properties were linearly interpolated within the temperature range of the simulations. Brownian force and thermophoresis were incorporated in the particle force balance as additional force terms. For the equation of Brownian force [7], the Cunningham correction factor was revised by the input of molecular mean free path of water instead of the default gas value. The default Talbot form for the thermophoretic force [7] is invalid for this study due to its sole applicability for ideal gas. Hence, another form for thermophoretic force in liquids suggested by Mahdavi et. al. [11] was employed as a user-defined function.

Due to the high number of nanoparticles in the pipe (1.0wt.%: 1.68583E+15), the nanoparticles were modelled as parcels, i.e. clusters of particles with equal diameter, position, and velocity, to reduce the computational effort. The simulations were carried out by setting the parcel mass as a constant to achieve a parcel concentration of 5 parcels per computational cell. Further rise in the parcel concentration had no effect on

the accuracy of the simulation results as revealed by 2D simulations. Moreover, the standard initialization method for the simulations was set with conditions that resemble the start of the experiment ($u = v = w = 0m/s$; $p - p_{op} = 0Pa$; $T = 300K$).

Discussion and Results: Various simulations were carried out to investigate the influence of the described forces on the heat transfer in nanofluids. The different forces were switched on alternatively in the respective simulations. To analyse the influence of the forces on the heat transfer between wall and fluid, the Nusselt numbers and the wall temperatures of the simulations were compared with those of single-phase nanofluid simulations and the experimental results for pure water and nanofluids. The simulation wall temperatures averaged over circumference of pipe were compared based on the percentage difference to the experimental counterpart. The results shown in Figure 2 are for a power input of 200 W and a mass fraction of 1 %-TiO_2 in the nanofluid.

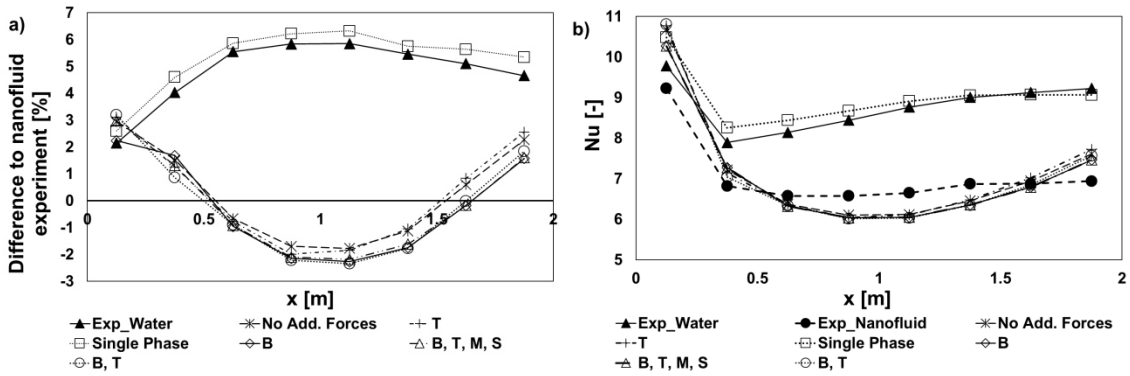

Figure 2: a) Difference of averaged wall temperature over pipe length to the experiment with nanofluid; b) Nusselt numbers of experiment and simulations (B = Brownian force, T = Thermophoretic force, M = Magnus force, S = Saffman lift force)

Overall, the results show that the experimental values are not exactly matched. The single-phase simulations show a deviation of about 6% and are close to the results of the experimental results of pure water. The results can be explained by the only slightly different material properties between water and nanofluid. Looking at the results for the two-phase simulation, the failure has been halved compared to the single-phase simulation. This shows that the single-phase model is not acceptable for such a simple simulation in a straight pipe with laminar flow.

The assumptions of Colla et al. [1] that thermophoresis and Brownian motion are responsible for the deterioration of the heat transfer, this statement cannot be confirmed based on the simulated results. The effect of delayed natural convection, however, can be confirmed in the simulation. Furthermore, it could be shown that the influences of the Saffman lift force and Magnus force on the heat transfer of nanofluids are negligible.

Summary/Conclusions: CFD simulations of a heated laminar flow straight pipe section with TiO_2-water nanofluids (1.0wt.%) were performed and compared with experimental data. It could be shown that neither Brownian motion nor thermophoresis causes the deterioration of heat transfer by this nanofluid. The simulation results indicate that the momentum and energy transport between base fluid and nanoparticles seems to influence this effect.

References:

[1] L. Colla, L. Fedele and M. Buschmann, *Laminar mixed convection of TiO_2–water nanofluid in horizontal uniformly heated pipe flow*, Int. J. of Thermal Sc., 26-40, November 2015.

[2] O. Mahian, L. Kolsi, M. Amani and a. et, *Recent advances in modeling and simulation of nanofluid flows-Part I: Fundamental and theory*, Physics Reports, Article in Press, 5 December 2018.

[3] M. Bahiraei, *A numerical study of heat transfer characteristics of CuO–water nanofluid by Euler–Lagrange approach*, Journal of Thermal Analysis and Calorimetry, 1591-1599, 23 September 2015.

[4] M. K. Moraveji and E. Esmaeili, *Comparison between single-phase and two-phases CFD modeling of laminar forced convection flow of nanofluids in a circular tube under constant heat flux*, Int. Communications in Heat and Mass Transfer, 1297–1302, 20 July 2012.

[5] A. Albojamal and K. Vafai, *Analysis of single phase, discrete and mixture models, in predicting nanofluid transport*, Int. J. of Heat and Mass Transfer 114, 225-237, June 2017.

[6] M. S. Mojarrad, A. Keshavarz and A. Shokouhi, *Nanofluids thermal behavior analysis using a new dispersion model along with single-phase*, Heat Mass Transfer, 1333–1343, September 2013.

[7] ANSYS, Inc., *ANSYS Fluent Theory Guide 19*, USA, Pennsylvania, 2018.

[8] Verein Deutsche Ingenieure, VDI Gesellschaft Verfahrenstechnik und Chemieingenieurwesen, *VDI - Wärmeatlas*, Springer-Verlag, Berlin, 10. Ed. 2006.

[9] D. de Ligny, P. Richet, E. F. Westrum Jr, J. Roux, *Heat capacity and entropy of rutile (TiO_2) and nepheline ($NaAlSiO_4$)*., Physics and Chemistry of Minerals, Volume 29, 2002.

[10] Deutsches Kupferinstitut, *Material Data Sheet Copper*, Düsseldorf, 2005.

[11] M. Mahdavi, M. Sharifpur, J. M. Meyer, *CFD modelling of heat transfer and pressure drops for nanofluids through vertical tubes in laminar flow by Lagrangian and Eulerian approaches*, Pretoria, South Africa, 2015.

1st International Conference on Nanofluids (ICNf2019)
2nd European Symposium on Nanofluids (ESNf2019)
26-28 June 2019, Castelló, Spain

Finite element formulation of Heat propagation in Nanoencapsulated Phase Change Materials

J. Forner-Escrig[1*], R. Mondragón[1] and R. Palma[1]

[1]Department of Mechanical Engineering and Construction, Universitat Jaume I, Av. de Vicent Sos Baynat, s/n 12071 Castellón de la Plana, Spain

[*]Corresponding author: jforner@uji.es

Keywords: Finite Element Method, Phase Change, Nanoparticles, Metal alloys.

Abstract: Nanoencapsulated phase change materials (nePCM) are currently under research for heat storage applications. Owing to the difficulty arising in this field, both experimental and numerical communities join efforts in order to reach a better understanding of the physical phenomena involved. One of the main concerns regarding these nePCMs is that after some cycles of heating and cooling, the shell that confines the PCM fails due to the stresses developed during these processes. Mechanically, the failure of the nanoparticle shell is due to thermal stresses and, consequently, the calculation of heat propagation in nanoparticles becomes a relevant issue. On this ground, the aim of this work is to develop a numerical formulation within the finite element method (FEM) for metallic pure substances and alloys since both are used as PCM in nanoparticles. The former case is of special relevance from a numerical perspective since regularization techniques are required to avoid numerical errors when describing phase change. Finally, temperature distributions inside nePCM are calculated, which will be used for thermal stress calculations in future works.

Introduction: Nowadays, thermal energy storage systems are under research since they can help to reduce the mismatch between supply and demand of energy [1]. From the different systems able to store energy, this work focuses on the ones based on nanofluids, which are the result of combining a heat transfer fluid (HTF) and nanoparticles. More specifically, this work aims to study only nanoencapsulated phase change materials (nePCMs). An inconvenient of these nePCMs is that after some cycles of heating/cooling, the shell is likely to break due to the stresses developed during these processes. According to literature, for instance [2,3], the nature of those stresses could be thermal. Therefore, studying heat propagation for different type of metallic materials – both pure and alloy substances- appears to be relevant and this is the main objective of the present work.

Methodology: The authors of this work have developed a numerical model considering thermal field with phase change for both pure substances and alloys. Thermal problems with phase change are governed by the following balance equation:

$$\frac{dH}{dT} + \underline{\nabla} H \cdot \underline{\dot{u}} = -\underline{\nabla} \cdot \underline{q} + Q \tag{1}$$

where H, $\underline{\dot{u}}$, $\underline{q}$ and Q denote enthalpy, velocity, heat flux vector and heat source/sink, respectively.

The difference in phase change between pure substances and alloy substances is grounded on the variation of enthalpy with temperature due to latent heat: a sharp change in enthalpy appears in pure substances, which require regularization techniques to solve phase change problems numerically [4]; for alloys, the variations of enthalpy with temperature occur gradually and, consequently, no numerical problems appear.

In order to obtain a numerical formulation of (1), this equation is expressed in weak form by means of standard finite element (FE) procedures, see [5] for more detail. Then, the FE formulation is implemented in the research code FEAP [6], which belongs to the University of California at Berkeley (USA).

Results: In this work, spherical aluminium nanoparticles and aluminium-copper nanoparticles are studied. Notice that, for comparison purposes, it is assumed that both materials are encapsulated by the same shell made out of alumina. The solution domain is formed by a single nanoparticle with a time-dependent temperature prescribed on the surface of the nanoparticle shell.

The diameter and shell thickness retained for nanoparticles is 42.5 nm and 7 nm, respectively. These nanoparticles are increasingly linearly heated from a reference temperature of 343 K up to a value of 1050 K in the case of aluminium nanoparticles and up to 893 K in the case of aluminium-copper nanoparticles. From numerical simulations, the results shown in Figure 1 are obtained after phase change.

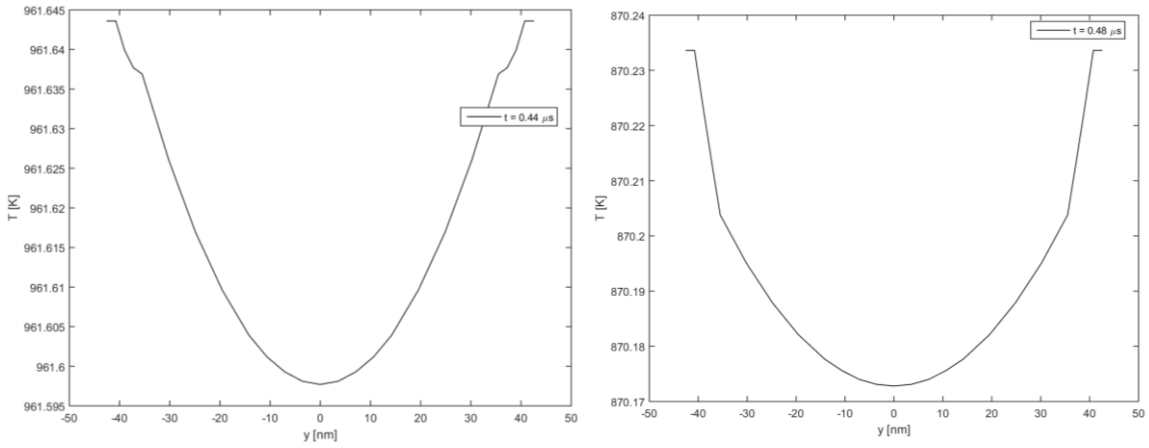

Figure 1. Temperature distribution along the nanoparticle diameter for pure substance (left) and alloys (right) after melting.

As shown in Figure 1, an abrupt change in the temperature distribution along the diameter for pure substance nanoparticles is observed. More precisely, this change in the temperature distribution occurs between the shell-core interface. However, the change in temperature distribution observed in alloys is softer than that of pure substances. This difference in heat propagation is likely to have a severe thermomechanical impact on the mechanical resistance of the nanoparticle shells since sudden changes in temperature may be associated to larger stresses developed during heating/cooling processes. Conversely, temperature change at the shell-core interface in alloy nanoparticles occurs in a smoother way than in pure PCM ones and this behaviour is likely to contribute to relaxing the state of stress in nanoparticles.

Conclusions: In this article, a FE analysis is conducted in order to compare heat propagation in pure substances and alloys. From numerical simulations, it can be concluded that the temperature distribution along the diameter of the nanoparticle exhibits an abrupt change in the core-shell interface for pure substance nePCMs, which could produce a more detrimental impact on stresses than a softer transition as that for alloy nePCMs. In conclusion, this preliminary result allows predicting that the nature of the phase change material may be relevant when assessing the mechanical strength of nanoparticle shells.

Acknowledgements: This research was partially funded by Ministerio de Economía y Competitividad (MINECO) of Spain through the project ENE2016-77694-R and Universitat Jaume I through the project UJI-B2016-47. Josep Forner-Escrig thanks Ministerio de Ciencia, Innovación y Universidades of Spain and Fondo Social Europeo for a pre-doctoral fellowship through Grant Ref. BES-2017-080217 (FPI program). This work has been developed by participants of the COST Action CA15119 Overcoming Barriers to Nanofluids Market Uptake (NANOUPTAKE).

References:

1. L. F. Cabeza, E. Galindo, C. Prieto, C. Barreneche and A. I. Fernández, Key performance indicators in thermal energy storage: Survey and assessment, *Renewable Energy* 83 (2015) 820-827
2. F. Pitié, C. Y. Zhao and G. Cáceres, Thermo-mechanical analysis of ceramic encapsulated phase-change-material (PCM) particles, *Energy Environ. Sci.* 4 (2011) 2117-2124
3. N. Maruoka and T. Akiyama, Thermal Stress Analysis of PCM Encapsulation for Heat Recovery of High Temperature Waste Heat, *Journal of Chemical Engineering of Japan* 36 (2003) 794-798
4. J. Forner-Escrig, R. Mondragón, R. Palma, Finite element formulation to investigate thermomechanical behaviour in nanoencapsulated phase change materials. *Submitted for publication*.
5. O. Zienkiewicz and R. Taylor, *The Finite Element Method 7th Edition*, Butterworth-Heinemann, 2013
6. R. Taylor, *FEAP A Finite Element Analysis Program: User Manual*. University of California, Berkeley, 2013. URL: http://www.ce.berkeley.edu/feap.

1st International Conference on Nanofluids (ICNf2019)
2nd European Symposium on Nanofluids (ESNf2019)
26-28 June 2019, Castelló, Spain

Nanofluid flow and heat transfer of Carbon Nanotubes and Graphene Platelettes Nanofluid in Entrance Region of Microchannels

J. T. C. Liu[1,*], M. E. Fuller[1]

[1] School of Engineering, Brown University, 69 Brown Street, Box D, Providence, Rhode Island 02912, U.S.A.

[*]Corresponding author: joseph_liu@brown.edu

Keywords: Nanofluids 1, Heat Transfer 2, Carbon Nanotubes 3, Graphene Platelettes 4

Abstract: Thermophysical properties of carbon nanotube nanofluids (CNTNf) and those of graphene nanoplatlette nanofluids (GNPNf) as functions of volume fraction are deduced from the literature. These properties are applied to a perturbative model to study nanofluid effects on the flow and heat transfer in the entrance region of microchannels. The increase in shear stress for GNPNf outweighs that for heat transfer by a factor of two. CNTNf shows anti-enhancement behaviour where there is an increase in shear stress coupled with a decrease in the surface heat transfer rate.

Introduction/Background: Since the pioneering work of Choi [1], nanofluids have become widespread in applications and stimulated much work on their fundamental understanding [2-8]. Dispersed metallic oxide nanoparticles were prevalent in studies. More recently, nano-sized carbon nanotubes (CNTNf) have become subjects of intense studies because of their thermophysical properties (e,g. [9]) as well as nanofluids with graphene nanoplatlettes (GNPNf) dispersed in liquid [10]. Our previous theoretical-numerical work [6-8] performed studies of nanofluids with dispersed spherical metallic nanoparticles (alumina and gold) using a perturbation method for small volume concentration. The present study is directed at CNTNf and GNPNf, with contrasting thermophysical properties. Application to the entrance region of microchannels is made, as measurements in alumina nanofluids indicate that the largest nanofluid effect is in this region [11] in which the flow is mimicked by the laminar boundary layer where convecting effects compete with the enhanced transport properties of the nanofluid.

Discussion and Results: The continuum description follows from [5] except that the thermophoresis effect, which has been found to be relatively unimportant in [5], is not considered at the outset. The resulting fundamental equations resemble that of the compressible boundary layer, because of the dependence of flow quantities on the volume fraction, which in turn is determined by its diffusion equation [6, 7]. The general

formulation of the perturbation problem represents flow quantities and thermophysical properties in ascending powers of the nanoparticle volume fraction, which is a small parameter as in nanofluid heat transfer experiments [11]. The zeroth order is that of the base fluid in the absence of nanoparticles. The first-order problem, which is linear, is the nanofluid effect at small volume fraction. The differential equations for the first-order momentum, heat, and mass transfer problems to be solved are discussed in [6-8] which was applied to spherical metallic nanoparticles. In the present paper, the applications to CNTNf and GNPNf are obtained. The thermophysical properties are obtained from [9, 10] for CNTNf and GNPNf, respectively and are summarized in Table 1.

Table 1. Nanofluid thermophysical properties

	CNTNf [9]	GNPNf [10]
$(\rho^*)'_{\phi=0}$	0.4 (exp)	1.3 (mix)
$(\rho^* c^*)'_{\phi=0}$	-1.62 (exp)	-0.62 (mix)
$(\mu^*)'_{\phi=0}$	200 (exp)	350 (exp)
$(k^*)'_{\phi=0}$	2.5 (exp)	210 (exp)
$(\mu^*)'_{\phi=0} - (\rho^*)'_{\phi=0}$	196.6	348.7
$(k^*)'_{\phi=0} - (\rho^* c^*)'_{\phi=0}$	4.12	210.62

The notation (exp) indicated experimentally obtained and (mix) obtained from mixture theory. The dimensionless quantities are defined similarly as in [6-8], using usual notion. The normalization quantities are those of the base fluid, the primes indicate differentiation with respect to the volume fraction and the slopes are at zero volume fraction. Nanoparticle effects are not limited to augmenting the molecular transport coefficients. In convective flows, both the perturbation temperature and velocity (and concentration) profiles are altered owning to convective transport effects. The net effect in the perturbation problem is revealed by the competition between molecular transport and convective transport, represented by the bottom two items in Table 1. The convective effects are also interpreted as inertia effects as they are reflected by the rate of change or adjustment process to be balanced by molecular transport. The volume concentration, for a solid wall, has a zero flux wall boundary condition. In the absence of sources (or sinks), it thus remains constant at the free stream value [6, 7].

In the Blasius similarity variable form, the first order velocity,(f_1'), problem to be solved is

$$f_1''' + (f_0 f_1'' + f_0'' f_1)/2 = [(\ )^*)'_{=0} \quad (\ )^*)'_{=0}] f_0 f_0''/2, \;\; f_1(0) = f_1'(0) = 0, \;\; f_1'(\infty) = 0$$

where f_1 is the stream function, subscript zero is base fluid problem corresponding to the Blasius boundary layer. The nanofluid effects appear on the right ride. The first order temperature (θ_1) problem is

$$f_1''' + (f_0 f_1'' + f_0' f_1)\mathrm{Pr}_f/2 = [(k^*)'_{\phi=0} \quad (\quad {}^*c^*)'_{\phi=0}]f_0 \quad {}_0'\mathrm{Pr}_f/2, \quad f_1(0) = f_1'(\infty) = 0$$

The direct nanofluid effects appear on the right ride; the inhomogeneous, convective effect of $\theta_0' f_1 \mathrm{Pr}_f/2$ is indirect. The profiles θ_1, f_1' for CNTNf and GNPNf are shown respectively in Figures 1 and 2. Because of the overwhelming viscosity effect relative to inertia for both nanofluids, (Table 1), the factor $(\mu^*)'_{\phi=0} - (\rho^*)'_{\phi=0} > 0$, in which case the velocity profile is stretched because of viscous diffusion and thus the first order correction is negative to "thin out" the velocity profile. The GNPNf correction is more severe, reaching a negative maxima larger than that of the CNTNf because of the stronger viscosity effect. This is in contrast to previous studies [6-8] of alumina and gold nanofluids where $(\mu^*)'_{\phi=0} - (\rho^*)'_{\phi=0} < 0$. The first-order nanofluid effect on the temperature profile is also shown in Figure 1. The GNPNf show stronger modification of the temperature profile because of the stronger convective transport effect.

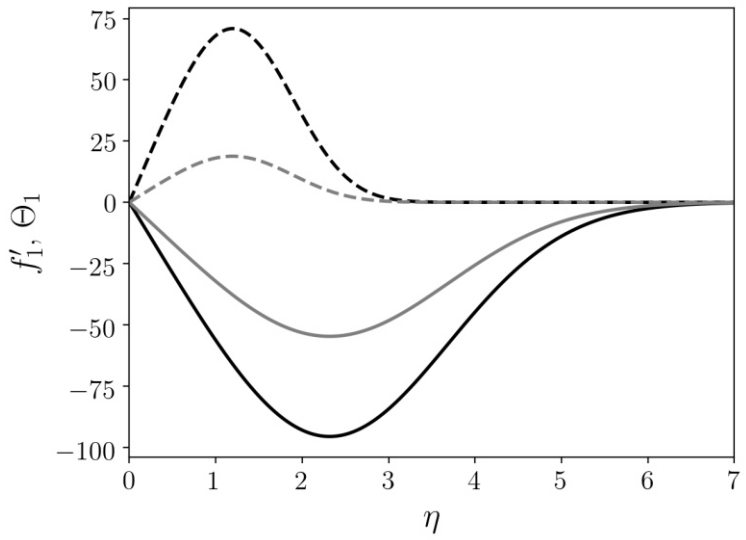

Figure 1. The first-order perturbation functions (GNPNf black, CNTNf grey): zero particle flux at the wall, $\mathrm{Pr}_f = 7.0$, $f_1'(\eta)$:——, $\theta_1(\eta; \mathrm{Pr}_f)$: – – –

In the first-order perturbation theory, the nanofluid effect is defined, and embedded in, the dimensionless slope times the volume fraction. The surface heat transfer and shear stress results are then expressed in terms of the slopes: for CNTNf, $(\tau^*)'_{\phi=0} = 100.2$, $(q^*)'_{\phi=0} = -31.54$. For GNPNf, $(\tau^*)'_{\phi=0} = 175.7$, $(q^*)'_{\phi=0} = 82.10$.

Concluding remarks: In previous studies [6, 7] of alumna and gold nanofluids, all the slopes are positive, i.e. such nanofluids increase the surface heat transfer and skin friction to the various degrees dictated by the respective thermophysical properties. The present studies indicate that both CNTNf and GNPNf incur very large increases in shear stress at the wall relative to alumina and gold nanofluids; similarly for surface heat

transfer for GNPNf but at about half the value of the shear stress. Of exception is the surface heat transfer for CNTNf, which shows anti-enhancement behaviour, principally due to the interaction of the convective effects of the strongly viscous dominated momentum problem. More accurate representations of nanofluid thermophysical properties as functions of the volume fraction and fluid temperature are suggested.

References:

1. S.U.S. Choi, *Enhancing thermal conductivity of fluids with nanoparticles,* in *Developments and Applications of Non-Newtonian Flows,* Eds., D.A. Siginer and H.P. Wang, FED-Vol. 231/MD-Vol. 66, pp. 99-105, ASME, New York, 1999.
2. S.K. Das, S.U.S. Choi and H.E. Patel, *Heat transfer in nanofluids—A review, Heat Transfer Engineering* 27 (2006) 3-18.
3. S.M.S. Murshed and C.A. Nieto de Castro, *Nanofluids: Synthesis, Properties and Applications*, Nova Science Publishers Inc., New York, 2014.
4. S.M.S. Murshed and C.A. Nieto de Castro, Nanofluids as advanced coolants, in *Green Solvents I: Properties and Applications in Chemistry,* Eds., Mohammad A. and Inamuddin, Chapter 14, pp.397-415, Springer, London, 2012.
5. J. Buongiorno, *Convective transport in nanofluids, J. Heat Transfer Engineering* 128 (2006) 240-250.
6. J.T.C. Liu, M.E. Fuller, K.L. Wu, A. Czulak, A.G. Kithes and C.J. Felten, *Nanofluid flow and heat transfer in boundary layers at small nanoparticle volume fraction: Zero nanoparticle flux at solid wall, Archive of Mechanics* 69 (2017) 75-100.
7. C.J.B. de Castillo, M.E. Fuller, A. Sane and J.T.C. Liu, *Nanofluid flow and heat transfer in boundary layers: The influence of Concentration diffusion on heat transfer enhancement, Heat Transfer Engineering* 39 (2018) doi.org/10.1080/01457632.2018.1442298
8. D. Hopper, D. Jaganathan, J.L. Orr, J. Shi, F. Simeski, M. Yin and J.T.C. Liu, *Heat transfer in nanofluid boundary layer near adiabatic wall, J. Nanofluids* 7 (2018) 1-6.
9. Y Li, S Suzuki, T Inagaki and N Yamauchi, *Carbon-nanotube nanofluid thermophysical properties and heat transfer by natural convection, J. Physics: Conference Series* 557 (2014) 012051
10. N. Ahammed, L.G. Asirvatham and S. Wongwises, *Effect of volume concentration and temperature on viscosity and surface tension of graphene-water nanofluid for heat transfer applications, J. Therm. Anal Calorim.* 123 (2016) 1399-1409.
11. D. Wen and Y. Ding, *Experimental investigation into convective heat transfer of nanofluids at the entrance region under laminar flow conditions, J. Heat Mass Transfer* 5181-5188.

1st International Conference on Nanofluids (ICNf2019)
2nd European Symposium on Nanofluids (ESNf2019)
26-28 June 2019, Castelló, Spain

Numerical Analysis of Erosion Phenomena by Nanofluids

A. Kosinska[1*], B.V. Balakin[1,2]

[1]Western Norway University of Applied Sciences, Dpt. Mech. Mar. Eng., Inndalsveien 28, 5063 Bergen, Norway

[2]NRNU Moscow Engineering Physics Institute, Russia, Inst. Nucl. Phys. Eng., Moscow, Kashirskoe sh. 31

[*]Corresponding author: adk@hvl.no

Keywords: Nanofluids, Modelling, CFD, Lagrangian approach, Erosion

Abstract: The objective of this research was investigation of erosion due to nanofluids, where the main focus was on flows through elbows. Small particles are usually expected to have a minor influence on erosion processes due to their low kinetic energy as they collide with solid surfaces. Nevertheless, in our numerical simulations we observe an increase of erosion rate for the case when the particles are of nano-size. An explanation is the significant increase of particle number for a given volume fraction of particles in the system, as well as their distribution towards the pipe wall due to the fluid flow through elbows.

Introduction/Background: It is well-known that liquids with suspended metallic nanoparticles (i.e. nanofluids) offer superior thermal properties in comparison with pure fluids. Therefore, they can potentially increase performance of e.g. cooling systems. However, the presence of particles in the system can result in an enhanced erosion of equipment that is subjected to nanofluid flow.

The issue of erosion due to flows with solid particles have been intensively studied in recent years. The main focus has been on investigation of flows in pipe elbows because this type of structure is frequently encountered in various industrial applications (see e.g. the review paper by Parsi et al. [1]). Also, an attention has been paid to particles of millimetre or micrometre-size. The main objective of those studies was to investigate the influence of particle size, material, velocity and pipe geometry. One of the tools was numerical analysis, where aspects such as influence of particle-particle and interphase interactions, as well as choice of mathematical models of erosion were also considered.

Nevertheless, the issue of erosion due to nanofluid flow through elbows has still not been widely investigated in the scientific literature. Therefore, the main objective of this paper is to study this problem using theoretical and numerical analysis.

Discussion and Results: Particle of larger size should usually result in higher erosion rates since their kinetic energy is higher. This may indicate that nanofluids should not lead to significant erosion of equipment, because they contain particles of nano-size. However, for a given volumetric or mass flow rate, the number of particles significantly increases when the diameter is lower. The difference is of order $(D_2/D_1)^3$, where D_1 is an average diameter of small particles, and D_2 is an average diameter of large particles. As a result, pipe surfaces are subjected to considerably higher collision rates, which may increase erosion.

According to [1-2], the erosion rate dependence on particle diameter is ~ D^m, where m is between 0.3 and 2.0. Combining with the analysis above, this shows that decreasing particle size from D_2 to D_1, results in a significant increase of erosion rate by a factor of $(D_2/D_1)^{3-m}$. It must be noted, however, that smaller particles track the flow when the flow changes direction so that the real particle-wall collision rate may be lower. Computer simulations of the whole process provide a more detailed insight into the problem. Therefore, in our research, we used the tool of numerical analysis where the commercial computational fluid dynamics software, Star-CCM+, was adopted. We studied a geometry that is shown in Figure 1 (left).

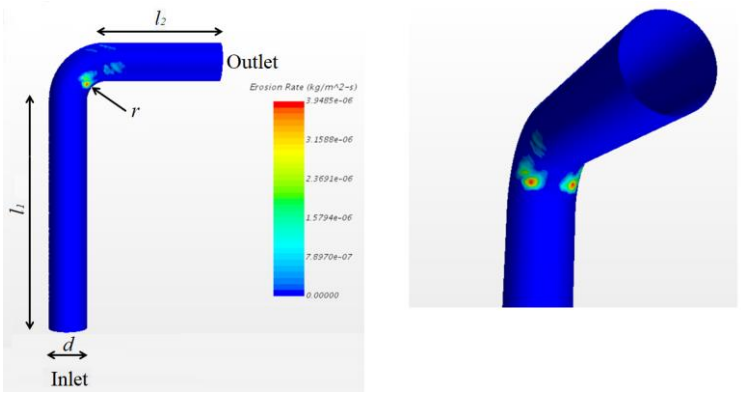

Figure 1. An illustration of the studied geometry and distribution of erosion rate on the pipe wall for diameter 10^{-5} m and velocity 1 m/s.

The geometry was inspired by the paper by Duarte et al. [2]. The pipe diameter d and curvature r were 2 in. (= 0.0508 m), lengths l_1 and l_2 were 0.3048 m and 0.1524 m, respectively. The mathematical model was described by the standard continuity and momentum equations:

$$\frac{\partial \phi_c \rho_c}{\partial t} + \nabla \cdot (\phi_c \rho_c \boldsymbol{u}) = 0, \qquad \frac{\partial \phi_c \rho_c \boldsymbol{u}}{\partial t} + \nabla \cdot (\phi_c \rho_c \boldsymbol{u}\boldsymbol{u}) = -\phi_c \nabla p + \nabla \cdot \left(\phi_c (\tau + \tau^t)\right) - f_\sigma, \qquad (1)$$

where ρ_c is fluid density, ϕ_c is fluid volume fraction, $\boldsymbol{u}$ is fluid velocity, p is pressure, τ and τ^t is the molecular and shear stress tensor, respectively, f_σ describes interphase forces (mainly the drag force). We assumed that the fluid was water with its standard properties. The flow was turbulent and modelled using the *k-ε* model. The computational domain contained 60 000 cells.

The particles were modelled using the Lagrangian approach, that is, they were treated as points tracked in the computational domain. Their motion was governed by the Newton 2. law. We assumed that there were no interactions between the particles. Nevertheless, collisions with the walls occurred and were described using a simplified hard-sphere model that considers two coefficients of restitution: along the normal and the tangential to plane of impact. In our research, we assumed that the collision was almost elastic with the coefficients being equal to 0.99. For modelling the erosion process upon particle-wall collisions, we adopted the model by Oka et al. [4] with the standard input parameters.

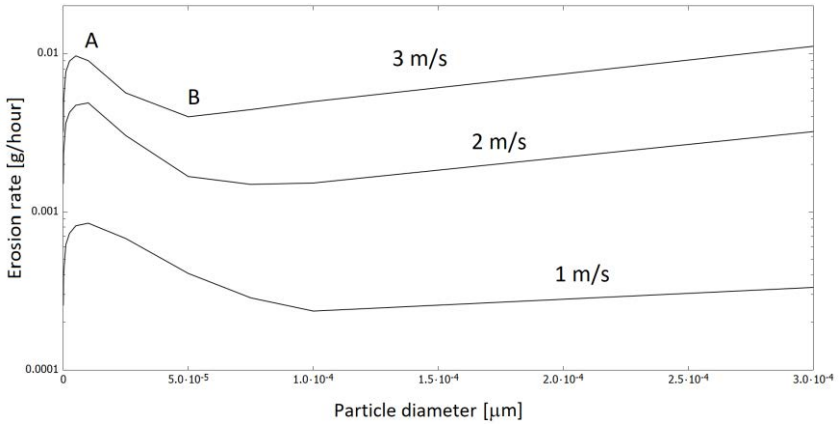

Figure 2. Overall erosion rate as a function of particle diameter for values of the inlet velocity. The local maximum is denoted by A and the local minimum by B and they occur for all the studied cases.

Fluid laden with particles was injected at the inlet (see Figure 1). We studied particles in which size was of order of 10^{-8} – 10^{-3} m. Thus, the smallest particles were of nano-size. The particle material density was 2600 kg/m^3 (aluminum). At first the fluid was introduced without particles until flow reached a steady state. In this paper, we consider three inlet velocities: 1.0, 2.0 and 3.0 m/s, i.e. the corresponding Dean numbers were about 40 000, 80 000 and 120 000. Afterwards, the particles were injected at the volumetric flow rate

equal to 10^{-4} m^3/s. The results of the simulations (erosion rate vs. particle diameter) are shown in Figure 2 and correspond to the point in time 4.7 s, where the flow became steady again.

For the case where the particle size was the largest, we observe the expected trend, in which the larger particles lead to the highest erosion. A similar observation was made also by other researchers, see e.g. [1]. This confirms that the high kinetic energy of the largest particles is a dominant process, even though the total number of particles is less. On the other hand, for the lowest particle size, an opposite trend appears where a decrease in the particle size results in the increase of the erosion rate. The first reason is that total number of particles is larger, but it has also to be noted the smallest particles are easier distributed towards the walls due to vortices that move the flow in the direction lateral to the main flow. Figure 1 shows erosion rate distribution on elbow wall for the case when this maximum occurs.

Conclusions: When comparing the influence of the inlet velocity, we notice that the local maximum and the minimum of the erosion rate do not occur for the same particle diameter. In is interesting to note, however, that they depend on the Stokes number. It must be noted that most researchers considered the case where the Stokes number was higher than the one corresponding to point B. Therefore, they did not observe the increase of erosion rate for low particle diameters.

Acknowledgments: This study was supported by Russian Science Foundation (project No. 17-79-10481).

References:

1. M. Parsi, K. Najmi, F. Najafifard, S. Hassani, B. S. McLaury and S. A. Shirazi, A comprehensive review of solid particle erosion modeling for oil and gas wells and pipelines applications, *Journal of Natural Gas Science and Engineering* 21 (2014) 850-873.
2. G.R. Desale, B.K. Gandhi and S.C. Jain, Particle size effects on the slurry erosion of aluminium alloy (AA 6063), *Wear* 266 (2009) 1066—1071.
3. C.A.R. Duarte, F.J. de Souza and V.F. dos Santos, Mitigating elbow erosion with a vortex chamber, *Powder Technology* 288 (2016) 6-25.
4. Y.I. Oka, K. Okamura and T. Yoshida, Practical estimation of erosion damage caused by solid particle impact Part 1: Effects of impact parameters on a predictive equation, *Wear* 259 (2005) 95-101.

1st International Conference on Nanofluids (ICNf2019)
2nd European Symposium on Nanofluids (ESNf2019)
26-28 June 2019, Castelló, Spain

Analysis of Thermophoretic Effects in Nanofluids

A. Sergis*, Y. Hardalupas

The Department of Mechanical Engineering, Imperial College London, London SW7 2AZ, UK

*Corresponding author: a.sergis09@imperial.ac.uk

Keywords: Nanofluids, Thermophoresis, MDS.

Abstract: Nanofluids are binary mixtures of nanosized solid particles (<100nm) and liquids with volumetric concentrations usually less than 5% that have exhibited enhanced thermal characteristics. The underlying heat transfer mechanisms of their behaviour are unconfirmed. The overall impact of global domain-wide thermophoretic effects in nanofluids for different nanoparticle sizes is believed to be one of the driving mechanisms giving rise to the observed phenomena. Thermophoresis is analysed with the use of a custom-made molecular dynamics simulation code that models the kinematic behaviour of a simplified nanofluid in a domain with a temperature gradient. Despite nanoparticles found to be significantly more mobile than fluid molecules, no net migration effects of nanoparticles are discovered across the temperature gradient of the system for all nanoparticle sizes tested throughout the simulation. It has been concluded that even though local stochastic nanoparticle-level thermophoretic effects are important, global domain-wide directional thermophoretic forces have not been observed under these circumstances.

Introduction/Background: Nanofluids are mixtures of coolants (e.g. water, ethylene glycol etc.) and solid particles, usually less than 100nm in size, in volumetric concentrations frequently less than 5% vol. These engineered fluids became interesting to the technological field of cooling, as they have exhibited increased thermal performance characteristics compared to their pure liquid counterparts. The physical mechanisms giving rise to the exhibited thermal enhancement are unconfirmed. As such, optimisation of these liquids is not straightforward [1].

The current authors' metadata statistical analysis investigation of a large proportion of the available literature indicated that thermal enhancements up to 200% could be achieved with nanofluids over conventional liquids [2]. The analysis indicated that the most popular mechanisms to explain these phenomena (in order of popularity) are the Brownian motion of nanoparticles (NP), the interfacial liquid layering (Kapitza resistance) theory, the aggregation and diffusion theory or simply a combination of all three.

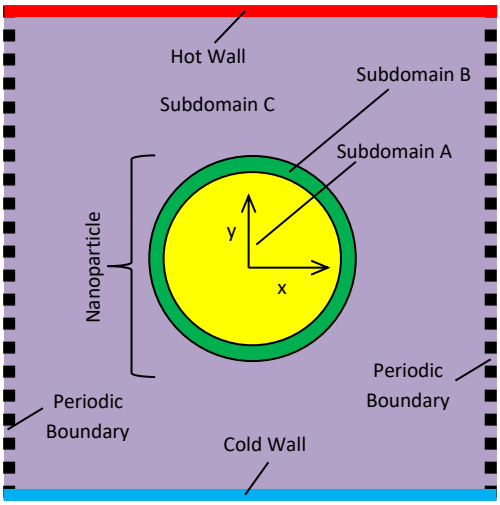

Figure 1. Schematic MDS domain set up, indicating main features

In recent Molecular Dynamics Simulation (MDS) of nanofluids by the current authors [3], [4], it was possible to demonstrate that NP appear to be highly mobile when a temperature gradient is applied – more mobile than fluid molecules. It was displayed that a complex heat transfer mechanism develops for NP dispersed inside liquids with an applied temperature gradient that gives rise to the observed increased nanoparticle thermal diffusion phenomena. The mechanism appears to confirm at large the speculations found in the literature. The increased mobility of NP was shown to be a result of local stochastic thermophoretic effects arising from mismatching local nanoparticle-liquid temperature differences across the surface of NP and the surrounding liquid molecules. Kapitza resistance seemed to play an important role in combination with the ability of the NP to rotate and translate inside the domain. In the current work, a custom-made MDS code is used to evaluate the influence of non-stochastic, collective, directional thermophoretic effects on dispersion of NP suspended in liquids with an applied temperature gradient for varying NP sizes.

Investigations of the physical slip mechanisms that might give rise to the increased mobility of NP in the literature are directing, amongst others, towards global effects of thermophoresis and enhanced Brownian motion. Thermophoresis is classically defined as a directional force applied on particles suspended in liquids and gases with temperature gradients. The force is defined as non-stochastic and aligned against or along a temperature gradient in the domain. Thermophoresis is expected to cause global particle migrations from hot towards colder parts of the domain and vice versa [5]–[7]. Buongiorno examined convective transport in nanofluids [8]. They identified that Brownian diffusion and thermophoresis are the most important NP/base-fluid slip mechanisms, explaining the thermal enhancement found in nanofluids. Bahiraei has analysed the impact of thermophoresis on NP distribution in nanofluids via a scale analysis [9]. It was concluded that thermophoresis has a significant effect on NP distribution in domains with an applied temperature gradient. A MDS study has also been performed by Han [10] for 1μm particle diameters and they concluded that thermophoresis could induce non-stochastic particle migrations from the hot to the cold side of the domain or vice versa.

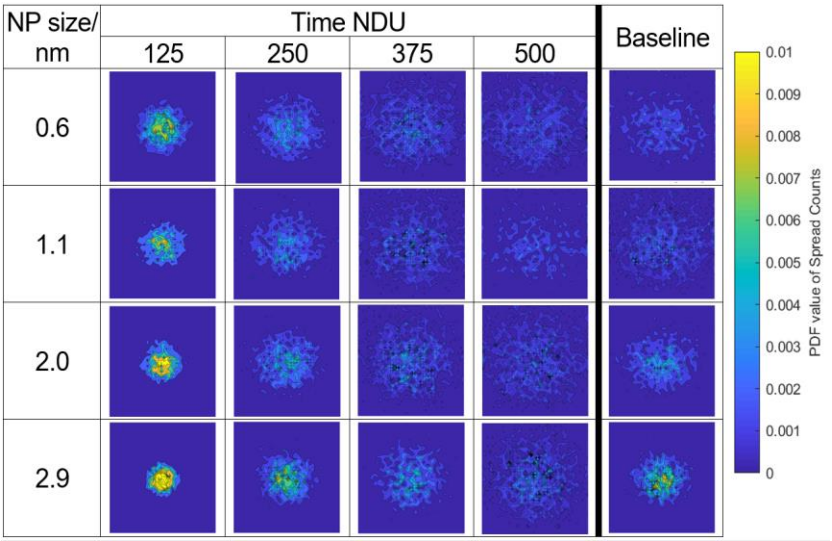

Figure 2. Topological PDF of nanoparticles and baseline spread

Since the details of the MDS code have been published [3], [4], the code setup is briefly summarised here with the help of the schematic of Fig. 1. The data presented in the current paper resulted from a simulation based on the Lennard Jones model [11] of Argon molecules in a 2D domain (Subdomain C) with horizontal adiabatic walls and periodic boundaries in the x direction. A temperature gradient is applied to the system via horizontal walls. A nanoparticle is formed by applying increased intermolecular attraction forces at the core (Subdomain A) and surface (Subdomain B) of the nanoparticle (Figure 1). The nanoparticles are formed at the centre of the domain. To avoid wall effects, the size of the domain scales to the size of the investigated NP, while, for all cases, a constant linear temperature gradient is applied. All quantities are presented in Non Dimensional Units (NDU) according to [11].

Discussion and Results: A collection of 1500 MDS realisations from stochastically initialised systems is used to compile the results. Each realisation includes 500NDU (100k time steps). Four nanoparticle sizes are examined, namely 0.6, 1.1, 2.0 and 2.7nm. Baseline reference cases are composed to facilitate a comparison between the scaled domain sizes without NP. A timeline of the Probability Density Function (PDF) of the topology for the nanoparticles is presented along with the baseline topology at the final iteration of the simulation in Figure 2.

Starting from the Baseline data, it is evident that no net accumulation of fluid molecules exists in the domain (as expected). The apparent shrinkage of the topological map is due to the effects of domain scaling to accommodate larger NP under the same temperature gradients. The spread geometry is symmetrical in both axes as expected. For the case of NP, these appear to be reaching further into the edges of the domain (higher penetrability). Their penetrability is intensifying with increasing NP size, which is a novel finding and complies with earlier studies of the current authors. The activity of NP is shown to be higher

in the hotter parts of the domain (as expected). However, there is no significant evidence of net migration effects taking place for the range of examined particle sizes. This indicates that system wide net thermophoretic effects, unlike to what has been reported in the literature so far, are either insignificant or stochastic from the mechanistic point of view of the system and for the size of nanoparticles examined.

Summary/Conclusions: A mechanistic MDS analysis of system wide net thermophoretic effects on NP of different sizes suspended in a liquid domain with a temperature gradient is performed. Unlike to what has been reported in the literature, system wise thermophoretic effects appear to be either insignificant or non-directional. Moreover, the global penetrability of NP in the cold/hot sides of the domain seems to increase with increasing NP size.

Acknowledgements: This work has been carried out within the framework of the EUROfusion Consortium and has received funding from the Euratom research and training programme 2014-2018 and 2019-2020 under grant agreement No 633053. The views and opinions expressed herein do not necessarily reflect those of the European Commission.

References:

1. S. K. Das, S. U. S. Choi, W. Yu, and T. Pradeep, *Nanofluids: Science and Technology*, First. Hoboken, NJ, USA: John Wiley & Sons, Inc., 2007.
2. A. Sergis and Y. Hardalupas, “Anomalous heat transfer modes of nanofluids: a review based on statistical analysis.,” *Nanoscale Res. Lett.*, vol. 6, no. 1, p. 391, 2011.
3. A. Sergis and Y. Hardalupas, “Revealing the complex conduction heat transfer mechanism of nanofluids,” *Nanoscale Res. Lett.*, vol. 10, no. 1, p. 954, Dec. 2015.
4. A. Sergis and Y. Hardalupas, “Molecular Dynamic Simulations of a Simplified Nanofluid,” *Comput. Methods Sci. Technol.*, vol. 20, no. 4, pp. 113–127, Dec. 2014.
5. S. Hottovy, G. Volpe, and J. Wehr, “Thermophoresis of Brownian particles driven by coloured noise,” *Epl*, vol. 99, no. 6, pp. 1–7, 2012.
6. G. S. McNab and A. Meisen, “Thermophoresis in liquids,” *J. Colloid Interface Sci.*, vol. 44, no. 2, pp. 339–346, 1973.
7. D. Liu, *Particle Deposition onto Enclosure Surfaces*, First Edit. Elsevier Inc., 2010.
8. J. Buongiorno, “Convective Transport in Nanofluids,” *J. Heat Transfer*, vol. 128, no. 3, p. 240, 2006.
9. M. Bahiraei, “Impact of thermophoresis on nanoparticle distribution in nanofluids,” *Results Phys.*, vol. 7, pp. 136–138, 2017.
10. M. Han, “Thermophoresis in liquids: A molecular dynamics simulation study,” *J. Colloid Interface Sci.*, vol. 284, no. 1, pp. 339–348, Apr. 2005.
11. D. C. Rapaport, *The Art of Molecular Dynamics Simulation*, 1st ed. Cambridge: Cambridge University Press, 2004.

1st International Conference on Nanofluids (ICNf2019)
2nd European Symposium on Nanofluids (ESNf2019)
26-28 June 2019, Castelló, Spain

Access resistance in a nanochannel

M. Aguilella-Arzo* and V.M. Aguilella

Laboratory of Molecular Biophysics, Department of Physics, Universitat Jaume I, 12071 Castellón, Spain

*Corresponding author: arzo@uji.es

Keywords: Access resistance, nanochannel, Poisson-Nernst-Planck.

Abstract: The access resistance of a nanometer-sized channel is important for channels with low pore length to radius ratio. This is specially important at low concentrations. We provide an analysis of the conditions under which the corresponding correction is important based both in the classical treatment of Hall and on numerical data in a model cylindrical pore.

Introduction/Background:

The transport of fluids and electrolytes through nanometric sized pores has recently received great interest [1]. This is due to the large number of applications expected from these devices, such as energy generation and storage [2], lab-on-chip nanodevices [3], Coulter counter [4], desalination [5], etc. In many of the mentioned applications the fluids that migrate in the system are electrolyte solutions that rearrange around the charged bodies over lengths that are of the order of the Debye length of the solution. The flows and electric currents generated in these cases depend on the transport of the solution as a whole (dependent on the pressure gradients and the fluid velocity) as well as on the electromigration of the electrolyte ions. The different contributions to the total flow of electric current are greatly simplified if a system without pressure gradients or solution flow is considered. In this simplified system, the total resistance under given conditions of external potential and concentrations will be determined primarily by the drift-diffusion ion properties and the geometry of the channel, but also by the pore-solution interfacial effects, i.e. by the access resistance [2,6–8]. The importance of the access resistance in the total resistance of the nanofluidic system can be critical, especially in the case of low concentrations and low channel aspect ratios (l/a). Traditionally this access resistance has been estimated using an analytical expression obtained by Hall [9],

$$R_{access} = \frac{1}{4\kappa a} \tag{1}$$

where κ is the conductivity of the solution medium, and a is the channel radius, however this equation assumes that conductivity in the vicinity of the pore opening is the same as bulk conductivity. However, this is not accurate except in some particular situations and it leads to misleading results for selective pores and/or charged pore substrates.

In this work, we analyse under what conditions the access resistance [7,10] should be accounted for the calculation of the current through an ideal cylindrical channel of nanometer size. In addition, we test the validity of Hall's equation to estimate the access resistance under various conditions of geometry (aspect ratio l/a), ion concentration and intrinsic charge of the pore and the substrate. To this end, we simulated numerically the pore-solution system. We obtained the currents and profiles of concentration and electric potential of an idealized nanometric channel as a function of a wide variety of boundary conditions similar to that used experimentally.

Model

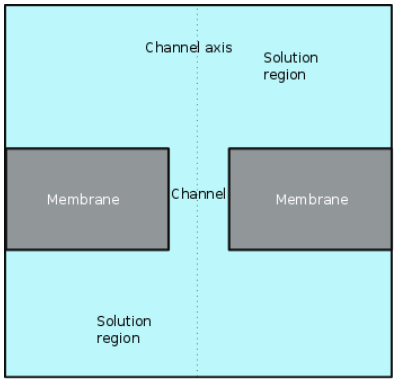

Figure 1. Sketch of the simulation box used to obtain the ion flows and profiles of concentration and electric potential.

The system shown un Figure 1 assumes cylindrical symmetry around the axis of the channel, so we can use cylindrical coordinates to solve the equations that describe the electromigration of ions through the solution, that is, the Nernst-Planck equations:

$$\vec{J}_i = -D_i(\vec{\nabla}c_i + \frac{z_i F}{RT}c_i\vec{\nabla}\phi) \tag{2}$$

where D_i is the diffusion coefficient of the ion i, c_i is its concentration, Φ is the total electric potential, z_i is the charge number of each species, F is the Faraday constant, R the ideal gas constant and T the absolute temperature. In the stationary state, the continuity equation applied to the ionic fluxes reads:

$$\vec{\nabla}\vec{J}_i = 0 \tag{3}$$

This leads to two second order partial differential equations on the concentrations and electric potential (for the case of a binary electrolyte). To these we should add the Poisson equation relating the electric field and the source charges present in the system:

$$\vec{\nabla}(\varepsilon\vec{\nabla}\phi) = -\rho \tag{4}$$

where the charge density (ρ) contains two contributions:

$$\rho = \rho_f + F\sum z_i F c_i \tag{5}$$

the first term (ρ_f) being the fixed charge (eg. for a charged channel) and the second term the charge carried by the ions in solution.

The equations (1-4) is a system of partial non-linear differential equations. In our case, we used FiPy [11] to solve the system numerically and obtain as a result both the concentrations of each ion and the electric field in the system. With this information it is possible to obtain the electric flows and currents flowing through the system, for given set of boundary conditions.

Discussion and Results:

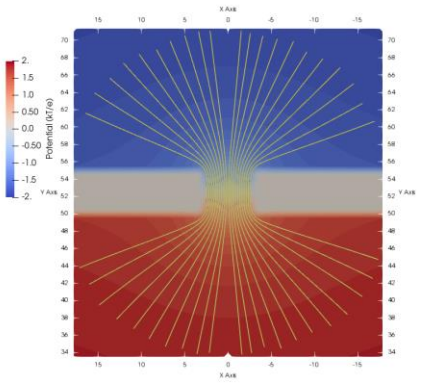

Figure 1. Electric potential through an ideal cylindrical channel at c=100 mM of KCl electrolyte. Applied potential was 100 mV.

Figure 2 shows the potential profile for a typical case. We have found that:

1) Access resistance is important at low concentration and/or with low aspect ratios. In this case there is good agreement (except at high concentrations) with Hall's equation.

2) The charge of the membrane and/or pore significantly reduces the importance of the access resistance. Discrepancies appear with respect to the analytical Hall's formula.

3) The charge of the membrane has influence both in the access resistance and in the resistance of the proper channel, especially at low concentrations. It is not possible to decouple both contributions.

Summary/Conclusions:

We show that access resistance in the total resistance of the nanofluidic system can be critical. Numerical results on the transport through an ideal cylindrical channel show that important discrepancies appear with the classical Hall formula, especially in the case of charged membranes and/or high concentrations.

Although the effects described here involve ions in an electrolytic solution, they may also be relevant in the case of particles that migrate in a base solution since these also respond to changes in local electrostatic fields in the vicinity of the microchannels.

References:

1. L. Bocquet, E. Charlaix, Nanofluidics, from bulk to interfaces. *Chemical Society Reviews* 39 (2010) 1073–1095.
2. Y. Yan, Q. Sheng, C. Wang, J. Xue, H.C. Chang, Energy conversion efficiency of nanofluidic batteries: Hydrodynamic slip and access resistance. *Journal of Physical Chemistry C* 117 (2013) 8050–8061.
3. S. Pennathur, J.C.T. Eijkel, A. Van Den Berg, Energy conversion in microsystems: Is there a role for micro/nanofluidics? *Lab on a Chip 7* (2007) 1234–1237.
4. S. Sahu, M. Zwolak, Maxwell-Hall access resistance in graphene nanopores. *Physical Chemistry Chemical Physics* 20 (2018) 4646–4651.
5. R.C. Rollings, A.T. Kuan, J.A. Golovchenko, Ion selectivity of graphene nanopores. *Nature Communications 7* (2016) 11408.
6. S. Sahu, M. Zwolak, Golden aspect ratio for ion transport simulation in nanopores. *Physical Review E 98* (2018) 012404.
7. Y. Ma, J. Guo, L. Jia, Y. Xie, Entrance Effects Induced Rectified Ionic Transport in a Nanopore/Channel. *ACS Sensors* 3 (2018) 167–173.
8. J. Wang, J. Ma, Z. Ni, L. Zhang, G. Hu, Effects of access resistance on the resistive-pulse caused by translocating of a nanoparticle through a nanopore. *RSC Advances* 4 (2014) 7601.
9. J.E. Hall, Access resistance of a small circular pore. *The Journal of General Physiology* 66 (1975) 531–532.
10. M. Aguilella-Arzo, V.M. Aguilella, R.S. Eisenberg, Computing numerically the access resistance of a pore. *European Biophysics Journal* 34 (2005) 314–322.
11. J.E. Guyer, D. Wheeler, J.A. Warren, FiPy: Partial Differential Equations with Python. *Computing in Science & Engineering* 11 (2009) 6–15.

1st International Conference on Nanofluids (ICNf2019)
2nd European Symposium on Nanofluids (ESNf2019)
26-28 June 2019, Castelló, Spain

Numerical analysis of thermophoresis phenomenon for size based exosome separation

A. Errarte[1#], M. Aginagalde[1], A. Martin[1], E. González[2], I. Iloro[2], J. M. Falcón-Pérez[2], F. Elorza[2], M. Mounir Bou-Ali[1*].

[1] Mechanical and Manufacturing Department, MGEP Mondragon Goi Eskola Politeknikoa, Loramendi 4 Apdo. 23, 20500 Mondragon, Spain

[2] CIC bioGUNE, Parque Técnológico de Bizkaia, Edificio 801 A, 48160 Derio, Spain.

[#]ane.errarte@alumni.mondragon.edu; [*]mbouali@mondragon.edu

Keywords: Exosome, Thermodiffusion, Microdevice, Separation.

Abstract: Microfluidic devices have shown to be a promising alternative to conventional separation and characterization processes. This work shows a numerical study where the thermodiffusion phenomenon is used to separate different populations of exosomes, nanovesicles liberated from most types of cells, within a microdevice. ANSYS Fluent software was used to analyse different geometries and temperature gradients to track the trajectories of exosomes and separate them into different populations. This work is focused on the procedure that was followed toward the final device design.

Introduction/Background: Medical detection and diagnosis techniques, as well as laboratory proceedings have advanced considerably during the last years, where taking into account the importance of miniaturization in biotechnology, microdevices have turned to be a promising alternative in front of actual techniques [1]. The study of exosomes is focused in this scenario. Exosomes are small vesicles (40-250 nm) liberated by most types of cells. These vesicles are formed by a lipid bilayer being able to contain in their interior proteins, messenger RNA (mRNA), microRNA (miRNA), metabolites or specific proteins of the liberator cell. The study of the internal components has demonstrated the potential in the discovery of new biological markers that can be directly associated to pathologies such as cancer or Alzheimer, as the vesicles work as cellular messengers [2, 3].

One of the principal objectives of the preventive medicine is the development of new techniques of purification that would help in biological marker analysis in a fast, cheap and non-invasive manner [4]. For this reason, this work is focused on the study of a new microdevice to separate populations of exosomes using thermal gradients.

Method: In this application thermal gradients are the principal driving force of the nanovesicles. For this reason thermodiffusion phenomenon must be studied. This phenomenon refers to a concentration gradient generation by means of thermal gradients. When a colloid is placed in front of a temperature gradient, particles move toward the cold or hot wall with a trawl velocity [5]. When particles move toward the cold wall, the suspension is determined as thermophobic, and when they move toward the hot one thermophylic. As a consequence of the components movement, a concentration gradient is generated, and with the aim of homogenizing the mixture, another flow acts in the opposite direction due to the diffusion. The mass flow of a multicomponent mixture can be described by expression (1) [6]:

$$\vec{J}_i = -\rho\left(\sum_{k-1}^{n-1} D_{ik}\nabla c_k + D'_{T,i}\nabla T\right) \qquad i = 1,...n-1 \qquad (1)$$

where $\vec{J}_i$ is the mass flow of component i, ρ is the mixtures density, D_{ik} is the molecular diffusion tensor, ∇c_k is the spatial gradient of mass fraction of component k, $D'_{T,i}$ is the thermodiffusion coefficient of i, T is the temperature y ∇T is the spatial temperature gradient across the mixture.

Numerical study: ANSYS Fluent software was used to carry out the numerical study. First exosomes displacement was studied, then the extraction was simulated and a final device was proposed.

The initial device was a bi-dimensional rectangular channel in order to analyse the displacement direction of the vesicles. In a second design, an exit was located in the bottom wall to extract a population. Finally, a second exit was located to extract two different populations. For the first device different channel heights were analysed; 50 µm, 100 µm, 200 µm, 400 µm, 800 µm and 1600 µm, adjusting for further studies the most adequate one. A cytometer was located in the entry of all analysed devices in order to limit the entry zone of the particles.

Cases were solved using Euler-Lagrange approach, considering the fluid phase as continuum and the dispersed as secondary. Particles were tracked in the laminar flow using the Discrete Phase Model (DPM) in a two way interaction. As particles were directed by thermal gradients, thermophoretic force was activated. Following the approach, stationary state 2D base mass, momentum and energy balance together with the particle force balance were solved. For the thermophoretic coefficient determination in the software ANSYS Fluent a unit change has to be done following expression (2) [5]

and it was then entered in the software as a User Defined Function, where the program detects automatically the size of the particle and determines it hermodiffusion coefficient.

$$D_{T\ fluent} = 6\pi \cdot \mu \cdot T \cdot D_{T\ \exp} \cdot \frac{P_{DIAM(p)}}{2} \quad (2)$$

Here μ is the viscosity, $D_{T\exp}$ is the experimental thermodiffusion coefficient and $P_{DIAM(p)}$ is the particle diameter. In addition, as particles are submicron size, Saffman lift force was activated.

For injection particles definition, vesicles ranging from 40 nm to 250 nm at 298.16 K were set from the central inlet of the cytometer. For material properties, the base fluid Phosphate Buffered Saline (PBS) properties and exosome nanoparticles properties were set. Finally, boundary conditions were defined. Top wall was heated up to 302.16 K and the bottom cooled to 294.16 K. Adiabatic lateral walls were set. Case to case the inlet velocity was changed to see the the velocity effect on population separation.

With the aim of analysing the population separation, different entry flows for the sample and the porter fluid were analysed. The $f_q = \frac{Q_c}{Q_T}$ parameter was defined as the relationship between the flow of the central cavity of the cytometer and the total flow. The defined entry flow relationship values were 0.2, 0.1, 0.05 and 0.025 for total flows of 50, 100 and 200 ml/min per channel height.

Discussion and Results: We saw that particles were displaced toward the cold wall, being the first ones the biggest ones and the last reaching the cool wall the smallest ones. Moreover, we saw that particles were stratified depending on their size, based on the boundary conditions applied. We also saw that the smaller the ratio between entry flows, the better the separation. In order to select the case to work with posterior simulations the parameter time was also taken into account. The 400 µm height and 100 ml/min entry flow case was selected; with a separation time around 100 min.

As for exosome extraction simulations, we saw that adjusting the boundary conditions gives the user the chance to select the cut size of populations. If a single outlet was located in the inferior wall only two populations could be separated in each lap. In order to separate faster and obtain two or three populations in each lap, a second exit was located next to the first one. Nevertheless, no suitable conditions were obtained to separate three populations. Figure 1 shows the first simulated device and the result of displacement and stratification.

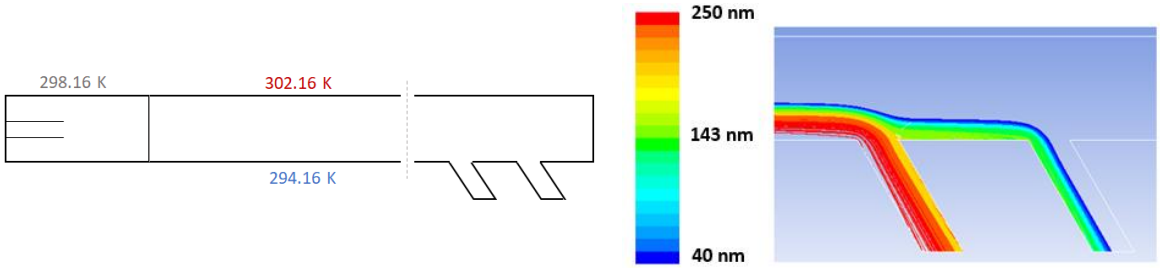

Figure 1: Geometry and boundary conditions used for simulation and extraction result.

Summary/Conclusions: This work studied numerically the thermodiffusion phenomenon applied to a biological mixture with the aim of separating different exosome populations by size. First, nanoparticles trajectory in front of thermal gradients was analysed, and then the extraction by outlets in the inferior wall was studied. Moreover, we saw that variations in boundary conditions allow the user to make a selective extraction. By this investigation it has been also demonstrated that thermodiffusion is an efficient mechanism for nanoparticle separation. All boundary conditions and geometries are patented in P20131380 and EP17382719.

Acknowledgements: Authors thank BG2018 (KK-2018/00054) and Research Groups (IT009-16) of Basque Government, ATNEMFLU (ESP2017-83544-C3-1-P) of the MINECO and FETRAFLU (2018-CIEN-000101-01) from Gipuzkoa Program for Science.

References:

1. S. J. Lee. S. Y. Lee, *Micro total analysis system (μ-TAS) in biotechnology,* Applied Microbiology and Biotechnology, 64 (2004), 289-299.
2. Stoorvogel, G. Raposo and Willem, *Extracellular vesicles: exosomes, microvesicles, and friends*, The Journal of Cell Biology, 200 (2013), 373-383.
3. H C. Anderson, D. Mulhall, R. Garimella, *Role of extracellular membrane vesicles in the pathogenesis of various diseases, including cancer, renal diseases, atherosclerosis, and arthritis*, Laboratory Investigation, 90 (2010), 1549-1557.
4. C. Théry, A. Clayton, S. Amigorena, and G. Raposo, *Isolation and characterization of exosomes from cell culture supernatants and biological fluids*, Current Protocols in Cell Biology, Chap 3 (2006).
5. M. Eslamian, M. Z. Saghir, *Novel thermophoretic particle separators: Numerical analysis and simulation*, Applied Thermal Engineering, 59 (2013), 527-534.
6. P. Blanco, M. Mounir Bou-Ali, J.K. Platten, D. Alonso De Mezquia , J.A. Madariaga, C. Santamaría. *Thermodiffusion coefficients of binary and ternary hydrocarbon mixtures*, J Chem Phys, 132 (2010).

1st International Conference on Nanofluids (ICNf2019)
2nd European Symposium on Nanofluids (ESNf2019)
26-28 June 2019, Castelló, Spain

Simulation of Heat Transfer in Nanofluids using a Multi-component Dissipative Particle Dynamics Model

Eiyad Abu-Nada*

Department of Mechanical Engineering, Khalifa University, P.O. Box 127788, Abu Dhabi, UAE

*Corresponding author: eiyad.abunada@ku.ac.ae

Keywords: nanofluids, dissipative particle dynamics, heat transfer enhancement

Abstract: The present work applies a multi-component Dissipative Particle Dynamics (DPD) model to investigate heat transfer enhancement in natural convection using nanofluids. The model gives a more realistic simulation technique by treating the base fluid and the dispersed nanoparticles as two different discrete phases. This approach helps in understanding heat transfer between nanoparticles and base fluid particles. The application selected in the current study is natural convection in a differentially heated enclosure filled with Al_2O_3 nanoparticles. It was found that heat transfer due to natural convection using Al_2O_3-water nanofluid is inversely proportional to the volume fraction of nanoparticles.

Introduction/Background: In recent years the topic of heat transfer enhancement using nanofluids has attracted numerous amount of work both from experimental and theoretical viewpoints. Basically, the nanofluid consists of nanoparticle dispersed inside a base fluid an attempt to enhance the intrinsic properties of the base fluid, such as the thermal conductivity. It is well known that poor thermal conductivity of pure fluids is considered a main drawback on their thermal performance. Many researchers reported a favorable enhancement in heat transfer in in forced convection applications using high conductive nanoparticles. However, there is a debate on the role of nanoparticles in natural convection applications in terms of heat transfer enhancement [1]. For example, theoretical investigation [2] reported a heat transfer enhancement due to the presence of nanoparticles opposing the experimental findings of Putra et al. [3] and Wen and Ding [4].

Theoretically speaking, most of the theoretical studies in literature relied on using continuum models in studying heat transfer between nanoparticles and base fluid particles and the big question here is whether at the nano transport scale, the continuum models still applicable. Recently, Abu-Nada [5, 6] presented a discrete heat transfer

model based on the dissipative particle dynamics (DPD) technique to analyze heat transfer in nanofluids. In the most recent publication [6], Abu-Nada presented a two-component model to study heat transfer in Al_2O_3-water nanofluids. Therefore, the scope of the present paper is to apply this discrete DPD model to study natural convection in a differentially heated enclosure using Al2O3-water nanofluid for a Rayleigh number of $Ra=2.5\times10^4$. The DPD particles motion is governed by conservation of momentum and energy and is described by the following set of equations using the Boussinesq approximation [6]:

$$\frac{d\vec{r}_i}{dt}=\vec{v}_i \tag{1}$$

$$\frac{d\vec{v}_i}{dt}=\left(\vec{f}_{ij}^{\,C}+\vec{f}_{ij}^{\,D}+\vec{f}_{ij}^{\,R}\right)+\vec{g}\beta(T-T_o) \tag{2}$$

$$C_v\frac{dT_i}{dt}=\left(q_{ij}^{visc}+q_{ij}^{cond}+q_{ij}^{R}\right) \tag{3}$$

where β is the thermal expansion coefficient and $\vec{g}$ is the gravity vector. The reader is referred to the work of Abu-Nada [6] for more details on the model.

Discussion and Results: A schematic of the square enclosure is shown in Fig. (1). The enclosure is filled with Al_2O_3-water nanofluid. Due to the scarce of experimental data at the nanoscale level to benchmark the current DPD model, the current problem is used to validate the DPD code at the extreme limit where it can be validated at the large scale with continuum based models, such as finite volume (FV) technique solutions.

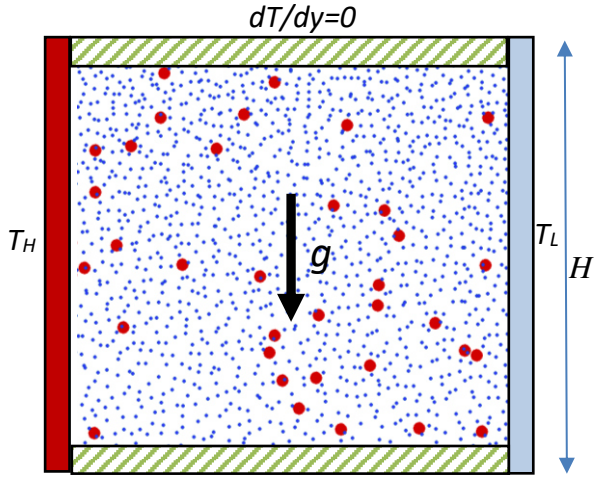

Figure 1. Schematic of problem geometry

The Prandtl number (Pr) and Rayleigh number (Ra) are given as:

$$\mathrm{Pr} = \frac{\nu_C}{\alpha_C} \qquad Ra = \frac{g\beta(T_H - T_C)H^3}{\nu_C \alpha_C}$$

Figure 2 presents the temperature isotherms and streamlines in the enclosure. The DDP captured the main features of fluid and heat transfer in the enclosure for the case of natural convection. For example, the isotherms get parallel to the hot and cold walls near walls due to the dominance of the boundary layer next to the walls; however, the isotherms become curve lines in the middle region of the enclosure due to the dominance of convection. Also, Fig. 2 shows the finite volume (FV) solution of the same problem where the dotted dashed lines represent the FV solutions. As seen from the figure, DPD agrees very well with the finite volume solutions, which gives a confidence in the ability of DPD to capture nanofluid heat transfer in natural convection applications. Also, the same figure shows that a single circulation cell is captured by the DPD approach and the results agree very well the finite volume results.

The Nusselt number is used here as an indicator of heat transfer enhancement. Figure 3 shows two cases: a nanoparticle volume fraction of φ= 5% and a pure fluid case. The figure demonstrates a decrease in Nusselt number with the increase of volume fraction of nanoparticles. The influence of nanoparticles has two opposing effects on the Nusselt number: a positive effect that is due to the presence of high thermal conductivity nanoparticles, and an adverse effect due to the high level of viscosity experienced at high volume fractions of nanoparticles. The heat transfer in natural convection at Ra= 2.5×10^4 is dominated by convection. The presence of nanoparticles will cause the nanofluid to behave as more viscous, which will decrease convection currents and accordingly reduce the temperature gradient and accordingly Nusselt number at the hot wall. This is accompanied by some enhancement in heat transfer due to the high thermal conductivity of nanoparticles but, such augmentation in heat transfer is small when compared to the deterioration brought by viscosity.

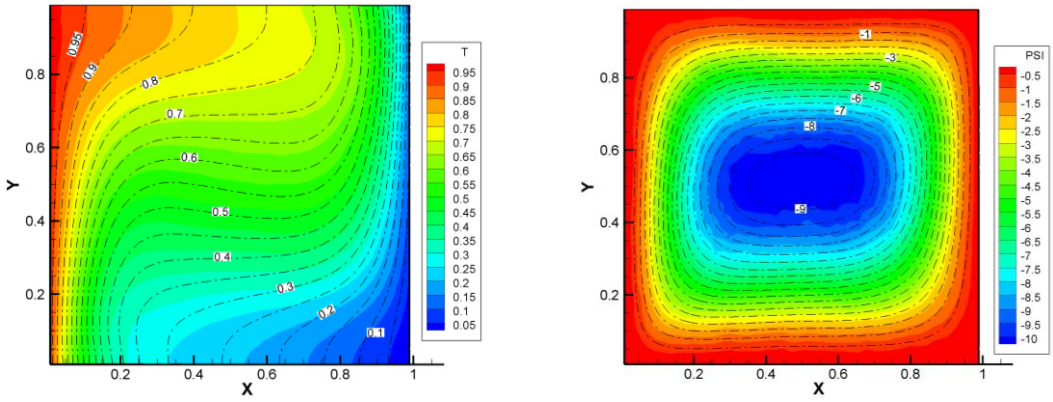

Figure 2. Isotherms (left) and streamlines (right) for φ = 5% Ra= 2.5×10^4

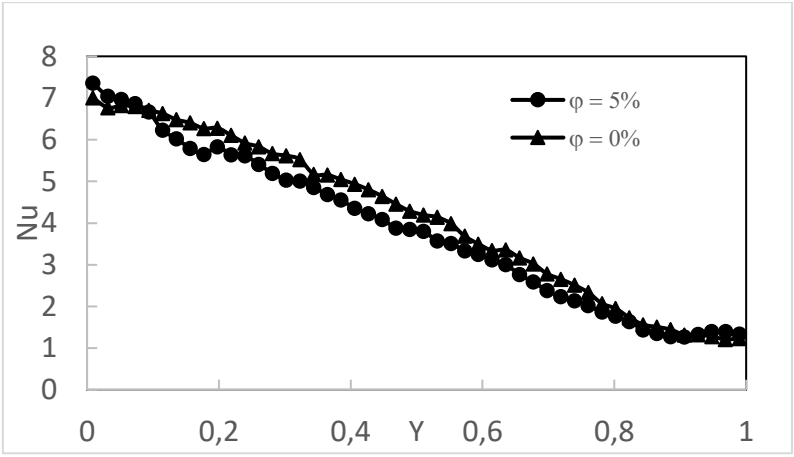

Figure 3. Nusslet number along the hot wall for φ = 5% and pure fluid case.

Conclusions: DPD was used to solve for temperature and velocities within the enclosure for natural convection of Al2O3-nanofluid. It was found that the addition of nanofluid has adverse effect on the enchantment in heat transfer as shown in the Nusselt number at the hot wall.

References:

1. E. Abu-Nada, Z. Masoud, H.F. Oztop, A. Campo, Effect of nanofluid variable properties on natural convection in enclosures, Int. J. Thermal Sciences 49 (2010) 479–491.
2. K. Khanafer, K. Vafai, M. Lightstone, Buoyancy-driven heat transfer enhancement in a two-dimensional enclosure utilizing nanofluids, Int. J. Heat Mass Transf., 46 (2003) 3639-3653.

3. N. Putra, W. Roetzel, S.K. Das, Natural convection of nano-fluids, Heat Mass Transf., 39 (2003) 775-784.
4. D. Wen, Y. Ding, Experimental investigation into convective heat transfer of nanofluids at the entrance region under laminar flow conditions, Int. J. Heat Mass Transf., 47 (2004) 5181–5188.
5. E. Abu-Nada, Dissipative particle dynamics investigation of heat transfer mechanisms in Al2O3-water nanofluid, Int. J. Thermal Sciences 123 (2018) 58–72.
6. E Abu-Nada, I Pop, O Mahian, A dissipative particle dynamics two-component nanofluid heat transfer model: Application to natural convection, Int. J. Heat Mass Transf. 133, 1086-1098

1st International Conference on Nanofluids (ICNf2019)
2nd European Symposium on Nanofluids (ESNf2019)
26-28 June 2019, Castelló, Spain

A Comparative Study of Multiphase Nanofluid Models of Ferromagnetic Nanofluids Flow in a Circular Pipe

M. Tekir[1], E. Gedik[2,*], M. Yiğit[3] and K. Arslan[1]

[1]Mechanical Engineering Department, Engineering Faculty, Karabük University, Turkey

[2]Energy Systems Engineering Department, Faculty of Technology, Karabük University, Turkey

[3]Graduate School of Natural and Applied Science, Karabük University, Turkey

[*]Corresponding author: egedik@karabuk.edu.tr

Keywords: Nanofluid, Multiphase, Laminar Flow, Convective Heat Transfer.

Abstract: Nanofluids have been greatly attracting the researchers, who mainly study on the heating and cooling process. Although numerous papers have been published on this field, there are still some lack of data for understanding and evaluating of nanofluid flow. Therefore, in this study, Fe_3O_4-water nanofluid flow in a pipe under laminar regime has been numerically investigated. Single-phase and multiphase approaches have been used in this study. VoF, Mixture, and Eulerian models have been used for multiphase modeling of the nanofluid. The results were compared with the experimental data obtained in the literature. As a result, it is obtained that Eulerian model represents the experimental data very well for lower nanoparticle volume concentrations. Furthermore, for higher nanoparticle volume concentration single-phase model shows better accuracy.

Introduction/Background: According to the literature, even though the investigation of the nanofluid concept has been greatly attracting the researchers and numerous papers on this field have been published, there are still some lack of studies for understanding and evaluating of the convective nanofluid flows. Especially, researches on performing of multiphase comparison in the literature are not adequate. Therefore, in this study, Fe_3O_4-water nanofluid flow in a pipe under laminar condition has been numerically investigated. Numerical results of single-phase and VoF, Mixture, and Eulerian multiphase modes have been compared with experimental data. Numerical calculations have been carried out for different nanoparticle volume concentrations (1.25%, 2.5% and 5.0%) of the nanofluid. Thus, an attempt in this study has been made assisting to close the gaps in the literature on this area. To solve nanofluid flow numerically, two approaches are employed in literature. In single-phase model, the nanofluid is treated as a homogeneous

fluid with effective properties due to nanoparticle dispersion. Bahiraei [1] studied the multiphase Eulerian method is to study heat transfer characteristics of the CuO–water nanofluid in a straight tube under laminar flow regime. All models have advantages and disadvantages. However, single-phase model comes forward among these since other approaches do not provide an insight into complicated numerical models. Besides, this model offers low computational cost and reasonable accuracy, whereas Eulerian models provide better results at the expense of high computational cost Minea [2]. In this study, the forced convective laminar flow condition of Fe_3O_4-water nanofluid flow has been investigated with an aim to perform hydrodynamic and thermal analyses. Internal diameter and length of the tube are 4.8 mm and 1245 mm, respectively. The walls of the channel were under the influence of constant heat flux ($q'' = 13\ kW/m^2$). In the laminar regime, different Reynolds numbers ranging from 670 to 1700 were taken into consideration. For numerical analyses, the single-phase, VoF, Mixture, Eulerian models were applied to investigate the fluid dynamic and thermal behaviours of the nanofluid. Steady-segregated solver has been used with second-order upwind scheme for convective terms in the mass, momentum, energy, and turbulence equations. For pressure discretization, the standard scheme has been employed while the SIMPLE-algorithm has been used for pressure–velocity coupling discretization. Each governing equation has been iterated until the residual falls below 10^{-6}. The numerical study results for pure water have been tested with Shah and London [3] correlation and experimental data by Dibaei and Kargarsharifabad [4]. It was found that the numerical results are compatible with literature as shown in Fig. 1.

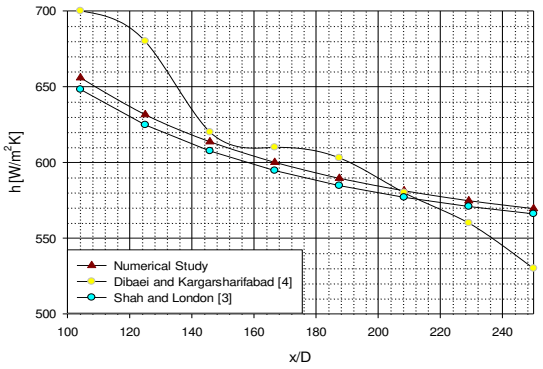

Figure 1. Comparison of the numerical study with literature.

These results are almost the same at the higher dimensionless axial length; however, the difference between the present study and Shah-London correlation increases at

lower dimensionless axial length. Specifically, numerical results are in the 2.5% error margin of Shah-London correlation and 7.0% error margin of experimental data.

Discussion and Results: After the mesh study and verification of results of pure water with experimental data and correlation, analyses were continued with multiphase models using nanofluids. It can be seen from Fig. 2 that convective heat transfer increases with increasing nanoparticle volume concentration throughout the pipe length. Nanofluid with 5.0% nanoparticle volume concentration offers up to 17.0% more heat transfer than pure water.

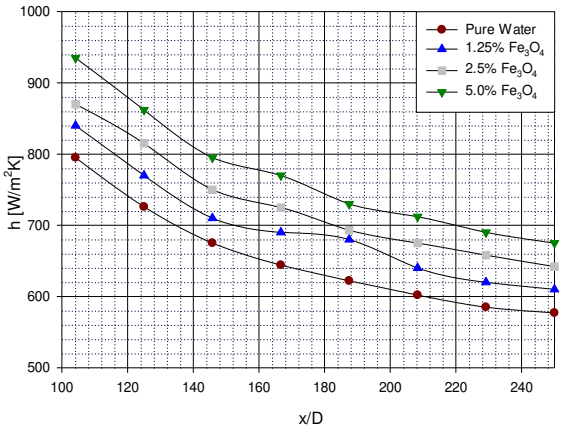

Figure 2. Variation of convective heat transfer with dimensionless axial length and nanoparticle volume concentration.

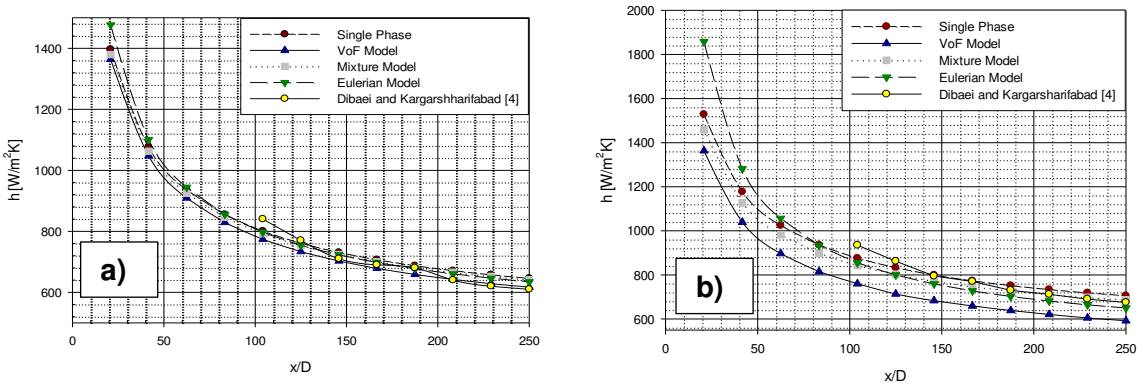

Figure 3. Variation of convective heat transfer coefficient of various models using nanofluid of (a) 1.25% and (b) 5.0% nanoparticle volume concentration.

Comparison of convective heat transfer coefficient from analyses of single-phase, VoF, Mixture, Eulerian models, and experimental study can be seen in Fig. 3a-b. Eulerian model is the best model to predict heat transfer coefficients compared to other models at lower

nanoparticle volume concentrations with an average range of ±0.75%, while single-phase model represents the experimental data very well at higher dimensionless axial lengths and higher nanoparticle volume concentrations.

Summary/Conclusions: In this study, an attempt has been made to perform the numerical analysis of Fe_3O_4-water nanofluid flow using single-phase and multiphase models. Analysis results have been compared and discussed with experimental data obtained from literature. Accordingly, the main findings that can be drawn from the present study are given below:

- Nanofluids present higher convective heat transfer coefficient comparing to the base fluid over a range of Reynolds numbers. The enhancement in laminar heat transfer coefficient is reached up to 17.0% in Fe_3O_4-water nanofluid with a volume concentration of 5.0%.
- Eulerian model is the best one among the multiphase approach models to predict the experimental data.
- All models underpredicts convective heat transfer coefficient at lower dimensionless axial lengths.
- With increasing nanoparticle volume concentration, the accuracy of Eulerian model declines while single-phase model provides better accuracy.
- Multiphase models have disadvantage of computational time. Extra cost of computation of nanoparticle tracking results higher computational time, whereas single-phase model approach provides reasonable result with lower computational time.

Acknowledgement: The authors would like to thank the Scientific and Technological Research Council of Turkey (TUBITAK) for providing the financial supports for this study under the 217M978 project.

References:

1. M. Bahiraei, A numerical study of heat transfer characteristics of CuO–water nanofluid by Euler–Lagrange approach, *Journal of Thermal Analysis and Calorimetry*, 123 (2016) 1591-1599.
2. A.A. Minea, Challenges in hybrid nanofluids behavior in turbulent flow: Recent research and numerical comparison, *Renewable and Sustainable Energy Reviews*, 71 (2017) 426-434.
3. R.K. Shah, and A.L. London, *Laminar Flow Forced Convection in Ducts. Supplement 1 to Advances in Heat Transfer*. Academic Press, NY. 1978.
4. M. Dibaei, H. Kargarsharifabad, New Achievements in Fe_3O_4 Nanofluid Fully Developed Forced Convection Heat Transfer under the Effect of a Magnetic Field: An Experimental Study. *Journal of Heat and Mass Transfer Research (JHMTR),* 4(1) (2017) 1-11.

SESSION 7

Nanofluids Materials, Nanofluid Preparation and Characterization Methods, Nanofluid Properties

S7

1st International Conference on Nanofluids (ICNf2019)
2nd European Symposium on Nanofluids (ESNf2019)
26-28 June 2019, Castelló, Spain

Effect of Time-Temperature Dependent Nanoclusters' Morphology and Stoke's Regime Induced Nano-convection on Thermal Conductivity of Nanofluids

Lal Kundan[1*], S.S. Mallick[2]

[1, 2] Mechanical Engineering Department, Thapar Institute of Engineering & Technology, Patiala, Punjab-147004

*Corresponding author: kundanlalrana@thapar.edu

Keywords: Nanoparticles, Brownian Reynolds' number, Nanocluster, Thermal conductivity

Abstract: The work represents the thermal conductivity enhancement of nanofluid due to perikinetic conduction and induced micro-convection (Al_2O_3 nanoparticles, size 25-30 nm in DI water). The theoretical and experimental investigations have been carried out to observe the effect of the time-temperature dependent volume concentration of nanoparticles on the overall thermal conductivity of nanofluid. The effect of time–temperature dependent Brownian Reynolds' number on the thermal conductivity has also been investigated. The improved model is found to be predicted well the thermal conductivity enhancement for nanofluid under investigation (± 5 to ±12%).

Introduction: The perikinetic heat conduction and Brownian motion induced micro-convection are the two main mechanisms which are assumed to be responsible for the thermal conductivity enhancements in a variety of nanofluids [1]. Brownian motion induced micro-convection is one of the main factors which contributes significantly in the enhancement of the thermal conductivity enhancement of nanofluids [2,3]. It has been observed that the nanoparticles' aggregation is one of the major mechanisms for enhancing the thermal conductivity of nanofluids [4,5]. However, nanofluids still face the challenges of knowing and clear understanding of mechanisms involved in the thermal transport. One of the key factors could be the use of a constant volume concentration of nanoparticles[6–8]. Whereas, the volume concentration of the nanoparticles in nanofluids changes continuously. This is a complex phenomenon and depends on the many factors related to nanofluids such as; settling rate of nanoparticles, nanocluster growth, cluster morphology and stability, Brownian movement of the nanoparticles, size distribution, temperature, liquid layering and aggregation kinetics. The present study focus on the investigation of such parameters based on the actual concentration of the nanoparticles

present in a particular nanofluid at a particular point of time and their effect on the thermal conductivity enhancement.

Discussion and Results: The commercial nanopowder of Al_2O_3 (γ) of an average size of 25-30nm has been used in experimentation. The XRD pattern analysis and Bragg profile confirm the existence of Al_2O_3 (γ) with 99% purity. Two step method is followed to prepare nanofluid samples of 20 ml each (0.05 % by vol. in DI water) followed by thermal conductivity measurements using a KD2 Pro [8,9]. The effect of pH and Zeta potential on the hydrodynamic size of the Al_2O_3-H_2O nanofluid has been shown in Figure 1 (a) and (b).

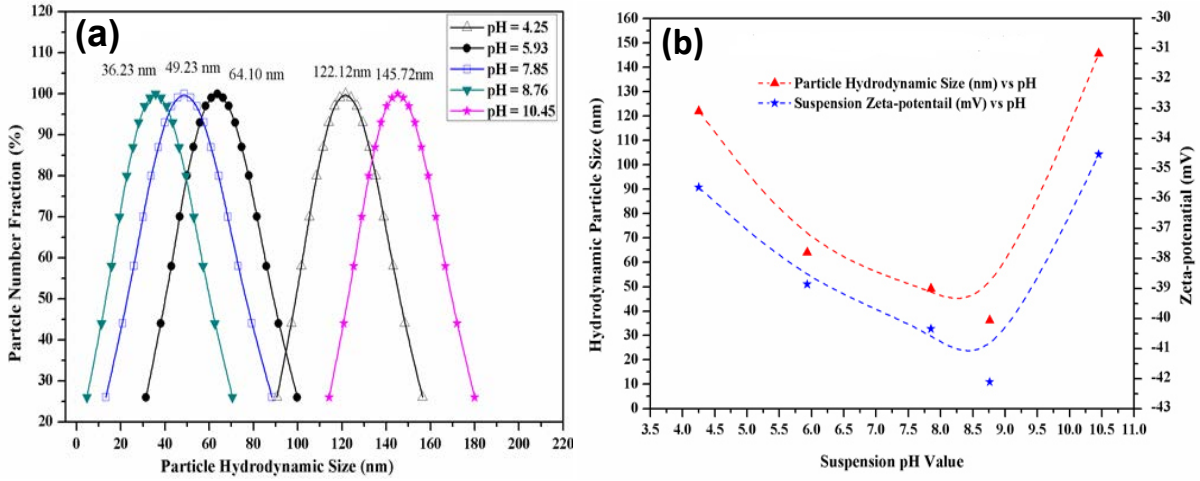

Figure 1 (a): Dispersion quality of Al_2O_3-H_2O nanofluid mix with SDS (by wt.1:1) at different values of pH (4.25 to 10.45) and (b) effect of pH on zeta potential and hydrodynamic size of Al_2O_3-H_2O nanofluid.

Nanofluid seems to be more stable when pH is around 8.5 to 9.5 and average nanoclusters size is minimum (around 40 nm), Figure 1 (a) and (b). This has been observed due to higher value of zeta potential of nanofluid (-42mv). In the assumed morphology, the governing equations have been identified and modified for the hydrodynamic size of the particles in suspension (*2a*), the fractal (d_f) and chemical (d_l) dimensions of nanoclusters. The aggregation in oxide based colloidal solutions is diffusion limited for which fractal dimension varies from 1.75 to 2.5 [10]. The volume fraction of the nanoparticles in a nanocluster (φ_a), volume of primary nanoparticles in the basefluid (φ_p) and total volume fraction of these nanoclusters presented in basefluid (φ_{at}) is found to be related by as, $\varphi_p = \varphi_a \varphi_{at}$.

Stoke's regime dependent induced convection: The temperature dependent Brownian movement of the nanoclusters cause the induced micro-convection and finally results into

thermal conductivity enhancement. The Brownian Reynolds number (R_{eB}) for the equivalent sphere as that of volume of the nanocluster which characteristic dimension is R_g is given as:

$$R_{eB} = \frac{3\,\rho_{nc}}{\mu_f} \frac{\left(\frac{k_B T}{\pi\,\rho_{nc}}\right)^{0.5}}{\left[\left(a\left(1+\frac{t}{t_p}\right)^{1/d_f}\right)^{0.5}\right]}$$

This relation can be used to study Brownian Reynolds number (R_{eb}) and its dependency on temperature, instantaneous volume fraction, nanoclusters growth and elapsed time.

Improved model of thermal conductivity: In order to bring down the gap between the theoretical and experimental values of the thermal conductivities, following aspects have been taken into account: (i) actual volume concentration of the nanoparticles, (ii) structural information about the nanoclusters, (iii) thermal conductivity of fluid enclosed in a nanocluster which is comparatively higher than the thermal conductivity of bulk fluid and lastly (iv) the effect of thermal conductivity of the bulk fluid due to induced micro convection. After knowing the thermal conductivities for different morphological parameters involved in a nanocluster, the thermal conductivity enhancement for the whole sample of nanofluid can be predicted by using a modified model, given as:

$$\frac{k_{eff}}{k_m} = \left\{\frac{[(k_{adb}+2k_l)+2\varphi_{at}(k_{adb}-k_l)]}{[(k_{adb}+2k_l)-\varphi_{at}\,(k_{adb}-k_l)]}\right\}$$

where, k_{eff}, is the effective thermal conductivity of the nanofluid under perikinetic heat conduction conditions and k_m, is the enhancement in thermal conductivity of the base fluid due to Brownian motion induced nano-convection. The final equation for the overall/effective thermal conductivity of a particular nanofluid which include the perikinetic heat condition and Brownian motion induced micro-convection can be defined as:

$$\frac{k_{overall}}{k_f} = \left\{\frac{[(k_{adb}+2k_l)+2\varphi_{at}(k_{adb}-k_l)]}{[(k_{adb}+2k_l)-\varphi_{at}\,(k_{adb}-k_l)]}\right\}\left(1 + A\;{R_{eB}}^{m}\,{P_r}^{0.333}\varphi_{at}\right).$$

This relation can be used to predict the thermal conductivity of a particular nanofluid with elapsed time, *t*. The enhancement in the overall thermal conductivity of Al_2O_3 nanofluid under the effect of time, temperature, instantaneous volume fraction, morphological parameters, perikinetic conduction, and Brownian induced micro-convection have been shown in Figure 3 (a) and (b).

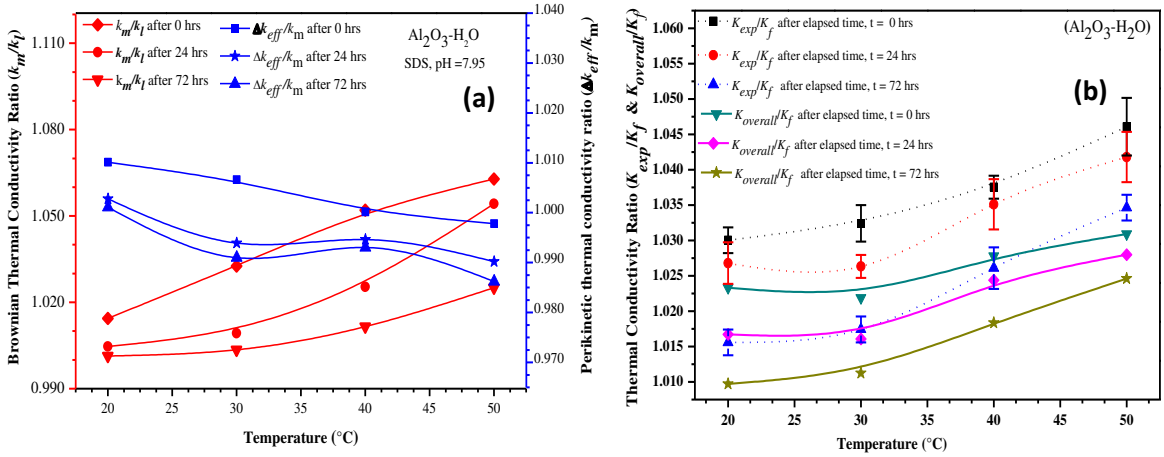

Figure 3 (a): Effect of temperature and time on the Brownian thermal conductivity and perikinetic thermal conductivity of Al_2O_3-H_2O and (b): A comparison between the experimental and theoretical values of thermal conductivity of Al_2O_3 nanofluid at pH =7.95.

Conclusions: Brownian Reynolds' number of nanofluid flow within the Stoke's regime has been expressed in term of nanocluster geometry, time and temperature and is found to be increasing (up to 0.50) with an increase in temperature (20-50°C). The heat transport takes place mainly through perikinetic heat conduction mechanism at temperature around 20-30°C, whereas, the induced nano-convection starts dominating as the temperature goes above 30°C. The experimental and theoretical results of the overall thermal conductivities differ by 5 to 12% for Al_2O_3-H_2O nanofluid in the temperature range of 20-50°C.

References

1. R. Prasher, W. Evans, P. Meakin, J. Fish, P. Phelan and P. Keblinski, Effect of aggregation on thermal conduction in colloidal nanofluids, *Appl. Phys. Lett.* 89 (2006) 143119-1–3.
2. A. Malvandi and D.D. Ganji, Brownian motion and thermophoresis effects on slip flow of alumina/water nanofluid inside a circular microchannel in the presence of a magnetic field, *Int. J. Therm. Sci.* 84 (2014) 196–206.
3. P.M. Kumar, J. Kumar, R. Tamilarasan, S. Sendhilnathan and S. Suresh, Review on nanofluids theoretical thermal conductivity models, *Eng. J.* 19 (2015) 67–83.
4. J. Sarkar, P. Ghosh and A. Adil, A review on hybrid nanofluids: Recent research, development and applications, *Renew. Sustain. Energy Rev.* 43 (2015) 164–177.
5. S.A. Angayarkanni and J. Philip, Review on thermal properties of nanofluids: Recent developments, *Adv. Colloid Interface Sci.* 225 (2015) 146–176.
6. S.Z. Miry, M. Roshani, P. Hanafizadeh, M. Ashjaee and F. Amini, Heat Transfer and

Hydrodynamic Performance Analysis of a Miniature Tangential Heat Sink Using Al_2O_3-H_2O and TiO_2-H_2O Nanofluids, *Exp. Heat Transf.* 29 (2016) 536–560.

7. R. Deepak Selvakumar and S. Dhinakaran, A multi-level homogenization model for thermal conductivity of nanofluids based on particle size distribution (PSD) analysis, *Powder Technol.* 301 (2016) 310–317.
8. S.P. Jang and S.U.S. Choi, Role of Brownian motion in the enhanced thermal conductivity of nanofluids, *Appl. Phys. Lett.* 84 (2004) 4316–8.
9. Y.H. Li, W. Qu and J.C. Feng, Temperature dependence of thermal conductivity of nanofluids, *Chinese Phys. Lett.* 25 (2008) 3319–3322.
10. W.B. Russel, D.A. Saville and W.R. Schowalter, Colloidal dispersions, Cambridge University Press, New York, 1989.

1st International Conference on Nanofluids (ICNf2019)
2nd European Symposium on Nanofluids (ESNf2019)
26-28 June 2019, Castelló, Spain

Ethylene glycol - water suspensions containing reduced graphene oxide particles for thermal management applications: formulation and characterisation

G. Zhang, H. Navarro and Y. Ding*

School of Chemical Engineering, University of Birmingham, UK

*Corresponding author: y.ding@bham.ac.uk

Keywords rGO/EG+DW nanofluids, thermal conductivity enhancement, viscosity

Abstract: Reduced graphene oxide (rGO) nanoparticles were suspended in an ethylene glycol - distilled water mixture at a mass ratio of 6:4. The resulting suspensions with different particle concentrations were characterised for their viscosities and thermal conductivities. The viscosity was measured at a temperature range of -45°C to 25°C. The results demonstrated that the suspension with 2.0 wt.% rGO nanoparticles was Newtonian and the temperature dependence of the viscosity followed the Arrenhius model. The suspension with 5.0 wt.% rGO particles showed a shear thinning behaviour. The thermal conductivity was measured over a temperature range between 5°C and 25°C. The results showed a 17% enhancement for the 2 wt.% rGO concentration over the entire temperature range, which agree well with the effective medium theory prediction.

Introduction/Background: The trend of higher power density in a smaller size [1] for high performance mini-and micro-scale electronic devices leads to a sharp increase of the local heat flux on the microchips. The quality of heat dissipation for the microchip plays an important role in the lifespan of the device[2]. Meanwhile, the temperature for electronic devices can be < -50°C [3] for outer space condition. Thus, thermal management (TM) is essential for microchips. One of key technologies to obtain a good TM is heat transfer intensification (HTI) which can be achieved via an efficient heat transfer fluid (HTF).

Recently, attention has been paid to nanofluids containing graphene nanoparticle due to its high thermal properties shown in Table 1. The base fluid: ethylene glycol (EG) mixed with distilled water (DW) for mass concentration of 6:4 has been formulated for its freezing point < -50°C[4]. As graphene is hydrophobic, to increase nanoparticle's stability, the surface of graphene has been modified to have hydrophilic properties[5].

Here, EG+DW based rGO nanofluids (rGO/EG+DW) are studied. A two-step method has been used to formulate nanofluids. The morphology, viscosity and thermal conductivity have been characterised and studied.

Discussion and Results:

(1) Nanofluids formulation

Graphene (>99.5% purity, purchased from Nanografi, Turkey) with a nominal diameter of ~150nm was used to formulate nanofluids of concentrations: 0.5wt.%~ 5.0wt.%. EG, HNO_3 and H_2SO_4 were all purchased from Sigma-Aldrich and used without further purification. H_2SO_4 and HNO_3 have been used as oxidizing agents for the acid treatment of graphene [6]. As is shown in

Figure **1**, 4g of graphene was added in 80mL of a 1:3 mixture of HNO_3(64-65wt.%)/H_2SO_4(>95 wt.%). The suspension was sonicated in water bath at 75°C for 6h. The resultant suspension was filtered with a 200nm pore membrane filter. After cleaning with distilled water, the filter cake was put into the vacuum oven for 45°C overnight to collect the dry rGO. The process of rGO/EG+DW nanofluids' formulation is as follows: 40 min ultrasonication was used to mix and homogenise the suspension. As is shown in

Figure **2**, graphene dry powders clearly agglomerated. Its size was roughly around 2 μm which is close to the manufacturer's given value. After the reaction and ultrasonication, rGO nanoparticle's size decreases to~800 nm.

(2) Viscosity

The viscosity was measured with a rheometer (MCR502 Anton Paar, Austria) in temperature range from -45 to 25°C. As is shown in

Figure **3**, the viscosity of the base fluids shows a Newtonian behaviour. For nanofluid, with concentration of nanoparticle up to 2.0 wt.%, the viscosity still shown Newtonian behaviour. Both of base fluid and 2.0 wt.% nanofluid follow Arrenhius model. The viscosity of rGO/EG+DW nanofluid increases with temperature decrease, the viscosity difference between nanofluid and base liquid decreases with temperature increase, which becomes very small at room temperature. However, with the concentration increase to 5.0 wt.%, an obvious shear thinning behaviour.

(3) Thermal conductivity

The thermal conductivity was measured using a lambda measuring system (PSL Systemtechnik GmbH, Germany) in the temperature range from 5 to 25°C. As is shown in Figure 4, thermal conductivity of the base fluid and nanofluid both increases with

temperature increase. Nanofluid thermal conductivity increases with concentration increase. Thermal conductivity enhancement in line with the effective medium theory prediction, Given in equation 1, Nan's model [7],which is likely to be due to good dispersion of nanoparticle. An enhancement of 17% achieved with 2.0 wt.% nanoparticles.

$$k/k_f = \{3 + \emptyset[2\beta_{11}(1 - L_{11}) + \beta_{33}(1 - L_{33})]\}/[3 - \emptyset(\beta_{11}L_{11} + \beta_{11}L_{11})] \quad [1]$$

Where L11=0 and L33=1, as the aspect ratio of rGO is very high.

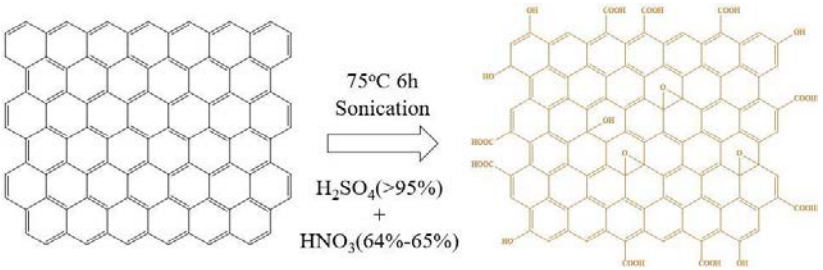

Figure 1. The reaction scheme for the acid treatment of Graphene

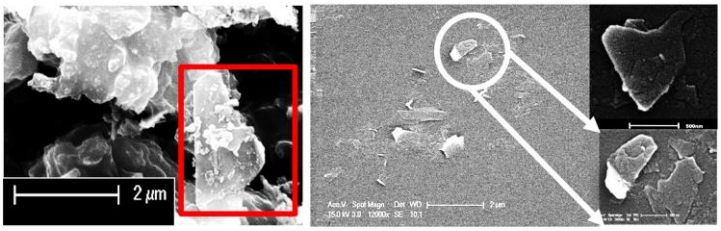

Figure 2. ESEM of graphene (left) and well dispersed rGO nanoparticles (right)

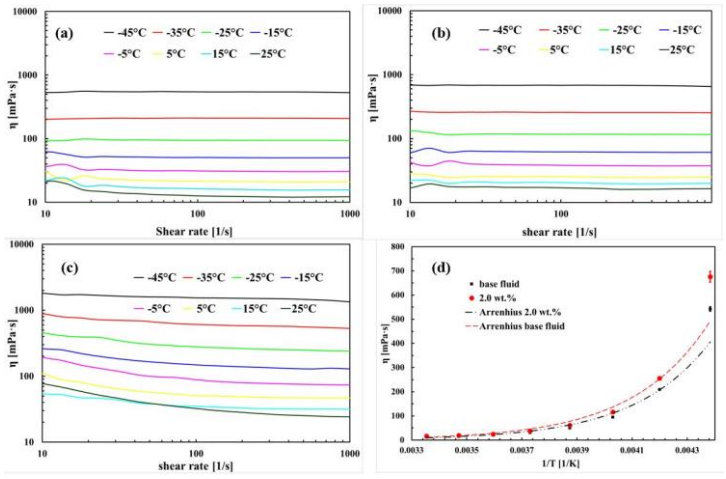

Figure 3. The viscosity of base fluids and rGO/EG+DW nanofluids (a) base fluids(b) 2.0 wt.%,(c) 5.0 wt% and (d) the viscosity with temperature.

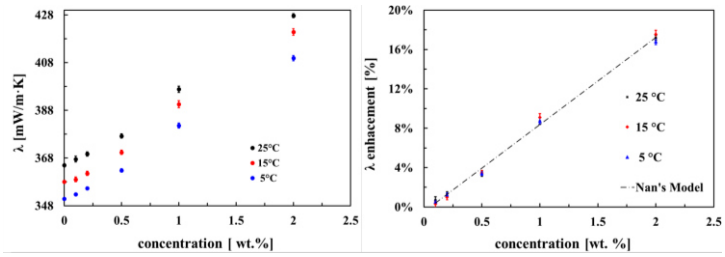

Figure 4. The thermal conductivity of rGO/EG+DW nanofluids and its enhancement

Table 1. Properties of the graphene nanoplatelet given by manufacturer

Thermal conductivity		diameter	thickness	specific surface area	Electrical conductivity	colour
Parallel	Perpendicular					
W/(mK)		μm	nm	m2/g	S/m	
3000[8]	6[8]	5	3	300	1400-1900	black

Summary/Conclusions:

In present study, rGO/EG+DW nanofluids have been formulated. Main outcomes are listed below:(1). The 2.0 wt% rGO/EG+DW nanofluids is a Newtonian fluids. Its viscosity with temperature follows Arrenhius model. However, with concentration increases to 5.0 wt.%, the nanofluids shows a shear thinning behaviour. (2) A 17% thermal conductivity enhancement with concentration of 2.0 wt.% is achieved. The thermal enhancement is in line with the effective medium theory prediction

Acknowledgements

The authors acknowledge the finance support from Engineering and Physical Sciences Research (EPSRC) Council, UK – Integrated GaN-Diamond Microwave Electronics: From Materials, Transistors to MMICs (EP/P00945X/1).

References:

1. A. Bar-Cohen, P. Wang, and E. Rahim, “Thermal management of high heat flux nanoelectronic chips,” *Microgravity Sci. Technol.*, vol. 19, no. 3–4, pp. 48–52, 2007.
2. S. M. Sohel Murshed and C. A. Nieto de Castro, “A critical review of traditional and emerging techniques and fluids for electronics cooling,” *Renewable and Sustainable Energy Reviews*. 2017.
3. A. Tang *et al.*, “CMOS (Sub)-mm-Wave System-on-Chip for exploration of deep space and outer planetary systems,” *Proc. IEEE 2014 Cust. Integr. Circuits Conf. CICC 2014*, 2014.

4. P. Wang, J. J. Kosinski, A. Anderko, R. D. Springer, M. M. Lencka, and J. Liu, "Ethylene glycol and its mixtures with water and electrolytes: Thermodynamic and transport properties," *Ind. Eng. Chem. Res.*, vol. 52, no. 45, pp. 15968–15987, 2013.

5. M. Kole and T. K. Dey, "Investigation of thermal conductivity, viscosity, and electrical conductivity of graphene based nanofluids," *J. Appl. Phys.*, vol. 113, no. 8, 2013.

6. W. S. Hummers and R. E. Offeman, "Preparation of Graphitic Oxide," *J. Am. Chem. Soc.*, vol. 80, no. 6, p. 1339, 1958.

7. C. W. Nan, Z. Shi, and Y. Lin, "A simple model for thermal conductivity of carbon nanotube-based composites," *Chem. Phys. Lett.*, vol. 375, no. 5–6, pp. 666–669, 2003.

8. M. Mehrali *et al.*, "Investigation of thermal conductivity and rheological properties of nanofluids containing graphene nanoplatelets," *Nanoscale Res. Lett.*, vol. 9, no. 1, p. 15, 2014.

1st International Conference on Nanofluids (ICNf2019)
2nd European Symposium on Nanofluids (ESNf2019)
26-28 June 2019, Castelló, Spain

Wettability control for correct thermophysical properties determination of molten salts and their nanofluids

Y. Grosu[1,*], L. Gonzalez-Fernandez[1], U. Nithiyanantham[1] and A. Faik[1,*]

[1] CIC Energigune, Albert Einstein, 48, 01510 Miñano, Spain

[*]Corresponding authors: ygrosu@cicenergigune.com; afaik@cicenergigune.com

Keywords: Molten salts, thermophysical properties determination, DSC, LFA

Abstract: Correct determination of thermophysical properties of molten salts (MSs) and molten salts based nanofluids (MSBNs) is of the highest importance in the field of thermal energy storage (TES) at concentrated solar power (CSP) plants. However, it is recognized that correct measurement of these properties is very complicated due to molten salts creeping (scaling) inside the crucible (sample container). In this work, we propose two strategies for controlling the wetting phenomena of MS and MSBNs to obtain correct results in such common techniques as differential scanning calorimetry (DSC) and laser flash apparatus (LFA). The proposed method can be extended for other techniques where creeping of molten salts is an issue.

Introduction: Molten salts, particularly Solar salt (60 - 40 wt% of $NaNO_3$ – KNO_3), are commonly used as a storage material at CSP plants [1], where their amount is thousands of tons [1]. Therefore the correct determination of their heat capacity (Cp) and thermal conductivity (λ) is of a paramount importance. However, it is recognized by the scientific and industrial communities to be very complicated, as reflected by the discrepancy of the published results. The same problem stands for molten salts based nanofluids [2]. For example, in 2016 a round Robin test was conducted within the NANOUPTAKE action by 11 institutions to determine Cp of the Solar salt [3].

For techniques like DSC or LFA a proper contact between the sample and the crucible is required. However, typically molten salts strongly wet the surface of the crucible, resulting in displacement (creeping) of the salt from the centre of the crucible to its walls – Scheme 1. As a result, a layer of non-uniform thickness is formed, bringing an unacceptable error to the measurement.

A larger mass of the sample can be used to confine the salt and to limit its movement inside the crucible [4]. However, due to the use of larger mass pressure builds up in the crucible during the measurement, which increases the risk of a salt leakage or crucible deformation, leading to critical damage of equipment due to the high corrosivity of molten

salts at high temperature. Often a small hole is constructed in the crucible to avoid pressure increase. However, in case of a crucible completely filled with molten salt such prevention measure is not effective as it leads to the leakage of the salt.

In this work, we demonstrate that the wetting phenomena responsible for displacement of the salt can be mitigated by introducing micro-roughness on the interior walls of the crucible or by using low-surface energy material crucibles – patent [5].

Materials and methods: Solar salt and Solar salt based nanofluids with 50 nm F_2O_3 nanoparticles (Sigma) were prepared according to the protocol described elsewhere [6].

DSC Q2500 (TA instruments) was used for Cp measurements (1% precision). Three types of T-zero hermetic Al-crucibles were used: 1) Pristine crucible from the supplier; 2) Partially leached Al-DSC crucible prepared as follows: 10 mg drop of 37%HCl acid was introduced into the pristine non-treated Al-DSC crucible and was kept for 15 min. Next the crucible was washed with distilled water and dried at 60°C. 3) Completely leached Al-DSC crucible prepared similar to the partially leached Al-DSC crucible, but repeating the leaching 5 times.

Thermal diffusivity (α) was measured with the LFA 457 MicroFlashTM (NETZSCH). Thermal conductivity was calculated as $\lambda=\alpha\cdot\rho\cdot Cp$, where ρ is density from [8]. Three types of LFA crucibles with similar dimensions were used for this work: 1) Standard PtRh-crucible provided by the supplier; 2) Custom made Zn-crucible; 3) Custom made Stainless Steel (SS) 316-crucible, with mechanically introduced roughness on its inner surfaces.

Discussion and results: It is well-known that the contact angle of a liquid on a surface depends on the roughness [7]. Hence, roughness at the inner surface of DSC or LFA crucibles can solve the creeping problem.

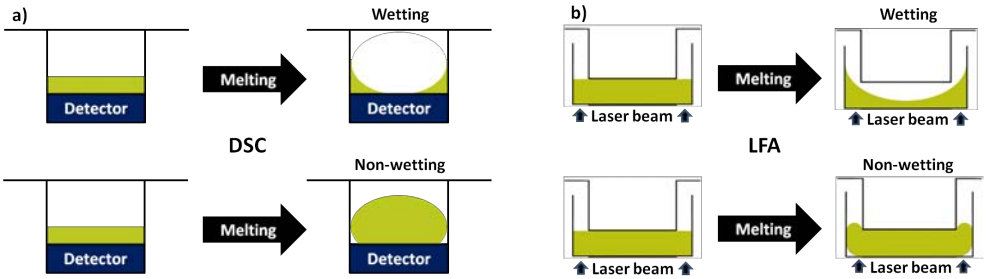

Scheme 1. Behavior of molten salt inside a) DSC and b) LFA crucible in case of wetting (top) and non-wetting (bottom) conditions

Figure 1a demonstrates Cp measurements for Solar salt using Al-crucibles with different roughness. One can clearly see that acid leaching resulted in the formation of micro-roughness on the surface of aluminium – Figure 1b, which considerably affects the wetting phenomena of the molten Solar salt – Figure 1c. One can see that if recommended by the

supplier mass of the salt is used (10 mg), the results obtained with the pristine non-treated Al-crucible strongly deviate from the correct values (Figure 1a). However, the use of rough crucible brings the results within a 3% error observed in the literature. Partial roughness has intermediate result between pristine and completely rough crucibles. It is also important to note that for the case of pristine crucible Cp decreases with temperature, this is because the creeping effect is gradual. From the successive cycling we found that Cp is decreasing with each cycle. While the slope of Cp is nearly absent for completely leached crucible.

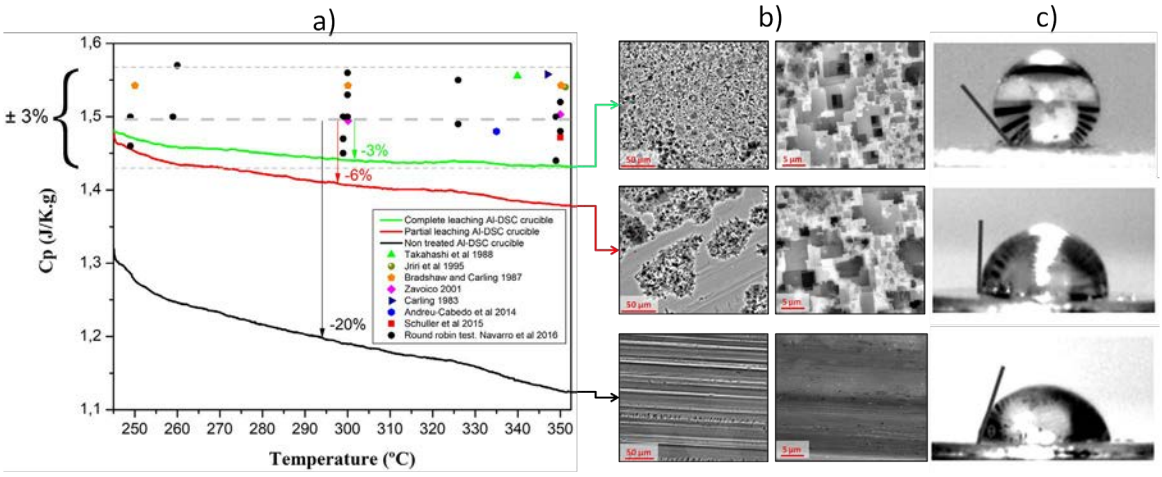

Figure 1. a) Heat capacity of Solar salt, b) SEM images of crucible surface and c) contact angle of Solar salt on the surface of the DSC crucible at 300°C for the cases of pristine non-treated Al-DSC crucible (bottom), partially leached Al-DSC crucible (middle) and completely leached Al-DSC crucible (top)

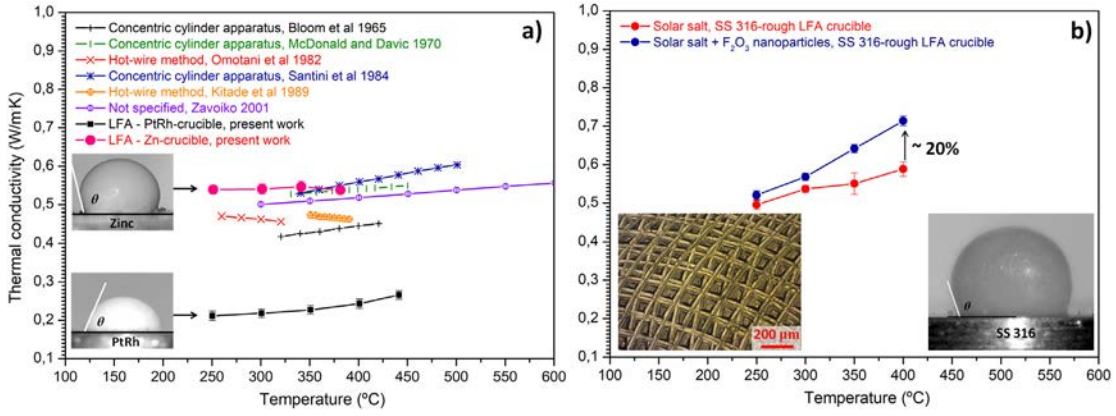

Figure 2. a) Thermal conductivity of Solar salt measured by LFA using PtRh- and Zn-crucibles; Inserts: contact angles of Solar salt on the surface of the PtRh- and Zn-LFA crucibles. b) Thermal conductivity of Solar salt and solar salt based nanofluid measured by LFA using rough SS 316-crucible; Inserts: roughness of SS 316-crucible and contact angle of solar salt on the surface of this crucible.

The effect similar to roughness can be reached by simply using crucibles with low-surface energy, which also results in a larger contact angle of molten salt – non-wetting condition. From Figure 2a, one can see that the use of low-surface energy Zn-crucible for LFA

results in values of thermal conductivity well agreed with the literature. While, unacceptably lower values are obtained with the standard PtRh-crucible due to strong wetting (creeping) phenomena. Similarly, the use of rough SS 316-crucible results in correct values of Solar salt and expected enhancement for {Solar salt + 50 nm F_2O_3 nanoparticles} nanofluid [2] – Figure 2b.

Conclusions: In this work, we propose two strategies for controlling the wetting (creeping) phenomena of molten salts inside crucibles used for such common techniques as DSC and LFA. The first method consists of the use of crucibles with micro-roughness, which considerably increases the contact angle of a molten salt, mitigating its creeping inside the crucible. The second method consists of the use of a crucible made of low surface energy materials, which ultimately leads to a high value of contact angle. We demonstrate the proposed methods using aluminium DSC crucibles with micro-roughness obtained by acid leaching. We also used LFA crucibles made of low-surface energy material (zinc) and stainless steel 316 with mechanically obtained roughness. The proposed methods resulted in obtaining the correct values of heat capacity and thermal conductivity compared to the literature data. Proposed methods are not specific for DSC and LFA techniques and can be extended for other techniques where creeping of molten salt is an issue.

References

1. K. Vignarooban, X. Xu, A. Arvay, K. Hsu, A. M. Kannan, Heat transfer fluids for concentrating solar power systems – a review. *Applied Energy*. 146 (2015) 383-396.
2. O. Arthur and M.A. Karim, An investigation into the thermophysical and rheological properties of nanofluids for solar thermal applications, *Renew. Sustain. Energy Rev.* 55 (2016) 739–755.
3. Navarro H. et al. Round robin test on the measurement of specific heat of solar salt, *SolarPaces 2016 Conference*, Abu Dhabi, United Arab Emirates, October 11-14, 2016.
4. B. Muñoz-Sánchez, et al. A precise method to measure the specific heat of solar salt-based nanofluids. *J Therm Anal Calorim*, 129 (2017) 905-914.
5. A. Faik, Y. Grosu, N. Udayashankar, L. González, Thermal analysis sample container. *European patent application number*: 18382688.2 - 1003.
6. Y. Grosu, et al., Unexpected effect of nanoparticles doping on the corrosivity of molten nitrate salt for thermal energy storage. *Sol Energy Mater Sol Cells*, 178 (2018) 91-97.
7. D. Quéré, Wetting and roughness. *Annu. Rev. Mater. Res.*, 38 (2008) 71-99.
8. Pfleger, N. et al. Thermal energy storage–overview and specific insight into nitrate salts for sensible and latent heat storage. *Beilstein J Nanotechnol*, 6 (2015) 1487-1497.

1st International Conference on Nanofluids (ICNf2019)
2nd European Symposium on Nanofluids (ESNf2019)
26-28 June 2019, Castelló, Spain

Electrical Conductivity and Thermal Conductivity of Nanofluids with Metal Particles

V. Rudyak[1,2,3], A. Minakov[3], M. Pryagnikov[3]

[1] Novosibirsk State University of Architecture and Civil Engineering
Leningradskay Str., 113, Novosibirsk, 630008, Russian Federation

[2] Novosibirsk State University, Novosibirsk, Russian Federation

[3] Siberian Federal University, Krasnoyarsk, Russian Federation

*Corresponding author: valery.rudyak@mail.ru

Keywords: Nanofluid, Electrical Conductivity, Thermal Conductivity, Rheology.

Abstract: The electrical conductivity and thermal conductivity of water and ethylene glycol based nanofluids with copper and aluminium particles are experimentally studied. It was shown that electrical conductivity of nanofluids increases practically linearly with growth of the particle concentration. The electrical conductivity of nanofluids on the contrary of the thermal conductivity increases with decreasing nanoparticle size. Finally, the rheological behavior of nanofluids is presented.

Introduction/Background: More than twenty years nanofluids are being actively studied. Today it has been reliably established that the thermophysical properties of nanofluids are radically different from those of conventional coarse dispersed fluids. It is shown that the nanofluids viscosity and thermal conductivity coefficients depend not only on the nanoparticles concentration but also on their size and material [1]. As a rule, the values of these coefficients significantly exceed those determined by classical theories. However, for various applications, it is extremely important to know the electrical conductivity of nanofluids. In recent years, a lot of research dealt with the studies of the electrical conductivity of liquids containing carbon nanotubes, have been published. However, only a few publications are dealt with the study of the electrical conductivity of nanofluids with spherical nanoparticles (see [2,3] and references therein). For this reason, it is still not clear how the electrical conductivity of nanofluids depends on the size of nanoparticles, how it relates to the thermal conductivity, and whether the nanofluid rheology affects its electrical conductivity. The present research answers these questions.

Distilled water (W) based and ethylene glycol (EG) based nanofluids with copper and aluminum (L-ALEXTM) particles were studied. According to the Brunauer-Emmett-Teller

method, the average size of copper and aluminum nanoparticles was 56, 98.8 and 90.7 nm, respectively. The weight concentration of nanoparticles *w* varied from 1.68 to 20%. These correspond to the following volume concentrations: for EG-Cu nanofluids from 0.32 to 3.2%, for EG-Al nanofluids from 1.05 to 9.3% and for W-Al nanofluids from 0.23 to 1.91%. A large variation of concentration was considered to investigate this dependance without considering the economic viability and stability of nanofluids under investigation. A standard two-step method was used to prepare nanofluids. The required amount of nanopowder was added to the liquid. Then the resulting suspension was thoroughly mixed mechanically. To destroy the nanoparticles aggregates, the suspensions were treated with UZTA-0.4/22-OM ultrasonic apparatus for 20 minutes. All measurements presented in this paper were conducted at a temperature of 20°C.

The electrical conductivity was measured by ANION-7025 conductometer. The measurement range of electrical conductivity was from 10^{-4} to 10 S/m. Nanofluid thermal conductivity and viscosity coefficients were measured simultaneously. In the first case, the hot-wire method was used [4], while the viscosity was measured by the Brookfield DV2T rotary viscometer. The measurement accuracy of the viscosity, the electrical conductivity and the thermal conductivity was no less than 2% in all cases.

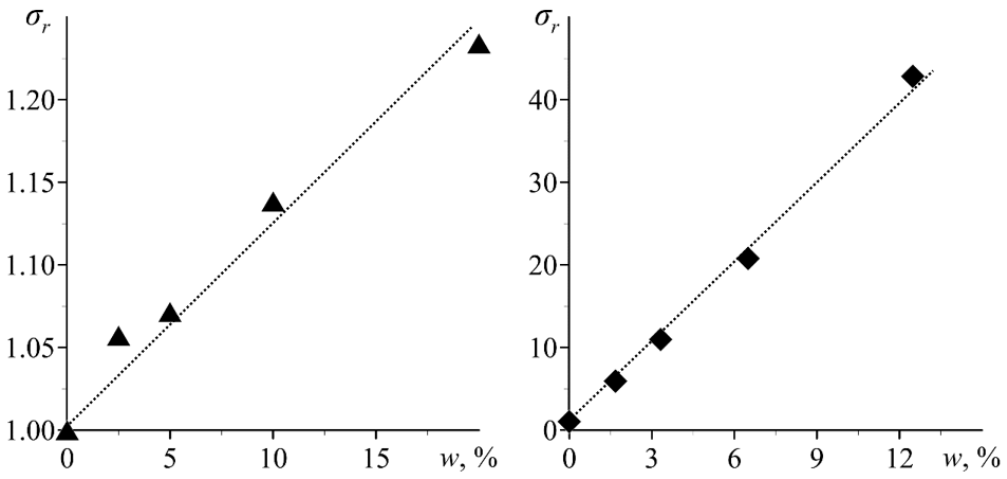

(a) (b)

Figure 1. The relative specific electrical conductivity of the EG-based (a) and W-based (b) nanofluids with aluminum particles versus their weight concentration

Discussion and Results: It was revealed that in all cases the specific electrical conductivity increases with the nanoparticles concentration. As an example, Fig. 1 presents the dependence of the specific relative electrical conductivity $\sigma_r = \sigma/\sigma_0$ of EG-based (a) and W-based (b) nanofluids with aluminum particles depending on particles weight concentration. Here σ and σ_0 are the electrical conductivities of the nanofluid

and the base fluid, respectively. In both cases, the electrical conductivity of nanofluids increases almost linear with the weight concentration of particles. The increase in the electrical conductivity of the EG-based nanofluid was just 23% (Fig. 1a) (the electrical conductivity of the ethylene glycol used was 0.91 μS/cm). On the other hand, the electrical conductivity of W-based nanofluid has increased by more than two orders of magnitude (Fig. 1b). The electrical conductivity coefficient of the water used was 3.1 μS/cm.

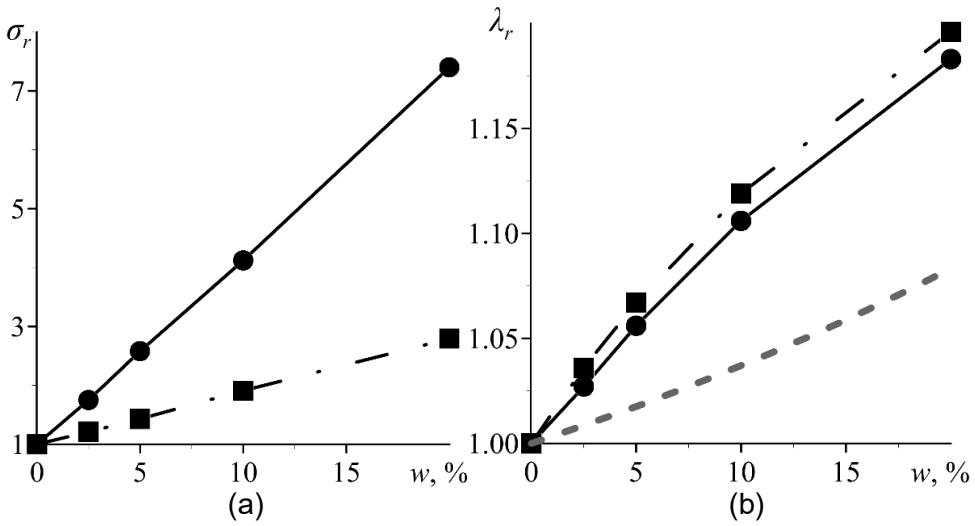

Figure 2. The relative specific electrical conductivity (a) and the relative thermal conductivity (b) of EG-based nanofluids with copper particles versus their weight concentration *w*. The labels ● and ■ correspond to particle size equal to 56 and 98.8 nm, respectively

It has already been noted above that both viscosity and thermal conductivity of nanofluids significantly depend on the size of nanoparticles. This dependence remains valid for electrical conductivity as well. The dependence of the electrical conductivity of the EG-based nanofluid with copper particles on their weight concentration is shown in Fig. 2a. Here, the dependence of electrical conductivity on the weight concentration of particles is also linear. It is important to note that the electrical conductivity of the nanofluid with small particles is greater than that of the fluid with large ones. At 20% weight concentration (the volume concentration is about 3%) of copper nanoparticles, this excess is two and a half times greater. On the contrary, the thermal conductivity coefficient increases with increasing particle size. The dependence of thermal conductivity on the nanoparticles concentration is presented in Fig. 2b for the same nanofluids as in Fig. 2a. Here, the black dotted line means the calculation according to Maxwell's theory [5].

Summary/Conclusions: We can make two main conclusions. First, the addition of metal nanoparticles to the weakly conductive base liquid significantly increases its electrical conductivity. This effect depends on the electrical conductivity of the nanoparticles

themselves. However, this relationship is not linear. Thus, the electrical conductivity of copper is 1.58 times higher than that of pure aluminum. However, the increments of the electrical conductivity of nanofluids with copper and aluminum particles at 20% weight concentration differ by an order of magnitude. Second, the electrical conductivity of nanofluids increases with decreasing nanoparticle size. On the other hand, the thermal conductivity of the nanofluid, on the contrary, increases with increasing particle size. Thus, the electrical conductivity and thermal conductivity mechanisms of nanofluids significantly differ. The final part of the paper discusses the rheology of the studied nanofluids. The rheology of the nanofluids studied was shown in Table 1. Here n-N and N correspond to non-Newtonian and Newtonian fluids, respectively. All non-Newtonian fluids are the pseudoplastic or viscoplastic.

This work was supported by the Russian Foundation for Basic Research (17-01-00040 and 17-58-45023).

Table 1. The rheology of nanofluids

Nanofluid	*w*=2.5%	*w*=5%	*w*=10%	*w*=20%
W-Al	N	n-N	n-N	n-N
EG-Al	N	N	N	n-N
EG-Cu (98.8 nm)	N	N	N	n-N
EG-Cu (56 nm)	N	n-N	n-N	n-N

References:

1. V.Ya. Rudyak and A.V. Minakov, Thermophysical properties of nanofluids, *European Physical Journal E* 41 (2018) 15(12 p.).
2. M. Dong, L.P. Shen, H. Wang, H.B. Wang and J. Miao, Investigation on the electrical conductivity of transformer oil-based AlN nanofluid, *Journal of Nanomaterials* 2013 (2013) ID 842963.
3. K.G.K. Sarojini, S.V. Manoj, P.K. Singh, T. Predeep and S.K. Das, Electrical conductivity of ceramic and metallic nanofluids, *Colloid and Surfaces A: Physicichemical and Engineering Aspects* 417 (2013) 39-46.
4. Minakov A.V., Rudyak V.Ya., Guzei D.V., Pryagnokov M.I. and Lobasov A.S. Measurements of the thermal conductivity coefficient of nanofluids by the hot-wire method, *J. Engineering Physics and Thermophysics* 88 (2015) 149-162.
5. J.C. Maxwell, *A treatise on electricity and magnetism,* Clarendon Press, Oxford, 1881.

1st International Conference on Nanofluids (ICNf2019)
2nd European Symposium on Nanofluids (ESNf2019)
26-28 June 2019, Castelló, Spain

Experimental study on thermal conductivity of Fe-Si hybrid nanofluids

G. Huminic, A. Huminic

[1]Transilvania University of Brasov, Mechanical Engineering Department,
29, Bulevardul Eroilor, 500036 Brasov, Romania

[*]Corresponding author: gabi.p@unitbv.ro

Keywords: Fe-Si nanoparticles, thermal conductivity

Abstract

The main goal of the present study was to investigate the effects of both temperature and mass concentration on the thermal conductivity of hybrid nanoparticle aggregates containing distinct iron-based and silicon nanophases (Fe-Si) dispersed in distilled water. The thermal conductivity was investigated within the range of the temperature of 20°C to 50°C for three mass concentrations of nanoparticles (0.25, 0.5 and 1.0 wt%). The experimental results show that the thermal conductivity is higher than of thermal conductivity of base fluid. Thus, the relative thermal conductivity was 13% for a concentration of 1.0 wt% and a temperature of 50°C.

Introduction/Background

Hybrid nanofluids are a new class of working fluids, intensely studied in last years, defined as the suspensions with two different solid materials into a conventional fluid (water, ethylene glycol or water/ethylene glycol mixture, engine oil, kerosene, vegetable oil and paraffin oil). The main research was focused on their thermal conductivity, and the most important results were reviewed in Refs. [1-2].

Esfe et al. [3] experimental studied the thermal conductivity of the SWCNTs-MgO/ethylene glycol hybrid nanofluids within the range of temperature and volume concentrations, 25 - 50°C and 0.015 - 0.55% respectively. Their results showed that the increase in thermal conductivity was approximately 37% at a volume concentration of 0.55% and a temperature of 50°C. Also, they proposed a new correlation based on the experimental data for SWCNTs-MgO/ethylene glycol hybrid nanofluids:

$$\frac{k_{nf}}{k_{bf}} = 0.97600 + 0.10579\,\phi + 0.00104\,T + 0.01017\,\phi\,T \quad (1)$$

Aparna et al. [4] investigated the effects of temperature and volume concentration on thermal conductivity of Al_2O_3-Ag/water hybrid nanofluids and found that the thermal conductivity values of the hybrid nanofluid were higher compared to Al_2O_3/water nanofluids and close of the thermal conductivity values of the Ag/water nanofluids.

The findings of Akhgar and Toghraie [5] showed that the addition of 1.0 vol.% TiO_2-MWCNTs nanoparticles in water-ethylene glycol mixture enhanced the thermal conductivity up to 38.7% at a temperature of 50°C. Two correlations for effective thermal conductivity of the TiO_2-MWCNTs / water-ethylene glycol were proposed:

- The first correlation:

$$\frac{k_{nf}}{k_{bf}} = 0.006\,(\phi^{1.099})\,T^{1.051} + 1.014,\ R^2 = 0.99 \tag{2}$$

- The second correlation:

$$\frac{k_{nf}}{k_{bf}} = 4.055\left(\frac{\phi}{34}^{1.09}\right)\exp\left(\frac{T}{34}\right) + 1.013,\ R^2 = 0.989 \tag{3}$$

As a continuous subject of research, this study presents new results concerning the thermal conductivity of Fe-Si/water hybrid nanofluids. Therefore, the main goal of the current study is to investigate the effects of the temperature and mass concentration of nanoparticles on the thermal conductivity of Fe-Si/water hybrid nanofluids.

Discussion and Results

In this paper, the measurements for the thermal conductivity was done using KD 2 Pro thermal properties analyzer (Decagon devices, Inc., USA), which consists of a handheld controller and one sensor with a length of 60 mm and a diameter of 1.3 mm. The accuracy of the analyzer is ±5%. Before the measurements, the analyzer was calibrated with tests on glycerine provided by the supplier. The thermal conductivity of each sample measured four times at each temperature. A Haake C10–P5/U thermostat bath for temperature control during the measurements was used.

The studied hybrid nanofluid were synthesized by laser pyrolysis using $Fe(CO)_5$ vapors and SiH_4 gas as Fe and Si precursors, and passivated and coated with a biocompatible agent (sodium carboxymethyl cellulose-(CMC-Na)) [6]. The concentration of the biocompatible agent for each type of nanofluids was 3 g/l.

Fig. 1 shows the variations of thermal conductivity of the Fe-Si hybrid nanofluid versus temperature at different mass concentrations of nanoparticles. As can be seen, the thermal conductivity increases by increasing temperature. According to the results, the

relative enhancement in thermal conductivity computed as $100[(k_{hnf} - k_{bf})/k_{bf}]$ is about 13% at a temperature of 323 K and a mass concentration of 1.0%.

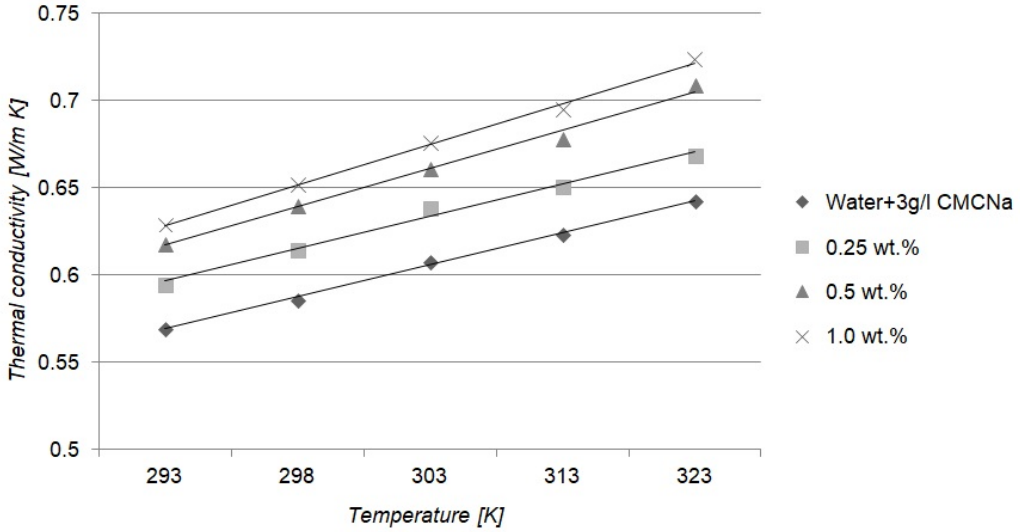

Figure 1. Thermal conductivity versus temperature at various mass concentrations

The variation of the thermal conductivity of the hybrid nanofluid with the mass concentration of nanoparticles at temperatures between 293-323 K is showed in Fig. 2.

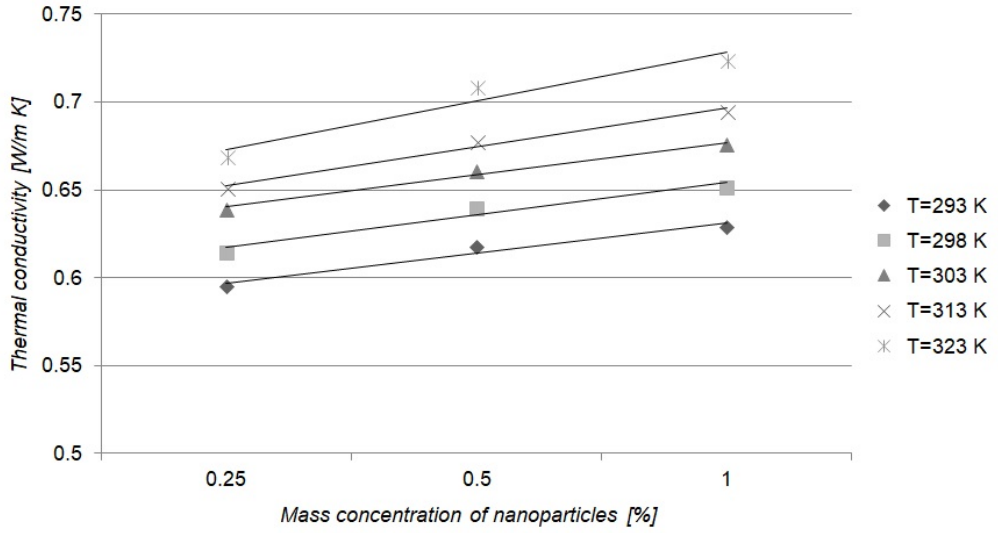

Figure 2. Thermal conductivity versus mass concentrations at various temperatures

As seen, the thermal conductivity increases with increase in concentration of Fe-Si hybrid nanoparticles in water. The majority of studies on thermal conductivity of the hybrid nanofluids from the open literature suggested that the thermal conductivity is highly dependent on the concentration of nanoparticles [1]. Moreover, the linear increase in thermal conductivity with increase in mass concentration of nanoparticles is an

indicator of well-dispersed nature of Fe-Si hybrid nanoparticles. The main reasons attributed to increased thermal conductivity to increase both the concentration and temperature were the increase in the number of collisions between nanoparticles, as well as the increase in Brownian motion [3-5].

Summary/Conclusions

Thermal conductivities of hybrid nanoparticle aggregates containing distinct iron-based and silicon nanophases (Fe-Si) dispersed in distilled water were determined experimentally as a function of mass concentration and temperature. The experimental results showed that the thermal conductivity of hybrid nanofluids is higher than the thermal conductivity of base fluid. Also, the thermal conductivities of the Fe-Si/water hybrid nanofluids increase linearly both with the mass concentration and the temperature. The future research will be focused on the viscosity, surface tension, contact angle as well on the efficiency of new type of hybrid nanofluids in thermal systems.

References

1. G. Huminic and A. Huminic, Hybrid nanofluids for heat transfer applications – A state-of-the-art Review, International Journal of Heat and Mass Transfer 125 (2018) 82–103.
2. Muhammad Usman Sajid, Hafiz Muhammad Ali, Thermal conductivity of hybrid nanofluids: A critical review, International Journal of Heat and Mass Transfer 126 (2018) 211–234.
3. M. H. Esfe, S. Esfandeh, M.K. Amiri, M. Afrand, A novel applicable experimental study on the thermal behavior of SWCNTs(60%)-MgO(40%)/EG hybrid nanofluid by focusing on the thermal conductivity, Powder Technology 342 (2019) 998–1007.
4. Z. Aparna, M. Michael, S.K. Pabi, S. Ghosh, Thermal conductivity of aqueous Al2O3/Ag hybrid nanofluid at different temperatures and volume concentrations: An experimental investigation and development of new correlation function, Powder Technology 343 (2019) 714–722.
5. A. Akhgar and D. Toghraie, An experimental study on the stability and thermal conductivity of water-ethylene glycol/TiO2-MWCNTs hybrid nanofluid: Developing a new correlation, Powder Technology 338 (2018) 806–818.
6. M. Balas, F. Dumitrache, M.A. Badea, C. Fleaca, A. Badoi, E. Tanasa, A. Dinischiotu, Coating Dependent In Vitro Biocompatibility of New Fe-Si Nanoparticles, *Nanomaterials* 8 (2018), 495-521.

1st International Conference on Nanofluids (ICNf2019)
2nd European Symposium on Nanofluids (ESNf2019)
26-28 June 2019, Castelló, Spain

Graphene nanofluid suitable for heat transfer in heat pipes

A. Huminic[1*], G. Huminic[1], M. Buschmann[2], A. Kujawska[3]

[1]Transilvania University of Brasov, Brasov 500036, Romania

[2]Institut für Luft- und Kältetechnik gGmbH Dresden, 01309 Dresden, Germany

[3]Wrocław University of Science and Technology, 50-370 Wrocław, Poland

[*]Corresponding author: angel.h@unitbv.ro

Keywords: graphene nanofluid, thermal conductivity, surface tension, contact angle

Abstract: The paper presents the experimental results concerning the physical properties of a graphene type nanofluid, which show great capability in heat transfer using passive devices, as heat pipes. Thermal conductivity, surface tension and dynamic contact angle have been measured in order to emphasise the suitability of this nanofluid for such practical applications.

Introduction

Heat pipes (HP) are particular applications of the two-phase closed thermosyphons, widely used in heat transfer against gravity, as the applications involving cooling of the electronic devices. They work through a continuous cycle of evaporation and condensation processes inside them, as shown in Figure 1. Transfer of the working fluid happens naturally through a wick structure, simple groves or porous media, from the liquid pool (condenser section) to the top of the enclosure (evaporator section). Thus, inside the wick structure, the adhesion and capillarity forces play a significant role in the mechanism of the fluid motion and heat transfer, and consequently the working fluids must have adequate physical properties, as high conductivity, large surface tension together with an increased adhesion/wettability. Currently, as shown by numerous research articles [1, 2, 3],

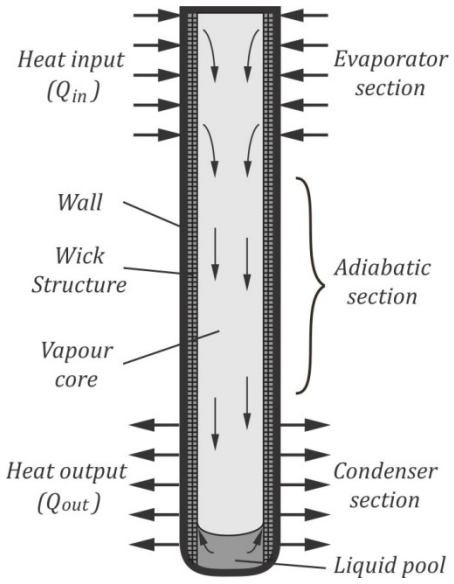

Figure 1. HP working principle

nanofluids are extensively used to increase thermal performances of the heat transfer devices. However, the addition of nanoparticles to the base fluid leads also to the decrease of the surface tension of the later ones, as shown by various studies reviewed in [4]. Thus, nanofluids with high thermal conductivity, which preserve also the surface tension of the base fluid, are found not frequently. Moreover, such fluids with high adhesion are quite rarely. This paper presents the experimental results concerning the main psychical properties of a graphene type nanofluid, which influence significantly the heat transfer using heat pipes.

Theoretical Foundation

In addition to a high thermal conductivity, the working fluids of heat pipes must have also high surface tension and adhesion, because they are both involved in transport of the liquid through the wick. Some large values of them could generate also high capillary forces, and facilitate the flow through the wick against gravity. Generally, thermal conductivity (k) and surface tension (γ) could be measured directly, and the adhesion/wettability is evaluated based on the contact angle the liquid makes with the surface in contact, as shown in Figure 2 in the case of static equilibrium. If the liquid is at rest on a surface, static contact angle (θ) can be computed from the Young equation of the phases equilibrium

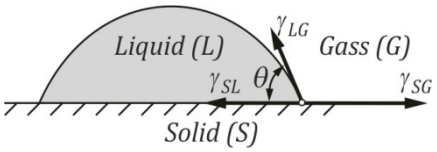

Figure 2. Static contact angle

$$\gamma_{LG}\cos\theta = \gamma_{SG} - \gamma_{SL}, \quad (1)$$

and, thus, it can express the wettability of the solid surface by a liquid. If $\gamma_{SG} - \gamma_{SL} > 0$ and $\gamma_{SG} - \gamma_{SL} < \gamma_{LG}$, then $0 < \theta \leq \pi/2$ and the liquid is wetting the surface as in previous picture. If $\gamma_{SG} - \gamma_{SL} < 0$ and $|\gamma_{SG} - \gamma_{SL}| < \gamma_{LG}$, it leads to $\pi/2 < \theta < \pi$, and the liquid is not wetting the surface. A particular situation is described by the relation $\gamma_{SG} - \gamma_{SL} > \gamma_{LG}$, when the equilibrium is not possible, no matter the value of θ. In such cases, $\theta \to 0$ and the liquid is stretching entirely over the surface indicating a high wettability.

If the liquid is in motion over the surface, the contact angle changes from its value at rest, and this situation refers to the dynamic contact angle(s). It provide information about the extreme values of the static contact angle, respectively the receding (θ_{re}) and advancing contact angles (θ_{ad}) as show in Figure 3 in the case of a liquid drop sliding on a tilting surface.

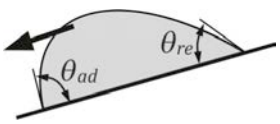

Figure 3. Dynamic contact angles

Materials and experimental procedures

Graphene oxide nanofluid (GOnf) of $0.1\ \mathrm{g}/l$ concentration was prepared at the Institute of Electronics Materials of Warsaw, Poland, through modified Hummers method [5]. The base fluid was water and no surfactant was used in this case.

Surface tension and dynamic contact angle were measured with the aid of a computer controlled Sigma force tensiometer (Biolin Scientific) which is based on force measurements of the interaction between probes with the liquid-air interface surface [6]. The tensiometer has an auto-calibrating microbalance which is capable to measure loads up to 210 g with an accuracy of ±0.01 mg. Thus, the maximum uncertainty of measurements is lower than 0.5%. Du Noüy ring method was employed in the case of surface tension, and for the experiments concerning contact angle, Wilhelmy plate method was used. When the plate submerges into the liquid, the advancing contact angle is measured. The receding contact angle is obtained when the sample is pulled out of the liquid. Thermal conductivity was measured using a KD 2 Pro thermal properties analyzer which has a specified accuracy of ±5%. A thermostatic vessel connected to a Haake bath C10–P5/U was used to control the temperature during measurements.

Results and discussion

Before experiments concerning thermal conductivity and surface tension of the nanofluid, several tests were performed concerning properties of the distilled water, in order to check the precision of the used procedures and devices, and to have a reference for the obtained values of GOnf. Figure 4 depicts the results of the measurements.

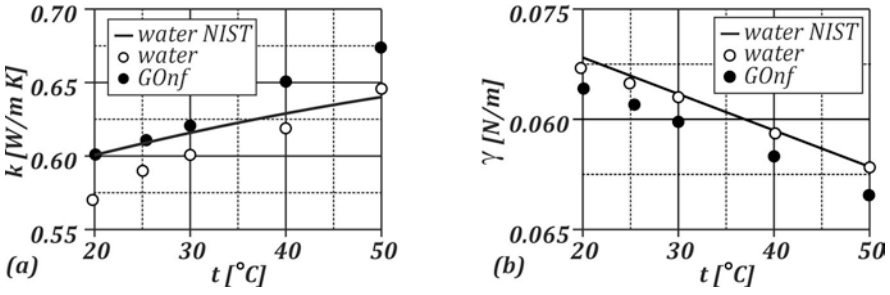

Figure 4. Thermal conductivity (a) and surface tension (b)

As shown in previous picture, the studied nanofluid has higher thermal conductivity than water (base fluid). The maximum relative variation is $\Delta k_m \cong 5\%$ at a temperature of $t = 50°$. The Increase of k is accompanied by a very small decrease of γ, the nanofluid preserving the high surface tension of water. The dynamic contact angles for a stainless steel plate are presented in Table 1 during a cycle of 5 consecutive measurements.

Table 1. Values of the dynamic contact angles, θ_{ad} and θ_{re}

Measurement	1	2	3	4	5
θ_{ad} [°]	76.30	37.13	16.97	0	0
θ_{re} [°]	29.90	27.23	25.60	24.87	24.61

The values reveal the dynamic contact angles are dependent on the surface state of the plate: if it dry, as for the first evaluation of θ_{ad}, or wet, as for all other measurements. Both of them decrease during experiments, decreasing of the advancing dynamic angle being much larger. Moreover, $\theta_{ad} \rightarrow 0$ when the surface becomes fully wet, revealing a situation when the liquid stretches over the surface, as explained in previous section.

Summary and conclusions

The paper presents the experiments concerning the physical properties of a graphene type nanofluid, and the results show that this sort of nanofluid is suitable in heat transfer through the heat pipes, where capillarity forces and wettability play a significant role in the mechanism fluid flow and heat transfer. Thus, it has a higher thermal conductivity than water, large surface tension and high capability to wet the stainless steel surfaces.

References

1. M.H. Buschmann, A. Huminic, S. Mancin, R.R. Riehl, G. Huminic, State of the art of heat transfer of heat pipes and thermosyphons employing nanofluids as working fluid, *Journal of Nanofluids*, 8 (2019), 253-266.
2. N.K. Gupta, A.K. Tiwaria, S.K. Ghosh, Heat transfer mechanisms in heat pipes using nanofluids – A review, *Experimental Thermal and Fluid Science* 90 (2018) 84–100.
3. G. Huminic, A. Huminic, C. Fleaca, F. Dumitrache, I. Morjan, Thermo-physical properties of water based SiC nanofluids for heat transfer applications, *International Communications in Heat and Mass Transfer,* 84 (2017), 94–101.
4. P. Estellé, D. Cabaleiro, G. Żyła , L. Lugob , S.M.S. Murshed, Current trends in surface tension and wetting behavior of nanofluids, *Renewable and Sustainable Energy Reviews*, 94 (2018), 931-944.
5. A. Wlazlak, B. Zajaczkowski, M. Woluntarski, M.H. Buschmann, Influence of graphene oxide nanofluids and surfactant on thermal behaviour of the thermosyphon, *Journal of Thermal Analysis and Calorimetry*, 2018, in Press.
6. A. Huminic, G. Huminic, C. Fleaca, F. Dumitrache, I. Morjan,, Thermal conductivity, viscosity and surface tension of nanofluids based on FeC nanoparticles, *Powder Technology*, 284 (2015), 78-84

1st International Conference on Nanofluids (ICNf2019)
2nd European Symposium on Nanofluids (ESNf2019)
26-28 June 2019, Castelló, Spain

Dynamic viscosity of purified MWCNT water and water-propylene glycol based nanofluids

S. Hamze[1*], N. Berrada[2], A. Desforges[2], B. Vigolo[2], T. Maré[1], D. Cabaleiro[1] and P. Estellé[1]

[1]Univ Rennes, LGCGM EA3913, 35704 Rennes, France

[2]Institut Jean Lamour, CNRS-Univ Lorraine, 54000 Nancy, France

[*]Corresponding author: samah.hamze@univ-rennes1.fr

Keywords: MWCNT, Water-based Nanofluids, Dynamic Viscosity

Abstract: Experimental results on the steady-state viscosity of purified carbon nanotubes dispersed in water and water-propylene glycol (Tyfocor® LS) are presented. The concentrations of the prepared nanofluids vary between 0.005 wt.% and 0.1 wt.%. It is shown that the nanofluids behave as shear-thinning materials for high particle content, and are Newtonian for lower particle content. Moreover, the relative viscosity of water-based nanofluids is well predicted by the modified Maron & Pierce model, also for higher concentrations of water-propylene glycol based nanofluids.

Introduction: The development of nanofluid research in different scientific fields as new energies, medicine, heat transfer, electronics and microelectronics, air conditioning, concentrating solar energy, and micro-channel cooling is continuously growing. This interest is due to the intrinsic thermal properties of nanoparticles introduced within common base fluids that enhance heat transfer properties. In this context, carbon nanomaterials as multi-walled carbon nanotubes (MWCNTs), diamond and graphene are promising. Among the different thermophysical properties, viscosity is very important to study the applications related to heat transfer involving fluid flow [1]. It was previously reported that rheological behavior of MWCNT-based nanofluids is influenced by several parameters such as base fluid, concentration, presence of surfactant or temperature. Thus, Halelfadl et al. [2] reported the influence of concentration (0.0055-0.55 vol.%) and temperature (0-40℃) on the viscosity of MWCNT-based nanofluids in water. A Newtonian behavior was noticed for lower concentrations, and a shear-thinning behavior was observed for higher particle content. Viscosity enhancement of nanofluids with concentration was also correlated to the presence of aggregates. MWCNT dispersed in water-ethylene glycol mixture at two weight concentrations, 0.015% and 0.15% were investigated by Kaman et al. [3]. They evidenced a strong shear-thinning effect for high concentration. Hameed et al. [4] studied the case of 0.1 wt.% of MWCNT-Kapok seed oil

based nanofluid. A non-Newtonian behavior was found for this nanofluid with an increase in viscosity in comparison to oil base fluid. In addition, Babita et al. [5] dispersed both pristine and functionalized MWCNTs in water with a mixture of sodium dodecyl benzene sulfonate (SDBS) and gum arabic (GA)(50:50 ratio by weight). Rheology measurements, done in shear rate range of 10-1000 s^{-1} and at room temperature, showed that nanofluids are Newtonian with a slight increase in viscosity compared to water. As a contribution on this topic, the present study aims to determine the rheological behavior of MWCNT nanofluids dispersed in water and Tyfocor® LS at different temperatures. Four weight concentrations of nanotubes are considered between 0.005% and 0.1%. Triton X-100 is used as surfactant to help disperse the nanotubes and stabilize the nanofluids.

Materials and experiments: The raw MWCNTs (Nanocyl™ NC7000) were purchased from Nanocyl S.A. (Belgium). The carried-out purification is a one-pot gas-phase treatment [6]. Briefly, the MWCNT powder is treated by chlorine at 1000°C for 2 h and heated under nitrogen for 2 additional hours. Then, the purified MWCNTs (p-MWCNT) are used to produce water and water-propylene glycol (Tyfocor® LS) based nanofluids by the two-step method with four weight concentrations: 0.005%, 0.01%, 0.05%, 0.1% and Triton X-100 as surfactant. Several amounts of surfactant with 0.1 wt.% of nanotubes and ultrasonication time were tested. The best dispersion state, evaluated from optical microscopy, was achieved for 5 wt.% of surfactant and 1 h of ultrasonication (probe sonicator, 125 W with a pulse mode 2 s ON/1 s OFF). This was used for all other concentrations. Flow curve experiments were performed between 0 and 80℃ using a Malvern Kinexus Pro rheometer (Malvern instruments, UK) working with a cone-plate geometry with a cone angle of 1º, a diameter of 60 mm and a gap of 0.03 mm. Tests were performed at shear rates between 10 and 1000 s^{-1} under steady-state conditions. Comprehensive experimental procedure and uncertainty in viscosity, less than 4%, were reported elsewhere [2].

Discussion and Results: Optical microscopy of nanofluids with 0.1 wt.% in nanotubes is shown in Figure 1. While good dispersion and stability are achieved, nanotube aggregates remain visible in the images. Their number and their size are greater when Tyfocor® LS is used as base fluid. The rheological behaviors of base fluids and nanofluids were investigated at different temperatures, between 10 and 40℃ for water based nanofluids, and between 0 and 80℃ for Tyfocor® LS based nanofluids. Figure 2 shows the flow curves obtained for the nanofluids prepared with water and Tyfocor® LS at 40℃ and 0℃ respectively. The rheological behavior of nanofluids is Newtonian for the two lower concentrations, and a decrease in dynamic viscosity as function of shear rate

was shown for the two highest concentrations at low shear rates (<200 s^{-1}), evidencing a shear-thinning behavior. In addition, nanofluid viscosity decreases with the reduction in nanotube content. Similar results are obtained for the other temperatures, with a decrease in viscosity with a temperature increase.

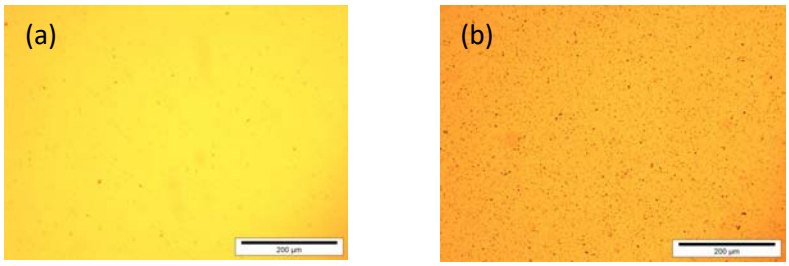

Figure 1. Optical microscopy of 0.1 wt.% nanofluid based in water (a) and Tyfocor® LS (b)

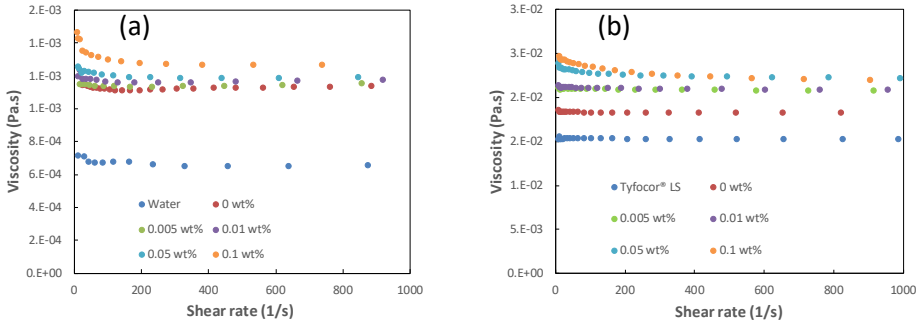

Figure 2. Flow curves of p-MWCNT nanofluids for all concentrations, at 40℃ for water based nanofluids (a), and at 0℃ for Tyfocor ® LS based nanofluids (b)

Moreover, relative viscosity of nanofluids at high shear rate that is presented in Figure 3(a) and 3(b), increases with volume concentration. These last values were obtained from densities of liquids, surfactant and nanotubes. Theoretical viscosity models such as Maron & Pierce and modified Maron & Pierce model [2] given by equations 1 and 2 respectively, were compared with experimental data. It is remarkable that the modified model taking into account the presence of aggregates, shows a good agreement with the experimental results of water based nanofluids at all concentrations, and mainly at higher concentrations for Tyfocor® LS based nanofluids.

$$\mu_r = \left(1 - \frac{\varphi}{\varphi_{max}}\right)^{-2} \quad (1) \; ; \; \mu_r = \left(1 - \frac{\varphi_a}{\varphi_{max}}\right)^{-2} \quad (2) \text{ where } \varphi_a = \varphi . \left(\frac{a_a}{a}\right)^{3-D} \quad (3)$$

In previous equations, μ_r is the relative viscosity, φ is the volume concentration of nanotubes, φ_{max} is the maximum volume fraction equal here to 3.61% [2], φ_a is the effective volume fraction of aggregates, a_a and a are the aggregates and primary nanoparticles radii respectively. The ratio $\frac{a_a}{a}$ here obtained is 4.41 for water based nanofluids and 8.4 for Tyfocor® LS based nanofluids, and D is fractal index and it is taken to 2.1 [2].

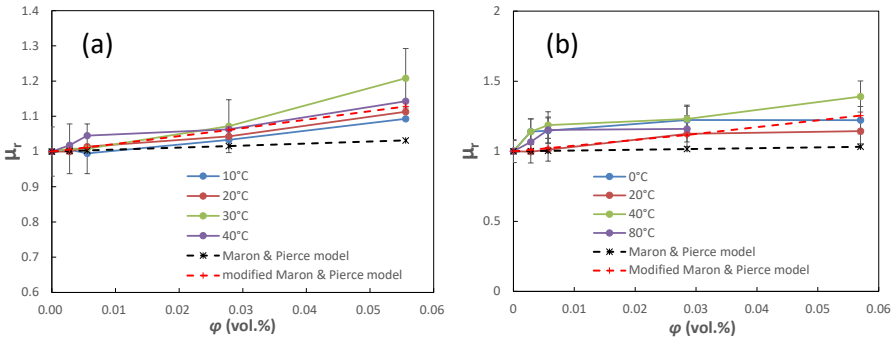

Figure 3. Relative viscosity of (a) water and (b) Tyfocor® LS based nanofluids as a function of volume particle content and temperature

Conclusions: Dynamic viscosity of stable purified MWCNT nanofluids was experimentally studied at temperatures between 0 and 80°C and under shear rates range of 10-1000 s^{-1}. A Newtonian behavior is observed for all nanofluids at low concentrations, and a shear-thinning behavior was found at higher concentrations. In addition, an agreement between the modified Maron & Pierce model and the experimental results of relative viscosity of all water based nanofluids and the higher two concentrations of Tyfocor® LS based nanofluids was obtained, in agreement with optical microscopy observations.

References:

1. S.M.S. Murshed and P. Estellé, A state of the art review on viscosity of nanofluids, *Renewable and Sustainable Energy Reviews* 76 (2017) 1134-1152.
2. S. Halelfadl, P. Estellé, et al., Viscosity of carbon nanotubes water-based nanofluids: Influence of concentration and temperature, *International Journal of Thermal Sciences* 71 (2013) 111-117.
3. M.D.K. Kaman, A. Sathishkumar, et al., Rheological analysis of MWCNT, TiO_2, CuO based Nano-Fluids under varying temperatures and concentrations, *Materials Science and Engineering* 402 (2018) 012178.
4. A. Hameed, A. Mukhtar, et al., Experimental investigation on synthesis, characterization, stability, thermo-physical properties and rheological behavior of MWCNTs-kapok seed oil based nanofluid, *Journal of Molecular Liquids* 277 (2019) 812-824.
5. Babita, S.K. Sharma and S.M. Gupta, Synergic effect of SDBS and GA to prepare stable dispersion of CNT in water for industrial heat transfer applications, *Materials Research Express* 5 (2018) 055511.
6. G. Mercier, C. Hérold, et al., Selective removal of metal impurities from single walled carbon nanotube samples, *New Journal of Chemistry* 37 (2013) 790-795.

1st International Conference on Nanofluids (ICNf2019)
2nd European Symposium on Nanofluids (ESNf2019)
26-28 June 2019, Castelló, Spain

Optimisation of nanofluid properties for reduced in situ nanoparticle agglomeration

K. Kouloulias, A. Sergis* and Y. Hardalupas

Imperial College London, Mechanical Engineering Department, London SW7 2AZ, UK

*Corresponding author: a.sergis09@imperial.ac.uk

Keywords: Nanofluids, nanoparticle agglomeration, TEM analysis, DLS analysis.

Abstract: For the formulation of stable and durable nanofluids, attention should be paid on the preparation method. Key parameters include the characteristics of the nanoparticles, the properties of the base fluids, the presence of surface-active agents and the pH value of the nanofluids. An optimisation study of nanofluid properties was conducted to minimise nanoparticle agglomeration, thus reducing sedimentation during turbulent Rayleigh-Bénard convection (RBC). Three types of Al_2O_3-H_2O nanofluids with different consistencies and characteristics were prepared, with and without employing the electrostatic stabilisation method, tested and compared in terms of the natural convective heat transfer performance. Transmission electron microscopy (TEM) and dynamic light scattering (DLS) measurements were performed to assess the characteristics of the nanofluids. It is reported that the electrostatic stabilization method and the use of suitable nanopowder in terms of physical characteristics and manufacturing process can improve nanofluid stability by reducing nanoparticle agglomeration and increase the natural convective heat transfer performance of nanofluids. By comparing data from TEM and DLS nanoparticle analysis, it is concluded that the average size of nanoparticles in the synthesized nanofluids is questionable in practice. A systematic approach for the formulation of nanofluids and presentation of data is required, so that reliable, reproducible and comparable results can be obtained that could eliminate discrepancies among findings in the literature.

Introduction/Background: The preparation method of nanofluids is one of the most critical aspects to consider in formulating stable suspensions with limited nanoparticle agglomeration. Effective ways to prepare high quality nanofluids include: the ultrasonication process, the electrostatic stabilisation method and the steric stabilisation method [1, 2]. In principle, ultrasonication can be used either individually or in combination with the other methods, depending on the requirements and the operating conditions set by the applications and the systems involved. In a previous study of the same authors [3], emphasis was given on the investigation of the natural convective heat transfer performance of “pure” nanofluids (nf-1), where neither the electrostatic nor the steric stabilisation methods were used.

In this work, an optimisation study of the nanofluid properties is presented for reduced nanoparticle agglomeration. Two types of nanofluids, nf-2 and nf-3, with different consistencies and characteristics were prepared and compared to nf-1. For the nanofluids, two high purity Al_2O_3 nanopowders P_a and P_b with different characteristics were used, along with high purity deionised (DI) water (grade 3, ISO 3696). On the onset of the experimental process, the TEM technique was employed to identify the average size and shape of the nanoparticles and calculate the nanopowder purity, in accordance to the process of [2, 4]. Figure 1 presents TEM images for the P_a and P_b nanopowders.

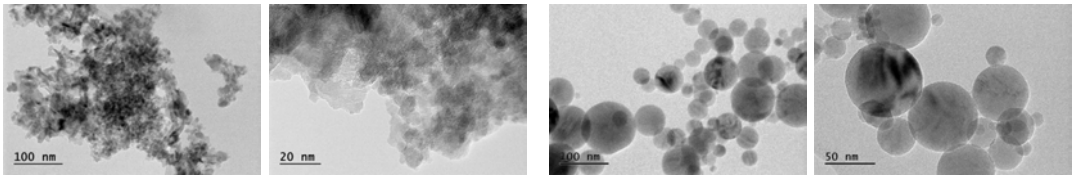

(a) (b)

Figure 1. TEM images of Al_2O_3 nanoparticles from (a) P_a and (b) P_b nanopowders

Fig.1 shows that the nanoparticles of P_a nanopowder have a flaky shape and an average size of 10 nm. Also, it is clearly depicted that the nanoparticles are highly agglomerated and form large clusters, possibly due to their large specific surface area. Regarding the P_b nanopowder, the nanoparticles have a spherical shape and an average diameter of 50 nm. As observed, the nanoparticles also tend to form agglomerates, however the agglomeration is less intense compared to the P_a nanopowder. The characteristics of nf-1, nf-2 and nf-3 nanofluids are included in Table 1. For nf-2 nanofluids, a pH controller was added to the suspension, to lower the pH value away from the isoelectric point (IEP) of alumina that varies between 7.7 and 9.1. For nf-3 nanofluids, instead of adding a pH controller, new nanoparticles that exhibited acidic behaviour once dispersed in water (due to the formulation process that was followed by the manufacturer) were used. The experimental apparatus of the study was a cubic Rayleigh-Bénard (RB) cell. Information for the RB cell and the control system can be found in [3]. With respect to the operating conditions of the RB cell, constant heat flux at the heating plate, q'' = 19.53 kW/m², and constant temperature at the cooling plate, T_c = 23.0°C (on average), were applied. Under these conditions, the Rayleigh number, Ra, varied between 2.6×10^9 and 2.8×10^9, and the Prandtl number, Pr, between 3.5 and 3.7.

Table 1. Characteristics of Al_2O_3-H_2O nanofluids

Nanofluids	Al_2O_3 powder	DI water	pH controller	Surface activator	pH (at 50°C)
nf-1	P_a	high quality	-	-	8.0
nf-2	P_a	high quality	~ 0.0005 vol.% acetic acid	-	4.9
nf-3	P_b	high quality	-	-	4.5

Discussion and Results: In Figure 2 (left), the heat transfer coefficient, h, of all three types of nanofluids as a function of the nanoparticle volume fraction, φ_v, is presented. It can be seen that the addition of Al_2O_3 nanoparticles deteriorates the heat transfer performance of DI water under turbulent RBC. The decrease of the heat transfer coefficient differs for the three types of nanofluids. For nf-1 nanofluids, the decrease of the heat transfer coefficient is quite intense, exhibiting a linear deteriorating trend as the nanoparticle concentration increases. For nf-2 and nf-3 nanofluids, minor deterioration of heat transfer is found that is notably less than that of nf-1 nanofluids within the bounds of experimental uncertainty. In Figure 2 (right), the temperature gradient between the heating and cooling plates, $\Delta T_{h,c}$, as a function of φ_v is depicted. For nf-2 and nf-3 nanofluids the increase of $\Delta T_{h,c}$ is insignificant, less than 2% compared to nf-1. Since the increase of $\Delta T_{h,c}$ is driven by the temperature at the heating plate, it is concluded that the use of acidic nanofluids can reduce the nanoparticle agglomeration, improve the nanofluid stability and eliminate the nanoparticle sedimentation during turbulent RBC, the latter confirmed through visual inspection.

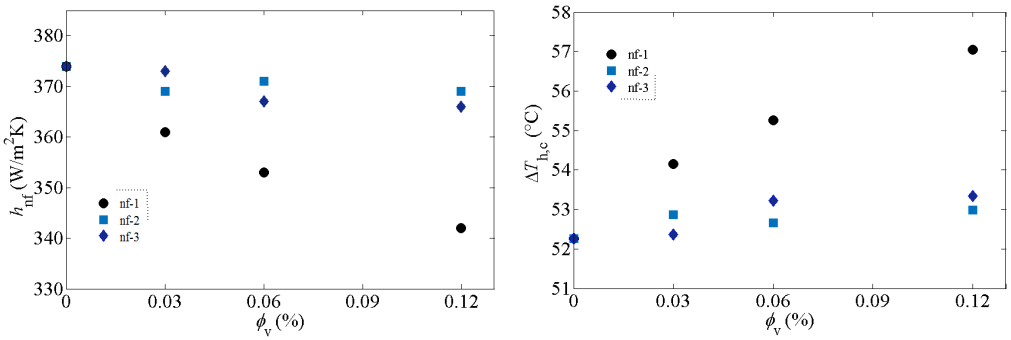

Figure 2. Natural convection heat transfer coefficient (left) and temperature gradient between the heating and cooling plates (right) as a function of the nanoparticle volume fraction

DLS measurements were also performed of the dispersed nanoparticles of the P_b nanopowder, which observed limited agglomeration. Figure 3 presents the measured multimodal size distribution of the nanoparticle diameter as a function of the number-weighted average. Accordingly, the mean diameter of the dispersed nanoparticles is D_{mn} = 162.6 nm. Concerning the lognormal size distribution (volume-weighted average), the effective diameter of the nanoparticles is D_{eff} = 253.4 nm with a polydispersity of 0.252. Therefore, the DLS measurements indicate that the average size of the nanoparticles is notably larger than the primary particle size of 50 nm that is given by the manufacturer and supported by the TEM images. This finding follows the same trend with similar results addressed in the literature, where the particle size of the dried form (TEM analysis) was different from that in the dispersed state (DLS analysis) [5, 6].

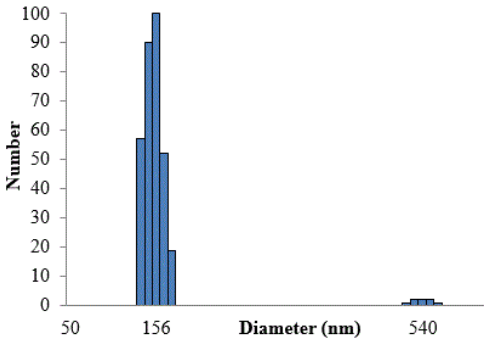

Figure 3. Multimodal size distribution of the Al_2O_3 nanoparticles (P_b nanopowder), measured by DLS

Summary/Conclusions: An optimisation study of nanofluid properties was conducted to reduce nanoparticle agglomeration. Al_2O_3-H_2O nanofluids with different consistencies and characteristics were prepared, tested and compared during turbulent Rayleigh-Bénard convection. By employing the electrostatic stabilisation method or using a suitable nanopowder in terms of physical characteristics and manufacturing process, it was found that the nanoparticle agglomeration is reduced, the attained stability is superior and the heat transfer deterioration is minimal. Therefore, it was demonstrated that the pH value of nanofluids and the resulting surface charge of the nanoparticles are of critical importance to nanofluids stability. The average size of the nanoparticles from DLS measurements were notably larger than the primary particle size from TEM measurements. In general, different particle analysis methods yield different equivalent sizes due to limitations in the applicable particle size, nanoparticle concentration and employed technique. Other reasons include the presence of difficult-to-break agglomerates during the preparation of nanofluids or the tendency of the nanoparticles to re-agglomerate, especially in the absence of a pH controller or a surface activator. Therefore, a systematic approach for the formulation of nanofluids and presentation of data is required to eliminate discrepancies among findings in the literature.

References:

1. Wen, D. and Y. Ding, *Formulation of nanofluids for natural convective heat transfer applications.* International Journal of Heat and Fluid Flow, 2005. **26**(6): p. 855-864.
2. Ghadimi, A., R. Saidur, and H.S.C. Metselaar, *A review of nanofluid stability properties and characterization in stationary conditions.* International Journal of Heat and Mass Transfer, 2011. **54**(17-18): p. 4051-4068.
3. Kouloulias, K., A. Sergis, and Y. Hardalupas, *Sedimentation in nanofluids during a natural convection experiment.* Int. J. Heat Mass Transfer, 2016. **101**: p. 1193-1203.
4. Barrett, T.R., et al., *Investigating the use of nanofluids to improve high heat flux cooling systems.* Fusion Engineering and Design, 2013. **88**(9-10): p. 2594-2597.
5. Taylor, R.A. and P.E. Phelan, *Pool boiling of nanofluids: comprehensive review of existing data and limited new data.* International Journal of Heat and Mass Transfer, 2009. **52**: p. 5339-5347.
6. Ghodsinezhad, H., M. Sharifpur, and J.P. Meyer, *Experimental investigation on cavity flow natural convection of Al2O3-water nanofluids.* International Communications in Heat and Mass Transfer, 2016. **76**: p. 316-324.

1st International Conference on Nanofluids (ICNf2019)
2nd European Symposium on Nanofluids (ESNf2019)
26-28 June 2019, Castelló, Spain

Dielectric properties of magnetic nanofluid based on transformer oil and Mn-Zn ferrite nanoparticles

M. Rajnak[1,2], B. Dolnik[2], J. Krempasky[2], K. Parekh[3], K. Paulovicova[1], Z. Mitroova[1], M. Timko[1], and P. Kopcansky[1*]

[1]Institute of experimental physics SAS, Watsonova 47, 04001 Kosice, Slovakia

[2]Faculty of Electrical Engineering and Informatics, Technical university of Kosice, Letná 9, 04200, Kosice, Slovakia

[3]K C Patel R & D Center, Charotar University of Science & Technology, CHARUSAT Campus, Changa, 388 421, Dist. Anand, Gujarat, India

[*]Corresponding author: kopcansky@saske.sk

Keywords: Magnetic nanofluid, Transformer oil, Dielectric permittivity, Nanoparticles.

Abstract: In this paper we present the investigation of dielectric properties of a transformer oil-based Mn-Zn ferrite magnetic nanofluid. A significant dielectric relaxation (dielectric losses) was found by means of a dielectric spectroscopy method. As the dielectric losses may be contradictory to the cooling efficiency of the nanofluid, we present two ways how to slightly control the maximum dielectric losses in the nanofluid. The first one is based on varying nanoparticle concentration, while the other relies on the application of an external DC electric field.

Introduction/Background: Magnetically responsive nanofluids (ferrofluids) are extensively studied as a potential medium for heat transfer devices. The most common dispersive phase consists of magnetite (Fe_3O_4) nanoparticles (NPs), which exhibit high domain magnetization resulting in high dipolar coupling coefficient [1]. On the other hand, the lower thermal conductivity of bulk magnetite (5 W/mK) stimulated researchers to synthesize magnetic NPs with higher thermal conductivity. Mn-Zn ferrite NPs with bulk thermal conductivity of 29 W/mK have been considered as a promising material with attractive thermo-magnetic properties [2], the presence of which in light hydrocarbon oil may increase its thermal conductivity up 45 % [3]. Recently, it was reported that transformer oil based Mn-Zn ferrite ferrofluid with high pyromagnetic coefficient (177 A/mK) can be used as an effective coolant in 3 kW power transformer [4]. In comparison to transformer oil, the authors observed 20 K decrease in transformer winding temperature when cooling with the ferrofluid. The maximum transformer cooling effect was achieved for overload conditions as a result of the effective thermomagnetic convection [5]. However, it is known that the ferrofluids exhibit dielectric losses around

the power frequency [6]. Then, along with Joule heating, the dielectric losses (polarization processes) may be contradictory to the cooling efficiency of the ferrofluid.

In this paper, we investigate complex dielectric permittivty of transformer oil-based Mn-Zn ferrite ferrofluid. After revealing a maximum dielectric loss, we demonstrate its dependence on NP concentration and an external DC bias voltage.

Discussion and Results: The investigated ferrofluid was prepared on transformer oil Tashoil-50. The Mn-Zn ferrite NPs were synthesized by chemical co-precipitation [3]. After the co-precipitation, oleic acid was used as a surfactant to create steric repulsion between the NPs. As shown in Fig. 1a, the final ferrofluid exhibits superparamagnetic behavior at room temperature (zero coercivity) and has magnetization of saturation 7.88 Am^2/kg, corresponding to NP volume fraction of 2.98 %. The temperature dependent magnetization of the prepared ferrofluid is plotted in Fig.1b, indicating the pyromagnetic effect. Fig. 1c shows the quasi spherical shape of the NP with the average diameter of 10 nm, as obtained from a low voltage electron microscope (Delong LVEM5). From the prepared ferrofluid (labeled as MF), three other samples were diluted with the estimated NP volume fraction of 1.5 %, 1 % and 0.43 %, labeled as MF1, MF2, and MF3, respectively.

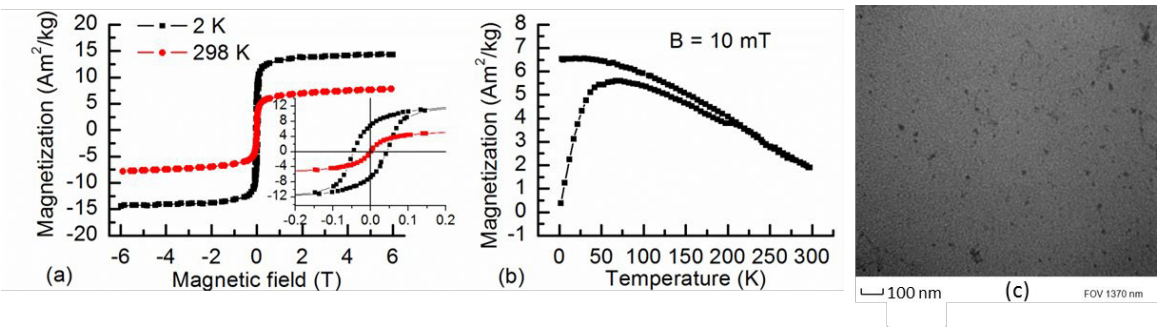

Figure 1. Magnetization curves of the prepared ferrofluid (a). Temperature dependent magnetization measured in zero field cooling (lower curve) and field cooling (upper curve) regime (b). TEM image of the synthesized nanoparticles (c).

In order to measure the complex dielectric permittivity of the prepared ferrofluids, LCR meters Agilent E4980A and IM3533 HIOKI were employed in the frequency range from 0.1 Hz to 200 kHz. Glass cells with Indium Tin Oxide (ITO) layers were used as measuring capacitors with the electrode separation distance of 5 μm, as depicted in Fig.2a. To influence the ferrofluid polarization and related dielectric losses with an external DC electric field, another pair of copper electrodes was attached to the outer walls of the capacitor (Fig.2b). In this way, the DC conductivity, which would contribute to the losses, was avoided. The complete experimental setup is shown in Fig.2c.

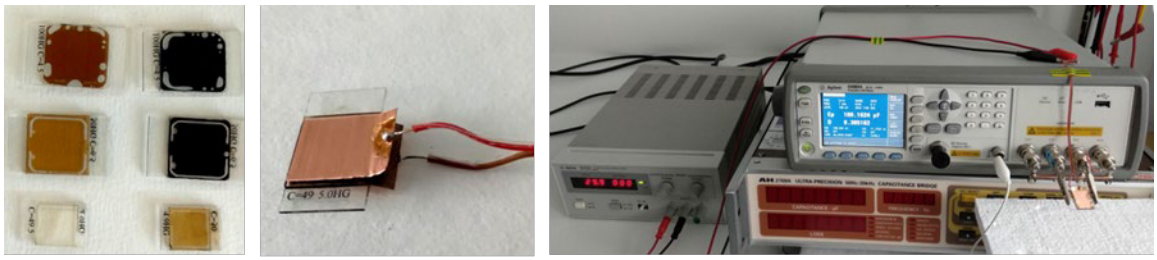

Figure 2. Glass plate capacitors with ITO layers filled with the ferrofluids (a). The glass plate capacitor with the attached copper electrodes connected to a DC voltage source (b). Complete experimental setup for dielectric measurements (c).

Measurements of dielectric permittivity of the transformer oil yielded the value of 2 practically in the whole frequency range. However, the presence of NPs in the oil results in a remarkable increase in the low frequency permittivity. In Fig.3a, one can see that the static ferrofluid permittivity increases with increasing NP concentration. It is therefore clear that the NP and interfacial polarizations significantly contribute to the total ferrofluid permittivity. Depending on the NP concentration, a dielectric dispersion occurs when approaching 10 Hz, which is accompanied with the relaxation maximum in the imaginary permittivity (dielectric loss). In a complex plane (Cole-Cole plot in Fig. 2b), this behavior is represented by a semicircle with the diameter dependent on the NP concentration.

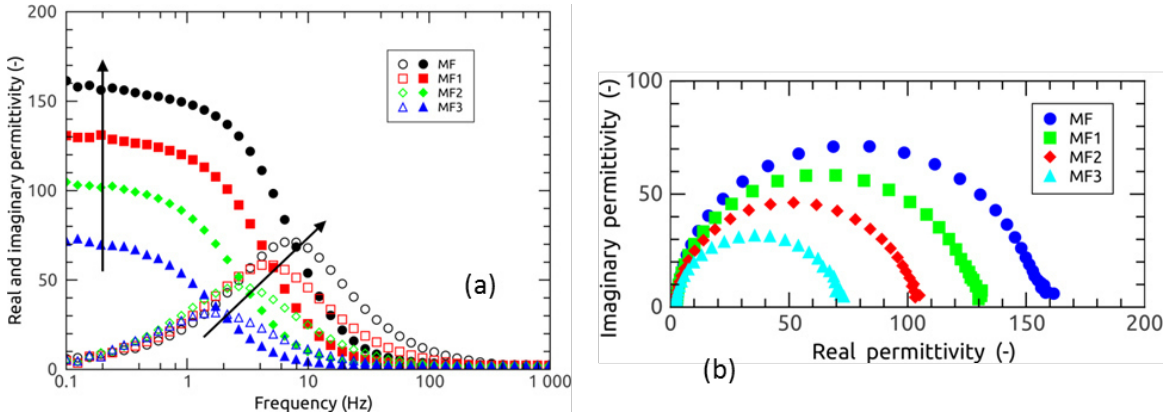

Figure 3. The complex dielectric permittivity of the ferrofluids. The arrows indicate the increasing concentration. The open and filled symbols represent imaginary (losses) and real permittivity, respectively (a). Cole-Cole plot (b).

While the increasing NP concentration shifts the maximum dielectric losses towards higher frequencies, the applied DC voltage has an opposite effect. This is presented in Fig.4 for the most concentrated sample (MF), when the DC voltage was applied on the external copper electrodes. It should be noted that the resulting DC electric field is much stronger than the AC measuring field, as the measuring voltage was set to 100 mV. Thus, without the Ohmic conductivity, the DC electric field induces another polarization

forces on the NPs, which can subsequently form assemblies [7]. This results in a slight shift (broadening) of the maximum losses towards lower frequencies. However, the static permittivity increases with increasing voltage.

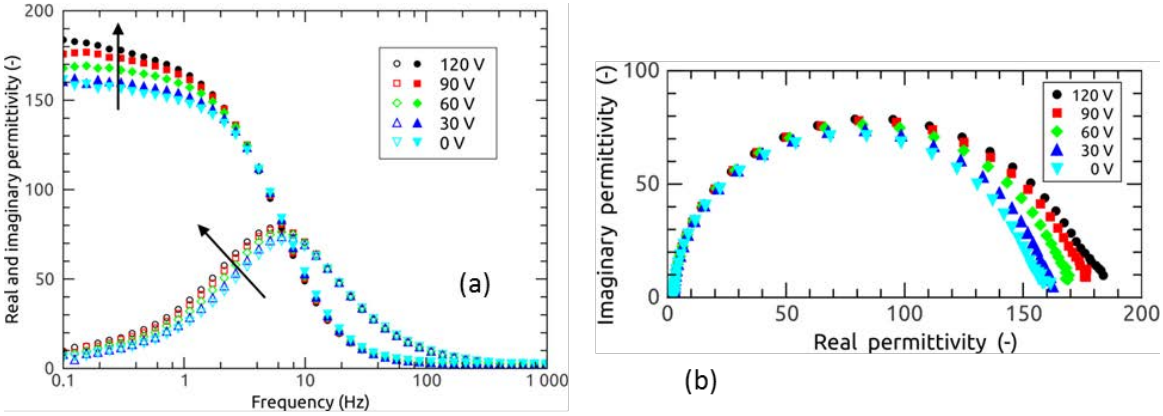

Figure 4. The complex dielectric permittivity of the most concentrated ferrofluid. The arrows indicate the increasing voltage. The open and filled symbols represent imaginary (losses) and real permittivity, respectively (a). Cole-Cole plot (b).

Summary/Conclusions: Transformer oil-based Mn-Zn ferrite ferrofluid, which is known for its attractive thermo-magnetic properties, was studied from a dielectric point of view. It was found that the dielectric losses reflected in the relaxation maximum can be slightly controlled by both, nanoparticle concentration and the external DC electric field. In this way, one could tailor the ferrofluid's dielectric properties to assure the best cooling effectiveness for a particular electrical engineering application.

References:

1. K. Parekh and H. S. Lee, Experimental investigation of thermal conductivity of magnetic nanofluids, *AIP Conf. Proc.*, 1447, 1, pp. 385–386, 2012.
2. R. Arulmurugan, G. Vaidyanathan, S. Sendhilnathan, and B. Jeyadevan, Mn–Zn ferrite nanoparticles for ferrofluid preparation: Study on thermal–magnetic properties, *J. Magn. Magn. Mater.*, 298, 2, pp. 83–94, 2006.
3. K. Parekh, Thermo-magnetic properties of ternary polydispersed Mn0.5Zn0.5Fe2O4 ferrite magnetic fluid, *Solid State Commun.*, 187, pp. 33–37, 2014.
4. J. Patel, K. Parekh, and R. V. Upadhyay, Prevention of hot spot temperature in a distribution transformer using magnetic fluid as a coolant, *Int. J. Therm. Sci.*, 103, pp. 35–40, 2016.
5. J. Patel, K. Parekh, and R. V. Upadhyay, Performance of Mn-Zn ferrite magnetic fluid in a prototype distribution transformer under varying loading conditions, *Int. J. Therm. Sci.*, 114, pp. 64–71, 2017.
6. M. Rajnak, J. Kurimsky, B. Dolnik, P. Kopcansky, N. Tomasovicova, E. Taculescu-Moaca, M. Timko, Dielectric-spectroscopy approach to ferrofluid nanoparticle clustering induced by an external electric field, *Phys. Rev. E*, 90, 3, p. 032310, 2014.
7. M. Rajnak, V.I. Petrenko, M.V. Avdeev, O.I. Ivankov, A. Feoktystov, B. Dolnik, J. Kurimsky, P. Kopcansky, M. Timko, Direct observation of electric field induced pattern formation and particle aggregation in ferrofluids, *Appl. Phys. Lett.*, 107, 7, p. 073108, 2015.

1st International Conference on Nanofluids (ICNf2019)
2nd European Symposium on Nanofluids (ESNf2019)
26-28 June 2019, Castelló, Spain

Thermodiffusive properties of colloidal dispersions of maghemite nanoparticles in ionic liquids

M. Sarkar[1*], J. Riedl[1], G. Demouchy[1,2], F. Gélébart[1], F. Cousin[3], G. Mériguet[1], V. Peyre[1], E. Dubois[1] and R. Perzynski[1]
[1] Sorbonne Univ., CNRS, PHENIX, F-75005, Paris, France.

[2] Univ. Cergy-Pontoise, Dpt. de Phys., F-95011, Cergy-Pontoise, France

[3] Lab. Léon Brillouin – CE-Saclay, F-91191 Gif-sur-Yvette cedex, France

[*]Corresponding author: mitradeep.sarkar@sorbonne-universite.fr

Keywords: Thermodiffusion, Colloidal dispersion in ionic liquid, Soret coefficient Thermoelectric effect, Forced Rayleigh scattering

Abstract: Thermodiffusive properties of maghemite nanoparticles dispersed in four different ionic liquids are studied here as a function of temperature by forced Rayleigh Scattering.

Introduction/Background: Ionic liquids (ILs) are a wide class of solvents, purely constituted of ions, and liquid at room temperature. Our work is aimed at developing new thermoelectric materials based on colloidal dispersions of maghemite nanoparticles (NPs) in ionic liquids that are versatile, cost-effective and non-toxic to assist the economically and environmentally sustainable energy transition.
Thermoelectric applications [1] require precise determination of several transport coefficients of the NPs under a thermal gradient, namely Ludwig-Soret (thermodiffusive) and Seebeck (thermoelectric) effects which are interlinked in such ionic systems. On applying a temperature gradient ∇T on the colloidal dispersions, the Soret effect induces a volume fraction gradient $\nabla\Phi$ of the NPs (Soret coefficient defined as $\Phi S_T \nabla T = -\nabla\Phi$) and the Seebeck effect induces an internal electric field E (Seebeck coefficient defined as $S_e^{S_t}\nabla T = E$) [2]. By a forced Rayleigh scattering (FRS) experiment, we determine the mass diffusion coefficient D_m and the S_T of the NPs as a function of temperature for four different ionic liquids.

Results and discussion: Aqueous colloidal dispersions of maghemite NP are synthesized following the Massart method (median diameter 8.7 nm). Following a pathway similar to that described in [3], these NPs coated with hydroxyl groups, are dispersed with [SMIM][TFSI] counter ions, at a volume fraction 1% in various Ionic Liquids (see Table 1).

Table 1. The ionic liquids (provided by SOLVIONIC) and their viscosity.

Sample name	Chemical formula	Viscosity (10^{-3} Pa.s)
[EMIM][TFSI]	1-Ethyl-3-Methyl Imidazolium bis(trifluoromethanesulfonyl)imide	42.6
[EMIM][FSI]	1-ethyl-3-methyl-1H-imidazolium bis (fluorosulfonyl) amide	18.7
[EMIM][AcO]	1-Ethyl-3-Methyl Imidazolium acetate	153
[Pyrr][TFSI]	N-(2-Methoxyethyl)-N-Methylpyrrolidinium bis(trifluoromethane sulfonyl)imide	72.2

In the FRS experiment [3,4] a1D sinusoidal grating with periodicity (Λ) is imaged in the fluid which causes a periodic modulation of temperature (ΔT), due to the light-absorbing NPs. Ludwig-Soret effect then induces a periodic array of NP's volume fraction (ΔΦ) in the fluid. By measuring ΔT and ΔΦ, we measure S_T in stationary conditions. The relaxation of the Φ-array at ΔT=0 leads to the determination of D_m. The FRS measurements are performed at 295K<T<463K.

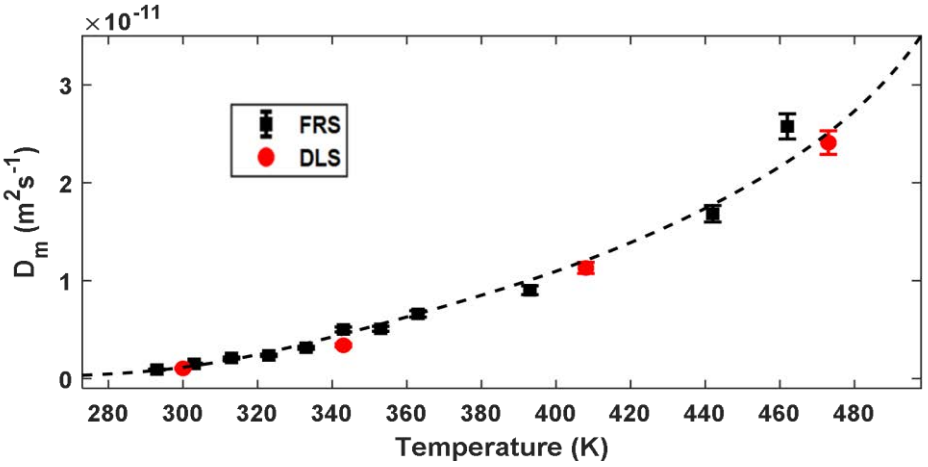

Figure 1 - Sample [EMIM][TFSI]: Diffusion coefficient D_m as a function of T measured by FRS and DLS. (Dashed) Calculated D_m with χ=0.8 and d_h=15nm.

Simultaneous Dynamic Light Scattering (DLS) and Small Angle Neutron Scattering (SANS) measurements are also performed at PAXY spectrometer in ORPHEE-LLB-Saclay-France in a controlled oven at 295K<T<473K.

SANS measurements are performed in the range of scattering vectors Q (2.4×10^{-3}Å to 4.3×10^{-1}Å). The scattering intensity I (Q) is seen to be almost independent of T, and the osmotic compressibility χ evaluated from I(Q=0) [3] is also found to be independent of T (value of χ=0.8±0.05 for [EMIM][TFSI] and χ=0.9±0.05 for [Pyrr][TFSI] at Φ=1%). The values of χ show that the inter-particle interaction is repulsive in these ILs with the two body interaction coefficient A_2 >0 for both of them.

D_m measured by DLS and FRS is shown as a function of temperature in Fig.1 for the NPs dispersed in [EMIM][TFSI]. D_m is given by the modified Stokes-Einstein formulation [2]:

$$D_m = KT/3\pi\eta\chi d_H \quad (1)$$

with η the solvent viscosity; d_H the hydrodynamic diameter and χ the osmotic compressibility of the NPs [2]. Fig.1 also shows D_m as deduced by Eq.1 with χ=0.8 and d_h=15nm. The close match of the measured and calculated values of D_m indicates that the T-dependence of D_m is ruled by the variation of IL viscosity.

The Soret coefficient measured by FRS is found to be positive for all IL-based NP's dispersions. In Fig 2, three ILs have the same [EMIM] cation and different anions, and two have the same anion [TFSI] and different cations.

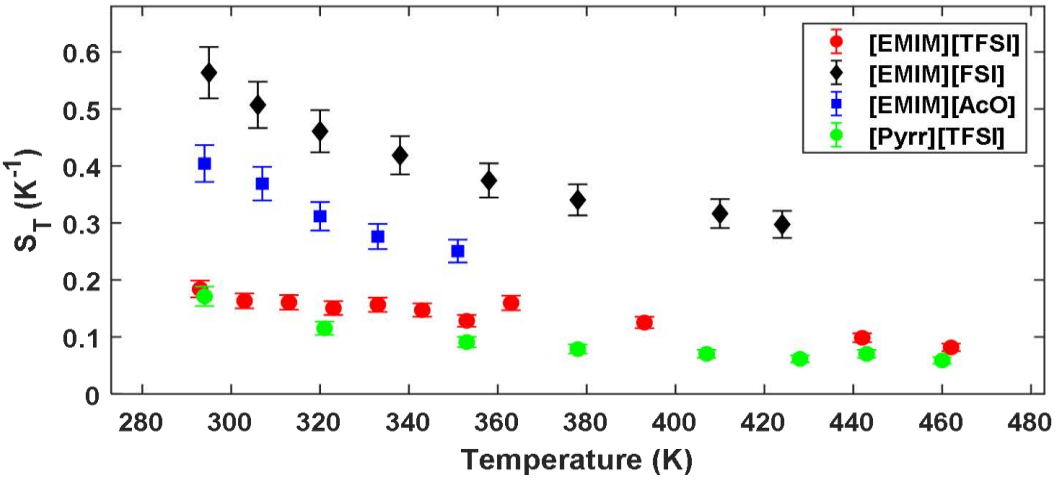

Figure 2. Soret coefficient as a function of T for the ferrofluids at Φ=1% in the four Ionic Liquids of table 1

As shown in Fig. 2 the colloids in [EMIM][TFSI] and [Pyrr][TFSI] are stable up to 463K and have similar values of S_T for all T. By changing the anion, the dispersion in [EMIM][FSI] is stable up to 433K while that in [EMIM][AcO] degrades for temperature over 353K. The two dispersions in those ILs have also values of S_T larger than the ones found with [TFSI] anions. So based on these initial results we see that the effect of anions on the Soret coefficient is more pronounced than that of the cations. In polar solvents S_T is linked to the stationary Seebeck coefficient S_e^{st} by the model described in [1,2,4]

$$S_T = \chi\left[\frac{\hat{S}_{NP} - e\xi_0 S_e^{st}}{kT}\right] \quad (2)$$

where ξ_0 is the dynamic electrophoretic charge number of the NPs and $\hat{S}_{NP}$ is the NP's Eastman entropy of transfer in the solvent. In first approximation the term $\mathrm{T}S_T/\chi = \left[\hat{\mathrm{S}}_{\mathrm{NP}}\text{-}\mathrm{e}\xi_0\mathrm{S}_{\mathrm{e}}^{\mathrm{st}}\right]/k$ can be evaluated with the quantity $3\pi\eta\mathrm{d}_{\mathrm{H}}\mathrm{S}_{\mathrm{T}}\mathrm{D}_{\mathrm{m}}$. This term is found to be positive and of the same order of magnitude (with a very weak variation with T) for the four ILs studied here. This indicates that for [EMIM][AcO] and [EMIM][FSI] a value of $\chi>1$ should be used in Eq.2 meaning that the interparticle interactions is slightly attractive in these ILs ($A_2<0$) while it is repulsive ($\chi<1$, $A_2>0$) in the other two ILs with [TFSI] anions.

Summary/Conclusions: We show that the temperature variations of the diffusion coefficient D_m scale with the IL viscosity. The Soret coefficient S_T has a weak dependence on the IL's cation nature and strongly depends on the nature of the IL's anion, through the interparticle interaction.

The authors thank F. Clement, A. Helary, A. Anfry for their help for the measurements and SOLVIONIC for providing the ILs. This work is supported by the European Union's Horizon 2020 research and innovation programme under grant agreement nº 731976 (MAGENTA).

References:

1. B. T. Huang, M. Roger, M. Bonetti, T. J. Salez, C. Wiertel-Gasquet, E. Dubois, R. Cabreira Gomes, G. Demouchy, G. Mériguet, V. Peyre, M. Kouyaté, C. L. Filomeno, J. Depeyrot, F. A. Tourinho, R. Perzynski, and S. Nakamae, Thermoelectricity and thermodiffusion in charged colloids, *The Journal of Chemical Physics.* 143 (2015) 054902.
2. R. C. Gomes, A. Ferreira da Silva, M. Kouyaté, G. Demouchy, G. Mériguet, R. Aquino, E. Dubois, S. Nakamae, M. Roger, J. Depeyrot and R. Perzynski, Thermodiffusion of repulsive charged nanoparticles – the interplay between single-particle and thermoelectric contributions, *Phys. Chem. Chem. Phys.* 20 (2018) 16402-16413.
3. C. L. Filomeno, M.Kouyaté, V.Peyre, G.Demouchy, A.F. C. Campos, R. Perzynski, F.A. Tourinho, and E. Dubois, Tuning the Solid/Liquid Interface in Ionic Colloidal Dispersions: Influence on Their Structure and Thermodiffusive Properties*, The Journal of Physical Chemistry C* 121 (2017) 5539-5550.
4. M. Kouyaté, C.L. Filomeno, G. Demouchy, G. Mériguet, S. Nakamae, V. Peyre, M. Roger, A Cēbers, J. Depeyrot, E. Dubois, R. Perzynski, Thermodiffusion of citrate-coated γ-Fe2O3 nanoparticles in aqueous dispersions with tuned counter-

ions - anisotropy of the Soret coefficient under a magnetic field, *Physical Chemistry Chemical Physics*. 21 (2019) 1895-1903

1st International Conference on Nanofluids (ICNf2019)
2nd European Symposium on Nanofluids (ESNf2019)
26-28 June 2019, Castelló, Spain

A preliminary study on Erythritol-based nanofluids for potential heat transfer and storage applications

F. Agresti[1*], L. Fedele[2], S. Bobbo[2], S. Rossi[2], S. Barison[1]

[1]Institute of Condensed Matter Chemistry and Technologies for Energy (ICMATE), National Research Council of Italy (CNR), Corso Stati Uniti 4, 35127 Padova, Italy

[2]Institute of Construction Technologies (ITC), National Research Council of Italy (CNR), Corso Stati Uniti 4, 35127 Padova, Italy

[*]Corresponding author: filippo.agresti@cnr.it

Keywords: Erythritol, Phase Change Material, Nanofluid, Emulsion, Supercooling.

Abstract: In this preliminary work, nanofluids based on Erythritol, a promising Phase Change Material (PCM) belonging to the class of Sugar Alcohols (SA), are studied as potential heat transfer and heat storage fluids in the form of Phase Change Material Emulsions (PCME). Suspensions of Erythritol into a commercial heat transfer fluid based on aromatic compounds have been obtained by an emulsification method. The nanofluids have been characterized by Dynamic Light Scattering (DLS) to estimate the hydrodynamic size of Erythritol particles and by Differential Scanning Calorimetry (DSC) to evaluate the melting and crystallization temperatures and the enthalpies involved. Work is under way to obtain more information regarding the thermal conductivity and viscosity of suspensions and to mitigate the phenomenon of supercooling, which is a major issue of this material for the use as a PCM.

Introduction/Background: Phase change material emulsions (PCMEs) or phase change slurries have risen interest in scientific community in the last years as potential heat transfer and heat storage fluids [1]. These systems consist on a base fluid, which, basically, is a suitable heat transfer fluid, and an emulsified phase change material that should be immiscible with the base fluid. The idea is to exploit the latent heat of melting and crystallization of PCM to increase the thermal energy storage capacity of the base fluid that from the other side confers higher thermal conductivity and lower viscosity with respect to PCM. Moreover, the large interface between base fluid and PCM favours the heat transfer between the two phases. The applications and the temperature ranges investigated so far include solar thermal storage, waste heat recovery and heat transfer.

Several issues currently hinder the application of PCME, as the colloidal stability of emulsions that is generally due to thermodynamic reasons, the phenomenon of

supercooling that is the PCM cooling below its melting point without crystallization and the reduction of the expected latent heats, both generally due to confinement.

Recently, a new class of organic materials called sugar alcohols (SA) have been proposed as PCM due to their high latent heat, compared to paraffin-based and fatty-acids PCMs, their environmental sustainability, and their low cost. They are industrially produced from naturally occurring sugars by reduction of the aldehyde group, leading to a series of polyols having a -OH group on each carbon. The melting temperatures of SAs useful for latent heat medium temperature storage applications are in the range 50-200 °C, depending on chain length, with latent heat in the range 250-320 J/g [2]. Erythritol is a natural occurring linear SA with 4 atoms of carbon having a melting temperature of 118 °C and a latent heat of melting of 340 J/g [3].

This work investigates the potential of Erythritol as a phase change material emulsified with an aromatic-based heat transfer oil.

Discussion and Results: In the preparation of PCMEs, meso-Erythritol (Sigma–Aldrich, >99%) has been used as the PCM dispersed phase. An aromatic-based heat transfer oil (Xceltherm SST), whose thermophysical properties are reported in table 1, has been used as the continuous phase. Docusate Sodium (AOT) (Sigma-Aldrich, >99%) has been used as a surfactant. 3 samples containing 4wt% Erythritol and 3 different amounts of AOT have been prepared, 0.75 wt% (sample A), 1 wt% (sample B) and 1.5 wt% (sample C). To prepare the 3 samples, 0.375, 0.05 and 0.75 g of AOT, respectively, have been dissolved into 2 g of deionised water at 45 °C and, after the complete dissolution, 0.2 g of Erythritol have been dissolved in the same solution. 5 g of SST oil have been added dropwise to the water solution under continuous stirring and ultrasound irradiation using a Sonics VCX130 (Sonics & Materials, Inc.) operating at 20 kHz and 130 W, equipped with a 2 mm diameter Ti6Al4V alloy tip, operated at 30% power. White opaque emulsions have been obtained after the complete addition of the oil phase. The water has been completely evaporated by heating the emulsion at 110 °C under stirring for 30 min, obtaining translucent nanofluids.

Table 1. Thermophysical properties of SST oil

	32 °C	**149 °C**
Density (Kg/m^3)	942	817
Viscosity (cP)	13.7	1.01
Specific heat (J/gK)	1.95	2.22
Thermal Conductivity (W/mK)	0.113	0.102

The hydrodynamic size of Erythritol particles has been estimated by Dynamic Light Scattering measurements (Zetasizer Nano-ZS90, Malvern Instruments Ltd., UK).

Simultaneous thermogravimetric analysis/differential scanning calorimetry TGA/DSC (SDT Q600-TA instruments) have been performed on nanofluids heating at 2 °C/min and cooling at 0.5 °C/min in nitrogen stream (20 ml/min) in the range 30-145 °C.

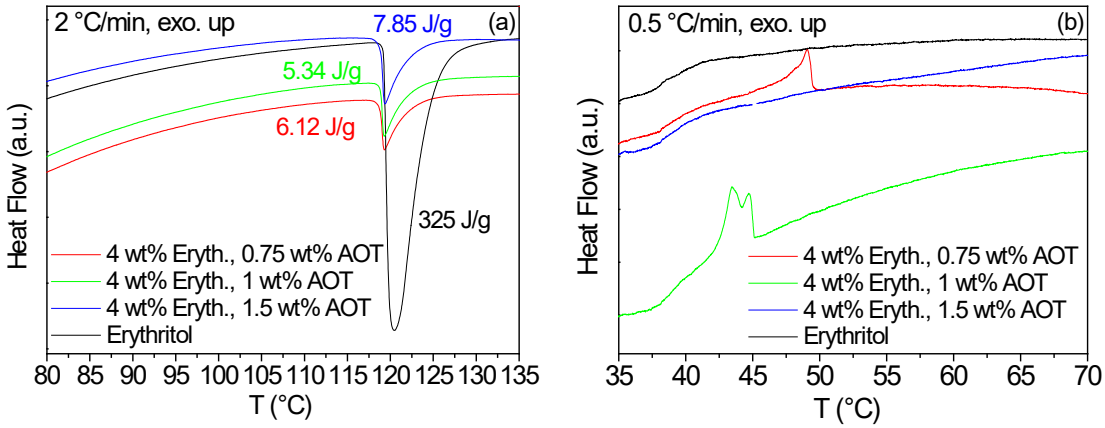

Figure 2. DSC peaks of melting (a) and crystallization (b) of pure Erythritol and suspensions in SST oil.

DLS measurements show that samples A and B have nearly the same average particle size that is 1000 nm and 1030 nm, respectively. Sample C shows a considerably higher particle size, 1900 nm.

DSC measurements on pure Erythritol reported in figure 1 shows a melting onset temperature of 118 °C and a latent heat of melting of 325 J/g, which is in agreement with literature data. As well known, Erythritol is characterized by a poor crystallization kinetics [3]. Actually, despite the slow cooling temperature of 0.5 °C/min, no crystallization peak is bserved in our experimental conditions down to 35°C. All suspensions show a melting peak with almost the same onset temperature of the pure compound. Anyway, the latent heats of melting are considerably lower than the theoretical value of 13 J/g. Sample A and B show a latent heat of 47 % and 41 % with respect to the theoretical value, while it is 60 % for sample C. Surprisingly, samples A and B show a clear crystallization peak with onset of 49 °C and 45 °C, respectively. While no crystallization peak is observed for sample C as in the case of pure Erythritol. The observed behavior could suggest that reducing the particle size

of Erythritol into suspensions could help the crystallization kinetics, maybe due to a better heat transfer or to the presence of interfaces that favor nucleation. However, reducing particle size also leads to reduced enthalpies, as already observed for other PCME systems.

Summary/Conclusions: From the reported preliminary data, suspensions of Erythritol into an aromatics-based heat transfer oil show that reducing the particle size leads to an improved crystallization kinetics, though with a considerable supercooling. Work is ongoing to confirm these results, to improve the colloidal stability of these suspensions by further reducing the particles size, which is still too high. Moreover, nucleating agents will be encapsulated along with Erythritol in order to mitigate the high supercooling, which is detrimental for heat transfer and storage applications.

References:

1. J. Shao, J. Darkwa, G. Kokogiannakis, Review of phase change emulsions (PCMEs) and their applications in HVAC systems, *Energy Build.* 94 (2015) 200–217. doi:10.1016/j.enbuild.2015.03.003.
2. E.P. del Barrio, A. Godin, M. Duquesne, J. Daranlot, J. Jolly, W. Alshaer, T. Kouadio, A. Sommier, Characterization of different sugar alcohols as phase change materials for thermal energy storage applications, *Sol. Energy Mater. Sol. Cells.* 159 (2017) 560–569. doi:10.1016/J.SOLMAT.2016.10.009.
3. A.J. Lopes Jesus, S.C.C. Nunes, M. Ramos Silva, A. Matos Beja, J.S. Redinha, Erythritol: Crystal growth from the melt, *Int. J. Pharm.* 388 (2010) 129–135. doi:10.1016/J.IJPHARM.2009.12.043.

1st International Conference on Nanofluids (ICNf2019)
2nd European Symposium on Nanofluids (ESNf2019)
26-28 June 2019, Castelló, Spain

Analytical Approximation to the Refractive Index of Nanofluids with Extended Applicability

A. Acevedo-Barrera and A. García-Valenzuela*

Instituto de Ciencias Aplicadas, Universidad Nacional Autónoma de México, Apartado Postal 70-186, Ciudad de México 04510, Mexico

*Corresponding author: augusto.garcia@icat.unam.mx

Keywords: Effective refractive index, Maxwell Garnett mixing formula, scattering corrections, dependent scattering, nanofluid properties.

Abstract: Currently there are available a few simple analytical approximations for the effective refractive index for nanofluids. These approximations are valid either for nanofluids of very small nanoparticles or very dilute. Here we propose a new simple analytical approximation, based on local-field corrections to the Foldy-Lax approximation, that coincides with the previously established approximations when they are expected to be valid, but remain valid also for denser nanofluids and for larger nanoparticles.

Introduction/Background:

We understand a nanofluid as a nanoparticle suspension of sizes smaller than 100 nm [1]. The optical properties of nanofluids are condensed in their complex effective Refractive Index (RI). It is possible to measure the effective RI of nanofluids using standard instrumentation. The effective RI can give information about the size and type of the nanoparticles, their spatial distribution or state of aggregation, therefore it is a useful tool to characterize a nanofluid.

The RI of nanofluids is a complex quantity, with both its real and imaginary parts, being functions of the optical properties of the medium surrounding the nanoparticles, the volume fraction occupied by the nanoparticles, their size and RI. To a very good approximation light refracts into the nanofluid according to Snell's Law with the real part of its effective RI and attenuates as it travels through the nanofluid exponentially (Fig.1), with an extinction coefficient α_{ext} proportional to the imaginary part of the effective RI: $\alpha_{ext} = 2k_0 \mathrm{Im}\left(n_{eff}\right)$. The extinction coefficient has contributions of absorption and scattering by the particles. In many nanofluids, when particles are larger than a few tens of nanometers, scattering losses are important and may dominate over absorption losses.

Calculating the optical properties of suspensions of particles has caught the attention of many researchers for more than 100 years [2]. When scattering losses may be ignored, the well-known Maxwell Garnett (MG) effective medium approximation to the effective dielectric function has been available for many years [2-4]. Simple analytical extensions to the MG approximation to include scattering losses to first order in the nanoparticles' volume concentration have been proposed [5,6]. However, the extended MG mixing formula is valid only for very dilute nanofluids. Also, the small particle limit of the so-called Quasi-Crystalline Approximation (QCA), developed for suspension of spherical particles of arbitrary size suspensions by Tsang and Kong [7], produces a simple analytical approximation that include scattering corrections to the MG mixing formula [4,7], and this formula can be used for relatively dense nanofluids [8,9]. However, for nanoparticles with sizes of a few tens of nanometers, this approximation yields non-physical predictions of the imaginary part of the effective RI. Therefore, there is still a large gap in particle size and volume concentrations values, within the realm of nanofluids, for which no available analytical approximation to the effective RI is valid. In this work we introduce a new analytical approximation to fill the mentioned gap.

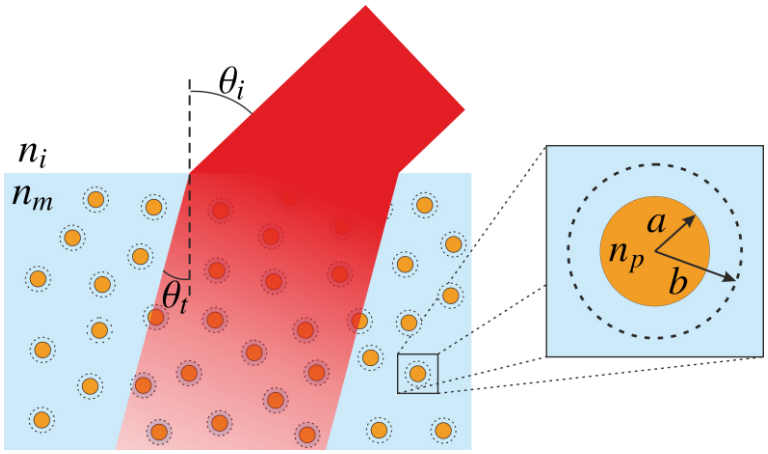

Figure 1. Refraction and attenuation of an optically collimated beam in a nanofluid

Discussion and Results:

The Maxwell Garnett mixing formula with scattering corrections (MGSC) derived in Refs. [5,6] is given by:

$$n_{eff}^{(MGSC)} = n_m \sqrt{1 + 3f\Gamma\left\{1 + i\frac{2}{3}x_m^3\Gamma\right\}}, \qquad (1)$$

where, $\Gamma = \chi/(1 - f\chi)$, $\chi = (n_p^2/n_m^2 - 1)/(n_p^2/n_m^2 + 2)$ and f is the volume fraction occupied by the particles. The quasi-crystalline approximation for nanofluids in the small

particles limit (QCA-SPL) assuming a "hole" correlation function of radius $b > a$, reduces to the following analytical approximation,

$$n_{eff}^{(QCA-SPL)} = n_m \sqrt{1 + 3f\Gamma\left\{1 + i\frac{2}{3}x_m^3\Gamma\left[1 - 8f\frac{b^3}{a^3}\right]\right\}}. \quad (2)$$

When scattering losses dominate over absorption losses, the prediction for the imaginary part of the effective RI from the latter two approximations do not coincide with each other, even for very small particles and very small particle concentrations.

The Foldy-Lax formula [10] is given by, $n_{eff}^{FL} = n_m\sqrt{1 + 3i\frac{f}{(ka)^3}S(0)}$, where $S(0)$ is the forward scattering amplitude of an isolated particle [2]. For spherical particles it is readily calculated with the so-called Mie theory [2]. n_{eff}^{FL} is generally considered valid for dilute particles suspensions but of particles of arbitrary size. However, for very small particles local field effects may become important even at low particle concentrations. In this work we propose a simple extension to the Foldy-Lax approximation by introducing local field effects (FL-LFC) assuming the "hole" pair distribution function $g(r)$ mentioned above. This new approximation takes the following form,

$$n_{eff}^{FL-LFC} = n_m \sqrt{1 + 3i\frac{f}{(ka)^3}S(0)\left\{1 + \frac{\tilde{\epsilon} - 1}{3}\left(1 - i\frac{16}{3}k^3b^3\right)\right\}}, \quad (3)$$

In Fig. 2 we present some predictions by the mentioned approximations.

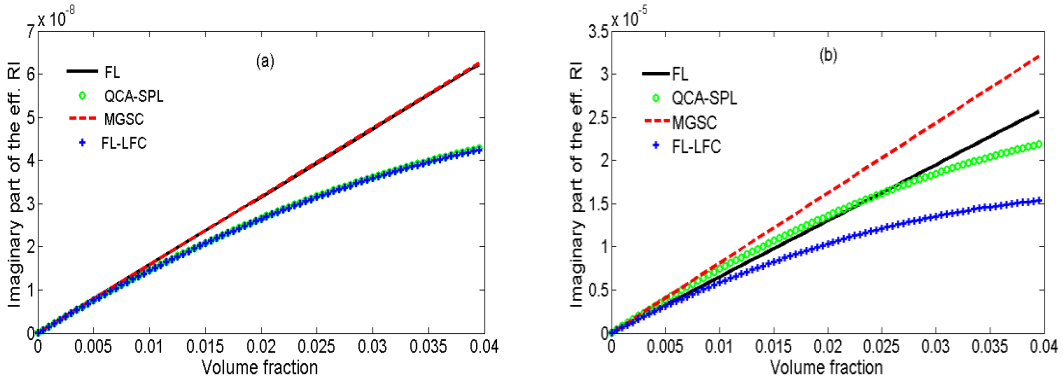

Figure 2. Plots of the imaginary part of the effective refractive index as a function of the particles volume concentration, f, predicted by Eqs. (1)-(4) for particles of radius of (a) 5 nm and (b) 40 nm. The refractive indices of the surrounding media and of the particles were supposed to be 1.33 and 1.4, respectively. For these graphs we chose $b = a$.

The graphs in Fig. 2a show that for particles of 5 nm radius and a volume fraction below 1% all approximations coincide with each other. For larger volume fractions the QCA-SPL and

the FL-LFC approximations deviates downwards from the FL and MGSC as expected due to the so-called dependent-scattering effects. However, for larger particles (Fig. 2b) the MGSC predicts a value of $\mathrm{Im}(n_{eff})$ larger than that predicted by the Foldy-Lax approximation, which is not physically possible. The FL-LFC still coincide with the FL approximation for very low particles' volume fraction and present the expected dependent-scattering effects.

Summary/Conclusions: In this work we introduce a new analytical approximation to the effective refractive index of nanofluids with a region of validity well beyond that of of the currently available approximations. It provides physically plausible predictions for particles' diameter up to about 100 nm and volume fractions up to about 5%.

References:

1. R. Taylor, S. Coulombe, T. Otanicar, P. Phelan, A. Gunawan, W. Lv, G. Rosengarten, R. Prasher and H. Tyagi, Small particles, big impacts: A review of the diverse applications of nanofluids, *J. Appl. Phys.* 113 (2013) 011301.
2. C. F. Bohren and D. R. Huffman, Absorption and Scattering of Light by Small Particles, Wiley-Interscience, 1983.
3. V. Merkel, Introduction to the Maxwell Garnett approximation: tutorial, J. Opt. Soc. Am. A 33 (2016) 1244-1256.
4. A. Sihvola, Electromagnetic Mixing Formulas and Applications, The Institution of Engineering and Technology, London UK, 1999.
5. Ari Sihvola and Reena Sharma, Scattering corrections for Maxwell Garnett mixing rule, Mocrowave and Optical Technology Letters 22 (4) (1999) 229-231.
6. C. A. Guérin, P. Mallet, A. Sentenac, Effective-medium theory for finite-size aggregates, J.Opt. Soc. Am. A 23 (2) (2006) 349-358.
7. L. Tsang, J.A. Kong, Theory of Microwave Remote Sensing, Wiley Series in Remote Sensing, Wiley, New York, 1985.
8. R. Márquez-Islas, A. García-Valenzuela, On the extinction coefficient of light in non-absorbing nanoparticle suspensions, *Applied Optics* 57 (13) (2018) 3390-3394.
9. A. García-Valenzuela, R. Márquez-Islas, R. G. Barrera, "Reducing light-scattering losses in nanocolloids by increasing average inter-particle distance", *Applied Physics A*, 123 (2017) 84.
10. M. Lax, Multiple scattering of waves. Rev. Mod. Phys. 23 (4) (1951) 287–310.

1st International Conference on Nanofluids (ICNf2019)
2nd European Symposium on Nanofluids (ESNf2019)
26-28 June 2019, Castelló, Spain

Effect of Preparation Method on the Wettability of Molten Salt Nanofluids

A. Anagnostopoulos[1*], U. Nithiyanantham[2], M.E. Navarro[1], Y. Grosu[2], S. Fereres[3] A. Faik[2], Y. Ding[1]

[1] *PhD A. Anagnostopoulos, Dr. M. E. Navarro, Prof. Y. Ding, Birmingham Centre for Energy Storage & School of Chemical Engineering, University of Birmingham, Birmingham B15 2TT, United Kingdom.*

[2] *PhD U. Nithiyanantham, Dr. Y. Grosu, Dr. A. Faik, CIC Energigune, Albert Einstein 48, 01510 Miñano (Álava), Spain*

[3] *Dr. S. Fereres, Abengoa, Calle Energia Solar 1, 41014 Sevilla, Spain*

[*]A. Anagnostopoulos: axa1217@student.bham.ac.uk

Keywords: solar energy, molten salt, nanofluid, preparation, contact angle

Abstract: Molten nitrate salts are the most common energy storage materials in concentrated solar power plants, with secondary applications as heat transfer fluids. Metal oxide nanoparticles are frequently suspended in molten salts to improve their thermal properties. Molten salt nanofluids are typically prepared by triple step method. An alternative method is the physical shaking method. In this study, the effect of the preparation methods on the wettability of molten salt nanofluid is investigated. It has been found that the contact angle of the base salt is similar in both preparation methods, in the absence of nanoparticles. However, the addition of nanoparticles has a significant impact on the wettability of the molten salt. The impact on the contact angle, is more prevalent in the second method.

Introduction/Background: Renewable energy technologies are key in solving the global energy crisis. In terms of power generation, solar energy is most commonly utilized through concentrated solar power (CSP) technologies [1]. Molten salts are the most common energy storage materials in CSP plants, with secondary applications as heat transfer fluids mainly due to their large operating temperature range and thermal stability [2]. However, they suffer from poor thermal properties. The addition of NPs can increase the thermal properties of the base fluid. For this reason, metal oxide nanoparticles (NPs) are suspended in the molten salts, to formulate molten salt nanofluids (NFs).

Typically, NFs are prepared by wet method, which has a long processing time, requires high ultrasonication power and is difficult to scale-up making it less feasible for large scale applications [3,4]. An alternative is the dry method with a shorter preparation time, ease of scale up, simplicity and reproducibility and purity control [4].

In this work a preliminary investigation on the effect of NPs and preparation method addition on the CA of the eutectic molten salt is conducted.

Materials and Methods: 51% $NaNO_3$- 49% KNO_3, is the material used for the measurements presented in this study. Amorphous SiO_2 NPs with 12 nm mean average diameter are suspended in the nanofluids. The salts used to compare the effect of the preparation method in the base case are purchased from Sigma Aldrich. In the NFs case, the wet method samples are prepared with Sigma Aldrich salts, while the dry ones with SQM. All individual materials have a purity >99.9%. The eutectic molten salt is synthesized by aqueous (wet) and non-aqueous (dry) method. In the wet method the salt is sonicated in the water and then dried in an oven at 105 °C. The second approach involves the mixture and static melting of the two independent salts. The nanofluid is synthesized using the three-step (wet) method and the dynamic shaking (dry) method [4,5]. In the wet method the nanoparticles are firstly sonicated in deionized water for 90 min, after which the salt is added, and a second sonication process occurs 180 min. The resulting solution is dried in the oven at 105 °C. In the second method, the NPs and the molten salt is added in an aluminium bottle, which is placed in a ball mill instrument. The mixture is then shaken up for 15 minutes to obtain the molten salt nanofluids. Dispersion and stability is studied for both methods. For the dry method a visual observation found that after 24 hours at 390 °C SiO_2 nanoparticles are floating on the surface. The mean NP's diameter is measured by Dynamic light scattering in the wet method and found to stabilize after 1h with a mean diameter of 1106 nm. The KRUSS HT-2 Contact Angle is used to perform the CA measurements. All CA measurements are conducted in air atmosphere, with a 2 °C/min heating rate up to the molten salt decomposition temperature or until complete wetting. The presented CA values are the average of 3 measurements. CA values dispersion is subject to several factors [6], where surface roughness and drop dimension are the most prevalent. To minimize their effect, a sample preparation protocol is followed. The salt eutectic powder was weighed, then milled and afterwards compressed at 40 MPa for 3 min in a 4 mm diameter round compression dye, to form identical dimension pellets of 0.1g. To minimize the impact of surface roughness, measurements are conducted on an alumina (Al_2O_3) substrate (30 mm x 30 mm x 10 mm), which roughness was measured before and after

each measurement using an EPS Interferometer. The surface roughness is found to have constant value of S=0.346±0.2 μm.

Discussion and Results: CA measurements are conducted on samples prepared with dry and wet method in the absence of NPs. No significant difference is observed between the CA of the two set of tests. Both present a CA linear reduction with the increase in temperature. Furthermore, also they are completely wetted at similar temperatures, 370 and 380 °C respectively (Fig. 1).

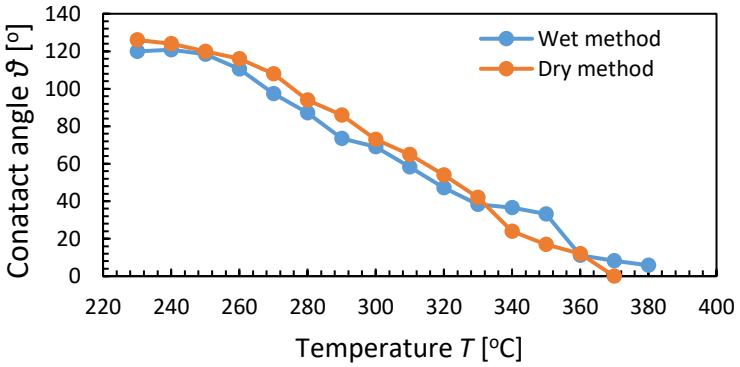

Figure 1. Effect of preparation method on the CA of the molten salt eutectic

NPs addition significantly affects the CA of the base salt in both cases. A liquid evidence to have a good wettability with a specific surface when its CA is <90°. It can be seen that in the base fluid case, the transition from poor to good wettability occurs around 280 °C (Fig.1). When NPs are added, the transition point is shifted to higher temperatures (Fig.2). This is observed in both NP formulation methods. In the wet method, the nanofluid wets the surface completely at 390 °C. In the dry one, the nanofluid does not achieve a complete wetting even at 450 °C. Furthermore, in the first case the salt retains the form of a liquid drop, while in the dry method, it initially forms a sessile drop, but at higher temperatures it presents a structural behavior similar to that of a composite material. Further research related to homogeneity and distribution of the NPs is required to provide a sufficient answer to this behavior.

1st International Conference on Nanofluids (ICNf2019)
2nd European Symposium on Nanofluids (ESNf2019)
26-28 June 2019, Castelló, Spain

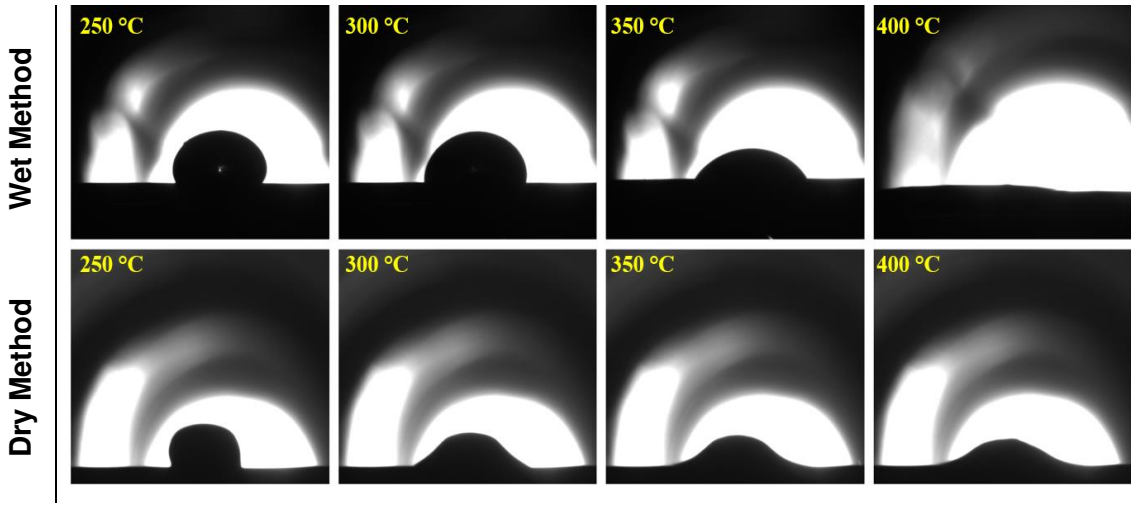

Figure 2. Effect of NPs addition and preparation method on the CA of the molten salt eutectic

Summary/Conclusions: Molten salts are used extensively as energy storage materials in CSP plants. Nanoparticles are frequently dispersed in molten salts to enhance their thermal properties. In this study the effect of the preparation method on the wettability of molten salt nanofluids is investigated. CA measurements are conducted for the eutectic salt with and without SiO_2-NPs, prepared both by wet and dry method. It can be seen that in the base fluid case, both preparation methods lead to a similar wetting behaviour. However, in the presence of silica NPs the CA of the molten salt nanofluid is increased. The effect of NPs on the CA is more prevalent in the case of the dry method. In both cases the transition point from poor to good wettability is shifted at higher temperatures. In the wet method the nanofluid is completely wetted at 390 °C, but in the dry method the complete wetting does not occur even at 450 °C. Further analysis is required to accurately profile the effect of the preparation method on the wetting behavior of the molten salt nanofluids.

Acknowledgments: The authors acknowledge the finance support from Engineering and Physical Sciences Research Council and the European Cooperation in Science and Technology, COST Action CA15119 for the funding of a short-term scientific mission (STSM), between CIC Energigune and University of Birmingham Center for Energy storage.

References:

1. B. Sørensen, *Renewable Energy: Physics, Engineering, Environmental Impacts, Economics and Planning: Fifth Edition*. 2017.

2. Z. Jiang *et al.*, “Novel key parameter for eutectic nitrates based nanofluids selection for concentrating solar power (CSP) system,” *Appl. Energy*, vol. 235, pp. 529–542, 2019.
3. P. K. Madathil *et al.*, “Preparation and characterization of molten salt based nanothermic fluids with enhanced thermal properties for solar thermal applications,” *Appl. Therm. Eng.*, vol. 109, pp. 901–905, 2016.
4. U. Nithiyanantham, Y. Grosu, L. González, A. Zaki, J. M. Igartua and A. Faik, Shape effect of Al_2O_3 nanoparticles on the thermophysical properties and viscosity of molten salt nanofluids for TES application. (*submitted to Solar Energy Materials and Solar Cells*)
5. N. A. Che Sidik, M. Mahmud Jamil, W. M. A. Aziz Japar, and I. Muhammad Adamu, “A review on preparation methods, stability and applications of hybrid nanofluids,” *Renewable and Sustainable Energy Reviews*, vol. 80. pp. 1112–1122, 2017.
6. Yuehua Yuan and T. Randall, *Surface science techniques*, vol. 51, no. 1. 2013.

1st International Conference on Nanofluids (ICNf2019)
2nd European Symposium on Nanofluids (ESNf2019)
26-28 June 2019, Castelló, Spain

Graphene-based nanofluids: structural quality of graphene vs. dispersion quality

N. Berrada[1*], A. Desforges[1], J. Ghanbaja[1], J. Gleize[2], D. Bégin[3], P. Estellé[4], S. Hamze[4], B. Vigolo[1]

[1]Institut Jean Lamour, CNRS-University of Lorraine, BP 70239, 54000 Nancy, France

[2]Laboratoire de Chimie et Physique Approche Multi-échelles des Milieux Complexes, University of Lorraine, 57000 Metz, France

[3] Institut de Chimie et Procédés pour l'Energie, l'Environnement et la Santé, CNRS-University of Strasbourg, 67087 Strasbourg, France

[4] Univ Rennes, LGCGM, EA3913, 35704 Rennes, France

[*]Corresponding author: nawal.berrada@univ-lorraine.fr

Keywords: Graphene-based nanofluids, Functionalization, Surface modification, Dispersion

Abstract: Graphene-based thermal nanofluids, innovative fluids where a small amount of nanoparticles is sufficient to significantly increase the conductivity of a solvent, have reached a great interest in recent years. Nevertheless, high aggregation tendency of graphene due to its hydrophobicity is one of the major issues to use it for applications. In this paper, various strategies to chemically modify graphene in order to overcome the dispersion difficulty are investigated. Several kinds of graphenic materials such as graphene oxide (GO), reduced graphene oxide (rGO) and high-quality few-layer graphene are synthesized and studied. Thanks to their in-depth characterization and to the preparation of graphene-based nanofluids, their ability to be dispersed will be discussed with respects to the respective defect amount within the graphene structure; structural damaging being prejudicial to thermal properties.

Background: By its theoretical unique and recorded intrinsic properties, single-layer high quality graphene is an impressive material. Indeed, it is the thinnest, the lightest and the strongest compound (between 100-300 times stronger than steel) known to human to date. It is also the best conductor of heat (5 $kW.m^{-1}.K^{-1}$) [1] at room temperature and the best conductor of electricity (a million times higher than copper) [2] due to the high electron mobility of its sp^2 network. Thus, this impressive new material has an application potential in a lot of fields, for instance, energy, medicine, electronics, mechanics… However, at the macroscopic scale and particularly in aqueous media, graphene sheets

being hydrophobic, suffer from aggregation and restacking, which leads to really decrease performances and to hinder their development. Thus, despite the well suitable characteristics of graphene which make it a new ideal nanomaterial for thermal nanofluids, dispersion of graphene in water is difficult. The strong van der Waals attraction between graphene nanosheets can be either counterbalanced by adding surfactant or by covalently grafting functional groups to the graphene surface. Chemical modification of graphene for nanofluid preparation has attracted much attention recently. It remains quite challenging since preserving high thermal properties requires to limit damaging of the sp^2 carbon network of graphene inevitably attacked through functionalization. We have investigated preparation of graphene-based nanofluids with different kinds of graphenic materials usually encountered in literature, including high quality few-layer graphene (HQ-FLG), graphene oxide (GO) and reduced GO (rGO). We have synthesized these materials which were eventually chemically modified. We will present their characterization by several complementary techniques (Scanning and Transmission Electron Microscopy (SEM and TEM), Thermogravimetric Analysis (TGA) and TGA coupled with Mass spectrometry (TGA-MS), Raman spectroscopy, InfraRed Spectroscopy) in order to determine the nature of the functional groups, the functionalisation rate and the amount of defects. Ability of each kind of graphenic material to be dispersed in water and in Tyfocor® LS base fluid in function of its defect level will be evaluated. These results will be put into perspective with the thermal properties of the prepared nanofluids.

Discussion and Results: The well-known way of increasing hydrophilicity is to oxidize graphite by the Hummers' method [3] in order to synthesize GO. This graphene-based material contains numerous hydroxyl and epoxy groups which lead to increase hydrophilicity and allow GO to be well dispersed in aqueous solutions [4]. However, adding functional groups on the surface of a graphenic compound decreases the number of sp^2 carbon hybridization in favour of sp^3 one. Thus, the structure of the conjugated network is disrupted and the thermal conductivity is expected to be consequently lower compared to that of HQ-FLG. A chemical reduction of the oxygen-containing groups of GO by reducing agents such as hydrazine [5] or sodium borohydride [6] to obtain rGO is reported to help in recovering this property (Figure 1). In our work, we have prepared GO, rGO and investigated both non-covalent and covalent functionalization of HQ-FLG.

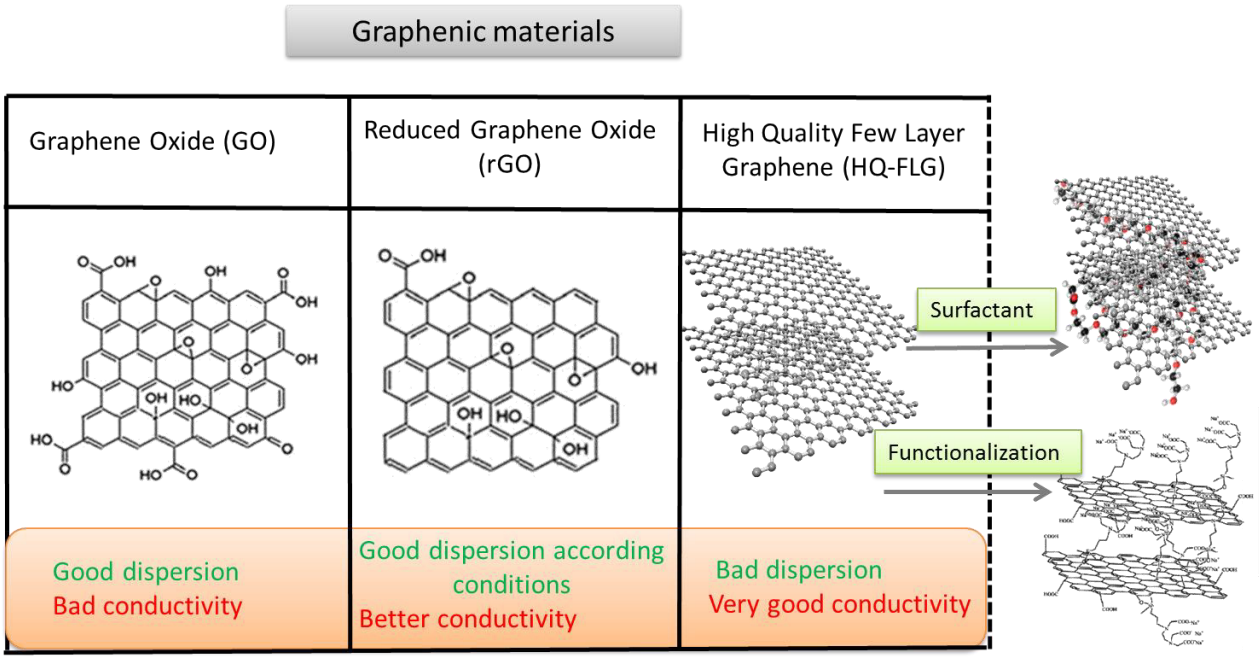

Figure 1. Different types of graphenic materials and their respective properties

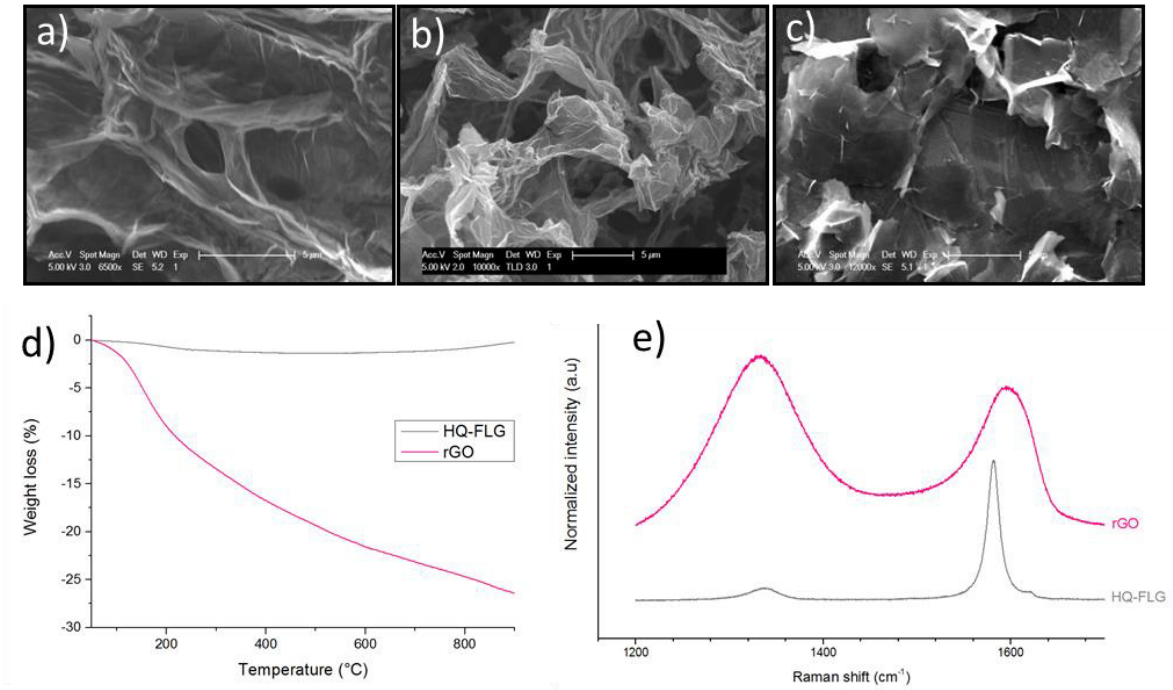

Figure 2. Typical SEM images of GO (a), rGO (b) and HQ-FLG (c). Thermograms recorded by TGA under helium with a temperature ramp of 5°C/min from 20 °C to 900 °C (d) and Raman spectra (incident wavelength 633 nm) (e) of HQ-FLG and rGO

SEM images of GO, rGO and HQ-FLG (Figure 2 a, b and c) reveal that for all these graphenic materials the thickness of sheets is quite similar.

TGA realized under helium, an inert gas towards carbon, shows thermograms strongly different for rGO and HQ-FLG (Figure 2 d). The sample weight loss is due to desorption of the grafted functional groups. Compared to HQ-FLG, rGO loses almost 30 wt. % of its weight meaning that, contrary to the generally accepted idea, rGO network is far from being completely restored. This assessment is confirmed by the Raman spectra showing that the band sensitive to the structural defects (D band: 1332 cm^{-1}) is more pronounced for rGO than for HQ-FLG (Figure 2 e).

Summary: Graphene can be found under various forms that have very different characteristics leading to a wide range of properties. Even if their morphological properties are quite similar, the structural and chemical properties of the graphenic materials usually encountered are strongly different. They can have a dramatic impact on their dispersion ability in aqueous media and consequently on the nanofluid properties.

References:

1. Zhu, Y., Murali, S., Cai, W., Li, X., Suk, J.W., Potts, J.R., Ruoff, R.S.: Graphene and Graphene Oxide: Synthesis, Properties, and Applications. Adv. Mater. 22, 3906–3924 (2010).

2. Novoselov, K.S., Fal'ko, V.I., Colombo, L., Gellert, P.R., Schwab, M.G., Kim, K.: A roadmap for graphene. Nature. 490, 192–200 (2012).

3. Dreyer, D.R., Park, S., Bielawski, C.W., Ruoff, R.S.: The chemistry of graphene oxide. Chem. Soc. Rev. 39, 228–240 (2009).

4. Bansal, P., Panwar, A.S., Bahadur, D.: Molecular-Level Insights into the Stability of Aqueous Graphene Oxide Dispersions. The Journal of Physical Chemistry C. 121, 9847–9859 (2017).

5. Si, Y., Samulski, E.T.: Synthesis of Water Soluble Graphene. Nano Letters. 8, 1679–1682 (2008).

6. Shin, H.-J., Kim, K.K., Benayad, A., Yoon, S.-M., Park, H.K., Jung, I.-S., Jin, M.H., Jeong, H.-K., Kim, J.M., Choi, J.-Y., Lee, Y.H.: Efficient Reduction of Graphite Oxide by Sodium Borohydride and Its Effect on Electrical Conductance. Adv. Funct. Mater. 19, 1987–1992 (2009).

1st International Conference on Nanofluids (ICNf2019)
2nd European Symposium on Nanofluids (ESNf2019)
26-28 June 2019, Castelló, Spain

Low Temperature Viscosity of Nanofluids with Water:Ethylene Glycol Base Fluid

A. Banisharif[1,2], M. Aghajani[1*], S. Van Vaerenbergh[2], P. Estellé[3*] and A. Rashidi[4]

[1]Gas Engineering Department, Petroleum University of Technology, Ahwaz, Iran

[2]Chimie-Physique (MRC), Université Libre de Bruxelles, 1050, Brussels, Belgium

[3]Univ Rennes 1, LGCGM, EA3913, 35704 Rennes, France

[4]Nanotechnology Research Centre, Research Institute of Petroleum Industry (RIPI), Tehran, Iran

[*]Corresponding author: patrice.estelle@univ-rennes1.fr m.aghajani@put.ac.ir

Keywords: Viscosity, Nanofluid, Low temperature, Rheological Behaviour.

Abstract: Experimental investigations of the dynamic viscosity of stable nanofluids water EG based are studied. For all temperatures, except for lower ones, a Newtonian behaviour is reported in the range -20°C to 20°C. No significant increase in viscosity was noticed for MWCNT nanofluids while a decrease in viscosity with nanoparticle content is observed for Cu and Fe_3O_4 nanofluids.

Introduction: Over the past decade, nanofluid transport properties have been extensively investigated. This has been driven by the use of nanosized systems for various applications. The viscosity of nanofluids is very important, as their flow properties are strongly linked to the potential application of nanofluids [1]. However, most researches have been performed at intermediate and high temperatures in particular to enhance the rate of heat transfer in heating applications. Because of the lack of nanofluid studies at low temperatures (sub-zero), the use of nanofluids remains debatable and hinders their marketing in the cooling industrial applications [2]. Aladag et al. [3] studied the viscosity of Al_2O_3 and CNT water-based nanofluids at low concentration and low temperatures and its changes caused by decreasing temperature and shearing time. Experiments also revealed that, depending on shear rate, the nanofluids behaved as Newtonian or non-Newtonian fluids [3]. The ability to lower the freezing point of water, low volatility, and relatively low corrosivity of the ethylene glycol make it a suitable adding fluid to use as aqueous freezing point depressants and heat transfer media in cooling systems [4]. In the literature, few rheological data at low temperature for such nanofluids is currently available. To expand its application in cold conditions, researching and reporting on the rheology of these nanofluids are very

important. In order to establish their applicability for use as a heat transfer fluid in the cold regions, Kulkarni et al. [4-5] investigated the rheological properties of ethylene and propylene-glycol and water mixtures 60:40 (by weight) with different volumetric percentages (0% to 6.12%) of copper oxide nanoparticles (CuO) over temperatures ranging from -35°C to 50°C. Naik et al. [6] measured the viscosity of the propylene glycol-water (60:40 by weight) mixture and derived nanofluids by adding different volume concentration (from 0.025 to 1.2%) of CuO nanoparticles at temperatures between -15°C and 30°C. They reported that viscosity increases exponentially with the decrease of temperature. In this work, the rheological behaviour of Water-Ethylene Glycol (WEG 50:50 by volume at 20ºC) mixture nanofluids is investigated at temperatures between -20ºC and 20ºC to verify the performance of such nanofluids through experimental studies in the cold condition.

Experimental Method: Several types of nanofluids (NFs) are prepared by selecting among metallic or non-metallic particles in given fluids. Copper (Cu) as metallic nanoparticles, Fe_3O_4 as metal oxides and MWCNT as non-metallic nanoparticles are selected for preparing nanofluids. The experimental study is performed to investigate the viscosity of Cu, Fe_3O_4, MWCNT nanoparticles suspended into W:EG base fluid over temperatures ranging from -20°C to 20°C with different volume concentrations of nanoparticles (0.01, 0.05 & 0.1%). The amount of 0.08wt% in Sodium Dodecyl Sulfonate (SDS), 0.2wt% in Chitosan (CH), and mixture of 0.2vol% in Oleic Acid (OA) and 0.2wt% in SDS are used to disperse and stabilize MWCNT, Cu, and Fe_3O_4 nanoparticles into base fluid, respectively. A series of W:EG based NFs (0.1 vol%) is prepared by dispersing a known weight of nanoparticles in the base fluid using ultrasonic mixing for 15 min. The NFs with 0.05 vol% and 0.01 vol% NPs are produced by diluting the 0.1 vol% NF with a proper amount of the base fluid. Rheological measurements of nanofluid and base fluid samples are carried out with a stress-controlled rheometer (Malvern Kinexus Pro, UK) with a cone-plate geometry with a diameter of 60 mm, a cone angle of 1° and a gap of 0.03 mm. The temperature is controlled using a Peltier temperature control device that is combined with a thermal bath circulator to reduce the temperature. Tests under the steady-state condition and imposed shear stress were performed to cover shear rate range from 10 to 1000 s^{-1} with at least 10 points per decade. The estimated uncertainty of the dynamic viscosities is previously reported less than 4% within the studied shear rate [7].

Discussion and Results: The dynamic viscosity of water-ethylene glycol with surfactants and nanoparticles is shown in Figure 1 and 2. An increase in viscosity is initially noted by

decreasing temperature for WEG, surfactant-base fluids, and nanofluids, but a corresponding reduction is occurred in the viscosity of nanofluid samples compared to their surfactant-base fluids. Nanostructures at concentration 0.1 vol.% in the surfactant-base fluids are observed to exhibit Newtonian behaviour in the studied shear rates range except Fe_3O_4 and Cu nanoparticles at low temperature (-10°C and especially -20°C) as well as their base fluid with OA and CH surfactants, respectively.

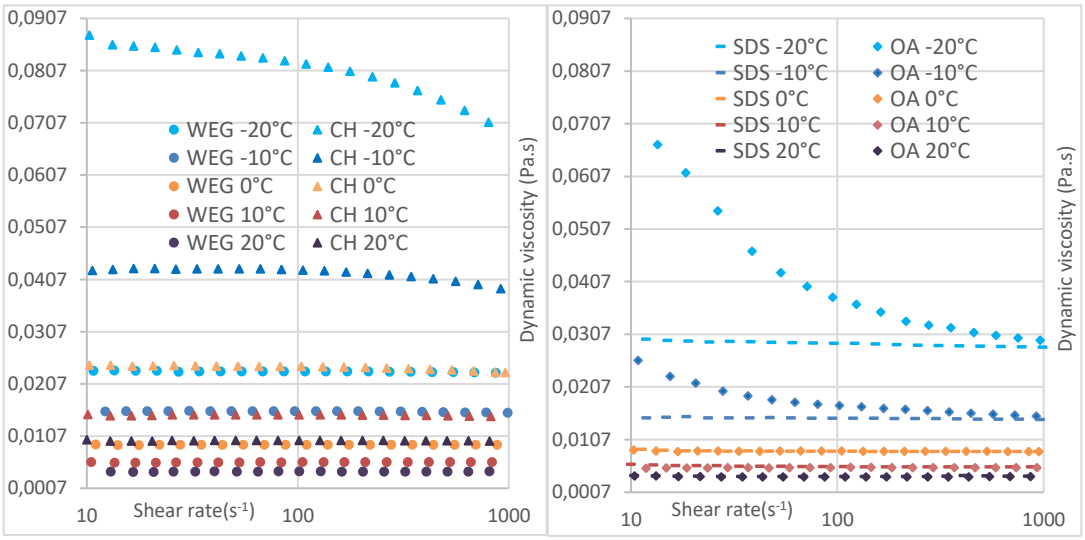

Figure 1. Flow curves of Base fluid Water-Ethylene Glycol (WEG) at different temperatures and with different surfactants.

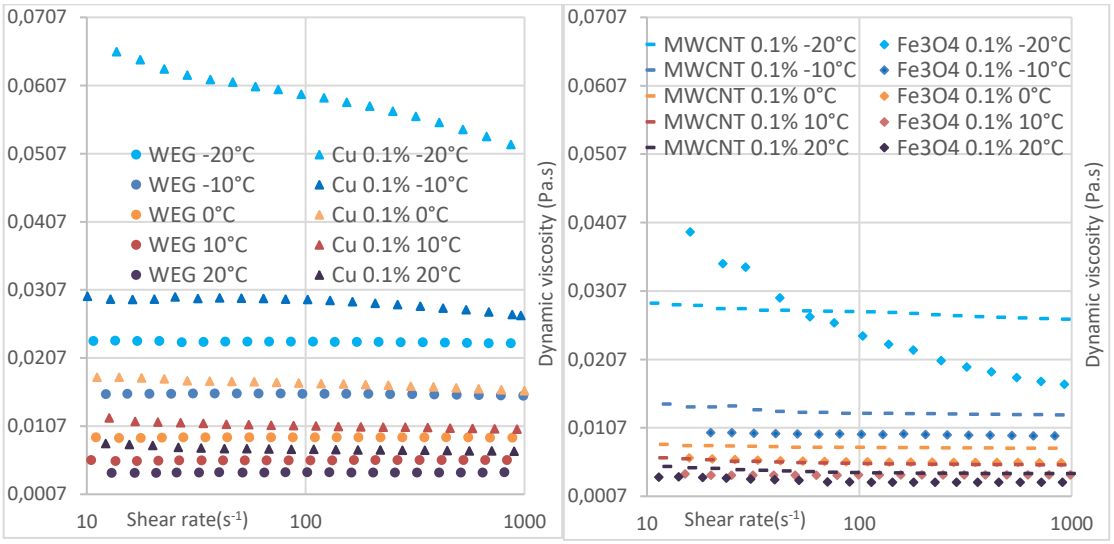

Figure 2. Flow curves of nanofluids

All viscosity data at high shear rate are compiled in Figure 3. At lower temperatures, the viscosity is increased more quickly than higher in agreement with [4-6]. There is no significant difference between MWCNT and the base fluid except at the lower temperature. The viscosity is reduced significantly by adding nanoparticles to surfactant-base fluids for both Cu and Fe_3O_4 nanofluids at all temperatures. For 0.1 vol% of Fe_3O_4 viscosity is lower

than the mixture of water and ethylene glycol, and also, the viscosity reduction is increased at the lower temperature. Such a behaviour should be attributed to the lubricating effect of nanoparticles as reported previously by Phouc et al. [8].

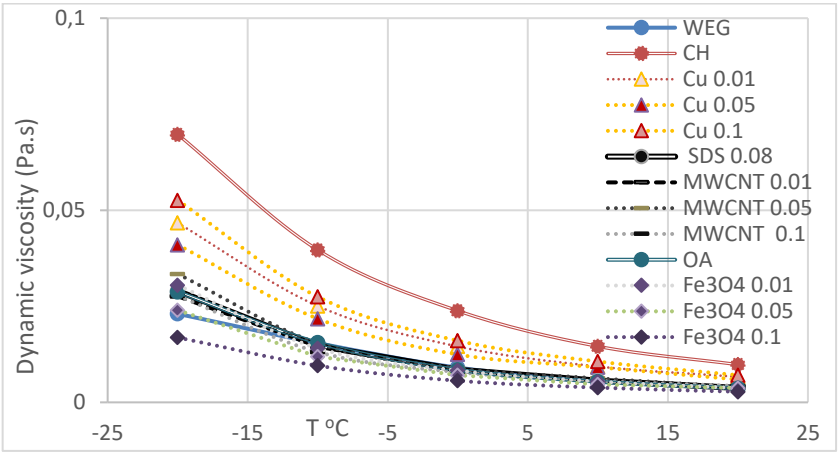

Figure 3. Viscosity of nanofluids against temperature

Conclusions: An experimental study is conducted on the dynamic viscosity of Cu, Fe_3O_4, and MWCNT nanofluids at low concentration stabilized by chitosan, oleic acid and SDS surfactants in a water ethylene glycol mixture. A Newtonian behaviour is observed for all nanofluids in the temperature range -20/+20°C except for the lowest one. No significant increase in viscosity was noticed for MWCNT nanofluids while a decrease in viscosity is observed for Cu and Fe_3O_4 nanofluids that is interesting for practical applications.

Acknowledgements: A. Banisharif acknowledges EU COST for the STMS grant ref. COST-STSM CA15119-42469 as well as the Iran Ministries of Oil and Science Research and Technology.

References:

1. V.Y. Rudyak, Viscosity of nanofluids. why it is not described by the classical theories. *Advances in Nanoparticles*, *02*(03) (2013)266–279.
2. G. Sekrani, and S. Poncet, Ethylene- and propylene-glycol based nanofluids: a literature review on their thermophysical properties and thermal performances. *Applied Sciences*, *8*(11) (2018) 2311.
3. B. Aladag, S. Halelfadl, et al., Experimental investigations of the viscosity of nanofluids at low temperatures. *Applied Energy*, 97, (2012) 876–880.
4. D.P. Kulkarni, D.K. Das, and S.L. Patil, Effect of temperature on rheological properties of copper oxide nanoparticles dispersed in propylene glycol and water mixture. *Journal of Nanoscience and Nanotechnology*, 7(7) (2007) 2318–2322.
5. P.K. Namburu, D.P. Kulkarni, D. Misra, and D.K. Das, Viscosity of copper oxide nanoparticles dispersed in ethylene glycol and water mixture. *Experimental Thermal and Fluid Science*, 32(2) (2007) 397–402.

6. M.T. Naik, G.R. Janardhana, et al., Experimental investigation into rheological property of copper oxide nanoparticles suspended in propylene glycol-water based fluids. *Journal of Engineering and Applied Sciences*, 5(6) (2010) 29–34.
7. D. Cabaleiro, P. Estellé, H. Navas, A. Desforges, and B. Vigolo, Dynamic viscosity and surface tension of stable graphene oxide and reduced graphene oxide aqueous nanofluids. *Journal of Nanofluids*, 7(6) (2018) 1081–1088.
8. T.X. Phuoc, M. Massoudi, And R. Chen, Viscosity and thermal conductivity of nanofluids containing multi-walled carbon nanotubes stabilized by chitosan. *International Journal of Thermal Sciences*, 50(1) (2011) 12–18.

1st International Conference on Nanofluids (ICNf2019)
2nd European Symposium on Nanofluids (ESNf2019)
26-28 June 2019, Castelló, Spain

Immunity Enhancement to Electrochemical Effect in 3omega Hot Wire Method for Thermal Conductivity Measurement of Nanofluids

I. Ates[1*], A. Turgut[2], L. Cetin[3] and M. Chirtoc[4]

[1]Department of Mechatronics Engineering, The Graduate School of Natural and Applied Sciences, Dokuz Eylül University, Buca, İzmir, Turkey.

[2]Department of Mechanical Engineering, Dokuz Eylül University, Buca, İzmir, Turkey.

[3]Department of Mechatronics Engineering, İzmir Kâtip Çelebi University, Çiğli, İzmir, Turkey.

[4]Thermophysics Lab., GRESPI, Université de Reims Champagne Ardenne URCA, Moulin de la Housse, Reims, France

[*]Corresponding author: iismetates@gmail.com

Keywords: Thermal Conductivity, 3omega Method, Electrochemical Effect, Hot Wire

Abstract: Thermal conductivity enhancement of nanofluids has been controversial for the last two decades due to contradicting results which could be attributed to several factors. A recent study has shown that electrochemical (EC) activity between measurement probe and nanofluid sample in some cases causes an error on thermal conductivity measurements in hot wire method. To use an electrically insulated hot wire was suggested as a solution to avoid this effect. The present contribution aims at enhancing immunity to EC activity and eliminating its error by using a Printed Circuit Board (PCB) based hot wire probe which has different insulated parts of prongs that was designed and tested in this focus. Thanks to fully insulated prongs of the probe, without insulating the hot wire, EC activity impact to thermal signals has been reduced drastically.

Introduction/Background: Thermal conductivity has been one of the most investigated property of nanofluids (Nfs), for the last two decades. Published studies show that there are still contradictions on this issue [1]. These contradicting results could be attributed to several factors [2,3]. A recent study [4] performed thermal conductivity measurements by a 3ω method and showed that electrochemical (EC) activity between measurement probe and Nf sample in some cases causes error which could be crucial on measured

thermal conductivity value of the sample. It is explained that for some Nfs, EC activity between bare parts of prongs of the probe that immersed in Nfs causes a nonlinear electrical impedance. This generates a disturbance voltage at higher harmonics when a potential is applied to the prongs of probe that act as electrodes. Theoretical background and practical implementation of the 3ω method for measurement of thermophysical properties of Nfs could be found in ref. [5] in details. When excitation current is applied to the hot wire, total thermal signal (V_{Th}) includes a small thermal component at 3ω dependent on the temperature θ_0 around the wire and temperature coefficient α, as given in Eq. 1[4]:

$$V_{Th} = V_0[sin(\omega t) - (1/2)\alpha\theta_0 sin(3\omega t - \varphi)] \quad (1)$$

During the measurement, due to the EC activity an EC signal is also generated:

$$V_{EC} = V_0\{sin(\omega t) + (1/2)r\beta V_0[1 - cos(2\omega t) - \beta V_0 sin(3\omega t)]\} \quad (2)$$

where $r=R_0/Z_0$ is ratio of the resistance of hot wire to the EC impedance. βV_0 is a nonlinearity term which depends directly on the ratio between 3rd and 2nd harmonics. V_0 is an applied voltage to the hot wire. Eq. 2 derives from equivalent resistance of R_0 and Z_0. Total EC signal includes component at 3ω, as seen in Eq. 2.

Eventually, total measured signal at 3rd harmonic includes both thermal and EC signals:

$$V_3\omega_{Tot} = V_3\omega_{Th} + V_3\omega_{EC} = -(1/2)[\alpha\theta_0 + r\beta^2 V_0^2]V_0 sin(3\omega t) \quad (3)$$

As seen from Eq. 3, the EC activity component might surpass the thermal component.

Discussion and Results: EC activity between the prongs and Nf sample was observed via two types of measurement setups. Nonlinearity setup (Fig.1a) is used for the detection of 2ω and 3ω signals related with EC activity. On/Off test setup (Fig.1b), is used for the observation of EC activity and its error influences on thermal conductivity measurement. When the switch in the system is set to On position, EC activity signal of the Nf is combined with thermal conductivity signal of the water as a base-fluid.

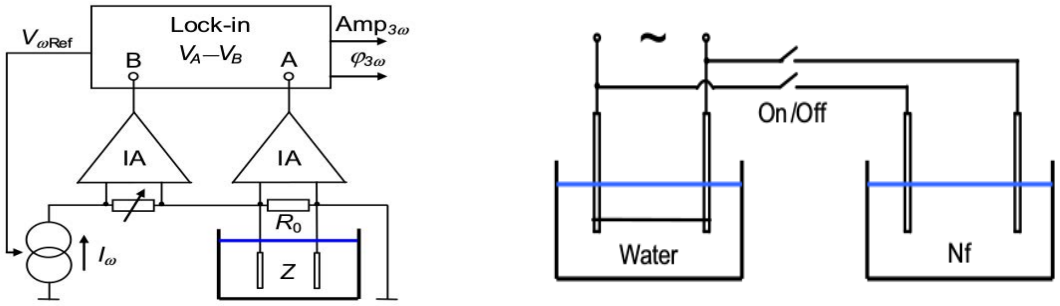

Figure 1. Nonlinearity detection setup(a), On/Off setup(b) [4]

Bare part of the probe decreases the EC impedance and so increases the EC activity. Effect of EC activity has been tested with bare prongs of electrode immersed in TiO_2 to show the influence clearly in a previous study [4]. In this scope, probe structure is important for eliminating the EC activity. Therefore, PCB based probes which have insulated prongs have been designed for optimization of immunity enhancement to the EC effect.

Totally, four types of probes were used in this study: Traditional probe (TP) has bare copper wire prongs, whereas PP, sdPP and isdPP are the PCB based probes and have insulated prongs. The difference between PP and sdPP is the diameter of solder pads on the prongs, respectively 1.93 mm and 1.01 mm. The last probe (isdPP) has fully insulated prongs including also the solder pads.

As given in Table 1, PP and sdPP increase the immunity to EC effects with increasing EC impedance and decreasing nonlinearity coefficient (β). The term $(R_0/Z_0)\beta^2V_0^2$ in Eq. 2 is defined as impact value of EC activity, and it is reduced in the 3 order of magnitude compared to the TP. However, as seen in Fig.2a, EC activity could not be suppressed completely and its effect has been still observed at On/Off test. This behaviour can be interpreted as the existence of the EC impedance on solder joints between the PCB and the hot wire. Therefore it is suggested to use improved version of sdPP, named as isdPP, for eliminating the observed shift on 3ω signal.

EC signals and characteristic of isdPP have been measured and given in Table1. EC impedance goes relatively to infinity (R_0/Z_0 goes to zero, where R_0=0.74Ω). Thus, impact value of EC activity has been reduced remarkably according to sdPP.

Table 1. EC Signals and Characteristic of TiO_2 Nf according to Probe Types

Probe type	EC Signals @ 1 Hz		EC Characteristic @ 1 Hz			
	2ω Amp(uV)	3ω Amp (uV)	Z_0 (kΩ)	V2ω /V3ω	β	Impact Value
TP	3.16	111.27	0.16	0.03	140.85	6.04E+00
PP	2.72	20.68	3.51	0.13	30.41	1.28E-02
sdPP	2.27	17.77	6.50	0.13	31.25	7.32E-03
isdPP	0.04	0.02	2.00E+04	2.06	1.94	9.17E-09

As shown in Fig.2a, On/Off test for error observation on TiO_2 Nf by using sdPP causes remarkable shift on signals. However, error ratio of EC effect is below 1% when isdPP is used (Fig.2b). EC effect of TiO_2 Nf can be suppressed remarkably with using isdPP.

Figure 2. EC effect on thermal 3ω signals in TiO_2 Nf: (a) sdPP and (b) isdPP

Summary/Conclusions: EC activity is related with hot wire probe design and prongs insulation. Improvement of the probe increases immunity to EC activity and it provides more accurate thermal conductivity measurement of Nfs. This study shows that fully insulated prongs of probe should be used to eliminate the error arising from EC characteristic of the Nfs. By using an improved probe, impact value of EC activity has been decreased below 0.1 μV level compared to 100 μV level of the traditional probe.

References:

1. M.H. Buschmann, R. Azizian, T. Kempe, J.E Juliá, R. Martínez-Cuenca, B. Sundén, Z. Wu, A. Seppälä and T. Ala-Nissila, Correct interpretation of nanofluid convective heat transfer, *International Journal of Thermal Sciences*, 129 (2018) 504-531.
2. G. Tertsinidou, M.J. Assael and W.A. Wakeham, The apparent thermal conductivity of liquids containing solid particles of nanometer dimensions: a critique, *International Journal of Thermophysics* 36 (2015) 1367-1395.

3. C.A Nieto de Castro, S.I Vieira, M.J. Lourenço, and S.M Murshed, Understanding Stability, Measurements, and Mechanisms of Thermal Conductivity of Nanofluids, *Journal of Nanofluids* 6 (2017) 804-811.
4. M. Chirtoc, J.F. Henry and N. Horny, Nonlinear electrochemical and electrokinetic effects in 3omega hot wire measurements of thermophysical properties of nanofluids, *Journal of Thermal Analysis and Calorimetry* (2018, online first) https://doi.org/10.1007/s10973-018-7807-5
5. A. Turgut, C. Sauter, M. Chirtoc, J.F. Henry, S Tavman, I. Tavman and J. Pelzl, AC hot wire measurement of thermophysical properties of nanofluids with 3ω method, *The European Physical Journal Special Topics*, 153 (2008) 349-352.

1st International Conference on Nanofluids (ICNf2019)
2nd European Symposium on Nanofluids (ESNf2019)
26-28 June 2019, Castelló, Spain

Challenges in the development of a database of thermophysical properties of nanofluids

M.E. Mondejar[1*], M. Regidor[1], G. Kontogeorgis[2] and F. Haglind[1]

[1]Department of Mechanical Engineering, Technical University of Denmark, Building 403, 2800 Kgs. Lyngby, Denmark

[2]Department of Chemical and Biochemical Engineering, Technical University of Denmark, Building 229, 2800 Kgs. Lyngby, Denmark

[*]Corresponding author: maemmo@mek.dtu.dk

Keywords: database, nanofluids, thermodynamic properties, transport properties.

Abstract: A comprehensive database of thermophysical properties of nanofluids composed of a base fluid and a single type of nanoparticle has been developed by collecting the available experimental data in published scientific literature. The database currently contains 5114 data records of thermophysical properties of nanofluids consisting of combinations of 12 base fluids and 18 nanoparticle types. The collected experimental data include a number of thermodynamic properties (i.e. density, heat capacity, vapor pressure) as well as transport properties (i.e. thermal conductivity, dynamic viscosity). The development process of the database and the faced challenges are described. Recommendations for reporting thermophysical properties of nanofluids are drawn, based on the current status of the available data.

Background: Since the introduction of the concept of nanofluids by Choi and Estman [1] in the early 90s as heat transfer fluids with substantially improved thermal properties, the research to explore their potential applications has increased exponentially. Over the last 10 years the number of scientific publications on nanofluids has multiplied by a factor of 20, being more than 1600 papers on nanofluids published only in 2018.

The properties which exhibit the most complex behavior and greatest interest for the scientific and engineering communities are their improved thermal conductivity [2] and their increased viscosity [3]. While the former brings up the attention on the potential use of nanofluids as heat transfer and/or working fluids, the later is of particular importance for the development of lubricants.

Despite the importance of an accurate determination of the thermal conductivity and dynamic viscosity of studied nanofluids, the experimental properties of similar systems

show large scatter of the property values [4,5]. A number of attempts have been made to develop correlations for the prediction of nanofluids' properties, accounting for the impact of different parameters (e.g. nanoparticle size, shape), but it has been observed that the developed correlations for thermal conductivity and dynamic viscosity perform well only for specific systems, or determined temperature ranges. Although a number of review papers have analyzed the thermophysical properties of nanofluids, covering specific types of nanofluids [6] or a broader group [7], a database gathering all the published experimental data of nanofluids is missing.

In order to overcome this gap in the field, a database collecting all of the published experimental data of thermophysical properties of nanofluids has been developed. The initial scope of the database focuses on nanofluids formed by a base fluid, and a single type of nanoparticle. Therefore, in this first stage of development of the database, hybrid nanofluids (i.e. containing more than one type of nanoparticle) or metal organic heat carriers (i.e. nanofluids containing metal organic frameworks) are not included. The considered thermophysical properties for which a high number of empirical data is available are the thermal conductivity (k), dynamic viscosity (μ), density (ρ), and isobaric heat capacity (c_p). Additionally, a few works analyzed the impact of nanoparticles in the vapor pressure (p_{sat}) of the base fluid, and its speed of sound (c). Because it is well known that some of these properties are sensitive to the nanoparticle shape and size, these data were also included in the database, if available in the sources.

Discussion and Results:

The developed database allows a comprehensive critical evaluation of the measured properties for selected base fluids, or nanoparticle material, and brings up insight on the significant scatter of some experimental data.

The development of this database provides two main contributions to the research in the field of thermophysical properties of nanofluids. First, during the data collection phase, the lack of a standard for the correct report of the experimental data of thermophysical properties of nanofluids has become patent. Second, the arrangement of all the experimental data available in the form of a database allows the quick comparison of existing data for different systems, thus facilitating the extraction of general conclusions.

With regards to the first contribution, it was observed that in many of the analyzed cases the reported data lack of enough quality as defined by Chirico et al. [8]. In this regard, the main inaccuracies found in the published literature on thermophysical properties of nanofluids are enumerated as follows by order of severity: i) experimental data reported only in the form of

plots (some with especial low resolution); ii) errors in the units of the reported values (especially in the case of dynamic viscosity); iii) describing the systems concentrations in volume basis; iv) incomplete definition of the characterized system (e.g. information on nanoparticle shape and dimensions missing); v) properties reported in the form of ratios with respect to the properties of the base fluid (in some cases for not well defined base fluids, such as lubrication oils).

The severity of the poor quality of some of the reported empirical data is here remarked, the thermophysical data of nanofluids can lead to overestimation of the thermal characteristics of the nanofluid, leading to under dimensioned heat exchangers, or failure in the design of lubricating systems.

When it comes to the second main contribution of the database, the organization and standardization of the available experimental data for different systems allows their straightforward comparison. This helps identifying trends on the impact of nanoparticles on different base fluids, recognizing discrepancies and outliers between data of the same or similar systems, or potential measurement errors. As an example of this feature, Figure 1 shows experimental dynamic viscosities of different authors versus temperature for the water/Al_2O_3 system. As it can be seen in Figure 1.a, the impact of small differences of the average diameter of the particles in the viscosity is not significant, but a larger difference in the nanoparticle size can have an important influence, even for low concentrations, as observed in Figure 1.b.

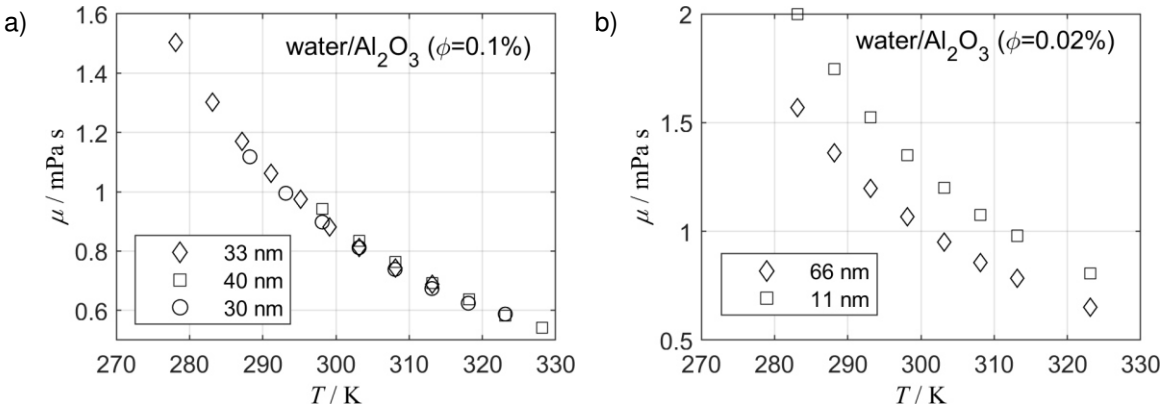

Figure 1. A comparison on the effect of particle size on dynamic viscosity.

Summary: A comprehensive database of experimental thermophysical property data of nanofluids consisting of a base fluid and a single type of nanoparticle has been developed. The database allows a comprehensive critical evaluation of the measured properties for

selected base fluids, nanoparticle material, or measurement conditions, and brings up insight on the significant scatter of some experimental data for specific similar systems.

The development of this database has been supported by the European Union's Horizon 2020 research and innovation programme with a Marie Skłodowska-Curie Fellowship under grant agreement No 704201 with the project NanoORC (see www.nanoorc.mek.dtu.dk).

References:

[1] Choi SUS, Eastman JA. Enhancing thermal conductivity of fluids with nanoparticles. ASME Int Mech Eng Congr Expo 1995;66:99–105. doi:10.1115/1.1532008.

[2] Buongiorno J, Venerus DC, Prabhat N, McKrell T, Townsend J, Christianson R, et al. A benchmark study on the thermal conductivity of nanofluids. J Appl Phys 2009;106. doi:10.1063/1.3245330.

[3] Venerus DC, Buongiorno J, Christianson R, Townsend J, Bang IC, Chen G, et al. Viscosity measurements on colloidal dispersions (nanofluids) for heat transfer applications. Appl Rheol 2010;20:2. doi:10.3933/ApplRheol-20-44582.

[4] Eggers JR, Kabelac S. Nanofluids revisited. Appl Therm Eng 2016;106:1114–26. doi:10.1016/j.applthermaleng.2016.06.100.

[5] Mondejar ME, Andreasen JG, Regidor M, Riva S, Kontogeorgis G, Persico G, et al. Prospects of the use of nanofluids as working fluids for organic Rankine cycle power systems. Energy Procedia 2017;129:160–7. doi:10.1016/j.egypro.2017.09.098.

[6] Mashali F, Languri EM, Davidson J, Kerns D, Johnson W, Nawaz K, et al. Thermo-physical properties of diamond nanofluids: A review. Int J Heat Mass Transf 2019;129:1123–35.

[7] Dey D, Kumar P, Samantaray S. A review of nanofluid preparation, stability, and thermo-physical properties. Heat Transf Res 2017;46:1413–42.

[8] Chirico RD, Frenkel M, Magee JW, Diky V, Muzny CD, Kazakov AF, et al. Improvement of quality in publication of experimental thermophysical property data: Challenges, assessment tools, global implementation, and online support. J Chem Eng Data 2013;58:2699–716. doi:10.1021/je400569s.

1st International Conference on Nanofluids (ICNf2019)
2nd European Symposium on Nanofluids (ESNf2019)
26-28 June 2019, Castelló, Spain

Stability and Thermal Conductivity of Carbon-based Aqueous Nanofluids

Tugce Fidan-Aslan[1], M. Batikan Kandemir[1], M. Ozgur Seydibeyoglu[1], Alpaslan Turgut[2] and Elif Alyamac-Seydibeyoglu[3*]

[1]Department of Materials Science and Engineering, Izmir Katip Celebi University, Cigli, 35620, Izmir, Turkey, [2]Department of Mechanical Engineering, Dokuz Eylul University, Buca, 35390, Izmir, Turkey, [3]Department of Petroleum and Natural Gas Engineering, Izmir Katip Celebi University, Cigli, 35620, Izmir, Turkey

[*]Corresponding author: elif.alyamac.seydibeyoglu@ikc.edu.tr

Keywords: Thermal conductivity, zeta potential, wettability, SWCNT, GNP.

Abstract: The aim of this study is to evaluate the stability, wettability, and thermal conductivity of nanofluids. Aqueous dispersions of single-walled carbon nanotubes (SWCNT) and graphene nanoplatelets (GNP) were successfully prepared through ultrasound technology in the presence of polyethylene glycol-polyhedral oligomeric silsesquioxane (PEG-POSS) as a stabilizer. Stability evaluations were carried out by Ultraviolet-Visible (UV-Vis) spectrophotometry and zeta potential measuring device (Zetasizer Nano). The contact angle values of dispersions were measured using the sessile drop method. The 3ω method was used for the determination of thermal conductivity of nanofluids. The highest zeta potential value was measured as -85.5 mV for 2.0 wt% SWCNT and 0.2 wt% PEG-POSS aqueous nanofluids. The 2.0 wt% GNP dispersion having a surface area 320 m^2/g, gave the highest thermal conductivity enhancement value as 12%.

Introduction: Heat transfer systems are important for many areas ranging from automotive industry to space industry, from electronic applications to solar thermal applications. In 1873, the theory of mixing millimeter and micrometer size metallic particles in base fluid, introduced by Maxwell, is the starting point for increasing thermal conductivity [1]. The term of “nanofluids” was first used by Choi in 1995 [2]. Compared to micron-sized particles, nanoparticles may remain suspended for longer periods. On the other hand, nanoparticles may enter a tendency to aggregate due to the strong Van der Waals forces between them [3]. Non-covalently functionalization (usage of surface active agents), covalently functionalization, pH control, and ultrasonication are basic methods to ensure stability. In the scope of this study, a method based on the principle of detection of the third harmonic (3ω method) using AC hot-wire and lock-in amplifier together, was used to measure the thermal conductivity of fluids. Although thermal conductivity studies have been conducted frequently, the stability of nanofluids has not

yet been elucidated. Additionally, due to the dark color and opacity of carbon-based nanofluids, zeta potential and UV-Vis spectrophotometry measurements are very challenging.

Discussion and Results: SWCNT (Tuball Matrix, Beta 302) was supplied from OcSiAl. PEG-POSS (PG1190) was purchased from Hybrid Plastics. GNPs with 800, 530, and 320 m^2/g surface areas were supplied from Nanografi. Ammonia (NH_3) anhydrous, ≥99.98% was purchased from Sigma-Aldrich. For preparation of SWCNT and GNP nanofluids, distilled water was used as a base fluid. Ultrasonicator (UP400S, Hielscher Ultrasonics GmbH, Teltow, Germany) at a setting cycle of 0.5 and amplitude of 50%, was used for aqueous dispersions. Nanofluids having 0.1, 0.5, 1.0, and 2.0 wt% carbon nanoparticle concentration and different amounts of PEG-POSS concentration were pre-sonicated before pH adjustment. 0.1 M NH_4OH solution was prepared and added into dispersions. During addition of NH_4OH solutions, Innolab Multi 9310 pHmeter was used for pH measurements of all samples at around 25 °C. After pH adjustment, dispersions were sonicated for 50 minutes. To prevent overheating, ice bath was used during sonication. Zetasizer Nano (Malvern Instruments) and UV-Vis Spectrophotometer (Perkin Elmer Lambda) were used for the stability measurements. Dispersions having an absolute value higher than 30 mV are regarded as stable. As shown in Figure 1 (A), the highest zeta potential value of -85.5 mV was measured for 2.0 wt% SWCNT and 0.2 wt% PEG-POSS included dispersion, resulting in an excellent stability. The high zeta potential values might be obtained due to the use of PEG-POSS and the effect of pH adjustment, as well as the prolonged ultrasonication.

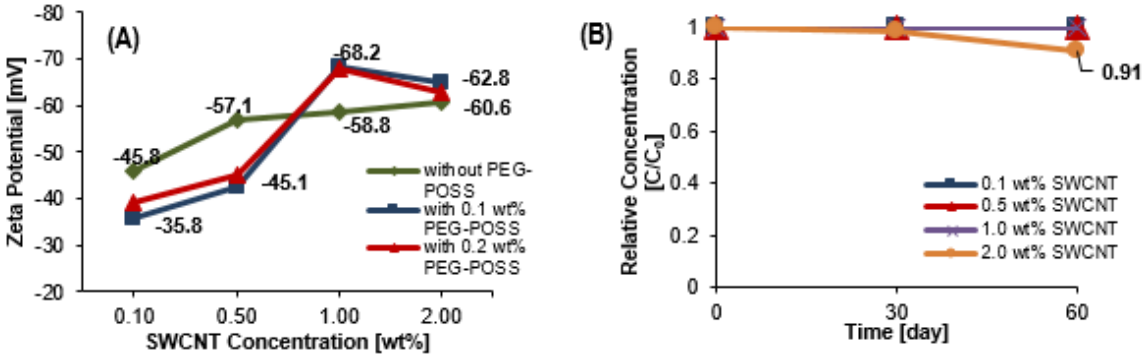

Figure 1. (A) Zeta potential change with different SWCNT and PEG-POSS concentrations, (B) Relative concentration of dispersions with 0.2 wt% PEG-POSS with respect to time.

To determine sedimentation amount, absorbance measurements of the dispersions prepared at different concentrations were performed at specific wavelength. At t_0 moment, UV-Vis was measured in dispersions and absorbance versus nanoparticle

concentration graph was plotted. Relative concentrations of dispersions after 60 days were determined by the linear correlation in the generated graph. A slight decrease in relative concentration is shown in Figure 1 (B) due to the increase in nanoparticle concentration of dispersions.

Attension Theta Lite Optical tensiometer (Biolin Scientific AB, Vastra Frolunda, Sweden) was used to measure contact angle values. Contact angle values in Figure 2 were calculated taking the average of 5 measurements for each sample by the sessile drop technique along with a straight line on the glass surface. GNPs with 3 different surface areas of 320, 530, and 800 m^2/g were used for PEG-POS free dispersions to compare the effect of surface area on wettability, shown in Figure 2. As the surface area of nanoparticles increased, an increase in contact angles was observed for dispersions having 0.1, 0.5, and 1.0 wt% GNP. Whereas, there was a decrease in the contact angle values of 2.0 wt% GNP nanofluids. The repulsive forces between the glass surface and the nanofluid cause a non-wetting behaviour, which increases with the concentration of the nanoparticles. Hence, an increase in the contact angle was observed for first three GNP concentrations. The effective surface tension of the nanofluid near the solid-particle-fluid line changes due to the cohesive and adhesive interactions between water molecules and nanoparticles at the interfacial surfaces. Therefore, the contact angle increases with the concentration of the nanofluid, reaches a peak, than decreases [4].

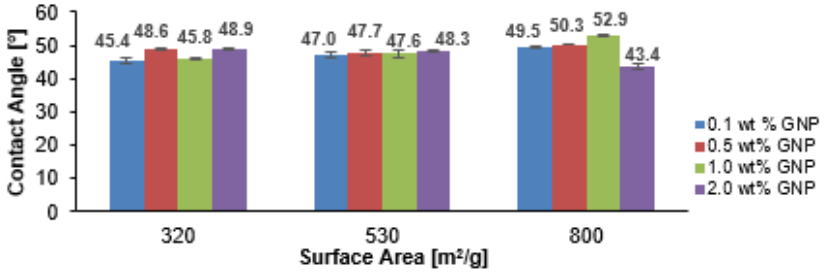

Figure 2. Contact angle measurements for dispersions without PEG-POSS having different surface area of GNP.

The thermal conductivity values decrease with the increase in surface area of GNP and increase with the increase in nanoparticle concentration, shown in Figure 3 (A). The highest value of thermal conductivity enhancement is 12% for 320 m^2/g GNP dispersions. The thermal conductivity decrement can be explained with clustering effect [5]. Smaller particles are more prone to clustering. Excessive clustering causes sedimentation and dispersions having small particles show lower thermal conductivity enhancement. The thermal conductivity results are supported by particle size distribution measurements via Mastersizer (Malvern Instruments), shown in Figure 3 (B).

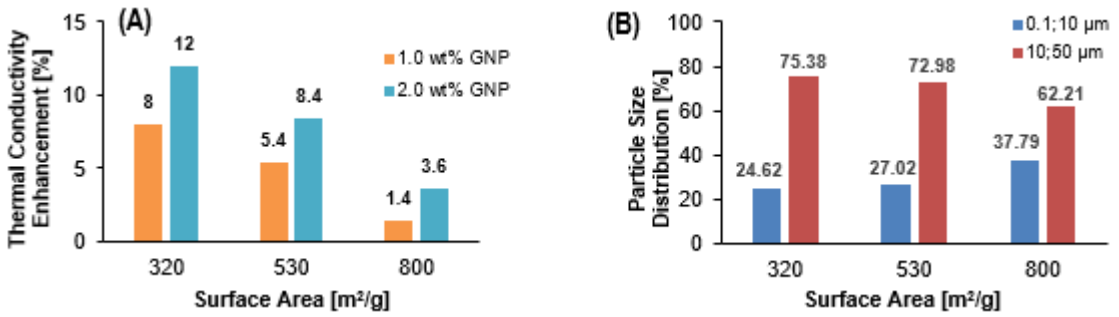

Figure 3. (A) Thermal conductivity enhancement for dispersions without PEG-POSS having different surface area of GNP, (B) Particle size distribution of different surface area of GNP.

Conclusions: In this study, aqueous SWCNT and GNP nanofluids were successfully prepared, using ultrasound technology. For stability enhancement, pH was adjusted to the value (around 8), where the nanofluids would be expected to be stable. Zeta potential analysis showed the highest value as -85.5 mV for 2.0 wt% SWCNT and 0.2 wt% PEG-POSS aqueous nanofluids. Decrease in surface area of GNP not only provided better wettability but also caused higher thermal conductivity values of nanofluids. The highest thermal conductivity enhancement was measured as 12% for 2.0 wt% GNP having a surface area of 320 m^2/g. Additionally, the nanofluids remain stable up to 60 days.

Ackowledgement: This study is supported by The Scientific and Technological Research Council of Turkey (TUBITAK) with the project no. 117M953.

References:

1. M.M. Tawfik, Experimental studies of nanofluid thermal conductivity enhancement and application: A review, *Renewable and Sustainable Energy Review* 75 (2017) 1239-1253.
2. S.U.S. Choi, Enhancing Thermal Conductivity of Fluids with Nanoparticles, Developments, and Application of Non-Newtonian Flows, *ASME Journal of Heat Transfer* 66 (1995) 99-105.
3. S. Mukherjee, P.C. Mishra and P. Caudhuri, Stability of heat transfer nanofluids – A review, *ChemBioEng Reviews* 5 (2018) 1-22.
4. S. Vafaei, T. Borca-Tasciuc, M. Z. Podowski, A. Purkayastha, G. Ramanath, and P. M. Ajayan, Effect of nanoparticles on sessile droplet contact angle, *Nanotechnology* 17 (2006) 2523-2527.
5. S. Ozerinc, S. Kakac, and A.G. Yazicioglu, Enhanced thermal conductivity of nanofluids: a state-of-the-art review, *Microfluid Nanofluid* 8 (2010) 145-170.

1st International Conference on Nanofluids (ICNf2019)
2nd European Symposium on Nanofluids (ESNf2019)
26-28 June 2019, Castelló, Spain

Design of ionic liquid-water mixture based nanofluids with aluminium oxide nanoparticles

Jose I. Prado[1], Elena Ionela Cherecheş[2], Marius Cherecheş[2], Alina Adriana Minea[2], and Luis Lugo[1*]

[1]Departamento de Física Aplicada, Facultade de Ciencias, Universidade de Vigo, Campus Lagoas-Marcosende, E-36310 Vigo (Spain)

[2]Technical University "Gheorghe Asachi" of Iasi, Iasi (Romania)

[*]Corresponding author: luis.lugo@uvigo.es

Keywords: Enhanced Ionic liquid, nanoparticles, Aluminium oxide, Nanofluid, NEILs, Al_2O_3.

Abstract: Interest in development of advanced heat transfer media has been encouraging worldwide researchers to perform investigations in the field of nanofluids, exploring different colloidal combinations of base fluids and nanomaterials. In this work, a binary mixture of an ionic liquid and water is used as base fluid to design new nanofluids containing aluminium oxide nanoparticles at different mass fractions. Stability assessment was performed by evaluating Al_2O_3 morphology and aggregation using electron microscopy techniques, measuring pH of prepared dispersions and studying temporal evolution of average apparent size of nanofluids.

Introduction:

Ionic liquids (ILs) are organic molten salts at room temperature. Their unique physicochemical properties make them excellent candidates to use as heat transfer fluids (HTFs) in renewable energy systems, especially in concentrated solar power (CSP) plants due to their low vapour pressure. Several ILs are completely miscible in water, having different chemical structures depending on the composition of binary mixtures. It is possible to develop advanced HTFs with specifically engineering properties combining effects of IL-water mixtures and nanomaterials.

This work was focused on the development of new nanofluids based on binary mixtures of water and 1-ethyl-3-methylimidazolium methanesulfonate. This imidazolium IL was selected due to its promising thermophysical properties and low toxicity as reported by Bioucas et al. [1]. Nanofluids were elaborated by dispersing aluminium oxide nanoparticles within an IL-water mixture. Their stability has been reported by means of measuring pH and determining size distributions of prepared nanofluids.

Discussion and Results:

Aluminium oxide nanoparticles (average size of 50 nm, according to manufacturer specifications) and 1-ethyl-3-methylimidazolium methanesulfonate, $[C_2mim][CH_3SO_3]$, with ≥ 95% purity and declared water content less than 0.5% were acquired from Sigma-Aldrich (St. Louis, USA). Milli-Q grade water was produced from a Millipore system (Billerica, USA) with a resistivity of 18.2 MΩ·cm at 298 K. All products were used without any further purification and were weighted in an analytical balance Sartorius CPA225 (Göttingen, Germany) whose resolution is 10^{-5} g.

Binary mixtures are named as x_w W + (1-x_w) IL, where x_w states for the water mole fraction. In this study, 0.25 W + 0.75 IL was prepared based on water mole fraction, x_w, by mixing both components at the specified mole fraction using a VELP Scientifica ZX3 Advanced Vortex Mixer (Usmate, Italy) for 2 minutes. Nanofluids were developed by dispersing Al_2O_3 into this base fluid at mass fractions of φ_m = 1, 2.5, 5, 10 and 15 wt% by means of an ultrasonic homogenizer Bandelin Sonopuls HD 2200 (Berlin, Germany), during 60 min.

Dry nanoparticles were characterized by means of Transmission Electron Microscopy (TEM) analyses. The used microscope is a JEOL JEM-1010 TEM (Tokyo, Japan) operating at an acceleration voltage of 100 kV. Nanoparticles were dispersed in analytical grade 1-buthanol and a drop of this solution was deposited in the top of 400-mesh copper grid coated with Formvar and sputtered with carbon, drying at atmospheric conditions. Al_2O_3 nanoparticles are pseudo-spherical and polydisperse, as can be seen in Fig. 1.

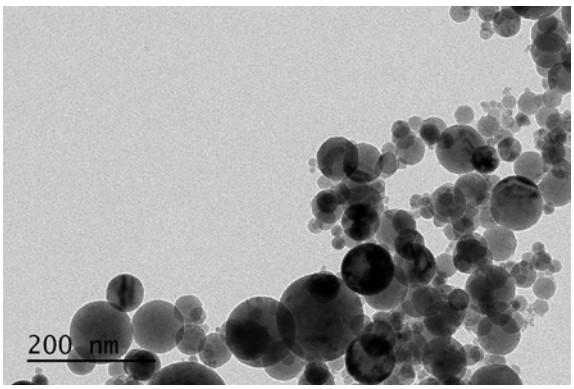

Figure 1. TEM image of Al_2O_3 nanoparticles.

It is known that several factors such as nanoparticle concentration, surfactant addition, viscosity of base fluid, and pH affect the stability of nanofluids [2]. There are plenty of works in the literature concerning the effect of pH on the zeta potential of nanofluids. This influence plays an active role in their stability. A change in pH value triggers a modification of surface charge of nanoparticles, which can be used to prevent the aggregation of

dispersed nanoparticles. Abdullah et al. [3] revealed that alumina dispersions in ethanol-water are highly stable at pH ranges from 0 to 3.5 and from 7 to 11.

Using a HACH pH-METRO SENSION+ ph3 (Loveland, USA), pH of studied nanofluids was measured with an estimated uncertainty better than 0.01. The obtained values, from 7.9 to 8.7, are within the stable range reported by Abdullah et al. [3], minimizing sedimentation effects. Moreover, values are around the optimized value of 8 recommended by Wang and Li [4] for nanofluids containing alumina, as can be seen in Table 1.

Table 1. pH of Al_2O_3/(0.25 W + 0.75 IL) nanofluids at different mass fractions of nanoparticles.

φ_m	pH
1 wt%	7.93
2.5 wt%	8.11
5 wt%	8.29
10 wt%	8.21
15 wt%	8.67

Another relevant tool to elucidate stability of nanofluids is the use of Dynamic Light Scattering (DLS) technique to obtain nanoparticle size distribution of these dispersions to study its evolution along time. Apparent average size was obtained by using a Zetasizer Nano ZS (Malvern, UK) operating at 298 K with a scattering angle of 173º. Aliquots of Al_2O_3/(0.25W + 0.75 IL) at φ_m = 1 wt%, were deposited in a measurement cell and remained in static conditions during 25 days, recording nanoparticle size distribution almost every day, as can be seen in Fig. 2.

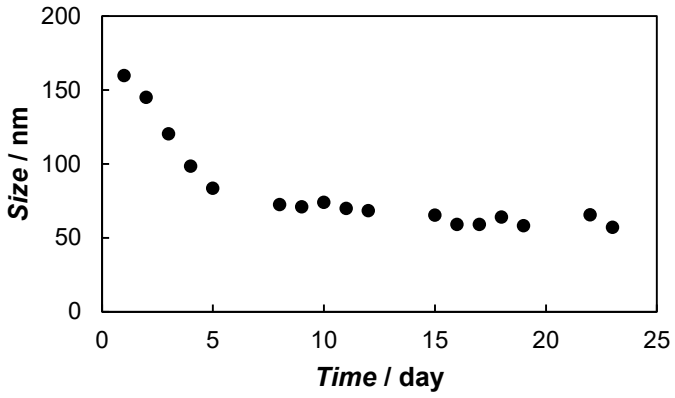

Figure 2. Temporal evolution of average size of Al_2O_3/(0.25 W + 0.75 IL) nanofluids at mass fraction of φ_m = 1 wt%.

Fig. 2 shows a decreasing in the mean size approximately from 160 nm to 72 nm, indicating that a controlled sedimentation of biggest agglomerates occurs in the sample

during first five days from preparation. After then, average size remains almost constant and close to the previous stated nanoparticle size (50 nm), as could be concluded from Fig. 1.

Conclusions:

This work aimed to design new nanofluids using a binary mixture of 1-ethyl-3-methylimidazolium methanesulfonate and water as base fluid and aluminium oxide nanoparticles. Stability of studied Al_2O_3/(0.25W + 0.75 IL) nanofluids has been confirmed by pH and size distribution measurements. Results showed that pH of nanofluids at all studied mass fractions is within the highly stable range reported in the literature. Since nanofluids exhibited, a good temporal stability for 25 days determined by DLS technique, the study of their thermophysical properties seems to be in priority and needs further elaboration. This future work may survey separately water and nanoparticles effects in volumetric and heat transfer behaviour of developed nanofluids to elucidate their feasibility as HTFs in commercial and domestic applications.

Acknowledgments: This work was partially supported by “Ministerio de Economía y Competitividad” (Spain) and FEDER program through ENE2017-86425-C2-1-R project and EU COST Action CA15119: Overcoming Barriers to Nanofluids Market Uptake. Authors also acknowledge the financial support by Xunta de Galicia, GRC ED431C 2016-034 and Galician Network on ILs, ED431D 2017/06. J.I.P. thanks a predoctoral fellowship from Xunta de Galicia (Spain).

References:

1. F.E.B. Bioucas, S.I.C. Vieira, M.J.V. Lourenço, F.J.V. Santos, C.A. Nieto de Castro and K. Massonne, [C_2mim][CH_3SO_3] – A Suitable New Heat Transfer Fluid? Part 1. Thermophysical and Toxicological Properties, *Industrial & Engineering Chemistry Research* 57 (2018) 8541-8551.
2. M. Zhao, W. Lv, Y. Li, C. Dai, H. Zhou, X. Song and Y. Wu, A Study on Preparation and Stabilizing Mechanism of Hydrophobic Silica Nanofluids, *Materials* 11 (2018) 1385-1394.
3. M. Abdullah, S.R. Malik, M.H. Iqbal, M.M. Sajid, N.A. Shad, S.Z. Hussain, W. Razzaq, Y. Javed, Sedimentation and stabilization of nano-fluids with dispersant, *Colloids and Surfaces A* 554 (2018) 86-92.
4. X.-J. Wang and X.-F. Li, Influence of pH on Nanofluids’ Viscosity and Thermal Conductivity, *Chinese Physics Letters* 5 (2009) 056601.

1st International Conference on Nanofluids (ICNf2019)
2nd European Symposium on Nanofluids (ESNf2019)
26-28 June 2019, Castelló, Spain

Colloidal stability of Fe_3O_4 nanofluids in water and ethylene glycol

Caio Carvalho dos Santos[1], Wesley Renato Vaili[1], Eloiza da Silva Nunes and Miguel Jafelicci Junior[1].

[1]Laboratory of Magnetic Materials and Colloids, Department of Physical Chemistry, Institute of Chemistry, São Paulo State University (UNESP), Araraquara - SP, Brazil.

*caio.c.santos@unesp.br; caio.cvs@hotmail.com

Keywords: magnetic nanoparticles, colloidal stability, coprecipitation, two-step nanofluid, magnetite, and oxide nanoparticles.

Abstract: In this work, we report the synthesis of new nanofluid (NF) based on magnetic nanoparticles (MNP) synthesized by coprecipitation method with high colloidal stability. The MNP were functionalized with citric acid (Cac) and after this polyethylene glycol 1000 (PEG1000) is bounded by polycondensation reactions with acid groups on the nanoparticle surface to increase the colloidal stability of the nanofluid. The amount MNP were dispersed in an aqueous medium to obtained NFMNPW and another amount of MNP was dispersed in ethylene glycol to obtained NFMNPE. The MNP were characterized by X-ray diffraction (XRD) which confirmed the formation of the crystalline phase of Fe_3O_4. The transmission electron microscopy (TEM) were used to characterize the size and morphology of the MNP the sample had an average diameter of 5.0 nm. FTIR spectrum of the MNP allowed proving the functionalization of the MNP by Cac and after by PEG1000. The colloidal stability of the NFMNPW and NFNPE were to evaluated by measurement of Zeta potential (ζ) and dynamic light scattering (DLS) -25 mV and 112 nm ± 1 nm, respectively. The DLS in function of temperature allowed to prove the stability of the NF in work conditions.

Introduction/Background: The combination of electronic components and the miniaturization of devices are responsible for the production of large amounts of heat flux. Although in recent years there has been a growth in the electronics industry, semiconductor technology still presents major challenges related to refrigeration, which may result in lower performance, lower longevity of the devices the combination of different cooling techniques has been used to meet the current energy demands [1]. As is generally known, high-efficiency electronic devices produce large amounts of heat in small areas and therefore traditional methods of refrigeration, as well as the use of traditional refrigerants, are not able to meet the demand for refrigeration [2]. To

overcome to demand related to high heat production, it has become increasingly intense new materials with more efficient refrigeration capacity [3]. In this context, the use of NF has shown to be promising because it presents a heat exchange capacity superior to the traditional fluids used in refrigeration [4]. In addition, their superior cooling can also be combined with microchannel systems and thus considerably increase the efficiency in the heat dissipation of the electronic devices. Although more than 20 years of research have been invested since the first report on the superior properties of heat exchange related to the use of NF as refrigerants. In this paper, we report the characterization of two NF (aqueous and ethylene glycol) based in MNP coated by Cac-PEG1000.

Materials and methods: All the chemical reagents used in this work presented analytical grade and were used without any purification. For the synthesis, iron (II) chloride tetrahydrate, iron (III) chloride hexahydrate, citric acid, polyethylene glycol, and triglyme, were purchased from Sigma-Aldrich Brazil. Sodium hydroxide, ethylene glycol, and absolute ethanol were acquired from Synth. Acetone acquired from J.T. Baker. The MNP was synthesized by coprecipitation of the mixture iron ions in alkaline medium [5], Briefly, An solution contains 0.04 mol of $FeCl_2$ and 0.08 mol of $FeCl_3$ were dropped into hydroxide solution 1.5 mol L^{-1} under mechanical stirring and inert atmosphere. This MNP produced was washed with distilled water until pH 9.0. After that, the MNP was functionalized with Cac, MNPCac, 0.37 mmol of Cac adds for each 1g of MNP and kept under stirring overnight. This MNPCac produced was washed with distilled water and ethanol. In the peglaytion step, PEG1000 was bounded by polycondensation with the citric acid on the surface of the nanoparticles to produce the MNPCacPEG1000. 1,5 g of wet MNPCac was dispersed in triglyme and to added 20 mL of PEG1000, this solution was kept in magnetic stirrer at 120°C for 3 hours under an Argon flow and then the temperature was raised to 150°C for 21 hours. This MNPCacPEG1000 produced was washed three times with acetone [6]. Finally, this material was divided into two parts, one was added to 50 mL water and the other one added to 50 mL ethylene glycol, to produce the NFMNPW e NFMNPE. The X-ray diffractogram was obtained in a model 5005 with CuKα radiation (I = 1.5418 Å) with a 40 kV and 40 mA, in the range of 20 to 80 degrees. The infrared spectra of the sample were performed using a VERTEX 70 FT-IR Spectrometer from Bruker using Diffuse Absorption spectroscopy in the medium infrared region by means of attenuated total reflection (diamond crystal). The analyze was measured using 64 scans to accumulation data and 4 cm^{-1} of resolution in 4000 at 400 cm^{-1} range. The micrograph of MNP has performed in a transmission electron microscope Philips CM120 microscope at 120. The colloidal stability to evaluated by the

analyses of the zeta potential (ζ) and DLS using a Zetasizer Nano series ZS equipment, from Malvern Instruments.

Discussion and Results: The characterization of the MNP was evaluated by XRD, TEM, and FTIR in the Figure 1a shows the XRD of the MNP, as observed the sample showed same peaks with standard of crystalline structure magnetite, as being cubic with a = 8.400 which is approximately equal to the standard of magnetite (pdf JPCDS-79-419) The size of the crystallites was calculated based on Scherrer's law, using the width at half height of the most intense peak and considering the approximately spherical MNP, the average size of the crystallites was of 3,97 nm [7]. Figure 1b shows of morphology approximately spherical of de MNP and the size calculated by the image of the TEM the MNP had an average diameter of 5.0 nm. Figure 1c shows the spectra in the infrared region allowed to confirm the coating of the MNP in different steps of the synthesis. The characteristics band was attributed to the C-O-C stretch present in the PEG 1000 framework observed at 1062 cm^{-1} and the bands present in1608 and 1386 cm^{-1} were attributed to the presence of carboxylates groups [8].

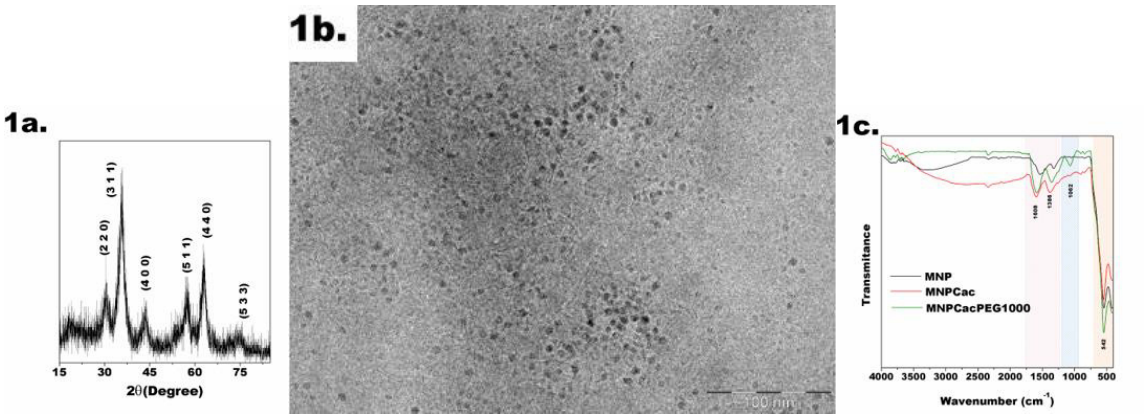

Figure 1. a. The XRD of the sample and the standard pdf JPCDS-79-419. b. The TEM of the MNP. c. The spectra of samples.

The colloidal stability of the NF was evaluated by measurements of the zeta potential and the DLS as a function of temperature shown in Figure 2. The isoelectric point (IEP) the MNP, MNPCac, and MNPCacPEG1000 were to pH 5.7, 3.2, and 4.9 respectively. Above pH 7.5, the sample shows a value the zeta potential in modulus (25 mV), which gives the minimum of electrostatic stability, therefore the final pH of the aqueous NF was adjusted to 8.0. The attachment of PEG onto the MNP surface added higher dispersibility and colloidal stability in aqueous media compared with citrate-coated [6]. As noted, the D_h of the two NF does not change significantly with the heating and cooling of the sample, which characterizes the colloidal stability of the NF against the working conditions of refrigerant fluid.

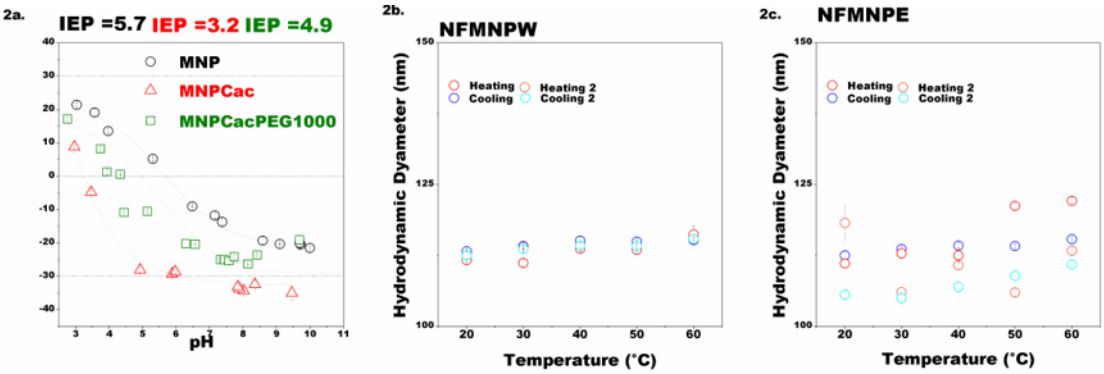

Figure 2. a. Show the Zeta potential of the samples. b. The Dh of the NFMNPW (Water). c. The Dh of the NFMNPE (Ethylene Glycol).

Summary/Conclusions: In this work, we used the peglaytion methodology to obtain stable NF based on Cac-PEG-functionalized magnetite dispersed in ethylene glycol and water. The MNPCacPEG1000 was shown to be easily dispersed in water and ethylene glycol and the resulting NF show good colloidal stability, D_h does not change significantly which the sample was submitted to heating and cooling heat cycles to evaluated.

References:

1. K. Zhu, Z. Cui, Y. Wang, H. Li, *et al*. Estimating the maximum energy-saving potential based on IT load and IT load shifting, Energy. 138 (2017) 902–909.
2. Y. Wang, B. Wang, K. Zhu, H. Li, *et al*, Energy saving potential of using heat pipes for CPU cooling, Appl. Therm. Eng. 143 (2018) 630–638.
3. K. V Wong, O. De Leon, Applications of Nanofluids : Current and Future, 2010 (2010).
4. W.H. Azmi, M.Z. Sharif, T.M. Yusof, R. Mamat, *et al*, Potential of nanorefrigerant and nanolubricant on energy saving in refrigeration system – A review, Renew. Sustain. Energy Rev. 69 (2017) 415–428.
5. R. Massart, Preparation of Aqueous Magnetic Liquids in Alkaline and Acidic Media, IEEE Trans. Magn. 17 (1981) 1247–1248.
6. W.R. Viali, E.S Nunes, C.C. Santos, *et al* PEGylation of SPIONs by polycondensation reactions : a new strategy to improve colloidal stability in biological media, J. Nanopart. Res. (2013) 15:1824.
7. M.F. Abdelbar, T.A. Fayed, T.M. Meaz, E.-Z.M. Ebeid, Spectrochimica Acta Part A : Molecular and Biomolecular Spectroscopy Photo-induced interaction of thioglycolic acid (TGA) -capped CdTe quantum dots with cyanine dyes, SAA. 168 (2016) 1–11.
8. K. Nakamoto. Infrared and Raman Spectra of Inorganic and Coordination Compounds. In Handbook of Vibrational Spectroscopy (eds J. M. Chalmers and P. R. Griffiths). (2006)

1st International Conference on Nanofluids (ICNf2019)
2nd European Symposium on Nanofluids (ESNf2019)
26-28 June 2019, Castelló, Spain

On the mixture model of the density of nanofluids

Gaweł Żyła

Department of Physics and Medical Engineering, Rzeszow University of Technology, Rzeszow, Poland
gzyla@prz.edu.pl

Keywords: nanofluid, density, mixture model.

Abstract: This paper tries to explain why predictions of often used two phase mixture rule and experimental results of nanofluids density differ. Presented here literature data shows that this model overestimates experimental results, and mechanism responsible for this situation is proposed.

Introduction/Background: Nanofluids, with its many potential applications, are quite interesting part of nanomaterials. For the last twenty years many research groups work on both experimental and theoretical studies of nanofluids physical properties. Most of them focus on thermal conductivity and viscosity of nanosuspension, which have great impact on heat transfer efficiency and determinate possibilities of using those materials in advanced heat exchange systems. Another properties like isobaric heat capacity, surface tension, density, etc. are out of main stream of research. In the case of the last mentioned above, density, problem is even more complex while many scientist and engineers consider density of nanofluids as exactly given by the mixture rule:

$$\rho_{nf} = (1 - \varphi_p)\rho_{bf} + \varphi_p \rho_p. \quad (1)$$

Rare experimental studies on this issue show that predictions of this model and experimental data differ, and deviations could reach several percent.

For the first time this model was used by Pak and Cho to describe ethylene glycol (EG) based nanofluids containing γ-Al_2O_3 and TiO_2 [1]. In the mentioned paper they have presented that experimental data shows lower values of density that predicted by mixture model with maximum deviation 0.6%. The same trend of overestimating density values of this model has been reported for another EG based nanofluids containing nanodiamonds [2] and six types of nitrides with various average particle sizes [3]. In these cases absolute average deviation (AAD) between model values and experimental data do not exceed 1%, so mixture model describe density of nanofluids with good accuracy, but still it was higher than relative measurement uncertainty (0.1%). Another experimental study on density of EG based nanofluids was conducted by Cabaleiro et al.

[4] and it employed two types of TiO_2 nanoparticles. They also reported that mixture model overpredicts density values in case of those nanofluids.

The same situation has been reported by Mahbubul et al. for density of some refrigerant based nanofluids containing Al_2O_3 [5].

Marcos et al. measured density of nanofluids containing low fractions of functionalized graphene nanoplatelets in poly(ethylene glycol) with the mass-average molecular mass of 400 g mol^{-1} (PEG(400)) [6]. Also there slightly deviations between experimental data and mixture rule has been reported.

Vajjha et al. present results of their study on density of three different nanofluids containing Al_2O_3, Sb_2O_5:SnO_2 and ZnO [7]. A mixture of EG and water (60:40 ratio) was used as base fluid. Authors evaluate uncertainty on the base of deviation between density value measured by them and literature data, and according to the paper it was 2%. For the first two nanofluids deviation between experimental data and predictions of mixture model do not exceed measurements uncertainty. In the case of nanofluids containing ZnO nanoparticles deviations reach 7% and mixture model overestimates the experimental data.

Interesting discussion of this issue was presented by Sharifpur et al. in recent paper presenting a new model for density of nanofluids [8]. They examined density of four different nanofluids and compare their experimental results with predictions of the mixture model. Again, values of density were lower in the case of experimental study than those calculated with eq. (1). Authors connected these deviations with existing "nanolayer" on the surface of nanoparticles. Development of this idea through the paper brings the new model of density of nanofluids, taking into account a nanolayer, in form of:

$$\rho_{nf} = \frac{\rho_{nf}}{(1-\varphi_p)+\varphi_p(r_p+t_v)^3/{r_p}^3}. \quad (2)$$

This model describes presented there experimental data with the better accuracy than the mixture rule.

In presented paper simple explanation of the deviation between experimental data and mixture model predictions has been proposed.

Discussion and Results: One must noted that all presented here experimental results refer to nanofluids prepared with the two-step method. This method is based on dispersing dry nanoparticles in a base fluid. Nanoparticles at dry form have tendency to create agglomerates, and after putting them into the base fluid they still could keep such

form. Various techniques are used to break agglomerates, including the mechanical mixing and sonication. After these processes most of agglomerates are break, but still some of them might occur. In this scenario the surface tension of base fluid might not allow it to fill the void in agglomerates, so real density of agglomerate is lower than the density of particles. Gas could be also adsorbed on the surface of nanofluids, and make a contribution to the decreasing real density of the particles.

Scheme of preparing nanofluids with two-step method and describe above situation was presented in Fig. 1.

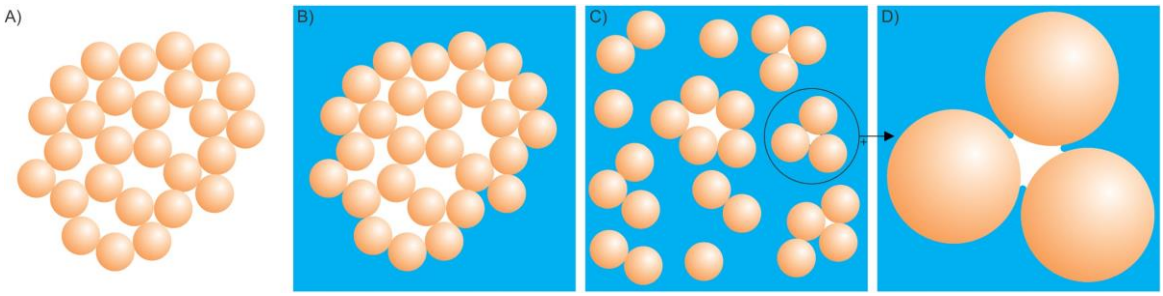

Figure 1. Scheme of preparing nanofluids with two-step method. A) agglomerate of dry nanoparticles, before adding the base fluid, B) agglomerate of nanoparticles in base fluid, C) dispersed nanoparticles after mixing and sonication action, some small agglomerates still occur D) the zoom on a single agglomerate in base fluid and gas trapped inside.

In that case real volume of additives in such nanofluids could be described as:

$$V_a = V_p + V_g, \tag{3}$$

and real volume fraction of additives is defined as:

$$\varphi_a = \frac{V_a}{V_{nf}} = \frac{V_p + V_g}{V_{nf}} = \frac{V_p}{V_{nf}} + \frac{V_g}{V_{nf}} = \varphi_p + \varphi_g. \tag{4}$$

So, finally, nanofluids prepared with two-step methods could be mixture of three phases: a) base fluid, b) solid particles and c) gas adsorbed on particles and trapped in agglomerates. The improved mixture formula of density is:

$$\rho_{nf} = (1 - \varphi_p - \varphi_g)\rho_{bf} + \varphi_p\rho_p + \varphi_g\rho_g, \tag{5}$$

which in absence of the gas fraction reduces to the simple mixture model (1).

Summary/Conclusions: In conclusion, mixture model of density of nanofluids is correct, but in the often used form proposed by Pak and Cho (1) is oversimplified. For nanofluids prepared with the two-step methods, it does not take into account all factors related to

the gas fraction (like adsorption of gas on nanoparticles surface and trapping gas inside the agglomerates).

Nomenclature: r is radius [nm], t - equivalent thickness [nm], V - volume [m^3], ρ - density [kg m^{-3}], φ - volume fraction [-]; subscripts *a*, *bf*, *g*, *nf*, *p*, *v* refers to additives, base fluid, gas, nanofluid, particle, and void respectively.

References:

1. Pak, B.C., Cho, Y.I., Hydrodynamic and heat transfer study of dispersed fluids with submicron metallic oxide particles. Experimental Heat Transfer an International Journal (1998), 11, 151–170.
2. Żyła, G., Vallejo, J.P., Fal, J., Lugo, L., Nanodiamonds–ethylene glycol nanofluids: experimental investigation of fundamental physical properties. International Journal of Heat and Mass Transfer (2018), 121, 1201–1213.
3. Żyła, G., Vallejo, J.P., Lugo, L., Isobaric heat capacity and density of ethylene glycol based nanofluids containing various nitride nanoparticle types: An experimental study. Journal of Molecular Liquids (2018), 261, 530–539.
4. Cabaleiro, D., Pastoriza-Gallego, M.J., Gracia-Fernández, C., Piñeiro, M.M., Lugo, L., Rheological and volumetric properties of TiO_2-ethylene glycol nanofluids. Nanoscale research letters (2013), 8, 286.
5. Mahbubul, I., Saidur, R., Amalina, M., Thermal conductivity, viscosity and density of R141b refrigerant based nanofluid. Procedia Engineering (2013), 56, 310–315.
6. Marcos, M.A., Cabaleiro, D., Guimarey, M.J., Comuñas, M.J., Fedele, L., Fernández, J., Lugo, L., PEG 400-Based Phase Change Materials Nano-Enhanced with Functionalized Graphene Nanoplatelets. Nanomaterials (2017), 8, 16.
7. Vajjha, R., Das, D., Mahagaonkar, B. Density measurement of different nanofluids and their comparison with theory. Petroleum Science and Technology (2009), 27, 612–624.
8. Sharifpur, M., Yousefi, S., Meyer, J.P. A new model for density of nanofluids including nanolayer. International Communications in Heat and Mass Transfer (2016), 78, 168–174.

1st International Conference on Nanofluids (ICNf2019)
2nd European Symposium on Nanofluids (ESNf2019)
26-28 June 2019, Castelló, Spain

Potential mechanisms responsible for the enhancement of thermal properties in graphene nanofluids

M. R. Rodríguez-Laguna[1,2*], A. Castro-Alvarez[3], M. Sledzinska[1], J. Maire[1], F. Costanzo[1], B. Ensing[1,4], M. Pruneda[1], P. Ordejón[1], C. M. Sotomayor Torres[1,5], P. Gómez-Romero[1] and E. Chávez-Ángel[1]

[1]Catalan Institute of Nanoscience and Nanotechnology (ICN2), CSIC and BIST, Campus UAB, Bellaterra, 08193 Barcelona, Spain

[2]Dept. Chemistry, Campus UAB, Bellaterra, 08193 Barcelona, Spain

[3]Organic Chemistry Section, Facultat de Química, Universitat de Barcelona, Av. Diagonal 645, 08028 Barcelona, Catalonia, Spain

[4]Van't Hoff Institute for Molecular Sciences, University of Amsterdam, 1098 XH Amsterdam, The Netherlands

[5]ICREA, Pg. Lluís Companys 23, 08010 Barcelona, Spain

[*]Corresponding author: rodriguez3laguna@gmail.com

Keywords: Graphene, enhancement of thermal properties, π-π stacking, liquid layering.

Abstract: Highly stable graphene nanofluids based on N,N-dimethylacetamide and N,N-dimethylformamide were prepared and thermally characterized. The thermal conductivity and specific heat capacity of both nanofluids suffered a dramatic enhancement with increasing graphene concentration. Raman spectroscopy showed a blue shift of certain Raman modes with increasing graphene concentration. This finding indicates that graphene affects the whole liquid in terms of vibrational energy. Furthermore, DFT and MD simulations showed that the liquid molecules tend to lay parallel towards graphene, favouring a possible π-π stacking. In addition, it was observed that graphene induces a local order of liquid molecules close to the flake. All these data are discussed in the paper to attempt to shed light on the mechanisms behind the enhancement of thermal transport in graphene nanofluids.

Introduction/Background: Heat transfer fluids have been used in a plethora of applications, from microelectronics [1] to concentrated solar power [2], among others. However, their poor thermal conductivity poses a challenge in terms of heat transfer efficiency. The dispersion of nanomaterials has been known for decades as an effective

strategy to upgrade the thermal properties of base fluids [3–5], such as the dispersion of graphene flakes in conventional fluids. Researchers have attempted to explain the outstanding enhancement of the effective thermal conductivity in nanofluids, however, although several theories have been proposed [6–9] there is still an ongoing debate.

Discussion and Results: In this work, we report on highly stable surfactant-free graphene nanofluids developed in-house, based on N,N-dimethylacetamide (DMAc) and N,N-dimethylformamide (DMF) with improved thermal properties. The influence of graphene concentration (0.00-0.27 % w/w), on thermal conductivity, specific heat capacity, sound velocity and Raman spectra was evaluated by means of experimental measurements. An increase of up to 48% in thermal conductivity and 18% in specific heat capacity were observed, see **Figure 1a**. Raman spectra showed a shift to higher frequencies with increasing graphene concentration in DMF. This finding indicates that the presence of graphene affects and modifies the vibrational energy of the whole liquid, even at long-range. Density functional theory and molecular dynamics simulations indicate that there is a strong interaction between graphene flakes and the nearest DMF molecules around them, suggesting a possible π-π stacking. In addition, a parallel orientation of the fluid molecules (**Figure 1b**) and a local solid-like nanolayer of DMF molecules around the graphene flakes is observed in the simulations [10].

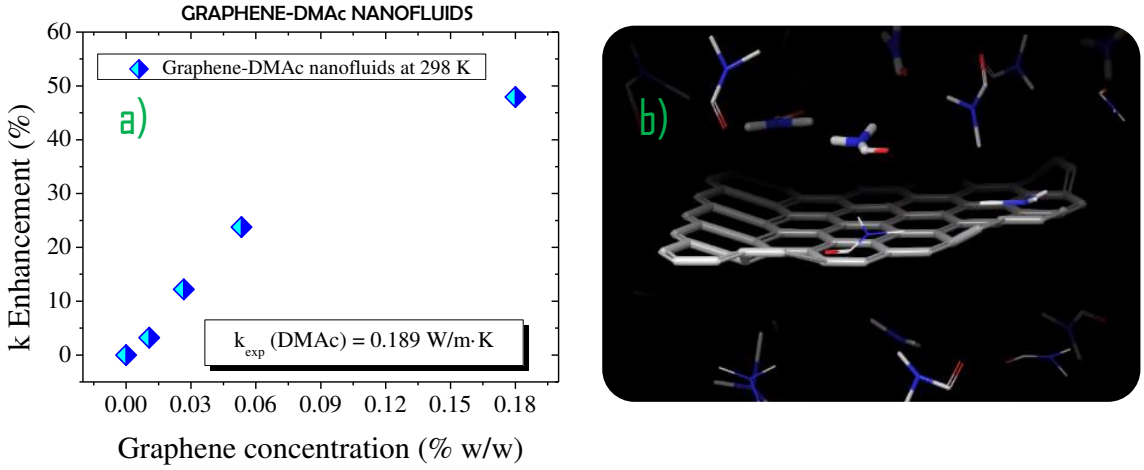

Figure 1. Thermal conductivity as a function of graphene concentration of DMAc-nanofluids and illustration of DMF molecules around a graphene flake; a) Thermal conductivity enhancement as a function of graphene concentration for DMAc nanofluids at room temperature; b) Frame from a MD simulation of a single layer graphene-DMF system.

Summary/Conclusions: Herein, we report on a set of highly stable graphene nanofluids prepared without the aid of surfactants. The selected base fluids have low thermal conductivity but a wider working temperature than water (most common coolant) and form very stable graphene dispersions. The addition and dispersion of small concentrations of graphene in these amides resulted in a dramatic improvement of their thermal properties. Furthermore, we discovered that the presence of graphene modifies the vibrational energy of liquid molecules, even of those far from graphene. Our simulations showed a special interaction between graphene and the molecules of liquid and a liquid solid-like structure around the graphene flake. Therefore, we can claim that our results are consistent with theories based on 1) the increase of interatomic interactions arising from the interatomic potential [7,9] and 2) solid-like layering of the liquid at the liquid/particle interface [6], but more work is needed to produce a comprehensive physical model.

References:

1. Sohel Murshed, S.M.; Nieto de Castro, C.A. A critical review of traditional and emerging techniques and fluids for electronics cooling. *Renew. Sustain. Energy Rev.* 2017, *78*, 821–833.

2. Vignarooban, K.; Xu, X.; Arvay, A.; Hsu, K.; Kannan, A.M. Heat transfer fluids for concentrating solar power systems – A review. *Appl. Energy* 2015, *146*, 383–396.

3. Tiznobaik, H.; Shin, D. Enhanced specific heat capacity of high-temperature molten salt-based nanofluids. *Int. J. Heat Mass Transf.* 2013, *57*, 542–548.

4. Tawfik, M.M. Experimental studies of nanofluid thermal conductivity enhancement and applications: A review. *Renew. Sustain. Energy Rev.* 2017, *75*, 1239–1253.

5. Kwek, D.; Crivoi, A.; Duan, F. Effects of Temperature and Particle Size on the Thermal Property Measurements of Al_2O_3 −Water Nanofluids. *J. Chem. Eng. Data* 2010, *55*, 5690–5695.

6. Keblinski, P.; Phillpot, S..; Choi, S.U..; Eastman, J.. Mechanisms of heat flow in suspensions of nano-sized particles (nanofluids). *Int. J. Heat Mass Transf.* 2002, *45*, 855–863.

7. Sarkar, S.; Selvam, R.P. Molecular dynamics simulation of effective thermal conductivity and study of enhanced thermal transport mechanism in nanofluids. *J.*

Appl. Phys. 2007, *102*, 074302.

8. Prasher, R.; Phelan, P.E.; Bhattacharya, P. Effect of Aggregation Kinetics on the Thermal Conductivity of Nanoscale Colloidal Solutions (Nanofluid). *Nano Lett.* 2006, *6*, 1529–1534.

9. Abou-tayoun, N.H. Molecular Dynamics Simulation of Thermal Conductivity Enhancement of Copper-Water Nanofluid, American University of Sharjah, 2012.

10. Rodríguez-Laguna, M.R.; Castro-Alvarez, A.; Sledzinska, M.; Maire, J.; Costanzo, F.; Ensing, B..; Pruneda, M.; Ordejón, P.; Sotomayor Torres, C.M.; Gómez-Romero, P.; et al. Mechanisms behind the enhancement of thermal properties of graphene nanofluids. *Nanoscale* 2018, *17*, 15402–15409.

1st International Conference on Nanofluids (ICNf2019)
2nd European Symposium on Nanofluids (ESNf2019)
26-28 June 2019, Castelló, Spain

Linking Thermodiffusion and Thermoelectricity in Magnetic Nanofluids

T. J. Salez [1], M. Roger[1], R. Perzynski[2], G. Mériguet[2], A. Cebers[3] and S. Nakamae[2]

[1]Service de Physique de l'État Condensé, CEA, CNRS, Université Paris-Saclay, 91191 Gif sur Yvette CEDEX, France

[2]Laboratoire Physicochimie des Electrolytes et Nanosystèmes Interfaciaux (PHENIX), Sorbonne Université, CNRS, 4 Place Jussieu, F-75005 Paris, France

[2]MMML Lab, Faculty of Physics and Mathematics, University of Latvia, Zellu-8, LV-1002 Riga, Latvia

[*]Corresponding author: Sawako.nakamae@cea.fr

Keywords: Seebeck effect, Thermodiffusion, Magnetic nanoparticles, Energy recovery.

Abstract: An analytical model describing the thermoelectric potential production in magnetic nanofluids (dispersions of magnetic and charged colloidal particles in liquid media) is presented. The two major entropy sources, the thermogalvanic and thermodiffusion processes are considered. The thermodiffusion term is described in terms of three physical quantities; the diffusion coefficient, the Eastman entropy of transfer and the effective dynamic charge number of colloidal particles, which all depend on the particle concentration and the applied magnetic field strength and direction. The results are combined with well-established formulation of thermoelectric potential in thermogalvanic cells, and compared to the recent observation of Seebeck coefficient enhancement/diminution in magnetic nanofluids in polar media.

Introduction/Background: Thermoelectric effects in liquid electrolytes is receiving increased attention as a potential source of renewable energy in recent years. Indeed, the Seebeck coefficients of complex fluids (ionic liquids, nanofluids, etc.) are one to two orders of magnitude larger than that of conventional solid-state thermoelectric materials owing to the thermogalvanic, the internal thermoelectric field, the ionic double layer formation at the electrodes or combination of these effects (see, for example [1-4]). In the case of ionic nanofluids [6], the thermodiffusion (Soret effect) of charged nanoparticles is also known to produce non-negligible contribution to the fluid's overall Seebeck coefficient [5, 6].

We have developed an analytical model linking the well-known macroscopic phenomena in nanofluids; *i.e.*, the Soret and the Seebeck effects, to the physical parameters (*i.e.*,

effective surface charges, diffusion coefficient and the transport entropy) of charged nanoparticles (NPs) [7]. In particular, we consider magnetic ionic nanofluids, where the inclusion of magnetic particles and the application of external magnetic field are found to enhance the fluids' Seebeck coefficient [6, 8].

Modelling Approach: A simple thermogalvanic cell considered here is filled with a solution composed of charged (magnetic) particles at a concentration ϕ with an effective (dynamic) charge number ξ, the counterions (for electric neutrality of the solution) and the redox couple molecules. The two ends of the cell are sealed hermetically with identical and metallic electrodes. An electrical potential, ΔV, appears across these electrodes upon application of a temperature gradient, $\overrightarrow{\nabla T}$ (Fig. 1) due to both the thermogalvanic effect of redox reactions and the internal electric field ($\overrightarrow{E_{int}}$) induced by the charged species in the bulk. Note that here, the cell is heated from the top, thus the convective movement of the fluid is ignored.

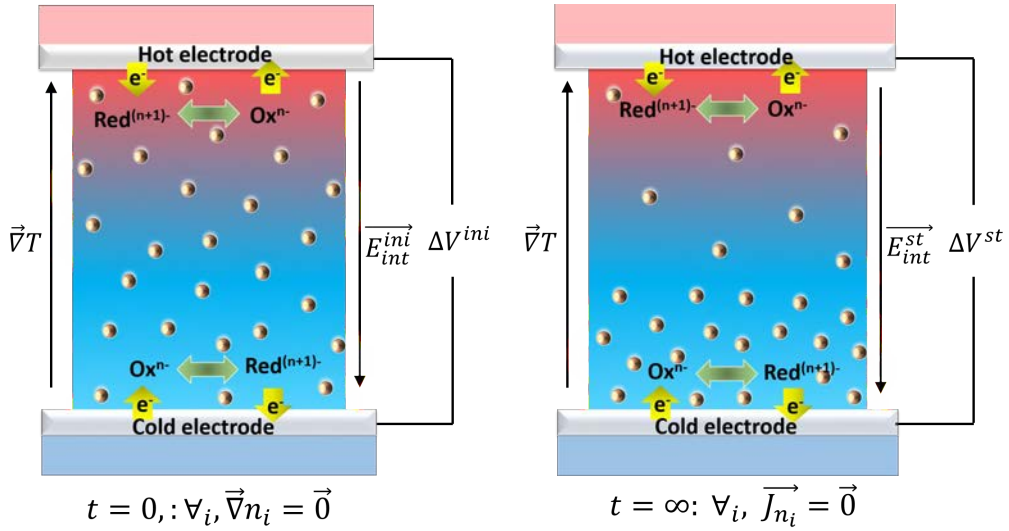

Figure 1. Open-circuit thermogalvanic cell modeled in this work, depicting the redox reaction at the electrodes and the thermodiffusion of charged nanoparticles at the initial state (left) and the steady state (right). See text for more explanation.

The total Seebeck coefficient is defined by: $Se_{tot} = -\Delta V/\Delta T$ (following the sign convention used in the solid state physics), which is the sum of two terms stemming from the thermogalvanic reactions and the internal electric field. The thermogalvanic term is produced by a temperature dependent Gibbs free energy $\Delta_r G$, of the redox half-reaction; *i.e*; $-\Delta(\Delta_r G)/(e.\Delta T)$. The internal electric field term, $\overrightarrow{E_{int}} = Se_{int}.\vec{\nabla}T$ is of fundamental importance for a large number of diffusion phenomena of charged species in electrolytes

(See for example, [9-11]). $\overrightarrow{E_{int}}$ can be determined from the particle current $\overrightarrow{J_{n_i}}$ of all charged and neutral species in the solution.

$$\overrightarrow{J_{n_i}} = -D_i\left[\vec{\nabla}n_i + n_i\frac{\widehat{S_i}}{k_BT}\vec{\nabla}T - n_i\frac{\xi_i e}{k_BT}\overrightarrow{E_{int}}\right]$$

where D_i, n_i, $\widehat{S_i}$ and ξ_i are the diffusion coefficient, the concentration, the Eastman entropy of transfer and the effective dynamic charge number of the i_{th} species. We first examine the particle flux using Onsager's theorem [12] to obtain a generic expression for $\overrightarrow{J_{n_i}}$ as an explicit function of physical quantities; D_i, $\widehat{S_i}$ and ξ_i, which all depend on n_i and the strength and the direction of applied magnetic field $\vec{H}$. This result is then used to calculate the internal electric field in ionic (and magnetic) nanofluids at the initial and steady-state conditions (as depicted in Fig. 1). Finally, combined with the thermogalvanic term, an analytic expression for the total Seebeck coefficient of a thermogalvanic cell containing nanofluid is reached.

Results and Discussions: The full derivation of the analytical expressions for the Seebeck coefficient is beyond the scope of this present communication. Here we simply present the final formulations for the initial and the steady state conditions, Se^{ini} and Se^{st}, respectively [7]. Assuming that the Eastman entropy of transfer is negligibly small for all species except for NPs,

$$Se^{ini} = \frac{1}{e}\left(-\Delta_r S + \sum_i \frac{t_i\widehat{S_i}}{\xi_i}\right) \qquad \text{and} \qquad Se^{st} \cong \frac{1}{e}(-\Delta_r S)$$

where $\Delta_r S$ is the redox half-reaction entropy and t_i is called Hittorf number that is equal to the partial conductivity of i^{th} charged species (nanoparticles, counterions, redox, etc.) with respect to the total conductivity of the nanofluid (For more exact expressions and their derivations, see [7].) The above expressions thus indicate that, it is possible to separate the thermogalvanic and the magneto-thermodiffusion components from the total Seebeck coefficient values obtained at initial and the steady states. These models had been applied to describe the experimental data of thermodiffusion and thermoelectric effects in magnetic nanofluids [5,6,14] where $\widehat{S_{NP}}$ of nanoparticles were found to be in the order of 10–100 meV/K per particle, two orders of magnitude larger than that of typical ions in aqueous electrolytes [15]. Furthermore, the signs of the dynamic charge of nanoparticles and the Eastman entropy of transfer with respect to the sign of the thermogalvanic Seebeck coefficient were found to play a decisive role in determining whether the thermodiffusion contribution enhances or reduces.

Summary/Conclusions: General expressions for the Seebeck coefficient of magnetic nanofluids are derived in the context of magneto-thermoelectric diffusion and thermogalvanic effects. The proposed model allows the extraction of key physical properties of nanoparticles from thermoelectric measurements in nanofluids containing charged particles (magnetic or non-magnetic). The next test step will be to compare the proposed model to the initial Seebeck coefficient measurement under applied magnetic field. The present work should serve to advance our understanding on the remarkable thermoelectric properties reported in complex fluids.

Acknowledgements: This work is supported by the European Union's Horizon 2020 research and innovation programme under grant agreement n° 731976 (MAGENTA), ANR TEFLIC (Grant No. ANR-12-PRGE-0011-01), LabEx PALM (ANR-10-LABX-0039-PALM) and PHC Osmose 2018 n°40033S.

References:

1. M.F. Dupont, *et al.*, *Chem. Comm*., 53 (2017) 6288–6302.
2. E. Laux, *et al.*, *J. Electron. Mater.* 47 (2018) 3193–3197.
3. A. H. Kazim, *et al.*, *Sustain. Energy Fuels* 1 (2017) 1381–1389.
4. H. Jia, *et al.*, *Langmuir* 33 (2017) 7600–7605.
5. B. T. Huang, *et al*., *J. Chem. Phys*. 143 (2015) 054902.
6. T. J. Salez, *et al., Phys. Chem. Chem. Phys*. 19 (2017) 9409–9416.
7. T. J. Salez, *et al.*, *Entropy* 20 (2018) 405.
8. T. J. Salez *et al*., *Nanoscale Advances* (2019) submitted.
9. A. Würger, *Physical Review Letters* 101 (2008) 108302.
10. K. A. Eslahian, *et al*., *Soft Matter* 10 (2014) 1931–1936.
11. J. Burelbach, *et al. European Physics Journal E* 41 (2018) 7.
12. L. Onsager, *Physical Review* 37 (1931) 405-426 and 38 (1931) 2265-2279.
13. R. Cabreira Gomes, *et al*., *Physical Chemistry Chemical Physics* 20 (2018) 16402-16413.
14. J. N. Agar, *et al., Journal of Physical Chem*istry 93 (1989) 2079–2082

1st International Conference on Nanofluids (ICNf2019)
2nd European Symposium on Nanofluids (ESNf2019)
26-28 June 2019, Castelló, Spain

Study on Electrical Conductivity of well-dispersed Transformer-Oil Based Fe_3O_4 Nanofluids

Yuzhen Lv *, Zhen Sun, Baixin Liu, Kai Yi, Meng Huang, Chengrong Li

State key Laboratory of Alternate Electrical Power System with Renewable Energy Sources, North China Electric Power University, Beijing 102206, China

*Corresponding author: yzlv@ncepu.edu.cn

Keywords: Fe_3O_4 nanoparticles, magnetic nanofluid, electrical conductivity, model

Abstract: Monodisperse Fe_3O_4 nanoparticles with an average size of 12.0 nm were synthesized and used to prepare Fe_3O_4 nanofluids with low volume fractions from 0.005% to 0.04%. These nanofluids exhibit good dispersibility and their electrical conductivity is greatly enhanced with increase in both fraction and temperature. The Maxwell model and electrophoresis motion of charged nanoparticles are employed to predict the transport process in Fe_3O_4 nanofluids. It was found that even at the low fractions of 0.02% and 0.04%, the prediction values of this electrical conductivity model are obviously less than the experimental data at higher temperatures. By considering the agglomeration state of nanoparticles and its effect on the electrophoresis conductivity, a modified electrical conductivity model is proposed to explain the mechanism of electrical conductivity of Fe_3O_4 nanofluids.

Introduction: Transformer oil-based nanofluids have attracted intensive attention for both experimental and theoretical researchers due to the great potential in improving the thermal and electrical properties of transformer oil [1,2]. The electrical conductivity of transformer oil-based nanofluids can be significantly increased by the presence of nanoparticles even at the low concentration [3,4]. An electrical conductivity model was developed to explain the transport mechanism of nanofluids and the calculated values agree well with experimental results. However, at the higher volume fractions the measured results are systematically higher than the predicted values. It may due to the lack of consideration of the nanoparticles agglomeration. Recently, investigation on Fe_3O_4 nanofluids has further confirmed that this model failed to predict results at the high volume fractions without considering agglomeration of nanoparticles [5, 6]. However, the effect mechanism of nanoparticles agglomeration on the electrical conductivity of nanofluids is still not very clear. Therefore, in this work, transformer oil-based Fe_3O_4 nanofluids with good dispersion stability were synthesized by adding monodisperse Fe_3O_4 nanoparticles into the oil and electrical conductivity of Fe_3O_4 nanofluids was measured and discussed by introducing a modified electrical conductivity model.

Experimental: Fe_3O_4 nanoparticles were prepared by a simple solvothermal method and oleic acid was used to modify the nanoparticle to ensure uniform dispersion [7]. Fe_3O_4 nanofluids were prepared by dispersing Fe_3O_4 nanoparticles into the filtered oil under stirring and ultrasonic treatment with the volume fractions of 0.005%, 0.010%, 0.020% and 0.040%, respectively. All nanofluids and pure oil were degassed at less than 1 kPa for 2 hours.

Discussion and Results: Monodisperse Fe_3O_4 nanoparticles (Figure 1a) have an average size of 12.0 nm and a cubic shape. Fe_3O_4 nanofluids are transparent and the color turns into light brown gradually with the increasing of nanoparticles concentration (Figure 1b). The dispersion of nanoparticles was characterized by testing UV-vis absorption spectra. The intensity of absorption peak (Figure 1c) has an approximate linear relation with the concentration of nanoparticles and keeps almost same after aging 14 days, exhibiting a good dispersion stability. Furthermore, the measured UV absorbance data obviously deviate from the calculated ones at the higher volume fractions, appearing agglomeration with the increasing of nanoparticle concentration [8].

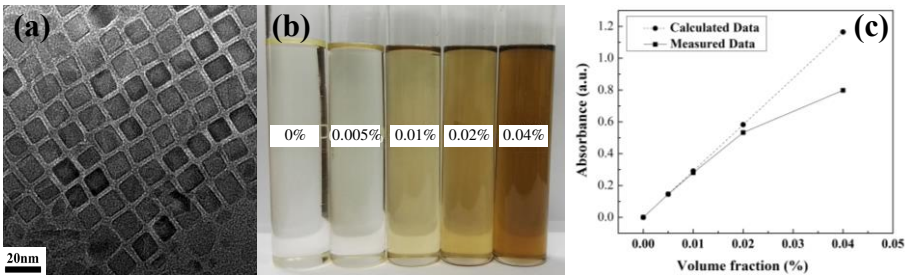

Figure 1. TEM image of Fe_3O_4 nanoparticles, image and UV-Vis absorption spectra of pure transformer oil and Fe_3O_4 nanofluids

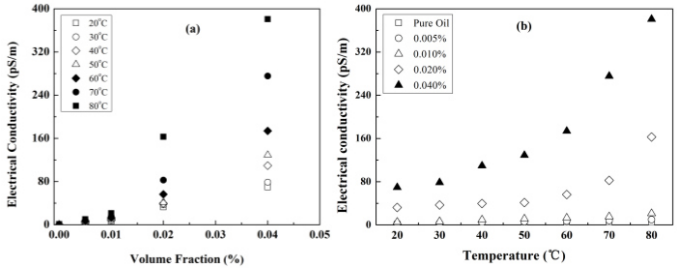

Figure 2. Electrical conductivity for pure oil and nanofluids vs. volume fraction (a) and temperature (b)

The DC electrical conductivity was measured by a Jiantong insulating oil dielectric loss and resistivity tester with a measuring range from 0.05 pS/m to 0.4 μS/m. The electrical conductivity of Fe_3O_4 nanofluids as the functions of volume fraction and temperature is depicted in Figure 2. The variation of electrical conductivity with temperature is not obvious for both pure oil and nanofluids at low concentrations of 0.005% and 0.010%. While at the high concentrations, the rate of enhancement is greatly increased as the

temperature rises. The electrical conductivity for the nanofluid of 0.04% is increased by 348 times in compared with that of the base oil at 80 °C. Previous studies has illustrated that electrical conductivity of nanofluids is closely related to EDL characteristics, volume fraction, and agglomeration of nanoparticles as well as natural properties of base fluid and nanoparticles [3-5]. In considering the contribution of electrophoresis conductivity of nanoparticles, an electrical conductivity model was developed and used successfully in predicting the electrical conductivity of nanofluids [3-5]. In view of that the electrical conductivity of Fe_3O_4 nanoparticles is much greater than that of transformer oil, the model can be approximated as Eq. (1):

$$\sigma = \sigma_f\left(1+\frac{3\varphi}{1-\varphi}\right)+\frac{2\varphi\varepsilon_0^2\varepsilon_{r1}^2\zeta^2}{\eta_0 r^2}e^{\lambda(T-T_0)} \qquad (1)$$

In this equation, where σ_f and σ_p is the electrical conductivity of the pure transformer oil and the nanoparticles. φ is the volume fraction of nanoparticles in nanofluids, ζ is the Zeta potential of the nanoparticles, λ is the viscosity index, and T is the absolute temperature. The values of important quantities used in calculations are as follows: the average nanoparticles radius is approximated to 6.0 nm, the dynamic viscosity of the fluid η_0 = 8.55 × 10^{-3} Pa.s at the temperature of 40 °C. The dielectric constant of the transformer oil ε_{r1} =2.2. The obtained results were compared with the experimental data as the functions of volume fraction and temperature. As shown in Figure 3a, the predicted values

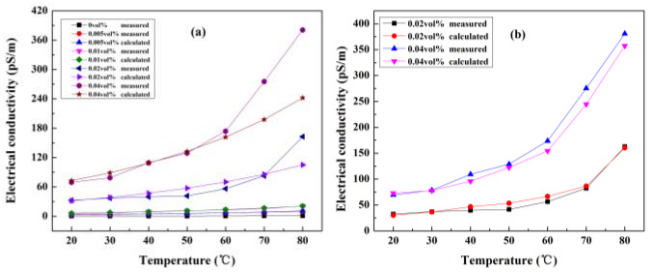

Figure 3. Experimental and calculated data for pure oil and nanofluids as a function of temperature

are well consistent with the measured data as the volume fractions of 0.005% and 0.010% respectively. While obvious deviation is observed for nanofluids with the volume fractions of 0.020% and 0.040% at the higher temperatures. This significant disagreement is consistent with ZnO and Fe_3O_4 nanofluids with the high volume fractions [3,5]. In order to investigate the agglomeration effect of nanoparticles on the electrical conductivity of Fe_3O_4 nanofluids, the hydrodynamic size of nanoparticles in the nanofluids of 0.020% and 0.040% were measured. It is 174 nm and 198 nm, respectively, which are much bigger than the radius of original solid nanoparticles used in the model. Therefore, it is more accurate to use hydrodynamic sizes of nanoparticles and the model is modified by

introducing two new parameters r_2 and φ_2 for the average size and content of agglomerated nanoparticles.

$$\sigma = \sigma_f \left(1+\frac{3\varphi}{1-\varphi}\right)+ \frac{2\varphi_1\varepsilon_0^2\varepsilon_r^2\zeta_1^{\,2}}{\eta_0 r_1^{\,2}} e^{\lambda(T-T_0)} + \frac{2\varphi_2\varepsilon_0^2\varepsilon_r^2\zeta_2^{\,2}}{\eta_0 r_2^{\,2}} e^{\lambda(T-T_0)} \qquad (2)$$

Where r_1, φ_1, ζ_1 and r_2, φ_2, ζ_2 is the average size, concentration and Zeta potential of non-aggregated nanoparticles and aggregated nanoparticles respectively. The concentration ratio for non-aggregated and aggregated nanoparticles calculated by UV absorption data is 9:1 and 6:4 for 0.020% and 0.040% Fe_3O_4 nanofluids respectively. The calculated values for nanofluids with volume fractions of 0.020% and 0.040% agree well with the measured results. This means that the electrical conductivity of nanofluids could be well predicted by considering the effect of nanoparticles agglomeration on the electrophoresis conductivity.

Conclusions: In this study, transformer oil-based Fe_3O_4 nanofluids were prepared and their electrical conductivity are greatly enhanced even at the relatively low volume fractions of 0.020% and 0.040%. A modified model has been proposed to well predict the change of electrical conductivity in nanofluids by introducing new parameters of agglomerated nanoparticles. This investigation provides a new way to further understand the electrical transport mechanism in transformer oil-based nanofluids.

References:

1. Y. M. Xuan, Q. Li, Heat transfer enhancement of nanofluids, *International Journal of Heat & Fluid Flow* 21 (2000) 58-64.
2. T. J. Taha, T. N. Narayanan, G. H. Gao, M. Rohde, D. A. Tsentalovich, M. Pasquali and P. M. Ajayan, Electrically insulating thermal nano-oils using 2D fillers, *ACS Nano* 6 (2012) 1214-1220.
3. L. P. Shen, H. Wang, M. Dong, Z. C. Ma and H. B. Wang, Solvothermal synthesis and electrical conductivity model for the zinc oxide-insulated oil nanofluid, *Physics Letters A* 376 (2012) 1053-1057.
4. M. Dong, L. P. Shen, H. Wang, H. B. Wang and J. Miao, Investigation on the electrical conductivity of transformer oil-based AlN nanofluid, *Journal of Nanomaterials* 2013 (2013) 842963.
5. S. Bagheli, H. K. Fadafan, R. L. Orimi and M. Ghaemi, Synthesis and experimental investigation of the electrical conductivity of water based magnetite nanofluids, *Powder Technology* 274 (2015) 426-430.
6. S. Chakraborty and S. Padhy, Anomalous electrical conductivity of nanoscale colloidal suspensions, *ACS Nano* 2 (2008) 2029-2036.
7. Y. Z. Lv, M. Rafiq, C. R. Li, B. L. Shan, Study of dielectric breakdown performance of transformer oil based magnetic nanofluids, *Energies* 10 (2017) 1025.
8. H. G. Cha, C. W. Kim, S. W. Kang, B. K. Kim and Y. S. Kang, Preparation and characterization of the magnetic fluid of trimethoxyhexadecylsiane-coated Fe_3O_4 nanoparticles, *Journal of Physical Chemistry C* 114 (2010) 9802-9807.
9. J. MIAO, M. Dong, Y. B. Yang, L. P. Shen and H. Wang, Modified electrical conductivity model for nanofluids-based transformer oil, *Journal of Xi'An Jiao Tong University* 47 (2013) 87.

1st International Conference on Nanofluids (ICNf2019)
2nd European Symposium on Nanofluids (ESNf2019)
26-28 June 2019, Castelló, Spain

Synthesis and characterization of aqueous silver nanofluid

Caio Carvalho dos Santos[1], Wesley Renato Vaili[1], Iasmin Louzada Herzog[2], and Miguel Jafelicci Junior[1].

[1]Laboratory of Magnetic Materials and Colloids, Department of Physical Chemistry, Institute of Chemistry, São Paulo State University (UNESP), Araraquara - SP, Brazil
[2]Federal University of Rio de Janeiro

*caio.c.santos@unesp.br; caio.cvs@hotmail.com

Keywords: metallic nanoparticles, colloidal stability, two-step nanofluid, and thermal conductivity.

Abstract: We report the synthesis of an aqueous nanofluid (NF) with improved thermal efficiency and with good colloidal stability. The NF is based on silver nanoparticles (NP) coated with glycine amino acid (Gly) synthesized by the chemical reduction method. The NP characterization by X-ray diffraction (XRD) indicated the formation of silver NP with a cubic crystalline structure. Transmission electron microscopy (TEM) allowed characterizing the morphology and size of the NP the sample had an average diameter of 15 ± 10 nm. To evaluate the colloidal stability of NF we performed Zeta potential (ζ) and dynamic light scattering (DLS) analysis, the NF showed values of the zeta potential (ζ) -28 mV and hydrodynamic diameter (D_h) of 110 nm ± 1 nm, respectively, in pH = 8. The thermal efficiency of the NF was evaluated by C-therm TCi show a 100% increase in thermal conductivity for NF with a volumetric fraction of 2,3 % and the NF was stable for over 30 days.

Introduction/Background: In recent years the advances in nanotechnology has intensified the search for new materials with efficient physical and chemical properties. The advances in different areas have allowed the miniaturization and increased the performance of amount systems and electronic devices. The search for ever smaller and integrated systems with a greater number of different functions has been a great technological objective today. Compact, lightweight and more efficient devices are a great challenge in terms of cooling [1-3]. To overcome these challenges related to high heat production in miniaturized systems, it has become increasingly intense by more efficient cooling methods capable of dissipating large amounts of heat [4]. In this context has intensified the search for ways to increase the thermal conductivity (k) heat

exchanger systems, through nanofluids employment, involving the dispersion of nanomaterials in a traditional fluid heat exchanger (water, ethylene glycol, and oils) [5]. This dispersion is designed to enable a large increase in the heat transfer rate of heat exchangers devices. To the commercial use, it is necessary that the nanofluids must be stable for long periods of time, so it should try to inhibit the aggregation trends of these nanomaterials, through the use of protective strategies and stabilization of nanoparticles that comprise it. The use of dispersion stabilization strategies is correlated to the study of the colloidal stability of these systems [6]. In this work, we report the synthesis and characterization of aqueous heat exchangers based in silver nanoparticles coated by glycine.

Materials and methods: All the chemical reagents used in this work presented analytical grade and were used as received from suppliers. Silver nitrate (98%), triethylene glycol (99%), glycine (99%), and were purchased from Sigma-Aldrich Brazil. The sodium chloride (99,3%) was acquired from Mallinckrodt. Sodium hydroxide (NaOH, 97%), and absolute ethanol were acquired from Labsynth® Ltda. Acetone acquired from J.T. Baker. The NP were synthesized by chemical reduction method [7]. Briefly, the silver nitrate was solubilized in distilled water with glycine in the molar ratio 1:10. This solution was added in the flask with 360 mL triethylene glycol, the mixture is heated at 30°C for two hours with magnetic stirring after de NP suspension was washed with ethanol, acetone and dialyzed for 14 days in water. After the suspension to add the aqueous base fluid to obtained the NF and the pH was adjusted at 8. The X-ray diffractogram was obtained in a model 5005 with CuKα radiation (I = 1.5418 Å) with a voltage of 40kV and current of 40 mA, in the range of 20 to 80 °, with a variation of 0.02 °. The infrared spectra of the sample were performed using a PerkinElmer FT-IR Spectrometer using Diffuse Reflectance Sampling Accessory module, the samples were prepared by diluting in potassium bromide. The analyze was measured using 128 scans to accumulation data and 4 cm^{-1} of resolution in 4000 at 400 cm^{-1} range. The micrograph of NP was performed in a transmission electron microscope FEI TECNAI G2 S-TWIN, LAb6, 200KV ASTAR. The colloidal stability to evaluated by the analyses of the zeta potential and DLS using a Zetasizer Nano series ZS equipment, from Malvern Instruments. The thermal conductivity of the sample was evaluated by C-therm TCi equipment, TH91-13-00554 instrument using H158 sensor at 25.08°C. The Thermal conductivity range device is: 0-100 W / m K with accuracy typically 5% for range 0 to 50°C and the precision typically

1.0%. The measurement time is less than 5 seconds to avoid errors associated with thermal convection of the samples.

Discussion and Results: In the Figure 1a shows the XRD of the NP, as observed the sample showed high crystallinity, and it was possible to index the characteristic peaks that allowed to identify the crystalline structure as being cubic with a = 4.086 which is approximately equal to the standard of silver (pdf JPCDS-89-3722) The other peaks were attributed to the crystalline phase of the amino acid coating (pdf JPCDS-7-718) the nanomaterials. Figure 1b shows the TEM of the sample. It was possible to observe that the morphology of the nanoparticles is approximately spherical. Based on the micrographs it was possible to determine the mean diameter of the same, plotting a lognormal curve in the histogram, the average diameter was 15 ± 10 nm. In the infrared spectra, figure 1c, it was possible to confirm the coating of the NP by the amino acid, which allows its dispersion in the base fluid and the obtention of an aqueous NF.

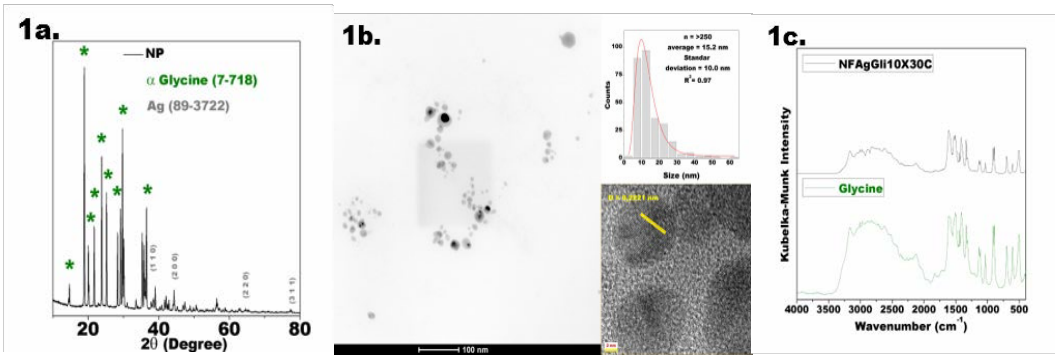

Figure 1. a. The XRD of the sample and the standard pdf of silver JPCDS-89-3722 and pdf of amino acid α - Glycine (7-718). b. The TEM of the silver NP. c . shows spectra in the FTIR of NP and Gly.

The colloidal stability of the synthesized NF was evaluated by zeta potential measurements and the hydrodynamic diameter in function of temperature. In the figure 2a it is shown the zeta potential titration curve of the NP, as can be observed above pH 7.5, the sample shows a high value the zeta potential in modulus (26,8 mV), which gives good electrostatic stability to the NP above that pH. Therefore, the final pH of the NF was adjusted to 8.0. The DLS as a function of temperature, figure 2b shows, that the D_h of the NF does not change significantly with the heating and cooling cycles (108 ±0.1 nm) which giving to the sample good colloidal stability under working conditions as a heat exchanger fluid. The NF was stable for over 30 days in the stationary state. In addition, the thermal conductivity of the NF was evaluated at 25.08 ° C, the NF had a k = 1.300 ± 0.005 W / m K which gave a gain of approximately 116% in the thermal conductivity of the NF produced in a volumetric fraction of 2,3% compare pure water. This high thermal

conductivity obtained is due to the higher concentration of the sample, in addition, this NP was coated with a large amount of amino acid that also has thermal conductivity superior to pure water and also contributed to the thermal conductivity of the sample [8].

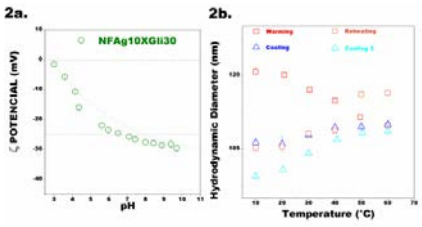

Figure 2. a The zeta titration of the silver Np. b. The Hydrodynamic Diameter of the silver NP in function of the temperature.

Summary/Conclusions: In this work, we presented an alternative synthetic route to obtain aqueous silver nanofluid with highly colloidal stability in heating and cooling cycles. The synthetic method used was outstanding for synthesizing cubic crystalline phase silver NP with a mean size of 15 nm functionalized with glycine. The new aqueous NF it exhibits an average increase of 116% in thermal conductivity at a volumetric fraction 2,3%. The NF show good colloidal stability 30 days in the stationary state and in function of temperature. The D_h of the sample does not change significantly when the sample was submitted to heating and cooling heat cycles.

References:

1. Rong H, Zhang H, Xiao S, Li C, Hu C. Optimizing energy consumption for data centers. Renew Sustain Energy Rev. 2016;58:674-691.
2. Sohel Murshed SM, Nieto de Castro CA. A critical review of traditional and emerging techniques and fluids for electronics cooling. Renew Sustain Energy Rev. 2017;78(May):821-833.
3. Colangelo G, Favale E, Milanese M, de Risi A, Laforgia D. Cooling of electronic devices: Nanofluids contribution. Appl Therm Eng. 2017;127:421-435.
4. Rodríguez-Muñoz JL, Belman-Flores JM. Review of diffusion-absorption refrigeration technologies. Renew Sustain Energy Rev. 2014;30:145-153.
5. Sezer N, Atieh MA, Koc M. A comprehensive review on synthesis, stability, thermophysical properties, and characterization of nanofluids. Powder Technol. 2018;344:404-431.
6. Gambinossi F, Mylon SE, Ferri JK. Aggregation kinetics and colloidal stability of functionalized nanoparticles. Adv Colloid Interface Sci. Volume 222, 2015: 332-349,

7. Manikam VR, Cheong KY, Razak KA. Chemical reduction methods for synthesizing Ag and Al nanoparticles and their respective nanoalloys. Mater Sci Eng B Solid-State Mater Adv Technol. 2011;176(3):187-203.
8. SIMMONS, J. A. Thermal Conductivity of Glycine. Nature. 1967 - 216: 1302.

1st International Conference on Nanofluids (ICNf2019)
2nd European Symposium on Nanofluids (ESNf2019)
26-28 June 2019, Castelló, Spain

Optical properties of colloidal suspensions of Goethite (α-FeOOH) nanorods under magnetic field

L. Mercatelli[1], E. Sani[1*], F. Agresti[2], V. Zin[2], S. Barison[2]

[1]National Institute of Optics (INO), National Research Council of Italy (CNR), Firenze, Italy

[2]Institute of Condensed Matter Chemistry and Technologies for Energy (ICMATE), National Research Council of Italy (CNR), Padova, Italy

[*]Corresponding author: elisa.sani@ino.it

Keywords: nanorods, magnetic field, goethite, magnetic nanoparticles

Abstract: The optical properties, and in particular the polarized transmittance, of colloidal suspensions of goethite (α-FeOOH) nanorods in water base fluid under the action of an external and tuneable magnetic field are investigated in the UV, visible and near infrared. As result we obtained that NIR transmittance changes in accordance with magnetic field direction and strength.

Introduction/Background:

Goethite-based colloids are mineral liquid crystals [1] with peculiar magnetic properties [2]; among all the fact that their optical properties can be tuned by the application of an external magnetic field.

Goethite (a-FeOOH) is investigated for many purposes as water purification, humidity sensing, organic pollutant degradation, coatings, pigments, lithium-ion batteries, as catalysts and for other applications thanks to their properties as high stability at room temperature, nontoxicity and low cost [3,4].

Goethite nanorods have been synthetized using various methods and several studies are still based on the development of their preparation processes, e.g. by the aging of ferrihydrite suspensions obtained through co-precipitation in different conditions, or by fast conversion of ferrihydrite through ultrasonic irradiation. The synthesis parameters can influence the morphology of nanoparticles as well as the optical properties of nanorods colloidal suspensions in water, thus optical characterization can represent a relatively simple method of characterization. Transmittance of colloids in the UV-Vis-NIR

range has been determined under different magnetic field intensities and directions with respect to light polarization.

Discussion and Results:

Samples obtained with different synthesis procedures (fig 1) were tested. After an ageing period, the obtained precipitate of each sample was washed, centrifuged and pH adjusted. Then stable colloids (0.1% wt) F1, T1, T2, US1 have been obtained by dilution. The spectral polarized transmittance, in two polarization directions, was measured as a function of strength and direction of external magnetic field (fig 2) by means of a spectrophotometer (Perkin Elmer Lambda900) equipped with a motorized polarizer.

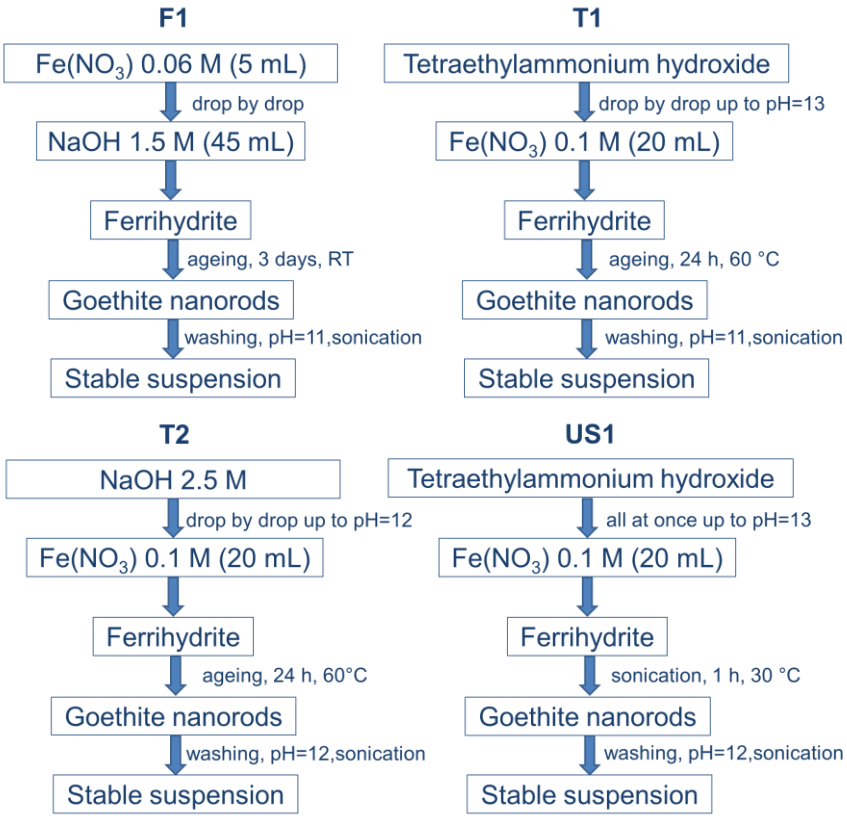

Fig 1. Synthesis of the 4 different samples

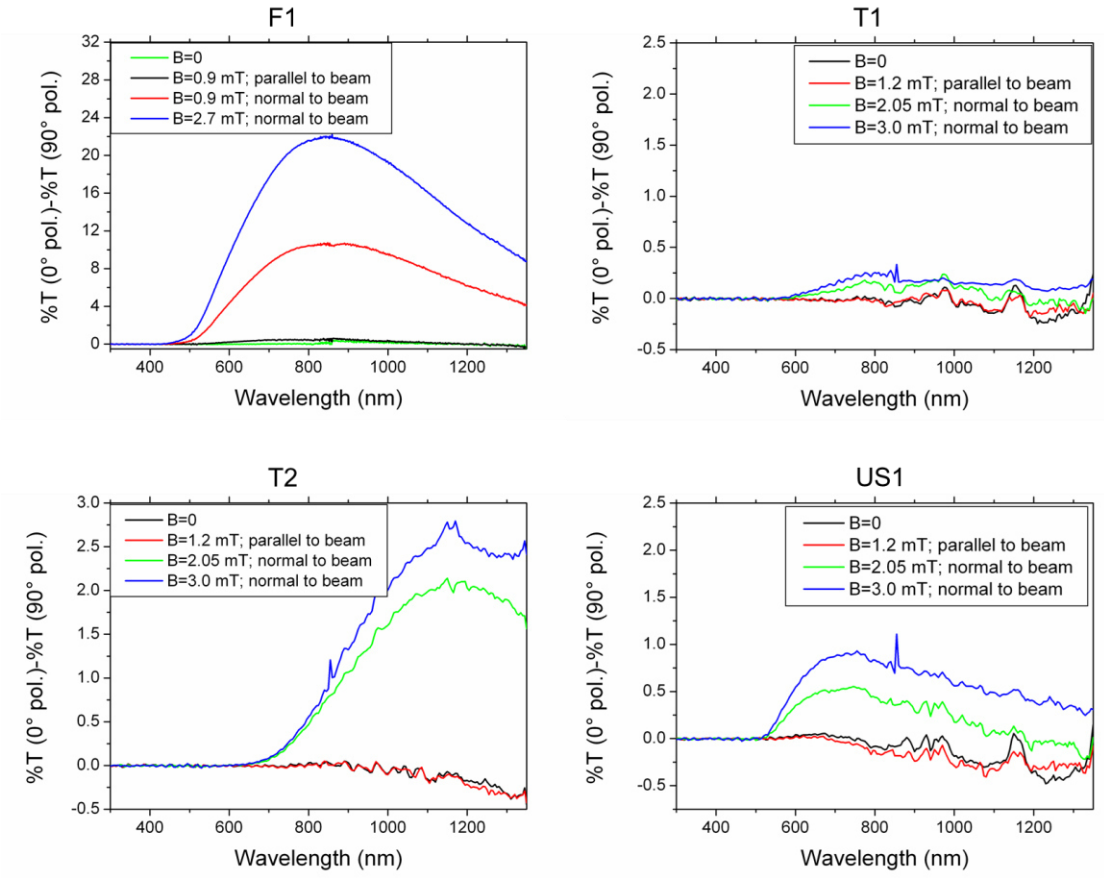

Fig 2. Difference between 0° and 90° spectral transmission as a function of magnetic field

Summary/Conclusions:

Goethite nanorods suspensions, synthetized with different morphologies, show the ability to change their transmittance of polarized light mainly in the NIR range. The transmittance can be tuned by changing the magnetic field intensity when normal to beam polarization, thus obtaining, as an example, a tunable optical filter. Samples show different responses with F1 being one order of magnitude more efficient than sample T2. F1 and US1 samples show high stability and their aggregates size are mainly a monodispersion (around 300 nm): this could play an important role in the efficiency of this interesting optical property.

References:

1. P.Davidson, P.Batail et al., Mineral liquid crystalline polymers, Progress in Polymer Science 22, 5, (1997) 913-936
2. B. Lemaire, P. Davidson et al., Outstanding Magnetic Properties of Nematic Suspensions of Goethite (α-FeOOH) Nanorods, Phys. Rev. Lett. 88 (2002), 125507
3. R. Baetens, B.P.Jelle et al. Properties, requirements and possibilities of smart windows for dynamic daylight and solar energy control in buildings: A state-of-the-art review, Solar Energy Materials and Solar Cells, 94, I 2 (2010) 87-105
4. M. Chu et al. Near-infrared laser light mediated cancer therapy by photothermal effect of Fe3O4 magnetic nanoparticles, Biomaterials, 34, 16 (2013) 4078-4088

1st International Conference on Nanofluids (ICNf2019)
2nd European Symposium on Nanofluids (ESNf2019)
26-28 June 2019, Castelló, Spain

Characterization and thermophysical properties of rutile and alumina nanofluids

J.L. Arjona-Escudero[1*], I.M. Santos-Ráez[1], and A.I. Gómez-Merino[2]

[1] Department of Mechanics, Thermal and Fluids Engineering, University of Málaga (Spain)

[2] Department of Applied Physics II, University of Málaga (Spain)

[*]Corresponding author: jae@uma.es

Keywords: nanofluids, thermal conductivity, DLS, viscosity.

Abstract: The characterization in relation to shape and particle size of alumina and rutile suspensions was performed. The intrinsic viscosity exhibited the presence of non-spherical aggregates in both suspensions although TEM images showed non monodisperse spherical shape of alumina particles. DLS indicated the existence of particle aggregates for both systems. In all cases, the increase in thermal conductivity with respect to the base fluid is verified. The thermal conductivities obtained experimentally were compared with three mathematical models, which yielded lower values than those measured. From rheological measurements and by means of the Peclet number defined in colloidal suspensions, values of thermal conductivity were also proposed.

Introduction/Background: Nanofluids are liquids containing nanoparticles with size generally less than 100 nm. They are very promising materials as high performance heat transfer fluids [1, 2]. The flow field of a suspension is mainly governed by the volume fraction occupied by the solid particles (ϕ). When the suspension is concentrated, the interactions of particles should be considered. In this case, several expressions for the relation between viscosity and volume fraction of particles have been proposed. The expressions used in this work are:

$$\eta_r = \left(1 - \frac{\phi}{\phi_m}\right)^{-[\eta]\phi_m} \quad \text{Krieger Dougherty model} \quad (1)$$

$$\eta_r = exp\left(\frac{[\eta]\phi}{1-\left({}^{\phi}/_{\phi_m}\right)}\right) \quad \text{Mooney model} \quad (2)$$

In these expressions, $\eta_r = {}^{\eta}/_{\eta_0}$, η_0 is the viscosity of the liquid phase, $[\eta]$ is the intrinsic viscosity, which depends on the aspect ratio, defined as the proportion between two characteristics lengths of the particle. When $[\eta] = 2{,}5$, particles are spheres. Finally, ϕ_m,

is the maximum packing fraction, which expresses the ability of particles to achieve the most compact distribution. The objective of this work is the characterization of the nanoparticles of alumina and rutile (titanium dioxide) aqueous suspensions in relation to size and shape, which exert a strong influence on the themophysical properties. The thermal conductivity of these nanofluids as a function of volume fraction was experimentally determined. These results were also compared with three models of thermal conductivity. Finally, another method of thermal conductivity determination from the shear stress values obtained by rheological measurements was proposed.

Discussion and Results:

TEM images showed spherical nanoparticles with a mean average diameter of 70±6 nm (Al_2O_3) or 100±10 nm (rutile) respectively, although polydispersity is observed, with a few particles of 200 nm in diameter (figure 1).

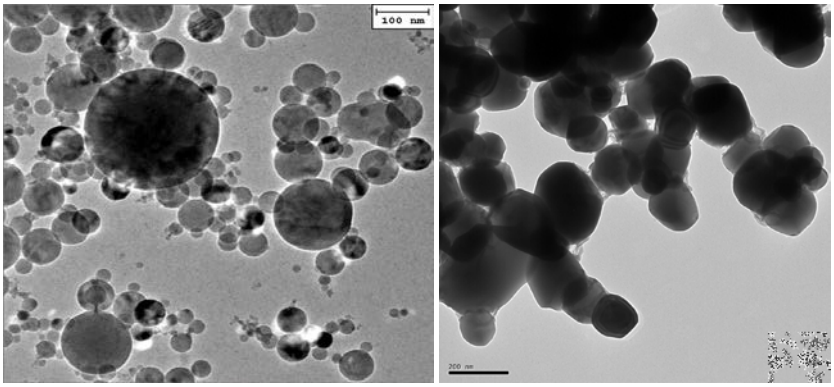

(a) (b)

Figure 1. Representative TEM micrograph and particle morphology of Al_2O_3 (a) and rutile (b) nanoparticles used in the study.

However, DLS technique was used to characterize the size of agglomerates in solution. These measurements indicated an average diameter of about 200 nm for alumina and 350 nm for rutile respectively, which remained significantly constant for at least five hours.

The steady shear flow was performed in a Haake Rheostress-600 rheometer. These rheological measurements showed a shear thinning behaviour, consequently the clusters deducted by DLS characterization, when they are at rest, are formed by highly branched aggregates that erode when shear rate increases, until a suspension of individual particles is achieved. These results are in good agreement with the intrinsic viscosity obtained by Mooney and Krieger-Dougherty models (table 1). In both cases, these values are far from the 2.5 corresponding to spherical particles. Consequently, both nanofluids showed the presence particle agglomerates, which produce a non-spherical system. This phenomenon

is more significant in alumina, according to the values of the intrinsic viscosity shown in table 1.

Table 1. Predicted values of $\emptyset_m$ and [η] at low and high shear rate obtained by fitting the measured data with the Krieger Dougherty and Mooney models.

	Alumina (25ºC)			Rutile (25ºC)		
Model	**Parameter**	**Low shear rate**	**High shear rate**	**Parameter**	**Low shear rate**	**High shear rate**
KD equ (1)	$[\eta]$	20±5	9.9±0.4	$[\eta]$	6.5±0.9	4.5±0.1
	ϕ_m	0.5±0.1	0.44±0.01	ϕ_m	0.6±0.1	0.52±0.02
M equ (2)	$[\eta]$	20±3	8.6±0.4	$[\eta]$	6±1	4.2±0.2
	ϕ_m	0.6±0.2	0.63±0.02	ϕ_m	0.9±0.3	0.81±0.05

The thermal conductivity was measured using the KD2 Pro equipment. The powder was dispersed water with a saline solution of 10^{-4} M KCl in order to stabilize the charged particles. Figure 2 indicates the experimentally measured relative thermal conductivity at different volume fractions for alumina and rutile suspensions. The comparison of these values with those estimated by means of Eqns. (3), (4) and (5) are also shown in Fig. 2.

$$K_{nf} = K_{bf}\frac{K_{np}+2\cdot K_{bf}+2\cdot(K_{np}-K_{bf})\cdot\emptyset}{K_{np}+2\cdot K_{bf}-(K_{np}-K_{bf})\cdot\emptyset} \quad \text{Maxwell model} \quad (3)$$

$$K_{nf} = K_{bf}\frac{(1+2\alpha)K_{np}+2\cdot K_{bf}+2\cdot(K_{np}\cdot(1-\alpha)-K_{bf})\cdot\emptyset}{(1+2\alpha)K_{np}+2\cdot K_{bf}-(K_{np}\cdot(1-\alpha)-K_{bf})\cdot\emptyset} \quad \text{Hasselman and Johnson model} \quad (4)$$

$$K_{nf} = \frac{K_{np}\cdot K_{bf}}{K_{np}-(K_{np}-K_{bf})\cdot\emptyset} \quad \text{Peñas et al. model} \quad (5)$$

Where K_{nf} is the thermal conductivity of the nanofluid, K_{bf} is the thermal conductivity of the base fluid, K_{np} is the thermal conductivity of the nanoparticles, ϕ is the volumetric fraction occupied by the nanoparticles, α is a dimensionless parameter including the boundary resistance.

A rheological study of the two systems was also carried out. Since Pe number and shear stress are connected by Eq. (6). This expression provides another method for the determination of the thermal conductivity in colloids system.

$$Pe = \frac{6\pi r^3}{k_B}\cdot\frac{1}{T}\cdot\tau = \frac{L\cdot v\cdot\rho_{nf}\cdot C_{p_{nf}}}{K_{nf}} \quad \text{Peclet number} \quad (6)$$

Where *r* is the particle radius, k_B is the Stefan-Boltzmann constant, *T* is the temperature, τ is the stress, *L* is a typical length, *v* is the velocity of the sample, ρ_{nf} is the density of nanofluid, and $C_{p_{nf}}$ is the specific heat of the nanofluid. The values of these thermal conductivities for the alumina and rutile suspensions at different volume fractions are shown in Fig. 2.a and 2.b. In alumina suspensions (Fig. 2.a), the theoretical models

underestimate the thermal conductivity. However, the values obtained by shear stress are closer to the experimental ones. On the other hand, in rutile suspensions, the differences in thermal conductivity with the volume fractions tested are very small, and the discrepancies with the mathematical models are very little and the rheological values are very close.

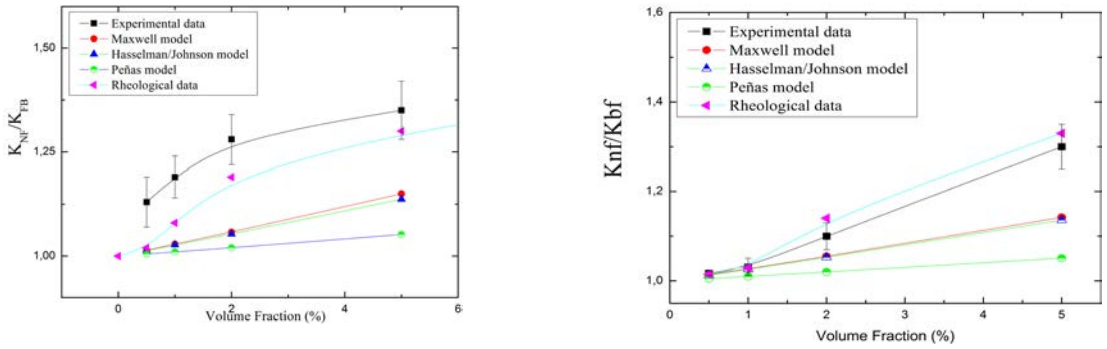

(a) (b)

Figure 2. Comparison among experimentally observed thermal conductivity and various models for alumina (a) and rutile (b).

Summary/Conclusions: DLS measurements showed the presence of agglomerates with spheroidal forms in both systems. Therefore, the influence of particle shape in thermal conductivity was not tested. The thermal conductivity of both nanofluids increased with volume fraction, as found in the literature [2-4], and showed some discrepancies with the three mathematical models checked, which was more pronounced in alumina suspensions. The experimental shear stress has demonstrated to provide thermal conductivity values in good agreement with the experimental measurements.

References:

1. S. P. Jang, S. U. Choi, Cooling performance of a microchannel heat sink with nanofluids, *Applied Thermal Engineering* 26 (17) (2006) 2457-2463.
2. J.R. Eggers, S. Kabelac, Nanofluids revisited, *Applied Thermal Engineering* 106 (2016) 1114-1126.
3. D. Cabaleiro, J. Nimo, M.J. Pastoriza-Gallego, M.M. Piñeiro, J.L. Legido, L. Lugo, Thermal conductivity of dry anatase and rutile nano-powders and ethylene and propylene glycol-based TiO_2 nanofluids, *J. Chem. Thermodynamics* 83 (2015) 67-76.
4. R. Agarwal, K. Verma, N.K: Agrawal, R. Singh, Sensitivity of thermal conductivity for Al_2O_3 nanofluids, *Experimental Thermal and Fluid Science* 80 (2017) 19-26.

1st International Conference on Nanofluids (ICNf2019)
2nd European Symposium on Nanofluids (ESNf2019)
26-28 June 2019, Castelló, Spain

Electrical Conductivity of Aqueous Alumina Nanofluids (15 nm or 40 nm) at Low Concentrations and Different Temperatures

M. A. Rivas[1], R. Iglesias[1], M. F. Coelho[1,3], G.Vilão[2] and T. P. Iglesias[1*]

[1*] Departamento de Física Aplicada, Facultad de Ciencias, Universidad de Vigo, Lagoas-Marcosende s/n, 36310 Vigo, Spain. E-mail address: tpigles@uvigo.es

[2] Departamento de Física-Politécnico do Porto, Instituto Superior de Engenharia, Portugal

[3] CIETI-Centro de Inovação em Engenharia e Tecnologia Industrial, ISEP, Porto, Portugal

Keywords: Alumina; nanofluids; nanoparticles; electrical conductivity.

Abstract: The electrical conductivity of alumina nanofluids (aluminium oxide) in water is studied. The nanoparticle sizes of 15 nm and 40 nm were considered and the measurements were carried out at various concentrations lower than that of 1.5% in volume and at six temperatures (from 298.15 K to 348.15 K). The empirical Hill's equation was used to describe the electrical conductivity of the experimental data. This equation can describe its rapid change with the variation of the alumina concentration. The enhancement of electrical conductivity was calculated and its behaviour analysed. Theoretical models in the study of electrical conductivity are applied.

Introduction/Background: From a scientific standpoint, electrical conductivity, σ, is a macroscopic thermo-physical magnitude that is related to certain microscopic mechanisms responsible for the electric current and it can give some information about them. As, from an industrial standpoint, it is important in the research of heating and cooling technologies, it is currently under study.

Literature has shown that the main factors involved in the behaviour of the thermophysical properties of nanofluids are size, morphology, nanoparticle content, the purity of the base fluid and also the possible addition of surfactants. The results presented in this work were carried out without addition of surfactants so as not to mask the effect of the nanoparticles and highlight the importance of another factors on the behaviour of electrical conductivity.

In previous works, [1, 2], the electrical conductivity of alumina nanofluids (15nm or 40nm) was studied at alumina concentrations higher than 0.25 % in volume. The present study

was performed in order to ascertain the behaviour of these nanofluids at lower concentrations.

Discussion and Results: At concentrations lower than 0.25% in volume the values of electrical conductivity rise with increasing alumina concentration at fixed temperature and with increasing temperature at fixed composition. Nanofluids with a nanoparticle size of 15 nm have a lower conductivity than that of nanofluids with nanoparticles of size 40 nm. These behaviours are the same at higher alumina concentrations [1, 2].

The experimental data can be accurately described in terms of composition by the empirical Hill's equation [3] which reads:

$$\sigma = \frac{K_0 \phi_A^n}{1 + K_0 \phi_A^n} \quad (1)$$

K_0 and n are two fitting parameters and ϕ_A the alumina volume fraction. This equation has been used in different branches of science to describe the degree cooperation in different kinetic processes. However, this is considered for some authors in literature as a merely fitting equation.

In order to describe their behaviour with temperature, an equation of Arrhenius type has been suitable as occurs at higher concentrations, [1, 2].

Figure 1 shows the electrical conductivity enhancement, σ/σ_W (where σ_W is the electrical conductivity of water) for the system α-Al_2O_3 (40nm) + water, for all studied alumina concentrations and temperatures. This figure shows that electrical conductivity is higher than that of the base fluid for all nanoparticle concentrations and temperatures. As occurs at higher concentrations, [1, 2], the observed values of $\sigma/\sigma_W > 1$ cannot be considered an expected behaviour because, at the experimental temperatures, the electrical conductivity of the alumina does not exceed 5pS·cm^{-1}, [4], which is about five orders of magnitude below that of the base fluid. As the electrical conductivity of alumina is lower than that of the water, the electrical conductivity of the nanofluids should be lower than that of the source fluid, which does not happen.

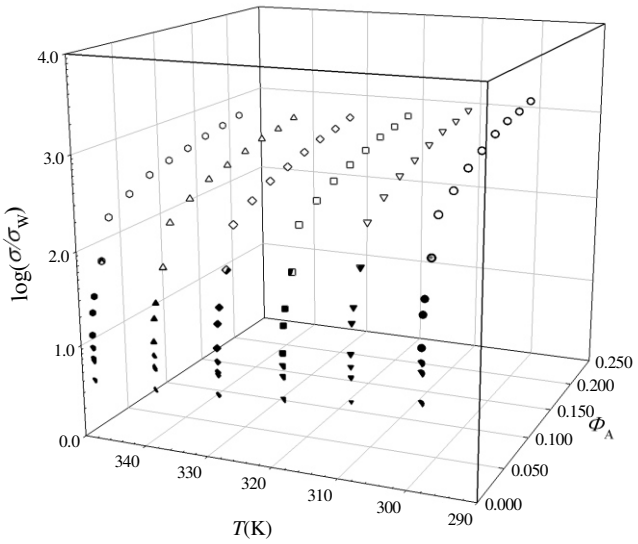

Figure 1. Electrical conductivity enhancement, σ/σ_W for the nanofluid α-Al_2O_3 (40nm) + water (open symbols) from [2] and (filled symbols) from this work as a function of alumina volume fraction, ϕ_A, at different temperatures.

Figure 1 shows that the electrical conductivity enhancement tends to one when the alumina concentration tends toward zero. A similar behaviour has been found for the γ-Al_2O_3 nanofluids (15 nm) in water. The two very different behaviours of the conductivity at lower and at higher concentrations can also be observed in this figure.

From a fundamental standpoint, the study of electrical conductivity of mixing $\Delta_{mix}\sigma$ is more interesting than electrical conductivity enhancement. For fixed temperature and pressure, this property is empirically defined by equation (2), in similitude to the theoretical definition of excess permittivity, [5].

$$\Delta_{mix}\,\sigma = \sigma - (\phi_W\,\sigma_W + \phi_A\,\sigma_A) \qquad (2)$$

As there is no theoretical definition of ideal electrical conductivity, the sum within the parenthesis will be empirically considered as the ideal conductivity. $\phi_W = 1 - \phi_A$ and σ_A is the electrical conductivity of bulk alumina. In these nanofluids, $\Delta_{mix}\,\sigma$ is positive and increases with increasing temperature.

Summary/Conclusions: We draw the following conclusions from the experimental determination of electrical conductivity of these nanofluids at low concentrations.

The electrical conductivity rises with increasing temperature and alumina concentration. This is the same behaviour as the previous obtained at higher alumina concentrations. The values of permittivity enhancement $\sigma/\sigma_W > 1$ is not an expected result as occurs at higher concentrations. The observed positive deviations of the electrical conductivity of mixing in relation to its considered ideal value ($\Delta_{mix}\sigma > 0$) indicate that the mechanisms of conduction improve when the components are in mixture. The rapid change of electrical conductivity at low concentrations can be described by a percolation model. The variable index equation [6] predicts that the water contribution to the electrical conductivity of these nanofluids does not depend on concentration and slightly on temperature. However, the alumina contribution depends on temperature and concentration, and for some alumina concentrations and temperatures its contribution exceeds that of the water.

Acknowledgements: We gratefully appreciate the financial support ED431C 2016-034 provided by the Xunta de Galicia (Spain). M.F.C. and G. V., thanks to the Instituto Superior de Engenharia do Porto for granting leave of absence to carry out experimental work at the University of Vigo.

References:

1. T. P. Iglesias, M. A. Rivas, R. Iglesias, J. Reis and F. Coelho, Electric permittivity and conductivity of nanofluids consisting of 15 nm particles of alumina in base Milli-Q and Milli-Ro water at different temperatures, *J. Chem. Thermodyn.* 66 (2013) 123-130.
2. R. Iglesias, M. A. Rivas, J. Reis, and T. P. Iglesias, Permittivity and electric conductivity of aqueous alumina (40 nm) nanofluids at different temperatures, *J. Chem. Thermodyn.* 89 (2015) 189–196.
3. S. Goutellea, M. Maurin, F. Rougier, X. Barbaut, L. Bourguignona, M. Ducher and P. Maire, The Hill equation: A review of its capabilities in pharmacological modeling, *Fundam. & Clinical Pharmacol*, 22, (2008) 633–648.
4. J.F. Shackelford, W. Alexander (Eds.), Handbook of Materials Science and Engineering, CRC Press, Boca Raton, Fl, third ed., 2001.
5. T.P. Iglesias, J.C.R. Reis, L. Fariña-Busto, On the definition of the excess permittivity of a fluid mixture. II, J. Chem. Thermodyn. 40 (2008) 1475-1476.
6. M. F. Coelho, M. A. Rivas, G.Vilão , E. M. Nogueira and T. P. Iglesias, Permittivity and electric conductivity of copper oxide nanofluid (12 nm) in water at different temperatures, J. Chem. Thermodyn. 132 (2019) 164–173.

1st International Conference on Nanofluids (ICNf2019)
2nd European Symposium on Nanofluids (ESNf2019)
26-28 June 2019, Castelló, Spain

Influence of measurement techniques on molten salt surface wetting characterization

A. Anagnostopoulos[1], A. Palacios[1], M.E. Navarro[1*], S. Fereres[2], Y. Ding[1]

[1] *PhD A. Anagnostopoulos, PhD A. Palacios, Dr. M. E. Navarro, Prof. Y. Ding, Birmingham Centre for Energy Storage & School of Chemical Engineering, University of Birmingham, Birmingham B15 2TT, United Kingdom.*

[2] *Dr. S. Fereres, Abengoa, Calle Energia Solar 1, 41014 Sevilla, Spain*

[*] M.E. Navarro: h.navarro@bham.ac.uk

Keywords: solar energy, molten salt, nanofluid, wettability, contact angle

Abstract: Molten nitrate salts have extended application in concentrated solar energy power plants as energy storage materials and heat transfer fluids. Due to their poor thermal properties, molten salts are doped with metal oxide nanoparticles to enhance their thermal performance, with varied reports of increased thermal conductivity and specific heat capacity. The stability of molten salt-based nanofluids is of paramount importance to understand their behaviour. Colloidal stability is determined by salt-particle surface interactions. Contact angle measurements are proposed to analyse the affinity of the molten salt components to the solid particle surfaces. In this work, the effect of environmental parameters and measurement techniques on the wettability of molten salts and molten salt nanofluids is investigated. The effect of time, surface, roughness and atmosphere are examined. The contact angle of solar salt is measured on different surfaces, to investigate the effect of surface energy and roughness on the wettability. Additionally, the time evolution of contact angle measurements is studied in air and vacuum. It is found that in vacuum the contact angle is stable with time, while in air it rapidly reduces in the first four hours. Different solid sample preparation processes are explored and their effect on the contact angle measurements is evaluated.

Introduction/Background: Renewable energy technologies are key solutions to the to the present environmental crisis. Solar energy, in an industrial scale, is applied in the form of concentrated solar power (CSP) [1]. Molten salts are the most common energy storage materials in CSP plants, with secondary applications as heat transfer fluids. They have a large temperature operating range and excellent thermal stability both detrimental properties for energy storage [2]. Their biggest disadvantage is their poor

thermal properties. To counter this, they are often doped with metal oxide nanoparticles (NP) to formulate molten salt nanofluids.

Wettability affects several factors that impact the performance of fluids in industrial processes. In molten salt energy storage, good wettability between salt and stainless steel, translates to corrosion issues in energy storage tanks. Additionally, pipe wettability has been found to relate to flow slip properties and turbulence in flow. From a fundamental perspective, a better understanding of the wettability behaviour of the molten salts with the materials used as nanoparticles can shed light on the electrostatic surface interactions that may explain some of the anomalous behaviour reported for molten salt based nanofluids [3]. The wettability between a fluid and a surface is most commonly assessed by measuring the contact angle (CA) between the two. CA measurement is greatly affected by the testing conditions. Surface roughness has been shown to be the most important parameter related to the wetting behaviour of a liquid. Additionally, each surface has a different crystalline orientation, that governs its surface energy and thus the CA of the material. Basic environmental testing conditions such as ambient pressure, temperature and time can also impact the CA [4]. Moreover, it is notoriously difficult to measure the CA of high temperature fluids, which are solid at ambient temperature, such as molten salts. Although temperature-controlled devices exist to keep the salts in a molten state during the measurement, the solid sample preparation method affects the CA results. In this work a preliminary investigation on the effect of environmental parameters on the CA of molten salt nanofluids is conducted.

Materials and Methods: Solar salt (SS) containing 60% $NaNO_3$- 40% KNO_3 (%wt.) is used for the CA measurements presented in this study. Amorphous SiO_2 NPs with a 10 nm mean average diameter are used in the nanofluid preparation. All individual component salts are purchased from Sigma Aldrich have a purity >99.9%. The molten salts are synthesized by the static melting of the two independent salts and the nanofluid using the three-step (wet) method [2]. A KRUSS HT-2 is used to perform the CA measurements in air and vacuum atmosphere, with a 2 °C/min heating rate. The presented CA values are the average of 3 measurements. CA values dispersion is subject to several factors [3]. Surface roughness and drop dimension are the most important. To minimize their effect, a sample preparation protocol is followed. The salt eutectic powder is weighed, then milled and afterwards compressed at 40 MPa for 3 min in a 4 mm diameter round compression dye, to form identical dimension pellets of 0.1g. To minimize the impact of surface roughness, measurements are conducted using an EPS Interferometer before and after each measurement, on all used surfaces. The surface roughness is found to have constant value

of S=0.346±0.2 μm for the alumina (Al_2O_3) substrate (30 mm x 30 mm x 10 mm), S=0.31 S=1.146±0.2 μm for the stainless steel and S=0.246±0.2 μm for the SiO2 {1 0 0}.

Discussion and Results: CA measurements are conducted using SS with 0 wt.% and 1 wt.% SiO_2 NPs on alumina, stainless steel and SiO_2 surfaces (Figure 1). Despite their similar surface roughness, the alumina and silica surfaces present differences in the CA, particularly between 220 and 280 °C. This temperature range roughly coincides with the "mushy" or sub-liquidus region for this salt mixture (220 to 260ºC), where the salt is not fully liquid. The most remarkable result is that (partially solid) solar salt has a much larger CA on the alumina surface, meaning that the mushy fluid has a worse wettability on this surface compared to the silica surface. At temperatures above 280ºC, the CA of solar salt on alumina and silica surfaces coincide. On the other hand, stainless steel with considerably higher roughness, leads to the CA retaining a stable value until 300 °C. A liquid is characterized as wetting a specific surface when its CA is <90°. In the presence of suspended SiO_2 nanoparticles in the salt mixture, all surfaces present an increase in the CA. In the case of the stainless steel, the effect is more prevalent with the CA retaining values higher than 90° even until 350 °C.

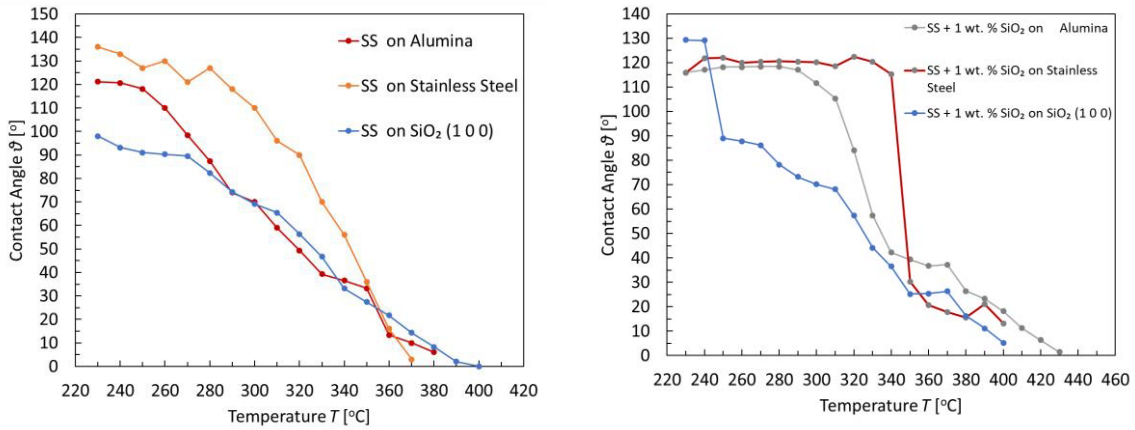

Figure 1. Effect of surface material on solar salt (SS) contact angle (left) and solar salt-based NPs suspension contact angle (right)

The effect of the CA with respect to time is also assessed. SS samples are tested in both air and vacuum with 0 wt.% and 1.0 wt.% SiO_2 nanoparticles (Figure 2). The CA decreases with time in all cases. The experiments conducted under vacuum present the least time variation. In the CA measurements conducted varying temperature, a 2°C/min heating rate is selected, to ensure that the measurements are not affected by time, since the CA remains stable in the 1st hour. After that, the CA drops at a fast rate in the first 4 hours after which it slowly stabilizes. In vacuum the CA remains relatively stable for the first 10 hours after which it reduces. This is to be expected as vacuum has a much lower density

than air. In the presence of silica NPs, the sample pellet compression influences the CA value mainly only during the first two hours.

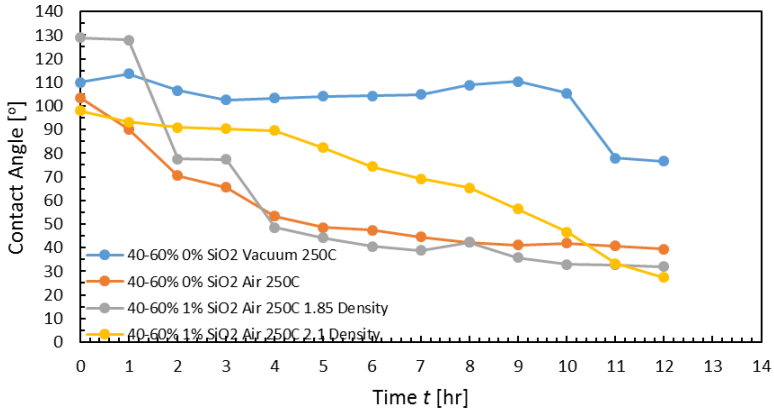

Figure 2. Effect of atmosphere, NP and pellet compression rate on the CA of molten salt and molten salt nanofluids.

Summary/Conclusions: CA measurements are conducted for SS without and with 1.0 wt. % SiO_2 on alumina, stainless steel and silica. Alumina and silica present different wettability in the mushy region of this salt mixture, suggesting that electrostatic interactions between the salt and SiO_2 or Al_2O_3 may be different. Stainless steel with a high roughness, presents non-wetting behaviour throughout the phase transition temperatures (220-300 °C). Additionally, the CA of the molten salt increases with nanoparticle addition. Studies with respect to time show that the CA is stable in the first hour, then rapidly reduces for 4 hours, after which it stabilized. In vacuum the CA remains stable for roughly 10hours after which it is suddenly reduced. Higher nanofluid pellet compression rates show a more stable CA, while lower ones have a higher initial CA followed by a rapid reduction, that matches the base case in 2 hours. Further research is required to evaluate the effect of air release during phase transition. These initial findings identify a difference in the wetting behaviour of binary nitrate salt mixtures on different materials. Future steps will investigate if differences in wetting behaviour may correlate to nanofluid property differences with different types of nanoparticles (i.e. rheology, specific heat capacity).

Acknowledgments: The authors acknowledge the finance support from Engineering and Physical Sciences Research Council (EPSRC).

References:

1. B. Sørensen, *Renewable Energy: Physics, Engineering, Environmental Impacts, Economics and Planning: Fifth Edition*. 2017.
2. Z. Jiang *et al.*, “Novel key parameter for eutectic nitrates based nanofluids selection for CSP system,” *Appl. Energy* 235 (2019) 529–542.
3. B. Muñoz-Sánchez *et al.*, “Rheology of Solar-Salt based nanofluids for

concentrated solar power. Influence of the salt purity, nanoparticle concentration, temperature and rheometer geometry," *Sol. Energy Mater. Sol. Cells*, 2018.

4. F. Sofos et al., "Surface wettability effects on flow in rough wall nanochannels," *Microfluid. Nanofluidics*, 2012.
5. Yuehua Yuan and T. Randall, *[9]Surface science techniques*, vol. 51, no. 1. 2013

1st International Conference on Nanofluids (ICNf2019)
2nd European Symposium on Nanofluids (ESNf2019)
26-28 June 2019, Castelló, Spain

Design of stable propylene glycol:water-based fAg–pGnP hybrid nanofluids

Javier P. Vallejo[1], Gaweł Żyła[2], Elisa Sani[3], Iván G. Cao[1], Luis Lugo[1*]

[1]Departamento de Física Aplicada, Facultade de Ciencias, Universidade de Vigo, E-36310 Vigo, Spain

[2]Department of Physics and Medical Engineering, Rzeszów University of Technology, 35-959 Rzeszów, Poland

[3]CNR-INO National Institute of Optics, Largo E. Fermi, 6, I-50125 Firenze, Italy

[*]Corresponding author: luis.lugo@uvigo.es

Keywords: Hybrid nanofluid, Graphene nanoplatelets, Silver nanoparticles, Propylene glycol, Stability.

Abstract: Hybrid nanofluids aim to improve the characteristics of classical nanofluids. In this study, different dispersions of fAg–pGnP nanoadditive at concentrations of 0.05, 0.10 and 1.0 wt% in propylene glycol:water 10:90 wt% were designed. The used fAg–pGnP nanopowder is composed by functionalized silver and polycarboxilate chemically modified graphene nanoplatelets. Various mass ratios between them were considered: 0:1, 1:4, 1:1, 4:1 and 1:0. A characterization of the hybrid nanopowder was developed by transmission electron microscopy. The long-term stability of the nanofluids was confirmed by dynamic light scattering measurements. Furthermore, the densities of the designed hybrid nanofluids was experimentally determined by the vibrating tube technique.

Introduction/Background: Nanoadditives based heat transfer fluids have received extensive consideration in the last two decades due to their exceptional potential qualities in different applications. Diverse nanostructured metals, metallic oxides and carbon-based have been stated to be outstanding additives for heat carrier fluids. Among them, it is quite well stablished that different carbon-derivatives have been considered as one of the most promising and attractive nanomaterials [1] and graphene nanofluids provided the best heat transfer coefficients [2]. In the recent years, the research in this field has started to pay attention on a new generation heat transfer fluids called hybrid nanofluids with the aim to further improve the characteristics of conventional nanofluids [3]. So, the synthesis of nanocomposite or nanoparticle-decorated and the preparation of nanofluids based on nanocomposites are a new and interesting topic, although hybrid nanofluids are prepared either by dispersing nanocomposite additives in the base fluid or by dispersing dissimilar nanoparticles as individual components [4]. Until now, the efforts

devoted to hybrid nanofluids are limited and a wide understanding based on systematic experimental investigations is missing. To propose new hybrid nanofluids for specific engineering applications with improved synergistic effects it is required to carry out systematic comprehensive experimental studies exploring thermophysical, rheological, optical and hydrodynamic profiles [3].

In this work, different dispersions of total nanoadditive concentrations of 0.05, 0.10 and 1.0 wt% in a propylene glycol:water 10:90 wt% mixture (PG:W) were designed by a two-step method. The employed nanoadditives were two commercial nanopowders: silver "NGAP NP Ag-2103" (NANOGAP S.A., A Coruña, Spain) and polycarboxilate chemically modified graphene nanoplatelets (NanoInnova Technologies S.L., Madrid, Spain). Hereinafter they are going to be named as fAg and pGnP, respectively. Different mass ratios between them were considered: 0:1, 1:4, 1:1, 4:1 and 1:0. The eleven designed nanofluids are described in Table 1.

Table 1. Designed fAg–pGnP hybrid nanofluids

Total nanoadditive concentration, wt%	fAg concentration, wt%	pGnP concentration, wt%	Nanofluid
0.05	0	0.05	0.05 wt% pGnP/PG:W
	0.04	0.01	(0.04 wt% fAg + 0.01 wt% pGnP)/PG:W
	0.05	0	0.05 wt% fAg/PG:W
0.10	0	0.10	0.10 wt% pGnP/PG:W
	0.02	0.08	(0.02 wt% fAg + 0.08 wt% pGnP)/PG:W
	0.05	0.05	(0.05 wt% fAg + 0.05 wt% pGnP)/PG:W
	0.08	0.02	(0.08 wt% fAg + 0.02 wt% pGnP)/PG:W
	0.10	0	0.10 wt% fAg/PG:W
1.0	0	1.0	1.0 wt% pGnP/PG:W
	0.80	0.20	(0.80 wt% fAg + 0.20 wt% pGnP)/PG:W
	1.0	0	1.0 wt% fAg/PG:W

A transmission electron microscope (TEM) JEM 2010 (JEOL, Tokyo, Japan) was employed to obtain TEM images of the hybrid nanopowder. The stability of the samples was assessed by means of dynamic light scattering measurements through a Zetasizer Nano ZS (Malvern Instruments Ltd, Malvern, United Kingdom) at room temperature. Density was determined by means of a DMA 500 densimeter (Anton Paar, Graz, Austria) based on the oscillating U-tube technique at 298.15, 308.15 and 318.15 K.

Discussion and Results: pGnP was characterized in a previous work [1] as staked graphene sheets with of up to 20 high and up to 500 nm wide/long while fAg are defined by the provider as quasi spherical and rod-like silver nanoparticles of 40-55 nm. Figure 1

shows a TEM image of the dried hybrid nanopowder, confirming these previous characterizations and evidencing the trend of the fAg to cluster around pGnP.

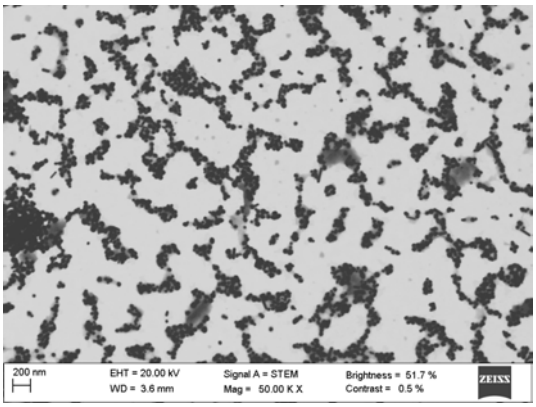

Figure 1. TEM image of the dried (0.08 wt% fAg + 0.02 wt% pGnP) hybrid nanopowder

The size distribution by intensity for the (0.08 wt% fAg + 0.02 wt% pGnP)/PG:W nanofluid is shown for the sample just after preparation in Figure 2 (a) and for the same sample five days later in static conditions in Figure 2 (b). Dynamic light scattering measurements assume spherical shape of nanoparticles while nanoplatelets do not present this shape. Thus, the reported size values should be assumed as “apparent” sizes. The first intensity peak observed in Figure 2 corresponds to fAg and the second to pGnP. As it can be seen, the obtained peaks are practically equal after preparation and five days later, confirming the stability of the dispersions that is also visually appreciated.

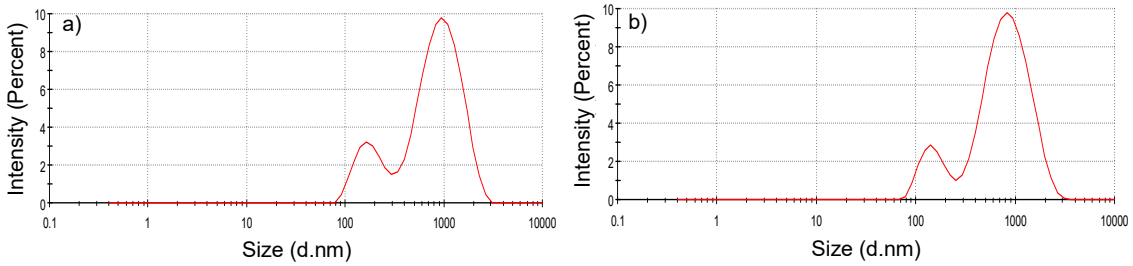

Figure 2. Apparent size distribution by intensity for the (0.08 wt% fAg + 0.02 wt% pGnP)/PG:W sample: (a) after preparation and (b) 5 days later.

Figure 3 shows the density results for the hybrid nanofluids with 0.10 wt% total nanoadditive concentration. For all the analysed samples, the one that only contains 1.0 wt% fAg showed the highest density increases, up to 2.4 % with respect to the base fluid, while the one that only contains 1.0 wt% pGnP, the lowest, up to 0.4 %. For a fixed total nanoadditives concentration of the hybrid nanofluids, the rising amount of fAg and the decreasing amount of pGnP leads to increasing density values.

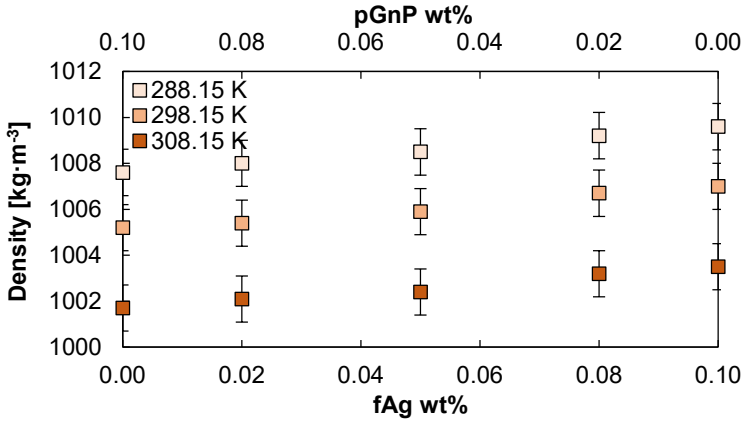

Figure 3. Density for the different hybrid nanofluids with total nanoadditive concentration of 0.10 wt% at 288.15, 298.15 and 308.15 K.

As follows, it is intended to perform a complete description of the thermophysical, rheological, optical and hydrodynamic profiles of the samples for heat transfer and direct solar absorption applications.

Summary/Conclusions: Eleven hybrid fAg–pGnP nanofluids based on PG:W were designed. TEM images of the dried hybrid nanopowder showed graphene nanoplateletes of a few hundred nm long clustered with ~50 nm silver nanoparticles. The apparent sizes determined by dynamic light scattering are practically equal after preparation and five days later in static conditions, confirming the stability of the dispersions. For a fixed total nanoadditive concentration of the hybrid nanofluids, the rising amount of fAg and the decreasing amount of pGnP leads to increasing density values. Different characterizations will be performed for the designed stable hybrid nanofluids for heat transfer and direct solar absorption applications.

Acknowledgements: This work was supported by “Ministerio de Economía y Competitividad” (Spain) and FEDER program through ENE2017-86425-C2-1-R project. Authors acknowledge EU COST Action CA15119: Overcoming Barriers to Nanofluids Market Uptake. J.P.V. acknowledges FPI Program of “Ministerio de Economía y Competitividad”.

References:

1. J.P. Vallejo, G. Żyła, J. Fernández-Seara, L. Lugo, Influence of Six Carbon-Based Nanomaterials on the Rheological Properties of Nanofluids, Nanomaterials, 9 (2019) 146.
2. H. Yarmand, S. Gharehkhani, G. Ahmadi, S.F.S. Shirazi, S. Baradaran, E. Montazer, M.N.M. Zubir, M.S. Alehashem, S.N. Kazi, M. Dahari, Graphene nanoplatelets–silver hybrid nanofluids for enhanced heat transfer, Energy Conversion and Management, 100 (2015) 419-428.
3. J.A. Ranga Babu, K.K. Kumar, S. Srinivasa Rao, State-of-art review on hybrid nanofluids, Renewable and Sustainable Energy Reviews, 77 (2017) 551-565.

4. J. Sarkar, P. Ghosh, A. Adil, A review on hybrid nanofluids: Recent research, development and applications, Renewable and Sustainable Energy Reviews, 43 (2015) 164-177.

1st International Conference on Nanofluids (ICNf2019)
2nd European Symposium on Nanofluids (ESNf2019)
26-28 June 2019, Castelló, Spain

Optical properties of nanodiamond suspensions in ethylene glycol

D. Di Rosa[1*], M. Wanic[2], G. Żyła[2], L. Mercatelli[1] and E. Sani[1*]

[1]National Institute of Optics (CNR-INO), Largo E. Fermi 6, 50125 Firenze, Italy

[2]Department of Physics and Medical Engineering,
Rzeszow University of Technology, Rzeszow, Poland

[*]Corresponding authors: daniele.dirosa@ino.it elisa.sani@ino.it

Keywords: Nanofluids, Nanodiamonds, Concentrating Solar Power, Extinction coefficient

Abstract

Nanodiamond-based nanofluids have attractive thermophysical properties, which make them good candidates for different energy applications. In this work, we report on the refractive index and the spectral extinction coefficient of nanofluids consisting in pure nanodiamonds suspended in ethylene glycol. We analysed two different sets of samples, differencing each other for the purity of the nanodiamond phase. For both of them, we investigated nanoparticles concentrations ranging from 0.01 to 0.1 wt%.

Background

Nanoparticle-laden fluids, briefly referred to as nanofluids, are recently experiencing a remarkable interest in many different scientific research fields, including concentrated solar power.

Among nanofluids, those containing nanodiamonds (ND) are receiving great attention recently, especially because they can greatly enhance the thermal conductivity of the base fluid [1]. In addition, their optical properties are of interest as well, e.g. for Direct Absorption Solar Collector (DASC) applications. As an example, the optical behavior of graphite/nanodiamond mixed suspensions in ethylene glycol (EG) was investigated in Ref. [2].

In the present work, we show some preliminary results concerning the refractive index values at 589.3 nm and the extinction coefficient spectra of nanofluids consisting of ethylene glycol and pure nanodiamonds, at concentrations ranging from 0.01 to 0.1 wt%.

1st International Conference on Nanofluids (ICNf2019)
2nd European Symposium on Nanofluids (ESNf2019)
26-28 June 2019, Castelló, Spain

Discussion and Results

We analysed two types of samples, which featured 87% and 97% purity of the nanodiamond (ND) phase. They will be referred to as ND87 and ND97 in the following, respectively. Figure 1 depicts the transmission electron microscopy (TEM) pictures of the nanoparticles we used.

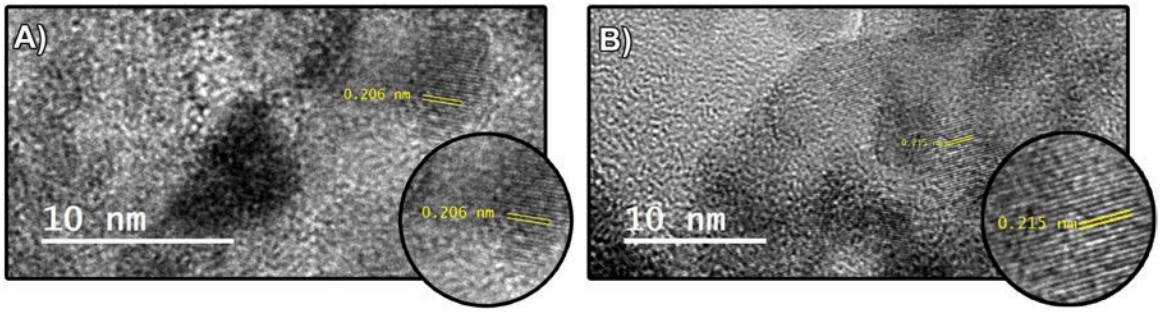

Figure 1. TEM pictures of: A) ND97; B) ND87. Reused with permission from Ref. [1].

Both for ND87 and ND97, we investigated four different nanoparticle concentrations: 0.010 wt%, 0.025 wt%, 0.050 wt% and 0.100 wt%. The nanofluid samples were prepared by a two-step method, starting from commercial powders. Then, we measured the refractive index of the samples, using an Abbemat 350 Refractometer (Anton Paar OptoTec GmbH, Seelze-Letter, Germany) operating at 589.3 nm. We found that the addition of nanoparticles, at the concentrations here studied, did not produced significant changes of the refractive index with respect to that of the pure ethylene glycol.

Transmittance spectra were acquired using a double-beam UV-VIS spectrophotometer (Perkin Elmer Lambda900). Figure 2 shows the obtained spectral extinction coefficient for the highest (0.1wt%) and the lowest (0.01wt%) nanoparticle concentrations, for both sample types. As it can be seen, the two samples did not show significant differences. This is an interesting result for practical applications, demonstrating that, at least from the point of view of optical properties, the use of less expensive ND87 nanopowders does not arise in a property degradation.

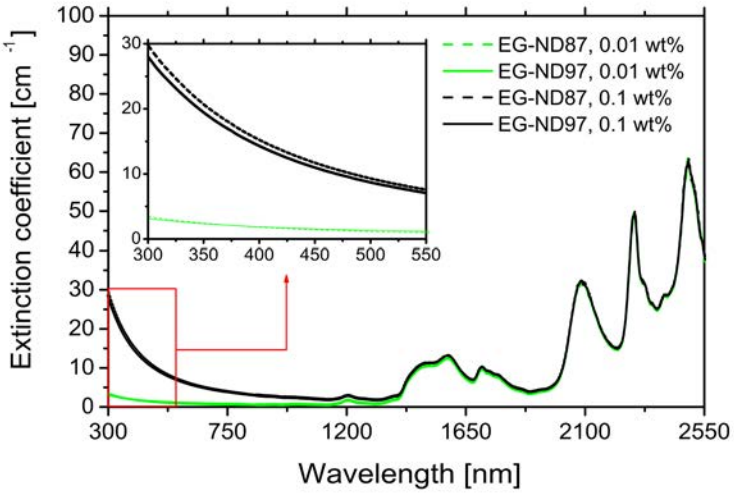

Figure 2. Comparison of spectral extinction coefficients of the EG-ND97 (solid lines) and EG-ND87 samples (dashed lines). At the lowest concentration (green lines), the two curves are practically superimposed.

Summary

In this work, we prepared two sets of nanofluids consisting in suspensions of pure nanodiamonds and ethylene glycol. Two powders with different nanodiamond purites were used (87% and 97%). The refractive index and the extinction coefficient were investigated as a function of nanoparticle concentrations, at 0.01, 0.025, 0.05 and 0.1 wt%. We obtained that the refractive index of the base fluid was unchanged. As a consequence, for all applications requiring the knowledge of refractive index (i.e. the optical design of novel solar collectors), the refractive index of the pure base fluid can be considered.

Differently, if the extinction coefficient is concerned, the nanoparticle addition considerably modifies this property with respect to the pure base fluid. The effect is more remarkable at shorter wavelengths and decreases towards infrared, with no significant differences among the two sample types.

Acknowledgements

This work was partially supported by EU COST Action CA15119: Overcoming Barriers to Nanofluids Market Uptake (NANOUPTAKE). D. Di Rosa acknowledges EU COST for the STSM grant ref. ECOST-STSM-Request-CA15119-42952.

References

1. G. Żyła, J. P. Vallejo, J. Fal and L. Lugo, Nanodiamonds – Ethylene Glycol nanofluids: Experimental investigation of fundamental physical properties, *International Journal of Heat and Mass Transfer* 121 (2018) 1201-1213.
2. E. Sani, N. Papi, L. Mercatelli and G. Żyła, Graphite/diamond ethylene glycol-nanofluids for solar energy applications, *Renewable Energy* 126 (2018) 692-698.

1st International Conference on Nanofluids (ICNf2019)
2nd European Symposium on Nanofluids (ESNf2019)
26-28 June 2019, Castelló, Spain

Dielectric properties of silicon nitride - ethylene glycol nanofluids

J. Fal[1*], M. Wanic[1], and G. Żyła[1]

[1] Department of Physics and Medical Engineering, Rzeszow University of Technology, Powstancow Warszawy 6, 35-959 Rzeszow, Poland

[*]Corresponding author: jacekfal@prz.edu.pl

Keywords: nanofluids, dielectric properties, silicon nitride, resonant absorption

Abstract: Experimental results of the dielectric properties of ethylene glycol (EG) with silicon nitride nanoparticles (Si_3N_4) are presented in this paper. All samples were prepared in a two-step method. Seven samples with various volume fractions of nanoparticles from 0.0033 to 0.0350 were prepared and their dielectric properties were investigated. The obtained results show relevant impact of Si_3N_4 nanoparticles on the dielectric properties of nanofluids. Also, according to the author's best knowledge, phenomena of resonant absorption so far unprecedented in fluids were observed.

Introduction/Background: In recent years nanofluids have attracted a huge amount of interest from researchers and scientists due to their unusual physical properties, which are different from their counterpart materials on the macro-scale. These types of nanomaterials, which are prepared as a mixture of solid particles with at least one nanometric dimension and a base fluid, are called "nanofluids". This term was introduced by Choi and Eastman in 1995 [1]. Among the most often studied properties of nanofluids are viscosity and thermal conductivity. This is related with the direct impact that these two properties of nanofluids can have on practical applications of nanosuspensions [2-4]. More recently, the surface tension and heat capacity of nanofluids have started to attract more attention of researchers [5, 6]. Despite the great interest in virtually all properties of nanofluids their electrical properties still remain out of mainstream investigation. In comparison to rheological and thermal properties, there are only a small number of publications considering the dielectric properties of nanofluids [7-9]. We demonstrate that even small amounts of nanoparticles can increase in a significant way the dielectric properties of nanofluids. Results of a study on the dynamic viscosity, thermal conductivity, and optical properties of silicon nitride ethylene glycol (Si_3N_4-EG) nanofluids have been presented in Ref. [10], where the authors show a huge enhancement of electrical conductivity with an increasing volume fraction of nanoparticles in the base

fluid. At the highest examined volume fraction (0.035) the electrical conductivity of this nanofluid was about 2400 times higher than that in pure ethylene glycol at 298.15 K.

This paper is a continuation of described above previous study on thermo-physical properties of Si_3N_4-EG nanofluids. In order to extend knowledge about the electrical properties of these types of nanofluids, dielectric properties were studied with a broadband dielectric spectroscopy device Concept 80 System (NOVOCONTROL Technologies GmbH & Co. KG, Montabaur, Germany). All samples were investigated at 298.15 K and controlled with 0.5 K accuracy, and frequency was changed between 10 MHz Hz and 0.1 Hz .

Discussion and Results: Seven samples with various volume fractions (0.0033, 0.0066, 0.0100, 0.0134, 0.0169, 0.0350) of Si_3N_4 nanoparticles with an average diameter size of 20 nm were prepared in a two step method as described in Ref. [10]. The conducted measurements confirm the strong impact of Si_3N_4 nanoparticles on the electrical conductivity of ethylene glycol base nanofluid [10]. Both direct measurements of electrical conductivity and the calculated value from dielectric spectra are in good agreement, as presented in Fig. 1, where on the ordinates axis are presented enhancement of electrical conductivity obtained from direct measurements and on the abscissa axis are presented values calculated from dielectric measurements.

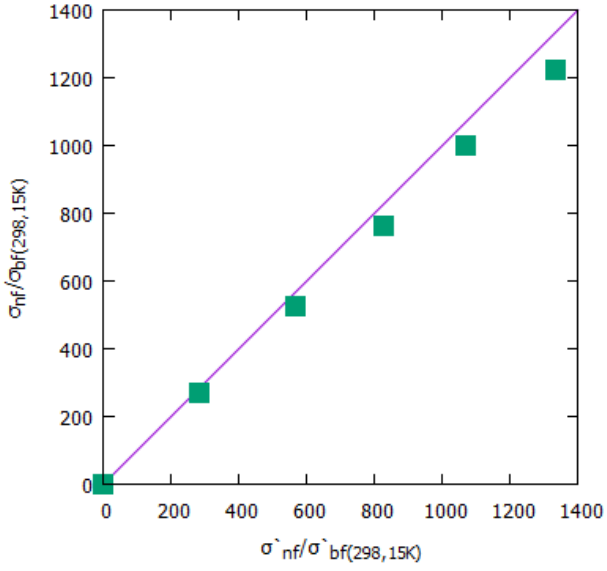

Figure 1. A comparison of results obtained from direct measurements of electrical conductivity and those calculated from dielectric spectra. Points are experimental data, the solid line presents the ideal agreement of results obtained with both methods.

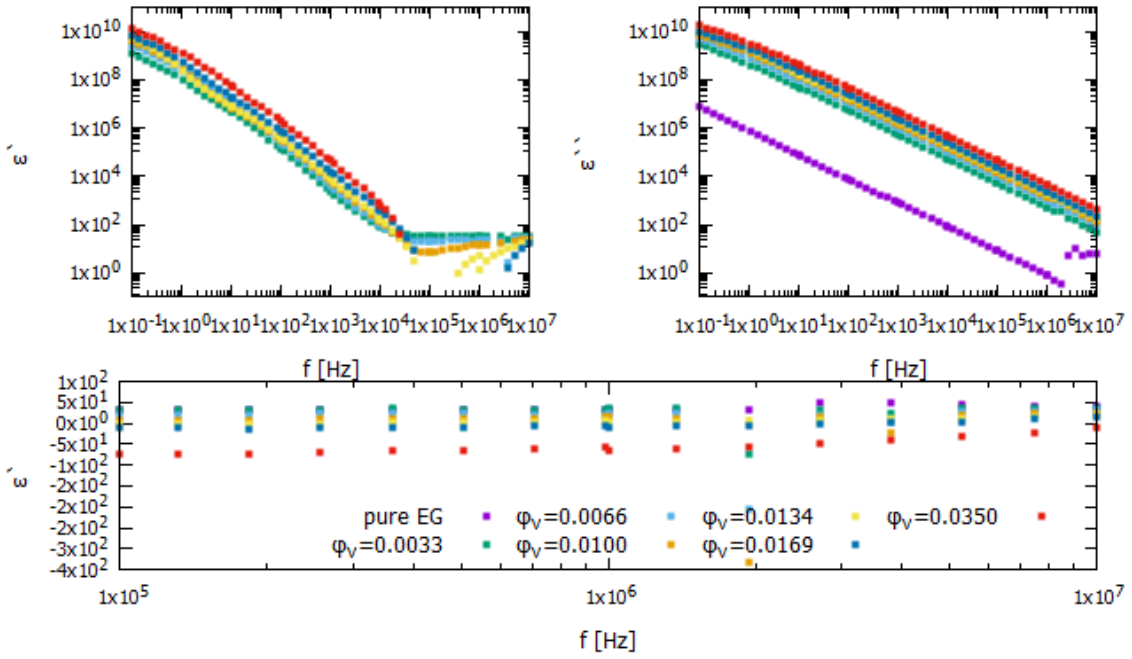

Figure 2. Real and imaginary part of permittivity of Si_3N_4 –EG nanofluids at 298.15 K.

Additionally, the effect on the complex permittivity of silicon nitride ethylene glycol nanofluid was observed for a range of frequencies. Figure 2 shows the real and imaginary part of the complex permittivity of Si_3N_4-EG nanofluids respectively, where changes in both parts of permittivity can be noticed. Dependence of the dissipation factor on frequency presented in Fig. 3 shows interesting phenomena in higher frequencies. For samples with a concentration of

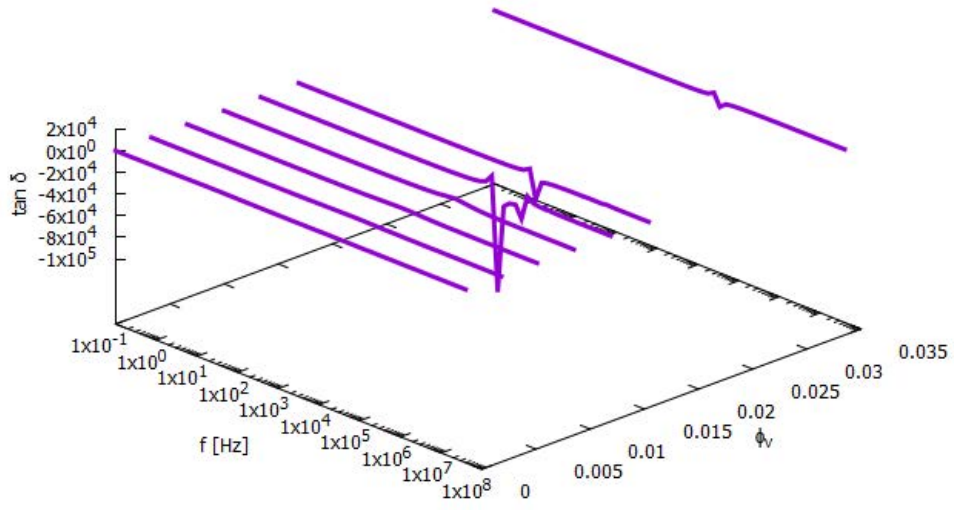

Figure 3. Dissipation factor of Si_3N_4 –EG nanofluids at 298.15 K.

nanoparticles at a level of 0.0134 the volume fraction and more, the discontinuity is visible, which can be assigned to resonant absorption related with damping of the oscillations forced by the external field [11].

Summary/Conclusions: This paper is a continuation of the study on the thermo-physical properties of silicon nitride ethylene glycol nanofluids presented in Ref [10]. Obtained results confirm the huge impact of Si_3N_4 nanoparticles on the electrical conductivity of ethylene glycol base nanofluids. The nanoparticles effect on the complex permittivity of silicon nitride ethylene glycol nanofluids was also presented and what we interpret as resonant absorption in the nanofluid was observed.

References:

1. S.U.S. Choi, Enhancing thermal conductivity of fluids with nanoparticles, *Developments Applications of Non-Newtonian Flows*, ASME, New York, 1995.
2. Y. Menni, A. J. Chamkha, A. Azzi, Nanofluid transport in porous media: A review, *Special Topics & Reviews in Porous Media: An International Journal* 10 (1) (2019).
3. M. U. Sajid, H. M. Ali, Recent advances in application of nanofluids in heat transfer devices: A critical review, *Renewable and Sustainable Energy Reviews* 103 (2019) 556–592.
4. A. Zendehboudi, R. Saidur, I. Mahbubul, S. Hosseini, Data-driven methods for estimating the effective thermal conductivity of nanofluids: A comprehensive review, *International Journal of Heat and Mass* Transfer 131 (2019) 1211–1231.
5. K. Khanafer, K. Vafai, A review on the applications of nanofluids in solar energy field, *Renewable Energy* 123 (2018) 398–406.
6. P. Estellé, D. Cabaleiro, G. Żyła, L. Lugo, S. S. Murshed, Current trends in surface tension and wetting behavior of nanofluids, *Renewable and Sustainable Energy Reviews* 94 (2018) 931–944.
7. P. Thakore, R. Patel, Effect of silica nanofiller concentration on dielectric properties of transformer oil, *2nd International Conference on Electronics, Materials Engineering & Nano-Technology (IEMENTec*h), IEEE, 2018, pp. 1–3.
8. G. Żyła, J. P. Vallejo, J. Fal, L. Lugo, Nanodiamonds–ethylene glycol nanofluids: experimental investigation of fundamental physical properties, *International Journal of Heat and Mass Transfer* 121 (2018) 1201–1213.
9. G. Żyła, J. Fal, Thermophysical and dielectric profiles of ethylene glycol based titanium nitride (TiN-EG) nanofluids with various size of particles*, International Journal of Heat and Mass Transfer* 637 (2016) 11–16.
10. G. Żyła, J. Fal, S. Bikić, M. Wanic, Ethylene glycol based silicon nitride nanofluids: An experimental study on their thermophysical, electrical and optical properties, *Physica E: Low-dimensional Systems and Nanostructures* 104 (2018) 82–90.
11. J. Janik, S. Urban, *Fizyka chemiczne: dynamika molekuł na tle różnych metod badawczych*, Państwowe Wydawnictwo Naukowe, Warszawa, 1989.

1st International Conference on Nanofluids (ICNf2019)
2nd European Symposium on Nanofluids (ESNf2019)
26-28 June 2019, Castelló, Spain

Thermophysical Properties of Nanoparticle Enhanced Ionic Liquids

M. Hothar[1*], Z. Wu[1] and B. Sundén[1]

[1]Division of Heat Transfer, Department of Energy Sciences, Lund University, SE-22100, Lund, Sweden.

[*]Corresponding author: marcus.hothar@energy.lth.se

Keywords: Nanofluid, Ionic liquid, thermal conductivity, specific heat

Abstract: Two very promising nanomaterials, magnesium oxide (MgO) and boron nitride (BN) as well as one of the most commonly studied materials in the field, aluminium oxide (Al_2O_3) have been selected to be used to enhance two ionic liquids that both show promise of being useful as heat transfer media, [emim][DCA] as well as [emim][TCM]. The goal of this study is to determine properties such as thermal conductivity, specific heat and viscosity and to analyse the effect of the nanoparticles as well as the difference in results when using the same substance with various particle sizes. Through this it's hoped that a clearer picture of the importance of the particle size both for stability as well as the properties for nanoparticle enhanced ionic liquids can be granted. A second goal with this study is to examine the stability of the various nanofluids mainly through the methods of dynamic light scattering (DLS) and zeta potential (ZP). It was however determined during the study that good ZP-measurements were not possibly for nanofluids based on ionic liquids.

Introduction/Background:

Nanofluids are a hot topic within the scientific community since the last decade and the number of published documents have been growing at an exponential rate. A nanofluid is a heterogeneous two-phase system where solid nanoparticles (of various shapes and generally with a size up to 100 nm) are suspended into a bulk liquid. The presence of even a very small amount of solid particles can have a noticeable effect on the properties of the fluid and for example increase its thermal conductivity and viscosity which both are essential parameters to consider during the development of efficient heat transfer media. The use of nanofluids specifically designed to function as enhanced heating and cooling media has been a growing research trend and it is possible that in the future they might be applied for applications such as solar energy systems. Nanofluids researched for this purpose usually consist of conventional heat transfer liquids as the base fluid (such as water and ethylene glycol etc.) but nanofluids consisting of ionic liquids (Nanoparticle Enhanced Ionic Liquids, NEILs) are also a research subject which is receiving more attention.

Ionic liquids consist of ions, namely an anion and a cation and are often referred to as molten salts. Room temperature ionic liquids (RTILs), are ionic liquids with a melting temperature beneath room temperature and these have attracted a lot of attention in several various research fields for purposes such as heat transfer, energy storage and drug delivery [1]. In general, ionic liquids are considered to be rather unique due to their low vapour pressure, thermal stability and solving capabilities. From a heat transfer perspective two ionic liquids that can catch the interest of a researcher are 1-ethyl-3-methylimidazolium dicyanamide ([emim][DCA]) and 1-ethyl-3-methylimidazolium tricyanomethanide ([emim][TCM]).

Table 1. Display of the density, thermal conductivity, dynamic viscosity and specific heat of four ionic liquids that all possess relatively high thermal conductivity in comparison with many others.

	Density (kg/m^3) T = 298 K	**Thermal conductivity (W/m*K)**	**Dynamic Viscosity (mPa*s) T = 298 K**	**Specific heat (kJ/kg*K) 1 atm, T= 296-298 K**
[emim][BF_4] **1-ethyl-3-methylimidazolium tetrafluoroborate**	1.29 [2]	0.188 - 0.199 [3] (300-390 K)	41.45 [4]	1.534 [5]
[emim][OAc] **1-ethyl-3-methylimidazolium acetate**	1.10 [6]	0.1915 -0.2137 [7] (273-353 K)	132.91[6]	1.915 [8]
[emim][DCA]	1.102 [6]	0.1914 -0.2053 [7] (273-353 K)	14.9 [6] - 15.1 [9]	~1.83 [9, 10]
[emim][TCM]	1.082 [10]	0.1815 –0.1956 [7] (273-353 K)	15.0 [10]	1.775 [10]

All the ionic liquids in Table 1 possess relatively high thermal conductivity when compared to many other ionic liquids [7]. Table 1 shows that [emim][DCA] and [emim][TCM] have a much lower viscosity than the other two ionic liquids while still having a relatively high thermal conductivity as well as specific heat. While a higher viscosity can be beneficial to the stability of the colloid suspension a lower viscosity is still favourable in general for heat transfer fluids since it will demand a lower amount of pumping power to reach a desired heat transfer rate. Concerning viscosity, it should also be mentioned that ionic liquids with a shorter non-polar tail tend to have a lower viscosity but that this improvement may come at the cost of less impressive solving capabilities [10]. This is the reason why only [emim]-kind ionic liquids are shown in the table and that for example [bmim][DCA] or [bmim][TCM] are not examined as

well in this study. The two ionic liquids in this research were acquired through IoLiTec GmbH and had the following mass purity: 1-ethyl-3-methylimidazolium dicyanamide, >98% and 1-ethyl-3-methylimidazolium tricyanomethanide, >98%.

In published articles, two interesting nanomaterials, boron nitride (BN) and magnesium oxide (MgO) have been used to create nanofluids. These have shown an impressive capability to enhance the thermal conductivity of the fluid [11, 12]. For this reason, the thermophysical properties of the mentioned ionic liquids enhanced with BN and MgO will be measured at room temperature and discussed in this article. The results will also be compared with the same ionic liquids enhanced with alumina (Al_2O_3) nanoparticles. Furthermore, the stability of the NEILs will also be examined and discussed through visual examinations, particle size measurements by dynamic light scattering (DLS) and zeta potential. The instruments that's used for measurements of the latter two is the *Zetasizer Nano ZSP* and the *Zetasizer Ultra* from Malvern. As several studies have shown that the size of the nanoparticle can have an impact on both the thermophysical properties as well as the stability of the nanofluid, several different sizes will be prepared, using the two step method, and examined for this reason. The various nanomaterials and their original average particle size are presented in **Table 2**.

Table 2. Average particle sizes of the three nanomaterials that have been selected to be used for this research. The BN with the particle size of 150 nm as well as the alumina with the aps 20 and 80 nm have been bought from Sigma Aldrich while the remaining ones are supplied by the US Research Nanomaterials Inc.

Nano Material:	**Average Particle Size (APS)**				
MgO	10 nm	20 nm	40 nm	60 nm	100 nm
BN	-	-	-	70-80 nm	150 nm
Al_2O_3	5 nm	13 nm	20 nm	50 nm	80 nm

The goal of the study is to provide a general indication of the stability of the various NEILs and to study the enhancement of the thermal conductivity, viscosity and specific heat that the three nanomaterials can provide to the two ionic liquids. Furthermore, the influence of different particle sizes of the same nanomaterial will provide is also of great interest in terms of the effect of the property enhancements as well as the stability of the nanofluids.

Discussion and Results: When it comes to measurements of the zeta potential by the Zetasizer Ultra it could be determined that an accurate and precise result was not achievable. Through using the diffusion barrier method (DBM) the sample was then separated from the electrode in hope that this would improve the readings but this was not enough to improve the precision of the results. When measuring for nanofluids consisting of

either of the two ionic liquids the deviations between the results were too large to be used as data whether the DBM was used or not, as can be seen in **Table 3**.

Nanofluid	Zeta potential [mV]		
[emim][DCa] + 2 wt-% Al_2O_3	-8.517	22.65	32.88
[emim][DCa] + 2 wt-% MgO (DBM)	-23.42	-92.98	
[emim][DCa] + 0.2 wt-% MgO (DBM)	55.97	-138.4	

The rest of the results will be gathered and analysed before the date of the conference.

References:

1. M. Smiglak, J.M. Pringle, X. Lu, L. Han, S. Zhang, H. Gao, D. R. MacFarlane and R. D. Rogers, Ionic liquids for energy materials and medicine, *Royal Society of Chemistry, Chem. Community,* 50, (2014) pp. 9228-9250.
2. X. Fan, Y. Chen, C. Su, Densities and viscosities of binary liquid mixtures of 1-ethyl-3-methylimidazolium tetrafluoroborate with acetone, methyl ethyl ketone and N-methyl-2-pyrrolidone, *Journal of the Taiwan Institute of Chemical Engineers*, Vol 61, (2017), pp.117-123
3. R. Haghbakhsh, S. Raeissi, A novel of correlative approach for ionic liquid thermal conductivities, *Journal of Molecular Liquids*, Vol 236, (2017), pp. 214-219
4. O. Ciocirlan, O. Croitoru, O. Iulian, Viscosity of binary mixtures of 1-ethyl-3-methylimidazolium tetrafluoroborate ionic liquid with four organic solvents, *Journal of Chemical Thermodynamics*, Vol 101, (2016), pp. 285-292
5. V.K. Sharma, S. Solanki, S. Bhagour, Excess heat capacities of binary and ternary mixtures containing 1-ethyl-3-methylimidazolium tetrafluoroborate and anilines, *Journal of Chemical & Engineering Data*, Vol 59, (2014), pp. 1852-1864
6. E. Quijada-Maldonado, S. van der Boogaart, J.H. Lijbers, G.W, Meindersma, A.B. de Haan, Experimental densities, dynamic viscosities and surface tension of ionic liquids series 1-ethyl-3-methylimidazolium acetate and dicyanamide and their binary and ternary mixtures with water and ethanol at T = (298.15-343-15 K), *Journal of Chemical Thermodynamics*, Vol 51, (2012), pp. 51-58
7. A. P. Fröba, M. H. Rausch, K. Krzeminski, D. Assenbaum, P. Wasserscheid, A. Leipertz, Thermal conductivity of ionic liquids: Measurement and prediction, *International Journal of Thermophysics,* Vol 31, (2010) pp. 2059-2077
8. C. Su, X. Liu, C. Zhu, M. He, Isobaric molar heat capacities of 1-ethyl-3-methylimidazolium acetate and 1-hexyl-3-methylimidazolium acetate up to 16 MPa, *Fluid Phase Equilibria*, Vol 427, (2016), pp. 187-193
9. P. Navarro, M. Larriba, E. Rojo, J. García, F. Rodríguez, Thermal properties of cyano-based ionic liquids, *Journal of Chemical & Engineering Data*, Vol 58, (2013), pp. 2187-2193
10. P. Navarro, M. Larriba, J. García, F. Rodríguez, Thermal stability and specific heats of [emim][DCA]+[emim][TCM] mixed ionic liquids, *Thermochimica Acta*, Vol 588, (2014), pp. 22-27
11. G. Żyla, J. Fal, J. Traciak, M. Gizowska & K. Perkowski, Huge thermal conductivity enhancement in boron nitride – ethylene glycol nanofluids, *Materials Chemistry and Physics*, Vol 180, (2016), pp. 250-255G. Żyla, Visosity and thermal conductivity of MgO-EG nanofluids Experimental results and theoretical models predictions, *Journal of Thermal Analysis and Calorimetry*, 2017, Vol 129, pp. 171-180

1st International Conference on Nanofluids (ICNf2019)
2nd European Symposium on Nanofluids (ESNf2019)
26-28 June 2019, Castelló, Spain

High versus low aspect ratio, helical and bamboo carbon nanotubes – synthesis and applications in nanofluids

S. Boncel[1*], M. Dzida[2], G. Dzido[3], B. Jóźwiak[1], R. Jędrysiak[1], A. Kolanowska[1] and A. Kuziel[1]

[1]Silesian University of Technology, Faculty of Chemistry, Department of Organic Chemistry, Bioorganic Chemistry and Biotechnology, Krzywoustego 4, 44-100 Gliwice, Poland
[2]University of Silesia in Katowice, Faculty of Mathematics, Physics and Chemistry, Institute of Chemistry, Szkolna 9, 40-006 Katowice, Poland
[3]Silesian University of Technology, Faculty of Chemistry, Department of Chemical and Process Engineering, Strzody 7, 44-100 Gliwice, Poland
[*]Corresponding author: slawomir.boncel@polsl.pl

Keywords: carbon nanotubes, helical carbon nanotubes, bamboo-like carbon nanotubes, nanofluids

Abstract: Four types of carbon nanotubes (CNTs) of various morphology, i.e. (1) high *versus* (2) low aspect ratio (length-to-diameter ratio), (3) helical and (4) bamboo-like CNTs have been synthesized *via* catalytic chemical vapor deposition (c-CVD) and comprehensively analyzed. CNTs were pre-designed toward their future applications as solid *quasi*-1D nanoparticle components of nanofluids.

Introduction/Background: The main challenge in the application of carbon nanotubes (CNTs) (of various morphologies) in the energy industry, including energy storage and heat-transfer fluids, is to 'translate' their excellent thermophysical properties from the individual nanotubes (thermal conductivity λ~3000 $Wm^{-1}K^{-1}$ for multi-wall CNT [1,2]) into the bulk systems such as nanofluids. So far, even the most remarkable results revealed that, among others, thermal conductivity for CNT nanofluids is a few orders of magnitude lower as compared to the individual CNTs [3,4]. Additionally, several other problems are related to CNT nanofluids, i.e. lower than theoretically predictable enhancements in thermal conductivity and convective heat transfer coefficients, medium time/operational stability, non-economic synthesis and manufacture as well as health and environmental concerns [5]. A promising solution in the

manufacture of nanofluids is to apply CNTs of pre-designed morphology and hence tunable physicochemical properties.

In the quest for addressing the fundamental questions in the area of nanofluids, we have synthesized CNTs of various morphologies *via* catalytic chemical vapor deposition (c-CVD) and performed their comprehensive analysis including scanning/transmission electron microscopy (SEM/TEM), thermogravimetric analysis (TGA), Raman spectroscopy and X-ray photoelectron spectroscopy (XPS). The analyses confirmed their prospective application as the thermoconductive components of nanofluids.

Discussion and Results: As the solid *quasi*-1D components of the future nanofluids two types of pure multi-wall CNTs (MWCNTs) of strikingly different morphology and aspect ratio were used, i.e. long MWCNTs (OD=50 nm, l=300 μm, aspect ratio=6000) and short MWCNTs (OD=10 nm, l=1.5 μm, aspect ratio=150). Additionally, helical (OD=250 nm, l>5 μm, turn=ca. 400 nm) and bamboo-like carbon nanotubes (OD=50 nm, l=40 μm, aspect ratio=800) have been used. MWCNTs were synthesized via c-CVD at 760 °C under argon using ferrocene as catalyst precursor and toluene as the main carbon source while the nanotube lengths were controlled by duration of the synthesis. Helical CNTs were grown similarly but using Cu precursor, elevated pressure (>1 atm) and partial recirculation of the non-reacted feedstock. Bamboo-like CNTs were synthesized from pyrazine (1,4-diazine) and toluene mixture under otherwise analogous conditions. Morphology of various CNTs as the future dispersed phases was presented in SEM and TEM images (**Figure 1**). TGA confirmed that the most thermally air-stable CNTs were the long MWCNTs – in the same time, as confirmed by Raman spectroscopy – exhibiting the lowest number of crystallographic defects. Bamboo-like CNTs – as revealed by XPS were nitrogen-doped (ca. 2 wt.%) – were found as more rigid nanoparticles of nano-needle aerodynamics while helical CNTs contained a regular turn length but the helicity was random. Systematic studies of their dispersibility in various fluids are being studied, nonetheless, e.g. non-ionic and ionic surfactants have been already found to form stable aqueous nanofluids.

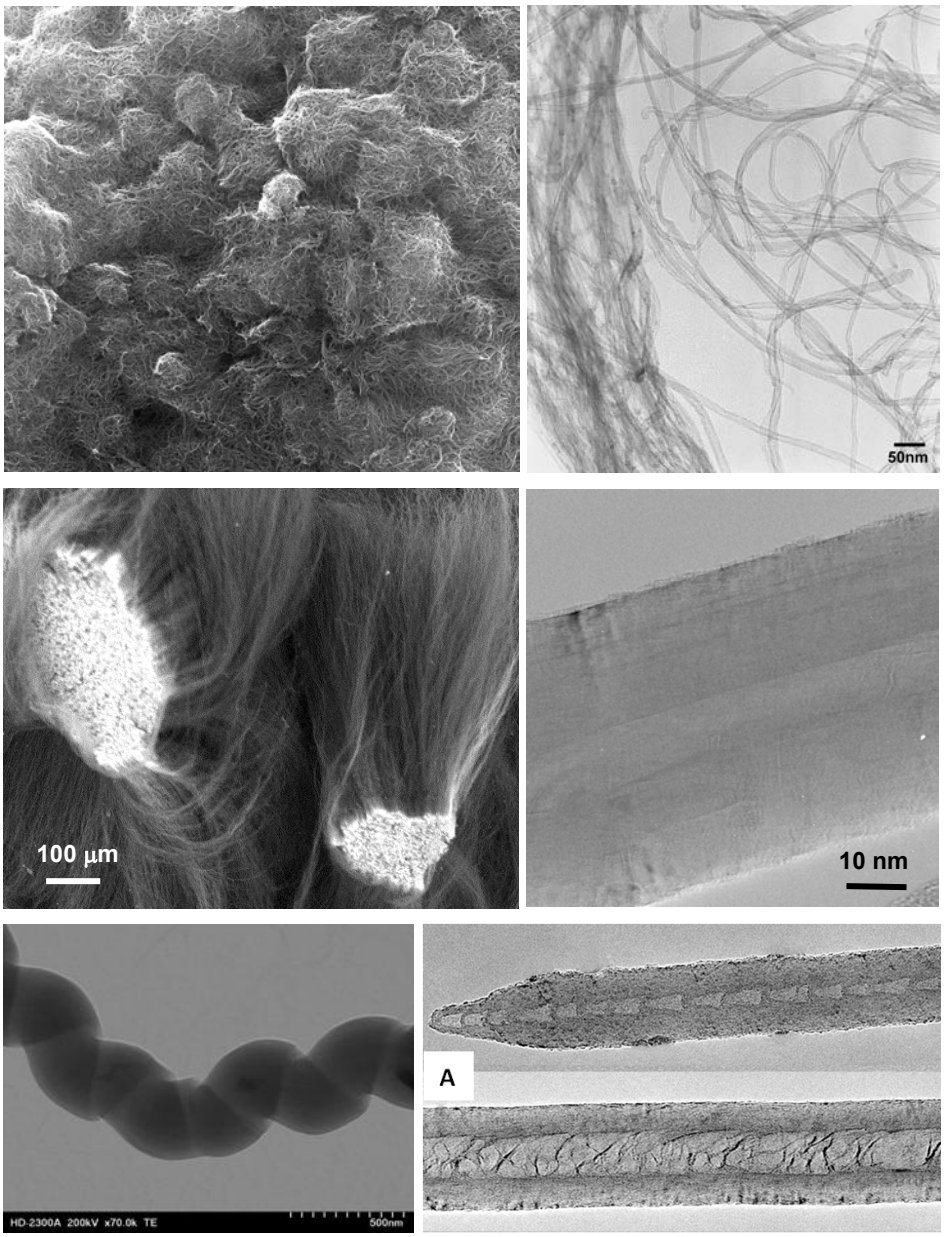

Figure 1. Micrographs of CNTs used in these studies: upper panel – short entangled MWCNTs, middle panel – long aligned MWNCTs, below panel – TEM images of helical and bamboo-like CNTs

Summary/Conclusions: The obtained CNTs of various morphologies were successfully synthesized under controllable conditions and their prospective application as active components of nanofluids is currently under investigation.

The authors are grateful for the financial support from the National Science Centre (Poland) Grant No. 2017/27/B/ST4/02748 in the framework of OPUS program.

References:

1. M.K. Samani, N. Khosravian, G.C.K. Chen et al, Thermal conductivity of individual multiwalled carbon nanotubes, *Int. J. Therm. Sci.* 62 (2012) 40-43.
2. P. Kim, L. Shi, A. Majumdar and P.L. McEuen, Thermal transport measurements of individual multiwalled nanotubes, *Phys. Rev. Lett.* 87 (2001) 215502.
3. I.V. Singh, M. Tanaka and M. Endo, Effect of interface on the thermal conductivity of carbon nanotube composites, *Int. J. Therm. Sci.* 46 (2007) 842-847.
4. S.Y. Kwon, I.M. Kwon, Y.-G. Kim et al, A large increase in the thermal conductivity of carbon nanotube/polymer composites produced by percolation phenomena, *Carbon* 55 (2013) 285-290.
5. S. Boncel, J. Kyziol-Komosińska, I. Krzyżewska and J. Czupiol, Interactions of carbon nanotubes with aqueous/aquatic media containing organic/inorganic contaminants and selected organisms of aquatic ecosystems – A review, *Chemosphere* 136 (2015) 211-221.

1st International Conference on Nanofluids (ICNf2019)
2nd European Symposium on Nanofluids (ESNf2019)
26-28 June 2019, Castelló, Spain

Carbon nanoparticles/polyethylene glycol solar nanofluid synthetized by pulsed laser fragmentation

C. Doñate-Buendía[1], M. Fernández-Alonso[1], W. K. Kipnusu[1], and G. Mínguez-Vega[1*]

[1] GROC·UJI, Institute of New Imaging Technologies, Universitat Jaume I, Avda. Sos Baynat s/n, 12071 Castellón, Spain

[*]Corresponding author: gminguez@uji.es

Keywords: nanosecond laser, laser fragmentation, solar nanofluids.

Abstract: Solar energy is becoming an essential tool to keep the ever-increasing demand of energy with a minimal environmental impact. A solar nanofluid is a colloidal suspension of nanoparticles in a heat transfer fluid and it is used as solar receiver for efficient harvesting of solar radiation based on volumetric absorption. In this contribution, the fabrication of a solar nanofluid of polyethylene glycol with carbon nanoparticles by pulsed laser fragmentation of a suspension is explored. A high stability of the sample over two years is observed without the use of surfactants.

Introduction/Background: The challenge of a environmental friendly nanotechnology is not only an ethical concern but a prerequisite for crossing the boundary between research and the general applicability at industrial scale. In this direction, laser-based synthesis of nanoparticles is an easy technique that fulfils the twelve principles of “green” chemistry. Specifically, laser fragmentation in liquids (LFL) consists of irradiating, with a pulsed laser source, a suspension composed by micrometric or nanometric solid particles dispersed in a liquid. The interaction between the intense laser radiation and the colloid may lead to transformations of particle morphology, crystallinity and/or chemical composition of the solid content through photothermal vaporization or Coulomb explosion mechanisms, depending on the laser fluence and pulse duration [1-3]. Conventional LFL is made with a batch processing configuration, where the powder material is dispersed into the liquid and the suspension is contained in a glass cell for laser irradiation.

Carbon and polyethylene glycol are two attractive materials in energy applications for harvesting solar radiation as they are non-toxic and biocompatible. Among others, the use of carbon nanohorns[4,5], graphene [6], carbon black [6,7] and graphite [8] has been

proposed for direct solar absorption applications. In this contribution we explore the fabrication of a carbon nanoparticle/PEG400 nanofluid with LFL technique.

Discussion and Results: The irradiated colloid is an 11 ml sample taken from an initial mixture of 40 mg of carbon glassy particles dispersed in 100 ml of polyethylene glycol (PEG) 400 (both purchased from Sigma Aldrich). The original size of carbon solid particles is 2-12 μm but the suspension was milled up till most of the particles had a size of around 1 μm. The experimental set up is shown in Figure 1 a). The laser irradiation was carried out using the second harmonic, with a wavelength of 532 nm, of a Nd:YAG pulsed laser (Brilliant, Quantel) at a mean power of 300 mW and a repetition rate of 10 Hz. The beam was focused by a cylindrical lens with a focal length of 300 mm providing a fluence of ~ 6 J/cm^2 at the focal spot. The focal spot was located 2 mm inside the cuvette containing the educt, and the liquid was constantly moving by means of a magnetic stirrer at 100 rpm. Due to laser irradiation, the solution changed its color progressively from grey to dark brown after 3 hours, which indicated the formation of the carbon nanoparticles [9], see inset Figure 1b).

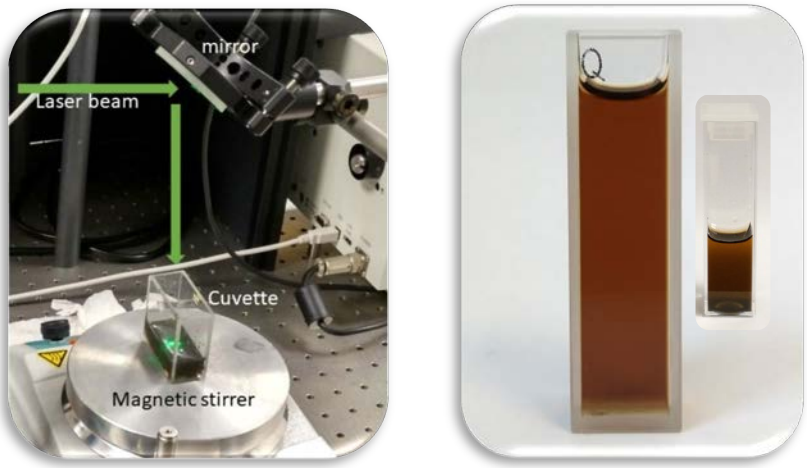

Figure 1. a) Experimental setup b) Image of the nanofluid after two years. The inset shows the image of the initial nanofluid

To further characterize the nanofluid, the hydrodynamic nanoparticle size distribution was measured by means of dynamic light scattering with a Zetasizer nano ZS (MalvernInstruments Ltd., UK). Results are shown in Figure 2 a), where we observe that the mean particle size of the nanoparticles of the nanofluid is about 50 nm with a dispersion size of about 40 nm. Also the morphology was studied by transmission

electron microscopy (TEM), where the nanoparticles show the characteristic spherical morphology of laser synthesis. Moreover, after strong centrifugation of the sample the presence of carbon dots (nanoparticles of less than 5 nm) is found. See Figure 2b).

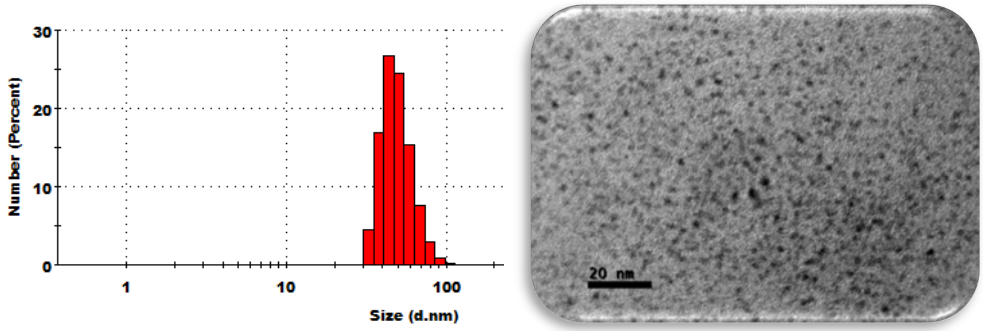

Figure 2. a) Histogram showing the statistical size distribution of NPs contained in the nanofluid. b) TEM micrograph showing the C-dots

The optical transmittance spectra were measured with a double beam UV/Vis spectrophotometer (Spectrophotometer Cary 300). The nanofluid was held in a quartz cuvette, with 10 mm beam path length. Figure 3a) shows the overall transmittance spectra of the nanofluid where the spectrum of PEG400 is shown for comparison. In order to evaluate the sunlight absorption capability of the nanofluid, the transmission solar spectral irradiance through 10 mm of the nanofluid was calculated, in Figure 3b). To this end, the reference solar spectral irradiance, ASTM G-173 for a mass air of 1.5 was considered. The transmission solar spectral irradiance through the nanofluid is obtained by multiplication of the reference solar spectral irradiance by the transmittance spectra in 10 mm of nanofluid. In this way, it is observed that the nanofluid synthesized by LFL shows a reduced transmitted solar irradiance for the visible wavelengths.

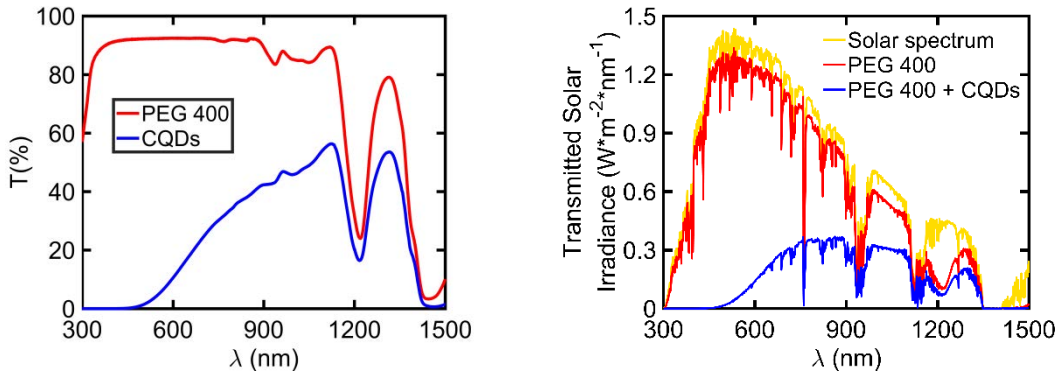

Figure 3. a) Transmittance spectra and b) transmission of solar spectral irradiance thorough 10 mm of the nanofluid.

Finally, a study of the stability over time demonstrates that the nanofluid shows outstanding properties with a very high stability even after 2 years of its synthesis.

Summary/Conclusions: The synthesis of a colloid by LFL composed by carbon nanoparticles and PEG400 is considered. First studies demonstrate that it has a high stability in time, nanoparticles are as small as few decenes of nanometres and a reduced spectral transmission in the visible and near infrared. Consequently, it is a good candidate for application as a solar nanofluid.

References:

1. D. Zhang, B. Gökce, and S. Barcikowski, Laser synthesis and processing of colloids: fundamentals and applications, *Chemical Review* 117 (2017), 3990–4103.
2. G. González-Rubio, A. Guerrero-Martínez, L. M. Liz-Marzán, Reshaping, fragmentation, and assembly of gold nanoparticles assisted by pulse lasers, *Accounts of Chemical Research* 49 (2016) 678–686.
3. A. Pyatenko, H. Wang, N. Koshizaki, and T. Tsuji, Mechanism of pulse laser interaction with colloidal nanoparticles. *Laser Photonics Review* 7(2013), 596–604.
4. E. Sani, S. Barison, C. Pagura, L. Mercatelli, P. Sansoni, D. Fontani, D. Jafrancesco, and F. Francini, Carbon nanohorns-based nanofluids as direct sunlight absorbers, *Optics Express* 18 (2010), 5179-5187.
5. A. Gimeno-Furio, J. E. Julia, S Barison, F. Agresti, C Friebe, and M. H. Buschmann, Nanofluids as directsolar energy absorbers, *Journal of Nanofluids* 8 (2019), 1-13.
6. G. Ni, N. Miljkovic, H. Ghasemi, X. Huang, S. V. Boriskina, C. T. Lin, J. Wang, Y. Xu, M. M. Rahman, T Zhang, and G. Chen, Volumetric solar heating of nanofluids for direct vapor generation. *Nano Energy*, 17(2015), 290-301.
7. D. Han, Z. Meng, D. Wu, C. Zhang, and H. Zhu, Thermal properties of carbon black aqueous nanofluids for solar absorption, *Nanoscale research letters* 6(2011), 457.
8. S. M. Ladjevardi, A. Asnaghi, P. S. Izadkhast, and A. H. Kashani. Applicability of graphite nanofluids in direct solar energy absorption. *Solar Energy* 94 (2013), 327-334.
9. C. Doñate-Buendia, R. Torres-Mendieta, A. Pyatenko, E. Falomir, M. Fernández-Alonso, G. Mínguez-Vega, Fabrication by Laser Irradiation in a Continuous Flow Jet of Carbon Quantum Dots for Fluorescence Imaging. *ACS omega 3* (2018), 2735-2742.

1st International Conference on Nanofluids (ICNf2019)
2nd European Symposium on Nanofluids (ESNf2019)
26-28 June 2019, Castelló, Spain

IoBiofluids – A Sustainable Alternative to Current Heat Transfer Fluids

C.S.G.P. Queirós[1*], M.J.V. Lourenço[1], F.J.V. Santos[1] and C.A. Nieto de Castro[1*]

[1]Centro de Química Estrutural, Faculdade de Ciências,

Universidade de Lisboa, 1749-016 Lisboa, Portugal

[*]Corresponding author: csqueiros@ciencias.ulisboa.pt

Keywords: Ionic Liquids, biomass, IoBiofluids, heat transfer fluids

Abstract: Energy efficiency is a cost-effective way to reduce energy consumption through existing and improved technologies and can play a significant role in reducing the threat of global climate change. By promoting the consumption of less energy, there will be less emission of greenhouse gases as the result of the burning of fossil fuels. Therefore, the development of energy saving practices and the use of energy from renewable sources constitute important measures. Ionic liquids have been wide study as potential heat transfer fluids. In this work, a new sustainable heat transfer fluid, IoBiofluids, was presented. The IoBiofluids produced used as base fluid a mixture of 1-ethyl-3-methylimidazolium acetate and water (x_{IL}=0.099) and lignocellulosic biomass particles dispersed. The thermal conductivity and viscosity of several IoBiofluids was presented.

Introduction/Background: In the heat transfer area, conventional liquid coolants used at low and moderate temperatures have very poor thermal conductivity and heat storage capacities and they are not recyclable. So, there is a need for more efficient and environmentally friendly heat transfer fluids (HTF), nanofluids being a more efficient alternative to the conventional HTF. The term nanofluid was invented by Choi et al.[1] to designate a new class of heat transfer fluids obtained by the dispersion of nanometer-sized solid particles, rods, or tubes in conventional heat transfer fluids. The most studied nanomaterials are the carbon nanotubes (CNT's), metal oxides and metals.

Recently, ionic liquids (ILs) have proven to be suitable alternatives for many applications in industry and chemical manufacturing, even in the field of heat transfer and energy storage[2]. With the current interest in the ionic liquids and the good thermal properties, Nieto de Castro et al.[3] reported a new class of nanofluids named IoNanofluids, defined as a dispersion of nanomaterials in an ionic liquid and it has been proved to increase the thermal conductivity of the IoNanofluid in relation to the base ionic liquid[4-6].

As a sustainable alternative to IoNanofluids, Queirós[7] proposed, for the first time in her MSc thesis, a new heat transfer fluid that correspond to a dispersion of biomass particles (micro or nano size) in an ionic liquid (or other "green" fluid). This type of dispersion was named IoBiofluids. In this work we present a new type of heat transfer fluids – IoBiofluids[8], a dispersion of lignocellulosic biomass particles in an ionic liquid or a mixture of ionic liquid and water. The thermal conductivity and viscosity of several IoBiofluids were studied and the first preliminary results indicated that these "green" heat transfer fluid can be a good alternative to Ionanofluids.

Discussion and Results: Before the preparation of the IoBiofluids, it was necessary to proceed to the anatomical and chemical characterization of the selected lignocellulosic biomass (almond shells, walnut shells, pine nut shells and *Hakea sericea* fruits) and to study the thermophysical properties of the selected ionic liquid, the 1-ethyl-3-methylimidazolium acetate ([emim][OAc]) and of its mixtures with water. Since the [emim][OAc] is highly hygroscopic, the mixture of [emim][OAc] with water (x_{IL} =0.099) was selected for the IoBiofluids studies and also due to its high thermal conductivity values, low viscosity (when compared with the pure IL) and also due to price of the IL. Since the ILs continue to be very expensive, especially when compared with the most used thermal fluids, water and ethylene glycol, the IL could be considered as an additive to water maintaining a high thermal conductivity and even work as lubricant avoiding the corrosive damages caused by hot water.

Figure 1. IoBiofluid with pine nut shells particles suspended.

The thermal conductivity and the viscosity of these systems were determined for a temperature range between 293 K and 343 K. The IoBiofluids produced were stable for almost 2 hours (figure 2), although more studies are needed to improve its stability.

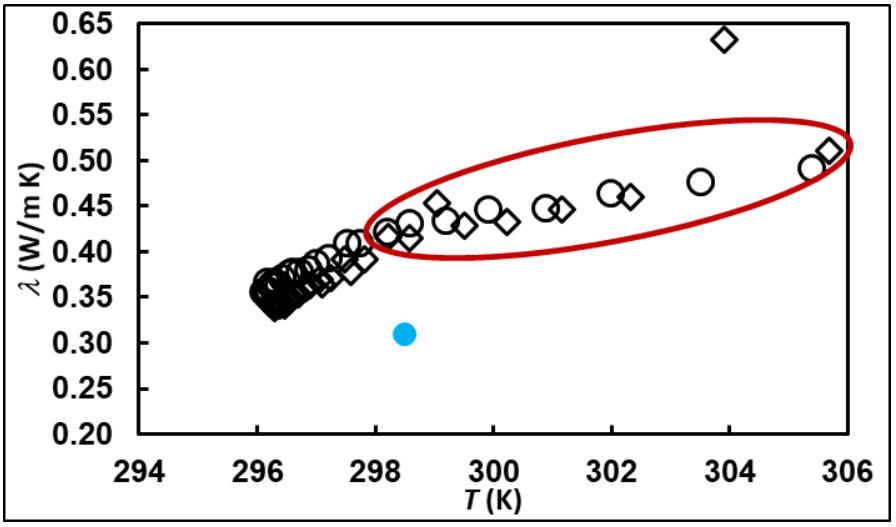

Figure 2. Evaluation of the thermal conductivity, at room temperature, for a IoBiofluid (3% w/w) for different days (◊ day 1; ○ day 2; ● base fluid). Measurements, in each day, lasted for 4 hours.

Summary/Conclusions: The thermal conductivity and viscosity of several IoBiofluids were studied. The viscosity didn't increase much compared with the viscosity of the base fluid. The small addition of biomass particles (< 1% w/w) to the based fluid didn't increase its thermal conductivity and at higher temperatures the thermal conductivity of the IoBiofluids decreased compared with the thermal conductivity of the base fluid. However, for mass concentrations of 3% (Figure 2) the enhancement is significant, of the order of 35% at room temperature. The IoBiofluids produced so far, are microfluids with biomass particles with a size inferior to 0.180 mm (Figure 3). The stability of the IoBiofluids is still a challenge and more studies are needed in order to improve it.

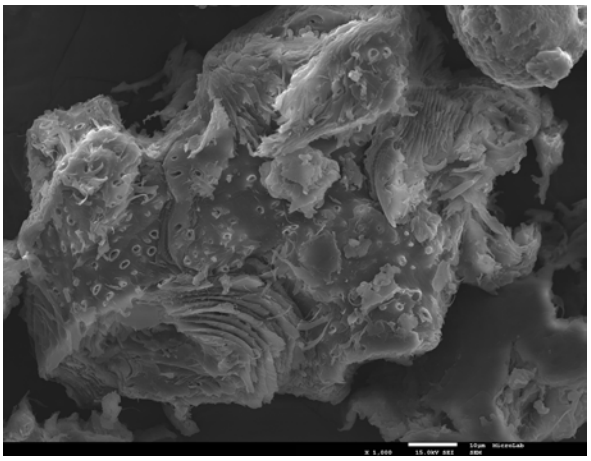

Figure 3. SEM images of pine nut shells particles.

References:

1. S.U.S. Choi. Nanofluid Technology: Current status and future research. 1998.
2. A.Z. Hezave, S. Raeissi, M. Lashkarbolooki. Estimation of Thermal Conductivity of Ionic Liquids Using a Perceptron Neural Network, *Industrial & Engineering Chemistry Research*, 51(29) (2012): 9886–9893.
3. C.A. Nieto de Castro, M.J.V. Lourenço, A.P.C. Ribeiro, E. Langa, S.I.C. Vieira, P. Goodrich, et al., Thermal Properties of Ionic Liquids and IoNanofluids of Imidazolium and Pyrrolidinium Liquids, *J. Chem. Eng. Data*, 55, 2 (2010), 653–661.
4. A. Kokorin, ed. Ionic Liquids: Theory, Properties, New Approaches. InTech, 2011.
5. S.M.S. Murshed, C.A. Nieto de Castro, M.J.L. Lourenço, J. França, A.P.C. Ribeiro, S.I.C. Vieira, et al., Ionanofluids as Novel Fluids for Advanced Heat Transfer Applications, *World Academy of Science, Engineering and Technology*, 5(4) (2011) 795–798.
6. J.M.P. França, M.J.V. Lourenço, S.M.S. Murshed, A.A.H. Pádua, C.A. Nieto de Castro, Thermal Conductivity of Ionic Liquids and IoNanofluids and Their Feasibility as Heat Transfer Fluids, *Ind. Eng. Chem. Res.*, 57(18) (2018), 6516–6529.
7. C.S.G.P. Queirós, Estudo do aproveitamento de resíduos de frutos como novos materiais absorvedores térmicos, Master thesis in Technological Chemistry, Faculdade de Ciências da Universidade de Lisboa, 2010.
8. C.S.G.P. Queirós, Lignocellulosic Biomass for a New Generation of Thermal Fluids, PhD thesis in Forestry Engineering and Natural Resources, Instituto superior de Agronomia, Universidade de Lisboa, 2019.

1st International Conference on Nanofluids (ICNf2019)
2nd European Symposium on Nanofluids (ESNf2019)
26-28 June 2019, Castelló, Spain

Towards the Correct Measurement of the Thermal Conductivity of Ionic Melts and Nanofluids

C. A. Nieto de Castro*, M. J. V. Lourenço

Centro de Química Estrutural, Faculdade de Ciências,

Universidade de Lisboa, 1749-016 Lisboa, Portugal

*Corresponding author: cacastro@ciencias.ulisboa.pt

Keywords: ionic melts, nanofluids, thermal conductivity, measurement.

Abstract: Measuring accurately the thermal conductivity of fluids is a successful task for decades. However, recent applications of the most accurate techniques to several systems with technological importance, like ionic liquids, nanofluids and molten salts, have not been made correctly, generating highly inaccurate data, not reflecting the real physical situation. It is the purpose of this paper to discuss the best available techniques for the measurement of thermal conductivity of ionic melts and nanofluids.

Introduction/Background: Thermal conductivity is the most difficult thermophysical property to be measured with high accuracy, due to different molecular mechanisms of heat transfer in solids, liquids and gases, with neutral or ionic media, and the need to isolate pure conduction from other mechanisms of heat transfer (convection and radiation). If in principle it is possible to establish the basic equations of heat transport and resolve them for selected geometries, the experimental realization of the instrument is difficult to obey completely to the desired physical situation, and the methods of measurement today, uses and abuses of the previous equations". It is the purpose of this paper to summarize the several existing methods and recommend its application in our field. Reference [1] has a more complete analysis of the problem.

Basic Theory: Details of the theory can be found in references [1-4]. The equation of change for non-isothermal systems, isotropic, and without convective (no fluid motion) or radiation processes involved can be transformed to:

$$\rho C_P \frac{\partial T}{\partial t} = \lambda \nabla^2 T \qquad (1)$$

Transport of energy by radiation is always present, and must be corrected for each measuring technique, especially if measurements are performed at high temperatures.

Equation (1) is the basis of all experimental methods for the measurement of thermal conductivity. As said in our previous work [2] a variety of experimental methods have been developed, for gaseous, liquid, supercritical or solid phases, over wide range of thermodynamic states. These methods are based on energy equation (1) and can be classified in two main categories [2,4]: The unsteady state or transient methods, in which the full equation is used, the principal measurement being the temporal history of the fluid temperature (transient hot-wire, transient hot-strip, the interferometric technique adapted to states near the critical point, laser flash, etc.); the steady state methods, for which $\partial T/\partial t = 0$ and the equation reduces to $\nabla^2 T=0$, integrable for a given geometry (parallel plates, concentric cylinders, etc.). However, making good measurements of thermophysical properties is difficult and tedious! Nowadays it is not fashionable or economically attractive, the need for accurate data on thermophysical properties of fluids being replaced by alternative methods of properties calculation, based on computer simulation or prediction/estimation methodologies (cheaper, but risky), and by the apparent contradiction between accurate (low uncertainty) or *fit for purpose*. This last approach supported many commercial types of equipment, with the main objective of being *friendly user* and fast. However, the use and misuse of *ill-designed* equipments, with methods of measurement not adequate to the object systems, can be a disaster in scientific and technological grounds! Current practice show that, in spite of being based in established methods, construction and type of fluid/solid to be applied to, led to several inaccuracies in the data obtained and sometimes to completely erroneous results. This is the case of their application in the fluids area to new and more complex systems like, ionic melts (molten salts and ionic liquids) and nanofluids.

Methods of Measuring Thermal Conductivity of Ionic Melts and Nanofluids: It is not possible to describe here all the methods developed so far, for the temperature range 300–1500 K, at ambient pressure, the main zone where ionic liquids, molten salts and nanofluids are important. A complete discussion of the situation can be seen in the paper by Mardolcar and Nieto de Castro (1992) [5]. From classical methods (transient hot-wire, concentric cylinders or parallel plates) to non-classical methods (laser flash, forced Rayleigh scattering, photon correlation spectroscopy, photothermal radiometry, transient thermoreflectance, photothermal detection, wave-front-shearing interferometry, heat flow, AC calorimetry, photoacoustic and radiation heat exchange), all are described there, identifying their advantages and disadvantages. To these, transient hot strip, the transient plane source or hot-disk and the 3ω method, all developed after 1992, must be

added. The methods can be classified as primary and secondary [6]. Attainable uncertainty correspond to the "state-of-art" instruments, not comparable to commercial instruments (high accuracy sacrificed to ease of operation and equipment cost). Transient methods are the only primary methods, in the sense of CIPM-BIPM. These methods include the transient hot-wire, and the transient hot-strip, this last one still needing the solution of 3D heat transfer equation for the geometries involved. Table 1 displays selected methods for the measurement of thermal conductivity (thermal diffusivity) and their applicability to ionic melts and nanofluids.

Table 1. Selected methods for the measurement of thermal conductivity (thermal diffusivity) and its applicability to ionic melts and nanofluids [1].

Method	Type	Attainable Uncertainty[3]	Applicability to Ionic Melts			Applicability to Nanofluids		
			Yes	No	Remarks	Yes	No	Remarks
Transient hot-wire for conducting liquids[4]	Primary	1 %	√		The best method to be applied with classical designs	√		The best method to be applied with classical designs
Transient hot-wire (bare wires)	Primary	1 %		√		√		Non-conducting base fluids and/or nanoparticles
Transient hot-strip for conducting liquids (insulated strip)	Primary/Secondary	2-3 %	√		Can be considered primary if the 3D heat transfer equation is solved for the geometries involved	√		Can be considered primary if the 3D heat transfer equation is solved for the geometries involved
Transient Plane Source or Hot-Disk	Secondary	3-5 %	√		Limited in temperature range	√		Limited in temperature range
Steady-state Parallel Plates (Guarded Hot-Plates)	Secondary	2-3 %	√			√		Small spacing between plates might induce phase separation
Steady-state Concentric Cylinders	Secondary	2-3 %	√		Small gaps. Guarded plates	√		Small gaps have to be used.
Laser Flash	Secondary	3-5 %	√		Difficulties with originated waves in the liquid surface (Marangoni effects)	√		Use low power lasers to avoid NP breakage and structure deployment
Forced Rayleigh Scattering	Secondary / Relative	3-5 %	√		Dyes necessary to enhance the signal compatible with molten salts or IL's	√		Dyes necessary to enhance the signal compatible with nanofluids.
Photon Correlation Spectroscopy	Secondary / Relative	2-3 %	√		Optically transparent fluids. Not explored for measurements above 473 K.	√		Optically transparent fluids.
Transient Grating	Secondary / Relative	3-5 %		√	Needs a big improvement in the calibration. Not recommended for high quality work		√	Needs a big improvement in the calibration. Not recommended for high quality work
3ω Method	Secondary	5 %	√		Needs improvement of the theory. However, alternating current, destroying the direction of the polarizing current, avoids current polarization	√		Needs improvement of the theory. However, alternating current, destroying the direction of the polarizing current, avoids nanoparticle deposition and electrically insulation problems.

[3] Uncertainty is defined using ISO criteria, using a coverage factor (k=2), that correspond to a 95% confidence level
[4] Both the insulated probe and the polarization technique can be used

Discussion and Results: In principle, the hot-wire method can be applied to ionic melts and nanofluids, if a careful design is made of the instrument [1,4]. Regarding molten salts (and nanosalts), we have high temperature measurements, radiation and convection corrected or minimized, electrical insulation of measuring probes absolutely necessary. Use of current commercial instrumentation like transient hot-probes, transient hot-strips/disks, sacrifice accuracy for cost of instrumentation and ease of handling of probes/samples. Many of the results available were taken with commercial instrumentation, not properly validated. Restricting to hot-wire, for instance, it is common to use just one wire, sometimes shorter than the model requires (end effects), affecting directly the accuracy. For the case of nanofluids [7] they can be electrically conducting (water, metal particles, nanocarbons, etc.), the generation of a high temperature gradient near the wire might create migration of nanoparticles and its deposition at the surface of the probes, creating nanostructures with organization dependent of surface of the

probe/hot-wire and changing the bulk concentration, making the sensing zone non-homogeneous, distorting the heating wave propagation, and originating a temperature discontinuity similar to the temperature jump in gases (Kapitza resistance). This is magnified when the nanoparticles have surface charges creating electrical double-layers and affect the modelling of the measurement and create erroneous results. Recent work in IoNanofluids of graphene and CNT's [8], using molecular simulation, showed that not only this interphase exists, has a finite value of thermal conductivity, of the order of 15-30% greater than that of the bulk ionic liquid. These problems are not considered by instrument manufacturers, and especial probes have to be designed on purpose.

Summary/Conclusions: The measurement of the thermal conductivity of ionic melts and nanofluids is proposed to be done with accurate methods of measurement, in order to have confidence in the quality of the results. The transient hot wire continues to be the best available technique to obtain good data, although methods like the transient hot strip, the laser flash, the hot disk and the photo-correlation spectroscopy (transparent fluids) might be a less accurate, but cheaper method. Most of the equipment manufactured sacrifice accuracy to easiness and speed of operation and in most cases, originate bad data, which cannot be validated with standard reference data or certified reference materials.

References:

1. C.A. Nieto de Castro, M.J.V. Lourenço, Thermal Conductivity of Ionic Melts and Nanofluids - Secrets of the Trade, in *The Art of Measuring in Thermal Sciences* Eds., Josua Meyer and Michel de Paepe. 2019, CRC Press (Taylor and Francis, Series: Heat Transfer, Series Editor: Prof Afshin Ghajar).
2. C.A. Nieto de Castro, Absolute Measurements of the Viscosity and Thermal Conductivity of Fluids", JSME Int. J., Series II, 31 (1988) 387- 401.
3. R.B. Bird, W.E. Stewart, and E.N. Lightfoot, *Transport Phenomena*, 2nd Ed., John Wiley Sons, Inc., New York, 2014.
4. W.A. Wakeham, A. Nagashima and J.V. Sengers, J. V. (eds), *Measurement of the Transport Properties of Fluids*, Experimental Thermodynamics, Vol. III, Blackwell Scientific Pubs, Oxford, UK, 1991, namely chapters 6, 7 and 8.
5. U.V. Mardolcar, C.A. Nieto de Castro, The measurement of thermal conductivity at high temperatures", High Temp. - High Press., 24 (1992), 551-580.
6. V.M.B. Nunes, M.J.V. Lourenço, F.J.V. Santos, M.L.S. Matos Lopes, C.A. Nieto de Castro, Accurate Measurement of Physico-Chemical Properties on Ionic Liquids and Molten Salts, in *Ionic Liquids and Molten Salts: Never the Twain*, Eds. K.E. Seddon and M. Gaune-Escard, Chapter 17, pp-229-263, John Wiley & Sons, Inc., New York, 2010.
7. C.A. Nieto de Castro, S.I.C. Vieira, M.J.V. Lourenço, S.M. Sohel Murshed, Understanding Stability, Measurements, and Mechanisms of Thermal Conductivity of Nanofluids, J. Nanofluids, 6 (5) (2017) 804-811.
8. J.M.P. França, C.A. Nieto de Castro, A.A.H. Pádua, Molecular Interactions and Thermal Transport in Ionic Liquids with Carbon Nanomaterials, Phys.Chem.Chem.Phys., 19 (2017),17075-17087.

1st International Conference on Nanofluids (ICNf2019)
2nd European Symposium on Nanofluids (ESNf2019)
26-28 June 2019, Castelló, Spain

Investigation of the Thermal Conductivity and the Viscosity of Carbon Black Heat Transfer Nanofluids

S.K. Mylona[1*], F. Chibante[2], L. Romero-Zeron[2], and D. Hume[1]

[1]Thermtest Inc., 34 Melissa Street, Unit 1, Fredericton, NB, Canada, E3A 6W1

[2]Dept of Chem Eng, Univ of New Brunswick, 15 Dineen Dr, Fredericton NB, Canada E3B 5A3

[*]Sofia Mylona: smylona@thermtest.com

Keywords: Carbon black, Ethylene glycol, Thermal conductivity, Viscoelastic behaviour

Abstract: In this work, the thermal conductivity and the rheological behavior of mixtures of spherical graphitized carbon black in ethylene glycol were measured. Seven mixtures of different concentrations were prepared and the thermal conductivity was measured at 20 and 30 °C using a Thermtest Transient Hot Wire (THW-L2) Liquid Thermal Conductivity Meter. The viscoelastic behaviour of the mixtures was investigated at 20 °C.

Introduction/Background:

Low thermal conductivity is a large limitation in the development of energy efficient heat transfer fluids required in many industrial and commercial applications. This has been addressed by a new class of heat transfer fluids (HTF) developed by suspending thermally conductive nanoparticles and carbon nanotubes in these fluids. The resulting heat transfer nanofluids possess significantly higher thermal conductivity compared to unfilled liquids.

This work attempts to examine the thermal and flow behavior of carbon-based fillers to further the heat transfer applications of nanofluids.

Experimental:

Materials: The nanofluid mixtures were prepared by mixing LITX® 50 Carbon Black purchased from Cabot Corporation, inside Ethylene glycol Dowtherm SR1. The mixtures prepared had composition 1%, 2%, 3%, 5%, 7%, 9%, 11 wt% and placed inside a Planetary Centrifugal Mixer "THINKY MIXER" ARE-310 for five minutes at speed 2000 rpm. The homogeneity of the mixtures is confirmed from the shinny surface of the samples and the shadows formed when we apply the mixture on a piece of paper. (Figure 1). The mixtures with composition (1-3) wt% where stable for more than 30

minutes and with a simple mixing with a spoon or shaking their container became homogeneous again.

Figure 1. homogeneous nanofluid mixture (left image), nanofluids applied on a piece of paper (right photo)

Thermal Conductivity Measurements: The transient hot-wire (THW) method is an accurate and precise method for thermal conductivity measurements of fluids and solids. The most common THW sensors consist from two wires of the same material and diameter but different length [1] or with a single wire [2,3]. The thermal conductivity device presented in this work is a Thermtest Transient Hot Wire (THW-L2) Liquid Thermal Conductivity Meter for direct determination of the thermal conductivity of liquids and pastes in accordance with ASTM D7896-14 [4].

The transient hot-wire method is based on recording the transient temperature rise of a thin vertical wire with effective infinite length when a step voltage is applied to it. The wire is immersed in a fluid and can act both as an electrical heating element and a resistance thermometer.

A slope of the temperature rise as a function of the logarithm of time can give the calculation of the thermal conductivity of the measured fluid.

$$\lambda = \frac{q}{4\pi}\frac{dlnt}{d\Delta T(r_0,t)} = \frac{q}{4\pi}\frac{dlnt}{d\Delta T(t)} \quad (1)$$

In figures 2 a) and b) the thermal conductivity results of SR1 ethylene glycol used for the preparation of the mixtures and the nanofluid mixtures for both 20 and 30°C are plotted as a function of temperature and as a function of concentration of carbon black in wt%.

In addition, the thermal conductivity of pure ethylene glycol was measured and found to be 0.251 W/m·K at 21.2 °C and 0.252 W/m·K at 32.6 °C. while the calculated from REFPROP values were 0.25134 W/m·K and 0.25209 W/m·K, respectively.

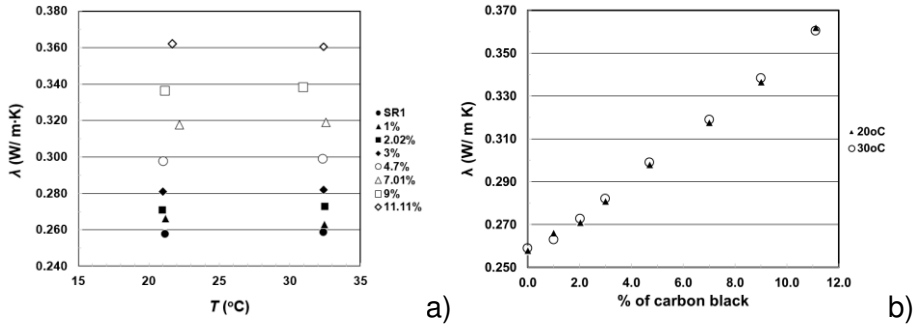

Figure 2. Thermal conductivity of the samples a) as a function of temperature, b) as a function of composition

Viscoelastic Behaviour

Viscoelasticity of materials can be seeing in between two extremes: flow of ideally viscous liquids on the one hand and deformation of ideally elastic solids on the other [5].

In this work, the rheological properties of the nanofluids were measured using a Bohlin Gemini rheometer using the parallel plate's geometry.

The use of this geometry is recommended when dispersions containing relative large particles and samples showing three-dimensional network structures are evaluated (as our samples) using a large gap between the plates, in this case H=1 mm (1000 μm). Although, this geometry could cause shear deformation during the measurements, this effect is negligible when performing small-angle oscillatory strain tests within the linear viscoelastic range [5].

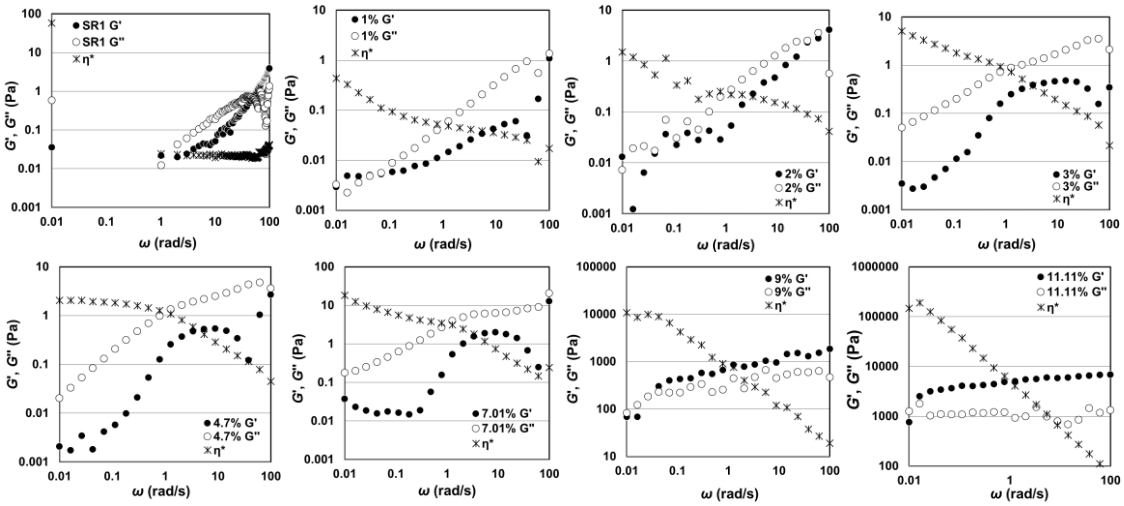

Figure 3. G', G', and η*as a function of angular frequency (ω) for all the mixtures

The rheological properties of the samples were investigated at 20 ºC. Figure 3 shows the elastic and viscous modulus as a function of the angular frequency. As it can been seen the mixtures with 9 and 11 wt% carbon black form network structures in which the elastic modulus dominates the viscous behavior (i.e. G'>G"). Furthermore, the complex viscosity indicates that the mixtures are shear thinning.

Summary/Conclusions: Thermal conductivity and viscoelastic behaviour of carbon black nanoparticles mixtures in ethylene glycol were measured. Thermal conductivity increases as the carbon black concentration increases in the mixtures. The rheological behavior indicates that at a concentration of 9 wt% of carbon black nanoparticles triggers the transition from a viscous liquid like behavior to an elastic dominated behavior (i.e. gel like behavior) typical of 3-D network structures developed through non-covalent interactions. Furthermore, the shear thinning performance of all the mixtures indicates the non-Newtonian behavior of these mixtures. Forthcoming research on the rheological properties of these carbon black nanoparticles mixtures and modeling of the experimental observations would provide more insights about the effect of nanofluids mixtures on the heat transfer properties of these materials.

References:

1. M.J. Assael, C.A. Nieto de Castro, H.M. Roder, W.A. Wakeham, "Transient methods for thermal conductivity", in: W.A. Wakeham, A. Nagashima, J.V. Sengers (Eds.), Measurement of the Transport Properties of Fluids, Blackwell Scientific Publications, London, 1991, p. 163.
2. N. Nagasaka and A. Nagashima, Review of Scientific Instruments 52:229 (1981).
3. M. Fujii, X. Zhang, N. Imaishi, S. Fujiwara, and T. Sakamoto, International Journal of Thermophysics 18:327 (1997).
4. ASTM D7896-14 Standard Test Method for Thermal Conductivity, Thermal Diffusivity and Volumetric Heat Capacity of Engine Coolants and Related Fluids by Transient Hot Wire Liquid Thermal Conductivity Method, ASTM International, West Conshohocken, PA, 2014, https://doi.org/10.1520/D7896-14.
5. T.G. Mezger, *The Rheology Handbook*, Vincentz Network, 4th Edition, Hanover, Germany, 2014.

1st International Conference on Nanofluids (ICNf2019)
2nd European Symposium on Nanofluids (ESNf2019)
26-28 June 2019, Castelló, Spain

Stability study of graphene nanofluid in liquid paraffin

G. Vilão [1,2], C.A. Ramos[2,3] and T.P. Iglesias[1*]

[1]Applied Physics Department, Faculty of Sciences of the University of Vigo, Lagoas-Marcosende s/n, 36310 Vigo, Spain.

[2]Physics Department of School of Engineering (ISEP), Polytechnic of Porto, Rua Dr. António Bernardino de Almeida, 431, 4200-072 Porto, Portugal.

[3]Research Centre in Industrial Technology and Engineering (CIETI), School of Engineering of Porto, Rua Dr. António Bernardino de Almeida, 431, 4200-072 Porto, Portugal

[*]Corresponding author: tpigles@uvigo.es

Keywords: Graphene, Nanofluid, UV-Visible Spectroscopic, stability.

Abstract: The study of the stability of nanofluid with 0.75% (V/V) of graphene in liquid paraffin at room temperature is presented. The nanoparticles with thickness 11–15 nm, surface area 50-80$m^2 \cdot g^{-1}$ and carbon content > 99.5 mass%, provided by MK-nano. Spectroscopy measurements were performed in the UV-visible zone for samples with different sonication times for the same concentration of graphene. The nanofluids were chosen with 40 min and 150 min of sonication, to study the permittivity and the electrical conductivity. The behaviour of the complex permittivity is shown as a function of the angular frequency.

Introduction/Background: The preparation of nanofluid is one of the most relevant tasks for the success of its characterization in function of its physical properties. Not because of the complexity of the execution method, but because of the need to control all surrounding experimental physical variables. The preparation of nanofluid is not a simple mixture between a solid and a liquid, the suspension and dispersion of the nanoparticles must be uniform, and the formation of agglomerates as small as possible. The nanofluid must exhibit stability and reproducibility during any experimental analysis to which it is subjected.

There are several methods of preparation of nanofluids, but they are all based primarily on two techniques, the single-step method and the two-step method. The two-step method is mostly the most usual method found in the studied literature, because it is more economical and easier to perform, however, it presents some difficulties in the stability of nanofluid. Another way to increase the dispersion of the nanoparticles in the

base fluid is the use of surfactant by controlling the pH of the solution [1]. However, the use of surfactants in the stabilization of nanofluids can alter the initial characteristics of the same.

In recent years there has been some progress in the preparation of stable nanofluids, with stability research being a "key" issue that influences the properties of nanofluids for technological and industrial application. Therefore, it is necessary to study and analyse which factors influence the stability of nanoparticle dispersion in nanofluids [2]. The mechanisms of stabilization of nanoparticle dispersions are discussed by studies of UV-Visible spectrophotometry, zeta potential, sediment photography, TEM (Electron Transmission Electron Microscopy) and SEM (Electron Microscopy Scanning), light scattering, of sedimentation, pH control, etc. One of the most reliable methods is the observation of nanoparticle size variation and / or their concentration variation in the base fluid over time, which method is relatively limited due to the need for observation over very long periods. Spectrometric measurements in the visible zone are used to characterize the dispersion stability of the nanoparticles on a micrometric scale [3], which allow to observe the variation of the nanofluid concentration. All methods referenced only allow to observe the stability of the nanofluid during a certain period, without quantifying or relating the different parameters that affect the stability of the same.

Discussion and Results: In the preparation of all samples was used the graphene nanoparticles provided by MK-nano, with thickness 11–15 nm, surface area 50–80$m^2 \cdot g^{-1}$ and carbon contents >99.5% mass. Liquid paraffin, CAS 8012-95-1, purity 99.5% mass and density 0.849 $g \cdot cm^{-3}$ at 298.15K was supplied by Guinama. Samples were prepared with a volume fraction of particles 0.75 % added to liquid paraffin. The nanofluids were homogenized by using intensive ultrasonic vibration with a Bandelin Sonoplus. During sonification, the fluid remained in a water bath with a controlled temperature of approximately 298 K [4].

In order to study the stability of the nanofluid, several samples were run as different sonication times. In this communication, we present the study for the volumetric concentration 0.75% of graphene in paraffin, this sample was chosen because it is an intermediate concentration of the concentration range of the studied samples. UV-visible spectroscopy measurements were performed for the various samples obtained and the absorption spectra were analysed. Due to the high absorption intensity of the nanofluid in the UV-visible zone (figure 1), it was diluted in 3 ml in base fluid and performed a new spectral analysis.

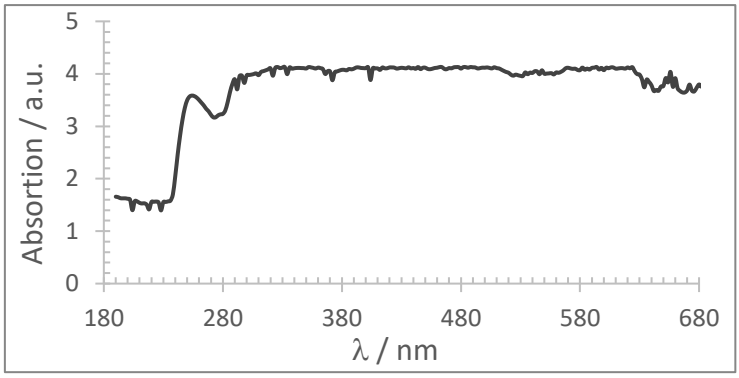

Figure 1. UV-visible spectrum of 0.75% (V / V) nanofluid graphene in liquid paraffin.

The graph of figure 2 represents the maximum relative intensity of one of the absorption peaks as a function of time that the samples were subjected to ultrasound.

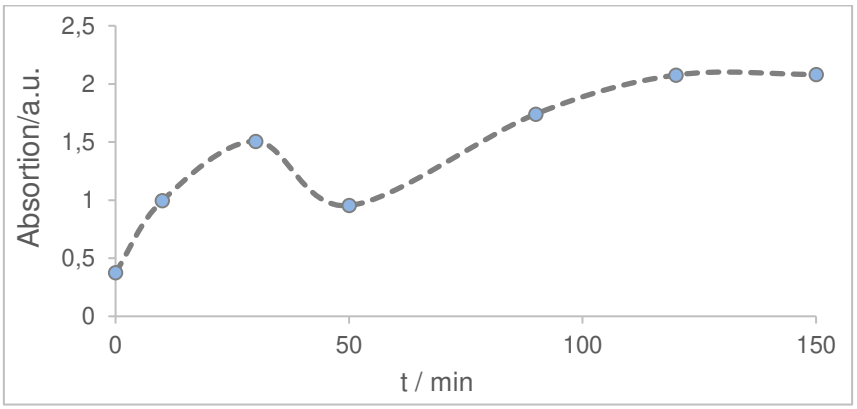

Figure 2. Relative peak of absorbance of the peak (282 nm) in relation to the sonication time, -●-sample of 0.75% (V / V) of graphene in liquid paraffin.

Electrical permittivity measurements as a function of the angular frequency of nanofluid were performed for the same sample with sonication times of 40 and 150 min, figure 3.

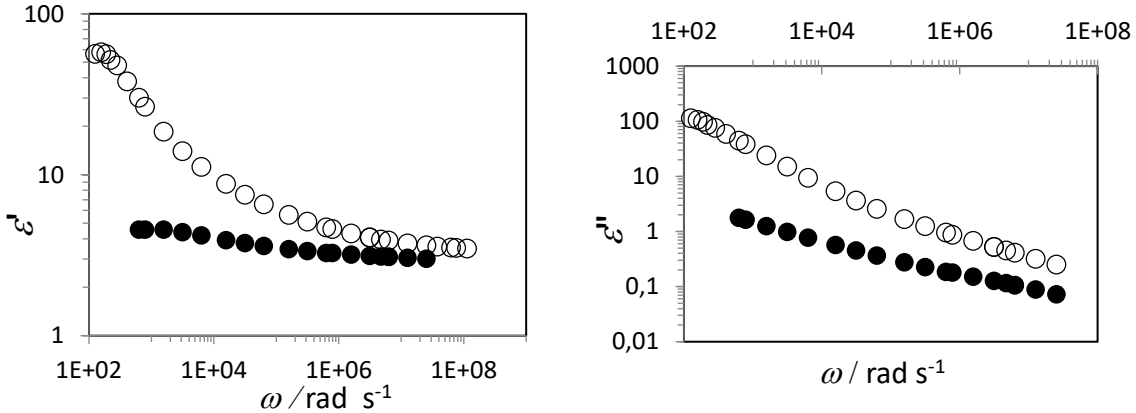

Figure 3. Complex permeability for nanofluid with 40 min (○) and 150 min (●) of sonication.

Summary/Conclusions: The intensity of absorption increases with the increase in the sonication time to which the nanofluid is subjected. Featuring a peak followed by a decrease, which follows a growth of the absorption intensity, from a certain time of sonication the intensity of absorption tends to a constant value. These results agree with the study by Sadeghi, et al., 2015 [5] in nanofluids of deionized water with alumina. It has been verified that the electrical permittivity presents higher values for the nanofluid with 40 min of sonication than the nanofluid with 150 min. The electrical conductivity was determined in d.c. of the nanofluids, verifying that the nanofluid with 40 min sonication has a conductivity of 9.77×10^{-8} $S \cdot m^{-1}$ whereas the nanofluid with 150 min has a conductivity of 5.68×10^{-9} $S \cdot m^{-1}$.

Acknowledgements: We gratefully appreciate the financial support ED431C 2016-034 provided by the Xunta de Galicia (Spain). G. V. thanks to the School of Engineering of Porto for granting leave of absence to carry out experimental work at the University of Vigo, and the laboratory of CIETI.

References:

1. C. Chen, Y. Chen and W. J Tseng, Surfactant-assisted de-agglomeration of graphite nanoparticles by wet ball mixing. *Journal of Materials Processing Technology*,190 (2007), 61-64.
2. A. Ghadimi, R. Saidur, and H.S.C. Metselaar, A review of nanofluid stability properties and characterization in stationary conditions. *International Journal of Heat and Mass Transfer* 54 (2011) 4051–4068.
3. R. Iglesias, M. A. Rivas, J. Reis, and T. P. Iglesias, Permittivity and electric conductivity of aqueous alumina (40 nm) nanofluids at different temperatures, *J. Chem. Thermodyn.* 89 (2015) 189–196.
4. M. F. Coelho, M. A. Rivas, G. Vilão, E. M. Nogueira and T. P. Iglesias, Permittivity and electric conductivity of copper oxide nanofluid (12 nm) in water at different temperatures, *J. Chem. Thermodyn*. 132 (2019) 164–173.
5. R. Sadeghi, S. Gh. Etemad, S. and E. Keshavarzi, Investigation of alumina nanofluid stability by UV–vis spectrum. *Microfluid Nanofluid* 18 (2015) 1023-1030.

1st International Conference on Nanofluids (ICNf2019)
2nd European Symposium on Nanofluids (ESNf2019)
26-28 June 2019, Castelló, Spain

Synthesis and analysis of PCM nano-emulsions for energy storage and heat transfer

S. Barison[1*], D. Cabaleiro[2,3], F. Agresti[1], L. Fedele[2], M.A. Marcos[3], S. Rossi[2] and S. Bobbo[2]

[1] Consiglio Nazionale delle Ricerche, ICMATE, Padova, Italy

[2] Consiglio Nazionale delle Ricerche, ITC, Padova, Italy

[3] Dpt. Física Aplicada, Universidade de Vigo, Vigo, Spain

[*]Corresponding author: simona.barison@cnr.it

Keywords: PCM, nano–emulsion, paraffin, stability, DSC, sub–cooling

Abstract: New phase change material emulsions (PCMEs) were developed and characterized as possible storage and heat transfer media for low–temperature thermal applications. RT21HC commercial paraffin (T_m ~21ºC) was investigated both in water and in an ethylene glycol+water mixture. A solvent–assisted emulsification method was used to prepare PCMEs. Paraffin droplet sizes were measured by DLS and emulsion stability evaluated during storage. Melting temperatures and latent heats were experimentally determined, and sub–cooling of up to 11 ºC were observed. Although thermal conductivity reduces by 9% for 10% paraffin mass concentration, enhancements in energy storage capacity overcome 20% for that same loading.

Introduction/Background: Phase change material emulsions (PCMEs) have been largely investigated in the last years as potential working fluids that could reduce energy consumption in HVAC systems [1]. They contain a fluid (mainly water or glycolated mixtures) and PCMs dispersed as fine droplets. PCMEs are especially attractive as PCMs are not encapsulated, but directly dispersed in the carrier fluid by means of an appropriately selected surfactant. Hence, PCMEs can combine the latent capacity provided by the PCM and the good transport properties of the carrier fluid. They have been investigated in the last years for many potential applications [2]. A barrier to practical implementation of PCMEs is the difficulty in maintaining stability with storage, freeze-thaw cycles or mechanical stress. Fine PCM droplets are usually preferred to avoid large increases in dynamic viscosity and to ensure long-term thermal stabilities. However, a size reduction can lead to large sub-cooling. Sub-cooling is an undesirable phenomenon due to which a material remains liquid below its melting temperature, thus enlarging the operating temperature ranges of the systems and worsening their energy efficiency. This behaviour has been attributed to isolation of nucleation sites [3]. A common strategy to reduce it is to introduce nucleation agents that act as impurities and

trigger heterogeneous solidification. Nanoparticles or PCMs with a higher melting point than the dispersed phase are commonly used as nucleating agents.

In this study a recently developed solvent–assisted method [5] was used to develop nanoemulsions using commercial RT21HC paraffin as dispersed phase in water and ethylene glycol+water. Stability through storage, phase change characteristics and thermal conductivity were investigated to elucidate the influence of dispersed phase droplets on the final performance of emulsions. Finally, the energy storage capacity versus temperature was estimated to define the working temperature range that would allow the best use of the latent heat provided by the PCM drops.

Materials and Sample Design: RT21HC paraffin was provided by Rubitherm Technologies GmbH (Germany). Water was deionized by a Millipore system (Billerica, USA) to obtain a resistivity of at least 18.2 MΩ cm, while ethylene glycol (mass purity >99%) was supplied by Sigma Aldrich. Sodium dodecyl sulphate (SDS, 98%, Sigma Aldrich) was used as emulsifier. In order to try to reduce sub–cooling effect, RT55 (T_m ~55ºC) and RT70HC (T_m ~70ºC) waxes (Rubitherm Technologies GmbH, Germany) were employed as nucleating agents.

Nano-emulsions were formulated by a solvent-assisted route presented in Agresti et al. [5]. Studied samples were prepared at 2, 4 and 10 wt.% of paraffin with a fixed SDS:PCM ratio of 1:8. Two different situations were considered: i) without nucleating agent (PCM drops only containing RT21HC) and ii) using a mixture of RT21HC:RT55 or RT21HC:RT70HC (at 90:10 wt.%) as dispersed phase. Hydrodynamic size and ζ–potential of nano-emulsions were determined by dynamic light scattering (DLS) using a Zetasizer Nano–ZS90 (Malvern Instruments Ltd., UK). Throughout the studied period (~ 1 month), PCM droplets showed average diameters ~90-110 nm (for samples at 2 and 4 wt.% paraffin contents) and ~125–160 nm (for 10 wt.% loadings), while ζ–potentials obtained for some representative samples were in the range ~72–82 mV (in negative value).

Experimental Methods: Solid–liquid transitions were characterized in terms of temperature, T, and latent heat, Δh, by means of a differential scanning calorimeter, DSC, Q2000 (TA Instruments, USA). Estimated temperatures and enthalpy uncertainties are 0.3ºC (repeatability of 0.1ºC) and 1.2 J/g (repeatability of 0.7 J/g), respectively. Thermal conductivities, λ, were obtained in the temperature interval from 2ºC to 60ºC using a hot disk thermal constants analyser TPS 2500 (Hot Disk AB, Sweden). Previous tests performed on stainless steel and deionized water reveal deviations lower than 2%.

Discussion and Results: DSC scans from -30ºC to +60ºC were performed for the bulk–RT21HC and different nano-emulsions. Table 1 gathers the measured melting and crystallization temperatures and the melting heats. As can be observed, while bulk–RT21HC sub–cooling is <1ºC, this value overcomes 11ºC for the emulsions without nucleating agents. The two paraffin with melting points higher than dispersed phase, tested as possible nucleating agents, only achieved small reductions in the undesirable sub–cooling effect (up to 3ºC in the case of RT55 and 2.2ºC for the RT70HC).

Table 1. Melting temperature, T_m, crystallization temperature, T_{cr}, and melting heats, Δh_m, measured for some representative samples

Sample	T_{cr} (ºC)	T_m (ºC)	Δh_m (J/g)
bulk–RT21HC	19.65	20.15	142.7
RT21HC(2 wt.%)	9.55	20.05	2.52
RT21HC(4 wt.%)	9.45	20.55	4.32
RT21HC(3.6 wt.%)+RT55(0.4 wt.%)	12.55	20.65	3.63
RT21HC(3.6 wt.%)+RT70HC(0.4 wt.%)	10.05	18.95	3.52
RT21HC(10 wt.%)	9.05	18.35	11.27

Latent heat stored by nanoemulsions increases with RT21HC concentration. However, these results are ~12–32% lower than Δh calculated from the melting heats of the bulk–RT21HC and the fraction of this material in the sample by using a weighted average equation. Results here presented as an example are similar to those obtained for PCMEs based on ethylene glycol+water.

Around the phase change, nanoemulsions are expected to store larger amounts of heat than their corresponding carrier fluids since paraffin drops absorb/release an additional amount of heat during solid–liquid transition.

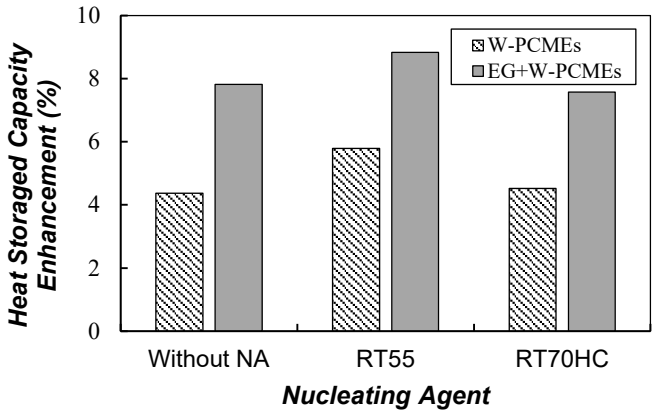

Fig. 2. Enhancements in heat storage capacity for PCM emulsions prepared at 4 wt.% with and without nucleating agent in both base fluids.

Fig. 1 shows the enhancement in heat storage capacity of some PCMEs considering a

temperature difference equal to the sub–cooling (minimum ideal interval to be covered by emulsions so that PCM drops reversely undergo solid–liquid phase change). In this case, nanoemulsions with nucleating agent exhibit better ideal heat storage capacities than samples containing only RT21HC in PCM droplets. This is consequence that sub–cooling reduction compensates the decrease in latent heat due to the addition of nucleating agent.

Given the lower thermal conductivity of RT21HC paraffin in comparison with the base fluids, λ is expected to decrease with the increasing concentration of PCM. In this case, reductions overcome 9% for 10 wt.% emulsions based on either water or glycol+water. Similar decreases were observed for samples prepared with and without nucleating agent.

Summary/Conclusions: PCM emulsions with fine drops were designed starting from a commercial paraffin with a melting transition ~21ºC. Samples proved to be resistant to storage under static conditions (no evidence of phase separation or significant growth in droplet size) but with large sub–cooling. In spite of the efforts to try to face that problem by promoting heterogeneous nucleation in dispersed drops with the addition of different nucleating agents, only partial decrease in sub–cooling effect (up to 3.2 K) was achieved with tested paraffin. Although the incorporation of a nucleating agent leads to a decrease in PCME latent heat, the reduction in sub–cooling effect of these nanoemulsions allows obtaining larger heat storage capacities. As expected, thermal conductivity decreases with increasing dispersed PCM concentrations. Reductions in this property overcome 9% for the highest paraffin loadings.

References:

1. J. Shao, J. Darkwa, G. Kokogiannakis, Review of phase change emulsions (PCMEs) and their applications in HVAC systems, *Energ. Build.* 94 (2015) 200.
2. M. Delgado, A. Lázaro, J. Mazo, B. Zalba, Review on phase change material emulsions and microencapsulated phase change material slurries: materials, heat transfer studies and applications, *Renew. Sust. Energy. Rev.* 16 (2012) 253-273.
3. E. Günther, L. Huang, H. Mehling, C. Dötsch, Subcooling in PCM emulsions-Part 2: Interpretation in terms of nucleation theory, *Thermochim. Acta* 522 (2011) 199-204.
4. L. Huang, E. Günther, C. Doetsch, H. Mehling, Subcooling in PCM emulsions-Part 1: Experimental, *Thermochim. Acta* 509 (2010) 93-99.
5. F. Agresti, L. Fedele, S. Rossi, D. Cabaleiro, S. Bobbo, G. Ischia, S. Barison, Nano-encapsulated PCM emulsions prepared by a solvent-assisted method for solar applications, *Solar Energy Materials & Solar Cells*, 194 (2019) 268-275.

1st International Conference on Nanofluids (ICNf2019)
2nd European Symposium on Nanofluids (ESNf2019)
26-28 June 2019, Castelló, Spain

Thermophysical properties and Thermodiffusion coefficient of Fullerene Nanofluids

A. Errarte[1#], M. Aginagalde[1] and M. Mounir Bou-Ali[1*]

[1] Mechanical and Manufacturing Department, MGEP Mondragon Goi Eskola Politeknikoa, Loramendi 4 Apdo. 23, 20500 Mondragon, Spain

[#]ane.errarte@alumni.mondragon.edu; [*]mbouali@mondragon.edu

Keywords: Thermodiffusion, Transport properties, Fullerene, Binary mixtures.

Abstract: This work studies the thermophysical properties and thermodiffusion coefficient measurements of the three binary mixtures correspondent of the ternary nanofluid mixture of the fourth mission of the project Diffusion coefficients Measurement in Ternary Mixtures (DCMIX4): 1,2,3,4-Tetrahydronaphthalene, Toluene and Fullerene. Thermogravitational columns were used to measure the thermodiffusion coefficient, analysing concentration variation across the column height. Nevertheless, previous knowledge about transport properties is necessary. So, density, viscosity, thermal and mass expansion and refractive index of all three mixtures were measured.

Introduction/Background: Fullerene is a carbon allotrope as the diamond or the graphite, a truncated icosahedron with an empty cavity surrounded by 60 atoms, 12 pentagons and 20 hexagons [1]. Fullerenes are considered nanoparticles with unique physical and chemical properties taking part in a wide range of applications such as lubricants or medicines.

The interest of the study of these nanoparticles has considerably increased in the last years. One of the characteristic that has been widely studied is its solubility [2]. They have low solubility in water and hydrogen bounding containing solvents, but they can easily be dissolved in solvents as the toluene. For this reason, it is necessary to study their properties in solvents of different characteristics.

At this scenario, the DCMIX4 project (Diffusion Coefficients Measurement in Ternary Mixtures) [3] selected the mixture composed by 1,2,3,4-Tetrahydronaphthalene, Toluene and Fullerene to study its transport properties in microgravity conditions, being the first time that those properties are analysed in the International Space Station (ISS) for a nanofluid. Results of the actual work contribute in the analysis of properties in ground conditions.

Experimental procedure: First steps were done in the determination of transport properties. As previously was mentioned three mixtures were analysed, where two of them are considered as nanofluids due to Fullerene nanoparticles:

- Tetrahydronaphthalene – Toluene (0.6004 in THN mass fraction)
- Fullerene – Tetrahydronaphthalene (0.0012 in C_{60} mass fraction)
- Fullerene – Toluene (0.0018 in C_{60} mass fraction)

Based on these concentrations, other surrounding mass fractions were also analysed.

Sample preparation was carried out in a Gram VXI-310 precision balance. An Anton Paar DMA 5000 density meter was used to measure the density. The same device was used to determine the mass and thermal expansion. The first one is determined measuring the density of the samples of five temperatures around the mean one. On the other hand, the mass expansion is determined by measuring the density of five samples close to the studied one. The dynamic viscosity was analysed by an Anton Paar AMVn falling ball micro-viscometer. Finally, the refractive index of the mixtures was measured by an Anton Paar Abbemat MW Multiwavelength refractometer with different wavelengths: 435.8 nm, 480.0 nm, 514.5 nm, 546.1 nm, 589.3 nm, 632.8 nm and 656.3 nm. Further information about thermophysical properties can be found in [4].

These thermophysical properties are necessary to determine the thermodiffusion coefficient. For this work two different thermogravitational techniques were used (Figure 1). On the one hand, Thermodiffusion coefficient (D_T) was determined by the traditional extraction method. On the other, the Digital Interferometry method was applied to a micro-thermogravitational column [5]. In both cases, the sample is placed between two parallel vertical walls, and a horizontal temperature gradient is applied; one of the lateral walls is heated and the other cooled. When the system reaches the stationary state, the concentration of each of the species is analysed along the height of the column.

In the traditional methodology, concentration along the column height is determined by extraction of five samples and the analysis of their density or refractive index. Then, the thermodiffusion coefficient is determined by the expression (1) [6].

$$D_T = -\frac{L_x^4}{504}\frac{\alpha g}{\beta \mu}\frac{1}{c_0(1-c_0)}\frac{\partial \rho}{\partial z} \qquad (1)$$

Here, L_x is the gap, β is the mass expansion, α is the thermal expansion, g is the gravitational force, μ is the dynamic viscosity, c_0 is the concentration of the densest component and $\frac{\partial \rho}{\partial z}$ is the variation of density along the column height.

The micro-column installation where Digital Interferometry is used is based on two lasers of 470 nm and 633 nm wavelengths, spatial filters, a Mach-Zehnder interferometer and a CCD camera to obtain the generated interferometry pattern. It is known that a change in phase is directly related to a refractive index change, thus to a concentration variation. Knowing contrast factors correspondent to the mixture, it is possible to determine directly the concentration from the refractive index and determine the thermodiffusion coefficient. As in this case only binary mixtures are studied, one laser would be enough to determine the concentration variation.

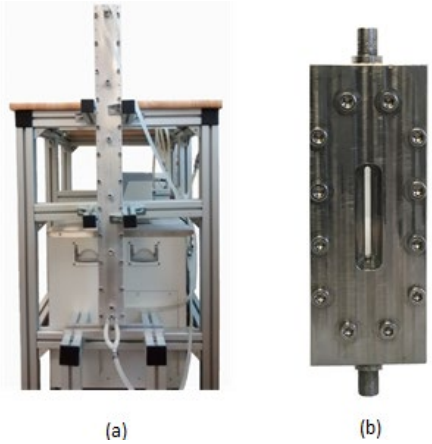

Figure 1: Thermogravitational columns used in this study. (a) Large Thermogravitational Column and (b) micro-Thermogravitational Column

Discussion and Results: Measurements were done in the temperatures that the ternary mixture is analysed in DCMIX4 project experiments in the ISS, 20ºC, 25ºC, 30ºC and 35ºC. Density approaches to pure solvents values when low fullerene concentrations are studied, increasing for higher C_{60} concentration. Moreover, it can be said that for lower temperatures the density increases. Figure 2 shows the variation of density used for mass and thermal expansion determination of C_{60}-THN mixture in a 0.0012 mass fraction.

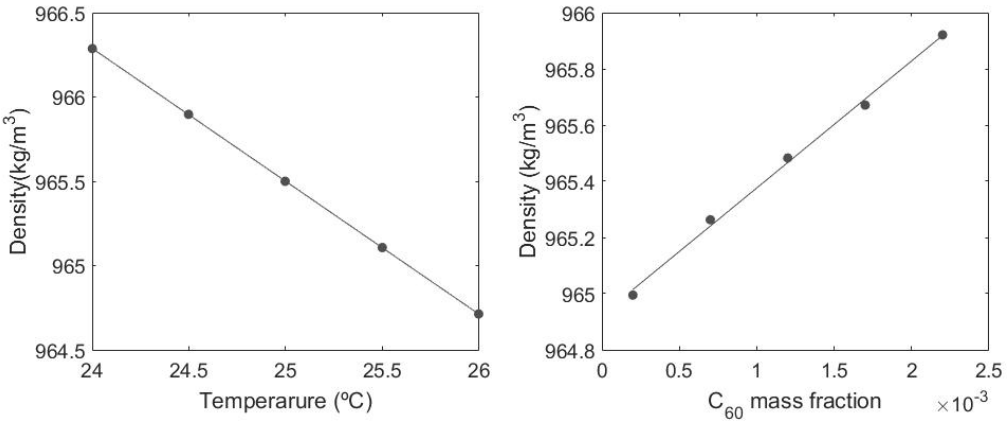

Figure 2: Density variation for different temperature and fullerene mass fraction at 25ºC

Moreover, it can be seen that the variation of the density of the nanofluids is higher than the ones formed by liquids, but no such difference was reported with thermal expansion.

Finally, in the case of the mixtures containing nanoparticles of fullerene, D_T shows higher order of magnitude than in the case of results obtained when pure liquids mixtures are analysed.

Summary/Conclusions: This work shows first insights about thermophysical and transport properties for the binary mixtures of fullerene based nanofluid of DCMIX4 project. We determined the density, viscosity, mass and thermal expansion, refractive index and thermodiffusion coefficient. It has been found that fullerene concentration generates variations in the studied properties even if the C_{60} concentration is very low, as in the case of thermodiffusion coefficient it increases its value in an order of magnitude.

New studies will be focused on the completion of this work and analysis of the ternary mixture. By this way, molecular diffusion will be also measured in order to be able to determine the Soret coefficient of the mixtures.

Acknowledgements:

The authors thank the support of the FETRAFLU (2018-CIEN-000101-01) from Gipuzkoa Program for Science, ATNEMFLU (ESP2017-83544-C3-1-P) of the MINECO, DCMIX (AO-2009-0858/1056) from the European Space Agency, and the Research Group Program (IT1009-16) from the Basque Government.

References:

1. H. W. Kroto, A. W. Allaf, and S. P. Balm, *C60: Buckminsterfullerene*, Chem. Rev., 91 (1991), pp. 1213–1235.
2. R. S. Ruoff, D. S. Tse, R. Malhotra, and D. C. Lorents, *Solubility of fullerene (C60) in a variety of solvents*, J. Phys. Chem., 97 (1993),pp. 3379–3383.
3. M. M. Bou-Ali et al., *Benchmark values for the Soret, thermodiffusion and molecular diffusion coefficients of the ternary mixture tetralin+isobutylbenzene+n-dodecane with 0.8-0.1-0.1 mass fraction*, Eur. Phys. J. E, 38(2015), pp.0–6.
4. J. K. Platten *et al.*, “Benchmark values for the Soret, thermal diffusion and diffusion coefficients of three binary organic liquid mixtures,” *Philos. Mag.*, vol. 83, no. 17–18, pp. 1965–1971, Jan. 2003.
5. E. Lapeira, A. Mialdun, V. Yasnou, P. Aristimuño, V. Shevtsova, and M. M. Bou-Ali, *Digital Interferometry Applied to Thermogravitational Technique*, Microgravity Sci. Technol., 30 (2018), pp. 635–64.
6. M. M. Bou-Ali, O. Ecenarro, J. A. Madariaga, C. M. Santamaría, and J. J. Valencia, *Thermogravitational measurement of the Soret coefficient of liquid mixtures*, J. Phys. Condens. Matter, 10 (1998), pp. 3321–3331.

1st International Conference on Nanofluids (ICNf2019)
2nd European Symposium on Nanofluids (ESNf2019)
26-28 June 2019, Castelló, Spain

Deagglomeration effects of hydrodynamic cavitation on Nanofluids

S. Niazi [1,2], M. Talebian Gevari [1,2], M. Ghorbani[1,2,3] and A. Kosar[1,2,4*]

[1] Sabanci University Nanotechnology Research and Application Center, 34956 Tuzla, Istanbul, Turkey
[2] Mechatronics Engineering Program, Faculty of Engineering and Natural Science, Sabanci University, 34956 Tuzla, Istanbul, Turkey
[3]Department of Biomedical Engineering and Health Systems, KTH Royal Institute of Technology, Stockholm, Sweden
[4]Center of Excellence for Functional Surfaces and Interfaces for Nano-Diagnostics (EFSUN), Sabanci University, Orhanli, 34956, Tuzla, Istanbul, Turkey
[*]Corresponding author: kosara@sabanciuniv.edu

Keywords: Nanofluid, deagglomeration, hydrodynamic cavitation

Abstract: Agglomeration issue for nanofluids in heat transfer applications has motivated the researchers to search for solutions to overcome this problem. The proposed technique in this paper is using the energy release of the cavitating bubbles to deagglomerate the nanoparticles. The agglomerated nanofluid passes through a microchannel with a micro orifice at different inlet pressures. DLS measurements are done at different inlet pressures to investigate the practicality of the system. The results show the mean size of the nanoparticles after being subjected to cavitating flow decreases by 87%.

Introduction/Background: Nanofluids have attracted the attention of many researchers during the past decades due to their wide applications in different areas such as heat transfer [1], drug delivery [2], and cancer therapy [3]. Nanofluids are known for their high convection heat transfer coefficient and high dispersion stability due to the Brownian motion of nanoparticles. Because of the heat transfer enhancement by nanofluids, they are frequently used in different industries for applications such as cooling systems and solar energy collectors. Also, nanofluids have adjustable properties like thermal conductivity and wettability by changing the weight fraction of nanoparticles in the base fluid. Although they have many applications and advantages, they also face some problems in the long run. For instance, they are not very stable and also they are not reusable after short use. Nanoparticles stick to each other and get agglomerated as they receive heat and consequently sedimentation occurs. Many efforts have been made to deagglomerate nanoparticles to increase their stability. One of the widely used techniques for deaggolomerating them is using surfactants in the nanofluids. However

they contaminate the heat transfer media and also they are not functional enough at high temperatures because the surfactants enlarge the thermal resistance between nanoparticles and the base fluid [4]. The other way to prevent agglomeration without surfactants is surface modification of nanoparticles. For example, grafting silanes directly to the surface of silica nanoparticles is a type of surface modifications that prevents the agglomeration [5]. Although this method is more functional than using surfactants, surface modification processes are hard and also expensive. Cavitation, as one of the main phase change mechanisms along with boiling, occurs due to the sudden pressure drop at a constant temperature. There are two methods to generate cavitation: i) hydrodynamic cavitation ii) acoustic cavitation. Hydrodynamic cavitation happens as a result of increasing the gravitational energy or kinetic energy of the fluid. A sudden reduction in cross-sectional area of the fluid flow path could decrease the pressure and cause hydrodynamic cavitation. The collapsing bubbles at the high pressure zone releases a massive amount of energy that could be used for different applications such as deagglomeration of nanoparticles [6, 7].

In this study, the proposed solution for nanoparticles deagglomeration exploits the energy release from the cavitation phenomenon in a microfluidic device. Titania-water nanofluid is prepared as the working fluid. The nanofluid is heated to make sure that agglomeration happens. Then, the effect of cavitating flow on the deagglomeration of the particles is investigated.

Experimental setup: Commercial TiO_2 rutile powder (Ionic Liquids Technologies, IoLiTec GmbH, Germany) with mean diameter of 30nm was mixed with the distilled water as the base fluid at the weight fraction of 0.05%. For nanofluid preparation, sonication and stirring were done simultaneously for 2 hours [8]. Then, it was heated up to 100℃ on the hot plate to agglomerate the particles. DLS measurement was used in each step to measure the average size of the dispersed particles.

As shown in Figure 1, the experimental setup consists of a high pressure nitrogen tank to drive the fluid into the system. The fluid container keeps the working fluid inside and the high speed camera monitors the fluid flow pattern while the microfluidic device is sandwiched between an aluminium package and Pyrex leads. Pressure gauges are installed at inlet, micro orifice, and outlet of the device. The microfluidic device is a dry etched micro orifice with the width of 152µm on a silicon substrate with one inlet and two outlets. The heated nanofluid is introduced to the system by increasing the inlet pressure. The high speed camera is used to ensure the inception, development, and supercavitation flow patterns.

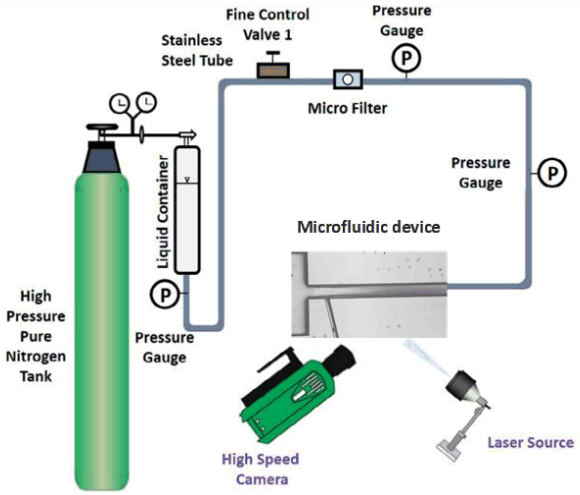

Figure 1. The experimental setup

Discussion and Results: The Dynamic Light Scattering (Zetasizer Nano ZS (Malvern)) technique is used for measuring the hydrodynamic diameter of the nanoparticles in the base fluid. DLS measurements were done in three stages; prepared nanofluid, heated nanofluid and after the experiments with different inlet pressures. The DLS results are shown in Figure 2. The mean diameter of the nanoparticles is measured as 255nm before heating while after heating, majority of the nanoparticles have a mean diameter of 1281nm. Since the cavitation intensity changes with alteration in inlet pressures, the size of the particles in the fluid decreases with increase in inlet pressure. The mean diameter of the nanoparticles as they passed through the micro orifice at 20bar, is 342 nm. At the inlet pressure of about 70 bar, the mean diameter of the nanoparticles reaches 164nm.

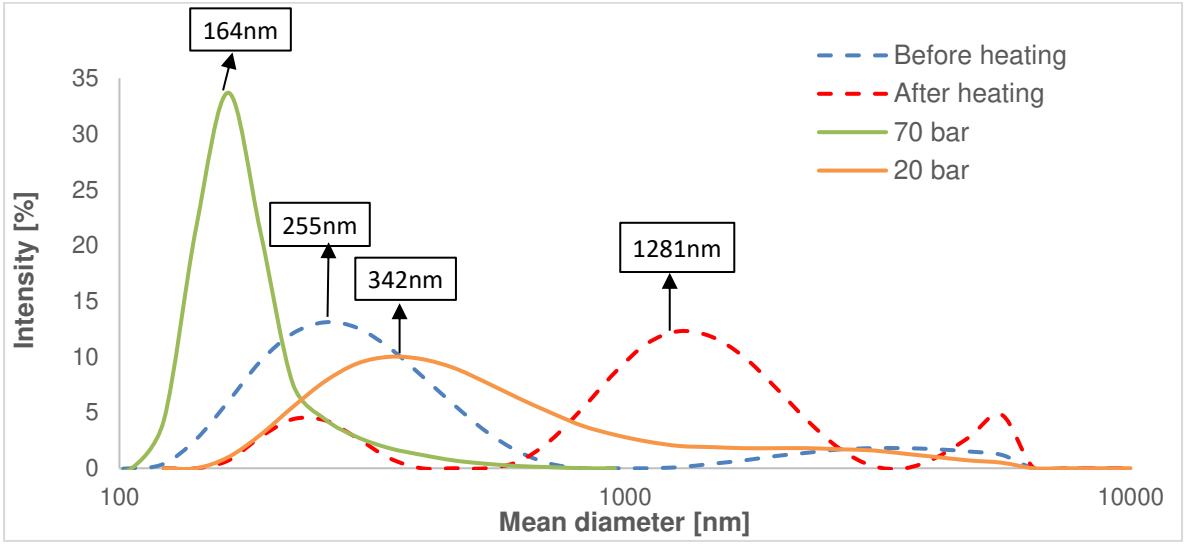

Figure 2. DLS results of the prepared nanofluid, heated nanofluid and after the experiments with two different inlet pressures

The DLS results show that the deagglomeration effect of this system has a direct relation with the cavitation intensity and inlet pressure.

Summary/Conclusions:

In this study, hydrodynamic cavitation is used as a technique to make the agglomerated nanoparticles inside nanofluid reusable. DLS measurements show that the mean dimeter of the nanoparticles decreases as they are subjected to cavitating flows. The experiments show that higher inlet pressures result in smaller mean dimeter of the nanoparticles, which is the result of enhanced shock wave propagation upon the collapse of the bubbles.

References:

1. Godson, L., et al., *Enhancement of heat transfer using nanofluids—an overview.* Renewable and sustainable energy reviews, 2010. 14(2): p. 629-641.
2. Tripathi, D. and O.A. Bég, *A study on peristaltic flow of nanofluids: Application in drug delivery systems.* International Journal of Heat and Mass Transfer, 2014. 70: p. 61-70.
3. Huang, H.S. and J.F. Hainfeld, *Intravenous magnetic nanoparticle cancer hyperthermia.* International journal of nanomedicine, 2013. 8: p. 2521.
4. Yu, W. and H. Xie, *A review on nanofluids: preparation, stability mechanisms, and applications.* Journal of nanomaterials, 2012. 2012: p. 1.
5. Yang, X. and Z.-h. Liu, *A Kind of Nanofluid Consisting of Surface-Functionalized Nanoparticles.* Nanoscale Research Letters, 2010. 5(8): p. 1324.
6. A. Kos¸ar, K.S.e., and M. P. Menguc *Flow system for avoiding particle agglomeration*, T.p. PCT/TR2015/050145, Editor. 2015.
7. Karimzadehkhouei, M., et al., *Increasing the stability of nanofluids with cavitating flows in micro orifices.* Applied Physics Letters, 2016. 109(10): p. 104101.
8. Haddad, Z., et al., *A review on how the researchers prepare their nanofluids.* International Journal of Thermal Sciences, 2014. 76: p. 168-189.

1st International Conference on Nanofluids (ICNf2019)
2nd European Symposium on Nanofluids (ESNf2019)
26-28 June 2019, Castelló, Spain

Thermoelectric-coupled hydrodynamic cavitation energy harvesting system

M. Talebian Gevari[1, 2], S. Niazi[1, 2], M. Ghorbani[1, 2, 3] and A. Kosar[1, 2, 4*]
[1] Sabanci University Nanotechnology Research and Application Center, 34956 Tuzla, Istanbul, Turkey
[2] Mechatronics Engineering Program, Faculty of Engineering and Natural Science, Sabanci University, 34956 Tuzla, Istanbul, Turkey
[3]Department of Biomedical Engineering and Health Systems, KTH Royal Institute of Technology, Stockholm, Sweden
[4]Center of Excellence for Functional Surfaces and Interfaces for Nano-Diagnostics (EFSUN), Sabanci University, Orhanli, 34956, Tuzla, Istanbul, Turkey
[*]Corresponding author: kosara@sabanciuniv.edu

Keywords: Nanofluid, Cavitation, Energy harvesting, μ-TEG

Abstract: The ever growing energy demand has led to the advent of different energy harvesting systems. This study investigates the performance of a thermoelectric coupled hydrodynamic cavitation system as an energy harvesting device. The effect of changing the working fluid from water to Titania-water nanofluid on the heat generation of the cavitation system is discussed in this study and also the coupling of the cavitation system with one of the micro thermoelectric generators in the literature is included. At the end, the device performance is quantified by comparing its power generation with the required power for the daily used miniature electrical devices.

Introduction/Background: As reported in the Annual Energy Outlook 2019 [1], the green resources share in power generation will continue with its increasing trend until 2050 and reach 13% by then. The decreasing share of coal and nuclear resources in this report as well as the increasing number of publications and patents in green energy harvesting systems reveal the growing attraction of researchers in this field.

During the past decade, the energy release from the cavitating flows has opened a new gate to the applications of this phenomenon, namely water treatment [2], surface cleaning [3], biomedical applications like breaking urinary stones [4], and energy harvesting [5]. The local high temperature $5000\ \mathrm{K}$ and high pressure $500\ \mathrm{atm}$ points upon bubble collapse is the main motivation behind these applications.

In this study, a hydrodynamic cavitation system is designed, and microfluidic devices are fabricated. Water and Titania-water nanofluid are introduced to the system as the working fluids to observe the inception, development, supercavitation, and chocked flow in the microfluidic device. The rate of temperature rise on the end wall as a result of the bubble collapse is estimated for both fluids. The energy harvesting system prototype, in

which the cavitation system is coupled with a micro thermoelectric generator is presented and the power generation is calculated. At the end, the amount of the power generation is compared with the common daily used miniature systems.

Experimental setup: The microfluidic device in this experiment is a dry etched micro orifice in a double side polished $< 100 >$ silicon wafer bonded to a Borofloat 33 glass. The geometry consists of an inlet with the width and length of $900\mu m$ and $2000\mu m$, respectively. The width of the orifice is $152\mu m$ with wall roughness of height $1.5\mu m$. The length of the orifice is $2000\mu m$ and the depth of the microfluidic device is $70\mu m$. Figure 1-a shows the geometry of the microfluidic device. The microfluidic device is sandwiched on an aluminium package with Pyrex caps so that the flow pattern visualization is possible. A high speed camera and a proper light source are used to see the fluid behaviour while doing the experiments. Three pressure gauges are installed at the inlet, micro orifice, and outlet of the microfluidic device to measure the static pressure. A high pressure nitrogen tank is used to push the working fluid to the system. The experimental setup is shown in Figure 1-b.

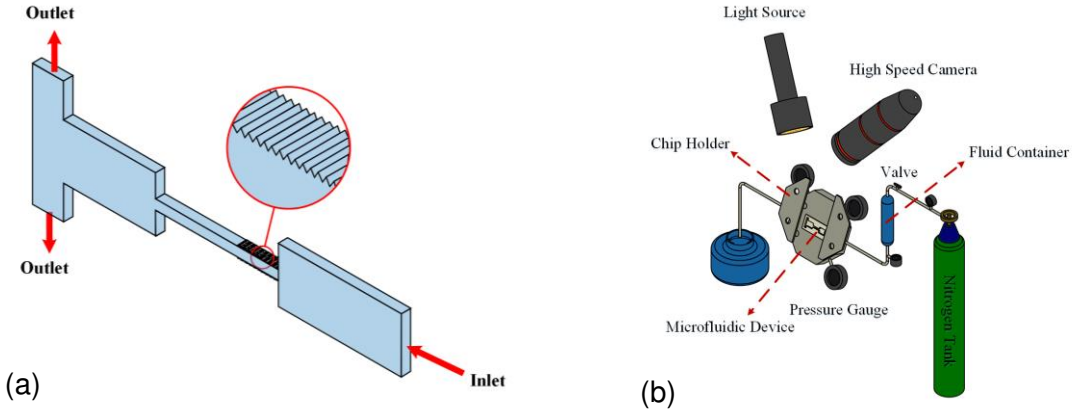

Figure 1 – a) the geometry of the microfluidic device with one inlet and two outlets, b) the experimental setup consisting of the high pressure nitrogen tank, fluid container, microfluidic device, high speed camera and light source

Two different working fluids (water and TiO_2-water nanofluid) are used to investigate the temperature rise on the end wall of the orifice as a result of the cavitating bubble collapse. The temperature rise in this location could be used to generate power using a thermoelectric device.

Nanofluid preparation: Spherical commercial titanium oxide powder rutile (Ionic Liquids Technologies, IoLiTec GmbH, Germany) with particle mean diameter of $10 - 30nm$ was used to make the suspension with the weight ratio of 0.05% in distilled water as the base fluid. Three sets of DLS measurements were done and in each measurement, the fluid was tested for 17 times. The reported z-average showed the mean diameter of the particles as $304.9\ nm$.

Device characterization: Increasing the inlet pressure leads to the increase in the flowrate of the working fluid in the microfluidic device. When the cross sectional area of the fluid flow path decreases dramatically in the micro orifice section, the velocity increases and consequently the static pressure decreases. The static pressure drop less than the vapor pressure leads to the cavitating bubble nucleation. The bubbles continue growing in size until they reach a high pressure zone and burst. The collapse of the cavitating bubbles releases a huge amount of energy within a very short time.

In the cavitation device, for water as the working fluid, inception was observed at $21.4\ \mathrm{bar}$, while the inception for the nanofluid occurred at $17.2\ \mathrm{bar}$. The reason for this is the heterogeneous bubble nucleation on the interface of the nanoparticles and the base fluid.

Discussion and Results: The potential energy of the bubbles could be calculated as $\mathrm{E_{pot}} = 4/3\,\pi \mathrm{R}^3(\mathrm{P_{stat}} - \mathrm{P_v})$ where $\mathrm{P_v}$ is the vapor pressure, $\mathrm{P_{stat}}$ is the static pressure, and R is the radius of the bubbles. Half of the potential energy turns to heat upon collapse [6]. On the other hand, the number of bubbles in the micro orifice can be calculated as $\mathrm{n} = \alpha/\frac{4}{3}\pi \mathrm{R}^3 \times \mathrm{V_{occ}}$ where α is the vapor volume fraction which is 1 at supercavitation and $\mathrm{V_{occ}}$ is the occupied volume by the vapor. The image processing of the pictures from the high speed camera shows that the diameter of the bubbles is $3.5\ \mu\mathrm{m}$. From the mentioned equations, the heat energy, which is released from the collapse of the cavitating bubbles occupying the micro orifice in the case working with water, is $1.053\mu\mathrm{J}$. The flowrate at supercavitation for water was measured as $719.49\ \mu\mathrm{L/s}$. As a result, the velocity of the working fluid at the micro orifice could be calculated as $67.57\mathrm{m/s}$. Therefore, the rate of the heat given to the end wall is $44.48\ \mu\mathrm{W}$.

The working fluid velocity in the case working with the nanofluid is $59.86\ \mathrm{m/s}$. With the same calculations, the generated heat on the end wall is $39.4\ \mu\mathrm{W}$. It is suggested that the cavitation system is coupled with a thermoelectric generator to harvest the generated heat energy to electricity. Considering a silicon dioxide wall as the thermoelectric generator, the rate of temperature rise on the bulk of the silicon dioxide could be calculated through $\dot{\mathrm{Q}} = \mathrm{mC}\frac{\mathrm{dT}}{\mathrm{dt}} = \rho.\mathrm{V}.\mathrm{C}.\frac{\mathrm{dT}}{\mathrm{dt}}$, where $\mathrm{m}\ [\mathrm{kg}]$ and $\mathrm{C}\ [\mathrm{j/Kg.K}]$ are the mass and specific heat capacity of silicon dioxide, respectively. m could be written as density multiplied by the volume of the silicon dioxide bulk. As a result, the rate of the temperature rise on a silicon dioxide plane with a nominal thickness of $500\ \mu\mathrm{m}$ with the area of $6.5 \times 5\ \mathrm{mm^2}$ would be $1.52 \times 10^{-3}\ \mathrm{K/s}$ and $1.35 \times 10^{-3}\ \mathrm{K/s}$ for water and nanofluid, respectively.

The μ-TEG, which is used in this design, consists of 127 pairs of micro pillars. The Seebeck coefficient of electroplated Bi_2Te_3 as the n-type material and Sb_2Te_3 as the p-type material are reported as $-63\,\mu V/K$ and $116\,\mu V/K$, respectively. The maximum power generation of the thermoelectric generators is calculated as $P_{max} = (S\Delta T)^2/4R$. Where S is the Seebeck coefficient and R is the resistance of the thermoelectric generator which is 13Ω in this study.

Figure 2 shows the power generation of the energy harvesting system working with water and nanofluid under super cavitation flow conditions.

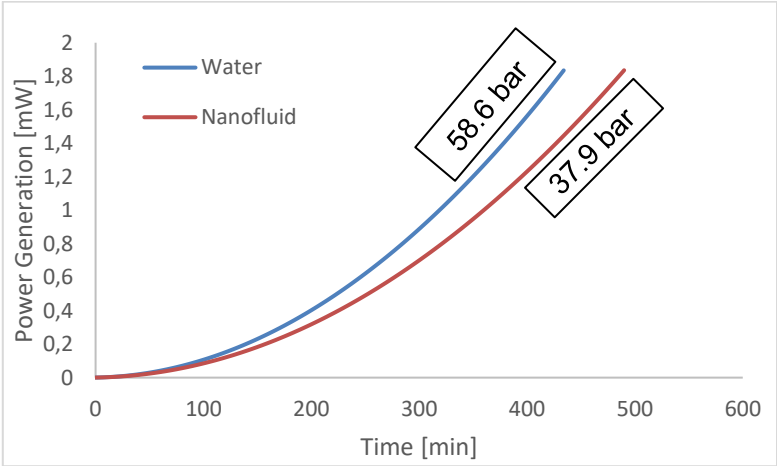

Figure 2 – The device performance working with water and nanofluid at supercavitation

The maximum power generation of the device is $3.96mW$. The power required to run most of the daily used miniature electrical devices are reported in our previous study [5]. The generated power by this system is in the range of the required power to run some electrical devices such as LEDs, antenna GPS, thermometers and other devices.

Summary/Conclusions

This study as the first part of an energy harvesting study shows the performance of a hydrodynamic cavitation system working with water and Titania-water nanofluid. The rate of the temperature rise on a silicon dioxide wall is estimated to show the feasibility of the energy harvesting system. The second part of the present study will show the performance of the thermoelectric coupled energy harvesting system.

References:

[1] S. Cases and I. T. Viewer, "Annual Energy Outlook 2019 Release date: January 24, 2019| Next release date: January 2020| full report."

[2] A. Šarc, T. Stepišnik-Perdih, M. Petkovšek, and M. J. U. s. Dular, "The issue of cavitation number value in studies of water treatment by hydrodynamic cavitation," vol. 34, pp. 51-59, 2017.

[3] B. Verhaagen and D. F. J. U. s. Rivas, "Measuring cavitation and its cleaning effect," vol. 29, pp. 619-628, 2016.
[4] M. Ghorbani et al., "Biomedical device prototype based on small scale hydrodynamic cavitation," vol. 8, no. 3, p. 035108, 2018.
[5] M. Ghorbani, A. Mohammadi, A. R. Motezakker, L. G. Villanueva, Y. Leblebici, and A. J. A. O. Kosar, "Energy Harvesting in Microscale with Cavitating Flows," vol. 2, no. 10, pp. 6870-6877, 2017.
[6] R. Pecha and B. J. P. r. l. Gompf, "Microimplosions: cavitation collapse and shock wave emission on a nanosecond time scale," vol. 84, no. 6, p. 1328, 2000.

SESSION 8
Industrial Applications

S8

1st International Conference on Nanofluids (ICNf2019)
2nd European Symposium on Nanofluids (ESNf2019)
26-28 June 2019, Castelló, Spain

Development of Composite Materials Based on the Interaction between Nanoparticles and Surfactants for Application on Chemical Enhanced Oil Recovery

Stefania Betancur[1,2,*], Francisco Carrasco-Marín[2], Camilo A. Franco[1] and Farid B. Cortés[1]

[1]Grupo de Investigación en Fenómenos de Superficie – Michael Polanyi, Facultad de Minas, Universidad Nacional de Colombia Sede Medellín, Kra 80 No. 65-223, Medellín, Colombia.

[2]Grupo de Investigación en Materiales de Carbón, Departamento de Química Inorgánica, Facultad de Ciencias, Universidad de Granada, 18071, Granada, Spain.

[*]Corresponding author: sbetancurm@unal.edu.co.

Keywords: Surfactant, Nanoparticles, Adsorption, Chemical Enhanced Oil Recovery (CEOR).

Abstract: The main objective of this work is to develop a nanofluid based on the adsorption/desorption process of ionic and nonionic surfactant onto nanoparticles and its application in enhancing process of oil recovery. The adsorption/desorption isotherms for determining the ability of nanoparticles to adsorb surfactants were carried out at 25 °C using batch-mode experiments. The surfactants used for the experiments were Cetyltrimethylammonium Bromide “CTAB” (cationic), Sodium Dodecyl Sulphate “SDS” (anionic) and Polyoxyethylenesorbitan Monolaurate “Tween 20” (nonionic). The amount adsorbed of surfactant onto nanoparticles decreased in the following order: CTAB > Tween 20 > SDS. Meanwhile, the desorption percentages obtained were below 2, 5.3 and 9.1% for CTAB, Tween 20 and SDS, respectively. From the adsorption/desorption isotherms, a composite nanomaterial for enhancing oil recovery was obtained and was evaluated through displacement tests using a micromodel. The composed material based on nanoparticles-surfactant increased the oil recovery up to 240% regarding surfactant flooding.

Introduction: In the production history of a reservoir, various stages of recovery are identified, namely: primary, secondary and tertiary stage. Among tertiary stage, surfactant flooding is applied to recover the residual oil of the reservoir by means of reduction of interfacial tension between water and crude oil. However, the efficiency of the surfactant flooding is affected mainly by the adsorption of the chemical in the porous medium. Hence, several researchers have studied the effect of the simultaneous application of nanoparticles and surfactants on enhanced oil recovery. For the

experiments, the researchers used different types of surfactants as SDS [1-3] and CTAB and different type of nanoparticles [1-4]. Based on results the authors concluded that the simultaneous use of surfactants and nanoparticles achieved to reduce the adsorption onto the rock up to 13.6% [1] and an oil recovery up to 51% [5]. These applications have been achieved mainly through nanoparticle-surfactant mixtures without considering the interaction between both components for the nanofluid design. The interaction between surfactant-nanoparticle based on the adsorption phenomena could be an essential factor for avoiding the synthesis process of a complex nanomaterial. Therefore, the main objective of this study is to evaluate the adsorption/desorption process of ionic and nonionic surfactants onto nanoparticles for the development of a nanofluid based on a composed material of nanoparticles-surfactant as an alternative chemical enhanced oil recovery (CEOR) method.

Materials and Methods: A cationic surfactant, cetyltrimethylammonium bromide (CTAB; 98%, PanReac, Spain), an anionic surfactant, sodium dodecyl sulfate (SDS; 85%, PanReac, Spain), and a nonionic surfactant, polyoxyethylene sorbitan monolaurate (Tween 20; ≥40%, Sigma-Aldrich, USA), were used for sorption experiments. Silica (SiO_2) nanoparticles were purchased from Sigma-Aldrich (USA). Light crude oil with 33.2 °API was used for the experiments. Ottawa sand (Minercol S.A., Colombia) of 50/60 sieve was used for the displacement tests in a micromodel.

For the adsorption isotherms, the surfactant is added to the brine with 10000 $mg \cdot L^{-1}$ of NaCl at concentrations between 100 and 8000 $mg \cdot L^{-1}$. The solutions are stirred for 2 h and left to stand for 24 h. Then, nanoparticles are added at a dosage of 10 $g \cdot L^{-1}$. The solutions are stirred and left to stand for 24 h. In desorption experiments, the nanoparticles with surfactant adsorbed obtained from the adsorption isotherms were added to brine with 10000 $mg \cdot L^{-1}$ of NaCl at a dosage of 10 $g \cdot L^{-1}$. Then, the solution was stirred for 2 h and left to stand for 24 h. An aliquot of each solution was taken from the supernatant to determine the percentages of desorption. Each measurement was performed in triplicate.

The micromodel was used to evaluate the performance of a surfactant solution and the designed nanofluid for enhancing oil recovery. The displacement tests were performed in a radial flow cell, packed with 50/60 sieve Ottawa sand at 25 °C. The injecting well and packed Ottawa sand, and injection pump (Eldex, USA), stainless steel displacement cylinders, and a pressure sensor were used for the experiments. The surfactant solution was prepared at a concentration of 100 $mg \cdot L^{-1}$ in a brine with 10000 $mg \cdot L^{-1}$ of NaCl. The nanoparticles dosage was 10 $mg \cdot L^{-1}$.

Discussion and Results: Figure 1 shows the adsorption isotherms for CTAB, Tween 20 and SDS onto SiO_2 nanoparticles at 25 °C. It is observed that CTAB and Tween 20 showed Type III isotherms and SDS presented Type I (a) isotherm, according to the International Union of Pure and Applied Chemistry (IUPAC) classification scheme [6]. Figure 1 shows the amount adsorbed of surfactant decreased in the order: CTAB > Tween 20 > SDS. In the experimental conditions, SiO_2 nanoparticles are negatively charged and therefore the negative charges of SiO_2 nanoparticles and the dodecyl sulfate anion of SDS results in an electrostatic repulsive interaction. These repulsive interactions difficult the adsorption of the surfactant molecules or micelles on the surface of the nanoparticles. Meanwhile, Tween 20 is adsorbed in multilayers on nanoparticles surface. The negative charges of SiO_2 nanoparticles could interact with the positive charges of hydroxyl functional groups of Tween 20 through dipole-dipole interactions. In this case, there are not repulsive electrostatic forces that difficult the adsorption of surfactant on nanoparticles, resulting in a higher adsorbed amount for Tween 20 than SDS. Finally, the adsorption of CTAB onto nanoparticles is mainly due to net electrostatic forces of CTAB cation with the silanol functional groups of SiO_2. The CTAB cations are attracted to SiO_2 surface in multilayer, and it is obtained, therefore, a higher adsorption capacity.

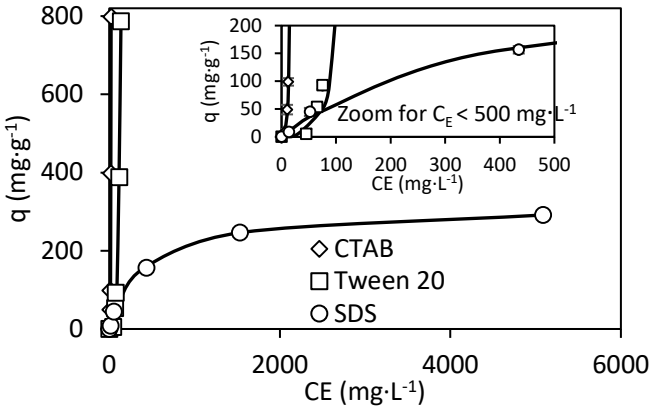

Figure 1. Adsorption isotherms for CTAB, Tween 20 and SDS onto SiO_2 nanoparticles at 25 °C.

The percentages of desorption for CTAB, Tween 20 and SDS, respectively, from SiO_2 nanoparticles at 25 °C were determined. CTAB presented percentages of desorption below 1.6% and 0.71% at 25 and 70 °C, respectively. These results indicate that the interactions of CTAB and nanoparticles surface are strong enough to prevent desorption of the surfactant. Meanwhile, it is observed the percentages of desorption of Tween 20 from SiO_2 nanoparticles are higher than obtained with CTAB. In this case, the

percentages of desorption were below 5.3%. However, SDS reached the percentages of desorption close to 90%.

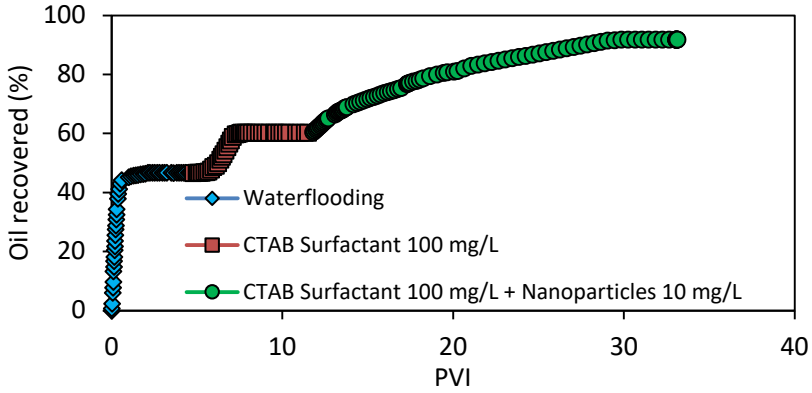

Figure 2. Oil recovered in a quarter five-spot pattern micromodel for waterflooding, followed by CTAB surfactant flooding at 100 mg·L^{-1} in absence and presence of SiO_2 nanoparticles at 10 mg·L^{-1} for a fixed temperature of 25 °C.

Displacement tests in a quarter five-spot pattern micromodel were performed for evaluating a nanofluid based on CTAB surfactant and SiO_2 nanoparticles interaction. The nanoparticles dosage for displacement tests was fixed at 10 mg·L^{-1}. Likewise, CTAB surfactant concentrations of 100 mg·L^{-1} was selected for the displacement tests. The displacement test was conducted in three steps: waterflooding emulating a secondary recovery, surfactant flooding, and nanoparticles-surfactant flooding. For all displacements tests, the fluid was injected until the oil production becomes zero. As observed in Figure 2, the oil recovered obtained with waterflooding was close to 47%. It is observed that surfactant flooding with 100 mg·L^{-1} of CTAB reached an oil recovery of 60% and increased to 92% when 100 mg·L^{-1} of CTAB surfactant and 10 mg·L^{-1} of nanoparticles were injected. This increase in the oil recovery represents about 240% more than that obtained with the injection of 100 mg·L^{-1} of CTAB in the absence of nanoparticles. The increase in oil recovery could be due to joint action of free surfactant and nanoparticles with adsorbed surfactant in their surface. In addition, the low concentration of composed material based on nanoparticles-surfactant used to obtain the nanofluid corroborates that this material can be cost-effective for an industrial application.

Conclusions: Adsorption isotherms were successfully constructed to evaluate the interactions between ionic and nonionic surfactants onto SiO_2 nanoparticles. CTAB showed the highest adsorptive capacity and the highest affinity adsorbate-adsorbent among the surfactants. Meanwhile, SDS presented the lowest adsorbed amount. This behavior can be related mainly due to the silanol functional groups of SiO_2 nanoparticles

presents attractive net electrostatic interactions with the cetyltrimethylammonium cation of CTAB, which can be stronger than the interactions of dipole-dipole showed by Tween 20 and the repulsive charges that are generated between SDS and SiO_2 nanoparticles. CTAB showed percentages of desorption from the nanoparticles surface below 1.6% at 25 °C and values below of 0.71% at 70 °C. The percentages of desorption of Tween 20 were lower than 5.3%. In contrast, SDS desorbed about 90%, which indicates that CTAB and Tween 20 adsorption is an irreversible process while SDS showed a reversible adsorption process. Thus, CTAB is the surfactant with the highest adsorbed amount and the lowest percentage of desorption, which could be a better alternative for nanoparticles- surfactant flooding for CEOR. On the other hand, the nanoparticles-surfactant flooding increased the oil recovery up to 240% regarding surfactant flooding. From this research, was obtained a new and alternative chemical composed material based on adsorption of surfactant onto nanoparticles surface for CEOR applications. In this way, a synthesis of a complex material that requires more costs and equipment can be avoided.

References:

1. M. A. Bagrezaie and P. Pourafshary, Improvement of Surfactant Flooding Performance by Application of Nanoparticles in Sandstone Reservoirs, Journal of the Japan Petroleum Institute 58 (2015) 97-102.

2. Y. Wu, W. Chen, C. Dai, Y. Huang, H. Li and M. Zhao, Reducing surfactant adsorption on rock by silica nanoparticles for enhanced oil recovery, Journal of Petroleum Science and Engineering 153 (2017) 283-287.

3. G. Cheraghian, S. Kiani, N. N. Nassar, S. Alexander, and A. R. Barron, Silica Nanoparticle Enhancement in the Efficiency of Surfactant Flooding of Heavy Oil in a Glass Micromodel, Industrial & Engineering Chemistry Research 56 (2017) 8528-8534.

4. M. Mohajeri, M. Hemmati, and A. S. Shekarabi, An experimental study on using a nanosurfactant in an EOR process of heavy oil in a fractured micromodel, Journal of Petroleum Science and Engineering 126 (2015) 162-173.

5. B. Suleimanov, F. Ismailov, and E. Veliyev, Nanofluid for enhanced oil recovery, Journal of Petroleum Science and Engineering 78 (2011) 431-437.

6. M. Thommes, K. Kaneko, A. V. Neimark, J. P. Olivier, F. Rodriguez-Reinoso and J. Rouquerol, Physisorption of gases, with special reference to the evaluation of surface area and pore size distribution (IUPAC Technical Report), Pure and Applied Chemistry 87 (2015) 1051-1069.

1st International Conference on Nanofluids (ICNf2019)
2nd European Symposium on Nanofluids (ESNf2019)
26-28 June 2019, Castelló, Spain

Magnetic Iron Core-Carbon Shell Nanoparticles for Ultra Low Interfacial Tension in Enhanced Oil Recovery

Stefania Betancur[1,2,*], Francisco Carrasco-Marín[2], Camilo A. Franco[1] and Farid B. Cortés[1]

[1]Grupo de Investigación en Fenómenos de Superficie – Michael Polanyi, Facultad de Minas, Universidad Nacional de Colombia Sede Medellín, Kra 80 No. 65-223, Medellín, Colombia.

[2]Grupo de Investigación en Materiales de Carbón, Departamento de Química Inorgánica, Facultad de Ciencias, Universidad de Granada, 18071, Granada, Spain.

[*]Corresponding author: sbetancurm@unal.edu.co

Keywords: Surfactant, Nanoparticle, Interfacial Tension, Enhanced Oil Recovery.

Abstract: The surfactant flooding is a commonly enhanced oil recovery (EOR) process to reduce the interfacial tension (IFT) between water and crude oil. However, the efficiency of surfactant flooding is affected IFT water/crude oil is not reduced enough to have an effect on trapped oil. As a result, the simultaneous use of surfactant and nanoparticles is presented as a promising alternative to improve the chemical flooding in EOR processes. Further, the main objective of this work is to synthesize, characterize and evaluate magnetic iron core-carbon shell nanoparticles for the reduction of IFT between a brine and crude oil and its effect in oil recovery. The magnetic iron core-carbon shell nanoparticles were obtained following a one-pot hydrothermal procedure. The core-shell nanoparticles were characterized by scanning electron microscopy (SEM), Dynamic light scattering (DLS), X-ray diffraction (XRD), X-ray photoelectron spectroscopy (XPS) and magnetometry measurements. On the other hand, to evaluate the simultaneous effect of core-shell nanoparticles and surfactant a displacement test to reservoir conditions was performed. The simultaneous use of nanoparticles and surfactant reached to decrease the IFT approximately to 10^{-4} mN/m. In addition, when core-shell nanoparticles and surfactant were simultaneously used in the injection fluid, increased the oil recovery up to 143% regarding the waterflooding process.

Introduction/Background: The surfactant flooding is a process applied to recover the residual oil after the waterflooding [1]. For a successful displacement process, the injected surfactant must achieve ultralow IFT to mobilize the residual oil. However, there were a numerous number of surfactant flooding that were ineffective, due to the IFT is not low enough to recover the trapped oil [2]. Hence, the use of nanoparticles as an alternative method of EOR has been studied by numerous researchers worldwide [1, 3-

6]. Most researchers focused on their work in the use of silica gel nanoparticles for EOR applications. However, there are different novel nanomaterials that involve two or more functionalities that give them unique properties as compared to their individual single-component materials. Magnetic core-shell nanostructured materials have recently great attention of researchers in the oil and gas area. The core determines the magnetic or electrical characteristic, while the shell determines the binding affinity for a specific target. This situation allows the synthesis and design of nanoparticles with desired properties. This study aims to synthesize, characterize and evaluate magnetic iron core-carbon shell nanoparticles applied to the reduction of IFT crude oil/water and improvement of oil recovery.

Discussion and Results: The particle size of the magnetic iron core-carbon shell nanoparticles was determined through SEM and DLS measurements, which corresponded to 60 nm. The peaks in the XRD pattern matched with the standard cubic Fe (0) structure data [7], which indicates the existence of Fe (0) in the core of nanoparticles. According to the results of the XPS spectrum, the Fe (0) of the core was adequately coating with a carbon shell. Similarly, the saturated magnetization are in agreement with the values reported in the literature for Fe (0) [8]. Figure 1 shows the interfacial tension values obtained for different nanoparticles concentration between 0 and 1000 mg L^{-1} at 25 °C. The aqueous phase was the synthetic brine and contains the surfactant mixture at a fixed concentration of 2000 mg L^{-1}. As observed in Figure 1, the dotted line represents the IFT of the surfactant mixture corresponding to 1×10^{-3} mN m^{-1}. It is observed, only the nanoparticles-surfactant solution with 100 mg L^{-1} of nanoparticles concentration achieves to reduce the IFT to 1×10^{-4} mN m^{-1}, a lower IFT value than obtained with the surfactant mixture solution. The reduction in IFT values can be due to the synergy between the free surfactant present in the bulk and the nanoparticles with adsorbed surfactant onto their surface.

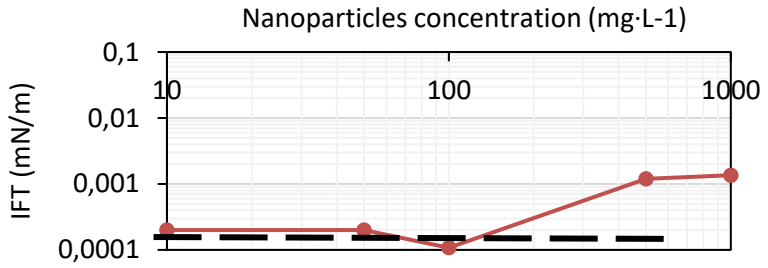

Figure 1. Interfacial tension of crude oil/synthetic brine in presence of magnetic iron core-carbon shell nanoparticles at concentrations between 10 and 1000 mg L-1 and at a fixed temperature of 25 °C.

Oil recovery curves for surfactant flooding and nanoparticles-surfactant flooding are presented in Figure 2. Each displacement test was conducted in different steps. The first displacement test included waterflooding, surfactant flooding, water drive, and a final surfactant flooding. The second displacement test comprised waterflooding, nanoparticles-surfactant flooding, water drive, and a final nanoparticles-surfactant flooding. As observed, in both cases, the oil recovered with waterflooding was approximately 66%. Similarly, the surfactant flooding in the first displacement test and the nanoparticles-surfactant flooding in the second displacement reached to increase the oil recovery close to 67%. The nanoparticles-surfactant flooding with 2000 mg L^{-1} of surfactant mixture and 100 mg L^{-1} of nanoparticles reached an oil recovery of approximately 95%. According to the results of displacement tests, the effect of magnetic iron core-carbon shell nanoparticles in the increase of oil recovery can be associated with the reduction in IFT between crude oil and aqueous phase generated by the weakening of the interactions between the molecules present in the interface.

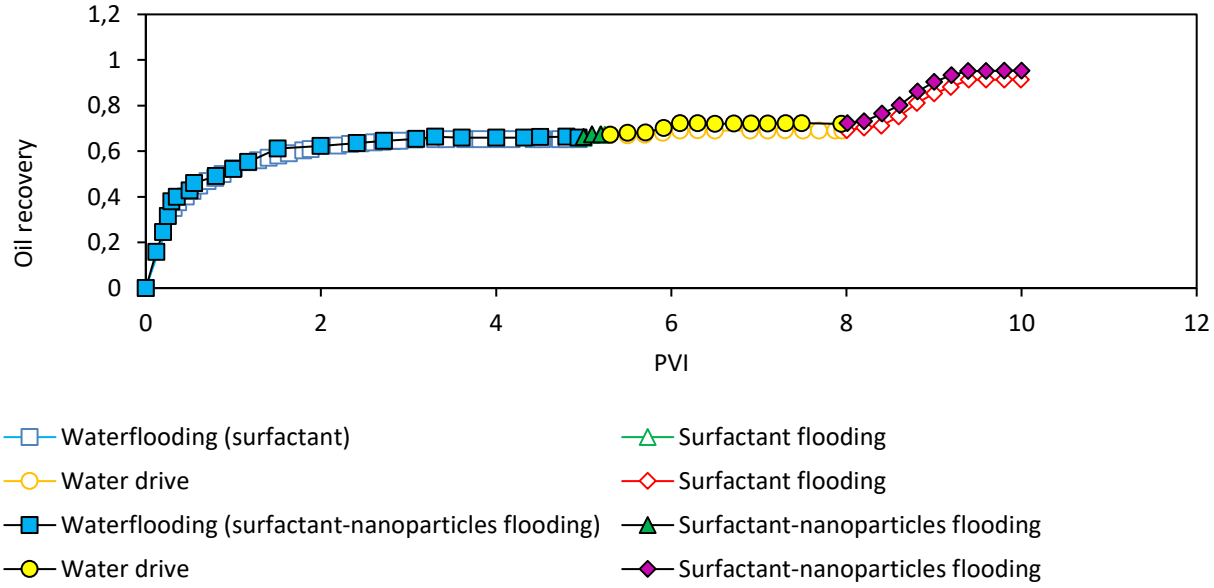

Figure 2. Oil recovery curves for the surfactant flooding and the nanoparticles-surfactant flooding.

Conclusions: Magnetic iron core-carbon shell nanoparticles were synthesized by one-pot hydrothermal procedure with a mean particle size of 60 nm and Fe (0) in the core of nanoparticles. XPS spectrum corroborated Fe in metallic state of the core was adequately coating with carbon shell. The nanoparticles-surfactant solution with 100 mg L^{-1} of nanoparticles concentration achieved to reduce the IFT to 1×10^{-4} mN m^{-1}, a lower IFT value than obtained with the surfactant mixture solution. This behavior can be related to the

synergy between the free surfactant and the nanoparticles with adsorbed surfactant onto their surface. The nanoparticles-surfactant flooding increased the oil recovery of about 143% more than obtained with waterflooding. The magnetic iron core-carbon shell nanoparticles synthesized and evaluated in this research represents a novel nanomaterial that takes advantage of the magnetism of Fe in metallic state and the high availability of the carbon for obtaining ultra-low IFT and increase oil recovery.

References:

1. G. Cheraghian and L. Hendraningrat, A review on applications of nanotechnology in the enhanced oil recovery part A: effects of nanoparticles on interfacial tension, International Nano Letters 6 (2016) 129-138.
2. S. Thomas, Enhanced oil recovery-an overview, Oil & Gas Science and Technology-Revue de l'IFP 63 (2008) 9-19.
3. A. Roustaei, S. Saffarzadeh, and M. Mohammadi, An evaluation of modified silica nanoparticles' efficiency in enhancing oil recovery of light and intermediate oil reservoirs, Egyptian Journal of Petroleum 22 (2013) 427-433.
4. T. F. Moghadam, S. Azizian, and S. Wettig, Synergistic behaviour of ZnO nanoparticles and gemini surfactants on the dynamic and equilibrium oil/water interfacial tension, Physical Chemistry Chemical Physics 17 (2015) 7122-7129.
5. M. Zargartalebi, R. Kharrat, and N. Barati, Enhancement of surfactant flooding performance by the use of silica nanoparticles, Fuel 143 (2015) 21-27.
6. M. Zargartalebi, N. Barati, and R. Kharrat, Influences of hydrophilic and hydrophobic silica nanoparticles on anionic surfactant properties: Interfacial and adsorption behaviors, Journal of Petroleum Science and Engineering 119 (2014) 36-43.
7. A. Mahto, A. Kumar, J. P. Chaudhary, M. Bhatt, A. K. Sharma, P. Paul, et al., Solvent-free production of nano-FeS anchored graphene from Ulva fasciata: A scalable synthesis of super-adsorbent for lead, chromium and dyes, Journal of hazardous materials 353 (2018) 190-203.
8. D. L. Huber, Synthesis, properties, and applications of iron nanoparticles, Small 1 (2005) 482-501.

1st International Conference on Nanofluids (ICNf2019)
2nd European Symposium on Nanofluids (ESNf2019)
26-28 June 2019, Castelló, Spain

Determination of the Magnetic Force Acting on Magnetic Nanofluids for MEMS Applications

S.Doganay[1*], L. Cetin[2] and A. Turgut[3]

[1]Department of Mechatronics Engineering, The Graduate School of Natural and Applied Sciences, Dokuz Eylül University, Buca, İzmir, Turkey.

[2]Department of Mechatronics Engineering, İzmir Kâtip Çelebi University, Çiğli, İzmir, Turkey.

[3]Department of Mechanical Engineering, Dokuz Eylül University, Buca, İzmir, Turkey.

[*]Corresponding author: serkan.doganay@outlook.com

Keywords: MEMS, magnetic nanofluid, microfluidic, magnetic force.

Abstract: The goal of this study is to determine the force acting on magnetic nanofluids with different particle concentrations in a micro sized channel for MEMS applications. In order to determine the magnetic force on magnetic nanofluids, in the first part magnetic properties of the nanofluid samples were determined. Secondly, the magnetic field generated by permanent magnets on the microchannel were analysed. According to the findings the magnetic force was calculated. The results indicated that the magnetic force acting on magnetic nanofluids increases while particle concentration increases.

Introduction/Background: Magnetic nanofluids are colloids which comprise of magnetic nanoparticles and a carrier liquid such as water, oil, ethylene glycol etc. Generally, the nano-sized ferromagnetic particles are maghemite (γ–Fe_2O_3), magnetite (Fe_3O_4) or cobalt-ferrite ($CoFe_2O_4$) etc. They have many potential application area such as electrical, mechanical and optical systems [1]. Magnetic nanofluids can be actuated under the influence of the external magnetic field. Moreover, their thermophysical properties can be tuned with varying magnetic field [2,3]. These make them attractive for micro-electromechanical systems (MEMS) such as micro sized heat sinks, micro operations, pumping and mixing [4]. The demand on micro sized mechanical and electronic systems contributes the expeditious development of the MEMS. Employing magnetic particles in MEMS is advantageous, since they provide distance free manipulation [5]. One of the most common particles in the MEMS application is superparamagnetic iron oxide nanoparticles (SPIONs).

In this study, the magnetic properties of Fe_3O_4-water magnetic nanofluids with different particle concentrations were measured. Then, magnetic flux density on a microchannel was modelled and analysed. Combining both results, the magnetic force acting on magnetic nanofluids in the microchannel was determined for different particle concentrations.

Discussion and Results: The Fe_3O_4-water magnetic nanofluid with 4.8 % vol. concentration was supplied commercially from US Research Nanomaterials Inc. Then, it was diluted to four different volumetric particle concentrations of 1, 2, 3, 4%. In order to investigate magnetic behaviour of the samples, a vibrating sample magnetometer (VSM) was used. VSM device was invented and reported by Simon Foner in 1955 that measures magnetic properties [6]. In this method, the sample is first magnetized in a uniform magnetic field. Then, it is sinusoidally vibrated, through the use of a piezoelectric material. The induced voltage in the pickup coil is proportional to the sample's magnetic moment.

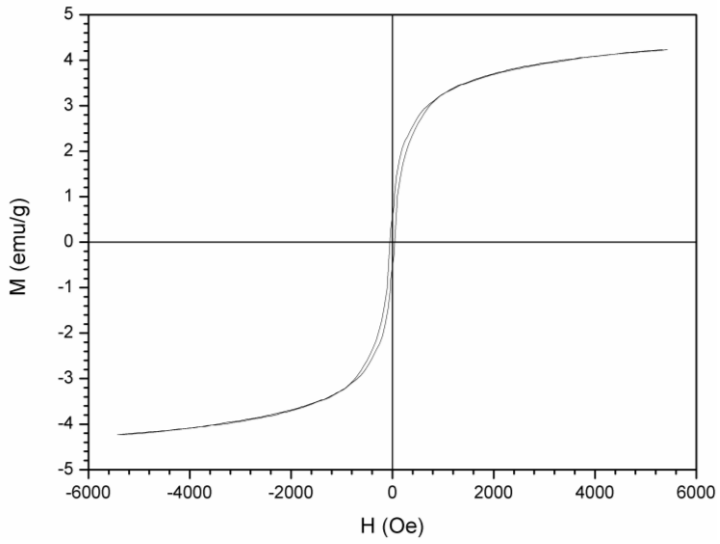

Figure 1. Magnetization behavior of the Fe_3O_4-water magnetic nanofluid with 4.8% vol. concentration

The magnetization curve for the 4.8% vol. concentrated sample is demonstrated in Figure 1. It can be seen the magnetic nanofluid sample reveals a superparamagnetic behaviour. There is almost no remenance when the magnetic field switched off. This behaviour was also observed for other samples with different particle concentrations.

Figure 2 shows the design of semi-circle shaped microchannel and magnetic actuator geometry. The cylindrical permanent magnet couple was mounted on a link which rotates

around the centre of the microchannel. The angle between magnets are kept constant as 45˚.

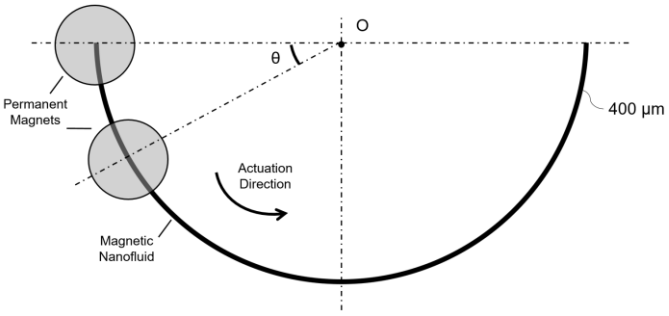

Figure 2. Schematic of the design.

Magnetic force acting on magnetic nanofluid can be expressed with Eq. 1 [7]:

$$F_m = \frac{V\chi}{\mu_o}(B.\nabla)B \tag{1}$$

where V is the volume, χ is the volume magnetic susceptibility, μ_o is the vacuum permeability and B is the magnetic flux density.

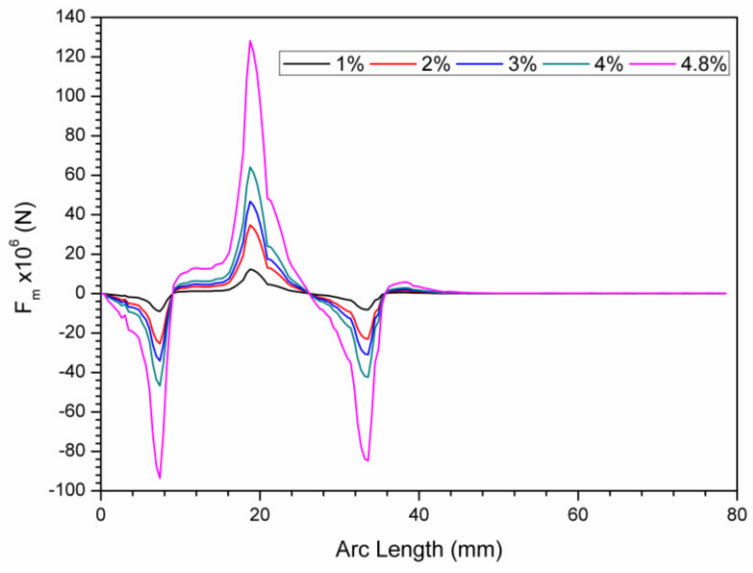

Figure 3. Tangential component of the magnetic force acting on different concentrated magnetic nanofluids for unit volume.

The volume magnetic susceptibility can be calculated from the H-M magnetization curve. It is the slope of the linear part. The driven force for the magnetic

nanofluid will be tangential component, due to the channel geometry. Therefore, tangential force for unit volume was calculated for all samples and shown in Figure 3. It is observed that the magnetic force acting on the magnetic nanofluid samples is higher for higher concentrated samples.

Summary/Conclusions: In this study, the magnetic force acting on Fe_3O_4 magnetic nanofluids with different particle concentrations were calculated. Conclusions below can be drawn:

- Magnetic nanofluids have the potential to be used in MEMS applications.
- They can be actuated by external magnetic field, this provides a distance free operations in small scales.
- All samples indicated superparamagnetic behaviour which means there is no remanence after the magnetic field removed.
- The magnetic force varies according to the particle concentration and it increases with increasing particle concentration.

References:

1. Felicia, L. J., Vinod, S. and Philip, J., Recent advances in magnetorheology of ferrofluids (magnetic nanofluids)—a critical review. *Journal of Nanofluids*, 5 (2016) 1-22.
2. Philip, J., Shima, P. D. and Raj, B., Nanofluid with tunable thermal properties. *Applied physics letters*, 92 (2008) 043108.
3. Doganay, S., Turgut, A. and Cetin, L., Magnetic field dependent thermal conductivity measurements of magnetic nanofluids by 3ω method. *Journal of Magnetism and Magnetic Materials* 474 (2019) 199-206.
4. Pal, S., Datta, A., Sen, S., Mukhopdhyay, A., Bandopadhyay, K. and Ganguly, R., Characterization of a ferrofluid-based thermomagnetic pump for microfluidic applications. *Journal of Magnetism and Magnetic Materials*, 323 (2011), 2701-2709.
5. Ganguly, R. and Puri, I. K., Microfluidic transport in magnetic MEMS and bioMEMS. Wiley Interdisciplinary Reviews: *Nanomedicine and Nanobiotechnology*, 2 (2010) 382-399.
6. Foner, S., Versatile and sensitive vibrating-sample magnetometer. *Review of Scientific Instruments*, 30 (1959), 548-557.
7. Nguyen, N. T. (2012). Micro-magnetofluidics: interactions between magnetism and fluid flow on the microscale. *Microfluids and Nanofluidics*, 12, 1-16.

1st International Conference on Nanofluids (ICNf2019)
2nd European Symposium on Nanofluids (ESNf2019)
26-28 June 2019, Castelló, Spain

Tribological assessment of nanoadditives for next generation of lubricants

I. Elexpe[1*], M. Hernaiz[1], G. Mendoza[1], V. Alonso[1], X. Fernandez[1], L. Muntada[2], E. Ortega[2]

[1]Tekniker. C/Iñaki Geonaga,5 Eibar. Basque Country. Spain
[2]Brugarolas, Camino de la Riera, 36-44. Barcelona. Spain
[*]iker.elexpe@tekniker.es

Keywords: Nanolubricant, Nanoparticle, tribological properties, EP properties

Abstract: The concept of additives for gear lubrication has gained importance in recent years, and nano-additives based on nanoparticles of different nature and geometries are being analysed with great interest by the scientific community and the business sector due to the potential, of this new generation of additives, related with energy efficiency and material protection. This research evaluates the effect of different nanoparticles, nature and geometry, used in the formulation of PAO based nanolubricant. Properties such us chemical compatibility, and tribological properties have been evaluated. Results showed that thanks to the developed dispersion methodology, including the use of a specific cost-effective surfactant, an appreciable dispersion capability and stability was achieved in de developed nanolubricant, resulting in an improvement in extreme pressure properties.

Introduction: In lubricants market there is a continuous tendency to minimize the machines components size, in order to reduce the weight, improve the energetic efficiency and reduce fuel consumption. This evolution has forced the lubricants to work at higher pressure contacts, displacing the lubrication regimen from hydrodynamic to mix or limit lubrication.

The hydrocarbon mixes derived from petroleum or the lubricants based on synthetic lubricants do not achieve all the requirements that lubricants used in nowadays applications should fulfil. A widely accepted solution is the addition of a relatively small amount of additive compounds that significantly improve the performance of the base oil in terms of oxidative degradation and tribological behaviour, among others [1]. However, conventional additives incorporating chemicals such as MoS2, cadmium chloride, sulphides and phosphides are not enough to cover new lubricants demands, hence the need to develop alternative lubricants to those that exist to date [2].

Nanolubricants are a new type of lubricants made from nanostructures, dispersants and oil, able to improve lubrication properties. The anti-wear, anti-friction and extreme

pressure properties of nano-lubricants containing different nanoparticles (NPs) such as fullerenes, titanium dioxide (TiO2), copper oxides (CuxO), nano-diamonds (ND) and graphite, have been analysed by several researchers [3-8]. One of the most fascinating materials for tribology is graphene, widely used as a solid lubricant in mechanical devices. Its lamellar structure and weak bonds between atomic layers facilitate shearing between layers of the structure, resulting in low friction [9]. Several studies have shown that including a minimum quantity of graphene flakes it is possible to generate a significant reduction in the friction and wear of steel. Z. Jia et al. [10] carried out tribological tests on chemically modified graphene flakes found that a 0.075wt% can provide a better load capacity than a base oil. [11].

Nanolubricants formulation: Working with nanomaterials, the main challenge is to obtain a stable dispersion with the minimum cluster size, and there are several technologies available to stabilize the NMs in the matrix. In this work the technology used to stabilize the NMs in oil, is through dispersing agents, these chemicals modify the electrostatic and steric forces between the NMs, and forces between the NMs and the oil, and as a result the wettability is improved and therefore the stability of the system is promoted. NMs dispersion process has been assisted by ultrasonication (UPI 1000 HDT230 Hielscher), with this process an energy density is applied to the system that allows to reduce the NM cluster size up to nanometric range.

A) Selected Nanomaterials properties: Proposed nanomaterials (NM) for this study are two commercial nanoparticles; Ti02 spherical NP (primary size 48nm and BET 5-50m^2/g) and graphene with laminar based structure (2D) (GP500 multilayer structure up to 40layers, lateral size 40-300nm, BET 500 m^2/g), supplied by Alfarben and Graphenetech, respectively. Tribological properties of spherical NM are based on rolling effect while multilayer structure-based NM present a tribological effect based on surface exfoliation. The proposed lubricant used to formulate the nanodispression is a Polyalphaolefin (PAO) based oil, provided by Brugarolas, for gears applications

B) Experimental: The experimental protocol developed to optimize the dispersion route consist on: with a fixed NM concentration the dispersibility of different surfactants was initially evaluated based on miscibility and wettability criteria, after this first screening, surfactant nature and concentration was evaluated measuring particle cluster sized by Laser diffraction (Mastersizer) in the case of spherical NP, and the required surfactant quantity for complete NM wetting in the case of graphene. As graphene is a laminar NM (2D nanomaterial) DLS technique does not

provide reliable size data (DLS is a reliable technique for spherical NP and not for laminar with high aspect ratio NM). The criteria used to select the optimal surfactant concentration working with spherical NP is that concentration that promotes the lower cluster size. Once this parameter is optimized the effect of sonication time is studied, by varying this parameter, it is possible to reduce nanoparticles cluster size. Figure 1 show both effect for TiO2 spherical NP

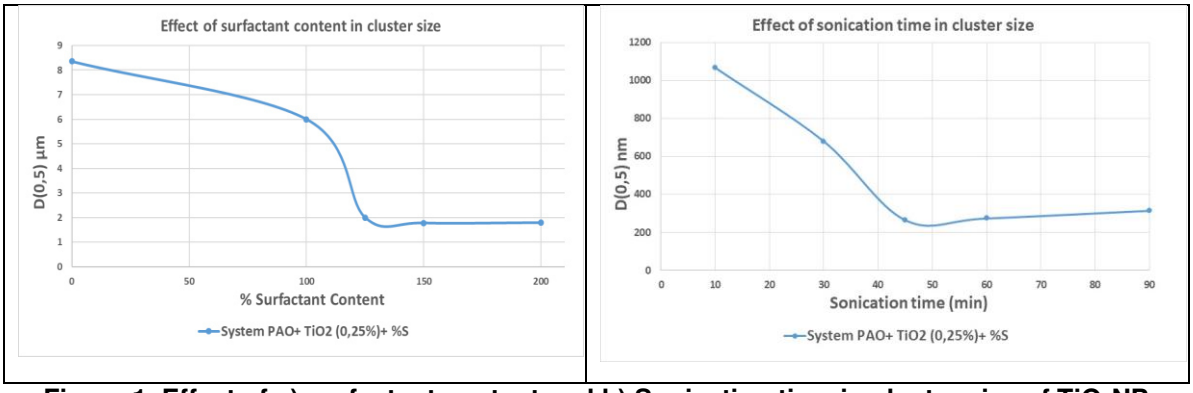

Figure 1. Effect of a) surfactant content and b) Sonication time in cluster size of TiO_2NP

Nanolubricants characterization: The determination of the optimal NM nature, and concentration, has been made by means of the tribological characterisation. A critical property in lubricants linked to dispersion stability is that the tribological effect must be maintained over time, it must be born in mind that a lubricant can be stored for a considerable time until it is shipped to installation, so it is necessary to ensure that the tribological properties are maintained over time, and therefore the NMs are kept dispersed in the oil in an optimal way.

The “ball on disc” test configuration has been selected to study friction, wear and extreme pressure properties of the reference PAO oils and the new developed nanofluids. The tribological system is a point to area contact under reciprocating movement. 2 types of tests have been performed

- Friction and wear tests (ASTM D6425). By means of these tests the ability to avoid wear mechanisms and maintain stable friction is evaluated.
- EP (Extreme Pressure) tests (ASTM D 7421). These tests are thought to evaluate the behaviour of the lubricants under high unitary loads. In this test the welding load is obtained.

Tribological Results: Working with optimized nanolubricants based on TiO2 nanoparticles, the effect of NP content on tribological properties are evaluated.

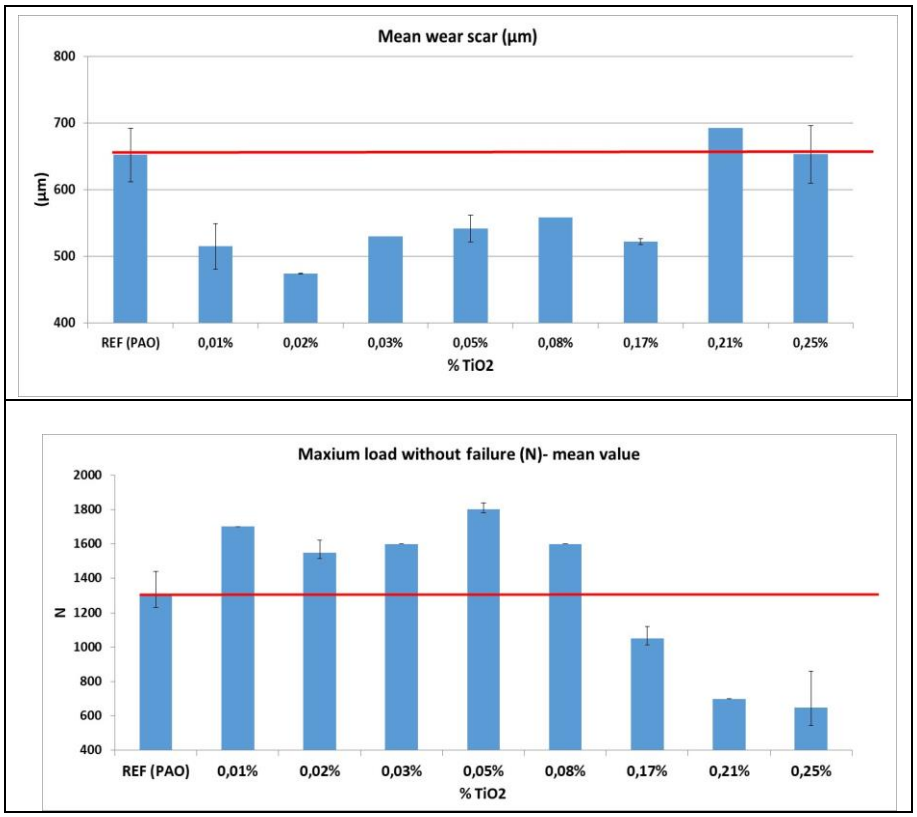

Figure 2. (a)Mean ball wear scars and (b) Seizure load obtained with the PAO oil additivated with different TiO2 concentrations

In this case attending to mean wear scar (Figure 2a) and EP properties (Figure 2b) the positive effects are found for a TiO2 concentration up to 0.21%. There seems to be an effective NP concentration, and an excess of additive promotes the formation of conglomerates at the friction interfaces, resulting in a poorer lubrication efficiency. [12] In this case the most promising results is found for a TiO2 concentration of 0.05%.

The effect on graphene at the same effective concentration (0.05%) was also evaluated from tribological point of view. Figure 3, shows how both NMs promote a positive effect compared with reference oil, using a low NM concentration.

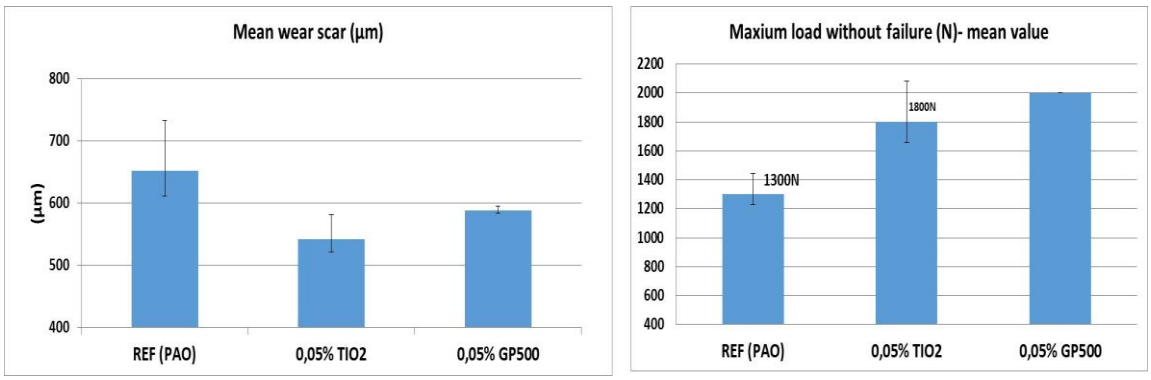

Figure 3. Mean wear scar and seizure load of the PAO and the PAO with proposed NM´s

Table 1 summarizes the tribological improvements achieved when adding both TiO2 NPs and graphene on the reference PAO oil.

Table 1. Improvement on tribological properties (%)

Nanomaterials	Wear scar improvement	Seizure load improvement
0.05%TiO2	17%	38%
0.05%Graphene	10%	54%

As can be observed, the addition of TiO2 and graphene results in an improvement in the wear protection properties, being slightly better for the TiO2 NPs. In a similar way both nanomaterials promote and enhancement of EP ability, being the results obtained with graphene significantly better. So, it can be concluded that the sample prepared with graphene nanoparticles with a concentration of 0.05% and using ionic surfactant, shows promising properties for its application as a nanolubricant.

SUMMARY

In this study nanolubricants formulation using a spherical and laminar nanoparticle has been optimized, for that two main parameters such us the minimum surfactant quantity, and sonication have been adjusted to promote lower cluster size and dispersion stability. Formulated Nanolubricants and the reference have been tribologically evaluated by means of wear and extreme pressure properties. The results show that the addition of TiO2 nanoparticles and graphene to the lubricant enhanced their ability to avoid wear as well as their capability to work under high loads

ACKNOWLEGGMENTS

The authors would like to acknowledge the from the National funding mechanisms in Spain (CDTI) for the financial support given to this work through the collective research project **NANOinTECH: "**Development and optimization of industrial processes for the efficient and secure production of nanomaterials". And specially to the companies **Graphene-Tech** and **Alfarben** for the development and characterisation of NPs.

REFERENCES

1. Zhenyu J. Zhang, Dorin Simionesie and Carl Schaschke; "Graphite and Hybrid Nanomaterials as Lubricant Additives"; Lubricants 2014, 2, 44-65; doi:10.3390/lubricants2020044
2. H. S. Kim, J. W. Park, S. M. Park, J. S. Lee, and Y. Z. Lee, "Tribological characteristics of paraffin liquid with nanodiamond based on the scuffing life and wear amount," Wear, vol. 301, no. 1–2, pp. 763–767, 2013.

3. Wu, et al. (2007) “Experimental analysis of tribological properties of lubricating oils with nanoparticles additives”, Wear 26
4. Liu et al. (2011) “Lubrication Effect of the Paraffin Oil Filled with Functionalized Multiwalled Carbon Nanotubes for Bismaleimide Resin”, Tribology Lett. 42 59–65
5. Peng et al. (2007) “Tribological behaviors of surfactant-functionalized carbon nanotubes as lubricant additive in water”, Tribology Lett. 25 (3) 247–253
6. Mingwu et al. (2001) “Nano-tribological properties and mechanisms of the liquid crystal as an additive”, Chinese Sci. Bull. 46 (14) 1227–1232
7. J. Jin et al. (2011) “Tribological properties of CaCO3 nanoparticles as an additive in lithium grease”, Tribology Lett. 41 113–119
8. Hwang et al. (2011) “Effect of the size and morphology of particles dispersed in nano-oil on friction performance between rotating discs”, Journal of Mechanical Science and Technology 25 (11), 2853–2857
9. Z.-L. Cheng and X.-X. Qin, “Study on friction performance of graphene-based semi-solid grease,” Chinese Chem. Lett., vol. 25, no. 9, pp. 1305–1307, 2014.
10. Z. Jia, T. Chen, J. Wang, J. Ni, H. Li, and X. Shao, “Synthesis, characterization and tribological properties of Cu/reduced graphene oxide composites,” Tribol. Int., vol. 88, pp. 17–24, 2015.
11. Diana Berman1, Ali Erdemir2 and Anirudha V. Sumant; “Graphene: a new emerging lubricant; Materials Today”; Volume 17, Number 1 January/February 2014 for tribological applications,” ACS Appl. Mater. Interfaces, vol. 3, no. 11, pp. 4221–4227, 2011.
12. Diana Berman, Ali Erdemir and Anirudha V. Sumant; “Graphene: a new emerging lubricant; Materials Today”; Volume 17, Number 1 January/February 2014 for tribological applications,” ACS Appl. Mater. Interfaces, vol. 3, no. 11, pp. 4221–4227, 2011.

1st International Conference on Nanofluids (ICNf2019)
2nd European Symposium on Nanofluids (ESNf2019)
26-28 June 2019, Castelló, Spain

Ferronematic as a special type of nanofluid for sensors of magnetic field

M. Timko[1], V. Lackova[1], N. Tomasovicova[1], N. Eber[2], T. Toth-Katona[2], J. Jadzyn[3], and P. Kopcansky[1*]

[1]Institute of Experimental Physics, Slovak Academy of Sciences, Watsonova 47, Kosice, Slovakia

[2]Institute for Solid State Physics and Optics, Wigner Research Centre for Physics, Hungarian Academy of Sciences, Budapest, H-1525, Hungary

[3]Institute of Molecular Physics, Polish Academy of Sciences, Poznan, 60179, Poland

[*]Corresponding author: kopcan@saske.sk

Keywords: liquid crystal, magnetic nanoparticles, ferronematics, Fréedericksz threshold.

Abstract: Suspension of magnetic nanoparticles in nematic liquid crystals, called ferronematics, have become a promising target for experimental and theoretical studies in many aspects, especially in enhancing the magneto-optical performance of such materials. In the presentation will be illustrated experimental data regarding the effect of how shape and size of used magnetic nanoparticles influence a liquid crystal and their response in low magnetic field region. Behaviour of these systems opens the doors towards their application such as low magnetic field sensors or basic logical elements for information storage technologies.

Introduction/Background: Liquid crystals (LCs) belong to a class of soft condensed matter that combine fluidity of ordinary liquids with the long-range order of crystalline solids. These materials- conventional thermotropic LCs are usually diamagnetic with a small anisotropy of diamagnetic susceptibility (~ 10^{-7}). Therefore, rather high magnetic fields (of the order of tesla) are required to change the orientation of LC molecules. One of the most important discoveries in the control of LCs by electric or magnetic fields was the threshold behaviour in their reorientational response, described by Fréedericksz and named after him as “Fréedericksz transition” [1]. Contrary to electro-optical effects, the magneto-optics effects have not found significant application in the industry of LC, so far. About 5 decades ago the idea was born to mix nano-sized magnetic particles with nematic LCs, in order to get fluids with a large magnetic susceptibility (frequently called ferronematics) (FNs) [2]. Doping LC with low volume concentration of nanoparticles has been shown to be a promising method to modify their properties. At such low

concentrations, nanosized particles do not disturb significantly the liquid crystalline order, hence, producing a macroscopically homogeneous structure. Therefore, these materials may give a strong push for the development of many kinds of new magnetically controlled LC-devices, serving as sensitive anisotropic magnetic materials (e.g. sensors of small magnetic fields).

Discussion and Results: Our results in study of composite systems showed that doping of LC 6CHBT with spherical, rod-like MNPs, single- wall carbon nanotubes (SWCNT), and SWCNT functionalized with Fe_3O_4 nanoparticles with volume concentration $\phi = 10^{-4}$ leads to increasing sensitivity of LC on the magnetic field, not only in high magnetic field region (order of several tesla- classical Fréedericksz transition) but also in low-magnetic field region (see Fig 1) [3]. The obtained results provide an evidence for a linear magnetic field dependence of the capacitance in this low magnetic field region (up to 0.1 T), even much below the magnetic Fréedericksz threshold.

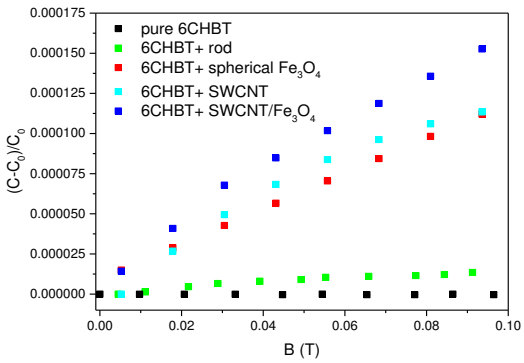

Figure 1. Relative capacitance variation vs. magnetic field for undoped 6CHBT and 6CHBT doped with rod-like nanoparticles, spherical Fe_3O_4 nanoparticles, SWCNT and SWCNT/Fe_3O_4.

Experimentally and theoretically were studied and described new types of FNs – LC 6CHBT doped with lath-like goethite MNPs, holding a permanent longitudinal magnetic moment along particle long axis. It was observed that these nanostructures have a negative magnetic susceptibility along the shortest particle dimension and therefore, they are oriented parallel with field at low intensities and perpendicular in case when magnetic field passes threshold intensity. It was shown that the presence of such nanoparticles influences not only on the sensitivity of studied samples to external magnetic fields, but also a reduction of phase transition temperature [4]. The modified variant of the Burylov–Raikher theory (dealing the coupling energy between MNPs and LC matrix) has been developed which describes the possible bistable behaviour of these FNs under the influence of magnetically induced phase transition.

A new method of detecting low magnetic fields by Whispering gallery mode (WGM) in a fiber microresonator infiltrated with 6CHBT LC doped with spherical or rod-like MNPs were used to study the influence of applied magnetic field on a spectral shift of the WGM resonances. The experimental results demonstrated that the proposed sensor was more sensitive for samples infiltrated with rod-like and spherical MNPs than for undoped LC [5]. Experimental observations point to the possibility of using such samples as sensors for magnetic field in range of 0-50 mT.

In our previous work [6] we have demonstrated that a small dc magnetic field (of the order of several Oe) applied in isotropic phase increases the magnetic susceptibility of a FN (LC 6CB@Fe_3O_4 with volume concentration $\phi = 10^{-4}$) sample. Driving it through the isotropic-to-nematic phase transition resets the magnetic susceptibility to the value measured prior to application of the dc bias field. After that, the sample could be "biased" again by repeated applications of the dc field in the isotropic phase. The understanding of this process and influence of doping MNPs on critical value of dc magnetic field could be useful for future utilization in various micro- and nanodevices.

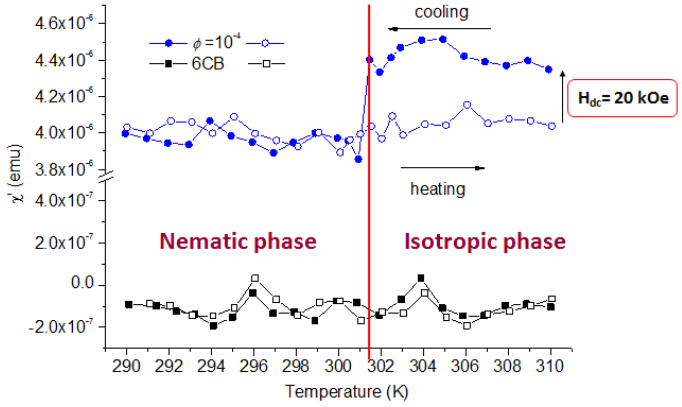

Figure 2. Temperature dependence of the real part χ´ of the ac susceptibility of the undoped 6CB (squares) and FN based on 6CB (circles) in the cooling-heating cycle with prior application of a dc magnetic field H_{dc}= 20 kOe.

Summary/Conclusions: We reviewed our experimental work focused on FNs, namely on LC doped with various types of MNPs, where the addition of MNPs influences the magnetic sensitivity of FNs. We have shown that shape and size of used MNPs have an impact on structural transitions. That is to say, the sensitivity range of FNs to magnetic fields can be extended significantly by optimization of the FN composition, and that, in principle, the effect may be used for sensing of low magnetic fields. Furthermore, a new modified version of FNs based on Burylov-Raikher theory has been developed, describing magnetically induced phase transitions of the first and/or second order

between different orientational states of FNs. On the basis of this theory, an elastic interaction of the elongated particles with line defects of the LC matrix of FN has been studied. The magnetic susceptibility of FNs was studied, mainly their response to a probing alternating magnetic field. It was found an unusual behaviour of the magnetic susceptibility while passing through the phase transition of the FN with prior presence of a small magnetic field. The experimental sensitivity of novel type of WGM fiber resonator infiltrated with FN was demonstrated. The obtained results showed that the proposed sensor was almost of 3 pm/mT more sensitive for samples infiltrated with MNPs than for undoped LC sample. This is the way to obtain magnetovision camera with the possibility of mapping the magnetic field in space.

References:

1. V. Freedericksz and V. Zolina, Forces causing the orientation of an anisotropic liquid, *Trans. Faraday. Soc.* 29 (1933) 919-930.
2. F. Brochard and P. G. de Gennes, Theory of magnetic suspensions in liquid crystals, *Journal de Physique* 31 (1970) 691-708.
3. N. Tomasovicova, M. Timko, Z. Mitroova, M. Koneracka, M. Rajnak, N. Eber, T. Toth-Katona, X. Chaud, J. Jadzyn and P. Kopcansky, Capacitance changes in ferronematics liquid crystals induced by low magnetic field, *Phys. Rev. E* 87 (2013) 014501.
4. P. Kopcansky, V. Gdovinova, S. Burylov, N. Burylova, A. Voroshilov, J. Majorosova, F. Agresti, V. Zin, S. Barison, J. Jadzyn and N. Tomasovicova, The influence of goethite nanorods on structural transitions in liquid crystal 6CHBT, *J. Magn. Magn. Mater.* 459 (2018) 26-32.
5. A. Mahmood, V. Kavungal, S. S. Ahmed, P. Kopcansky, V. Zavisova, G. Farrell and Y. Semenova, Magnetic field sensing using whispering-gallery modes in a cylindrical microresonator infiltrated with ferronematic liquid crystal, *Optics Express* 25 (2017) 12195-12202.
6. N. Tomasovicova, J. Kovac, Y. Raikher, N. Eber, T. Toth-Katona, V. Gdovinova, J. Jadzyn, R. Pincak and P. Kopcansky, Biasing a ferronematic- a new way to detect weak magnetic field, Soft Matter 12 (2016) 5780-5786.

1st International Conference on Nanofluids (ICNf2019)
2nd European Symposium on Nanofluids (ESNf2019)
26-28 June 2019, Castelló, Spain

Comparison Study for Different Experimental Models of Nanofluid/Pressboard Configuration

El-Sayed M. El-Refaie[1], Diaa-Eldin A. Mansour[2], M. K. Abd Elrahmen[1], and Mohamed H. Abdo[1*]

[1]Department of Electrical Power and Machines Engineering
Faculty of Engineering, Helwan University
Cairo, Egypt

[2]High Voltage and Superconductivity Laboratory
Department of Electrical Power and Machines Engineering
Faculty of Engineering, Tanta University
Seperbay, Tanta 31521, Egypt

[*]Corresponding author: drmhsa3ed@h-eng.helwan.edu.eg

Keywords: Alumina Nanofluid 1, Pressboard 2

Abstract: This paper aims to compare between experimental models for vertical and horizontal configurations of a needle to plane with constant gap length which implemented on the surface of pressboard under the AC supply application, that to study electrical discharge on pressboard surface using alumina nanofluid prepared with different weight fractions. The value of applied AC voltage during electrical discharge (Break Down: BD) was measured. Also, using a finite element package electric field distribution was obtained.

Introduction/Background: Although pressboards play important role in the insulation system in large power transformers [1], but space charge can be formed at an oil/pressboard interface under a high electric field due to interfacial polarization arising from the difference in permittivity between adjacent materials causing one of the most reasons of discharge initiation and propagation [2]. Several trials were suggested to solve the mentioned problem, from the pressboard side coating by a thin solid layer of epoxy resin and Teflon was considered [3] and nano additives were applied in [4]. On the other hand, benzotriazol and ditertiary-butyl para-cresol additives to oil presented in [5]. However, the long-term effect of these additives is not guaranteed. Recent researches applied the technique of nanofluids with transformer oil to enhance its dielectric and thermal properties [6]. So, it is proposed in this study to use alumina nanofluid in suppressing electrical discharge at the oil/pressboard interface under AC voltage application with weight fractions 0.01 g/L, 0.04 g/L, 0.07 g/L, and 0.1 g/L of nanoparticles.

EXPERIMENTAL PROCEDURES AND SETUP: In the last researches [7:9], preparation of nanofluid and impregnated pressboard samples was explained in detail.

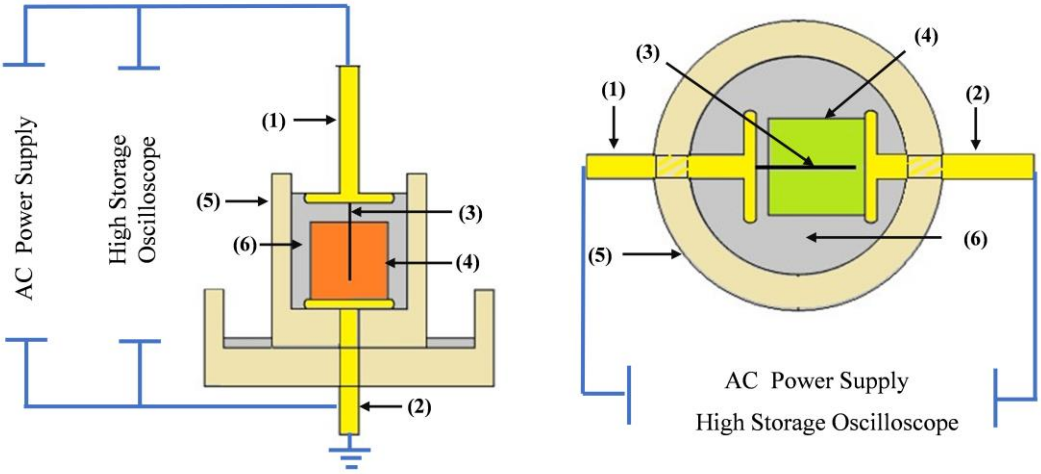

Figure 1. Vertical and Horizontal Electrode systems used for flashover tests. (1)H.V Elec., (2) Ground Elec., (3) Needle, (4) Pressboard, (5) Beaker, (6) Nanofluid

From figure (1) shown, at vertical system gap distance between needle tip and ground electrode equal 1cm and 0.5 cm at the horizontal system.

Discussion and Results:

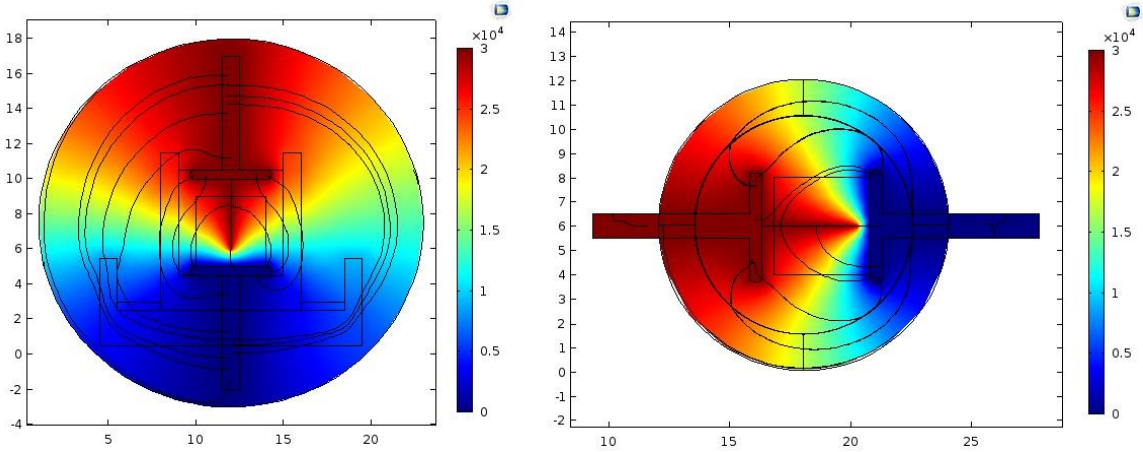

Figure 2. Electrical Potential and Electrical Field Distribution.

The two applied configurations have been simulated by models illustrated in figure (2) which executed using COMSOL package based on finite element analysis. Comparing the two models clarify that the direction of configuration (vertical or horizontal) does not affect the electrical potential distribution (gradient of colors degree) and electrical field distribution represented by shown lines. It also explains the reason behind electrical discharge occurrence on the pressboard surface which appears in gap distance between needle tip (HV part that may be reached to 30 kV) and the ground electrode.

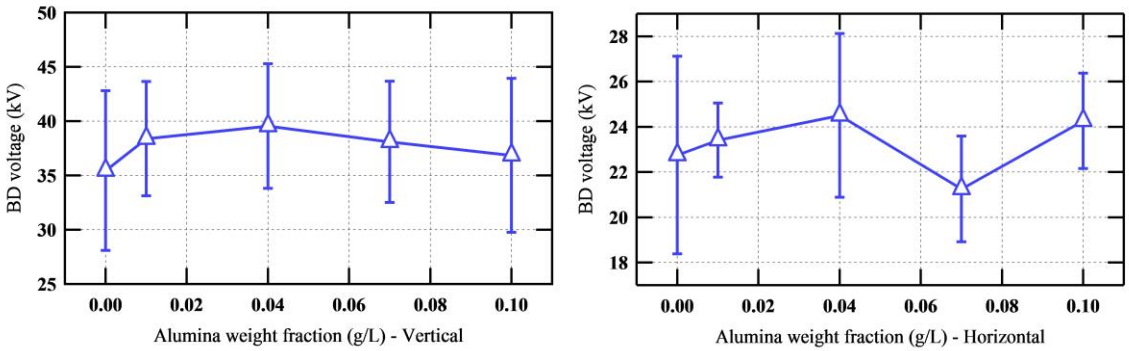

Figure 3. BD Voltage vs. Alumina Weight Fraction at Vertical and Horizontal Cases.

Table 1. Percentage Change of Alumina BD Voltage Results Based on Oil.

Alumina Weight Fraction (g/L)	0.01	0.04	0.07	0.1
Improvement Increasing % - Vertical	8.255	11.535	7.451	3.948
Improvement Increasing % - Horizontal	2.93	7.69	-6.59	6.67

Figure (3) and table (1) present the results of BD. Voltage using alumina nanofluid which improved up to 0.04 g/L and decayed at 0.07 and 0.1 g/L weight fractions for the vertical configuration; But at the horizontal configuration there was an improvement at (0.01,0.04 and 0.1 g/L) concentrations and collapse at 0.07 g/L. Of course, the noticeable change in the magnitude of BD voltage values returns to the gap distance length which changed from 1 cm at vertical to 0.5 cm at horizontal configuration.

Agglomeration negative charges on the pressboard surface are the major cause behind electric discharge, which can be explained by space charge polarization theory and variation in dielectric constant (ε) between adjacent materials (oil and pressboard) under a high electric field. As the applied AC voltage and corresponding electric field increase, the negative charges accumulated on the pressboard surface also increase. It was found that the surface of alumina nanoparticles is positively charged (cationic) [9]; besides that electronegativity property that specialized the mentioned nanoparticles [10].so, can explain the reason behind progressing the results of alumina nanofluid results to the capability of nanoparticles to hold negative charges from disassociation. The stability of the dissociated negative charges in a horizontal configuration more than vertical one and that makes charges diffusion more difficult.

Summary/Conclusions: The comparison between the two configurations of a needle to plan (vertical and horizontal) applied in this paper proved the similarity of Break Down voltage results improvement trend and electrical field distribution despite changing the gap length and direction of electrical discharge. The best results have been achieved at 0.04 g/L concentration of alumina nanoparticles at both applied configurations. The results of BD voltage were better in the vertical model than the horizontal one.

References:

1. T. A. Prevost, et al, “Cellulose insulation in oil-filled power transformers: Part I - history and development,” IEEE Electr. Insul. Mag., vol. 22, no. 1, pp. 28-35, 2006.
2. L. Lundgaard, et al., “Propagation of positive and negative streamers in oil with and without pressboard interfaces,” IEEE Trans. Dielectr. Electr. Insul., pp. 388-395, 1998.
3. K. H. Jang, S. Yoshida, M. Kozako and M. Hikita, “Effect of thin solid layer coating on creepage discharge characteristics in oil/pressboard composite insulation system,” IEEE Conf. Electr. Insul. Dielectr. Phenomena (CEIDP), USA, pp. 832-835, 2015.
4. J. Huang, et al., “Enhancing mechanical strength and breakdown behavior of insulating presspaper by introduction of nanofibrillated cellulose,” IEEE Int’l. Conf. High Voltage Engineering and Application (ICHVE), China, pp. 1-4, 2016.
5. S. Okabe, M. Kohtoh and T. Amimoto, “Suppression of increase in electrostatic charging tendency of insulating oil by aging used for power transformer insulation,” IEEE Trans. Dielectr. Electr. Insul., vol. 17, pp. 294-301, 2010.
6. D. A. Mansour and A. M. Elsaeed, “Heat transfer properties of transformer oil-based nanofluids filled with Al_2O_3 nanoparticles,” IEEE Int’l. Conf. Power and Energy (PECON), Malaysia, pp. 123-127, 2014.
7. Sayed M. El-Refaie, Diaa-Eldin A. Mansour, M. K. Abd Elrahman and Mohamed H. Abd, "Electrical Discharge Analysis on Nanofluid/Pressboard Surface under AC Voltage Application", Nineteenth International Middle East Power Systems Conference, Egypt, 19-21 December 2017.
8. J. Dai, Z. D. Wang and P. Jarman, “Creepage discharge on insulation barriers in aged power transformers,” IEEE Trans. Dielectr. Electr. Insul., vol. 17, pp. 1327-1335, 2010.
9. D. A. Mansour, Ahmed M. El saeed and Mohamed A. Izzularab “The role of interfacial zone in dielectric properties of transformer oil-based nanofluids,” IEEE Trans. Dielectr. Electr. Insul., vol. 23, pp.3364-3372, 2016.

10. Manal M. Emara, Diaa-Eldin A. Mansour and Ahmed M. Azmy, "Mitigating the impact of aging by products in transformer oil using TiO_2 nanofillers", IEEE Transactions on Dielectrics and Electrical Insulation, Volume 24 , Issue 6 , Dec. 2017.

1st International Conference on Nanofluids (ICNf2019)
2nd European Symposium on Nanofluids (ESNf2019)
26-28 June 2019, Castelló, Spain

Tailoring the surface properties of nanoparticles by ALD nanocoatings

D. Valdesueiro[1*], S. Moitzheim[1], J.A. Moulijn[1,2], R. Colen[1]

[1] Delft IMP B.V., Molengraaffsingel 10, 2629 JD, The Netherlands

[2] Delft University of Technology, Department of Chemical Engineering, Van der Maasweg 9, 2629 HZ, Delft, The Netherlands

[*]Corresponding author: d.valdesueiro@delft-imp.nl

Keywords: Atomic layer deposition, nanoencapsulation, nanoparticles, nanocoatings.

Abstract: In this paper we present a gas-phase coating technology, atomic layer deposition (ALD), that allows the deposition of nanometer-thin conformal coatings with low waste generation and sub-nanometer control over the thickness of the deposited coatings. This technique, originally developed to coat wafers for the semiconductor industry, has been widely applied to encapsulate different types of particles and nanoparticles regarding composition, size, geometry and porosity. This technique is versatile with the coating materials, since allows the deposition of compounds in metallic form, oxides, nitrides, etc…, organic films and even inorganic-organic hybrid coatings, just by selecting the right precursors. Several fields are currently applying ALD films to enhance the performance of materials, such as to protect the substrate from degradation as in the case of powders used in the production of Li-ion batteries, or to increase the activity of the substrates as in the case of catalysts production. These and other applications are benefiting from the functionalities added by these nanometer-thin films that do not alter the bulk properties of the substrates. All this has converted ALD in a common technique used in nanotechnology, and this could potentially be extended to the application of coating particles to be used for nanofluids.

Introduction: Atomic layer deposition (ALD) is a gas-phase coating technology that allows the deposition of nanometer-thin conformal coatings on a wide variety of particles (Fig. 1 left). The versatility of ALD covers both the nature and size of the particles, as well as the chemistry of the coating. For example, particles ranging from nanoparticles to particles of several hundreds of micrometers can be coated with this technique. Additionally, the nature of the substrate can be ceramic (e.g. Al_2O_3, TiO_2, SiO_2), metallic (Ti), and polymeric (powder coating paints), amongst many others. The nature of the coating (Fig. 1 bottom) can be also selected from metal oxides (Al_2O_3) or nitrides (e.g.

AlN), pure metals (e.g. Pt), organic coatings and even inorganic-organic hybrid coatings [1]. These thin films could potentially be used for nanofluid applications, aiming at encapsulating the nanoparticles comprising the nanofluids without interfering with their intrinsic heat properties.

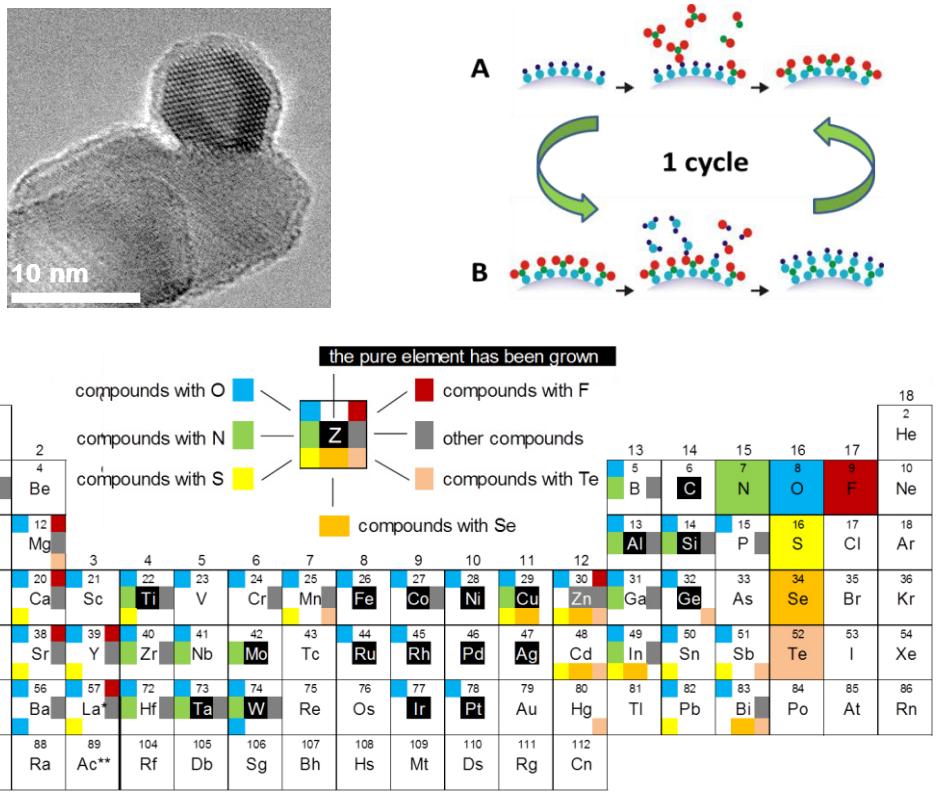

Figure 1. (top left) Titanium oxide nanoparticles coated with aluminium oxide using ALD [2]. (top right) Reaction mechanism of one cycle of atomic layer deposition. (bottom) Periodic table of ALD, showing the compounds reported in literature as oxides, nitrides, metals, etc. [1]

ALD is a coating process that relies on a layer-by-layer growth mechanism in which the coating chemistry is split into two half-reactions (Fig. 1 top right). Each of these reactions is self-limiting, such that at most a monolayer of a compound can be deposited per cycle. In this way, we have full control over the coating thickness: the number of times that the alternating feed of the two precursors is repeated determines the thickness of the achieved coating [3].

In recent years, atomic layer deposition (ALD) has become a standard tool to apply ultrathin and conformal coatings on substrates of complex geometries, mostly driven by an interest from semiconductor industry applications. The intrinsic advantages of controlling the structure growth at the (sub)nanometer level, while coating complex

surfaces – either for providing protection to the substrate or boosting its activity – are also relevant for other industrial applications related to particle technology, such as nanofluids.

In this presentation we will show an example of the influence of nanometer-thin aluminium oxide films used to encapsulate a polymer-based powder. These thin alumina films were able to confine the softened core material without altering the thermal properties when heating the coated particles above the glass transition temperature of the core material. That can be of use with nanofluids based on phase change materials.

This example aimed at tuning the surface finish of a standard polyester-based powder coating paint, from gloss to matt (Fig. 2 left), by depositing ultrathin films of Al_2O_3 on the powder coating particles [4]. The coating experiments were performed in a fluidized bed reactor at 1 bar and 27 °C, using an alternating exposure of the particles to the two precursors (trimethylaluminium and water). By varying the number of coating cycles from 1 to 9, we deposited alumina films ranging from 1 to 30 nm. When the average alumina shell was thicker than 6 nm, the shell prevented the core particles from flowing, even though the powder particles did soften above their glass transition temperature. With the particles morphology intact, this resulted in a rough and matte surface finish of the coating after curing. Additionally, the alumina coating acted as a barrier able to encapsulate the softened powder coating above the glass transition temperature, without altering other thermal properties as such as the glass transition temperature (Fig. 2 right). This type of application can be extended to the encapsulation of phase change materials with thin alumina films that would contain a molten core without modifying the thermal properties, which is of crucial importance in the development of efficient nanofluids.

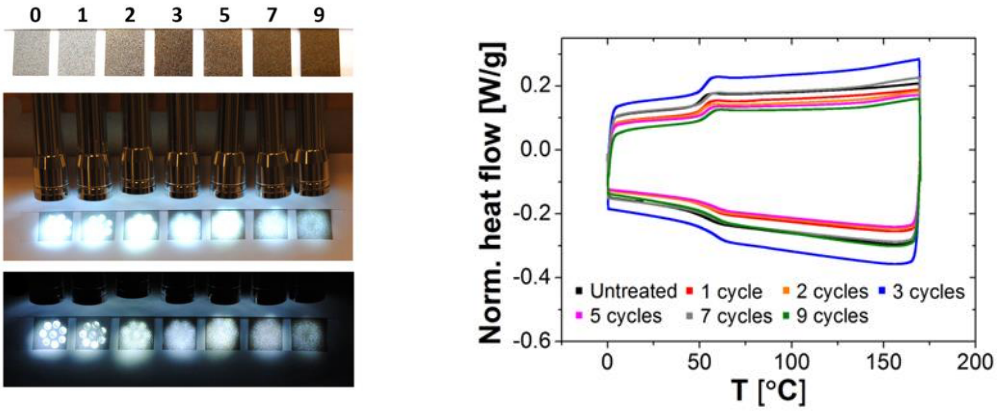

Figure 2. (left) Tuning of the surface finish of the paint from gloss to matte depending on the thickness of the deposited aluminium oxide film. (right) Differential scanning calorimetry profiles of the uncoated and coated powder coating samples.

Summary/Conclusions

In this presentation we will show the process of depositing ultrathin films on particles with the coating technique atomic layer deposition, and we will present an example on how the performance of a material can be tuned without altering other physical properties such as density, heat capacity, shape or size. Additionally, we will explain how the coating process works, and what can be further done with this versatile technique, aiming at a scaled up process able to produce coated particles at industrially relevant volumes. Finally, we will discuss how this technique could contribute to the development of new nanofluids. This technique can be interesting for this emerging application, since from other fields it has been proven that ultrathin films can enhance the performance of other materials, perhaps applications for nanofluids being the next one.

References

1. V. Mikkulainen, M. Leskela, M. Ritala and R.L. Puurunen, Crystallinity of inorganic films grown by atomic layer deposition: Overview and general trends, *Journal of Applied Physics* 113 (2013) 1-101.
2. D. Valdesueiro, G.M.H. Meesters, M.T. Kreutzer and J.R. van Ommen, Gas-Phase Deposition of Ultrathin Aluminium Oxide Films on Nanoparticles at Ambient Conditions, *Materials*, 8 (2015) 1249-1263.
3. S.M. George, Atomic layer deposition: An overview, *Chemical Reviews*, 110 (2010) 111-131.
4. D. Valdesueiro, H. Hettinga, J.P. Drijfhour, P. Lips, G.M.H. Meesters, M.T. Kreutzer and J.R. van Ommen, Tuning roughness and gloss of powder coating paint by encapsulating the coating particles with thin Al_2O_3 films, *Powder Technology* 318 (2017) 401-410

1st International Conference on Nanofluids (ICNf2019)
2nd European Symposium on Nanofluids (ESNf2019)
26-28 June 2019, Castelló, Spain

Graphene nanofluids.
From thermal to electrochemical applications

P. Gomez-Romero*, R. Rodriguez-Laguna, E. Chavez-Angel, D. P. Dubal, D. Rueda-García, R. Benages

[1]Catalan Institute of Nanoscience and Nanotechnology, ICN2 (CSIC-BIST)

*Corresponding author: pedro.gomez@icn2.cat

Keywords: Graphene nanofluids, thermal properties, HTFs, electrochemical properties, energy storage, Reduced Graphene Oxide.

Abstract: Recent work on graphene nanofluids in organic solvents and reduced graphene oxide in aqueous electrolytes are described. In addition to a thorough study of thermal properties of the former, the potential of RGO nanofluids for electrochemical energy storage (i.e. in novel flow cells) was studied.

Introduction/Background: Graphene is the advanced material of choice for a wealth of applications, but it has customarily been used as a solid. Yet, fluids are key materials for a variety of industrial applications, from thermal to electrochemical devices. Furthermore, nanofluids are a ground-breaking type of materials with exciting new properties and opportunities to improved performance in a wide variety of fields, from magnetic ferrofluids to thermal to health applications. [1]

Graphene Nanofluids, formed by graphene nanosheets dispersed in suitable base fluids can be prepared as stable dispersions in organic or aqueous solvents [2-5] either as pure graphene [5] or RGO [2] or as hybrid derivatives, [3,4] and they show most interesting thermal and electrochemical properties as it is briefly described below.

Discussion and Results: In the field of thermal energy conversion and storage, we have developed stable graphene nanofluids of different concentrations in suitable organic solvents as base fluids (dimethylacetamide /dimethylformamide). Figure 1 (LEFT) shows thermal conductivity data for DMAc and nanofluids of graphene (0.09% and 0.18%) in this same solvent. Notably, the measurements were carried out using a modified 3-ω technique adapted to liquid samples [5]. Thermal conductivity (as well as other thermal properties [5]) is substantially enhanced proportionally to the graphene

concentration. Thus, the 0.18% nanofluid leads to a thermal conductivity enhanced by a 48% with respect to the pure solvent.

In a different area, related to electrochemical energy storage, we have developed electroactive nanofluids based on Reduced Graphene Oxide (rGO) dispersed in acidic aqueous electrolytes showing ultrafast charge transfer. [2-4] Thus, a surfactant-stabilized dispersion of rGO in 1M H_2SO_4 aqueous solution was shown to have capacitive energy storage capabilities (Figure 1 RIGHT) parallel to those of solid electrode supercapacitors (169 F g−1(rGO)) but working up to much faster rates (from 1mV s−1 to the highest scan rate of 10 V s−1) in nanofluids with 0.025, 0.1 and 0.4 wt% rGO, featuring viscosities veryclose to that of water, these characteristics and the capacitive response which suggest the possible application of these nanofluids in novel flowing supercapacitor cells. Indeed we were able to show that the dispersed solid nanoparticles can be fully utilized even in the dilute sols prepared. Furthermore, it should be noted that the CVs can be run at the very fast scan rate of 10000 mV/s (Figure 1 RIGHT) which suggest ultrafast charge-transfer in these novel nanofluids.

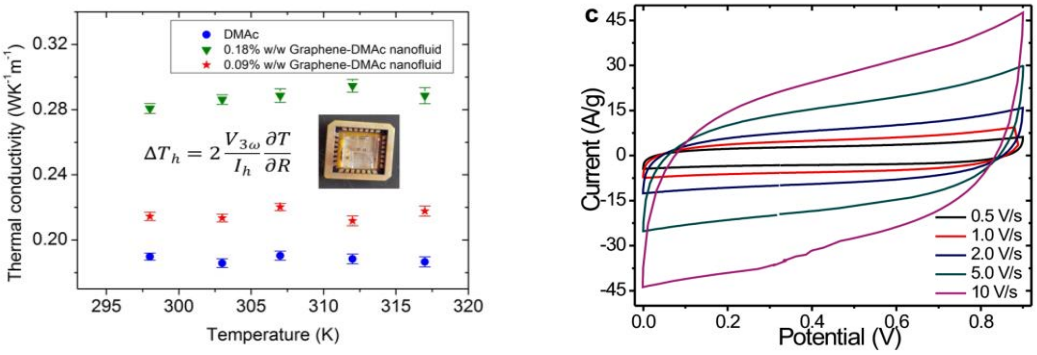

Figure 1. LEFT: Thermal conductivity measurements carried out through the 3-omega technique for graphene nanofluids in Dymethylacetamide solvent. RIGHT: Cyclic Voltammograms of Reduced Graphene Oxide Nanofluids in aqueous acidic electrolytes at various fast scan rates

But in addition to pure graphene nanofluids, we have also developed hybrid nanofluids with graphene as a capacitive and charge-transfer booster, but also incorporating additional inorganic species with redox activity. In this way, our hybrid electroactive nanofluids (HENFs) combine capacitive and faradaic energy storage mechanisms in a single fluid material. In particular we have developed true “liquid electrodes” composed of reduced graphene oxide and polyoxometalates (rGO-POMs) forming a stable nanocomposite for

electrochemical energy storage in novel Nanofluid Flow Cells. Two series of hybrid materials (rGO-phosphomolybdate, rGO-PMo12 and rGO-phosphotungstate, rGO-PW12) were synthesized and dispersed with the aid of a surfactant in 1 M H2SO4 aqueous electrolyte to yield highly stable hybrid electroactive nanofluids (HENFs) of low viscosity which were tested in a home-made flow cell under static and continuous flowing conditions [3]. Remarkably, even low concentration rGO-POMs HENFs (0.025 wt%) exhibited high specific capacitances of 273 F/g(rGO-PW12) and 305 F/g(rGO-PMo12) with high specific energy and specific power (Figure 2). Moreover, rGO-POM HENFs show excellent cycling stability (~ 95%) as well as Coulombic efficiency (~77–79%) after 2000 cycles. Thus, rGO-POM HENFs effectively behave as real liquid electrodes with excellent properties, demonstrating the possible future application of HENFs for dual energy storage in a new generation of Nanofluid FlowCells.

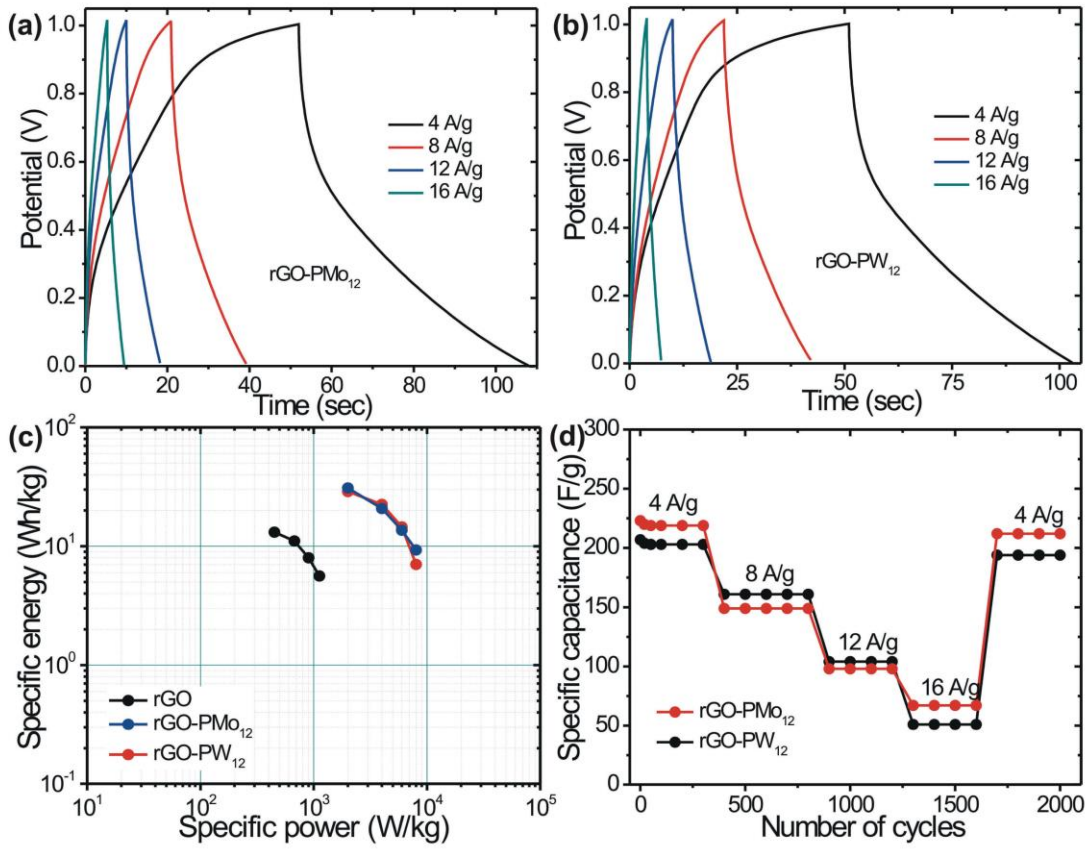

Figure 2. (a–b) Galvanostatic charge-discharge curves for rGO-PW12 and rGO-PMo12 HENFs of 0.025% at different current densities in static condition, (b) Plot of specific energy versus specific power in Ragone plot for rGO, rGO-PW12 and rGO-PMo12 in flow cell (d) Galvanostatic charge/discharge cycling test for rGO-POMs HENFs of 0.025% at different current densities for 2000 cycles.

Summary/Conclusions: From the better known thermal properties (thermal conductivity, specific heat capacity), to the more novel studies of electrochemical performance we have been able to design graphene as well as graphene-based nanofluids that present enhanced performance and open possibilities to new applications such as energy storage in novel flow cells.

References:

1 R. Taylor, S. Coulombe, T. Otanicar, P. Phelan, A. Gunawan, W. Lv, G. Rosengarten, R. Prasher, H. Tyagi, Small particles, big impacts: A review of the diverse applications of nanofluids, Journal of Applied Physics 2013, 113, 10.1063/1.4754271.

2 D. P. Dubal and P. Gomez-Romero, Electroactive Graphene Nanofluids for Fast Energy Storage, 2D Mater., 2016, vol. 3(3), p. 31004.

3 D. P. Dubal, D. Rueda-Garcia, C. Marchante, R. Benages and P. Gomez-Romero, Hybrid Graphene-Polyoxometalates Nanofluids as Liquid Electrodes for Dual Energy Storage in Novel Flow Cells, Chem. Rec. 2018, 18, 1076 –1084

4 D. Rueda-Garcia, Z. Caban-Huertas, S. Sanchez-Ribot, C. Marchante, R. Benages, D. P. Dubal, O. Ayyad, P. Gómez-Romero* , Battery and supercapacitor materials in flow cells. Electrochemical energy storage in a LiFePO4/reduced graphene oxide aqueous nanofluid, Electrochimica Acta, 2018, 281, 594-600.

5 M. R. Rodríguez-Laguna, A. Castro-Alvarez, M. Sledzinska, J. Maire, F. Costanzo, B. Ensing, P. Ordejón, C. M. Sotomayor-Torres, P. Gómez-Romero and E. Chávez-Ángel, Mechanisms behind the enhancement of thermal properties of graphene nanofluids, Nanoscale, 2018, 10, 15402-15409

1st International Conference on Nanofluids (ICNf2019)
2nd European Symposium on Nanofluids (ESNf2019)
26-28 June 2019, Castelló, Spain

Heat transfer enhancement using nanofluids in the compression exchanger in a solar Stirling engine

I.M. Santos-Ráez[1], J.L. Arjona-Escudero[1*], A.I. Gómez-Merino[2]

[1] Department of Mechanics, Thermal and Fluids Engineering, University of Málaga (Spain)

[2] Department of Applied Physics II, University of Málaga (Spain)

[*]Corresponding author: jae@uma.es

Keywords: Nanofluids, Stirling engine, Heat transfer enhancement, Alumina.

Abstract: In this paper a improvement in the heat exchange of a solar Stirling engine during the compression phase was studied. The viability of using nanoparticles as ceramic oxide (Al_2O_3 in water) at different concentrations instead of conventional refrigerants (water or air) was evaluated. Since these systems could behave as non-Newtonian fluids the dynamic viscosity was measured, as well as other thermophysical properties. The results showed that the convective heat transfer coefficient could raise one order of magnitude respect to the conventional heat transfer fluids at moderately volume fractions (over 0.15).

Introduction/Background: Heat transfer is involved in many industrial processes, either in the form of input energy in complex systems, or as output energy produced by the systems themselves, which needs to be removed by means of cooling devices. In particular, the problem of heat removal and/or temperature control has become crucial in some critical applications involving high temperature flows: power electronics systems, electromechanical systems, etc. The importance of research in the field of nanofluids as a new generation of transfer heat fluids may be demonstrated by the large number of publications on this field especially by rapid advances in nanotechnology in recent decades [1,2,3]. The main advantage of its use is the increase in thermal conductivity, compared to conventional coolants [4].

Stirling engine is an external combustion engine based on the Stirling cycle. This engine generates mechanical energy thanks to the difference in temperature caused by a fixed mass of gas (usually air, hydrogen or helium), which increases its temperature in the zone of expansion and cools in the compression zone. A mechanical drive generates a power of net output (Figure 1a). Compression zone must be cooled to keep the gas temperature as low as possible (compression exchanger, Figure 1b and 1c). As the temperature of the coolant increases there is a considerable drop in thermal efficiency.

Almost all engine designers have opted for conventional refrigerants, but there are other fluids which offer interesting features in heat transfer processes. The studies carried out with nanofluids show a considerable improvement in the heat transfer, especially in the thermal conductivity and convection heat transmission [5,6].

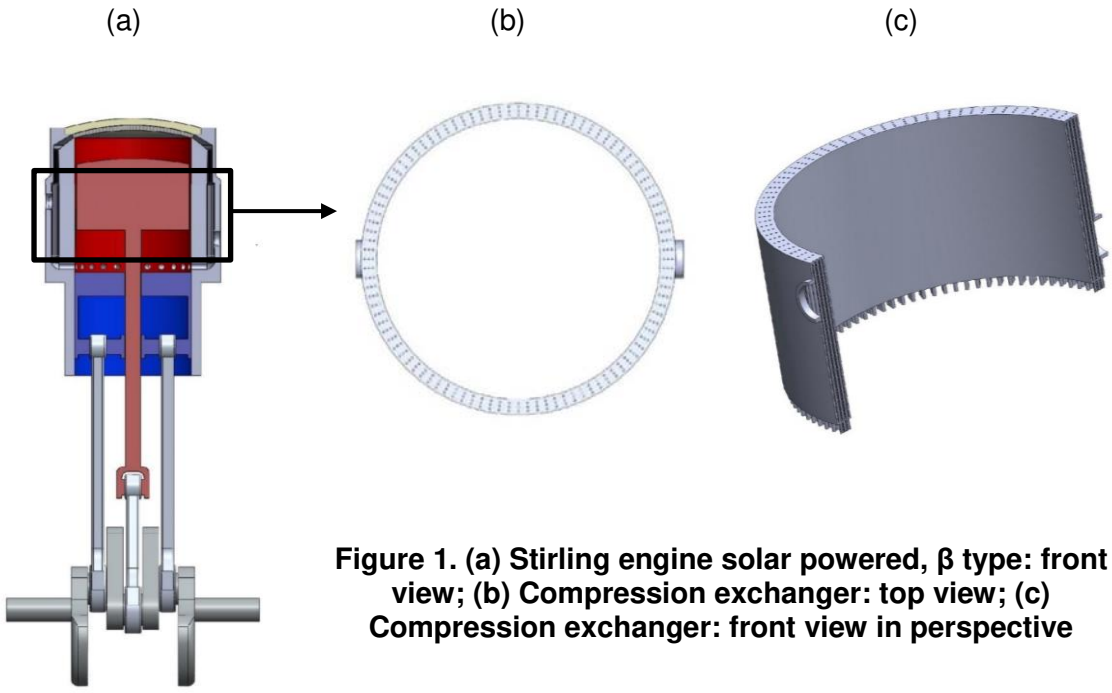

Figure 1. (a) Stirling engine solar powered, β type: front view; (b) Compression exchanger: top view; (c) Compression exchanger: front view in perspective

In this paper, the results obtained from rheological and thermophysical analyses on the use of a cooling agent in the compression exchanger of a solar Stirling engine based on aluminum oxide (Al_2O_3) at different concentrations (0.05, 0.1, 0.15 and 0.18 v/v) were exposed.

Discussion and Results: Table 1 shows the thermophysical experimentally measured values of specifc heat capacity (c_p), density (ρ) and thermal conductivity (κ) at different volume fractions (ϕ). Zero concentration indicates pure water. The values of dynamic viscosity (η_{nf}) were obtained from rheological measurements in steady shear flow, since at low shear rate and volume fractions over 0.05 non Newtonian behaviour is usually observed in ceramic colloid systems. From the thermophysical properties the dimensionless numbers of Reynolds (Re_{nf}) and Prandtl (Pr_{nf}) were calculated. Nusselt number (Nu_{nf}) was evaluated using the correlation proposed by Xuan and Li [7] for laminar flow (Eq. 1).

Table 2. Thermophysical properties of nanofluids (subscript "nf" refers to nanofluids), 311 K

ϕ (v/v)	c_{pnf} (J/kgK)	ρ_{nf} (kg/m^3)	K_{nf} (W/mK)
0	4170	997	0.6
0.05	3598	1140	1.1
0.1	3140	1281	1.2
0.15	2780	1430	1.35
0.18	2380	1630	1.5

$$Nu_{nf} = \frac{h_{nf} D_h}{\kappa_{nf}} = 0,4328 \left(1 + 11,285\ \phi^{0,754}\ Pe^{0,218}\right) Re^{0,333}\ Pr^{0,4} \qquad \text{Eq. 1}$$

where h_{nf} is the convective coefficient, and D_h the hydraulic diameter, which value was 2.11 cm, depending on compression exchanger geometrical parameters, *Pe* Peclet number, *Re* Reynold number an *Pr* Prandtl number.

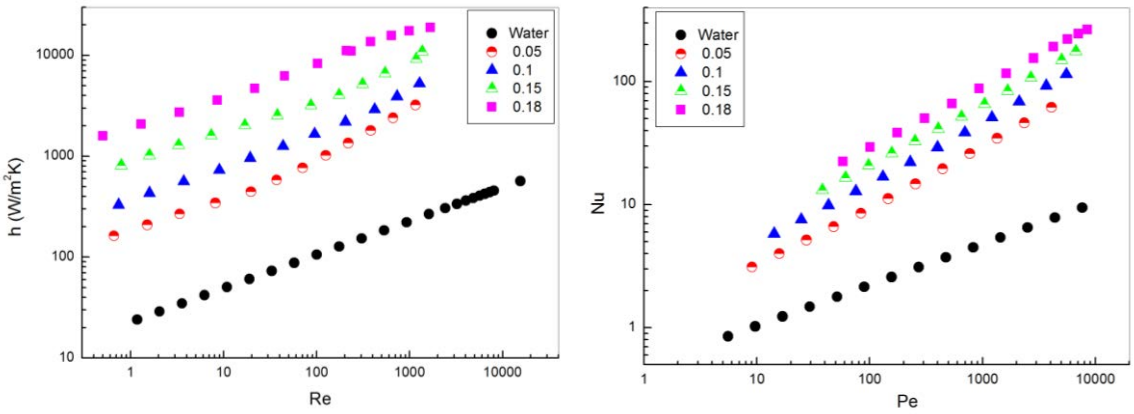

Figure 2. (a) Convective coefficient Vs Reynolds number; (b) Nusselt Vs Peclet. Both graphs at different volume fractions.

Fig. 2a shows the effect of solid particles on the convective coefficient at different *Re*. Fig. 2b exhibits the effect of *Pe* on the *Nu* number at 0.5<Re<1500. The higher the *Re* the better the heat exchange was and the lower the viscosity. At higher *Re* the flow rate of the nanofluid increased, and better mixing of particles was observed (reduction of viscosity), which improved thermal transport properties and caused an enhancement in heat transfer rate. At higher volume fractions the increase in thermal Brownian motion and the migration of particles enhance the Pe number and accordingly the *Nu* number and the convective coefficient, *h*. This can be explained considering that the presence of nanoparticles causes a reduction in the thickness of the particle boundary layer (electric double layer) and produces particle clustering, which also improves the heat transmission [8].

Summary/Conclusions: In this work, the addition of nanoparticles to the base fluid has demonstrated an increase of the efficiency of the heat transfer. In order to have more reliable results the viscosity was measured at different *Re* with a rheometer. The use of alumina suspensions of moderately volume fractions could arise the convective coefficient in more than one order of magnitude. For example, for Φ=0.1 the heat transfer in the Stirling engine increases in a 15-20 %. At higher volume fractions the increase of the nanofluid viscosity may require more pumping power reducing the potential of nanofluids as heat exchangers. For this reason, an optimum concentration of nanoparticles should be used, in order to balance minimum viscosity and high thermal conductivity.

References:

1. Saidur, R., K.Y. Leong, and HaA Mohammad. "A review on applications and challenges of nanofluids." Renewable and sustainable energy reviews 15.3 (2011): 1646-1668.
2. Ganvir, R. B., P. V. Walke, and V. M. Kriplani. "Heat transfer characteristics in nanofluid—a review." Renewable and Sustainable Energy Reviews 75 (2017): 451-460.
3. Huminic, G., & Huminic, A. Hybrid nanofluids for heat transfer applications–a state-of-the-art review. International Journal of Heat and Mass Transfer, 125, (2018) 82-103.
4. Lomascolo, Mauro, et al. "Review of heat transfer in nanofluids: conductive, convective and radiative experimental results." Renewable and Sustainable Energy Reviews 43 (2015): 1182-1198.
5. Kim, Doohyun, et al. "Convective heat transfer characteristics of nanofluids under laminar and turbulent flow conditions." Current Applied Physics 9.2 (2009): 119-123.
6. Saidur, R., K. Y. Leong, and HaA Mohammad. "A review on applications and challenges of nanofluids." Renewable and sustainable energy reviews 15.3 (2011): 1646-1668.
7. Xuan, Yimin, and Qiang Li. "Investigation on convective heat transfer and flow features of nanofluids." Journal of Heat transfer 125.1 (2003): 151-155.
8. Sajid, Muhammad Usman, and Hafiz Muhammad Ali. "Recent advances in application of nanofluids in heat transfer devices: a critical review." Renewable and Sustainable Energy Reviews 103 (2019): 556-592.

1st International Conference on Nanofluids (ICNf2019)
2nd European Symposium on Nanofluids (ESNf2019)
26-28June 2019, Castelló, Spain

Numerical study of the influence of nanofluids on thermal exchange in mini-channels

K. Chadi[1], B. Guerira[2], N. BELGHAR[1], M. Falek[2], C.E. Bensaci[2] and A. Messaoudi[1]

[1]Laboratory of Materials and Energy Engineering LGEM Mohamed Khider University of Biskra 07000, Algeria

[2]Laboratory of Mechanical Engineering, LGM Mohamed Khider University of Biskra 07000, Algeria

Keywords: minichannelscooler, numerical simulation, thermal exchange, nanofluid

Abstract: In the present work, the effect of the nature of the nanofliud and the Reynolds number, on thermal exchange in a silicon mini-channels cooler for cooling electronic components, have been numerically studied Three different types of nanofluids have been considered(Cu-water; Ag-water; Diamond-water), using three dimensional (3D) simulation. In this study, the volumetric fraction of the nanoparticles has been taken 5%, Reynolds number (Re) between 200 and 800 and the flow regime has been assumed to be stationary. The commercial software, ANSYS Fluent 15.0 has been used as a computation tool. The obtained results show that: the maximum temperature of the electronic component decreases with the increasing of Reynolds number. The temperature decrease of the electronic component is most notable for the Diamond-Water nanofluid. The best heat transfer fluid among the studied nanofluids is the one that contains the diamond nanoparticles.

Introduction: Temperature plays an important role in the functioning of electronic components. This temperature can be high enough to reduce in a significant manner the life of the component, to improve this temperature. It is necessary to choose the appropriate liquid for cooling electronic components. Among works in this domain of cooling electronic component, the work donne by C. T. Nguyen et al. [1]. Indeed the authors proceed to an experimental investigation for the enhancement of heat transfer coefficient of Al_2O_3–H_2O nanofluid. They concluded that an increase of particle concentration has produced a clear decrease of the heated component temperature and Increasing nanoparticles in water leads to a significant improvement of heat transfer coefficient, S. S. Khaleduzzaman et al. [2] present an analytical study of the thermal performance improvement of three nanofluids (Al_2O_3-water, CuO-water, SiC-water) for a copper rectangular micro channel heat sink for electronic device cooling. They concluded that CuO-water nanofluid is the most suitable for cooling of electronics among three

nanofluids. The objective of this study is to study the effect of three types of the nanofliuds on the temperature of the electronic component and heat transfer in a silicon mini-channels cooler.

Geometries studied: Figure 1 shows the geometry of the studied mini channels cooler, using fluent industrial software. The dimensions of the mini-channel cooler are of the order of 42 x 52 mm with a thickness of 6 mm. This cooler is formed of 13 channels. The power of the electronic component is equal to 200W with thermal insulation on all the outside faces of the cooler; the inlet temperature of the nanofluid in the cooler is 293K.

Due to symmetry, and in order to reduce the grid size and the computational time, only half of the mini channel has been modeled.

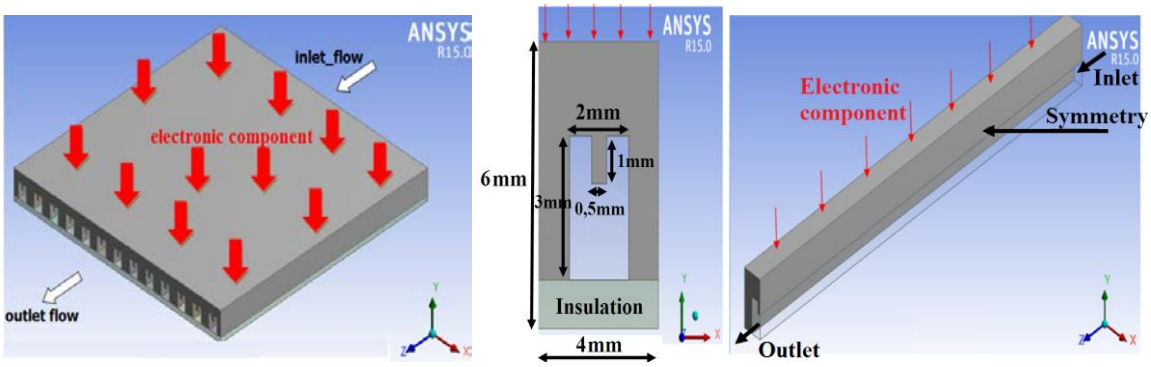

Figure1. Schematic of the mini channels cooler studied and computational domain of mini channel heat sink

Mathematical formulation: In this study, we assumed that the flow is stationary. The three nano-fluids considered are the Cu-water, diamond-water and Ag-water, these nanofluids are supposed to be incompressible and the thermo physical properties of nanofluids are constant. The heat transfer by radiation is considered negligible.

The boundary conditions are:

- zero pressure at the outlet of the mini channels
- the velocity components of the fluid at the level of the channel wall are equal to zero.
- The effect of body force and viscosity dissipation is neglected

The governing equations are conservation of mass, momentum equation, energy conservation equation and equation of the solid [3, 4].

The formulas for the calculation of the thermo-physical properties of the nano fluids used in our work are written as follows:

The effective thermal conductivity of the nanofluid is approximated by Maxwell-Granetts as follows:

$$k_{nf} = \frac{k_S + 2k_f - 2\varphi(k_f - k_s)}{k_S + 2k_f + \varphi(k_f - k_s)} k_f \quad (1)$$

The dynamic viscosity is approximated by Brinkman model as: $\mu_{nf} = \mu_f / (1-\varphi)^{2,5}$ (2)

The density of the nanofluid is given as: $\rho_{nf} = (1-\varphi)\rho_f + \varphi\rho_s$ (3)

The heat capacitance of the nanofluid given as: $(\rho C_p)_{nf} = (1-\varphi)(\rho C_p)_f + \varphi(\rho C_p)_s$ (4)

Results and interpretations: In the simulation, we obtained a convergence for the studied model. The nodes used for meshing of the physical domain are affecting the results. The figure 2 shows the number of nodes used for analysis of mini channel heat sink with result of temperature of the electronic component. According to these figure the results from 1500,000 nodes can be considered to be grid independence.

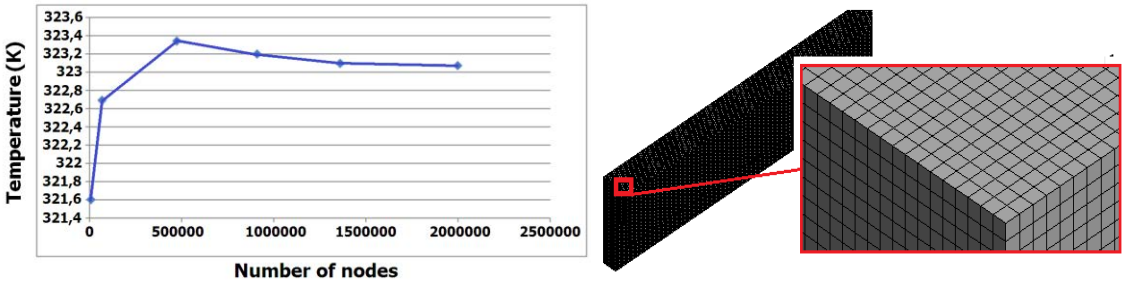

(a) A Temperature vs. number of nodes **(b) Type the mesh: hexahedral (972362 nodes)**

Figure2. Grid independence examination

Figure 3, shows the evolution of the temperature value of the electronic component with respect to the Reynolds number. The temperature decreases substantially for the three types of nanofluids, when the Reynolds number increases. The electronic components have a high temperature for lowest values of Reynolds number and a minimum temperature for highest one. the more effective nanofluid to reduce the temperature of the electronic component among the three coolants is diamond-water

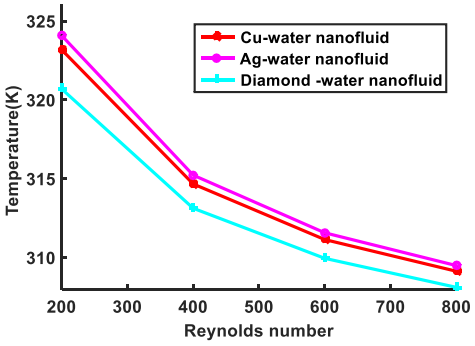

Figure3.The variation of the temperature of the electronic component according to the number of Reynolds

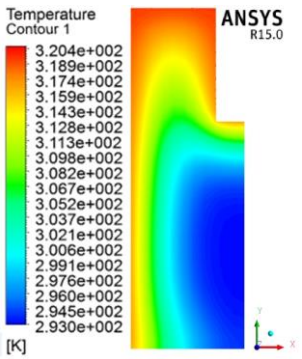

Figure4.The distribution of the temperature in outlet of mini channel for diamond-water

Figure 4 shows that for a Reynolds number equal to 200, and the volume concentration of nanoparticles equal to 0,05, the isotherms become more curved and tighter on the walls of the mini-channel. The comparison between the three nanofluids used shows that diamond has a greater heat transfer than copper Cu and silver Ag, as shown in Figure 5

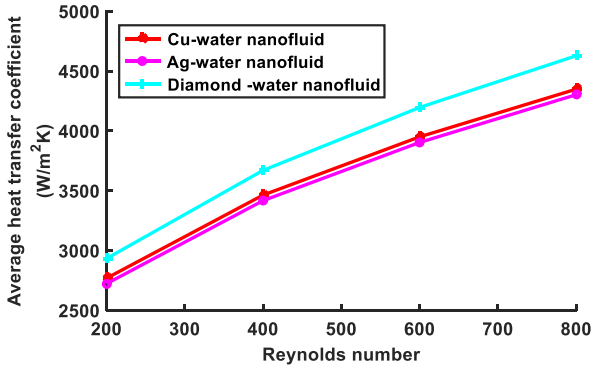

Figure5. The average heat transfer coefficient calculated as a function of the Reynolds number at volume fraction =0,05

Conclusions: In the present work, a numerical study, on the effect of the nanofliud nature on the electronic component temperature and thermal exchange, has been carried out. The obtained results, confirm that the electronic component temperature decreases with the increase of Reynolds number. This decrease of the electronic component temperature is most notable for the nanofluid diamond-Water.

- The use of diamond-water nano-fluid gives significantly higher heat transfer coefficients than water-Ag and water-Cu.

References:

1. C. T. Nguyen, G. Roy, C. Gauthier, and N. Galanis, “Heat transfer enhancement using Al_2O_3-water nanofluid for an electronic liquid cooling system”, Applied Thermal Engineering, vol. 27, no. 8-9, pp. 1501–1506, 2007.
2. S.S. Khaleduzzaman, R. Saidur, Jeyraj Selvaraj, I.M. Mahbubul,M.R. Sohel, I.M. Shahrul“Nanofluids for Thermal Performance Improvement in Cooling of Electronic Device”, Advanced Materials Research Vol 832 (2014) pp 218-223
3. Irnie Zakaria, W.A.N.W Mohamed A.M.I Bin Mamat, R.Saidur, W.H. Azmi , Rizalman Mamat K.I Sainana and H.Ismail, Thermal analysis of heat transfer enhancement and fluid flow for low concentration of Al_2O_3 Water – Ethylene Glycol Mixture Nanofluid in a Single PEMFC Cooling Plate, Energy Procedia79 pp 259–264, 2015
4. Mostafa Keshavarz Moraveji, Reza Mohammadi Ardehali and Ali Ijam, CFD investigation of nanofluid effects (cooling performance and pressure drop) in mini-channel heat sink, International Communications in Heat and Mass Transfer 40 pp58–66, 2013

1st International Conference on Nanofluids (ICNf2019)
2nd European Symposium on Nanofluids (ESNf2019)
26-28June 2019, Castelló, Spain

Numerical study of the thermal transfer in different geometries of the mini-channels

K. Chadi[1], N. Belghar[1], B. Guerira[2], M. Falek[2], C.E. Bensaci[2] and A. Messaoudi[1]

[1]Laboratory of Materials and Energy Engineering LGEMMohamed Khider University of Biskra 07000, Algeria

[2]Laboratory of Mechanical Engineering,LGM Mohamed Khider University of Biskra 07000, Algeria

Keywords: thermal transfer, cooler, minichannels, numerical simulation, nanofluid

Abstract: In the present work, a numerical study of the thermal exchanges between different geometries of a cooler mini channels of dimensions (21 × 21 × 3.5 mm^3) has been carried out. Three different shapes have been considered to cool an electronic component of dimensions (100 × 0.25 mm^3) using a nanofluid (Cu-water) as a coolant. The simulation has been carried out using the software ANSYS Fluent. Reynolds number (Re) has been taken between 300 and 1500 and the flow regime has been assumed to be stationary. The obtained results for the three proposed forms of mini-channels shows that the increase of the exchange surface between the walls of the mini-channels and the cooling fluid leads to the increase of the thermal transfer coefficient and to the improvement of the maximum of the electronic component junction temperature by increasing the value of Reynolds number

Introduction: The improvement of heat transfer is directly related to factors like the Reynolds number, materials thermal properties, geometric forms and dimensions. Several works have been carried out in this field. P. Gunnasegaran et al. [1] undertook a numerical study on the effect of geometric parameters on the heat transfer characteristics, for three different forms of micro-channels (rectangular, trapezoidal and triangular). They concluded that the heat transfer coefficient and the Poiseuille number increase with the increase of Reynolds number. Heat transfer coefficient and Poiseuille number have the highest values in case of rectangular form. However, for the micro channels of triangular form they have the weakest one. The intermediate values have been obtained for the micro channels of trapezoidal form. The results of a numerical simulation [2] using the Ansys-Fluent thermal characteristics software for a mini-channel radiator structure show that the maximum temperature and the thermal resistance, decrease with the increase of the speed of the flow. Muhammad Saeed et al. [3] present a numerical and experimental investigation on the heat transfer enhancement

characteristics using three different volume concentrations of nanoparticles Al_2O_3 in water as a base fluid, and with four different channel configurations of mini-channel heatsink. They observed that the convective heat transfer coefficient of the heat sink with fin spacing. And they observed also that enhancement factor increases by dreading the fin spacing (hydraulic diameter) of the flow channel at the same value of volume concentration and coolant flow rate.

Studied Geometries: The geometry of the mini channel of the cooler is represented by Figure. 1 Three different shapes using a fluent software.15 have been studied. The dimensions of the cooler are in the order of 21 x 21mm^2 with a thickness of 3.5 mm. This cooler is composed of 10 channels and 11 fins, we impose the maximum flux of the electronic component is constant with thermal insulation on all external faces of the cooler, The inlet temperature of the nanofluid in the three cases of the mini channels is set at 298.15K. For reasons of symmetry, only half of the cooler have been simulated.

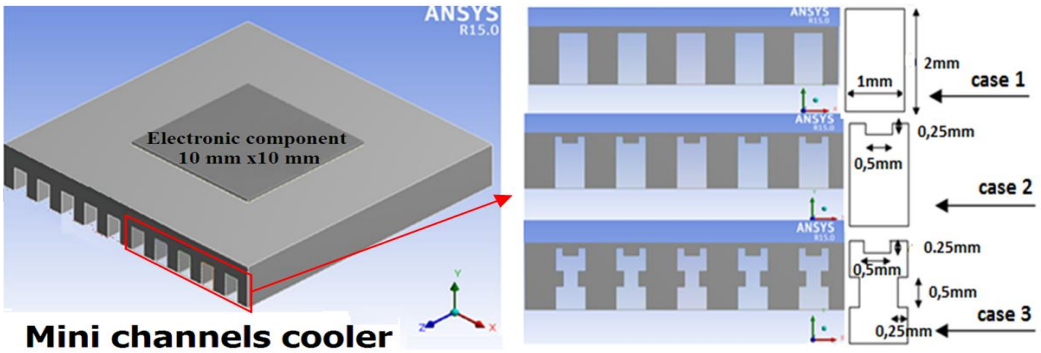

Figure 1. The different cases of the studied mini-channels

Mathematical formulation: In this study, we assumed that the flow is stationary. The base fluid is supposed to be Newtonian and incompressible. The thermo physical properties of the nano-fluid are taken as constant. The radiation heat transfer is negligible.

The boundary conditions are: Zero pressure at the outlet of the mini channels.

- The velocity components of the fluid at the level of the channel wall are equal to zero, and no-slip boundary conditions are applied to all micro channel walls.
- The effect of body force and viscosity dissipation is neglected.
- At the inlet, the speed and the temperature of fluid are constant (V_{in}=Re*μ/ρ*D_h)

Governing equations are given in term mass conservation equation, momentum equation, energy conservation equation and solid equation [4].

The formulas for the calculation of the thermo-physical properties of the nano fluids used in our work are written as follows: The effective thermal conductivity of the nanofluid is approximated by Maxwell-Granetts as follows: $k_{nf} = \frac{k_S+2k_f-2\varphi(k_f-k_s)}{k_S+2k_f+\varphi(k_f-k_s)} k_f$ (1)

The dynamic viscosity is approximated by Brinkman model as: $\mu_{nf} = \mu_f / (1-\varphi)^{2,5}$ (2)

The density of the nanofluid is given as: $\rho_{nf} = (1-\varphi)\rho_f + \varphi\rho_s$ (3)

The heat capacitance of the nanofluid given as: $(\rho C_p)_{nf} = (1-\varphi)(\rho C_p)_f + \varphi(\rho C_p)_s$ (4)

Results and interpretations: The mesh is realized using the fluent software 'Meshing'. After convergence of the calculations of the simulation, the results are represented as follows: Figure. 2 shows the variation of the temperature of the upper surface of the mini-channel cooler of the second case along the plane of symmetry for the different meshes applied. Therefore conclude that the solution is independent of the mesh.

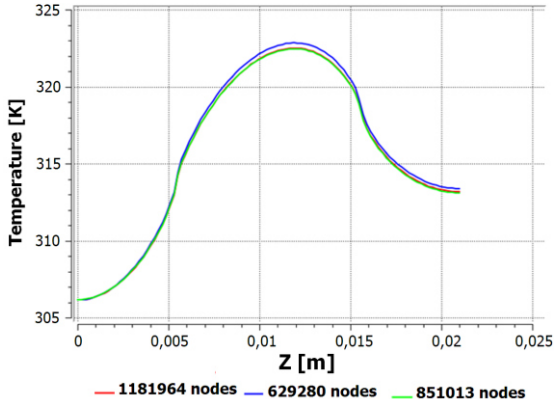

Figure 2. Influence of the mesh on the temperature of the upper surface of the mini-channel cooler of the 2nd case

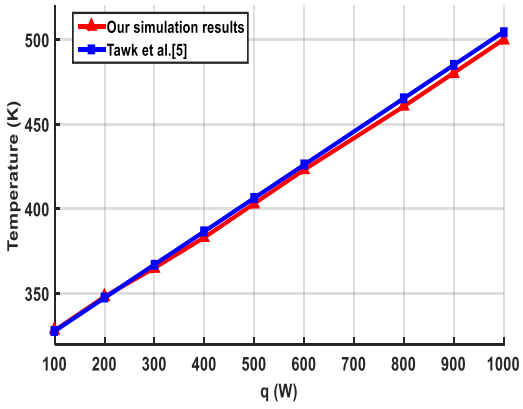

Figure 3. The temperature according to the power dissipated in the chip

Figure 3 shows a comparison of the temperature of this simulation with earlier experimental study [5]. A good agreement was obtained for the cooler case of copper and water (such as liquid cooling). We notice that the temperature increases with the increase of the power dissipated in the chip.

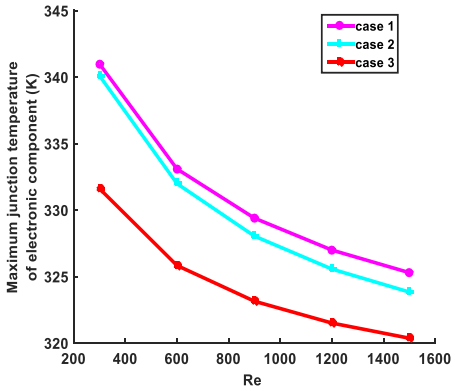

Figure 4. The values maximum junction temperature of electronic component obtained by simulations for a volume concentration of Cu-water nanofluid of 0.05

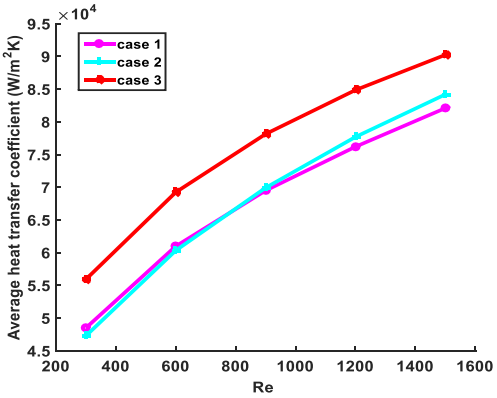

Figure 5. The average heat transfer coefficients as a function of the Reynolds number for a volume fraction of 0.05

Figure.4 shows the evolution of the maximum junction temperature of electronic component as a function of the Reynolds number. It is observed that the profile of the junction temperature decreases substantially for the three cases of the mini-channels when the Reynolds number increases. The temperature of the electronic component has the highest values for low values of Re. Figure5 shows the average heat transfer coefficient calculated as a function of Reynolds number for a volume fraction of 0.05, the average heat transfer coefficient is proportional to Reynolds number, varying from 300 to 1500. The comparison of the obtained results of the three studied cases of mini-channels, shows that the average heat transfer coefficient of the mini-channel of the third case is greater than those of the mini-channels of the first and second cases.

Conclusions: In the present work, the thermal exchanges of the different geometries of the mini channels of a cooler has been studied numerically, using the Fluent 15.0 software, according to the obtained results, it can be concluded that for the three cases of the mini-channels and with a Reynolds number between 300 and 1500, the mini-channels of the third case improve the heat transfer compared to the other cases as well as the value of the maximum temperature of the junction of the electronic component.

References:

1. C P. Gunnasegaran, H.A. Mohammed, N.H. Shuaib, R. Saidur, The effect of geometrical parameters on heat transfer characteristics of microchannels heat sink with different shapes, International Communications in Heat and Mass Transfer 37 pp 1078–1086, 2010.

2. Jing Hongqi, Zhong Li, Ni Yuxi, Zhang Junjie, Liu Suping, and Ma Xiaoyu, Design and simulation of a novel high-efficiency cooling heat-sink structure using fluid-thermodynamics, Journal of Semiconductors, Vol. 36, No. 10,October 2015
3. Muhammad Saeed, Man-Hoe Kim, Heat transfer enhancement using nanofluids (Al2 O 3 -H2 O)in mini-channel heat sinks, International Journal of Heat and Mass Transfer 120 ,671–682, 2018
4. Mostafa Keshavarz Moraveji, Reza Mohammadi Ardehali and Ali Ijam, CFD investigation of nanofluid effects (cooling performance and pressure drop) in mini-channel heat sink, International Communications in Heat and Mass Transfer 40 pp58–66, 2013
5. Yvan Avenas, Afef Kedous-Lebouc, David Charalampous, Emanuelle Dubois, Jean Chevalet, Mansour Tawk, Study of a system of cooling of electronic components of power by liquid metal, University of Pierre and Marie Curie, Paris VI, 2010

1st International Conference on Nanofluids (ICNf2019)
2nd European Symposium on Nanofluids (ESNf2019)
26-28 June 2019, Castelló, Spain

Stability of molten salt nanofluids under industrial operation conditions

P. Giménez-Gavarrell[1*], S. Fereres[2] , and M. Zurita-Gotor [2, 3]

[1]School of Engineering, University of Seville, Spain

[2]Abengoa Innovación, 41014, Seville, Spain

[3]Universidad Loyola Andalucia, Energía Solar 1, 41014 Seville, Spain

[*]Corresponding author: pgimenez7@us.es

Keywords: thermal energy storage, nanofluids, molten salts, dispersion stability

Abstract: This study experimentally investigates the dispersion stability of high temperature molten salt based nanofluids after repeated freezing and thawing cycles through successive measurements of specific heat and phase change characteristics of the colloids. The dispersion of nano-salt based PCM during the energy storage and release processes were investigated with an experimental setup where small cylindrical vials (1.5 ml) filled with the nano-PCM samples are heated in direct contact melting on a hot plate. The experiments show a visible convective flow within the nanofluid, where particles are aggregated to micron-size clusters moving in a clearly buoyant flow. No previous studies have shown the evolution of the initially well-dispersed nanoparticles in high temperature nanofluids after several freezing and melting thermal cycles.

Introduction/Background: Solar thermal power plants are an attractive renewable energy option for electricity generation as long as they incorporate economical and efficient thermal energy storage, allowing electricity production beyond daylight hours. Thermal energy storage can involve two primary mechanisms: sensible heat, where the storage capacity is directly proportional to the material´s temperature and specific heat, and latent heat storage (PCM), using the phase change transition to store heat.

One of the basic shortcomings of PCM is their low thermal conductivity, typically less than 1 W $(m\ K)^{-1}$ [1]. This leads to insufficient heat exchange rates in thermal energy storage systems, where power is as important as the amount of energy stored. Enhancing the heat transfer characteristics of PCM through the addition of nanoparticles has been the subject of increased research in the past decades [2-4], since the improvement of their thermo-physical properties and performance is critical to their adoption. However, sometimes this property enhancement is not observed, its magnitude varies significantly among different authors and it is not maintained over time. Nanoparticles may increase the material´s thermal conductivity [4], decreasing the

storage charge and discharge time. The specific heat [5-8] and the phase change properties (melting point and latent heat) [8-11] are other thermo-physical properties that may be modified by the addition of nanoparticles.

The applicability of these colloids at a large scale is highly dependent on the nanoparticle dispersion stability. Limited experiments have investigated the stability of the nanoparticle suspension and if these modified property values can be easily maintained during thermal cycling and operation. The objective of this work is to investigate heterogeneities in the molten salt nanofluids due to particle agglomeration. This might be crucial in PCM systems, subjected to daily freezing/thawing cycles during operation, as well as in molten salt sensible storage system. We evaluate the effect of adding different types of metal oxide nanoparticles (1 wt. %) to the binary nitrate system KNO_3-$NaNO_3$ commonly used in solar thermal plants by testing the eutectic mixture (49% $NaNO_3$ by mol).

Materials and methods: sodium and potassium nitrate eutectic mixture (49 mol% $NaNO_3$) has been used as the base salt, prepared using laboratory grade $NaNO_3$ and KNO_3 (99+%, Acros Organics). A series of near-spherical metal oxide nanoparticles (SiO_2 (Io-li-tec nanomaterials, 10-20 nm, 99+%), CuO (Io-li-tec nanomaterials, 40-80 nm, 99.9%), Al_2O_3 (Aldrich Chemistry, 13 nm, 99.8%)) are used to produce the nanoparticle dispersions. The concentration of the different nanoparticle types was fixed to 1 wt. %. The nanofluid synthesis procedure to prepare the salt mixture with the different nanoparticle types is a two-step water solution method as described in [5, 6].

To assess the dispersion quality of the nanofluid PCM powder in its operational state small cylindrical vials filled with the nano-salt samples were heated from below in a direct contact melting on a hot plate. Differential Scanning Calorimeter (DSC) (Q2000, TA-Instruments) was used for the analysis of the solid/liquid phase change properties.

Discussion and Results: Figure 1 shows the nanoparticle dispersions during the water-solution step after sonicating the dissolved nanofluids and after the evaporation process. The main difference between the three nanoparticle dispersions synthesized while they are dissolved in water is the colour of the sonicated solution. While SiO_2 and Al_2O_3 make the salt-water solution slightly whiter and less transparent, CuO presents brownish translucent solution. After sonication, the nanofluids are stable homogeneous mixtures. Note that a good nanoparticle dispersion during the synthesis water solution step in addition to subsequent solid phase SEM images have been typically used to assess the nanofluid particle dispersion quality.

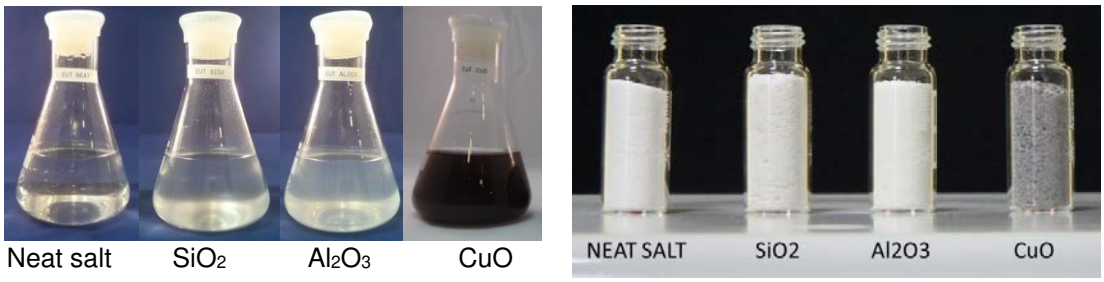

Figure 1. Neat salt and nanofluids: dissolved in water after sonication step (left); nanofluid powder after solvent water evaporation, grinding & mixing (right)

The hypothesis proposed is that a similar appearance to the dissolved nanofluid would be expected for the molten salt nanofluid indicating a uniform nanoparticle. However, Figure 2 shows a visible convective flow within the molten nanofluid at 350ºC, where particles are aggregated to micron size clusters moving in a clearly buoyant flow. These observations in molten state are completely different from the homogeneous dispersion in the initial water solution.

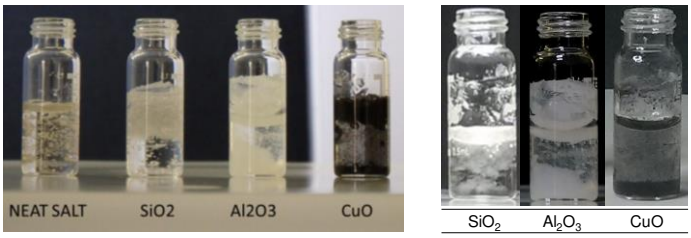

Figure 2. Molten nano-enhanced PCM at 350ºC: during the first melting (left), after 6 melting and freezing cycles (right)

Figure 3 shows the phase change characteristics of the nanofluids measured with DSC after several freezing and melting thermal cycles. There is great variability in the latent heat measurement depending on melting cycle and particle type. The specific heat of the modified molten salt nanofluids shows a moderate enhancement in the first cycle, although it is within the measurement uncertainty. After several melting/thawing cycles, the specific heat decreases for SiO_2 samples, and slightly increases for Al_2O_3 nanofluids, suggesting particle-salt interactions might be responsible for these variations and they do not seem stable throughout thermal cycling.

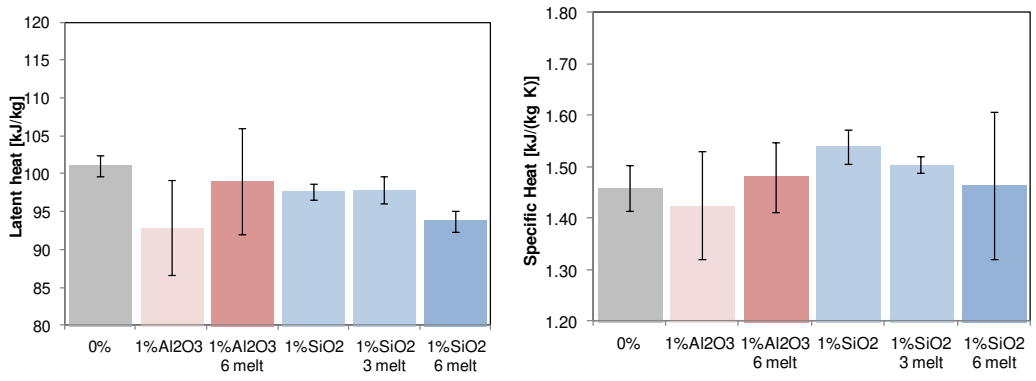

Figure 3. Melting latent heat (left) and specific heat at 350ºC (right) of neat salt and nanofluids after several melting and freezing cycles.

Summary/Conclusions: A series of experiments analyzing the macroscopic behaviour of the molten eutectic $NaNO_3$-KNO_3 mixture adding 1 wt. % of different nanoparticle types (SiO_2, CuO, and Al_2O_3) has been performed investigating whether different types of nanoparticles can be kept homogeneously dispersed in nitrate base molten salts after several melting and freezing cycles. The qualitative results presented in this paper show that, although well-dispersed when all components are dissolved in water, nanoparticles tend to agglomerate and stratify even during the first melting cycle. None of the nanofluids tested are able to maintain the stability of the nanoparticle suspension in liquid form. The results clearly indicate that more effort is needed to design a stable, functional, and realistic heat transfer nanofluid for any engineering application which should include supplementary mixing mechanisms.

References:

1. A. Sharma, et al., *Review on thermal energy storage with phase change materials and applications*, Renew. Sust. Energ Rev. 13 (2009) 318-345.
2. J. Buongiorno et al., *A benchmark study on the thermal conductivity of nanofluids*, J. Applied Physics (2009) 106 094312.
3. X.Q. Wang and A.S. Mujumdar, *Heat transfer characteristics of nanofluids: a review*, Int J Thermal Sciences (2007) 46 1–19.
4. J.M. Khodadadi et al., *Thermal conductivity enhancement of nanostructure-based colloidal suspensions utilized as phase change materials for thermal energy storage: A review*, Renew. Sust. Energ Rev. 24 (2013) 418–444.
5. D. Shin and D. Banerjee, *Enhanced Specific Heat of Silica Nanofluid*, J Heat Transfer 133 (2011) 024501.
6. B. Dudda and D. Shin, *Effect of nanoparticle dispersion on specific heat capacity of a binary nitrate salt eutectic for concentrated solar power applications*, Int J. Thermal Sciences 69 (2013) 37-42.
7. M. Chieruzzi, et al., *Effect of nanoparticles on heat capacity of nanofluids based on molten salts as PCM for thermal energy storage*, Nanoscale Res. Lett 8 (2013) 448
8. A. Zabalegui, D. Lokapur and H. Lee, *Nanofluid PCMs for thermal energy storage: Latent heat reduction mechanisms and a numerical study of effective thermal storage performance*, Int J Heat Mass Tran 78 (2014) 1145–1154.
9. P. Gimenez-Gavarrell et al., *Latent Heat of Fusion and Melting Temperature of Molten Salt Based Carbon Nanotube Suspensions used as Phase Change Materials*, Proc. 9th ASME Int Conf Energy Sustainability (2015), San Diego, USA.

1st International Conference on Nanofluids (ICNf2019)
2nd European Symposium on Nanofluids (ESNf2019)
26-28 June 2019, Castelló, Spain

Nanoemulsion absorbents for CO_2 absorption application

Seonggon Kim[1], Ronghuan Xu[1], Wonhyeok Lee[1] and Yong Tae Kang[1*]

[1]School of Mechanical Engineering, Korea University

145 Anam-ro, Seongbuk-gu, Seoul 02841, Republic of Korea

[*]Corresponding author: sa7122@korea.ac.kr

Keywords: CO_2 absorption, Dodecane, Nanoemulsion, Methanol.

Abstract: One of the CO_2 capture technologies, the physical absorption is widely used. According to the Henry's law, the physical absorption system must be operated at very low temperature (-40°C), and a large freezing energy is required. The objective of this study is to develop novel nanoemulsion absorbents that can operate at room temperature. The dodecane/methanol nanoemulsion absorbents are fabricated by the ultrasonication method. The CO_2 absorption performance of nanoemulsion absorbents (0.01-0.1 vol%) is evaluated using a porous nozzle absorber at room temperature (25°C). As a result, 0.05 vol% nanoemulsion absorbents show the highest CO_2 absorption rate, which is 10% higher than that of pure methanol. The enhancement mechanisms of CO_2 mass transfer are explained based on the Einstein-Stokes' equation and the average droplet size of dodecane droplets. It is found that the nano-sized dodecane droplets (smaller than 100 nm) transport the CO_2 molecules to the low concentration region by the Brownian motion.

Introduction: Due to the the global warming problem, many researchers focus on the CO_2 treatment technology, which is called as carbon capture and storage (CCS). Among the CO_2 capture methods, the physical absorption is widely used. However, according to the Henry's law, it must be operated at very low temperature (-40°C) and the large freezing energy is required. The absorption performance should be improved so that it can operate at room temperature. To do this, nanofluids have been developed in which nano-sized solid particles are dispersed in the base fluid, which is methanol in this study. CO_2 absorption and regeneration performance of nanofluids is found to be significantly higher than that of pure methanol [1, 2]. Even though the performance is enhanced, there are critical problems that particles may cause the clogging or corrosion problems. In this study, dodecane/methanol nanoemulsion absorbents are developed to solve these problems, in which nano-sized oil droplets are dispersed instead of solid particles.

Experiment: Dodecane/methanol nanoemulsion absorbents are prepared by using ultrasonication method. Considering the chemical conditions of the hydrocarbon (dodecane), Span 60 and Tween 60 are added to absorbents, and mixed at a ratio of 4:6 to match hydrophile-lipophile balance (HLB). The schematic of the CO_2 absorption experiment is shown in Figure 1. CO_2 is supplied from the CO_2 tank (1), and steady conditions are maintained by the regulator (2), mass flow controller (3), and thermostat (7). In the absorber (4), the absorbents are maintained at a constant temperature by the thermostat (7). As CO_2 flows to the absorber by the porous nozzle, the absorption occurs. The unabsorbed CO_2 is discharged to the purifier (5), and the mass flow rate is measured. The detailed experimental conditions are summarized in Table 1.

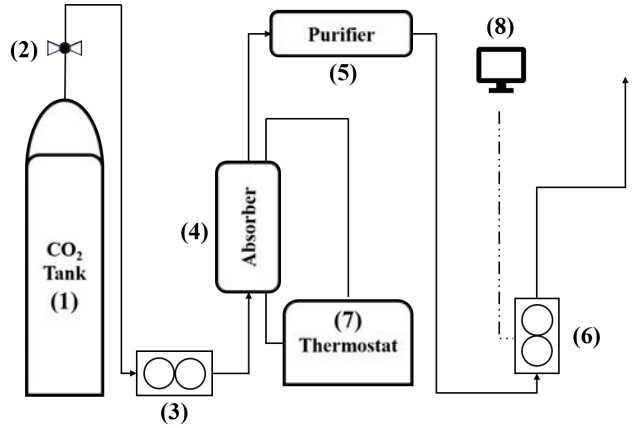

Figure 1. The experimental apparatus of CO_2 absorption test

Table 1. Experimental conditions of the CO_2 absorption test

CO_2 inlet flow rate	0.06 g/s
Initial conditions of CO_2	3 bar and 25°C
Dodecane concentrations	0.01-0.1 vol%
Absorber temperature	25°C
Measurement interval	4 s

Discussion and Results: Figure 2 shows the results of CO_2 absorption experiments. When the concentration of nanoemulsion absorbents is 0.05 vol%, the CO_2 absorption rate is the highest, which is 10% higher than that of pure methanol. The enhancement mechanisms of CO_2 mass transfer are explained by two steps. First, the nano-sized dodecane droplets are attached to the CO_2 molecule. Then, dodecane droplets diffuses

by the Brownian motion effect, which makes CO_2 molecule to migrate quickly to the low concentration region. As shown in Figure 3, the cryogenic transmission electron microscope is taken to verify that the dodecane droplets and CO_2 molecule stick together. Instead of CO_2 molecule, the SiO_2 nanoparticles (15 nm) are used. It exists in the form of networks structure and is non-polar, which is same as CO_2. As a result, it is reasonable to consider that dodecane droplets attach to the CO_2 molecule. The Brownian motion of dodecane droplets can be calculated by the Einstein-Stokes' diffusion and the average droplet size (Figure 4). When the concentration is lower than 0.05 vol%, the average droplet size is almost constant. On the other hand, the size increases significantly after 0.05 vol%. As droplet size increases, the Brownian diffusion coefficient decreases, and the mass transfer enhancement is reduced.

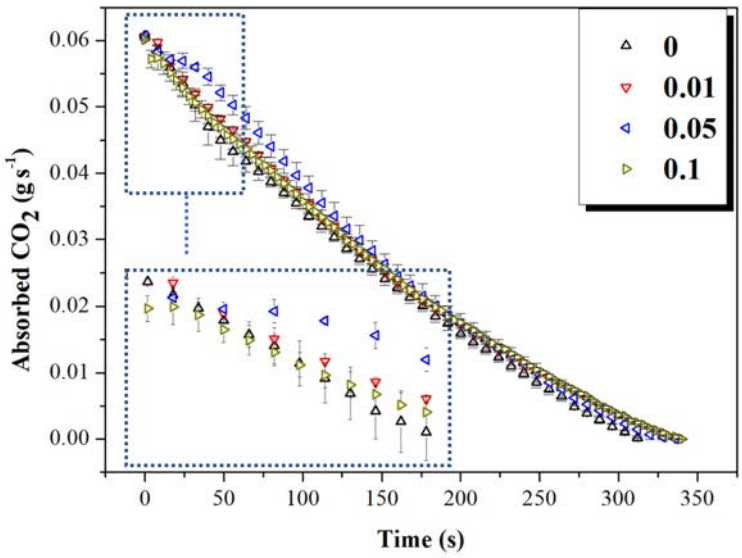

Figure 2. CO_2 absorption performances of nanoemulsion absorbents. CO_2 flow rates are 0.06 g/s

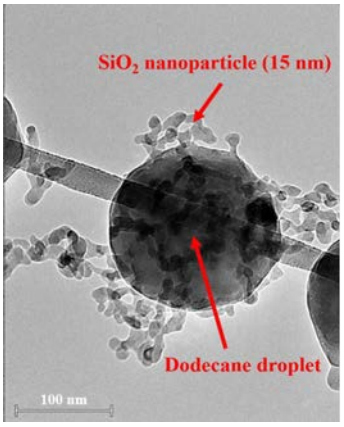

Figure 3. Cryogenic transmission electron microscope image of the nanoparticles and dodecane droplets in the methanol.

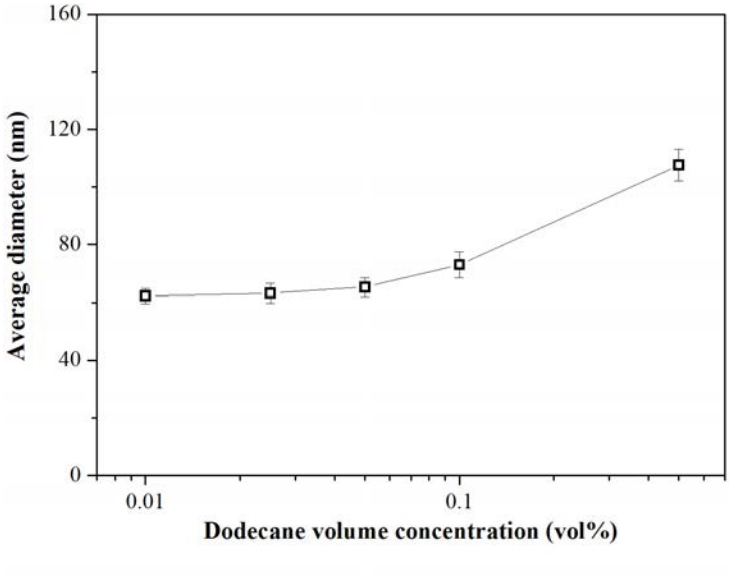

Figure 4. Average diameter of dodecane droplets

Summary/Conclusions: Dodecane/methanol nanoemulsion absorbents are prepared by using the ultrasonic emulsification method. Considering the chemical conditions, Span 60 and Tween 60 are added to the absorbents and mixed at a ratio of 4:6. The CO_2 absorption performance is evaluated using a porous nozzle absorber for various dodecane concentration (0.01-0.1 vol%). As a result, 0.05 vol% nanoemulsion absorbents show 10% enhanced performance compared with pure methanol. The mass transfer enhancement can be explained by the Einstein-Stokes' diffusion, average droplet size and cryogenic transmission electron microscope image.

References:

1. I. Tm Pineda, D. Kim and Y.T. Kang, Mass transfer analysis for CO_2 bubble absorption in methanol/Al2O3 nanoabsorbents, *International Journal of Heat and Mass Transfer* 114 (2017): 1295-1303.
2. J. W. Lee, I. T. Pineda, J.H. Lee and Y.T. Kang, Combined CO_2 absorption/regeneration performance enhancement by using nanoabsorbents, *Applied Energy* 178 (2016): 164-176.

1st International Conference on Nanofluids (ICNf2019)
2nd European Symposium on Nanofluids (ESNf2019)
26-28 June 2019, Castelló, Spain

Benefits of the Arbitrary Shaping of Fiber Laser Pulse Properties in the Pulsed Laser Ablation on Liquid Technique

A. Almagro-Ruiz[1*], V. Otgon[1], A. Ortigosa-Claveria[1], J. Abreu-Afonso[1], P. Pérez-Millán[1]

[1] FYLA LASER S.L. Ronda Guglielmo Marconi, 12, 46980 Paterna, Valencia.

[*]Corresponding author: aalmagro@fyla.com

Keywords: Boiling, Ultrafast fiber lasers, nanoparticles, PLAL.

Abstract:

An optical fiber laser of ultrashort-ultraintense pulses (up to 50 W of average power) is presented as a potential and versatile tool for synthesizing nanoparticles through the Pulsed Laser Ablation on Liquids (PLAL) technique. FYLA PS50 is a 1064 nm pulsed laser with selectable pulse properties. The time width and the repetition rate of the emitted pulses can be tuned from 400 ps to 400 fs and from 20 MHz to 500 kHz, respectively. The laser system includes the option of emission of a single pulse and of arbitrary bursts of pulses. New advances on nanoparticles growth through the PLAL technique can be boosted by this availability to arbitrarily shape the parameters of exposition to radiation of the samples from a single laser source.

Introduction/Background:

Interest of technological applications of nanomaterials in fields like medical diagnosis, biology or energy is growing steadily. In these applications nanoparticles are used to induce specific effects over different materials. For this, the nanoparticles have to present certain surface activity, which has to be achieved irrespective of the production method of the nanoparticles. Some of the usual production methods as chemical synthesis or gas-phase processes introduce impurities which reduce the desired performance of the nanoparticles [1]. When the solid targets used to synthesize the nanoparticles are immersed in liquid less impurities are introduced. The nanoparticles grown in the liquid are stabilized straight into the solvent and, depending on the chosen solvent, it is also possible to change the properties of the synthesized nanoparticles. Thus, since PLAL is performed with the targets immersed in liquids, the stability or size distribution can be changed (e.g., adding surfactants to the liquid), enabling the synthesis of nanoparticles on a wide range of materials [2]. The growth of the

nanoparticles depends strongly on the composition of the solid target and on the laser parameters, since the nucleation of the nanoparticles depends on the light-matter interaction processes. Previous studies have found that the productivity on the growth of nanoparticles increases with the repetition rate of the pulsed laser emission. The ablation efficiency increases with wavelength, whilst fluence and pulse duration change the amount of generated nanoparticles and their morphology, respectively. Furthermore, fluence can affect nanoparticles already synthesized in a re-ablation process if irradiation time is long enough.

PLAL occurs when an ultrafast pulsed laser interacts with the target material immersed in a liquid and creates a hot and dense plasma from the evaporated material [2]. The process can be thermal or non-thermal depending on the pulse duration. If the temporal width is higher than the time in which energy transfer from carriers to the target lattice occurs, then it is a thermal process. The thermal process that allows enough mass removal is phase explosion (explosive boiling). This leads to homogeneous nucleation and the creation of vapor bubbles which collapse releasing ligand-free nanoparticles in the liquid medium.

Therefore, the PS50 optical fiber laser is an optimum tool for the arbitrary design of properties of synthesized nanoparticles by the PLAL technique, since such properties depend on laser parameters that can be changed arbitrarily in this laser.

Discussion and Results:

The PS50 laser we developed could be a versatile PLAL tool as it has tunable optic-temporal properties thanks to its different modules at high average powers. Designed as fiber optic laser, it is a compact solution which allows users to have pulse temporal widths from 400 ps to 400 fs. Selection of the pulse duration is achieved through a stretching/compressor pair which varies the introduced dispersion. Tunable Pulsed Stretcher (TPSR) introduces a certain amount of chirp which is then compensated with the same amount but different sign of chirp introduced by the compressor. Both are Bragg Grating based elements: TPSR uses a Fiber Bragg Grating (FBG) of temperature-dependent variable dispersion. The compressor introduces chirp through a Volume Bragg Grating (VBG). It is designed in double pass configuration (fig. 1) so that a smaller VBG can be used to reduce the compressor size.

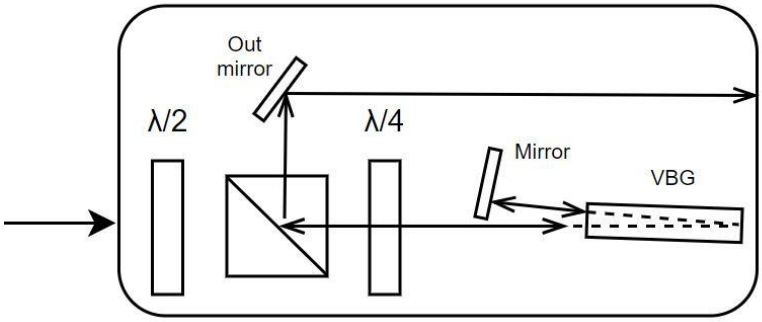

Figure 1. Scheme of the VBG temporal compressor.

About the burst module, it allows to set a single-shot configuration or to select a train of pulses to reach the solid target. With a fast-acousto-optic modulator of crystal quartz, it is possible to pick just one pulse or set a temporal window to let pass a desired number of pulses at the repetition rate selected from 500 kHz to 20MHz. This is an excellent property in PLAL applications as it makes it possible to study the effects on synthesized nanoparticles related to the number of pulses.

Summary/Conclusions: To conclude, we have presented a high-power laser for PLAL nanoparticle generation that offers arbitrary shaping of the properties of its emitted pulses. It is all-fiber designed, cost effective and compact. Thanks to those characteristics, research on effects of pulse duration and number of pulses on the PLAL technique can be done, providing different synthesizing options with just one tool.

References:

1. S. Barcikowski and G. Compagnini, Advanced nanoparticle generation and excitation by lasers in liquids, *Physical Chemistry Chemical Physics* 15 (2013), 3022-3026.
2. J. Lam, *Pulsed Laser Ablation on Liquids: towards the comprehension of the growth processes*, Université Claude Bernard – Lyon I, France, 2015.

SESSION 9
Health, Safety and Environment

S9

1st International Conference on Nanofluids (ICNf2019)
2nd European Symposium on Nanofluids (ESNf2019)
26-28 June 2019, Castelló, Spain

NanoSafety – A survey on the safety of nanofluid use

J. Kaur[1,3], L. Hernandez[2] and M.H. Buschmann[3*]

[1]Hochschule für Technik und Wirtschaft Dresden, Friedrich-List-Platz 1, 01069 Dresden, Germany

[2]Departamento de Ingeniería Mecánica y Construcción, Universitat Jaume I, Castelló de la Plana 12071, Spain

[3]Institut für Luft- und Kältetechnik gGmbH Dresden, 01309 Dresden, Germany

[*]Matthias.Buschmann@ilkdresden.de

Keywords: nanoparticles, nanofluids, safety, survey

Abstract: The first results of a survey conducted on safety of nanoparticles/nanofluids handling are presented. One of the major findings is, that despite the participants being very much aware of the risks related to nanofluids, hardly any specific regulations exist to avoid these risks.

Introduction: Nanofluids offer new options to improve heat transfer [1]. However, as most new technologies nanofluids are related to certain risks that have not been specified yet and demand special regulation. Within the framework of the COST Action CA15119 NanoUptake [2] a survey has been carried out in October 2018, including institutions from 19 countries, majority being from Europe. Goal is to investigate how the risks related to nanofluids are estimated, which measures are undertaken to handle them and if special regulations exist for treating nanoparticles/nanofluids in laboratories. The survey consists of 45 questions divided into 6 sections, which are sent to about 220 individuals. The answers received from 68 participants are analysed and presented here. It must be emphasised, that these results do not necessarily give a complete picture of the institutions/countries involved. However, it is expected that the survey is a sufficient sample out of the population and gives reliable information.

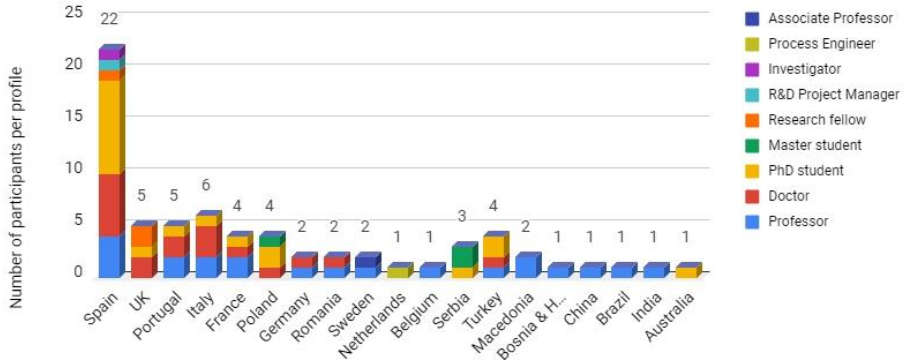

Figure 1. Country wise distribution of participants

Results: Figure 1 gives the country wise distribution of participants. Out of these 60 (88.2%) participants deal with nanoparticles/nanofluids. The overall trend in the survey shows that more than half of the participants (61.7%)[1] are of the opinion, that nanoparticles/nanofluids both pose a risk to human's health. About 18.3% of the participants are of the opinion that only nanoparticles are harmful. Just one participant believes, that only nanofluids are injurious to health. Another 18.3% of the participants are unsure of the health risks. No participant is of the view, that neither nanoparticles nor nanofluids are harmful.

For a similar analysis for environmental risk, 65% hold the opinion that both nanoparticles and nanofluids pose an environmental risk. However, the level of unsurety is really high. Around 28.3% of the participants believe, that nanoparticles/nanofluids may or may not cause risk to environment. Merely three people hold the view that only nanoparticles are harmful. None of the participants credit nanofluids for posing risk to environment. One participant believes, that neither nanoparticles nor nanofluids are harmful to the environment.

Figure 2 indicates, the share of participants with (53.3%) and without (46.7%) health and safety regulations in their institution and the results are almost comparable. Some institutions do not have health and safety regulations so far. It becomes clear from the survey, that most of the organisations do not provide special health and safety training to their employees. In Spain alone, only 43% of all participating organisations have health and safety training. Portugal, Poland, Romania, Sweden, Belgium, Turkey, Macedonia, India and Australia provide no provision for training at all. Similarly the question with respect to criteria for risk assessment indicates, that majority of the institutions do not have any criteria. Only 38.3% of the participants have risk assessment criteria of which majority are from Spain and the UK. About 47% of all countries involved do not to have any criteria.

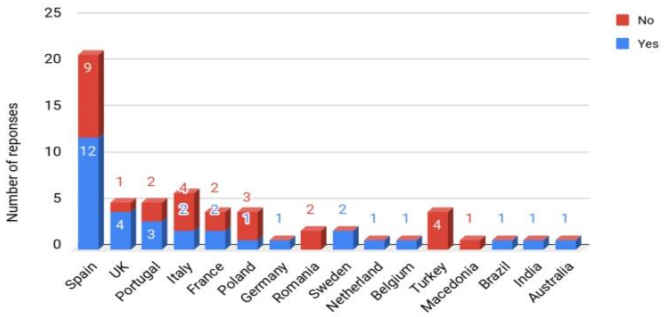

Figure 2. Existence of health and safety regulations

[1] Note all percentages are related to the number of 68 responses obtained. There are cases with no response at all, whereas some had multiple answers. Therefore, completion to 100% based on the data given might not be possible in all cases.

The survey indicates, that the amount of nanoparticles/nanofluid handled by the different institutions spans a wide range from nothing (theoretical/numerical research only) to 1 kg/month (nanoparticles) and 26 l/per month (nanofluids) respectively. The majority of the participants (65%) think that inhalation is a main route of exposure to nanoparticles, followed by the dermal route (44%) and ingestion (13%). About 66% of the participants responded that the dermal is the major route of exposure to nanofluids. Some proportion (28%) of participants from each of the country find injection of nanofluids to be of main concern. Just 20% consider ingestion as a problem.

Most of the participants dispose of the waste nanoparticles either as ordinary chemical waste (35%) or hand it over to special waste disposal companies (29%). A few organisations in the UK and Portugal follow their own procedures. Interestingly 10% of the organisations claim to have no waste nanoparticles at all. The majority of the countries dispose of the nanofluids as ordinary chemical waste (44%) or handover it over to special waste disposal organisations (24%). One participant in Turkey follows its own waste disposal method along with standard methods. Consequently, most of the groups (51 to 53%) have specific storage places for nanoparticles/nanofluids in their laboratories and employ appropriate measures to reduce the risk of exposure (Fig. 3).

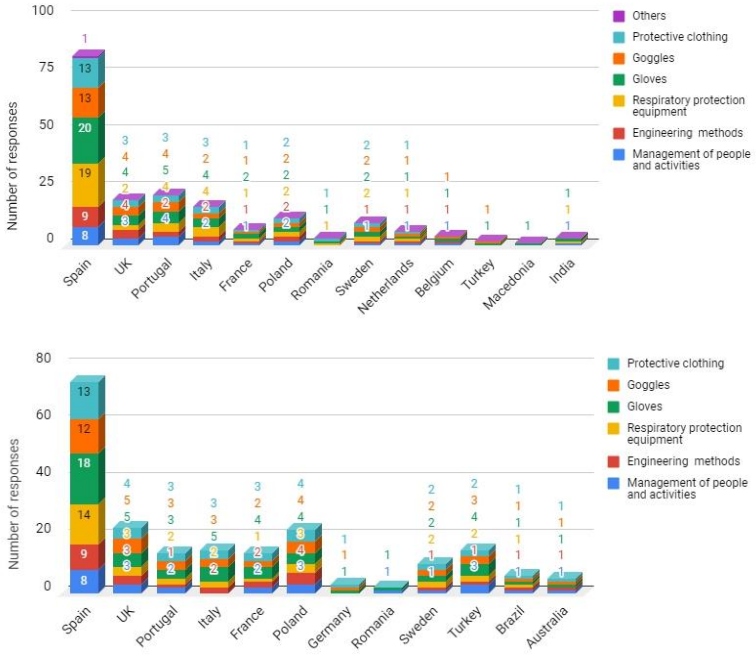

Figure 3. Measures to reduce risk of exposure.

Conclusions: A survey on the safety requirements while using nanoparticles/nanofluids has been carried out under 19 countries. From the 68 responses, first conclusions are

drawn. The majority of the answers indicate a very careful handling of these special materials based on standard safety rules usually employed to similar chemical substances. However, it seems that there are no specific rules for handling nanofluids/nanoparticles. Especially the nanofluids seem to be treated as any other comparable chemical risky liquids. This goes along with the finding that there is no special literature on the subject of nanofluid safety. The found and analysed references deal with safety aspects of solid nanomaterials and their processing but not with nanofluids (see e.g. [3]). Moreover, no references on the subject could be provided.

All participants are obviously aware of the specific risks which are related to nanoparticles/nanofluids. However, special training of employees or monitoring of workplaces is very limited. Merely 6 to 7% monitor workplace for nanoparticles/nanofluids and only 28% provide special training to employees. This is really surprising because the survey reveals that more than 750 people are working either with nanoparticles or with nanofluids or with both. It is hypothesised, that the reason for this finding is, that majority of the nanoparticles/nanofluids handling has research character and is still carried out in laboratories. Anyway, the expected future industrial applications demand the development of clear European standards for handling these specific nanomaterials.

Acknowledgement: First of all the authors like to thank sincerely all the people who responded to the survey. This work is part of the Grant 49VF170005 and the NanoUptake COST Action (European Cooperation in Science and Technology) CA15119: Overcoming Barriers to Nanofluids Market Uptake.

References:

1. M.H. Buschmann, R. Azizian, T. Kempe, J.E. Juliá, R. Martínez-Cuenca, B. Sundén, Z. Wu, A. Seppälä, and T. Ala-Nissila, *Correct interpretation of nanofluid convective heat transfer*, Int. J. Therm. Sci. 129 (2018) 504–531.
2. http://www.cost.eu/COST_Actions/ca/CA15119, http://www.nanouptake.eu/
3. B. Fadeel et al., Safety assessment of graphene-based materials: Focus on human health and the environment, ACS Nano. 12(11) (2018) 10582–10620.

1st International Conference on Nanofluids (ICNf2019)
2nd European Symposium on Nanofluids (ESNf2019)
26-28 June 2019, Castelló, Spain

Environmental performance of nanofluids in Life Cycle Perspective

J. Krupanek[1]

[1]Instytut Ekologii Terenów Uprzemysłowionych, Katowice, Kossutha 6

[*]Corresponding author: j.krupanek@ietu.pl

Keywords: nanofluids, human health, environmental performance, Life Cycle Perspective

Abstract:

Nanofluids have novel properties that make them potentially useful in many applications. Production of nanofluids, their application, use in products and final disposal can generate health and safety risks and environmental impacts but at the same time provide environmental benefits. These aspects should be carefully considered in implementing of nano-based solutions in practice. A review of current studies concerning these issues in Life Cycle Perspective was performed to provide an insight into the potential drivers and obstacles to nanofluid applications.

Introduction

The health, safety and environmental aspects of nano-based solutions have been the subject of research and activities of international and national organisations in recent years. It is widely recognised that Life Cycle approach should be applied in assessing the impacts on environment and human health [1, 2]. A set of methodological approaches are used for this purpose including Life Cycle Assessment and Health Risk Assessment. To conduct the assessment on a wider scale further extensive research is needed with regard to particular life cycle phases: production, use and disposal and such aspects as hazards to humans and environment [1]. The results of the studies should serve the purpose of products design and establishing appropriate regulations securing high protection of human health and environmental performance.

Key health and environmental aspects of nanofluids implementation

Nanofluids contain nanoparticles which have been recognized as one of the major occupational health and safety risks. The nanoparticles and their by-products can be released into surrounding atmosphere, soil and water at each stage of their life cycle: production, use, waste, and disposal [1]. The influence of nanoparticles on humans and environment vary during different stages of their life cycle. On the other hand use of

nanofluids can be beneficial in terms of energy savings, reduction of carbon footprint and toxicity impact.

The Life Cycle Assessment studies performed for promising nanofluids applications quantified potential environmental impacts and benefits [2,3,4]. The results are in general positive with regard to their environmental performance indicating main advantages and potential drawbacks.

The harmfulness of nanomaterials is still ambiguous. Health Risk Assessment studies show that exposure to nanomaterials may occur through inhalation, dermal contact, accidental injection and ingestion. Inhalation of airborne exposure presents the greatest exposure hazard. Human hazards were characterised for nanoparticles such as iron oxide, copper, chromium, zinc oxide, silicon carbide and titanium dioxide [5]. Nanoparticles emitted to the environment would accumulate in water, soil, and plants and depending on their characteristics can pose risk for biota [6, 7]. Modelling studies show essential potential for distribution of nanoparticles in the environment [8]. Despite the efforts undertaken so far, the current knowledge of the nanotechnology threat to human health and environment is still insufficient. It is widely recognized that the impacts need to be examined by employing Life Cycle Assessment and Health Risk Assessment in an integrated manner [1, 4].

In Life Cycle Perspective the impact of nanomaterials production can be an important factor, depending on their type and content. For example carbon nanoparticles can be produced in energy and emission intensive processes. In some cases, as the synthesis of ionic liquid, the risks can be also attributed to use of organic reagents and solvents. On the other hand there are reported opportunities for production of nanoparticles from wastes in a sustainable manner. Another essential issue are the requirements for design of the functional components dedicated to application of nanoparticles which can be beneficial or detrimental from Life Cycle Perspective.

For the service phase of nanofluids there are not sufficient predictions concerning such aspects as their lifetime, degradation/wearing out, stability and energy efficiency. Potential improvements in environmental performance, including the aspects of energy efficiency and carbon footprint, are reported for selected applications such as nanofluid-based concentrating solar water heating and photovoltaic systems [9, 10].

It is recognised and required that after the service life the functional components containing nanofluids should be safely dismantled from the utility/product and disposed in a strict way. There is limited experience regarding this aspect. Many conventional

waste treatment processes (incineration, scrubbing/filtering etc.) do not decompose nanoparticles, allowing their direct release into the environment. Current studies show some opportunities for recovery of nanoparticles from nanofluids using various techniques [11]: extraction, separation, and re-use of gold nanoparticles [12], palladium cadmium and zinc [13] and iron-containing nanoparticles [14].

The potential threat to environment by nanoparticles can be reduced by using efficient way of production, preparation, transportation, use and waste management. Aspects of environment assessment, health risk and safety of nanomaterials are the subject of research strategies in Europe and USA. These themes include the need for standardization and nomenclature. The International Organization for Standardization (ISO) and the European Committee for Standardization (CEN) are taking leading roles on these issues. In Europe, safety of nanomaterials is regulated by the REACH Regulation and the CLP (Classification, Labelling and Packaging) Regulation. For Occupational exposure a set of guidelines was prepared including OSHA and NIOSH. Up to date, there is no specific legislation to control the release of nanoparticles into the environment. Recommendations concerning protection measures, includes laboratory good practices, codes of conduct, safety standards, Occupational Health and Safety regulations, national and international guidelines [15, 16].

Regulatory schemes for market introduction of nanomaterials are proposed by responsible agencies and research institutions [17]. It is suggested that manufacturers and retailers of nano-enhanced products should build plans for recovering and recycling the nanomaterials into the product lifecycle. Products should be designed so that nanoparticles can be separated out and re-used as easily as possible. Recovery and re-use of these materials could speed up commercial application of nanotechnology, reducing risk related to nano-waste and decreasing production costs [17].

Conclusions

Up to date the results of research on environmental and health aspects of the nanomaterials and nanofluids are a good indication of strong and weak points of nanofluids applications in practice and the best opportunities to gain the environmental benefits in the Life Cycle Perspective. More comprehensive integration of results from toxicity and environmental studies in the development of engineered nanomaterials is recommended from occupational point of view and at the same time from environmental perspective. Results of the research should provide a sound basis for actions, policies and regulations concerning health, safety and environmental aspects of nanofluids.

References (Selected):

1. M. Miseljic, S. I. Olsen Life-cycle assessment of engineered nanomaterials: a literature review of assessment status, J Nanopart Res., 2014, 16, pp 2427 -2460.
2. R. Harder, H. Holmquist, S. Molander, M. Svanström, G. M. Peters, Review of Environmental Assessment Case Studies Blending Elements of Risk Assessment and Life Cycle Assessment Environ. Sci. Technol. 2015, 49, pp 13083−13093.
3. S. Scalbi, P. Masoni, Procedia Comparative Environmental Assessment Of Nanofluid Application In Refrigeration Of Power Electronic Traction Systems Environmental Science, Engineering and Management 2, 2015 (1) pp 93-106.
4. G. Barberio, S. Scalbi, P. Buttol, P. Masoni, S. Righi, Combining life cycle assessment and qualitative risk assessment: the case study of alumina nanofluid production. Sci Total Environ. 2014; 496, pp122-131.
5. M. Rafiq, Y. Lv, C. Li A Review on Properties, Opportunities, and Challenges of Transformer Oil-Based Nanofluids, Journal of Nanomaterials, vol. 2016, 23 p., 2016.
6. A. Mottier, F. Mouchet, É. Pinelli, L. Gauthier, E. Flahaut, Environmental impact of engineered carbon nanoparticles: from releases to effects on the aquatic biota, Current Opinion in Biotechnology, Volume 46, 2017, pp 1-6.
7. L. E. Ogden Nanoparticles in the Environment: Tiny Size, Large Consequences? BioScience, 2013, Volume 63, Issue 3, p 236.
8. C Coll, D Notter, F Gottschalk, T Sun, C Som, B. Nowack Probabilistic environmental risk assessment of five nanomaterials (nano-TiO2, nano-Ag, nano-ZnO, CNT, and fullerenes) Nanotoxicology. 2016;10(4), pp 436-44.
9. V. Khullar & H. Tyagi A study on environmental impact of nanofluid-based concentrating solar water heating system, International Journal of Environmental Studies - Issue 2: Energy Conservation, Conversion and Storage, 2012, Volume 69, pp 220-232.
10. Z. Said, S. Arora, E. Bellos, A review on performance and environmental effects of conventional and nanofluid-based thermal photovoltaics Renewable and Sustainable Energy Reviews 2018, 94, pp 302–316,
11. A. Deep; K. Kumar; P. Kumar, P. Kumar, A. L. Sharma, B. Gupta; L. M. Bharadwaj, Recovery of Pure ZnO Nanoparticles from Spent Zn-MnO2 Alkaline Batteries. Environmental Science & Technology, 2011, 45 (24), pp 10551-10556.
12. P. Pati, S. McGinnis; P. J. Vikesland, Waste not want not: life cycle implications of gold recovery and recycling from nanowaste. Environmental Science-Nano, 2016, 3 (5), pp 1133-1143.
13. O. Myakonkaya, C. Guibert, J. Eastoe, I. Grillo, Recovery of Nanoparticles Made Easy, Langmuir, 2010, 26 (6), pp 3794–3797.
14. O. Myakonkaya, Z. Y. Hu; M. F. Nazar, J. Eastoe, Recycling Functional Colloids and Nanoparticles. Chemistry-a European Journal, 2010, 16 (39), pp 11784-11790.
15. K. Moore, I. Stuart, F. O'Brien, A. Lewis, 2016, Innovating Nanoparticle Safety: Storage, Handling, and Disposal Processes An Interactive Qualifying Project, Final Report, WPI, NTB.
16. World Health Organization, 2017, WHO guidelines on protecting workers from potential risks of manufactured nanomaterials. Geneva Licence: CC BY-NC-SA 3.0 IGO.
17. T. Faunce, B. Kolodziejczyk, Need for Disposal and Recycling Standards POLICY AREA: 2030 Agenda Nanowaste: April 27, 2017, www.G20-insights.org.

1st International Conference on Nanofluids (ICNf2019)
2nd European Symposium on Nanofluids (ESNf2019)
26-28 June 2019, Castelló, Spain

Real World: Safety Nanofluids

M.J.V. Lourenço[1]

[1]Centro de Química Estrutural, Faculdade de Ciências,

Universidade de Lisboa, 1749-016 Lisboa, Portugal

*Corresponding author: mjlourenco@ciencias.ulisboa.pt

Keywords: nanomaterial, nanofluid, safety, sustainability

Abstract: Nowadays, numerous studies on nanomaterials (NM) and Nanofluids (NF) are currently accounted for. With the common goal of the scientific society in fulfilling the sustainable development proposed by the UN until 2030, it is necessary to merge efforts based on the scientific and technological knowledge already acquired. There are thousands of publications on the technological advantages in the use of NF, its benefits and harm, properties, behaviors, etc., but little or nothing is known about the safety of some of these systems in the short and medium term, what is the correct form of storing or even destroy, what its life circle and whether it is likely or not to reuse it. Depending on the characteristics of the base fluid (water, ethylene glycol or even an ionic liquid (IL)) and the addition or not of surfactants, this problematic becomes complex. All these factors need an organization and prediction methodology like Dmitry Mendeleev (DM) achieved 150 years ago with the chemical elements of the periodic table. In this study NF (natural NF are also included) general data are discussed, for a profound reflection leading to the elaboration of a methodology that respects a near future, intended to be sustainable at the level of existing resources, health and environmental protection.

Introduction/Background: UNESCO proclaimed 2019 The International Year of the Periodic Table of Chemical Elements (PT) (www.IYPT2019.org). We celebrate the 150th anniversary of the publication of the first model of the PT, established by DM in 1869. A profound reflection on the visionary ideas of DM makes us think about organization. DM get involved in other areas of knowledge, like aeronautics, meteorology, Arctic exploration (Ice breaker design), education, legal expertise, economics, metrology, and painting, among others. But the major part of his research was devoted to what we now call the concept of sustainable development, rational management of natural resources and ecology. In his time DM perceived the need to prevent the excessive exploitation of natural resources, informed people about the exhaustion of minerals and that they

should decrease consumption, and restrain the use of oil, water and coal. He defended the careful use of soil to improve its fertility. Thus, his prophecies on the management of natural resources and sustainable development are as important as the Periodic Law and his PT.

I do believe that we have a complex mission to fulfil in the development of energy-efficient, low-polluting (CO_2 footprint) systems, with secondary resources and which must be based, whenever possible in a sustainable circular economy without irreversible environmental damage. In this context the NM, NF and INF (IoNanofluids) can play a key role. However, this sustainability language arrives to 2019 with little effective demonstration. If on one hand there is recognition of exhaustion of natural resources, case of the Critical Raw materials (CRM), on the other hand there seems to be no unanimous awareness for this global problem.

The effects of the addition of NM to base fluids and of NF prepared by various methods are well known, and we all recognize large changes in properties such as viscosity and thermal conductivity. There is also knowledge that the literature on NF and INF encompasses in these results a set of different techniques of measurement, characterization and preparation, totally different, and without informing correctly about the errors associated to each of them. There are experimental limitations, for example, in the transient hot-wire technique, not always fulfilled or accounted for. This results in infinite comparisons and tables of data that are never validated [1]. There is a need to define a special organization for the NF and to know the degree of toxicity appropriate to the intended use. I draw attention to the urgent need for NM and Standard Reference Methods for the so-called NF. In addition, there is an urgent need of Certified Reference Materials for NM and Standard Reference Methods for the NF [2].

The number of phases involved in the NF (at least two) is also important in this strategy. The biphasic system is preferable, as it is a dispersion (and water is many times involved in the base fluid). Dispersion, by definition, is a material that consists of a dispersing medium and a dispersed phase. Both the dispersing medium and the dispersed phase can be solid, liquid or gaseous, leading to a number of possible combinations [3]. In the NF case the dispersing medium is a fluid and the dispersed phase a NM. A common term to denote a similar class of materials is the term 'colloid', but the upper size limit of the particles in a colloid system varies in different definitions of the term between 100 nm [4], and 1000 nm [5]. By distinguishing dispersions from colloids, guiding our research and analysis to all systems that have particles below 100nm (definition of NM) we

achieve an organization. JCR report [6] and the European Initiative for Sustainable Development through Nanotechnologies (Nanofutures.eu) provides recommendations for a harmonized and coherent implementation of the NM definition in any specific regulatory context at European Union and at national level. The need for stabilization of NF necessarily implies the use of DLS techniques [7] or equivalents to characterize the system under study. The stability of a NF is very important even for safety reasons. Any sedimentation occurring and not accounted for may jeopardize the safety and operation of, for example, flow systems, clog process equipments and cause accidents.

Discussion and Results: The use of NM points to the resource saving action line, as we use a much smaller amount of matter and, by definition, we get completely different properties of the material from it originates. However, we will have to know the useful life of the NM used and its final destination. The same happens with the NF. The total characterization of NM (www.nanoreg.eu) and NF will allow a recovery and reuse of the entities involved and a control over the environment and safer human exposure, as they know the NM and the NF already used, and where it is. The use of NF with natural origin NM may solve some problems of production, scarcity and toxicity as is also the case of melanin and biomass [8]. Silver and copper nanoparticles are known to be strongly ecotoxic. There are also many studies on titanium dioxide and zinc oxide, showing diverging results, depending on the forms of nanoparticles studied. These studies should be considered in the work to be performed with NF and INF of these NM [9-13].

INF are complex systems with NM dispersed in ILs. The reputation of these solvents as "environmentally friendly" chemicals is mainly based on their insignificant vapor pressure. However, the solubility of ILs in water and a number of literature documenting the toxicity of ILs for aquatic organisms highlight a real cause of concern. The importance of IL in medical and pharmaceutical applications is now relevant and it has already been realized that its antimicrobial and cytotoxic activity may have several benefits in the future. It will then be necessary to assess the levels of toxicity and tolerances for health without uncontrolled environmental hazards [14 e 15].

The Globally Harmonized System of Classification and Labelling of Chemicals (GHS) contains a standard specification for safety data sheets (SDS) (www.osha.gov); the SDS follows a 16 section format which is internationally agreed and for substances especially, the SDS should be followed with an Annex which contains the exposure scenarios of this particular substance (http://guidance.echa.europa.eu); (https://euon.echa.europa.eu/safety); (https://osha.europa.eu/) and (www.unece.org).

Summary/Conclusions: The approach of relevant challenges for sustainable societies, in fields as diverse as health, food security or energy, quickly imposes a methodology for the operation of the systems involved, the measurement of permissible levels without disturbing environmental balances, and the evaluation of the toxicity applied to cure health problems. Human food and transport systems in the future (8.5 billion by 2030) will have to consider the release of CO_2 generated, with the direct consequences this implies. NF has the potential to play an important role in increasing the sustainability of a wide range of sectors. NM, NF and INF could contribute to more sustainable uses through cleaner, less wasteful production processes and can substitute conventional materials, leading to savings in raw materials and energy.

References:

1. Nurettin Sezer, Muataz A. Atieh, Muammer Koc, *A comprehensive review on synthesis, stability, thermophysical properties, and characterization of nanofluids*, Powder Technology, Volume 344, Pages 404-431, 2018
2. Y. Ramaye, V. Kestens, K.A. Braun, T. Linsinger, A. Held, G. Roebben, *The certification of equivalent diameters of silica nanoparticles in aqueous solution,* Certified Reference Material ERM®- FD101b, JRC 105046, Luxembourg, 2017
3. ISO TS 80004-1: *Nanotechnologies – Vocabulary – Part 1: Core terms*, 2010
4. ISO 1942-2-1989: *Dental vocabulary – Part 2: Dental materials*, 1989
5. R.J. Hunter*, Foundations of Colloid Science*, Oxford University Press, 2001
6. Hubert Rauscher, Gert Roebben, Agnieszka Mech, Neil Gibson, Vikram Kestens, Thomas P. J. Linsinger and Juan Riego Sintes, *An overview of concepts and terms used in the European Commission's definition of nanomaterial"*, Joint Research Centre (JRC), Publications Office of the European Union, ISBN 978-92-79-99660-3, European Union, 2019
7. F. Babick, C. Ullmann, *Error propagation at the conversion of particle size distributions*, Powder Technology 301: 503–510, 2016
8. R. Madavan, S. Senthil Kumar, M. Willuice Iruthyarajan, *A Comparative Investigation on Effects of Nanoparticles on Characteristics of Natural Esters - based Nanofluids.* Colloids and Surfaces A: 556, 30-36, 2018
9. European Commission, Types and Uses of Nanomaterials, Including Safety Aspects, Commission Staff Working Paper SWD (2012), European Commission, Brussels, 2012
10. Fedora Grande, Paola Tucci, *Titanium Dioxide Nanoparticles: a Risk for Human Health?* Mini-Reviews in Medicinal Chemistry, Vol. 16, Issue 9, 2016

11. Engineered Nanoparticles - Review of Health and Environmental Safety (ENRHES), final-report; conclusions on p. 359 – 360 and EC4SafeNano: European Centre for Risk Management and Safe Innovation in Nanomaterials Nanotechnologies
12. COMMISSION STAFF WORKING PAPER *Types and uses of nanomaterials, including safety aspects*; Appendix 6 Nanomaterials and worker protection; Appendix 9 Standardisation, Brussels, 3.10.2012, SWD (2012), 2012
13. David Rickerby, Nanotechnology for Sustainable Manufacturing, 1st Edition, CRC Press, ISBN 9781482214826, 2014
14. Wendel Wohlleben, Thomas A.J. Kuhlbusch, Jürgen Schnekenburger, Claus-Michael Lehr, *Safety of Nanomaterials along Their Lifecycle: Release, Exposure, and Human Hazards*, CRC Press, 2014
15. Ksenia S. Egorova, Evgeniy G. Gordeev and Valentine P. Ananikov, “Biological Activity of Ionic Liquids and Their Application in Pharmaceutics and Medicine”, Chem. Rev., 117, 7132−7189, 2017

1st International Conference on Nanofluids (ICNf2019)
2nd European Symposium on Nanofluids (ESNf2019)
26-28 June 2019, Castelló, Spain

Occupational exposure to engineered nanoparticles – industrial case studies

V. Sanfélix[1], M. Domat[2], E. Monfort[1], A. López-Lilao[1], A. García[1], and A. Ballesteros[2]

[1]Instituto de Tecnología Cerámica-AICE, Universitat Jaume I.

[2]ITENE-Instituto Tecnológico del Embalaje, Transporte y Logística.

[*]Corresponding author: vsanfelix@itc.uji.es

Keywords: Occupational exposure, engineered nanoparticles, dustiness, toxicity

Abstract:

Exposure assessment to nanomaterials in industrial workplaces shows that the handling of manufactured nanomaterials may give rise to occupational exposure to primary nanoparticles. Other workplace-related sources include releases from conventional compounds which may contain a significant fraction of nano-sized particles. This work aims to evaluate occupational exposure to engineered nanoparticles under real-world operating conditions and to assess the dustiness index as an exposure predictor metric. The studied operations, due to their representativeness, were milling, dosing, weighing and synthesis. The nanomaterials studied were Au, Ag, Perovskitas, TiO_2 and SiO_2. The results showed the influence of the intrinsic properties of material (dustiness) and the engineered controls on the concentrations obtained in the industrial scenarios studied.

Introduction/Background:

Nanomaterials are present in everyday products such as cosmetics, paints, electronics and medicines. For instance, nano-titanium dioxide is used as a UV-blocking agent in paints or sunscreen; nano-silver as an anti-microbial in paints, textile and medical applications; silica powders in pharmaceutical industry, printer toners and electronic parts.

However, although nanomaterials have many beneficial properties, there are large gaps in the knowledge about their associated health hazards. The Scientific Committee on Emerging and Newly Identified Health Risks found that there are enough evidences of health hazards associated with different manufactured nanomaterials. Not all nanomaterials have necessarily a toxic effect, however, a case-by-case approach is necessary while ongoing research continues.

In this regard, nanoparticle exposure (<100 nm; NPs) in workplaces has been an issue of concern for the last decades, and the subject of numerous research studies. The health impacts deriving from inhalation of NPs are related with their capacity to penetrate into the deeper sections of the respiratory tract due to their small size (Oberdorster, 2000).

NPs found in industrial workplaces come generally from two sources: (i) emissions resulting from industrial activities and (ii) background aerosols. The NPs emitted by industrial activities may be engineered and used as input/output in the manufacturing process, or non-engineered and formed unintentionally as a result of an industrial activity.

Regarding the exposure mitigation strategies, they are based on the control methods hierarchy (E.U., 2014). Primarily, recommended methods to minimize exposures to hazardous substances in workplaces are the elimination or isolation of their sources. If these measures are not applicable, engineering controls should be applied (e.g. ventilation, extraction) and finally, personal protective equipment (respirators or masks).

The present work aims to evaluate the occupational exposure to engineered nanoparticles under real-world operating conditions. The study was assessed by a case-study approach. The methodology presented consists of NPs exposure level determination, characterization of these collected NPs (physical, morphological, chemical and toxicological) and the dustiness of the handled nanomaterial. It should be noted that this study did not aim to discuss the exposure concentrations from a regulatory compliance perspective, because when evaluating the occupational exposure under real operating conditions in industrial scenarios, it was not possible to isolate the handling of the nanomaterial to be studied from other sources.

Discussion and Results:

Workplace exposure assessments were carried out by monitoring particle number concentration and their mean diameter, using online instrumentation. The monitors measured particle diameters from 4nm to 1.5µm. All instruments were intercompared prior to the measurements for quality assurance purposes. A real-time, self-designed instrument was also used and validated in the real scenarios.

Particle number concentrations were monitored at the emission source, in the worker area or in the breathing zone (depending on the scenario), in indoor (background) and outdoor locations (OECD, 2015). The outdoor location was to evaluate the possible contribution of outdoor sources (e.g., road traffic).

Particles for chemical and morphological analysis by TEM were collected onto Au grids and attached to air sample cassettes. In addition, a toxicological characterization was performed on some samples. Considering inhalation as the most common route of exposure, cytotoxic assays were developed. Samples in bioaerosol form were collected in cell culture medium by a BioSampler®.

Finally, the nanomaterial dustiness as an exposure predictor metric was also assessed by using an adapted rotating drum method for NPs (EN 15051-2) (Ribalta et al., 2018).

Worker exposure was here analyzed considering the operation and the handled nanomaterial. The selected operations, due to their representativeness, were milling, dosing, weighing and synthesis. The nanomateriales studied were Au, Ag, Perovskitas, TiO_2 and SiO_2. In some industrial scenarios engineering controls had been implemented.

Particle number concentrations increased significantly during the dosing and weighing of TiO_2 and SiO_2, obtaining average values higher than 120000 cm^{-3}. In this scenario, engineering controls were not implemented. In addition, the indoor background prior to the studied operations was high (>70000 cm^{-3}). Extensively, the same operations have been evaluated in other industrial scenario, in which a local extraction was implemented. In this case, an average concentration of 30000 cm^{-3} was recorded when TiO_2 was weighed and dosed during the production of a paint. On the other hand, it should be noted that different TiO_2 nanomaterials presented different dustiness index (concentrations in the range 10-200 cm^{-3}), which influence the natural tendency of the material to emit dust. Moreover in the TEM analysis, it has been observed micro sized agglomerates of NPs. Therefore, to adequately assess exposure it is important to be able to measure in a wide size range (from nanometres to microns).

The handling of nano-silver, showed a similar average concentration (30000 cm^{-3}) both when the nanomaterial was dosed into a composition and when the operations required for weighing were carried out, despite having a localised extraction ventilation (LEV) system operating during dosing.

Finally, during gold grinding a concentration of about 14000 cm^{-3} was obtained without using corrective measures, and during the synthesis of perovskites an average concentration of 5000 cm^{-3} was recorded, when an extractor hood was being used.

In the TEM analysis of samples taken, the presence of the finest particles of conventional products used in the manufacture of paints, e.g. $CaCO_3$, was generally observed when they were used as a dry powders. On the other hand, particles in the

nano range associated with the use of diesel-powered forklifts inside the company were also identified in some scenarios.

Finally, the results in toxicity assays showed an average cellular viability of 65%, which means that approximately 65% of the cells have continued to live (without rupture of their cell wall) after the exposure to the enviromental pollutants.

Summary/Conclusions:

The exposure assessment to engineered NPs in real industrial scenarios showed that the handling of some nanomaterials (TiO_2, SiO_2) entails a significant NPs concentration increase. However, these concentrations cannot be associated only with the handling of these nanomaterials. Other sources, such as the dosing of some conventional materials to the composition also contributed to the total work-related NPs exposure, because they may contain a significant fraction of nano-sized particles. In addition, the TEM analysis showed the tendency of nanomaterials to rapidly agglomerate, therefore, to adequately assess exposure it is important to be able to measure in a wide size range (from nanometres to microns). Finally, to minimize the exposure, it has been observed that the implementation of widespread engineering controls (such as LEV) can significantly reduce the NPs exposure.

Acknowledgements: This work has been funded by IVACE, Instituto Valenciano de Competitividad Empresarial, through the Fondos europeos FEDER de Desarrollo Regional, by funding the projects NanoImpulsa and ProSafe (IMDEEA/2017/96, IMDEEA/2017/87, IMDEEA/201/78, IMDEEA/2018/106).

References:

1. E.U., 2014 COUNCIL DIRECTIVE 98/24/EC. Off. J. Eur. Communities.
2. European Committee for Standardization (CEN), 2017. EN 15051-2 Workplace exposure - Measurement of the dustiness of bulk materials – Part 2: Rotating drum method.
3. Oberdorster, G., 2000. Pulmonary effects of inhaled ultrafine particles. Int. Arch. Occup. Environ. Health 74, 1-8. https://doi.org/10.1007/s00400000185
4. OECD, 2015. Harmonized Tiered Approach to Measure and Assess the Potential Exposure to Airborne Emissions of Engineered Nano-Objects and their Agglomerates and Aggregates at Workplaces. Ser. Saf. Manuf. Nanomater. No.55 55, JT03378848-JT03378848.

5. Ribalta, C., Viana, M., López-Lilao, A., & Monfort, E. (2018). On the relationship between exposure to particles and dustiness during handling of powders in industrial settings. Annals of work exposures and health, 63(1), 107-123.

Funded by the Horizon 2020 Framework Programme
of the European Union